Investigating the Molecular Pathogenesis of Tuberculosis-associated Immune Reconstitution Inflammatory Syndrome

Thesis Submitted in Fulfilment of the Requirements for the Degree of:

Doctor of Philosophy in Medicine

Author:

Raymond Moseki

Department of Medicine

University of Cape Town

September 2024

Table of Contents

Declaration

I, Raymond Moeketsi Moseki, hereby declare that this thesis is entirely original work produced by myself, except in instances noted in the acknowledgments and in the section below. The entirety of this work nor its portions has ever been, is currently being, nor will ever be submitted for another degree at this university or any other.

The conceptual framework for each study was developed collaboratively with Prof. Graeme Meintjes, Dr. Rachel Lai, Prof. Robert J Wilkinson, Dr. Catherine Riou, Associate Prof. Muki Shey, Dr. Elsa Du Bruyn, and Dr. Daniel Barber. The funding for the various studies was contributed by Prof. Graeme Meintjes.

Statement of work done by the PhD candidate

This PhD contains certain wet lab-based experiments which were not conducted by myself. The study in chapter 4 contains experiments performed in mice and ex vivo experiments using peripheral blood mononuclear cells (PBMC) collected from TB inpatients that were enrolled in the TBART cohort study. The flow cytometry experiments performed in human PBMC, including the data analyses, data interpretation and compilation of the manuscript were performed by myself. Murine experiments including the generation of Eomes and Tbet floxed mice, infection with *Mycobacterium avium*, flow cytometry experiments and data analyses were performed in the United States of America by Dr. Daniel Barber and his team.

Work presented in chapter 5 contains RNA sequencing findings which can be divided into wet lab-based experimental manipulations and computational biology analysis. The wet lab aspects in chapter 5 including RNA isolation from whole blood was performed by Associate Professor Muki Shey. The RNA samples were shipped to Francis Crick Institute, London, United Kingdom, for sequencing. Prof. Graeme Meintjes arrange the material transfer documentation associated with sample shipping. RNA sequencing libraries were prepared by Dr. Rachel Lai prior to sequencing. The data from the sequenced samples was shipped on a hard drive by air to South Africa. All data analyses and interpretation presented in chapter 5 were conducted by myself.

All the wet lab experiments, data analyses and data interpretation in chapter 6 and 7 were conducted by myself.

"I confirm that I have been granted permission by the University of Cape Town's Doctoral Degrees Board to include the following publication(s) in my PhD thesis, and where co-authorships are involved, my co-authors have agreed that I may include the publication(s): Phenotypic profile of *Mycobacterium tuberculosis*-specific CD4 T-cell responses in people with advanced human immunodeficiency virus infection who develop Tuberculosis-associated Immune Reconstitution Inflammatory Syndrome", the content of which is identical to Chapter 4 in this thesis.

Moseki, RM

September 2024

Acknowledgements

This body of work reflects the human resource that was available to me throughout my PhD journey. These are the people who have afforded me unconditional support which enabled me to weather the many challenges without crumbling.

First, I acknowledge Jesus Christ my Lord and Savior who keeps me. Lord Jesus, you have done all things well and I thank you for offering me the gifts of grace, mercy and favor.

To the administrators of the Fogarty HIV-associated TB Training Program at UCT, thank you for putting together such a comprehensive fellowship which has contributed tremendously to my growth as a scientist.

I extend my sincere gratitude and appreciation to the current and former MSc, PhD students and Postdoctoral fellows in CIDRI-Africa in no specific order Nomfundo Sibiya, Rudranil Hazra, Mthawelanga Ndengane, Avuyonke Balfour, Robert Rousseau, Kate Haigh, Nomawetho Masina and Abulele Bekiswa. Thank you for your warm, caring and inviting demeanor. I relished the thought-provoking discourse around all things science. Your dedication to excel in a dynamic and competitive field of immunology is inspiring. Your selfless aspiration to impact the lives of the sick is unknown to many yet it shows in your daily commitment which is admirable.

To the CIDRI-Africa office personnel. Thank you for making the office a professional working space. Thank you for your great spirit of Ubuntu which many embodied. I enjoyed the food and snacks we shared from time to time. To Sis' Nonzwakazi Bangani, all the fruit you carried for me every now and then kept me well-nourished when I was stubborn to find the time to eat. Me and my stomach thank you profusely.

For the few light-hearted conversations we had with Ms Rene Goliath, Ms Megan McMaster and Mr Franscisco Lakay, I say thank you. Those conversations were a welcomed reprieve from the grueling pace of working constantly at the highest level. To Mrs. Celeste Worship, thank you for all the deep conversations we shared about spirituality. Our conversations were enlightening and often helped put life in perspective. I feel blessed to have met you. To Ms. Nompumelelo Maxebengula, your friendship is like medicine, it helped me heal the traumas I never knew existed.

A particular note of appreciation to Mrs Erica Morey, Ms. Crystal Geduld, Mrs. Sohana Ranglal, and Mrs. Kathryn Wood for helping with all the administrative work. Your service which was rendered with a smile and remarkable finesse simplified my stressful academic life. To Mrs. Kathryn Wood, I have learned so much from your remarkable humanity. Thank you for serving as a quiet example that demonstrated what daily committed work looks like. You have set a standard for me. Thank you. Mrs Sohana Ranglal, your kind and gentle nature is truly incredible and endearing. Thank you for everything.

To my long-time friends, Mampoa Windy Thekiso, August Vuitton Moatlhodi, Mosedi Mphuthi thank you for constantly keeping in touch. May your pain be champagne!

A note of gratitude, and appreciation to all my supervisors. Your support and guidance is embedded in me and I'm grateful for your tutelage. At the very initial stages, hands on training on cell culture, cell staining for flow cytometry, cytometer set-up, acquisition and data analysis were provided by Dr Catherine Riou, who additionally provided support in writing the manuscript.

Dr Rachel Lai provided hands on training on the *ex vivo* cell culture and drug treatment experiments and provided additional feedback on data analysis. Mr Francisco Lakay provided hands-on training in the biosafety level 3 facility, for handling *Mycobacterium tuberculosis* cultures.

Dr Cari Stek was an investigator for the Pred-ART intervention trial from which the biological samples for the transcriptomics study are derived. Associate Prof. Muki Shey extracted RNA from whole blood samples collected from all patients. Prof. Graeme Meintjes facilitated the material transfer documents for shipping the RNA samples to the United Kingdom. Dr Rachel Lai prepared the sequencing libraries, sent the samples for sequencing, and shipped the data back to South Africa for analysis. Dr Jon Ambler provided initial hands-on support on the command-line prompt code that was used for running the data through the RNA-sequencing pipeline and provided feedback on the R code used for data analysis.

The murine experiments including the deletion of Eomes and Tbet, subsequent infection with *Mycobacterium avium* and data analysis were performed by Prof. Daniel Barber and his team in the United States of America.

Prof. Graeme Meintjes read and edited all ethics application and renewal documentation. All supervisors and authors provided feedback on all written work, including study proposal, standard operating procedure protocols, abstracts, manuscripts, power point presentations, funding applications, and drafts of this thesis.

Moreover, I want to acknowledge the various funders. I extend my warm gratitude to the funders for taking interest in my career development. The Fogarty HIV-associated TB Training Program (HATTP) fellowship which was secured by myself with support from Prof. Graeme Meintjes. This fellowship supported my living expenses and family. The NRF-SARChI fund secured by Prof. Graeme Meintjes, supported both my living expenses and the laboratory consumables for the various studies. The Wellcome Trust funding secured by Prof. Robert Wilkinson, supported my living expenses. All the funding made it possible to complete my studies.

Finally, to the patients for the clinical specimen that I was entrusted with to contribute insights into important clinical questions pertaining to the complications arising from the co-treatment of HIV and TB. The precious samples were handled with a sense of respect and purpose. Thank you for contributing towards these efforts.

Dedication

This body of work is dedicated to my sweet mother, Catherine Sedibe and her now late substitute, Monica Makabela. Thank you both for your undying love and enduring support.

Thesis summary

This thesis comprises a series of studies that adapted a reverse translational approach to investigate the mechanisms underlying the immunopathogenesis of paradoxical tuberculosis-associated immune reconstitution inflammatory syndrome (TB-IRIS).

Paradoxical TB-IRIS is an aberrant immune response targeted against *Mycobacterium tuberculosis* or its residual antigens in patients with advanced human immunodeficiency virus (HIV) infection shortly after commencement of antiretroviral therapy (ART). TB-IRIS is characterized by hyperinflammation and tissue damage. Pulmonary and lymph node involvement are the most common clinical manifestations. The incidence of TB-IRIS can reach up to 54% in settings where both HIV and TB are endemic, such as the sub-Saharan-Africa region of the African continent. Approximately 25% of patients with paradoxical TB-IRIS will require hospitalization for syndromic management. The management and prevention of paradoxical TB-IRIS rely on the use of anti-inflammatories such as immunosuppressive corticosteroid intervention, which is associated with an increased risk of Kaposi sarcoma. Paradoxical TB-IRIS is potentially fatal, with cases of central nervous system (CNS) involvement having the highest fatalities (up to 56%). The underlying cause of paradoxical TB-IRIS is thought to arise from a dysregulated hyperinflammatory immune response during ART-mediated immune recovery, although the causal mechanisms and associated molecular pathways are incompletely defined. This knowledge gap compromises efforts to develop new diagnostic and prognostic modalities as well as safer and more efficacious therapeutic interventions. This served as the rationale for undertaking the studies reported in this thesis.

Using clinical samples from the PredART intervention trial and the TB-ART observational study, this thesis investigated the cellular and molecular determinants of paradoxical TB-IRIS. Conventional scientific hypothesis-based approaches as well as unbiased hypothesis-generating approaches were used, with major experimental approaches including ribonucleic acid (RNA) sequencing, flow cytometry and soluble analyte analyses.

RNA extracted from whole blood of consenting participants from the Pred-ART intervention trial was sequenced to profile global gene expression. Cross-sectional and longitudinal analyses were performed to compare transcriptomic profiles in participants who developed paradoxical TB-IRIS to those who did not, at week 0, 2 and 12 on ART.

Using pathway analysis, samples collected prior to the initiation of ART (week 0) in patients who later developed paradoxical TB-IRIS (cases) were characterized by the upregulation of transcripts encoding neutrophil-derived antimicrobial peptides and defensins and associated with hypoxemia compared to the TB-non-IRIS controls. These largely reflected biological processes involved in neutrophilic responses and adaptation to metabolic stress and dysfunction. Furthermore, pathways that were significantly downregulated in patients who later developed paradoxical TB-IRIS compared to those who did not, included chondroitin sulfate biosynthesis and interleukin (IL)-6. These finding suggest that paradoxical TB-IRIS is preceded by increased expression of antimicrobial peptides and the impairment of immune cellular function controlled by the extracellular matrix.

Pathway analysis at week 2 on ART, which coincided with the median time of clinical manifestations in patients that developed paradoxical TB-IRIS, revealed the significant enrichment of neutrophil degranulation, interleukin (IL)-1 signalling, as well as type I and II interferon (IFN). Moreover, biological pathways that were significantly downregulated in cases as opposed to controls at week 2 on ART were largely overrepresented by epigenetic biological processes. These data suggested that neutrophil degranulation preceded and characterized the onset of paradoxical TB-IRIS.

To validate these findings, we evaluated the associations between absolute neutrophil counts and neutrophil soluble markers, with paradoxical TB-IRIS at week 0 and week 2 on ART. No significant differences in absolute neutrophil counts were reported in participants who later developed paradoxical TB-IRIS compared to those who did not at week 0. However, azurocidin measured in plasma samples by enzyme-linked immunosorbent assay (ELISA) was significantly

lower in samples from participants who later developed paradoxical TB-IRIS at week 0. This suggests that participants who are likely to develop paradoxical TB-IRIS might have impaired innate immune responses at week 0 compared to those who did not develop the syndrome. Absolute neutrophil counts were higher in cases compared to controls at week 2 on ART. Soluble neutrophil markers including human neutrophil peptide 1-3, myeloperoxidase, and neutrophil elastase were significantly higher in cases compared to controls at week 2 on ART. These data suggest that patients who develop paradoxical TB-IRIS have heightened neutrophil degranulation at the time of symptoms onset.

Longitudinal perturbation of gene expression was investigated between week 0 and week 2 in people who developed paradoxical TB-IRIS and TB-non-IRIS controls, respectively. Among the top significantly upregulated biological pathways in samples of participants that developed paradoxical TB-IRIS were neutrophil degranulation, type I and II interferon signaling, IL-1 cytokine signalling, and pyroptosis. Biological pathways that were significantly downregulated in these patients included heme biosynthesis and oxygen-carbon dioxide gaseous exchange signalling metabolic dysfunction. In TB-non-IRIS controls, biological pathways that were significantly upregulated included epigenetic modulation of gene expression, collagen biosynthesis and extracellular cytoskeleton remodelling indicating anabolic processes that restore or maintain proper cellular functionality such as cellular signalling. Type I interferon signalling and immune responses to viral pathogens were among biological pathways that were significantly downregulated in people who did not develop paradoxical TB-IRIS at week 2 on ART compared to week 0, likely indicating decrease in antiviral responses as HIV viral load declined.

The management and prevention of paradoxical TB-IRIS rely on the use of corticosteroids which is associated with an increased risk of Kaposi Sarcoma and herpes reactivations. Thus, there is a need to explore other anti-inflammatory but non-immunosuppressive drugs that can be repurposed for the management of IRIS-related pathologies. Gene expression data at week 2 on ART and previous published data indicated that aberrant inflammasome activation represent one of the molecular mechanisms that underpins the pathogenesis of paradoxical TB-IRIS. We proposed that chemical inhibition of the inflammasome would result in a targeted reduction of inflammation.

Two candidate drugs (anakinra and parthenolide) were evaluated and benchmarked against the standard of care (prednisolone) in an *ex vivo* mycobacterial cell stimulation model using patient samples. Both anakinra and parthenolide significantly reduced several markers of inflammation compared to prednisolone. However, parthenolide was the more potent in reducing cytokine production including IL-1β among others. These findings provide experimental evidence of *in vitro* use of novel anti-inflammatory agents. Anakinra has been approved for clinical use in inflammatory conditions such as rheumatoid arthritis and could potentially be repurposed for use in the context of paradoxical TB-IRIS.

A hallmark of paradoxical TB-IRIS includes the partial reconstitution of *Mtb*-specific CD4 T cell responses within 3 months of initiating ART while on effective antituberculosis therapy.

The phenotype and transcription factors of antigen-specific interferon-gamma producing (IFNγ+) CD4+ T cells and their potential involvement in the pathogenesis of paradoxical TB-IRIS were characterized in an experimental mouse model of IRIS (by collaborators) as well as in human peripheral blood mononuclear cells (PBMC). In mice, antigen-specific CD4 T cells knocked out for Eomes showed significantly higher proportion of survival compared to wildtype mice. No significant differences in Eomes expression were observed in Mtb-300 specific, IFNγ+ CD4 T cells in PBMC from paradoxical TB-IRIS cases compared to controls at the onset of clinical symptoms. However, Eomes expression was higher in cases compared to controls in bulk CD4 T cells at week 2 on ART. HLA-DR expression was higher in cases compared to controls in Mtb300-specific IFNγ+ CD4 T cells at week 2 on ART. Additionally, Granzyme B producing, Mtb300-specific IFNγ+ CD4 T cells co-expressing Eomes and Tbet were significantly higher in cases compared to controls at week 2 on ART. These data indicate that HLA-DR expression on Mtb300-specific CD4 T cells producing IFNγ+ can potentially be developed as a diagnostic tool to identify individuals with paradoxical TB-IRIS.

Collectively, these findings highlight the key contribution of neutrophils and Mtb-specific CD4 lymphocytes in the pathogenesis of paradoxical TB-IRIS. The gene expression findings suggest that the underlying mechanism involves interferon stimulated genes which trigger the secretion of

proinflammatory cytokines and the aberrant activation of the inflammasome. Members of the IL-1 family of cytokines are secreted as catalytically inactive proenzymes that require the action of mature inflammasome for activation. IL-1a is the only exception since its proform and mature form are both fully functional. Active IL-1 family of cytokines are potent modulators of inflammation which is a defining feature in people who develop paradoxical TB-IRIS at the time of clinical symptom onset. In addition, the pathogenesis of paradoxical TB-IRIS appears to be mediated by the heightened degranulation of neutrophils which may cause acute inflammation and tissue damage.

List of Figures

List of Tables

List of Conferences

1. Phenotypic profile of Mtb-specific CD4 T cells in patients who develop paradoxical tuberculosis-associated immune reconstitution inflammatory syndrome. **Poster Presentation. 2018. Infectious Diseases in Africa (IDA). 8th Annual International Symposium.**

2. Phenotypic profile of Mtb-specific CD4 T cells in patients who develop paradoxical tuberculosis-associated immune reconstitution inflammatory syndrome. **Oral Presentation. 2019 Department of Medicine annual research day.**

3. Whole blood RNA-sequencing in people who develop paradoxical tuberculosis-associated immune reconstitution inflammatory syndrome: An exploratory analysis. **Oral Presentation. 2022 CIDRI-Africa annual symposium.**

4. Neutrophil degranulation precedes and characterizes the onset of paradoxical tuberculosis-associated immune reconstitution inflammatory syndrome. **Oral Presentation. 2023 Department of Medicine annual research day.**

List of publications

1. **Moseki RM**, Barber DL, Du Bruyn E, et al. Phenotypic Profile of *Mycobacterium tuberculosis*-Specific CD4 T-Cell Responses in People With Advanced Human Immunodeficiency Virus Who Develop Tuberculosis-Associated Immune Reconstitution Inflammatory Syndrome. In: Open Forum Infectious Diseases. Oxford University Press US:ofac546.

List of Grants and Fellowships

After school's programme community outreach award: IDM1002 - 475078 August **2022**-August **2023.**

The HIV-associated TB Training Programme (HATTP) Fogarty Doctoral Fellowship (**2021-2023**)

Abbreviations

A Adenine

AFB Acid Fast Bacilli

AIDS Acquired Immmuno-Deficiency Syndrome

AM Alveolar Macrophages

ANC Absolute Neutrophil Count

APC Antigen Presenting Cell

ART Antiretroviral Therapy

ATP Adenosine Triphosphate

ATT Anti-Tuberculosis Therapy

BCG Bacille Calmette Guerin

BH Benjamini-Hochberg

C Cytosine

cART Combined Antiretroviral Therapy

CCR Chemokine receptor

CD Cluster of Differentiation

CFP10 Culture Filtrate Protein 10

CNS Central Nervous System

CRP C-Reactive Protein

CSF Cerebrospinal Fluid

CT Computed Tomography

DAMP Danger Associated Molecular Patterns

DC Dendritic Cell

DEGs Differentially Expressed Genes

DGEA Differential Gene Expression Analysis

DMSO Dimethyl Sulfoxide

DNA Deoxyribose Nucleic Acid

DST Drug Sensitivity Testing

ECM Extracellular Matrix

EDTA Ethylene diamine tetra acetic acid

ELISA Enzyme-linked-Immunosorbent Assay

Eomes Eomesodermin

ESAT-6 Early Secreted Antigenic Target 6

EMB Ethambutol

EPTB Extra Pulmonary Tuberculosis

ES Enrichment Score

FCS Fetal Calf Serum

FDA Food and Drug Administration

FDR False Discovery Rate

FEV Forced Expiratory Volume

G Guanine

GO Gene Ontology

GSEA Gene Set Enrichment Analysis

HAART High Active Antiretroviral Therapy

HIV Human Immune deficiency Virus

HLA Human Leukocyte Antigen

HPC High Performance Computing

IFN Interferon

IGRA Interferon gamma release assay

IL Interleukin

ILC Innate Lymphoid Cells

INH Isoniazid

INSHI International Network for the Study of HIV-associated IRIS

IPT Isoniazid Preventative Therapy

IQR Interquartile Range

IRIS Immune Reconstitution Inflammatory Syndrome

Kg Kilogram

KS Kolmogorov-Smirnov

LAM Lipoarabinomannan

LDH Lactate Dehydrogenase

LFC Log2 Fold Change

LJ Lewis-Jenson

LPA Line Probe Assay

LPS Lipopolysaccharide

LTBI Latent TB Infection

mAb Monoclonal antibody

MAC *Mycobacterium avium* Complex

mg milligram

mL Milliliter

MDR-TB Multiple Drug Resistant tuberculosis

ME Module Eigengene

MGIT Mycobacterial Growth Indicator Tube

MHC Major Histocompatibility Complex

MM Module Membership

MMP Matrix metalloprotease

MOI Multiplicity of Infection

MRI Magnetic Resonance Imaging

MSM Men having Sex with Men

MSMD Mendelian Susceptibility to Mycobacterial Disease

Mtb *Mycobacterium tuberculosis*

Mtb-300 300 peptide pool derived from *Mycobacterium tuberculosis*

n Number

NAAT Nucleic Acid Amplification Test

NAD+ Nicotinamide Adenine Dinucleotide

NADH Nicotinamide Adenine Dinucleotide Hydrogen

NES Normalized Enrichment Score

NADPH Nicotinamide Adenine Dinucleotide Phosphate

NFkB Nuclear Factor Kappa light chain enhancer of activated B cells

ng nanogram

NGS Next Generation Sequencing

NK Natural Killer

nM nano Molar

NSAID Non-Steroidal Anti-Inflammatory Drugs

NTM Non-Tuberculous Mycobacteria

OD Optical Density

OI Opportunistic Infection

PAMP Pathogen Associated Molecular Patterns

PBMC Peripheral Blood Mononuclear Cell

PBS Phosphate Buffer Saline

PC Principal Component

PCA Principal Component Analysis

PCR Polymerase Chain Reaction

PE-Cy5.5 Phycoerythrin cyanine 5.5

PE Phycoerythrin

PEP Post Exposure Prophylaxis

pg Picogram

PLWHIV People Living With HIV

PMN Polymorphonuclear

PPD Purified Protein Derivative

Pred-ART Prednisone-ART clinical trial

PrEP Pre-exposure Prophylaxis

PRR Pattern Recognition Receptor

PTB Pulmonary Tuberculosis

PZA Pyrazinamide

RCF Relative Centrifugal Force

RIF Rifampicin

ROS Reactive Oxygen Species

RNS Reactive Nitrogen Species

RNA Ribose Nucleic acid

RNA-seq Ribose Nucleic acid Sequencing

Rpm Revolutions Per Minute

RPMI Rosewell Park Media Institute

SA South Africa

SSA Sub-Saharan Africa

T Thymine

TB10.4 Tuberculosis antigen 10.4

TB Tuberculosis

TB-ART Tuberculosis-Antiretroviral therapy observational trial

T-bet T-Box Expressed in T cells

TB-IRIS Tuberculosis associated Immune Reconstitution Inflammatory Syndrome

TCR T Cell Receptor

Th-1 T-helper-1

Th-2 T-helper-2

Th-17 T-helper-17

Th-22 T-helper-22

TLR Toll Like Receptor

TNF Tumor necrosis Factor

TOM Topological Overlap Matrix

Treg Regulatory T cell

TST Tuberculin Skin Test

UCT University of Cape Town

UK United Kingdom

mL Microliter

WC Western Cape

WGCNA Weighted Gene Co-expression Network Analysis

WGS Whole Genome Sequencing

WHO World Health Organization

xg x (times) gravity

ZN Ziehl-Neelsen

1. Chapter 1 outline: Investigating the molecular pathogenesis of paradoxical tuberculosis inflammatory syndrome.

This chapter provides a high-level introduction to the thesis. The chapter details the rationale for the studies contained in the thesis and the relevance of this work. It briefly discusses the hypotheses addressed in each chapter, the research questions and the main aims. The chapter also discusses in broad terms the study populations, ethical compliance, study design, laboratory assays, statistical methods and approaches and provides a chapter-by-chapter summary of the thesis.

1.1 Rationale

Disease and death due to tuberculosis (TB) represents a global scourge. The incidence of TB in 2022 involved an excess of 10 million cases and it resulted in 1.4 million deaths across the globe [1]. The brunt of the TB crisis is particularly severe in developing countries such as sub-Sahara Africa where healthcare resources are often limited.

Several factors contribute to the success of *Mycobacterium tuberculosis (Mtb)*, the most common cause of TB in humans. First, Mtb can exist in a non-replicative, metabolically quiescent state during TB therapy and in a setting of an effective immune response [2]. Infection with Mtb does not lead to clinical disease in 90% of cases but establishes a state of bacterial latency responsible for a global latent reservoir of approximately 2 billion people, 10 % of which will develop reactivation TB disease in their lifetime [3]. This latently infected global pool of asymptomatic people therefore feeds the vicious cycle of TB transmission. Additionally, the emergence of resistance towards first-line drugs undermines efforts to eradicate TB [4]. Co-infection with the human immunodeficiency virus (HIV) represents a major hindrance to TB control programmes in sub-Saharan Africa and other third world countries [1, 5]. Although the advent of antiretroviral therapy (ART) has significantly advanced the management of TB in people living with HIV, this is not without challenges. While the incidence of HIV-associated TB represents the minority of overall TB incidence globally, the mortality rate attributed to HIV-associated TB is excessive relative to HIV-negative individuals with TB [1]. Additionally, HIV-associated TB is associated with significant treatment complications including drug-drug interactions among others [6, 7]. The most common complication related to co-treatment of HIV-associated TB is the emergence of localized or systemic hyper-inflammatory features with new or recurrent TB symptoms despite effective control of HIV viremia and the exclusion of other causes for clinical deterioration [6]. This is known as paradoxical TB-associated Immune Reconstitution Inflammatory Syndrome (TB-IRIS), the focus point for the body of research presented in the thesis.

The burden of paradoxical TB-IRIS in sub-Saharan Africa is substantial, particularly given that guidelines shifted to advise early ART in patients with TB and low CD4 lymphocyte counts [8]. Paradoxical TB-IRIS has an incidence of 18% across adult cohorts [9, 10]. However, its incidence is as high as 54% in cohorts where risk factors for the condition are frequent [9]. The incidence in children is not well documented.

Pulmonary and lymph node involvement are the most common clinical manifestations of paradoxical TB-IRIS [9, 11]. Patients often require hospitalization for diagnostic and therapeutic intervention [12, 13]. Paradoxical TB-IRIS is potentially fatal for a minority of patients especially when the brain is affected [14]. The mortality rate attributed to paradoxical TB-IRIS is 2% [9]. Fatality rates can be as high as 56% in instances of central nervous system (CNS) involvement, which is the most severe form of paradoxical TB-IRIS [15-17]. Notably, paradoxical TB-IRIS is self-limiting in most patients, with the resolution of clinical symptoms in 2 months on average [18]. Corticosteroids are the mainstay therapy and the only evidence-based therapy for the prevention and management of symptoms of TB-IRIS. Corticosteroid therapy is associated with shorter symptom duration as well as reduced length of hospital stay [19]. However, the use of corticosteroids in severely immunocompromised patients is not entirely safe and is prescribed with caution due to the increased risk of Kaposi's sarcoma and potentially other opportunistic infections [20].

Lastly, a moderate dose of prednisone was evaluated for preventing complications with paradoxical TB-IRIS in a double-blind placebo-controlled randomized clinical trial. The authors reported a reduction in the incidence of paradoxical TB-IRIS by 30% [21]. There are important knowledge gaps regarding the molecular mechanisms underlying paradoxical TB-IRIS and the mechanisms of action of corticosteroids in this condition. This hinders the design and development of effective prognostic and diagnostic interventions. Additionally, safer anti-inflammatory and less immunosuppressive agents that modulate these molecular mechanisms in a more targeted manner need to be identified for the prevention and management of paradoxical TB-IRIS.

1.2 Relevance

The diagnosis of paradoxical TB-IRIS relies on clinical features at presentation and the exclusion of conditions that mimic TB-IRIS [18, 22]. The molecular mechanisms underlying the immunopathology of paradoxical TB-IRIS are poorly understood, and their thorough elucidation could aid in the design and development of better diagnostic tools. Prior research has focused on characterizing immune responses during TB-IRIS episodes to derive a diagnostic biosignature. These studies have suggested that paradoxical TB-IRIS is an aberrant and excessive immune response that is targeted at live Mtb and/or its residual antigens, which results in tissue damage [18, 23]. This thesis addresses knowledge gaps in the molecular aspects

underlying the pathogenesis of paradoxical TB-IRIS which hinders efforts to design and develop diagnostic tools and safer preventive and therapeutic interventions.

This thesis reports a series of studies that used a blend of traditional immune phenotyping techniques and reverse translational approaches to investigate the molecular phenomena underlying the immunopathogenesis of HIV-associated paradoxical TB-IRIS. Cryogenically preserved clinical material obtained from consenting patients enrolled in one randomized placebo-controlled clinical trial and one prospective observational cohort study, were used to experimentally interrogate several related hypotheses.

1.3 Study population and sample collection

1.3.1 Pred-ART intervention trial

Biological materials used in this study were obtained from two separate studies. The first was a double blind placebo-controlled randomized clinical trial that assessed the efficacy and safety of prednisone in preventing paradoxical TB-IRIS in high risk patients with HIV-associated TB starting ART [24]. The second was a prospective observational cohort study monitoring complications related to the initiation of ART in HIV-immunosuppressed TB patients in an inpatient TB facility [6, 25]. Both studies enrolled consenting, ART naïve, HIV-infected patients with microbiologically confirmed active TB as well as patients who displayed robust clinical or radiological evidence of TB and had a favorable symptomatic response to TB treatment prior to ART initiation. Participants in the Pred-ART trial were recruited from four clinics dedicated to HIV and TB care in Khayelitsha Cape Town, from August 2013 to February 2016. Other inclusion criteria included age of 18 years or older and a CD4 cell count of 100 cells per microliter or less. Patients were excluded if they were not on first line TB treatment, had poor clinical response to TB treatment, were pregnant, had tuberculomas or TB meningitis, had pericardial TB at diagnosis or had rifampicin resistance. Patients with uncontrolled diabetes mellitus, Kaposi sarcoma or Hepatitis B were also excluded. Lastly, patients with an absolute neutrophil count of less than 500 cells per microliter, levels of alanine transferase greater than 200 units per liter or those on corticosteroid therapy for another disease within 7 days before enrolment were excluded from the study. Within 4 weeks of starting the intensive phase of TB treatment, recruits were randomized to four weeks of prophylactic prednisone or placebo and initiated on ART. Prednisone or placebo was given for 4 weeks (40mg/day for 2 weeks followed by 20mg/day for 2 weeks). 240 participants were enrolled

(120 to each arm). Peripheral blood samples were taken at baseline, 2, 4 and 12 weeks. Biological material including ribonucleic acid (RNA), deoxyribonucleic acid (DNA), plasma and peripheral blood mononuclear cells (PBMC) for each patient were cryogenically preserved. The main findings of the study were that prednisone reduced the incidence of TB-IRIS by 30% relative to placebo (relative risk is 0.70, 95%CI 0.51-0.96) without significant complications [24]. Ethical clearance for the studies was granted by the Human Research Ethics Committee in the Faculty of Health Sciences at the University of Cape Town (HREC REF:136/2013 and 213/2014)

1.3.2 TB-ART observational cohort study

Peripheral blood mononuclear samples (PBMC) used in this study (chapter 4) were obtained from patients that were enrolled in the TB-ART observational study which evaluated the adverse effects associated with HIV-associated TB cotreatment during ART scale-up [6]. The authors reported many complications with cotreatment with paradoxical TB-IRIS being the most common complication. Patients were enrolled in a prospective observational study conducted at Brooklyn Chest TB Hospital between May 2009 and November 2010 in Cape Town, South Africa [6]. All patients were ART naïve and those with rifampicin-resistant TB were excluded. TB diagnosis was based on smear, culture, or clinical diagnosis. The first TB episode was treated with standard first line regimen of rifampicin (R), isoniazid (H), pyrazinamide and ethambutol for two months followed by four months of RH regimen. In patients with subsequent episodes, streptomycin was added for 2 months. Paradoxical TB-IRIS was diagnosed per International Network for the Study of HIV-associated IRIS (INSHI) criteria [26]. HIV-1 treatment included lamivudine and efavirenz with stavudine or tenofovir depending on guidelines at the time. Written informed consent was obtained from all participants. The study was approved by the Human Research Ethics Committee (HREC REF: 049/2009 and 809/2018) of the University of Cape Town. Clinical and other immunological findings from this cohort have been published [6, 27-29].

Additionally, ethical approval was granted by the same body to collect peripheral blood samples for biobanking. Different components of the blood were extracted and preserved for long term storage and used to investigate the molecular pathogenesis underlying paradoxical TB-IRIS (see Chapter 4).

1.4 Overall aims of the studies in thesis

- To derive a transcriptional signature associated with TB-IRIS occurrence both prior to ART and at the time of symptom onset.
- To investigate the effect of prednisone on the transcriptional expression profile associated with TB-IRIS to identify biological pathways modulated by prednisone.
- To investigate the role of the T-cell transcription factor Eomesodermin in TB-IRIS pathogenesis.
- To investigate the anti-inflammatory capacity of agents directed at inflammasome-related targets in an *ex vivo* cell culture model with *Mycobacterium tuberculosis* stimulation.

1.5 Main objective: To broaden the understanding of the molecular pathogenesis of paradoxical TB-IRIS

Studies aimed at understanding the pathogenesis underlying paradoxical TB-IRIS have historically explored cellular assays and analysis of soluble analytes primarily. Recently, studies have used untargeted, hypothesis-generating approaches to assess differential transcript abundance and subsequent pathway analysis to gain better insights into the pathogenesis of different diseases. For instance, studies have demonstrated the dysregulation of immune responses in blood and PBMC at the onset of paradoxical TB-IRIS using high throughput technologies [30-32]. This thesis used a blended approach of classic cellular assays and high throughput techniques to investigate the molecular aspects of the pathogenesis of paradoxical TB-IRIS. Below are the major hypotheses and research question addressed in these studies.

1.5.1 Hypotheses

1.5.1.1. The onset of paradoxical TB-IRIS is characterised by a series of immune perturbations at the gene expression level that can be predicted and detected prior to the manifestation of symptoms.

Research question 1

What are the genes that are differentially expressed in patients who develop paradoxical TB-IRIS and those who do not (TB-non-IRIS controls) prior to the initiation of ART?

The derivation of such a biosignature from these findings could be useful in identifying individuals at high risk of developing paradoxical TB-IRIS, allowing for targeted prevention.

1.5.1.2. The diagnosis of paradoxical TB-IRIS is empiric, relying on characteristic symptom onset and timing and the exclusion of other causes for clinical deterioration. The lack of laboratory-based diagnostic tools complicates the management of paradoxical TB-IRIS. The second hypothesis was that the onset of TB-IRIS symptoms is characterised by a distinct transcriptional biosignature.

Research question 2

What genes are differentially expressed in patients who develop paradoxical TB-IRIS and those who do not (TB-non-IRIS controls), at the onset of clinical symptoms?

Such a transcriptional biosignature could be used for the diagnosis and clinical management and to elucidate the pathological mechanism underlying paradoxical TB-IRIS.

1.5.1.3. A recent double blind, placebo-controlled clinical trial demonstrated the efficacy and safety of moderate dose of prednisone in preventing TB-IRIS. The hypothesis related to this is that prednisone exerts its preventive effect by modulating the proinflammatory transcriptomic signature associated with TB-IRIS.

Research question 3

Does prednisone modulate the gene expression profile in patients with HIV-associated TB at the time of onset of paradoxical TB-IRIS when compared to patients who received placebo? Identifying significantly differentially expressed genes could provide an indication of the mechanisms of action of prednisone in this context.

1.5.1.4. Previous *ex vivo* work has shown that hypercytokinemia in paradoxical TB-IRIS is contributed to by activation of canonical and non-canonical inflammasomes [25]. Inhibition by non-selective pan-Caspase inhibitors such as prednisone can significantly reduce the production of proinflammatory cytokines including IL-1α and IL-1β [33, 34]. Prednisone is an anti-inflammatory, immunosuppressive drug, and the only evidence-based treatment for

paradoxical TB-IRIS. Its use in already severely immunocompromised individuals is associated with complications [20]. As such, safer therapeutic interventions are needed. The hypothesis related to this is that anakinra (an IL-1 receptor blocker) and parthenolide (inflammasome inhibitor among other targets) have a greater effect in suppressing pro-inflammatory cytokine release than prednisone in *ex vivo* cell culture experiments.

Research question 4

Does specific inhibition of inflammasome related targets, with anakinra and parthenolide, significantly reduce pro-inflammatory cytokine compared to prednisolone in an *ex vivo* model involving mycobacterial stimulation of PBMC collected from patients who developed paradoxical TB-IRIS? Anakinra is approved for treatment of inflammatory disorders by the Food and Drug Administration and could potentially be repurposed for use in cases of paradoxical TB-IRIS, particularly in severe or steroid refractory cases [35, 36].

1.5.1.5. The role of *Mycobacterium tuberculosis* (Mtb) specific CD4 T lymphocytes in the pathogenesis of paradoxical TB-IRIS has been the subject to much prior investigation [37-39]. Much of the earlier work characterized the quantity of Mtb-specific CD4 T cell responses and showed that in most cases of paradoxical TB-IRIS, the onset of symptoms was accompanied by significant increases in CD4 T cell compartment compared to those who did not develop paradoxical TB-IRIS, but some patients who did not develop TB-IRIS also had substantial increases [37]. Recently, efforts were directed at characterizing the nature of these pathogen-specific CD4 T cell responses. In one study, Eomesodermin, a transcription factor that mediates cytotoxicity had increased frequency in *Mycobacterium* (*M). avium* specific CD4 T-cells in patients who developed *M. avium*-IRIS [40]. The hypothesis related to this is that Eomesodermin expression in CD4 lymphocytes is associated with the development of paradoxical TB-IRIS in patients with HIV-associated TB starting ART.

Research question 5

Do patients who develop paradoxical TB-IRIS have higher frequencies of Mtb-specific IFNγ+ CD4 T cell responses expressing Eomesodermin than TB-non-IRIS controls at the time of paradoxical TB-IRIS symptom onset?

1.6 Ethical compliance

These wet-lab based studies used biological specimen collected from the Pred-ART clinical trial and the TB-ART cohort study. Each study was approved by the Human Research Ethics Committee (HREC reference: 809/2018, 213/2014) of the Faculty of Health Sciences of the University of Cape Town.

1.7 Case definition and cut-offs

The diagnosis of paradoxical TB-IRIS was based on a consensus case definition. Paradoxical TB-IRIS in participants enrolled in the TB-ART observational study and the Pred-ART trial was defined according to the International Network for the Study of HIV-associated IRIS (INSHI) criteria [22]. Paradoxical TB-IRIS was defined as the worsening of the signs and symptoms of TB with distinct inflammatory features, upon starting effective ART while on anti-TB treatment.

1.8 Design of studies

The laboratory studies were designed to answer questions relating to the molecular pathogenesis of paradoxical TB-IRIS using samples collected in the aforementioned clinical studies including RNA, plasma and PBMC collected prior to the initiation of ART (week 0), at the median time on paradoxical TB-IRIS symptom onset (week 2 on ART) and at symptoms resolution (week 12 on ART). Cases (participants who develop paradoxical TB-IRIS) were compared to controls (participants with HIV-associated TB starting ART who did not develop paradoxical TB-IRIS).

1.9 Statistical software and analyses

The laboratory studies were nested within previously completed clinical studies based on available samples. Therefore, formal power calculations were not performed. Graphpad Prism, linux based command-line prompt scripting and the R-statistical programming language were used for data analyses. Each chapter contains a detailed statistical analysis section.

1.10 Broad overview of laboratory assays

1.10.1 Flow cytometry

The underlying principle of flow cytometry is to phenotypically study single cells. In chapter 4, flow cytometry was used to study the expression of 14 markers on the surface and the intracellular compartment of CD4 lymphocytes in patients enrolled in the TB-ART observational study who developed paradoxical TB-IRIS compared with controls. The expression of the various markers were reported as median frequencies in bulk and Mtb specific CD4 lymphocytes.

1.10.2 Luminex

Luminex is an analyte capture assay in which the concentration of an unknown analyte in a sample is determined in relation to the known concentration of a standard. It provides the benefit of multiplexing different analytes of interest and assaying for their abundance in a single sample by measuring absorbance. In chapter 7, a total of 15 inflammatory cytokines, many that were previously shown to be significantly upregulated in patients who developed paradoxical TB-IRIS relative to TB-non-IRIS controls at symptom onset, were measured by Luminex in supernatants from stimulation experiments involving samples collected from participants that were enrolled in the Pred-ART trial. Samples were stimulated with heat-killed Mtb and subsequently treated with inflammasome targeting drug candidates. The anti-inflammatory effect of candidate drugs relative to stimulated but untreated samples was assessed. Prednisolone, the current drug of choice for managing severe inflammatory symptoms associated with paradoxical TB-IRIS, was used for drug benchmarking.

1.10.3 ELISA

Enzyme linked immunosorbent assay (ELISA) is an analyte capture assay in which the concentration of an unknown sample can be determined by absorbance based on the known concentration of a standard. In chapter 6, ELISA was used for the detection of four analytes in diluted plasma samples collected from participants that were enrolled in the Pred-ART trial.

1.10.4 RNA sequencing

Nucleic acids are biological macro-molecules. They serve as templates for the storage and/or expression of the genetic information inside a living organism. Two types of nucleic acids include deoxyribonucleic acid (DNA) and ribonucleic acid (RNA). DNA is made up of four molecules known as nucleotides comprising adenine (A), guanine (G), thymine (T), and cytosine (C) [41]. Each nucleotide interacts with a phosphate group and a pentose sugar to form a nucleotide base which interact with one another through phosphodiester bonds to form a repetitive stretch of a phosphate sugar backbone. Each DNA molecule is composed of two such sequences known as DNA strands. The strands interact via hydrogen bonds between specific nucleotide residues: A with T and G with C to form an alpha helix. Due to this, the two strands contain the same information and are complementary to each other. The totality of the organism's DNA or RNA is known as the genome. The genome of eukaryotic organisms is DNA and it is spooled around histone proteins and organized into structures called chromosomes in the cell nucleus. Notably, DNA is the preferred format of preserving the genome from which all other functional biological products are derived [41].

The genome of eukaryotic organisms is evolutionarily conserved. In fact, virtually all cells of an organism are an exact copy of the inherited DNA. Its cells, however, can vary in appearance, function and respond differentially to external stimuli. These differences are possible because cells make use of different stretches of the DNA, called genes as templates to build functional cellular products in a process called gene expression. Cellular products and their abundance are a result of the integration of the cells prevailing state and extracellular stimuli controlled by a complex regulatory system which is encoded in the DNA structure.

In the first step of gene expression (in humans), one strand of DNA is used as a template to generate RNA molecules in a process known as transcription. RNA has the same chemical composition as DNA except that thymine is replaced with uracil (U). Of note, certain RNA species can be the end-product by themselves, while others serve as templates for the synthesis of other complex biological macro-molecules, such as proteins in a process called translation. According to this distinction, RNAs are classified as either messenger RNAs (mRNAs) or non-coding RNAs (ncRNAs). Proteins are functional gene products synthesized from mature mRNA molecules. Each protein is composed of sequences of molecules called amino acids. Each amino acid is derived from an RNA nucleotide sequence in which each successive triplet corresponds to one amino acid [42].

Due to intrinsic regulatory mechanisms at various levels along specific pathways, the presence of RNA molecules in a cell does not always reflect the presence of their functional end products. Changes in gene expression levels have been exploited to investigate the phenotypic differences in disease conditions, and analyzing the regulatory mechanisms underpinning these changes is an important aspect of molecular biology. RNA levels are often used as a surrogate for different phenotypes such as disease states [42]. Furthermore, although the cell transcriptome is dynamic and temporally regulated, it is more easily and reproducibly quantified in high-throughput fashion compared to other cellular products.

Recently, new technologies have offered sequencing methodologies for characterizing the transcriptome and quantifying gene expression patterns in biological conditions of interest with high throughput and unprecedented resolution [43]. Two have the capacity to measure thousands of transcripts simultaneously: the original microarray technology and the more recent RNA-sequencing (RNA-seq) technology which has emerged as the preferred technology [44].

Bulk RNA sequencing was used to study the global gene expression in whole blood samples of participants enrolled in the Pred-ART trial. Samples collected at week 0, 2 and 12 were sequenced and analyzed to identify differentially expressed genes which were mapped into biological pathways to gain insights into which biological pathways are differentially regulated between paradoxical TB-IRIS cases and controls and prednisone and placebo-treated participants.

1.11 Summary description of chapters:

Chapter 1 provides a high-level introduction of the entire thesis and explores the rationale and relevance for the studies.

Chapter 2 reviews and summarizes the literature on paradoxical TB-IRIS with emphasis on its molecular pathogenesis.

Chapter 3 details the methods, study design and statistical approaches used throughout the thesis.

Chapter 4 reports the findings of a study that characterized the quantity and quality of *Mycobacterium tuberculosis*-specific conventional CD4 lymphocytes and the expression of specific immune markers on these cells using flow cytometry. The samples from this study were obtained from TB inpatients that were enrolled in the TB-ART cohort study.

Chapter 5 is the core chapter of the thesis and explores the molecular mechanisms of paradoxical TB-IRIS pathogenesis using RNA-sequencing to characterize gene expression. Data analyses of the transcriptomic findings comparing placebo and prednisone-treated participants and those who developed TB-IRIS and controls are presented. The findings are discussed in the context of the existing literature.

Chapter 6 reports a study that sought to extend and validate the transcriptomic findings presented in chapter 5. The neutrophil response signature observed in the transcriptomic analysis was validated using ELISA assays for neutrophil products using available plasma samples at week 0 and 2, collected from participants that were enrolled in the Pred-ART trial. Absolute neutrophil counts were also analyzed.

Chapter 7 reports a proof-of-concept study that explored the use of anti-inflammatory and non-immunosuppressive, inflammasome targeting drugs in an *ex vivo* Mtb lysate stimulation experiment. To understand if specific inhibition of inflammasomes or their downstream effectors (e.g. IL-1 cytokines) results in greater modulation of the pro-inflammatory response than non-selective pan-Caspase anti-inflammatory targets such as prednisone, the effect of two drugs were assessed: a specific-inflammasome targeting drug (parthenolide) and anakinra which acts downstream of the inflammasome by blocking IL-1 receptor. Comparisons were made with prednisolone in cell culture stimulation experiments using PBMC collected from patients in the Pred-ART trial. Caspase-1 ELISA, and a custom 15-plex Luminex assay,

including among others IL-1 family of cytokines, were tested on cell supernatants as a measure of inflammasome inhibition.

Chapter 8 discusses and summarizes the findings from each study, highlights a working model of paradoxical TB-IRIS pathogenesis, provides overall conclusions, and highlights future research directions.

2 Chapter 2 outline: Literature review of human immunodeficiency virus -associated paradoxical tuberculosis immune reconstitution inflammatory syndrome (TB-IRIS)

This section provides an overview of TB disease in the context of HIV infection by introducing the epidemiology of TB and how it is transmitted. It discusses the possible outcomes of TB infection and explores the prevailing paradigm of the molecular pathogenesis underlying active TB disease. Further explored is the clinical diagnosis of TB and the current diagnostic modalities and their limitations. It also covers the management of TB with a particular focus on the challenges that complicate its management including the emergence of drug-resistant TB and how co-treatment of TB and HIV may lead to complications with paradoxical TB-associated immune reconstitution inflammatory syndrome (TB-IRIS).

2.1 The spectrum of tuberculosis (TB) disease and its complications in people living with the human immunodeficiency virus (HIV)

2.1.1. Epidemiology of TB

Tuberculosis (TB) is the most prevalent cause of infectious morbidity and mortality throughout the world [1, 45]. Although it is commonly associated with chronic pulmonary disease, TB can spread beyond the lungs to cause extrapulmonary and/or disseminated TB disease [46]. There were over 10 million incident TB cases in 2022 across the globe. The brunt of the TB epidemic is often severe in Sub-Saharan Africa where healthcare infrastructure is often limited. Although TB is curable, it is associated with a significant death toll, reaching 1.5 million approximated fatalities worldwide in 2022 [1].

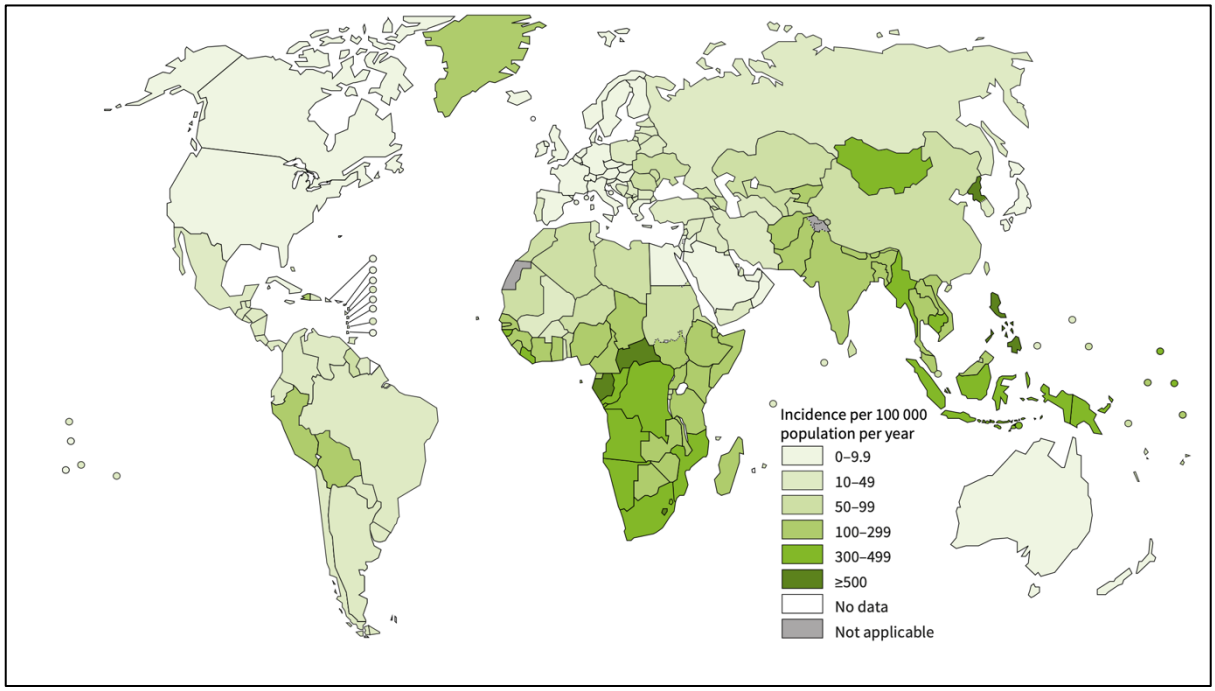

Figure 2. Annual estimates of global incidence rates of tuberculosis (TB) per 100 000 people in 2022. *Darker shades of green are correlated with higher incidence rates. Of note, the sub-Sahara region of the African continent has some of the highest incident rates compared to the rest of the world [1]*

2.1.2 Transmission and pathogenesis of TB

The success of *Mycobacterium tuberculosis* (Mtb), the etiological agent of TB disease, is attributed to its ease of spread. Mtb is an airborne pathogen that is transmitted via the inhalation of infected respiratory nuclei that are produced through coughing by an individual with

subclinical or active pulmonary TB disease [47, 48]. Recent evidence suggests that bioaerosols that are released through talking or sneezing are also able to transmit Mtb [47]. TB transmission is common in overcrowded and poorly ventilated spaces. Notably, most TB cases are recorded in young adult populations [49].

Upon inhalation, Mtb travels via the respiratory airways and is seeded in the apices of the lung where there exists both delayed immunity and high oxygen tension which promote Mtb proliferation [50]. In the alveoli of the lungs, Mtb is rapidly engulfed by resident alveolar macrophages [51, 52]. The initial interaction of Mtb with these cells and epithelial cells in the alveoli culminates in the production of cytokines and chemokines which trigger the migration of phagocytic innate immune antigen presenting cells (APC) such as monocytes, neutrophils, and dendritic cells (DC) into the focal lesion [53]. This interaction leads to one of several outcomes depending on a myriad of factors such as age, level of immunity, and genetic susceptibility to TB disease among others.

First, Mtb infected individuals may develop primary progressive TB disease [54, 55]. This occurs in approximately 10% of otherwise healthy adults but its incidence is estimated to be higher in patients with mendelian susceptibility to mycobacterial disease (MSMD), in young children with poorly developed immune systems and those with immunosuppressive disorders such as HIV [56]. Second, robust and regulated innate immune responses may sterilize the lesions without resulting in immune sensitization in some individuals [57, 58]. Third, Mtb infected individuals may contain Mtb and develop immune sensitization without the signs and symptoms that are typical of active TB disease [3, 55, 59]. This is known as latent TB infection (LTBI). It is estimated that 25% of the worlds' population has LTBI [1, 3, 60]. Failure to sterilize Mtb lesions during LTBI culminates in the containment of Mtb in a highly structured barrier of immune cells known as a solid granuloma [61]. The solid granuloma is composed of a variety of macrophages including foamy macrophages which are surrounded by a lymphocytic cuff. Notably, a solid granuloma has a hypoxic cellular environment that is devoid of nutrients and is maintained by the persistence of mycobacterial antigens [62, 63]. The persistence of Mtb antigens establishes a chronic inflammatory state in which Mtb is contained in a viable but non-replicative metabolic state under immune pressure [64, 65]. Individuals with LTBI can persist for a lifetime in this non-symptomatic state , except in cases of immune decline [66, 67]. In activated macrophages, Mtb is killed through a process which may involve cellular apoptosis [68-71]. However, in some macrophages, Mtb actively subverts macrophage responses by inhibiting phagosome maturation, thus allowing Mtb to replicate intracellularly

[72-74]. Alternatively, Mtb may escape the phagosome through the upregulation of virulence factors such as ESAT6 [75-78]. Both instances lead to host cell death by necrosis which results in the formation of a caseous granuloma [70, 79, 80]. In the hypoxic caseum, Mtb has a nutrient source comprising the lipid debris of dead macrophages. The gradual degradation of the caseous granuloma through necrosis results in the formation of the necrotic granuloma which breaks down and thereby enables the spread of Mtb through nearby blood vessels and the lymphatic system [80]. This culminates in clinical TB disease. This is known as secondary TB disease and is accountable for approximately 80% of the TB cases worldwide [55]. Secondary TB disease occurs because of reactivation in the global pool of the latently infected individuals.

2.1.3 TB diagnosis and the spectrum of disease

The screening for TB in countries with an incidence greater than 20 per 100,000 people follows a standardized algorithm that is based on age and HIV status [81]. Because most cases of TB are reported in young adults and older adult populations, clinical suspicion of TB disease in these age groups following patient history evaluation and physical examination, prompt chest radiological examination to assess the lungs for abnormalities associated with TB disease [82-84]. A chest X-ray that is consistent with TB is followed up by the collection of a respiratory specimen. Typically, a sputum sample is sent for nucleic acid amplification testing (NAAT) using the polymerase chain reaction (PCR) based MTB/RIF Gene-Xpert technology [85]. A sputum sample may also be used for microbiological confirmation using both Ziehl-Neelsen staining for the direct detection of acid-fast bacilli (AFB) using microscopy and the liquid culture technology from BACTEC known as the mycobacterium growth indicator tubes (MGIT) assay [81].

Optimal TB management including treatment initiation relies on timeous and accurate detection of Mtb and its drug susceptibility profile. NAAT has significantly reduced the turn-around time for TB diagnosis. Moreover, NAAT modalities provide rapid drug susceptibility testing information which is a major drawback associated with microbiological staining modalities. Despite these benefits, its inherent limitation lies in its incapacity to differentiate live and dead pathogen [86-89].

Furthermore, these diagnostic modalities rely on sputum which can be challenging to obtain particularly when extrapulmonary disease predominates [88, 90].

2.1.4 Prevention of TB disease

Vaccination is a major scientific milestone in public health and remains a key preventive strategy for severe forms of TB disease in infants and young children [91-93]. The Bacille Calmette Guerin (BCG) vaccine developed in the early 20th century, is the only licensed vaccine for the prevention of TB disease [94, 95]. It is a live attenuated vaccine generated through multiple passages of *Mycobacterium bovis* [96, 97]. BCG is highly immunogenic and has also been evaluated as a preventive measure against other diseases, however, it fails to provide robust and long-lasting protection, including in the context of TB disease [98, 99]. BCG prevents extrapulmonary forms of TB disease in neonates and young children by inducing the development of T-helper (Th)-1 responses, such as interferon-gamma (IFNγ) [100, 101]. Notably, the use of BCG in neonates or children with MSMD or in individuals with other forms of compromised immunity has documented serious adverse effects [102].

The efficacy of BCG is highly variable in adults who are the reservoir and main spreaders of TB and confers protection in the range between 0 and 80% [98, 103]. This is attributed in part to the waning immune response induced by BCG over time. BCG "masking" and "blocking" are two hypotheses that could potentially explain the geographical variability in the efficacy of BCG [104]. Both terms refer to a pre-existing immune response due to immune sensitization with environmental mycobacteria. BCG "masking" refers to BCG being masked by a pre-existing immune response probably due to shared antigens between the BCG vaccine and ubiquitous environmental mycobacteria [105]. On the other hand, the "blocking" effect on the BCG vaccine refers to the early containment of BCG replication due to a pre-existing immune response preventing vaccine uptake [106]. Lastly, the multiple vaccine strains could potentially explain the varying efficacy of BCG [107].

The prevention of TB disease is also possible through antibiotic intervention. Isoniazid preventative therapy (IPT) is one prophylactic measure that is used to combat progression to active TB disease, especially in HIV-infected individuals. In such cases, IPT is recommended for a minimum duration of 6 months [108-111]. One-month daily rifapentine plus isoniazid (1HP) or three-months weekly rifapentine plus isoniazid (3HP) regimens are available and represent a significant reduction in duration required for TB preventive therapy [112, 113].

2.1.5 Treatment of TB disease

The main objectives of TB treatment are to achieve patient cure, reduce transmission, minimize disability, and the risk of death and prevent emergence of drug resistance. A fixed dose short-course of first-line, combination chemotherapy for 6-months is used in programmatic settings for the management of drug sensitive TB [114, 115]. This standard of care comprises rifampicin (RIF), isoniazid (INH), ethambutol (EMB) and pyrazinamide (PZA) for a treatment intensive phase lasting 2 months. In the treatment continuation phase of two months, the number of drugs are subsequently reduced to two (RIF and INH) [116-118]. Although, most bacteria are eliminated within the first 8 weeks of chemotherapy, the longer treatment duration is necessary to eliminate the persistent Mtb population. Failure to eliminate "persisters" may lead to relapse at the end of treatment, potentially associated with the emergence of drug resistance [119]. Resistance to both RIF and INH is known as multi-drug resistant (MDR) TB [120]. The treatment of MDR-TB has historically required longer durations of second-line drugs which are more toxic and expensive [121, 122]. Many factors such as poor adherence to TB treatment, long treatment duration, and high pill burden contribute towards the emergence of Mtb drug resistance [123]. Drug resistant TB is one of the major factors that complicate the eradication of TB disease. Recently, the World Health Organization approved the daily use of bedaquilline, pretomanid, linezolid and moxifloxacin (BPaLM) in the management of MDR-TB for a duration of 6 months [4, 124].

2.1.6 HIV-associated TB and attendant clinical challenges

Recent global trends indicate a decrease in HIV-associated incident TB cases and deaths [125]. This is likely due to antiretroviral therapy (ART) scale-up. Yet infection with HIV still represents a serious epidemic in sub-Saharan Africa which carries a disproportionate burden accounting for approximately 70% of the global burden of infection [126, 127]. Sub-Saharan Africa contributed 670 000 cases of the 1.5 million HIV incident cases and 280 000 of the 650 000 AIDS-related deaths estimated in 2021 globally [125].

HIV is transmitted in adults mainly through sexual intercourse and the sharing of needles among people who inject drugs [128]. The transmission of HIV is higher in key populations because of higher risk behaviors and structural factors [129]. Key populations include men who have sex with men (MSM), sex workers, people in prison and people who inject drugs.

The pathogenesis of HIV involves the progressive depletion of pathogen specific CD4 T cells and other immune cells expressing CD4 and chemokine receptors CCR5 or CXCR4, resulting in susceptibility to opportunistic infections and cancers. Infection with HIV represents a major impediment to TB epidemic control particularly in sub-Saharan Africa [126, 127]. TB is the commonest opportunistic infection associated with advanced stages of HIV infection [127, 130, 131].

Until recently, TB was mostly described as a binary disease state (active and latent), however, infection with HIV has highlighted nuances in the spectrum of TB disease and has consequently shifted this paradigm [130]. Recent technological advances in medical imaging have facilitated the characterization of early manifestations of TB disease prior to the onset of TB symptoms [132, 133]. The new paradigm proposes that LTBI and active TB disease represent polar extremes of the TB spectrum, where incipient and subclinical TB are intervening disease states that may progress in either direction towards containment as latent TB or active disease [3, 133]. Incipient TB defines a clinical state where the infecting bacilli are actively replicating but in check by the immune system, whereas subclinical TB defines a state without clinical symptoms but with positive microbiological tests and abnormal chest radiographic findings [133, 134]. TB transmission during these transient disease states is thought to be possible. Consequently, intervening along the spectrum of TB transmission is anticipated to have a dramatic impact in the control of the TB epidemic.

Furthermore, the detection of Mtb using sputum based microbiological assays is made challenging by the dynamics of TB disease manifestations in people with HIV. The presentation of TB disease in people with HIV is often characterized by limited pulmonary involvement and extrapulmonary TB disease manifestations [135]. The paucibacillary nature of sputum in people with HIV limits the diagnostic sensitivity of sputum based microbiological assays [136]. The use of sputum-based microbiological assays for the screening of TB in people living with HIV is associated with reduced sensitivity and specificity that are below the thresholds that are recommended by the World Health Organization (WHO) [137]. This has necessitated the development of more rigorous screening and diagnostic modalities which do not rely on the availability of sputum for TB diagnosis in people with HIV [138].

This includes the urine lipoarabinomannan (LAM) assay which is a lateral flow test that detects components of the outer immunogenic layer of the mycobacterial cell wall [139, 140]. Urine LAM is recommended for use in the diagnosis of extra pulmonary TB in people with HIV.

Additionally, urine GeneXpert Ultra have improved sensitivity, specificity and diagnostic yield compared to the use of LAM.

Different tests are available for testing for TB infection. The interferon gamma release assay (IGRA) is a blood-based test [141, 142] that is an immunological assay in which a tube coated with Mtb antigens including ESAT6, CFP10 and TB10.4 is incubated with blood. A positive IFN gamma readout (> 0.35 international units, IU) is indicative of immune sensitization to Mtb antigens [143, 144]. Alternatively, the screening of TB in resource constrained settings may depend on the use of the tuberculin skin test (TST) [145, 146]. The latest iteration of the TST is called purified protein derivative (PPD) which is a concoction of a variety of Mtb antigens that are injected intradermally to evaluate immune sensitization to Mtb antigens. A positive reaction is indicated by a region of induration of 5 mm or more [147]. The TST is in less clinical use today due to the widespread use of IGRA. Individuals with a positive IGRA are programmatically targeted for TB prevention using IPT. Notably, these assays exploit an important principle of immunological memory-an intrinsic trait of the adaptive antigen specific CD4 T cell immune response. Dendritic cells (DC) are antigen presenting cells (APC) that drain to the nearby lymph nodes where they present antigens for the activation of the adaptive CD4 T cell responses. Proper activation of CD4 T cells culminates in the proliferation of long-lived antigen specific CD4 T cells that respond by secreting interferon (IFN) gamma which functions to activate Mtb infected macrophages, increasing their killing efficiency. Therefore, these assays function by detecting a central memory CD4 T cell response that signals previous encounter with Mtb [148]. More importantly, these assays provide rapid screening but cannot distinguish between LTBI and active TB disease [141, 144].

2.1.7 Clinical management of the human immunodeficiency virus

Infection with HIV leads to chronic immunosuppression which culminates in opportunistic infections, cancers and death if not appropriately treated with antiretroviral therapy (ART) [149]. The significant global reduction in AIDS-related deaths in recent years can be largely attributed to ART and its rapid scale up, which has also contributed to prevention of transmission [150, 151]. ART is now typically a combination of different drugs in a single pill regimen [152]. Different drug classes have different mechanisms of action with unique molecular targets. Combination therapy is used to potentiate the effect of ART and prevent the emergence of drug resistance [153].

In developing countries, TB is the commonest opportunistic disease and the most prevalent cause of hospitalization and death in people living with HIV [154]. HIV-associated TB has high case fatality rates, with an attributable mortality rate of up to 25% [155]. Effective ART in people with HIV is associated with a decline in the incidence of HIV-associated TB [156, 157].

Despite the availability of effective therapy for both HIV and TB, concurrent treatment can be challenging. Challenges include potential drug-drug interactions, increased pill burden-compromising adherence, clinical deteriorations, and programmatic challenges [7]. Delays in ART in patients with HIV-associated TB are associated with increases in AIDS related deaths, while early initiation of ART can be associated with the development of the TB-associated immune reconstitution inflammatory syndrome (TB-IRIS) [6, 158, 159].

Several observational studies and randomized controlled trials have established the survival benefit of integrated TB therapy and early ART in patients with HIV-associated TB. In the SAPiT trial, patients with a CD4 counts less than 50 cells/mm^3 who were administered ART early during the course of TB therapy demonstrated a significant reduction in mortality, relative to those who initiated ART following the completion of the intensive phase of TB treatment [160].

The following section will review the literature on paradoxical tuberculosis-associated immune reconstitution inflammatory syndrome.

2.2. The recurrence of TB symptoms and signs with inflammatory features in HIV-immunosuppressed patients after initiating ART

The most common complication of HIV-associated TB after ART initiation is the recurrence of TB symptoms and signs, with marked features of inflammation. This occurs despite the initial indication of improvement on TB treatment and effective suppression of HIV viremia [6]. This complication is known as TB-associated immune reconstitution inflammatory syndrome (TB-IRIS) [22, 161]. TB-IRIS is an aberrant and excessive inflammatory immune response that is targeted at live Mtb and/or its residual antigens [162]. For this reason, it often occurs during co-treatment with antituberculosis therapy and ART or less conventionally, following the successful completion of antituberculosis therapy. TB-IRIS is characterized by inflammation which causes tissue damage [18].

The lack of a standardized case definition for TB-IRIS early on during the roll out of ART prompted the International Network for HIV-associated IRIS (INSHI) to develop a consensus case definition and distinguish between two forms of TB-IRIS, namely unmasking and paradoxical TB-IRIS. The main distinction between the two is the sequence of initiation of antituberculosis therapy and ART. The following sections provide a review on paradoxical TB-IRIS, its incidence, diagnosis, mechanisms of pathophysiology, prognosis, clinical management, and prevention. In addition, knowledge gaps and key questions are highlighted, certain of which are addressed in the studies reported in this thesis.

2.2.1 Unmasking TB-IRIS

ART-associated TB is active TB that is diagnosed after the initiation of ART in people living with HIV not receiving antituberculosis therapy. Unmasking TB-IRIS occurs in a subgroup of these patients and is characterized by the onset of exaggerated inflammatory manifestations within the first 3 months of initiating ART, similar to those of paradoxical TB-IRIS.

2.2.2 Paradoxical TB-IRIS

Paradoxical TB-IRIS occurs in a proportion of HIV-immunosuppressed patients with TB diagnosis while on effective antituberculosis therapy. People who develop paradoxical TB-IRIS exhibit new, recurrent or worsening signs and symptoms of TB shortly after the initiation of ART. Paradoxical TB-IRIS occurs with effective HIV viremic control (between 50 and 2000 HIV copies/mL) and despite the initial indication of TB symptom improvement [22]. The case

definition for paradoxical TB-IRIS is described in two reviews by Meintjes, and French colleagues respectively [22, 89, 163].

Case definition for paradoxical tuberculosis-associated IRIS

There are three components to this case definition:

(1) Antecedent requirements

The following two requirements must be met:

- Diagnosis of tuberculosis: the diagnosis of tuberculosis was made before starting ART and this should fulfil WHO criteria for diagnosis of smear-positive pulmonary tuberculosis, smear-negative pulmonary tuberculosis, or extrapulmonary tuberculosis.
- Initial response to tuberculosis treatment: the patient's condition should have stabilized or improved on appropriate tuberculosis treatment before ART initiation—eg, cessation of night sweats, fevers, cough, weight loss. (Note: this does not apply to patients starting ART within 2 weeks of starting tuberculosis treatment since insufficient time may have elapsed for a clinical response to be reported)

(2) Clinical criteria

The onset of tuberculosis-associated IRIS manifestations should be within 3 months of ART initiation, re-initiation, or regimen change because of treatment failure.

Of the following, at least one major criterion or two minor clinical criteria are required:

Major criteria

- New or enlarging lymph nodes, cold abscesses, or other focal tissue involvement—eg, tuberculous arthritis.
- New or worsening radiological features of tuberculosis (found by chest radiography, abdominal ultrasonography, CT, or MRI)
- New or worsening CNS tuberculosis (meningitis or focal neurological deficit—eg, caused by tuberculoma)
- New or worsening serositis (pleural effusion, ascites, or pericardial effusion)

Minor criteria

- New or worsening constitutional symptoms such as fever, night sweats, or weight loss
- New or worsening respiratory symptoms such as cough, dyspnoea, or stridor
- New or worsening abdominal pain accompanied by peritonitis, hepatomegaly, splenomegaly, or abdominal adenopathy

(3) Alternative explanations for clinical deterioration must be excluded if possible*

- Failure of tuberculosis treatment because of tuberculosis drug resistance
- Poor adherence to tuberculosis treatment
- Another opportunistic infection or neoplasm (it is particularly important to exclude an alternative diagnosis in patients with smear-negative pulmonary tuberculosis and extrapulmonary tuberculosis where the initial tuberculosis diagnosis has not been microbiologically confirmed)
- Drug toxicity or reaction.

ART = antiretroviral therapy. IRIS = immune reconstitution inflammatory syndrome.

2.3 Epidemiology

Paradoxical TB-IRIS is the most studied form of IRIS, and by extension, the best characterized of the two types. Its incidence is approximately 18% across adult cohorts with HIV-associated TB from different settings [9, 10]. However, in HIV/TB endemic settings such as sub-Saharan Africa, the incidence of paradoxical TB-IRIS in adult populations is as high as 54% [10]. In pediatric cases, the incidence of paradoxical TB-IRIS is not well documented, however, one study reported an incidence of 7% [164].

Paradoxical TB-IRIS is an acute hyperinflammatory condition caused by activated immune cells which have been triggered by *Mycobacterium tuberculosis* (Mtb) or its residual antigens during immune restoration [39, 162]. Unlike the risk factors for TB disease itself, the known risk factors for paradoxical TB-IRIS are neither genetic nor socio-economic. Instead, they are rooted in the infectious load and severity of disease due to the two interacting pathogens and the timing of management in the host.

2.4 Determinants of paradoxical TB-IRIS

The answer to why only a certain proportion of HIV immunosuppressed patients with TB develop paradoxical TB-IRIS remains elusive. However, several risk factors including high viral load, a CD4 count of less than 200 cells/mL, disseminated TB disease, a short interval between the initiation of anti-tuberculosis therapy and ART, and the rapid reduction in HIV viral load on ART are known risk factors [22, 165-167].

In a study that evaluated the efficacy of ART, different ART regimens led to at least a 2 $\log_{10}$ -fold reduction in HIV viral load within the first 2 weeks of therapy and a concomitant early and partial reconstitution of the CD4 T cell compartment due to effective HIV replication inhibition [168].

The timing of ART is important in managing the risk of paradoxical TB-IRIS. This is because the risk of developing paradoxical TB-IRIS is increased in patients with higher bacterial burden or higher antigen load and HIV viremia [8]. Early ART in TB coinfected patients with CD4 T cell counts < 50 cells/µL is also associated with increased risk to TB-IRIS, but has a benefit of reducing mortality due to HIV mediated immunosuppression [169]. Therefore, a short delay in ART is a counter measure to minimize the risk of ART mediated complications in patients with severely reduced CD4 lymphocyte counts, higher HIV viremia and bacterial burden [18, 22].

Consequently, ART is initiated within 2 weeks of antitubercular therapy in patients with CD4 count <50 cells/μL but can be delayed up to 2 months in those with a CD4 counts >50 cells/μL according to South African guidelines [169]. On the other hand, the WHO guidelines recommend initiating ART within two weeks of anti-tubercular therapy initiation regardless of CD4 count [170-172]. The initiation of ART in patients with tuberculous meningitis requires longer delay of ART by 4-8 weeks [173, 174].

2.5 Clinical manifestations

The clinical manifestations of paradoxical TB-IRIS are varied and may include deteriorating radiological findings, inflamed and enlarged lymph nodes, cold abscesses and worsening symptoms [18]. The burden on health systems of paradoxical TB-IRIS is significant in HIV/TB endemic settings and approximately 25% of the cases will require hospitalization for diagnostic work-up and syndromic management [19]. Pulmonary and lymph node involvement are the most prevalent clinical manifestations of paradoxical TB-IRIS comprising 40% and 38% of cases respectively [9, 11, 175, 176]. The duration of TB-IRIS symptoms is highly variable with reported median durations between 19-87 days [9]. However, longer durations of paradoxical TB-IRIS of up to a year have been reported and often require intervention with corticosteroids which are associated with significant complications [14].

2.6 Diagnosis

The clinical presentation of paradoxical TB-IRIS may be similar to that of superimposed infections, treatment failure resulting from inadequate TB treatment, or MDR-TB, and it is important to consider and exclude these diagnoses before diagnosing paradoxical TB-IRIS. For this reason, there exist standardized criteria for its diagnosis.

The diagnosis of paradoxical TB-IRIS is empirical and is predicated on the sequence of therapeutic intervention with antituberculosis therapy then ART; the combination of which triggers clinical deterioration with marked features of inflammation in some patients [177]. Several imaging modalities can aid in the diagnosis of paradoxical TB-IRIS. Worsening of chest radiological findings even in the absence of clinical deterioration may be indicative of paradoxical TB-IRIS. According to Fishman and colleagues, approximately 45% of patients

with pulmonary TB experienced radiographic deterioration within the first 5 weeks of initiating ART and the inflammatory lesions resolved within two weeks to three months [178]. Radiological findings on thoracic imaging may include enlarged thoracic lymph nodes, progression to miliary disease, pleural effusions, and worsening consolidation [179]. In instances of disseminated TB disease, other imaging tools that can aid in the diagnosis of extrapulmonary TB-IRIS include ultrasound for intra-abdominal TB-IRIS, brain computed tomography (CT) and magnetic resonance imaging (MRI) scans for paradoxical TB-IRIS involving the central nervous system (CNS), and chest CT for intrathoracic IRIS [16, 179, 180].

Furthermore, markers of immune system activation such as elevated plasma C-reactive protein (CRP), and/or significant increases in CD4 count between the start of ART and paradoxical TB-IRIS onset, may support the diagnosis of paradoxical TB-IRIS [181, 182]. Michailidis and colleagues reported a 0.6–5.6, and a 0.2–1.0-fold increase in absolute CD4 T-cell counts among patients on ART who developed TB-IRIS and those who did not develop TB-IRIS respectively [183]. In rare cases, there is a decline in absolute CD4 T-cell count at the time of IRIS onset. This is attributed to bone marrow suppression due to TB, but may also reflect the fact that, blood and tissue dynamic of immune restoration may not occur synchronously [180, 184].

Paradoxical TB-IRIS may present with non-specific clinical manifestations including systemic illness and lymphadenopathy. In such cases, INSHI definition is investigated to rule-out potential IRIS mimics [22].

Poor adherence to either ART or anti-TB regimen respectively is not uncommon in patients with HIV-associated TB and may lead to treatment failure, and the subsequent emergence of resistance to ART or antituberculosis therapy [185]. This can lead to clinical deterioration, which can be indistinguishable from paradoxical TB-IRIS [186, 187]. Although evidence suggests it is not more frequent in people with HIV, MDR-TB is a major problem in many HIV/TB endemic countries. Therefore, investigating drug susceptibility when TB-IRIS is suspected is important to rule out drug resistance before diagnosing TB-IRIS [187, 188].

Adverse effects associated with antituberculosis therapy can mimic certain TB-IRIS manifestations [189]. For example, hepatotoxicity due to antituberculosis therapy should be considered in cases of suspected abdominal TB-IRIS [190].

Testing for alternate infectious agents is recommended and should be guided by localizing symptoms and signs; for example, worsening pulmonary symptoms should trigger

consideration of bacterial pneumonia, *Pneumocystis jirovecci,* pneumonia or pulmonary Kaposi Sarcoma [22, 191]. Based on the patient's location, endemic opportunistic and non-opportunistic pathogens may cause superimposed infections such as malaria causing the recurrence of fever which can be misdiagnosed as TB-IRIS [192]. Additionally, HIV immunosuppressed patients have a disproportionate risk for cervical or penile carcinomas, Kaposi Sarcoma, and non-Hodgkin's lymphoma which can present with lymphadenopathy mimicking TB-IRIS [193]. Histopathologic examination of lymph node biopsies or other tissues can distinguish malignancies from the non-caseating granulomas that characterize the tissue pathology of TB-IRIS [178].

2.7 The immunopathogenesis of paradoxical TB-IRIS

The immune system provides a defense mechanism against pathogens and other foreign, noxious agents. It also regulates aberrant biological processes that may occur due to age or cellular dysfunction related to lifestyle. The immune system is traditionally simplified into two divisions, namely: the innate and adaptive immunity respectively. Innate immunity is the first line of defense that counteracts or eliminates pathogens. There are two main features that distinguish innate immunity from adaptive immunity. First, it is activated within minutes after infection, unlike the adaptive immunity that takes days or weeks to optimally respond. Second, the receptors of the innate immunity which are a surveillance mechanism that functions to detect pathogens, foreign particles, or abnormal cells and are germline encoded and do not require a previous encounter with a pathogen to recognize it. The receptors are generally referred to as pattern recognition receptors that recognize conserved structural features or moieties on different microorganisms. Therefore, the receptors of the innate immunity have broad specificity. This is in contrast with the receptors of the adaptive immunity (B and T cells) that have pathogen specificity. Mature B and T lymphocyte reside in primary and secondary lymphoid organs and are activated by antigen presenting cells such as dendritic cells. Following activation, they migrate to sites of infection to coordinate a robust immune response [63, 194, 195].

Adaptive cell-mediated immunity is vital for facilitating inhibition of Mtb replication inside the phagosome of phagocytes in 90% of the individuals with uncompromised immunity. However, HIV targets and depletes Mtb-specific CD4 T lymphocytes in particular, due to their

activation and the elevated expression of chemokine receptor (CCR)-5 [196, 197]. In the remaining CD4 T lymphocytes, HIV additionally impairs their capacity to recognize processed antigens and their ability secrete cytokines [198]. Moreover, infection with HIV also targets innate immune cells such as resident alveolar macrophages which are the first immune cells to interact with Mtb. HIV dysregulates Mtb recognition, impairs the phagocytic capacity and subsequent intracellular signaling of macrophages, thereby hampering their ability to effectively control Mtb proliferation [199]. This occurs through the impairment of TLR signaling which has a knock on effect on downstream processes including phagocytosis [200]. Furthermore, HIV impairs the ability of macrophages to undergo apoptosis; a process that regulates intracellular growth of Mtb, through the inhibition of Mtb-induced tumor necrosis factor alpha (TNF-α) [201]. Due to these impairments in macrophages and CD4 T cells in advanced HIV infection, disseminated TB disease is more frequent [202]. For instance, in patients with advanced HIV infection, TB spreads hematogenously to cause extrapulmonary and disseminated TB [16]. Phagocytes such as macrophages, monocytes and neutrophils are the main immunological barrier of defense against Mtb infection in the absence of adaptive CD4 T cell mediated immune responses which aid in the activation of tissue resident macrophages enabling the control Mtb growth [203-205].

The lymphatic system filters Mtb, its antigens and infected leukocytes from the blood or drains these from diseased tissue to the nearest lymph nodes. Commonly affected lymph nodes include the thoracic, cervical and mesenteric, where nodal TB disease often develops [206]. In TB disease, granulocytes sequester Mtb in the phagosome, where Mtb subverts the immune responses by preventing phagosome maturation thereby continuing to replicate [52, 77, 78]. In paradoxical TB-IRIS, ART initiation leads to a restoration of many aspects of the immune response to TB, while others remain impaired. For example, CD4 T cell counts may increase, but ratios of memory to naïve subsets remain unbalanced [207].

The initiation of ART during antituberculosis therapy may result in excessive production of cytokines and chemokines resulting in the activation of immune cells and a chemokine gradient which causes the trafficking on immune cells from the vasculature to the site of disease, thereby causing excessive inflammation which is a hallmark of paradoxical TB-IRIS pathology [177, 208]. This results in a pathologic hyperinflammatory response against Mtb and its residual antigens in tissues, manifesting clinically as paradoxical TB-IRIS with new or recurrent or

worsening signs and symptoms associated with TB disease with distinct inflammatory features [18, 22, 209].

Advances in the understanding of paradoxical TB-IRIS immunopathology are hampered by a lack of a suitable animal model that encompasses the two interacting pathogens and their respective therapies. However, the recent breakthrough in the establishment of a humanized murine model of HIV/TB coinfection could be repurposed for studying TB-IRIS [210]. Additionally, Barber and colleagues established a murine model of *Mycobacterium avium* IRIS which has enabled advances in understanding mycobacterial IRIS immunopathogenesis [211-213]. Research into TB-IRIS has mainly relied on the use of human samples such as plasma cytokine assessment, ex vivo stimulation of PBMCs, the analysis of the transcriptome, proteome and metabolome comparing patients who developed paradoxical TB-IRIS to control groups from the same cohorts who did not [15, 177, 214]. The current literature on the pathogenesis of paradoxical TB-IRIS highlights a synergistic role of dysregulated innate and adaptive immune responses mediated through a positive feedback loop of elevated pro-inflammatory cytokine responses.

2.7.1 The involvement of adaptive immune responses in the pathogenesis of TB-IRIS.

The onset of paradoxical TB-IRIS is characterized by a significant increase in absolute counts of CD4 T lymphocytes and frequencies of Mtb-specific IFNγ CD4 T cell in cases compared to TB-non-IRIS controls [29]. However, similar expansions were reported in some TB-non-IRIS controls although not quite as robust as in patients with TB-IRIS [37]. These expansions are attributed to ART mediated reversal of immune suppression, culminating in the restoration of Mtb-specific CD4 immune cells and do not fully explain the phenomena underlying TB-IRIS pathogenesis [37]. The work of Bourgarit and colleagues reported that PPD-specific CD4 T cells that expanded during TB-IRIS were indeed functional as evidenced by their ability to secrete IFNγ which was significantly higher in patients with paradoxical TB-IRIS compared to TB-non-IRIS controls at the median time of IRIS onset [39]. IFNγ is important for the activation of Mtb primed phagocytes and enhances their capacity to control Mtb [215]. The polyfunctionality of Mtb-specific CD4 T cells was investigated in people with TB-IRIS by Wilson and co-workers and they documented the loss of polyfunctional responses in the CD4

T cell compartment [216]. The implications of these findings are that restored Mtb-specific CD4 T cell responses may be impaired in their capacity to form granulomas and control Mtb growth. However, many studies have demonstrated that Mtb-specific CD4 T cells are polyfunctional as indicated by expression and significant secretion of IFNγ and TNFα in Mtb stimulated PBMC from patients with paradoxical TB-IRIS compared to TB-non-IRIS controls at the median time of TB-IRIS onset [217]. The characterization of pathogen specific CD4 T cell responses by Elliot and colleagues demonstrated that IFNγ responses differed on the basis of ART status but not TB-IRIS status [218]. However, many studies have since reported that responses differed based on TB-IRIS outcome [29, 37, 177].

Other analyses of Mtb-specific CD4 T cell response revealed that they retained the ability to proliferate as evidenced by increased expression and secretion of IL-2 following immune recovery in patients who developed paradoxical TB-IRIS. ART mediated Th-1 immune recovery is additionally associated with elevated expression of IL-12, IFNγ inducible protein 10 (IP10), IL-18, and soluble IL-2 receptor (sCD25) [25, 162, 216]. Haridas and co-workers characterized Mtb-specific IFNγ expressing CD4 T lymphocytes and reported that responses were highly activated as evidenced by elevated expression of HLADR in patients with TB-IRIS compared to TB-non-IRIS controls at the median onset time of paradoxical TB-IRIS [219]. Other studies demonstrated that Mtb-specific CD4 T cell responses were not anergic as evidenced by the comparable expression profiles of exhaustion markers such as PD-1 and Lag3 in cases compared to TB-non-IRIS controls at the median time of paradoxical TB-IRIS onset. Finally, Meintjes and colleagues reported comparable frequencies of regulatory CD4 T cells (Tregs) between cases and TB-non-IRIS controls at the median time of paradoxical TB-IRIS onset [37]. This suggests that the ability to regulate CD4 T cell responses was not impaired or heightened in patients who developed paradoxical TB-IRIS. An increase in effector-memory CD4 T cells, and a decrease in central-memory CD4 T cells has been described in patients with paradoxical TB-IRIS compared to TB-non-IRIS controls, at the median time of TB-IRIS onset [38]. This may reflect that the effector memory phenotype contributes disproportionately to Mtb-specific CD4 T lymphocyte dysregulation during paradoxical TB-IRIS.

Besides conventional T and B cells, innate lymphoid cells (ILCs) which bridge the innate and adaptive immunity were recently described [220]. ILCs retain characteristics of both the innate and adaptive immunity and comprise a sizeable proportion of immune cells that contribute

towards pathogen responses and can produce interleukin-5 (IL-5), IL-13, IL-17 and/or IL-22 helping to initiate immune responses against pathogens. Natural killer (NK) cells are now recognized as a subset of cytotoxic ILCs that express the transcription factor E4BP4/ Nfil3. NK cells also secrete cytokines, such as interferon-γ (IFN-γ), that participate in shaping the adaptive immune response [221]. A defining and crucial feature of NK cells is their ability to distinguish stressed cells (such as infected cells, chemically or physically damaged cells, and tumour cells) from normal cells.

Natural Killer T (NKT) are a subset that is further divided into four different categories including type I-IV NKT cells [222]. Type I NKT cells or invariant NKT cells (iNKT cells) are the most studied and conserved in mammals [220, 223]. The development of iNKT cells occurs in the thymus, and they develop from a common lymphoid progenitor cell from which conventional T cells develop [223, 224]. Lineage commitment for iNKT cells occurs after the formation of double positive thymocytes following the αβ T cell commitment step [224, 225]. iNKT cell precursors are selected following α-chain rearrangement and expression of the semi-invariant T cell receptor (Vα14-Jα18 in mice, Vα24-Jα18 in humans) [226]. In contrast to conventional T cells that are selected by antagonist ligands, it is believed that iNKT cells are selected by agonist glycolipids [227].

The role of both NK cells and iNKT cells in TB-IRIS pathogenesis has been investigated in several studies. NK cells have robust cytotoxic effector capabilities such as perforin and granzyme B production which are constituents of cytotoxic granules in NK cells. NK cells were reported to be highly activated, with higher capacity to degranulate in TB-IRIS patients compared to TB-non-IRIS controls [228, 229]. iNKT derived perforin and granzyme B were significantly elevated in patients who developed paradoxical TB-IRIS compared to TB-non-IRIS controls at the time of symptom onset [229]. Walker and colleagues observed perturbations of iNKT and regulatory iNKT subsets, with higher frequencies of iNKT cells displaying evidence of recent degranulation in patient samples with paradoxical TB-IRIS compared to TB-non-IRIS controls [230].

Another lineage of T cells with cytotoxic potential, CD8 T cells, have been investigated in TB-IRIS. Evidence regarding the involvement of CD8 lymphocytes in TB-IRIS pathogenesis is conflicting. There were comparable frequencies of CD8 T cells between TB-IRIS cases and

TB-non-IRIS controls at baseline. However these were significantly expanded in participants who developed paradoxical TB-IRIS compared to TB-non-IRIS controls at the median manifestations of inflammatory features [231]. Phenotypic characterization of Mtb-specific CD8 T cells revealed decreased activation of CD8 T cells prior to the initiation of ART, and reduced CD8-signaling were reported in patients who developed TB-IRIS compared to TB-non-IRIS controls [216, 232]. However, Bourgarit and colleagues reported increased frequencies of an activated distinct lineage of CD8 T cells called the γδ CD8 T cells in patients who developed TB-IRIS compared to TB-non-IRIS controls [38, 233, 234]. Additionally, expression of killer cell ligand like receptor g1 (KLRG1) and programmed cell death protein 1 (PD-1) indicating immune exhaustion were significantly higher in Mtb-specific CD8 T cells of patients who developed TB-IRIS compared to TB-non-IRIS controls [233].

2.7.2 The involvement of innate immune responses in the pathogenesis of TB-IRIS.

Systems biology has substantially enriched our understanding of TB-IRIS immunopathogenesis by integrating genome wide analysis such as RNA (transcriptomics) with phenotypes (clinical diagnosis of TB-IRIS). These discovery approaches involve hypothesis generating frameworks with subsequent validation of findings in downstream experiments. Mounting evidence derived from systems biology approaches suggests that macrophage and monocyte effector responses are central to the pathogenesis of paradoxical TB-IRIS. Whole blood transcriptomics studies performed by Lai and colleagues reported that macrophage signaling was the leading enriched biological process shortly following the initiation of ART and at the median onset of paradoxical TB-IRIS [25]. Moreover, Tran and colleagues reported the role of monocytes in TB-IRIS pathogenesis with the aid of microarray analysis. The authors reported the significant enrichment of pattern recognition receptors and the complement system at baseline in patients who later developed TB-IRIS compared to TB-non-IRIS controls. At the onset of TB-IRIS, one biological pathway that was significantly enriched in patients who developed paradoxical TB-IRIS compared to TB-non-IRIS controls was complement pathway [235]. The same group used microarray technology to study gene expression profiles in purified monocytes that were extracted from PBMC. Pathway analysis highlighted impaired complement responses in patients who were predisposed to developing paradoxical TB-IRIS; while perturbations in components of the complement including C5q, C1q (effector) and C1Inh

(its inhibitor) were reported at the median onset of inflammatory symptoms in patients who developed paradoxical TB-IRIS compared to matched TB-non-IRIS controls [236]. These findings have been corroborated by other studies [237].

Experimental validation of these discovery approaches has elucidated important aspects of paradoxical TB-IRIS pathogenesis and led to a rational paradigm of how IRIS occurs. For instance, Andrade and colleagues characterized soluble markers of monocyte activation including sCD14, sCD163, and soluble tissue factor during TB-IRIS. The authors demonstrated perturbations in monocyte populations and the upregulation of monocyte soluble markers at IRIS onset. The reported perturbations were significantly correlated with inflammatory cytokines [237].

Inflammatory immune responses in patients who develop paradoxical TB-IRIS have been extensively analyzed. They are characterized by a cytokine storm that has been associated with tissue damage [162]. Biological processes that precede hypercytokinaemia and clinical features include elevated expression of pattern recognition receptors (PRR) [25, 235]. Findings also implicate TLR signaling and inflammasome activation in paradoxical TB-IRIS [15, 177]. The expression of TLR2 is elevated in monocytes and dendritic cells, and is positively correlated with the secretion of downstream cytokines (TNF-α, IL-12p40) [32]. These findings were corroborated by Lai and colleagues who experimentally demonstrated that the identified myeloid signature predicted the activation of a number of proinflammatory cytokines such as IL-12, IFNγ and TNFα at the median time of paradoxical TB-IRIS onset; and that the inhibition of downstream adaptor of TLR2 (myeloid differentiation primary response 88 / MyD88) abrogated the secretion of downstream cytokines in samples from patients with paradoxical TB-IRIS [177]. The authors additionally demonstrated elevated expression and secretion of multiple components of the inflammasome (Caspase-1 and 5, triggering receptor expressed on myeloid cells-1 [TREM-1] and IL-1 family of cytokines) in patients that developed TB-IRIS compared to TB-non-IRIS controls at the median onset of inflammatory features [177]. Downstream cytokine responses, the secretion of IL-1 family of cytokines in particular, depend on the activation and maturation of the inflammasome complex [31, 177, 238].

The involvement of neutrophils in paradoxical TB-IRIS pathology is increasingly being recognized. TB-IRIS patients had increased expression of calprotectins (S100 calcium binding

protein A9 (S100 A9) compared to TB-non-IRIS controls [239]. S100A9 concentrations reflect perishing neutrophils in their activated state. Calprotectins are DAMPs which recruit more neutrophils to the site of disease. Other studies have corroborated the overexpression of S100A8 and A9, thereby emphasizing the importance of neutrophils in the pathogenesis of TB-IRIS [15, 16, 240, 241]. The NLR pyrin domain containing 12 (NLRP12), and cyclooxygenase 1 (COX-1) were significantly higher in TB-IRIS patients compared to TB-non-IRIS controls at the median time of TB-IRIS onset [239]. NLRP12 and COX-1 are components of different signaling processes; NLRP12 is a component of the inflammasome complex which amplifies the inflammatory cascade through the maturation of IL-1 family of cytokines (such as IL-1α and IL-1β) which are potent modulators of inflammation; while Cox-1 is a component of the eicosanoid biosynthetic pathway and is postulated to activate neutrophils. The authors additionally reported significantly higher absolute neutrophil counts in peripheral blood in patients who developed paradoxical TB-IRIS compared to TB-non-IRIS controls at the median time of symptom onset. Soluble markers of neutrophils, including neutrophil elastase and human neutrophil peptides in the CSF, were similarly significantly higher at the onset of inflammatory symptoms in patients who developed paradoxical tuberculous meningitis (TBM)-IRIS compared to TBM-non-IRIS controls [241]. Lastly, immunohistochemistry staining revealed the presence of neutrophils in lymph node biopsies of patients who developed paradoxical TB-IRIS [239, 242].

Matrix metalloproteinases (MMPs) are endopeptidases that are important in tissue remodeling and repair. MMPs were highly upregulated at the median onset of inflammatory symptom in patients who developed TB-IRIS compared to TB-non-IRIS controls [162, 241, 243, 244]. Walker and colleagues and Marais and colleagues reported MMP involvement in the inflammatory response observed in patients who developed paradoxical TB-IRIS and in paradoxical TBM-IRIS [15]. MMPs were significantly higher in plasma samples of patients who developed TBM-IRIS compared to those who did not (TBM-non-IRIS controls) at the time of symptom manifestation [243].

Dissemination of TB to the central nervous system most frequently results in infection of the meninges enveloping the brain. CNS involvement is associated with 56% mortality because it is challenging to manage [245, 246]. There are notable differences in the immune responses of TBM-IRIS patients in the CSF and peripheral blood despite certain parallels. At baseline as

well as at the time of TBM-IRIS onset, there were significant differences in the secretion of proinflammatory cytokines, chemokines and matrix metalloproteinases (soluble plasma mediators) in the cerebrospinal fluid (CSF) compartment of people that were at high risk of developing TBM-IRIS compared to those who did not (TBM-non-IRIS controls). Conversely, no significant differences in soluble plasma mediators in peripheral blood of people who developed TBM-IRIS compared to TBM-non-IRIS controls at baseline as well as at the time of TBM-IRIS onset [241]. Additionally, there were significant differences in soluble plasma mediators between the CSF and peripheral blood compartments in patients that developed TBM-IRIS at symptom onset. Similarly, this was true for TBM-non-IRIS controls [241]. By contrast, there are no significant differences in neutrophil and inflammasome derived cytokine response in peripheral blood of TBM-non-IRIS controls compared to TBM-IRIS patients at the time of TBM-IRIS onset. This is likely due to the compartmentalization of immune responses in TBM-IRIS patients. The number of participants enrolled in these studies are historically limited. Therefore, larger studies are needed to validate these patterns [15, 241]. Notably, humoral and Th-2 immune responses have not been implicated in the hyper-inflammatory response underlying paradoxical TB-IRIS immunopathogenesis or its regulation [247, 248].

2.8 Prognosis

Paradoxical TB-IRIS is a potentially life-threatening condition for a minority of patients. In many patients, it is self-limiting within a few weeks and in most patients clinical symptoms resolve within 2 months [18]. Prognosis depends on the site of disease and the implemented treatment. Lack of standardized follow up time and criteria defining paradoxical TB-IRIS associated death are accountable for a wide range in mortality attributable to paradoxical TB-IRIS [17, 249, 250]. The most recent systematic review reported a 2% mortality rate due to paradoxical TB-IRIS [9]. Mortality rates can reach up to 56% in instances of CNS involvement which is the most severe form of paradoxical TB-IRIS [15-17]. Studies have reported varied findings regarding pulmonary consequences of paradoxical TB-IRIS and lung function. Auld and colleagues reported significant decline in lung function (forced expiratory volume [FEV]) in 50% of patients with paradoxical TB-IRIS while 18% shows sustained long term impairment [251]. By contrast, Stek and colleagues reported no association between lung function and pulmonary disease in patients with paradoxical TB-IRIS disease who either received placebo or prednisone prophylactic intervention in a clinical trial [252].

2.9 Clinical management

2.9.1 Treatment

The management of paradoxical TB-IRIS is complicated and evidence-based intervention are limited. Corticosteroid therapy tapered over the course of four weeks is the treatment of choice to manage significant symptoms resulting from TB-IRIS [9, 19]. Evidence supporting this intervention was provided by Meintjes and colleagues, in which TB-IRIS patients who received prednisone had decreased duration of hospitalization, and more rapid recovery based on the improvement of symptoms and inflammatory markers [19].

In vitro studies indicate that corticosteroid treatment can effectively lower proinflammatory cytokines including IL-6 and TNF-α, and MMP proteins such as MMP-7, 8 and 9, suggesting a mechanism for their efficacy in treating IRIS [162].

In cases of protracted symptoms or symptom recurrence after stopping prednisone, the duration of prednisone may need to be extended with more gradual weaning, but continuation beyond four months is not recommended because of cumulative side effects [21, 209]. In cases of steroid refractory paradoxical TB-IRIS, biologics and other immunomodulators including thalidomide, TNF-α inhibitors, interleukin (IL)-6 blockers, montelukast, and pentoxifylline have been used in isolated cases; albeit with insufficient evidence to recommend for routine use [209, 253, 254].

Similarly, there is no randomized clinical trial-based evidence for the use of nonsteroidal anti-inflammatory drugs (NSAIDs). However, NSAIDs have been used to manage symptoms of mild or localized paradoxical TB-IRIS [9, 253].

In severe cases of paradoxical TB-IRIS, invasive procedures including lymph node aspiration, pericardiocentesis, paracentesis, and thoracentesis have been performed to alleviate symptoms or manage complications [21, 209]. The extension of antituberculosis therapy is not necessary following successful completion of TB treatment, except in patients with abscesses or tuberculomas that have persisted despite six months of TB treatment as it may be difficult to exclude ongoing Mtb replication at the site of inflammation [158]. Importantly, ART is continued during TB-IRIS, except in cases of life-threatening neurologic disease [9, 18, 158].

2.9.2 Prevention

Prednisone is the only evidence-based intervention for the prevention of paradoxical TB-IRIS. Meintjes and colleagues reported a 30% reduction in the incidence of paradoxical TB-IRIS, in HIV-TB coinfected patients allocated a moderate dose of prednisone (40 mg/kg tapered down to 20 mg/kg after 2 weeks) starting ART; compared to patients that were allocated placebo [21].

Peripheral blood was collected from enrolled participants in this trial. Cellular components including (DNA, RNA, PBMC, Plasma) were extracted from the blood samples and were used in studies reported in chapter 5, 6 and 7.

3. Chapter 3 outline: Materials and Methods

This chapter discusses the methodological approaches used to address several different hypotheses discussed in subsequent chapters. This chapter describes the TB-ART and Pred-ART cohorts from which the samples used in this sub-study were derived. The section describes the patient demographics and criteria used to include and exclude patients into the parent studies. The chapter also describes how biological samples were obtained from the patients and the methods used to extract cellular fractions of interest and their subsequent storage. The chapter continues by describing in depth protocols used in various experimental assays including immunoassays such as Luminex, enzyme linked immunosorbent assay (ELISA), flow cytometry, the extraction of ribonucleic acid (RNA), preparation of RNA libraries, sequencing of RNA libraries, and the downstream processing and workflows for data analyses of sequenced samples.

3. Background

Cryopreserved biological human samples from different clinical studies were used to investigate several related hypotheses. The various studies collectively enhanced our understanding of the cellular mechanisms that underlie the pathogenesis of paradoxical TB-IRIS. The work presented herein was designed as four separate studies each addressing specific hypotheses. In the first study, we characterized the quantity and quality of Mtb-specific conventional CD4 T cells and the expression of specific immune markers in TB-IRIS using flow cytometry (chapter 4). The second study (chapter 5) used RNA sequencing to discover differentially abundant transcripts in whole blood and summarized them into biological pathways in patients who received either placebo or prednisone, a proportion of whom subsequently developed paradoxical TB-IRIS and compared to those who did not. The third study validated the neutrophil signature using immunoassays (chapter 6). The last chapter evaluated the capacity of inflammasome related drugs to reduce inflammatory markers using peripheral blood mononuclear cells (PBMC) from patients who previously developed paradoxical TB-IRIS (chapter 7). The following sub-section will describe the clinical cohorts and outline the scientific methods that were used to investigate the postulated hypotheses in each sub-study.

3.1 Patient recruitment: TB-ART observational study

To investigate the phenotype of *Mycobacterium tuberculosis* (Mtb)-specific IFNγ+ CD4 T cells, bio-archived patient PBMC from the TB-ART observational trial were used [19]. Briefly, patients were enrolled in a prospective observational study conducted at Brooklyn Chest TB Hospital between May 2009 and November 2010 in Cape Town, South Africa [6]. All patients were ART naïve and those with rifampicin-resistant TB were excluded. TB diagnosis was based on smear, culture, or clinical diagnosis. The first TB episode was treated with standard first line regimen of rifampicin (R), isoniazid (H), pyrazinamide and ethambutol for two months followed by four months of RH regimen. In patients with subsequent episodes, streptomycin was added for 2 months. Paradoxical TB-IRIS was diagnosed per International Network for the Study of HIV-associated IRIS (INSHI) criteria [26]. HIV treatment included lamivudine and efavirenz with stavudine or tenofovir depending on guidelines at the time. Written informed consent was obtained from all participants to collect and biobank cellular fractions derived from peripheral blood samples. A proportion of the participants subsequently

developed paradoxical TB associated immune reconstitution inflammatory syndrome (IRIS) and their samples were used phenotype Mtb-specific responses, investigating the hypothesis that patients who developed paradoxical TB-IRIS might have more cytotoxic CD4 lymphocyte responses following ART mediated immune reconstitution. The study was approved by the Human Research Ethics Committee (HREC REF: 049/2009 and 809/2018) of the University of Cape Town. Clinical and other immunological findings from this cohort have been published [6, 27-29].

3.2 Isolation of peripheral blood mononuclear cells by ficoll

For optimizing experimental conditions, peripheral blood was collected by a qualified healthcare practitioner, from a consenting healthy adult with sensitization to mycobacterial antigens. Peripheral blood was collected in 10 mL blood collection tubes containing ethylenediamine tetra-acetic acid (EDTA)/ heparin as an anticoagulant of choice. PBMC were isolated from whole blood according to Gill et al [255]. Briefly, peripheral blood was aseptically diluted in 10 mL of sterile 1X phosphate buffer saline (PBS) inside a sterile biosafety level II cabinet (BSC) and gently layered into a 50 mL falcon tube containing 15 mL ficoll to avoid disturbing the ficoll-blood interface. The falcon tubes were subsequently spun at 500 xg for 25 minutes (min) at 22 °C with acceleration and deceleration set at maximum and zero respectively. Following gradient centrifugation, the tubes were carefully transported to the BSC, taking caution not to disturb the resultant solid and liquid interfaces, namely: the sedimented blood pellet, the toxic ficoll, the PBMC and the plasma layers respectively. The caps of the falcon tubes were gently removed and the PBMC layer was transferred to a properly labelled and sterile 50 mL falcon tube and topped up to 40 mL with fresh and sterile Rosewell park media institute (RPMI) medium supplemented with 2% heat inactivated fetal calf serum (FCS). PBMC were washed by centrifugation at 400 xg for 10 min with both acceleration and deceleration set to maximum. The tubes were carefully transported to the BSC where the supernatant was discarded into a beaker containing 10% biocide and the tubes gently blotted on sterile gauze. The PBMC pellet was resuspended in 40 mL of RPMI supplemented with 2% FCS and washed as previous. The supernatant was discarded as previous and the PBMC pellet was gently resuspended by flicking. Subsequent steps were performed on wet ice. For complete resuspension of the PBMC pellet, the convention is to resuspend in 0.5 mL of RPMI (supplemented with 10% FCS) for each 10 mL of blood collected. The PBMC pellet was resuspended in 5 mL of RPMI supplemented with 10% FCS. For cryopreservation, freezing

media comprised of a mixture of 20% dimethyl sulfoxide (DMSO) in 40 mL FCS. Freezing media was added slowly in drop-wise fashion while swirling the PBMC suspension. Approximately 1 mL of the PBMC with freezing solution was aliquoted to labelled and sterile corning cryogenic vials. The cryovials were subsequently transported from ice to -80 °C overnight (O/N; minimum of 12 hours) before transferring to liquid nitrogen for long term storage. Of note, all the used chemicals were within their expiration date.

3.3 PBMC recovery from cryopreservation

Patient and healthy participant PBMC were recovered from cryo-preservation as described by Honge et al. [256]. Briefly, cryopreserved PBMC were rapidly thawed in a uniformly heated water bath with temperature set to 37 °C and transferred to 50 mL falcon tubes. To collect residual PBMC, cryovials were rinsed with 1 mL of phosphate buffer saline (PBS) supplemented with 20% FCS and transferred drop wise to the 50 mL falcon tube containing cells. The suspension was topped up to 20 mL with warm PBS supplemented with 20% FCS. Cells were washed by centrifugation at 1200 rpm for 6 min at room temperature (RT). The supernatant was discarded in a liquid waste bucket containing biocide and the tubes containing the PBMC pellet were blotted on sterile paper gauze to completely remove supernatant. The PBMC pellet was resuspended in 20 mL PBS supplemented with 20% FCS. Washing was repeated and the supernatant was discarded as previous. The tubes were blotted on sterile gauze, taking precaution not to lose the cell pellet. Cells were resuspended in appropriate volume of RPMI supplemented with 10% FCS and allowed to recover by resting in an incubator calibrated to 37 °C with 5% CO_2 between four and 12 hours.

3.4 Optimizations

3.4.1 Optimizing cell number recovery: V vs U bottom 96 well cell culture plates.

The strength of flow cytometry lies in analyzing single cells in high numbers. Compounding the fact that variable PBMC numbers for each participant enrolled in the TB-ART observational study were stored, our flow cytometry cell staining workflow entailed several steps of manual cell washing which often result in significant loss of cells. To mitigate the potential short falls of low cell numbers when processing patient samples for flow cytometry, our experimental workflow was optimized to recover maximum number of cells. Cells from one healthy participant were seeded (up to 10 million cells/mL) either in a 96 well V or U

bottom cell culture plate. PBMC stimulation with a peptide pool of 300 of Mtb antigens and subsequent staining with classical T cell surface markers (CD3, CD4), markers of immune activation (HLADR) and intracellular staining (IFNγ, TNFα, Tbet, Eomes, Granzyme B) were performed and cells were analyzed for cell number recovery by flow cytometry.

3.4.2 Antibody titration protocol

Mouse raised human monoclonal antibodies were procured from different suppliers for single cell analysis using flow cytometry. To avoid antibody wastage and allow for optimal fluorescence on dim and bright populations, the 15-color antibody panel was optimized. The antibodies were titrated to determine the appropriate titers to use for standardized staining protocol. Antibody titration experiments were set up for classical T cell markers spanning the various phenotypes or functions, in a sterile 96 well V bottom plate. For instance, titration of antibodies was performed for T cell surface markers (CD3, CD4), intracellular function markers (IFNγ, and TNFα), T-box transcription factors (Eomesodermin, Tbet), markers that served as proxies for cytotoxic potential (Granzyme B), markers for immune activation (HLA-DR), and exclusion markers (CD19, CD20). Briefly, a volume of 132 µL of PBS supplemented with 2% FCS (diluent) was added to the first well of the plate. To the same well, 6 µL of CD4-PerCPcy5.5, and CD3-BV785 (all from BioLegend, San Diego, CA) were added. The contents of the well were thoroughly mixed by pipetting up and down. A volume of 75 µL of PBS supplemented with 2% FCS was added to the subsequent 6 wells. A two-fold dilution series was performed by pipetting 75 µL of the antibody concoction from the first well down to the sixth well. A volume of 75 µL of the antibody dilution in the last well was discarded into a liquid waste containing biocide. The 2-fold serial dilution of classical T cell surface markers were kept at 4 °C in the dark until use (Figure 3).

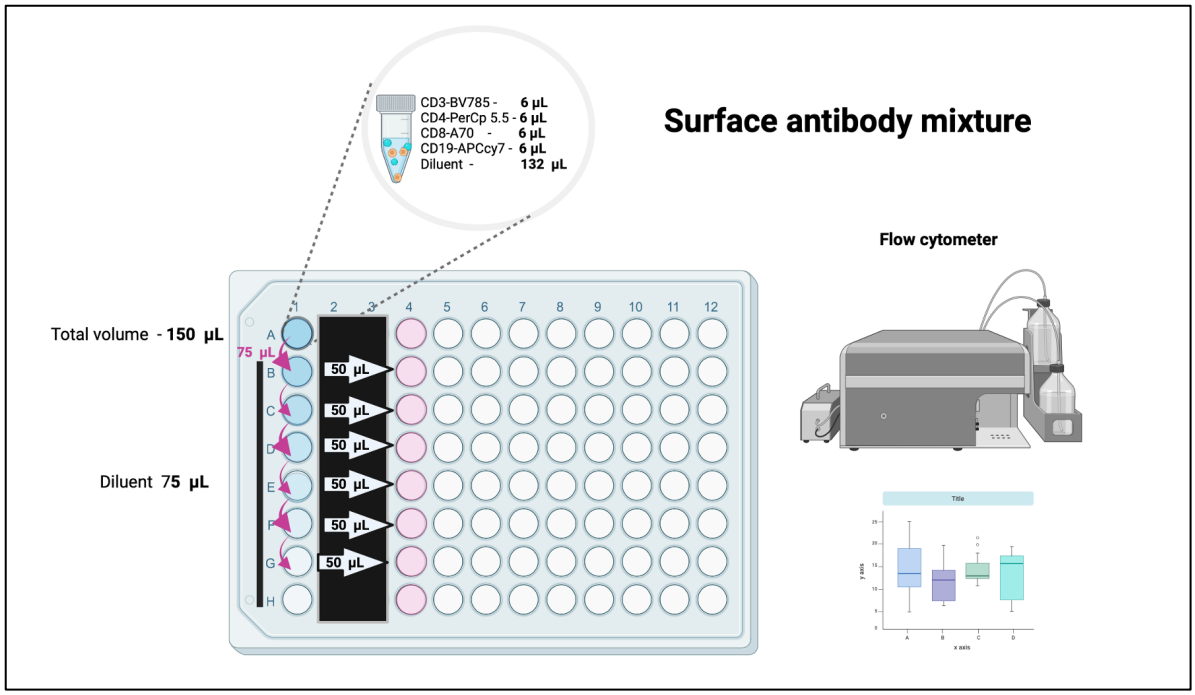

Figure 3. Diagrammatic illustration of antibody titration set up. *Surface staining antibodies with the same recommended titers were titrated together. Similarly for antibody markers for intracellular cytokines and transcription factors.*

Similarly, titration experiments were set up for all antibodies included in the final panel according to Figure 3 above. The final volume in the first well for all titration reactions was 150 µL which was used to generate a 2-fold dilution series in RPMI supplemented with 2% FCS per dilutions shown in Table 3.1. A total of 50 µL of the dilutions were added to cells for staining. Stained cells were incubated for 30 min for staining classical T cell surface markers (CD4-PerCPcy5.5, CD8-A700, CD19-APCcy7, HLADR-BV605). Staining of intracellular markers (CD3-BV785, IFNγ-BV711, TNFα-FITC, IL-2-BV421, GranzymeB-BV510, Tbet-PEcy7, and Eomes-APC) was performed by resuspending in the brefeldin treated PBMC with 200 µL of 1X eBio fixation buffer to permeabilize cells prior to staining with the intracellular concoction. The cells were washed twice by gradient centrifugation at 1600 rpm for 6 minutes in RPMI supplemented with 2% FCS to remove unbound antibody. Cells were resuspended in 1% formaldehyde and acquired in BD LSR II cytometer.

Table 3.1. Optimization of antibody titers for flow cytometry. *A total of 9 antibodies were titrated to determine the optimal volume for staining.*

Antibody	Titer (µL)	Fold dilution
CD3-BV785	2	2
		1
		0.5
		0.25
		0.125
		0.0625
TNFα-FITC	0.8	0.8
		0.4
		0.2
		0.1
		0.05
		0.025
GrB-BV510	5	5
		2.5
		1.25
		0.625
		0.313
		0.156

Representative antibody titers for surface and intracellular staining markers. Manufacturer recommended titers which were tested for CD3-BV785, CD4-PerCP-cy5.5, IFNγ-BV711, HLA-DR-BV605, Tbet-PEcy7 and CD19-APC-cy7 were the same. Similarly for titers for Granzyme B-BV510 and Eomes-APC.

3.4.3 PBMC surface staining for antibody titration

For optimization of antibody staining workflows for flow cytometry, all human samples were handled in a biosafety level 2 in a class 2 biosafety cabinet. Briefly, a single vial of cryo-preserved PBMC from one healthy individual with sensitization to mycobacterial antigens was recovered from cryopreservation as previously described (**see Section 3.3**) and resuspended in RPMI supplemented with 10% FCS to achieve a cell concentration of 10 million cells/ mL.

Cells were allowed to recover by resting in a stationary incubator at 37 °C, 5% CO_2 for 4 hours and were subsequently pelleted by centrifugation at 1800 rpm for 3 min at RT. The supernatant was discarded by rapid flicking motion and blotting of the 96 well plate on a sterile paper towel. Cells were subsequently washed in plain PBS by centrifugation at 1600 rpm for 6 min at RT and the supernatant discarded as previous. Cells were resuspended in 50 µL near infrared (NIR) live/dead stain, incubated in the dark for 10 min and were subsequently washed as previous in PBS supplemented with 2% FCS and the supernatant properly discarded. The cells were resuspended in 50 µL of the antibody titration mixture for 30 min and incubated in the dark for 30 min at RT. Cells were subsequently pelleted by centrifugation at 1800 rpm for 3 min and the supernatant was subsequently discarded as previous. Cells were washed in 200 µL PBS supplemented with 2% FCS by centrifugation at 1600 rpm for 6 min at RT and the supernatant discarded as previous. Cells were fixed in 1% formaldehyde and up to 1 million cells acquired by flow cytometry.

3.4.4 Preparation of compensations controls (for optimizations)

Compensation tubes for 3 fluorophores and one negative control were prepared in the following manner. A volume of 100 µL of PBS supplemented with 2% FCS was added to properly labelled 5 mL FACS tubes. A volume of 60 µL of anti-mouse immunoglobulin (Ig) compensation beads were added to each tube. A 1X reaction volume of each antibody was added to corresponding tubes (**see figure 3.1**). The tubes were thoroughly mixed by vortexing and incubated in the dark at RT for 10 min. A volume of 2 mL of PBS supplemented with 2% FCS was added to the tubes. The contents of the tubes were mixed thoroughly and centrifugated at1600 rpm for 6 min at RT. The supernatant was carefully discarded, and tubes blotted on paper towel. A total of 200 µL of 1% formaldehyde (for cell fixation) was added to the tubes and the contents of the tubes thoroughly mixed by vortexing. The tubes were kept at 4 °C in the dark until further use.

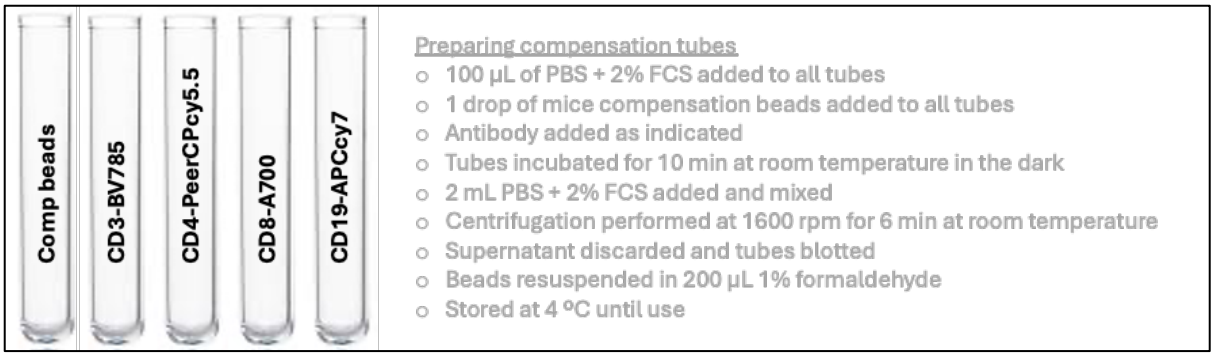

Figure 3.1. Preparation of compensation tubes for antibody titration assay optimization

3.5 Optimized 9 color antibody panel standard operating procedure pilot run on PBMC from the TB-ART cohort.

3.5.1 Cell recovery

PBMC from the TB-ART observational study were retrieved from long-term liquid nitrogen storage and recovered from cryopreservation as previously described (**Section 3.3**). Cells were resuspended at 10 million cells per mL and rested for 4 hours in a sterile U bottom 96 well plate in an incubator set at 37 °C and 5% CO_2.

3.5.2 Measure of cell viability

Twenty (20) µL of cells from each participant were taken for viability staining by performing a 1:2 dilution in trypan blue. Trypan blue is a viability dye that permeates cells whose cell membrane has lost integrity. The percentage of viable cells was determined by a BioRad TC 20 automated cell counter.

3.5.3 Cellular Stimulation

PBMC were stimulated with a peptide pool consisting of 300 Mtb-derived peptides (Mtb300, 1.5 µg/mL) [257]. Briefly, a vial containing 5 µL Mtb300 with a concentration of 0.7 µg/ µL was thawed on wet ice and diluted 1:20 by resuspending in 95 µL of PBS to obtain a final working concentration of 0.035 µg/mL. A volume of 8.5 µL of Mtb300 (final concentration 1.5ug/mL) was used to stimulate PBMC in the presence of co-stimulatory molecules and Golgi blockers. The co-stimulatory concoction included CD49d, CD28 (both at 1 µg/mL; BD, Franklin Lakes, NJ) and Brefeldin-A (10 µg/mL; Sigma, St. Louis, MO) resuspended in plain RPMI 1640. The master mix for this concoction was prepared for 22 reactions according to

table 3.2. A volume of 10 µL of the co-stimulatory mixture was added to corresponding wells, mixed thoroughly and subsequently incubated for 6 hours at 37 °C.

Table 3.2. Stimulation master mix for single cell gene expression analysis using flow cytometry.

Components of the co-stimulation master mix	1X reaction (µL)	Master mix for 22.5 reactions (µL)
CD49d	0.2	4.5
CD28	0.2	4.5
Brefeldin	0.2	4.5
RPMI (max 10 µL)	9.4	212

3.5.4 Cellular staining

Following the 6-hour stimulation step, PBMC were pelleted by centrifugation at 1800 rpm for 3 min at RT. The supernatant was properly discarded in a liquid waste bucket containing biocite and the plate was blotted. PBMC were resuspended in 200 µL plain and sterile PBS and transferred to a V-bottom 96 well plate. Cells were washed by centrifugation at 1600 rpm for 6 min at RT and the supernatant discarded as previous. The lights in the BSCII were turned off and a NIR live/dead stain was prepared by diluting 1 µL of NIR in 39 µL of plain and sterile PBS. The master mix for the NIR live/dead mixture was prepared on wet ice for 22 reactions according to table 3.3. The cells were incubated for 10 min in the dark at RT in the presence of 50 µL NIR live/dead master mix after which 190 µL PBS supplemented with 2% FCS was used to top up the reaction.

Table 3.3. Live/dead staining master mix for single cell gene expression analysis using flow cytometry.

Live/dead stain components	1X reaction (µL)	Master mix for 22.5 reactions (µL)
NIR (1:40) in PBS	1	22.5
PBS	49	1103

Cells were pelleted as previous, and the supernatant was discarded appropriately. Cells were stained with a cocktail of antibody targeting the following surface proteins: CD4 (PerCPcy5.5), CD19 (APCcy7) and HLA-DR (BV605) (see table 3.4). A volume of 50 µL of the surface stain master mix was added to each well and incubated for 30 min at room temperature in the dark. A total of 190 µL of PBS supplemented with 2% FCS was added to the cells which were subsequently pelleted at 1800 rpm for 3 min at RT.

Table 3.4. Surface staining master mix for single cell gene expression analysis using flow cytometry.

Surface staining master mix components	1X reaction (µL)	Master mix for 22.5 reactions (µL)
CD4-PerCPcy5.5	0.5	11.3
CD19-APCcy7	1	22.5
HLA-DR-BV605	2	45
Brilliant Violet buffer (to 50 µL)	43.4	976.5

The supernatant was discarded as previous, and the cell pellet resuspended in 200 µL of 1X eBio fixation buffer to permeabilize cells for intracellular staining. The cells were subsequently incubated in the dark for 30 min at RT. Cells were pelleted as previous and resuspended in 200 µL 1X eBio wash buffer. Cells were centrifuged at 1800 rpm for 3 min at RT and the supernatant was subsequently discarded as previous. Intracellular staining (ICS) was performed by adding 50 µL of antibody cocktail containing CD3-BV785, TNFα-FITC, IFNγ-BV711, Tbet-PEcy7, Eomes-APC, and GranzymeB-BV510 prepared in 1/3 of BV buffer and 2/3 1X eBio wash buffer (see Table 3.5). The reaction was mixed thoroughly and incubated in the dark for 45 min at 4 °C and subsequently washed by centrifugation at 1600 rpm for 6 min at RT in 190 µL 1X eBio wash buffer. The supernatant was discarded properly in a liquid waste bucket containing biocite and the washing repeated. The supernatant was discarded as previous, and the cells fixed by resuspending in 1% formaldehyde. The cells were transferred to properly labelled sterile FACs tubes and stored at 4 °C until further use.

Table 3.5. Preparation of intracellular staining master mix for single cell gene expression analysis using flow cytometry.

Intracellular staining master mix components	1X reaction (µL)	Master mix for 22.5 reactions (µL)
TNFα-FITC	0.1	2.3
IFNγ-BV711	0.5	11.3
CD3-BV785	0.5	11.3
Tbet-PEcy7	0.1	2.3
Eomes-APC	2	45
GrB-BV510	2	45
BV $_{(1/3)}$ +1X e-Bio Wash $_{(2/3)}$ buffer (to 50 µL)	42.3 (14.1+28.2)	317.3 BV+ Wash 635

3.5.5 Preparation of compensation controls

For each fluorophore used in the experiment, a single-stained bead sample and one unstained control were prepared. Briefly, 100 µL of PBS supplemented with 2% FCS was added to appropriately labelled FACs tubes. 50 µL of anti-mouse Ig compensation beads were added to each tube and antibody was added to FACs tubes with corresponding labels. The reaction mixture was incubated for 10 min in the dark at RT and topped up with 2 mL of PBS supplemented with 2% FCS and thoroughly mixed. The tubes were centrifuged at 1600 rpm for 6 min at RT and the supernatant appropriately discarded. The beads were resuspended in 200 µL of 1% formaldehyde and mixed by vortexing and kept in the dark at 4 °C until further use. Of note, compensation controls were prepared newly for each experiment and the samples were acquired within 4 hours of staining (**Figure 3.2**).

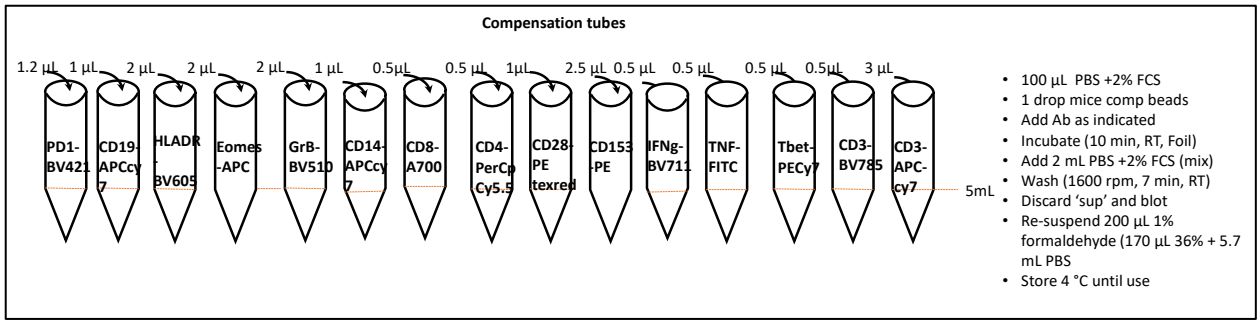

Figure 3.2. Preparation of compensation tubes for antibody staining for all the staining antibodies in the panel.

3.6 Cytometer calibration and data acquisition

Samples were acquired on a four laser BD LSRII flow cytometer. The cytometer was properly calibrated each day prior to use.

3.7 Data analysis and visualization software

Data was analyzed in FlowJo version 9.9.6 and visualized in Prism version 8.0.2 (GraphPad Software Inc., San Diego CA).

3.8 RNA sequencing methods and materials

3.8.1 Pred-ART cohort: Patient recruitment and enrolment

To better understand the cross-sectional and longitudinal perturbations in global gene expression in patients who developed paradoxical TB-IRIS, RNA-sequencing was performed using whole blood collected from the Pred-ART clinical trial for which the study protocol and findings have been reported [21, 258]. The protocol for the parent study was approved by the Human Research Ethics Committee of the University of Cape Town (UCT). The parent study enrolled HIV immunosuppressed patients with confirmed TB disease. Adult patients above the age of 18 were recruited from four clinic sites in Khayelitsha, Cape Town, South Africa between August 2013 and February 2016. All participants provided written informed consent to participate in the trial and for collection of peripheral blood samples. A total of 240 participants with confirmed HIV-associated TB were enrolled in the double blind, placebo-controlled randomized trial which assessed the efficacy and safety of prednisone in preventing TB-IRIS [21, 258]. At enrolment, patients had not initiated ART and 73% had microbiologically confirmed TB. Patients were on standard first line antitubercular treatment for a median of 16-17 days prior to randomization. A total of 120 patients were randomized to 40 mg/kg of prophylactic prednisone for 2 weeks which was tapered down to 20 mg/kg for 2 weeks, or identical placebo [21, 258]. The case definition for paradoxical TB-IRIS was defined according to the criteria outlined by the international network for the study of HIV-associated IRIS (INSHI) [22].

The trial found that the incidence of TB-IRIS was lowered by 30% in the prednisone compared to the placebo arm and no serious complications were recorded in the prednisone arm [21]. Paradoxical TB-IRIS diagnosis was confirmed in 39 patients (32.5%) allocated to prednisone prophylaxis compared to 56 (46.7%) who were allocated placebo (p=0.03). Lastly, open label prednisone was used to treat paradoxical TB-IRIS in 16 patients (13.3%) in the prednisone arm compared to 34 (28.3%) in the placebo arm.

3.8.2 Sample collection

Peripheral blood samples (where available) were collected in PAXgene tubes from patients prior to ART initiation (week 0), and at 2, 4 and 12 weeks longitudinally on ART. The samples were transported on ice to the laboratories at the Institute of Infectious disease and Molecular Medicine (IDM) at the University of Cape Town (UCT) and stored at -80 °C until ready for RNA extraction using PAXgene blood RNA kit (QIAGEN). Extracted total RNA were stored

at -80 °C until the sequencing libraries were constructed. The quality of the total extracted RNA per sample was assessed with Qubit fluorometer. Nanodrop 2000 was used to analyse RNA quantity and purity per sample. Tape Station 2000 was used to assess RNA integrity per sample. For this sub-study, available RNA samples at 3 time points (week 0, 2 and 12, as summarized in Table 6) were used to construct libraries for downstream RNA-sequencing.

***Table 3.6. Summary of the number of samples that were available by patient intervention and outcomes at different study visits**, prior to antiretroviral therapy (ART) initiation (week 0) and up to week 12 on ART.*

Time-point (weeks)	Number of samples Placebo/Prednisone (TB-IRIS)	Number of samples Placebo/Prednisone (TB-non-IRIS)	Total (Placebo/Prednisone)
Week 0	56/36	58/75	114/111
Week 2	44/26	51/69	95/95
Week 12	42/34	50/62	92/96

3.9 RNA sequencing workflow

Several technologies are available for the high-throughput sequencing of RNA and due to their proprietary technology and software, each requires a customized experimental protocol [44]. Illumina technology, which was used for sequencing, comprises several steps discussed below.

3.9.1 RNA extraction

The PAXgene 96 Blood RNA Kit offers high-throughput purification of cellular RNA in a manual format. RNA was extracted following manufacturer's guidelines and specifications. The blood samples (2.5 ml) had been collected in PAXgene Blood RNA Tubes (available from BD, cat. no. 762165). The PAXgene blood RNA tubes were centrifuged to pellet nucleic acids. The pellet was washed, and proteins were digested using proteinase K. Alcohol was added to adjust binding conditions. Lysates were applied to the PAXgene 96 filter plate and centrifuged to remove cell debris. The lysate was then applied to a PAXgene 96 RNA Plate. RNA extracts were shipped on dry ice to the Francis Crick Institute (London, UK) for library preparation and RNA sequencing. RNA extracts were constructed into short fragment length sequences for directional sequencing as described below. To reduce batch effects, libraries were constructed from samples that were collected prior to the initiation of ART (week 0), and at week 2 and 12 on ART and were randomised and pooled for high throughput sequencing.

3.9.2 Library construction

Sequencing libraries were prepared using Tecan Genomics's Universal Plus Total RNA-Sequencing kit with build-in depletion step of globin RNA and ribosomal RNA [259].

3.9.3 Sample preparation

All reagents were thawed at room temperature, mixed by vortexing, spun down by gradient centrifugation at 1800 rpm for 1 min and kept on ice. Approximately 200 ng of total RNA was aliquoted into 0.2 mL sterile tubes. The RNA was subsequently diluted to a final volume of 10 µL with nuclease free water and kept on ice. The libraries were prepared in 4 randomised batches, of which 603 samples were successfully sequenced.

3.9.4 RNA fragmentation

Approximately10 µL of 2X fragmentation buffer was added to each sample. The solution was mixed thoroughly by pipetting up and down at least 10 times. The tubes were placed in a pre-warmed thermal cycler and fragmented at 86 °C for 8 min.

3.9.5 First strand cDNA synthesis

Samples were processed in batches of 4, each containing 160 samples. A master mix for 160 samples plus adjusting for pipetting error was prepared according to table 3.7 to a final volume of 805.1 µL. Briefly, 201 µL of actinomycin D was mixed in a 0.5 mL sterile container with 443 µL of first strand buffer mix and 161 µL of first strand enzyme mix. A total of 5 µL of first strand master mix was added to each sample to make up a final reaction volume of 25 µL. The suspension was mixed thoroughly by pipetting up and down at least 10 times and kept on wet ice.

Table 3.7. First strand synthesis constituents and master mix preparation.

Reagent	Actinomycin D	First strand buffer mix	First strand enzyme mix
1X reaction volume (µL)	1.25	2.75	1
161 reaction volume (µL)	201.3	442.8	161

The tubes were placed in a prewarmed thermocycler for first strand cDNA synthesis with the following cycling conditions: 25 °C for 5 min, 42 °C for 15 min and 70 °C for 15 min. The tubes were subsequently removed from the thermocycler and spun down at 1800 rpm for 1 min to collect condensation and subsequently kept on ice.

3.9.6 Second strand cDNA synthesis constituents and master mix preparation

The second strand cDNA synthesis master mix was prepared according to table 3.8. Briefly, a total of 7728 µL second strand buffer mix was combined with 322 µL of second strand enzyme mix for a 160 reaction. A total of 50 µL of the second strand master mix was added to each sample to make up a total volume of 75 µL. The suspension was mixed thoroughly as previous.

Table 3.8. Second strand master mix

Reagent	Second strand buffer mix	First strand enzyme mix
1X reaction volume (µL)	48	2
161 reaction volume (µL)	7728	322

The tubes were placed in a pre-heated thermocycler for second strand cDNA synthesis. Briefly, the cycling conditions for second strand cDNA synthesis entailed incubating the tubes at 16 °C for 60 min. The tubes were subsequently removed from the thermocycler and the condensation collected as previous.

3.9.7 cDNA purification

The Agencourt beads (AMPure XP beads) were thawed at room temperature and mixed by vortexing for a minimum of 2 min. The beads were subsequently kept on ice. Fresh 70% ethanol wash solution was prepared on the day of the experiment. The beads were fully resuspended by gently inverting and tapping the tube prior to use. A total of 135 µL of the AMPure XP beads were added to the samples at room temperature and the suspension was mixed as previous. The suspension was subsequently incubated at room temperature for 10 min. To allow the suspension to clear up, the tubes were transferred to a magnet and allowed to stand for 5 min after which the binding buffer was carefully removed and discarded. Approximately 200 µL of 70% ethanol was added to the tubes and allowed to stand for 30 sec while on the magnet. The 70% ethanol wash solution was removed by pipetting. To remove residual ethanol, the beads were air-dried on the magnet for 5 min and removed from the magnet. A total of 11 µL of nuclease free water was added to the dry beads and resuspended by pipetting up and down. The tubes were subsequently incubated at room temperature for 5 min and transferred to the magnet for an additional 5 min to sediment the beads. A total of 10 µL of the samples were subsequently transferred to sterile 0.2 mL tubes.

3.9.8 End repair

End repair master mix was prepared by combining 644 µL of end repair buffer mix with 80.5 end repair enhancer and enzyme mix respectively according to table 3.9. The concoction was mixed by pipetting up and down and kept on wet ice. A total of 5 µL of the end repair master mix was added to each sample to make up a total volume of 15 µL.

Table 3.9. End repair constituents and master mix preparation.

Reagent	End repair buffer mix	End repair enzyme mix	End repair enhancer
1X reaction volume (µL)	4	0.5	0.5
161 reaction volume (µL)	644	80.5	80.5

The suspension was mixed well and placed on ice. The samples were placed on a thermocycler and the end repair protocol executed. Briefly, the cycling condition for end repair were as follows: 25 °C for 30 min, 70 °C for 10 min and the tubes were removed from the thermocycler and spun down at 1800 rpm for 1 min to collect condensation and kept on wet ice.

3.9.9 Adapter ligation

The adapter plate was thawed on ice, spun down via centrifugation at 1800 rpm for 1 min and placed back on ice. All samples were transferred to the appropriate adapter wells and mixed well by pipetting. The entire suspension was subsequently transferred to a PCR tube. The master mix was prepared according to table 10. Briefly, 966 µL of ligation buffer was mixed with 241.5 µL of nuclease free water and 725 µL ligation enzyme. The ligation master mix was thoroughly mixed and kept on ice. Due to the viscosity of the ligation buffer component in the master mix, 12 µL of the master mix was added slowly to each sample to make up a final volume of 30 µL.

Table 3.10. Adapter ligation constituents and master mix preparation.

Reagent	Ligation buffer mix	Ligation enzyme mix	Nuclease free water
1X reaction volume (µL)	6	1.5	4.5
161 reaction volume (µL)	966	241.5	724.5

The suspension was mixed well as previous, spun down and placed on ice. The tubes were placed in the thermocycler to execute the ligation reaction. Briefly, the thermocycler was set to 25 °C for 30 min and the tubes subsequently removed from the thermocycler, spun down as previous to collect condensation and kept on ice.

3.9.10 Strand selection

Thawed strand selection buffer mix 1 and strand selection enzyme mix 1 were mixed in a sterile 0.5 mL bottle to prepare a master mix according to the volumes on table 3.11.

Table 3.11. Adapter ligation constituents and master mix preparation.

Reagent	Strand selection buffer mix I	Strand selection enzyme mix I
1X reaction volume (µL)	69	1
161 reaction volume (µL)	11109	161

Briefly, 11109 µL of strand selection buffer mix 1 was mixed with 161 µL of strand selection enzyme mix I. A total of 70 µL of strand selection master mix was added to 30 µL of each sample to make up a total of 100 µL. The suspension was mixed thoroughly by pipetting, spun down by gradient centrifugation at 1800 rpm for 1 min and kept on ice. All the tubes were placed in a pre-warmed thermocycler to execute the strand selection programme. Briefly, the thermocycler was calibrated to 72°C for 10 min and the tubes were removed from the thermocycler. The tubes were subsequently spun-down to collect condensation and placed on ice.

3.9.11 Strand selection purification

The AMPure XP beads were allowed to equilibrate to room temperature and subsequently resuspended as previous. A total of 80 µL AMPure XP beads were added to the strand selection reaction product and mixed thoroughly by pipetting up and down at least 10 times. The suspension was incubated for 10 min at room temperature prior to transferring the tubes and incubating on a magnet for an additional 5 min to enhance the sedimentation of the beads. The buffer was carefully removed and discarded while the tubes stayed incubated on the magnet. Approximately 200 µL of 70% freshly prepared ethanol was added to the samples and incubated on the magnet for 30 sec. The ethanol was carefully removed by pipetting and the beads air dried for 5 min to remove residual ethanol wash solution. The tubes were removed from the magnet and 16 µL of nuclease free water was added to the dried beads and resuspended by pipetting. The tubes were transferred to the magnet and incubated for 3 min to allow the solution to clear. Approximately 15 µL of the eluate was removed, caution was taken not to carry over beads. The eluate was transferred to a sterile set of PCR tubes and kept on ice.

3.9.12 Probe binding

A master mix for probe binding was prepared according to table 3.12.

Table 3.12. Probe binding constituents and master mix preparation

Reagent	AnyDeplete buffer mix	AnyDeplete enzyme mix I	AnyDeplete probe mix	Strand selection enzyme mix II
1X reaction volume (µL)	5	0.5	4	0.5
161 reaction volume (µL)	805	80.5	644	80.5

Briefly, all reagents were thawed at room temperature, spun down by gradient centrifugation and kept on ice. The master mix concoction was prepared in a sterile 0.5 mL tube by combining 805 µL of anydeplete buffer mix, 644 µL anydeplete probe mix, 80.5anydeplete enzyme mix and strand selection enzyme mix II respectively. A total of 10 µL of the probe binding master mix was added to each sample to obtain a final volume of 25 µL. The suspension was mixed thoroughly and kept on ice. The tube was placed in a pre-heated thermocycler programmed to run the probe binding protocol according to the following cycling conditions: 37 °C for 10 min, 5x(95 °C for 2 min, 50 °C for 30 s) and 65 °C for 5 min. The tubes were removed from the thermocycler and spun down as previous to collect the condensation and kept on ice.

3.9.13 Targeted depletion.

The targeted depletion master mix to remove globin and ribosomal RNA was prepared according to table 3.13 below.

Table 3.13. Targeted depletion constituents and master mix preparation.

Reagent	AnyDeplete buffer mix	AnyDeplete enzyme mix II	Nuclease free water
1X reaction volume (µL)	5	4	16
161 reaction volume (µL)	805	644	2576

Briefly, 805 µL anydeplete buffer mix was added to a 0.5 mL containing 2576 µL nuclease free water and 644 µL anydeplete enzyme mix II. Approximately 25 µL of targeted depletion master mix was added to each sample to make up a final volume of 50 µL. The suspension was mixed well, spun down as previous and placed on a pre warmed thermocycler programmed to

execute the targeted depletion protocol according to the following cycling conditions: 65°C for 30 min, 95°C for 5 min. The tubes were removed from the thermocycler and spun down to collect condensation and placed on ice.

3.9.14 Library amplification

The library amplification master mix was prepared according to table 3.14 below.

Table 3.14. Library amplification constituents and master mix preparation.

Reagent	Amplification reagent I	Amplification reagent II	Amplification enzyme mix	Nuclease free water
1X reaction volume (µL)	10	8	0.5	31.5
161 reaction volume (µL)	1610	1288	80.5	5071.5

Briefly, 1610 µL of amplification reagent I was added to a 0.5 mL containing 5072 µL nuclease free water and 1288 µL amplification reagent II and 80.5 µL amplification enzyme mix. The concoction was mixed thoroughly by pipetting and approximately 50 µL of library amplification master mix was added to each sample to produce a final volume of 100 µL. The suspension was mixed well, spun down as previous and placed on a pre warmed thermocycler programmed to execute the library amplification protocol according to the following cycling conditions: 95°C for 2 min, 2x(95°C for 30 s, 60°C for 90 s), 13x(95°C for 30 s, 65°C for 90 s), 65°C for 5 min. The tubes were removed from the thermocycler and spun down to collect condensation and placed on ice.

3.9.15 Amplified library purification

The AMPure XP beads were removed from storage and allowed to equilibrate at room temperature before vortexing. A total of 70 µL of AMPure XP beads beads were added to 100 µL of the library amplification product. The suspension was mixed thoroughly by pipetting and subsequently incubated for 10 min at room temperature. The tubes were transferred to the magnet and incubated for an additional 5 min to allow the solution to clear. The supernatant was carefully removed and discarded before adding 50 µL of nuclease free water to resuspend the bead pellet. The suspension was incubated for 2 min at room temperature prior to adding 40 µL of the bead suspension to 50 µL of the library amplification product. The suspension was mixed thoroughly as previous and the tubes removed from the magnet. A total of 200 µL

of freshly prepared 70% ethanol wash solution was added to the tubes and mixed thoroughly by pipetting. The tubes were transferred back to the magnet and incubated for 5 min to allow the beads to settle. The ethanol was removed by pipetting and the beads resuspended in fresh 70% ethanol for the second time and incubated as previous. The ethanol was removed by pipetting and subsequently air dried for a minimum of 5 min to remove residual ethanol. The tubes were removed from the magnet and the dried beads resuspended in 26 µL of nuclease free water. The tubes were incubated at room temperature for 5 min before being transferred back to the magnet and incubated for a minimum of 2 min for the beads to settle. Approximately 25 µL of the eluate was removed and transferred to sterile PCR tubes and kept on ice.

3.9.16 Library quantification

Approximately 200 µL of NuQuant buffer was aliquoted into a sterile thin walled, clear, 0.5 mL tube labelled S1. A total of 195 µL of NuQuant buffer was aliquoted into separate sterile, clear-thin walled 0.5 mL tubes (diluted standard tube and one for each library). The diluted standard tube was labelled S2 which represents the universal plus total RNA-seq NuQuant library with a concentration of approximately16.1 nM. A total of 5 µL of diluted NuQuant standard or library was added to each tube containing the NuQuant buffer. The lids were securely closed and mixed by vortexing and subsequently spun down to collect all the liquid. The prepared libraries were quality and quantity assessed using TapeStation 2000 (Agilent) where 2 µL of each sample was tested for quality.

3.9.17 Library pooling and assessment

The libraries were subsequently pooled at a concentration of 4nmol per sample. The library pool was validated for sequencer loading following the Hi-Seq 4000 Illumina platform guidelines. Finally, the libraries were denatured and diluted for sequencing according to the guidelines and specifications of the Hi-Seq 4000 Illumina platform.

3.9.18 Sequencing by synthesis

High quality libraries were sequenced on the Illumina HiSeq 4000 platform at Francis Crick Institute, London, UK. Briefly, the fragments were sequenced on both ends (paired-end sequencing or PE). In the first step of sequencing the double stranded molecules were denatured into single strands and passed over a flow cell with oligo sequences complementary to the

adapters immobilized on its surface. Fragments bind to the oligonucleotides, and each was bridge amplified on the spot to create a cluster of identical molecules that serve as templates for the formation of complementary strands. Sequencing primers were added to each molecule and the millions of molecules in the clusters were reverse complemented simultaneously. In each sequencing step, fluorescently labelled reversibly terminated nucleotides compete to bind with the template strands. In each step only one nucleotide is added to each growing complementary strand. Each new nucleotide is labelled with a dye (different for each nucleotide type) and a laser is used to identify where and which nucleotide was incorporated in each cluster. The fluorescent dye and terminal group were subsequently removed from the new nucleotides and the process was repeated approximately 200 times.

At the end of this process the result is a sequence of images (one for each sequencing step), in which each lighted spot corresponds to a cluster and the color of each cluster represents a different base type. While it is possible to analyze the images themselves to obtain the nucleotide sequences for each cluster using software tools called Base Callers [260, 261], for most analyses this is done at the sequencing facility and users start from text files containing the nucleotide sequence for each cluster. These files are typically in the FASTQ file format which includes for each cluster (read): a unique id, the nucleotide sequence and a Phred quality score per base. These Phred quality scores Q are set by the Base Callers and are defined as $Q = -10\log10(P)$, where P is the probability of the base call being incorrect [261]. In paired end experiments, reads are typically split over two ordered files, one with the first end and the other with the second.

3.9.19 Raw data handling

The raw reads obtained from the sequencer are stored in text format which represents the sequence output for each sample. This text data about the sample is stored in FastQ file format which is the default output of the sequencer. Raw sequenced data were shipped stored on a hard drive by air to UCT in South Africa for further analysis. The raw data were accompanied by sequencing report from Illumina. The Md5 checksum computational tool (indexing algorithm) was used to index both orientations of each FastQ file. Both the raw files, a total of 603 samples and the indexed checksum file were uploaded to the UCT high performance computing (HPC) facility using command line scripting. The indexes used ascertained that all the files that were uploaded to the UCT server were intact and complete.

3.10 RNA sequencing analysis pipeline

Various workflows are available to handle distinct analytical aspects of RNA-seq data. However, configuring the available tools and chaining them into a robust analytical pipeline has proven to be a study-specific task, demanding refined expertise for each tool and its behavior. Furthermore, RNA-seq methods typically generate a plethora of raw reads requiring terabytes of storage, and extensive computational capacity that render the analysis impossible without the use of powerful servers. This trend between experimental high throughput and processing capacity is widening, with the processing aspect slightly trailing.

The Nextflow (nf)-core/rnaseq analytical pipeline which is developed and validated by the data scientists at Bioconductor was adapted for processing of our raw data and for data analysis [262, 263]. Nf-core is a bioinformatics workflow manager that allows for the development of portable and reproducible workflows. NF-core offers the benefit of parallelization and distributed computing, which significantly increases the speed of computing tasks.

The nf-core/rnaseq pipeline is an automated linux-based pipeline for pre-processing, quantifying gene expression and assessment of RNA-seq datasets quality. For deployment, the nf-core/rnaseq pipeline required three inputs. First, a sample sheet containing information about the samples to be analyzed. This is a comma-separated file with a header, 4 columns and rows. Second, the actual raw sequences from the samples. Third, the human reference genome (GRC-37). Using linux, the sample sheet was imported from Bioconductor and it was modified appropriately to reflect the 603 samples that were analyzed. We also imported and deployed the nf-core/rnaseq pipeline (v3.5) from Bioconductor, with the end goal of quantifying transcript abundance across the 603 patient samples. All 603 patient samples were processed with the nf-core/rnaseq pipeline which executes several tasks as outlined below.

3.10.1 Data Preprocessing

For data preprocessing, the pipeline ran a series of computational tools which prepared the raw sequences for quantification by “cleaning” the raw unprocessed sequences. The tools are described below.

3.10.1.1 Concatenation of identical sample file names

Identical sample names may arise from RNA library preparation or multiple sequencing runs as an attempt to increase sequencing depth. The first step of data preprocessing included screening and merging all samples with identical names using the concatenation (cat) tool. This

improves consistency in sample naming throughout the pipeline. Of note, there were no re-sequenced samples, as such, no samples were merged.

3.10.1.2 FastQC

FastQC is a tool that provides several informative quality metrics with regards to the raw reads. These include the quality score distribution across reads, per base sequence content (%A/T/G/C), adapter contamination and overrepresented sequences for each sample [264].

3.10.1.3 Unique molecular identifier (UMI)-tools extract

During library preparation, amplicon duplication can occur. This is undesirable because it can result in overrepresentation of certain transcripts which results in overestimation of their expression in downstream analysis. This duplication in amplicons generates what is known as PCR bias. To address issues relating to PCR-bias, UMI-tools performs read deduplication based on unique molecular identifiers (UMIs) [265]. Deduplication refers to the process of removing PCR duplicates were the reads have UMIs incorporated. This works efficiently in paired end reads. First, the extract command removes the UMI barcode from the read sequence and incorporates it to the read name. Notably, reads must first be mapped with the splice-aware STAR aligner before read deduplication. This step was omitted because it can remove biologically meaningful reads and not those that are due to technical artefacts.

3.10.1.4 TrimGalore

TrimGalore was used to assess read quality and detect and trim off adapters.

3.10.1.5 BBSplit

BBSplit is a tool that groups reads and stores them in different containers (to bin) by mapping to multiple references simultaneously. BBSplit uses one of its features called BBMap to bin reads of the reference they map to best. There are also disambiguation options, such as reads that map to multiple references can be binned with all of them, none of them, one of them, or put in a special "ambiguous" file for each of them. This functionality was not entirely useful for our dataset since mRNA was extracted from human blood.

3.10.1.6 SortMeRNA

SortMeRNA has important functionality that removes ribosomal RNA which constitutes most of the RNA in peripheral blood [266]. Moreover, our samples were enriched for mRNA, nonetheless, this functionality of SortMeRNA was helpful in cleaning the data further.

3.11 Alignment

RNA-seq studies typically have a myriad of objectives, most are used for estimating expression of specific genomic regions which could be genes, isoforms, exons, splice junctions or novel transcribed regions. The first step to achieve this requires the identification of which features are present in the sequencing library. Mapping of reads to these features can be challenging given that reads are very short when compared to most genome sizes. There are three principal approaches for mapping reads to features of interest. Here, reads were mapped to genes of an indexed human reference genome (GRCh-37).

The nf-core/rnaseq pipeline provided several tools for read alignment and quantification. The default splice aware mapping tool called spliced transcripts alignment to a reference (STAR) aligner was used for mapping reads to GRCh-37. STAR is a hyper-efficient aligner with high accuracy [267]. The default options of the nf-core/rnaseq pipeline were used to map the reads from all the samples to the indexed GRCh37 reference genome.

3.12 Read quantification.

For read quantification, salmon was employed. Salmon is a super-fast read quantifier that can perform both pseudo and mapped read quantification [268]. The pseudo quantification option provided by salmon entails counting reads albeit without alignment to a reference genome. This functionality provides an expedited method for running the pipeline. The second read quantifier option inherent to salmon requires binary alignment map (BAM) files as input. The latter functionality of salmon was used for quantifying reads. This allowed us the potential benefit of identifying novel genes and isoforms down the analysis pipeline if our discovery approach for identifying differentially abundant transcripts was not successful.

One major concern when quantifying gene expression was to identify multi-reads, also known as multi mapping reads to avoid double counting. Multi reads are reads that map well to several

regions of the reference genome. The reason for this occurring is two-fold: 1. The reads may have low complexity (i.e contains sequences that map to repetitive sequences in the genome). Alternatively, the reads map to paralogs and/or 2. The reads overlap transcripts from either different or the same genes. We elected not to remove multi reads to avoid both the significant underestimation and loss of vital information about gene expression. The reason for this is, reads generated by RNA-seq are typically short between (100-500 bp). As such, removing multi-reads could have resulted in a catastrophic loss of gene expression information. Finally, because multi-reads were left distributed according to the neighboring coverage at each site, salmon dealt with this predicament by assigning a count to each of the overlapping side. It is clear how this could lead to overestimation of some of the genes that are expressed in low abundance. Discussed below are the tools that the pipeline used for gene quantitation.

3.12.1 SAMtools

BAM files generated by the STAR/Salmon alignment algorithm were additionally processed with SAMtools, for indexing, sorting by coordinates, and to generate read mapping statistics [269].

3.12.2 UMI-tools deduplication

The downstream second step of UMI-barcode removal in the pipeline involved the actual removal of duplicated reads (read deduplication) once reads are aligned to the indexed GRC37 reference genome. The duplicated reads are removed based on mapping and UMI-barcode information. Of note, this step of the pipeline was omitted because previous findings indicated that removing PCR duplicates carries an inherent risk of removing biologically meaningful reads that might distort downstream findings. Moreover, neglecting to remove duplicated reads has been reported to not cause significant artifacts in the data provided the sequencing depth or library complexity is sufficient. Lastly, short reads and highly abundant transcripts normally account for most duplicated reads. Data normalization in downstream analyses additionally helps in eliminating this bias.

3.12.3 Picard MarkDuplicates

To distinguish between true biological duplication and PCR bias is virtually impossible without incorporating UMI-barcodes in the library preparation step. Where duplicate reads have not

been removed either on purpose or through a glitch in the pipeline, the Picard MarkDuplicate tool facilitates the flagging of read duplicates to gauge the level of duplication for each sample.

3.12.4 StringTie

StringTie assembles RNA-seq alignments into potential transcripts [270]. It is ultra-efficient owing to its novel network flow algorithm. The output of StringTie can be readily used in standalone algorithms for determining differentially abundant transcripts.

3.12.5 BEDTools and bedGraphToBigWig

The pipeline used BEDTools to generate less cumbersome file sizes that are often not convenient to use. BEDTools was utilized to generate a binary indexed file format known as bigwig. It overcomes the limitation of working with large file formats such as the BAM files which consume a lot of memory and are less ideal for data visualization. Importantly, bigwig is supported by many bioinformatics tools for downstream processing and analyses [271].

3.13 Quality control using RSeQC

The pipeline uses a collection of packages called RSeQC to assess the quality of the resultant RNA sequencing processed data [272]. A range of parameters that are evaluated by different packages in the RSeQC suite for quality control are discussed below.

3.13.1 Infer experiment.

The strandedness of each sample must be provided to the pipeline in the input sample-sheet. This information is not always available. Consequently, additional features have been incorporated into the pipeline to automatically detect whether the correct information in the sample-sheet was provided. The script run by infer experiment predicts the strandedness of the protocol that was used to prepare the sample for sequencing. The script achieves this by determining the orientation in which aligned reads overlay gene features in the reference genome.

3.13.2 Read distribution.

Read distribution computes how mapped reads are distributed over genomic features. A good result for a standard RNA-seq experiments is generally to have as many exons as possible. A

large amount of intronic reads can be expected for a total RNA preparation and this potentially indicates DNA contamination in samples.

3.13.3 Junction annotation

Splicing annotation is performed at two levels: splice event level and splice junction level. Junction annotation compares detected splice junctions to a reference gene model.

3.13.4 Inner distance

For paired end reads, the distance between the end of one read and the start of the second read is the inner distance. The inner distance script was used to determine the inner distance between two paired-end reads. The result is indicative of the integrity of the sample which might be affected by experimental procedure or other factors like the age of the sample.

3.13.5 Read duplication

Read duplicates may arise during library preparation as technical noise or due to valid biological effect. Quality control to quantify level of read duplication was carried out to gauge the level of gene duplication. Generally, samples with many duplicates are indicative of excessive technical duplication.

3.13.6 BAM statistics

Part of the report is numerous statistics on the aligned BAM files. Detailing many metrics such as reads that failed alignment and PCR duplicates.

3.13.7 Transcript integrity number (TIN)

The script assessed RNA integrity at transcript level. Transcript integrity number (TIN) is analogous to RNA integrity number (RIN) which is a widely used metric to evaluate RNA integrity at sample level. TIN is a useful measure to ensure good RNA quality and robust, reproducible RNA sequencing.

3.13.8 DupRadar

DupRadar generates several different QC metrics and plots relating the duplication rate to gene expression levels. This identifies experiments with high technical duplication. A good sample with little technical duplication will show only high numbers of duplicates for highly expressed

genes. Samples with technical duplication typically show high duplication for all genes, irrespective of transcription level.

3.13.9 MultiQC report

The pipeline also produces a multiQC report where all the QC and all the statistics for the QC check points are included [273].

3.14 Differential gene expression analysis

To assess for quantitative differences between the samples of patients who developed paradoxical TB-IRIS and TB-non-IRIS controls at different sampling time points, differential gene expression analysis was performed. Several statistical tools are available for the identification of differentially expressed genes (DEGs) across groups of samples [274]. Among the many, one method that models the heteroscedastic nature of RNA-seq data better than others but with some reservations, is the generalized linear-fit model (GLM) offered by the negative binomial (NB) model. Heteroscedasticity in RNA-seq data occurs when the variance of the predicted variable (gene expression) across a range of samples in not constant [274].

For technical replicates in RNA-seq experiments, heteroscedasticity is modelled well by the linear Poisson model which assumes that the mean expression of a gene across all samples is equal to the variance. However, the model struggles to account for the typical extra variability also known as over-dispersion which is inherent to biological replicates (reflecting intra group variance). Over-dispersion is problematic particularly in RNA-seq expression data sets containing few biological replicates (less or equal to 10) which is common. Huber and colleagues developed a statistical algorithm called DESeq2, which accounts for over dispersion by sharing statistical data between the biological replicates. In our RNA-seq experiment, we had access to a minimum of 44 samples per group which theoretically would negate many of the limitations posed by lack of experimental power.

3.14.1 DESeq2

Following successful completion of the nf-core/rnaseq pipeline, the results generated by the pipeline were downloaded from the UCT-HPC server to a local machine where further analyses were performed. The sequencing results included a read count matrix, which represents genes as rows, different samples as columns and the values as counts. The counts reflect the number of reads mapping to a particular gene in a particular sample and as such, are the basic unit for measuring gene expression in RNA-seq data sets. Counts have several important properties. They are discrete data and are represented as whole numbers having a dynamic range and more notably, are not normally distributed.

DESeq2 is a statistical method available as a package in the dynamic R programming language [275]. The R statistical language provides built-in functions and algorithms that can transform the raw counts into expression data that has been normalized for size factors, discreteness, large

dynamic range, outliers and modeled to generate a list of DEGs between two biologically distinct conditions [276]. It accomplishes this by calculating shrinkage estimates for dispersions and fold changes with improved interpretability and stability. DESeq2 accepts as input a raw counts matrix with genes and samples as attributes. Additionally, DESeq2 requires a sample information table with the number and order of the samples corresponding to the counts-matrix. Lastly, DESeq2 requires a design formula which specifies the conditions to be compared. Of note, the conditions must have a factorial design. Several key operations performed by DESeq2 are elaborated below.

3.14.1.1 Normalization

Normalization is the process of scaling raw count values to account for the size factors. In this way, the expression levels are more comparable between and/or within samples. Size factors include sequencing depth and gene length. Both sequencing depth and gene length were accounted for because our analysis included both cross-sectional and longitudinal analysis strategies. Sequencing depth is defined as the average number of reads mapping to a particular locus in the reference genome. It is vital to account for sequencing depth when comparing gene expression between samples because if one sample has more sequencing depth than the other, it might appear that the gene in a sample with more sequencing depth is more expressed than the gene in a sample with less sequencing depth at a particular time point. Additionally, it is important to account for gene length when performing differential gene expression analysis within the same sample. This is because a short gene with more reads mapping to it might seem like it is more expressed compared to a longer gene with fewer reads. Lastly, another factor that is normalized for size factors is the type of RNA. Contamination with other RNA species has the potential to skew other normalization methods.

In the backend of DESeq2, multiple steps are computed for data normalization which relies on the median of ratios method. The null hypothesis (H_0) for DGEA using DESeq2 is that none of the genes are differentially expressed and as a result, the computed normalization factor accounts for library size and RNA composition bias when comparing two biologically distinct groups. Briefly, DESeq2 creates a pseudo reference sample and computes the geometric mean for each gene across all samples. The counts for each gene are subsequently divided by the computed geometric mean. This results in similar ratios for genes that are not differentially expressed. The median of these ratios in each sample, is called the normalization factor also

known as the size factor for each sample. Finally, multiplying the raw counts with the computed normalization factor produces normalized counts.

3.14.1.2 Estimating size factors

The reliable estimation for intra-group variance using a small number of biological replicates (typically less than 10) is a challenging task. DESeq2 employs shrinkage estimation for dispersions and fold changes to do this effectively. Using biological replicates, DESeq2 utilizes a modeling algorithm to estimate a dispersion value for each gene.

Inferential methods that treat each gene separately suffer here from lack of power, due to the high uncertainty of within-group variance estimates. Many methods available for differential gene expression analysis overcome this limitation by sharing information across genes, by exploiting the assumptions made about the similarity of the variances of different genes measured in the same experiment. DESeq2 detects and corrects low dispersion estimates through modeling of the dependence of the dispersion on the average expression strength over all samples by exploiting the mean-variance relationship across all samples.

3.14.1.3 Model fitting

For modeling, DESeq2 fits the generalized linear model called the negative binomial distribution model for each gene. The Wald test is employed for significance testing and hypothesis testing and generates a p-value to distinguish between DEGs and non-DEGs. The Wald statistic is generated as part of the computation and includes other parameters including the base mean expression of a gene across all samples, the log2 fold change which describes the effect size or the magnitude by which the expression of a gene changes, the log2fold change standard error which accounts for the accuracy of the log2 fold change metric, the Wald statistics, the p-value indicating the level of significance and the adjusted p-value which corrects the p-value for multiple comparisons or multiple hypothesis testing. Moreover, DESeq2 uses the Cooks' distance to automatically detect and remove genes with outliers from the count matrix to avoid spurious findings. Finally, DESeq2 automatically excludes genes whose mean of normalized counts is below a threshold determined by an optimization procedure. This improves the detection power by making the multiple testing adjustment of the p-values less severe.

3.14.1.3 Multiple hypothesis testing problem

Adjusting for multiple hypothesis testing is essential in RNA-seq data analysis. An alpha level of 0.05 was applied to 10 000 permutation tests for which roughly 500 false positives were expected. Many statistical methods are available to deal with the problem of multiple hypothesis testing. By default, DESeq2 uses False Discovery Rate (FDR) to address this. FDR is calculated as the ratio of estimated falsely significant genes over the number of significant genes declared. The number of false positive genes is estimated by the average of significant genes from all permutations.

3.15 Exploratory analysis

To evaluate trends in our data, exploratory data analysis (EDA) was performed prior to ART initiation (week 0), at week 2 and 12 on ART in samples from patients who were allocated either placebo or prophylactic prednisone who developed paradoxical TB-IRIS and those who did not (TB-non-IRIS controls). Discussed below are the EDA that were performed.

3.15.1 Principal component analysis (PCA)

Principal component analysis (PCA) is a dimensionality reduction technique used in high throughput datasets to cluster samples with similar variance [277]. A DESeq2 inherited method called plotPCA was used to visualize the 500 most variable genes in samples from patients who either received placebo or prophylactic prednisone who developed paradoxical TB-IRIS compared to TB-non-IRIS controls at week 0, week 2 or 12 on ART respectively.

3.15.2 Minus over average (MA) plots

For preliminary analysis, the results were explored using a DESeq2 inherited method called Minus over Average (MA) plot. MAplot enables the visualization of genes that are up or downregulated by contrasting the mean of the normalized counts against the log2 fold change metric for all tested genes. The DEGs are traditionally colored for ease of identification. The MAplot provides the benefit of quickly evaluating the magnitude of the log2fold change metric and its distribution across the mean expression.

3.15.3 Heatmap of DEGs

Other unsupervised learning utilities such as heatmaps which provide visual summary of the gene expression data were capitalized upon. A pHeatmap package from CRAN repository was

employed for this task [278]. Heatmap functions accept matrices of counts as input together with several customizable and default arguments. DEGs from patients who received either placebo or prophylactic prednisone who developed paradoxical TB-IRIS and TB-non-IRIS controls were visualized at week 0, 2 or 12 respectively.

3.16 Functional enrichment scoring

The process of extracting both accurate and concise gene information from RNA-seq derived differential expression data is both tedious and challenging. Recent methodological advances have enabled researchers to accurately identify the genes underlying a condition under investigation and evaluate their level of significance. However, one major limitation behind this approach is that individual-gene level analysis often yields a plethora of significant genes, with a small fraction underpinning the condition under investigation. This presents a challenge for scientists to accurately interpret the data. Recent efforts have yielded innovative approaches for studying DEGs and they rely on the discovery of significant biological pathways using a set of *a priori* defined genes as opposed to data mining a list of individual DEGs. One major benefit behind discovery approaches is that the gene set of interest may include moderate effects of individual genes that are not captured by the analysis of individual DEGs.

The statistical methods for testing the multivariate null hypothesis associated with gene set discovery approaches is well established [279]. Maciejewski and Henryk distinguished between the utility of "self-contained null hypothesis" and "competitive null hypothesis" which underlie discovery approaches such as gene set analysis. "Self-contained null hypotheses" are defined as hypothesis testing that no gene in the gene set of interest is differentially expressed; while a competitive null hypothesis is defined as the proportion of genes that are different between the two groups [280]. This is equivalent to the proportion of genes which are differentially expressed among the genes in experimental comparators outside the gene set. The corresponding test statistic in both cases is determined by calculating sample and gene permutations respectively.

I present below gene set enrichment analysis which was used in chapter 5 to summarize DEGs into biological pathways. Gene set enrichment analysis is a hybrid approach between competitive and self-contained hypothesis testing methods [281].

3.16.1 Gene set enrichment analysis (GSEA)

Gene set enrichment analysis (GSEA) is a type of gene set analysis technique that takes as input all of the DESeq2 derived gene list that are pre-ranked by some metric. Log2fold change values otherwise known as effect size were used for pre-ranking. The Reactome C2CP curated database was used in conjunction with the ranked gene list to summarise genes into functional profiles. GSEA subsequently groups the gene list into biological pathways based on a curated gene set. In this way, GSEA overcomes the limitations associated with individual gene analysis methods [282, 283]. Briefly, based on the experimental design, all genes in the DESeq2 derived gene list are ranked based on some metric of differential expression, typically log2 fold change,. The hypergeometric enrichment test or the Fisher's exact test was used to iterate between a curated, predefined gene-set and a pre-ranked gene list and calculates the enrichment score using the random walk test statistic. Subsequently, a p-value that indicates the probability of significance is calculated for each gene-set. The latter metric indicates the distribution of genes in the gene-set located in the ranked gene list. For each gene-set, an enrichment score based on the genes that are up or downregulated is calculated. Permutation tests are used to evaluate the significance of the enrichment score for each gene-set and an false discovery rate (FDR) value is calculated for a collection of sets of genes [283]. Ultimately, identifying biological pathways that underlie the condition under investigation is more meaningful than searching for individual genes for the following reasons: in a biological system, genes function together in biological pathways as opposed to functioning in isolation; the interpretation of a list of significantly enriched biological pathways based on *a priori* knowledge of the biological functions is more intuitive than interpreting and data mining individual genes; RNA-sequencing data is inherently noisy, as such, pathway analysis is well suited for detecting subtle changes in gene expression that underlie a condition under investigation as opposed to using individual gene analysis. Finally, the identification of significantly enriched biological pathways is more reproducible across different platforms in todays' dynamic and fast paced clinical research that seeks to translate research into clinical practice. Therefore, the overarching aim behind computational pathway analysis tools is to identify pathways that are over- or under- represented in a phenotype of interest. We used the C2 canonical Hallmark gene-set from Molecular Signature Database (MSigDb) and Reactome database which currently contain 50 curated gene-sets which add up to over 4500 genes [284-286].

3.16.1.1 Computing the gene level statistic

The required input for computing GSEA includes a pre-ranked list of differentially abundant transcripts derived from DESeq2 or any other statistical tool with synonymous functionality. Transcripts were pre-ranked by log2fold change (LFC) metric. The LFC values indicate the direction and magnitude of the change in gene expression. The p-value indicates whether the change in gene expression is significant or not. The calculated statistic is known as a gene level or the local statistic. The top and bottom of the ranked gene list contain all the significantly upregulated and downregulated genes respectively; the middle of the ranked gene list contains the genes with no significant change in gene expression.

3.16.1.2 Computing the global statistic.

The algorithm used to calculate global statistic is over-simplistic but the underlying statistical approach for summarising genes into biological pathways is complex. To calculate the global statistic, two inputs are required, the pre-ranked gene list and candidate gene sets from a curated database. The Human MSigDB collections C2 canonical pathway (CP) candidate gene-sets from Reactome were used in conjunction with a pre-ranked gene list to establish gene membership [286]. The enrichment score which is the global statistic for each candidate gene-set was subsequently calculated.

3.16.1.3 Computing random walk test statistic

GSEA employs a permutation-based approach using Kolmogorov Smirnov statistic to determine if a pre-defined gene-set is differentially expressed between the two tested conditions [283]. In a curated database, GSEA evaluates a single gene-set candidate at a time against a ranked gene list to establish gene membership. The iteration begins at the top of the rank containing upregulated transcripts. If a gene constitutes a member of the candidate gene set, it is added to a running sum, otherwise, it is subtracted. The value that is added or subtracted is called the running sum and is proportional to the quantitative value of each gene that was used for ranking. This process is repeated for each gene in the ranked list. The enrichment score (ES) for each candidate gene-set is calculated as the largest absolute value that the running sum achieved. Therefore, the enrichment score plot depicts how the running sum changes as one

iterates from the top of the ranked gene list to the bottom. The ES is one of the most important features of the ES plot. The ES is the height or the maximum point on the plot. It is defined as the maximum deviation from zero and it indicates the extent to which the gene set is at the top or the bottom of the ranked gene list. A positive ES indicates upregulated genes or gene-sets that are at the top of the ranked gene list and conversely for a negative ES [283].

3.16.1.4 Leading edge subset

The leading edge genes is a subset of candidate gene members that contribute most to the ES. These appear in the ranked gene list before the peak of the ES. Because these influence the ES dramatically, they are highly associated with the phenotype in question [283].

3.16.1.5 Computing the statistical significance level of the global statistic

The statistical significance of the ES was determined by calculating a p-value using the Kolmogorov-Smirnov test (KS-test). This entails performing a minimum of 1000 permutations of the phenotype labels. Following this, the statistical significance of each gene set is evaluated by comparing the ES to the 1,000 permuted ES values. The KS-test essentially evaluates normality of the generated ES. For instance, if the ES follows normal distribution then the KS is greater than 0.05. Alternatively, the KS generates a p-value of less than 0.05. This means there is a significant difference from normal distribution. Therefore, the null hypothesis is rejected [283].

3.16.1.6 Adjusting for multiple hypothesis testing

After calculating the ES for different gene sets and determining their level of significance, the differences in gene set sizes were adjusted for. This made possible the comparison of the results across different gene sets. The outcome was a new score called the normalized enrichment score (NES). The NES is calculated by dividing the corresponding observed ES (for each gene set) by the average of ES over all permutations. An adjusted p-value was calculated to infer statistical significance when comparing different gene sets, a process known as estimating the

false discovery rate (FDR). The FDR represents the expected proportion of gene sets falsely identified as significant. The Benjamini Hochberg (BH) test was used to calculate the FDR, which computes the ratio of two percentages: the numerator containing NES from all the permutations of all gene sets; and the denominator containing NES from only significant gene sets and multiplied by a chosen threshold [287]. Typically a threshold of 20% is used, which has an assumption that 20% of all positive findings are potentially false positives. However, in our analyses, a more stringent threshold of 10% was used.

3.17 Biological Networks

Biological networks are graphical depictions of associative or probabilistic interactions between components of a biological system such as genes, proteins, or metabolites. Different types of networks such as directed and undirected networks exist. In this study, weighted directed networks with edges between genes that represent co-expression associations between the nodes were used as exploratory tools to analyze system level gene topology and functionality [288].

3.17.1 Co-expression gene networks

A gene co-expression network consists of gene expression profiles, depicted as nodes (also known as vertices) and gene connections depicted as edges (or arcs) [289]. Edges occur conditionally when two genes are significantly correlated or co-expressed. A co-expression gene network can be undirected or directed. In an undirected co-expression network, each node is connected to another node with at least one edge. In contrast, a directed co-expression network has nodes that are connected together where all edges are directed from one node to another [288]. With expression profiles from several RNA samples, co-expression similarity for each gene pair can be computed. Co-expressed genes are biologically meaningful because nodes in a co-expression network may represent biological functions or pathways. Numerous computational methods and tools have been developed to construct co-expression gene networks [288, 290]. Such methods measure the expression similarity between each gene pair in the data by ranking correlations that are represented in a topology overlap matrix (TOM) (e.g. by using Pearson or Spearman), where weak (i.e., non-significant) correlations are

removed. We explored one such method known as weighted gene co-expression network analysis.

3.17.1.1 Weighted gene co-expression network analysis (WGCNA)

When constructing a weighted gene co-expression network, a soft threshold is applied to assign each pair of genes a connection weight. This helps identify genes that are upregulated and downregulated, respectively. In WGCNA, highly correlated nodes form clusters, which are characterized by highly interconnected genes, also collectively known as modules. Within each module, module eigengenes are identified as representative of the module's overall gene expression pattern. A module eigengene is technically defined as the first principal component of that module, capturing the largest proportion of the variance in gene expression within the module, thus serving as a generalizable gene expression pattern of the given module [288].

3.17.1.1.1 Sample pre-processing

Normalized and variance stabilized expression counts that were filtered for low counts were provided as input for WGCNA using the R statistical language. Hierarchical clustering approaches were used to identify and exclude outlier samples from both the expression matrix and the database containing information pertaining to the samples. This was done for analyses conducted at week 0 and week 2 on ART.

3.17.1.1.2 Network construction- from a gene expression matrix to a similarity matrix

The gene expression matrix was transformed into a similarity matrix. This was achieved by computing the absolute value of the Pearson correlation between each gene pair. The resulting similarity matrix provides a measure of the level of similarity between gene expression profiles across genes otherwise known as co-expression [288].

3.17.1.1.3 From a similarity matrix to an adjacency matrix

An adjacency function was used to transform a similarity matrix containing co-expression similarity values into an adjacency matrix. The choice of the adjacency function depends on the weight properties of the network. The term weight properties reflects whether a network is weighted or unweighted. For WGCNA, soft thresholds were applied to the similarity matrix to generate a weighted adjacency matrix. The application of soft thresholds helps to identify genes that are either up or downregulated. Soft thresholding is used to define a power for the adjacency function, where power or beta values that allows for the generation of a network that satisfies scale free topology are calculated [288, 291].

3.17.1.1.4 Scale-free Topology

An important characteristic of a scale-free network is that the frequency of node connectivity follows the power law. In a power-law distribution, scale-free topology is directly related to the growth of the network, where new nodes prefer to connect with existing nodes. As a result, a network with scale-free topology is characterized by nodes with high connectivity. The Pearson correlation measures the strength of the linear relationship between two variables, and in this instance, gene pairs. The square of the Pearson correlation (R^2) is used to illustrate the extent to which a network satisfies scale-free topology [288]. An R^2 approaching 1 approximates a straight line which signals a good fit for the data, thus signifying a scale-free network. Trade-offs exist between maximizing R^2 and retaining a high mean number of connections. Only adjacency function parameter values leading to a scale-free topology fitting index of $R^2 > 0.80$ should be considered. The mean connectivity should also be high enough to contain enough information for module detection [288]. Therefore, an R^2 value above 80% with a corresponding mean connectivity was chosen as the power or beta value. The similarity matrix was raised to this Beta value to generate a weighted adjacency matrix which contains the connection strengths between node pairs. The topology of scale-free networks is largely controlled by highly connected nodes called hubs . One of the implications of scale-free topology is that relatively few hubs exist in the network. Less-connected nodes are linked to the hub, forming a network. An important characteristic of scale-free networks is that they have a relatively large error tolerance [292].

3.17.1.1.5 Selecting Adjacency Function Parameters

Several factors are accounted for when determining the parameters of the adjacency function. These include sensitivity and specificity since they define the gene pair connection strengths. The connectivity of a node is defined as the number of its direct connections with other nodes. The resulting weighted adjacency matrix was transformed into a topological overlap matrix (TOM) which is another important measure of node connectivity which has been shown to be superior to other standard measures. Finally, the TOM was transformed into a dissimilarity matrix which was subsequently used for unsupervised hierarchical linkage clustering of genes [288, 291].

3.18 Gene Module Identification

Subsequent to network construction is module detection. Modules are clusters of closely interconnected nodes (i.e. genes with high overlap). A weighted topological overlap measure has been shown to deliver more interconnected modules than an unweighted measure. The WGCNA package uses unsupervised clustering to identify gene modules. Using a TOM-based dissimilarity, average linkage hierarchical clustering is performed using the standard R function *hclust*. Modules are depicted as dendrogram branches, and cutting is performed using the dynamic hybrid tree cut algorithm [288]. A TOM plot is a color-coded matrix representation of a summary of the co-expression network, which depicts the values of the dissimilarity matrix. Rows and columns are sorted by the hierarchical clustering dendrogram. Red and yellow indicate low and high dissimilarity respectively (see Figure 5). Modules are described as red squares along the diagonal. Of note, the TOM plots are symmetric along the diagonal because they are graphical representations of the topological overlap matrix which is also symmetric.

3. 19 Intramodular Connectivity and Module Membership

Network connectivity can also be defined with respect to each individual module. The intramodular connectivity and the TOM-based intramodular connectivity can be defined similarly to whole-network connectivity. Intramodular connectivity measures have been shown to be more biologically significant than whole-network connectivity. Hierarchical clustering results in a binary module assignment. Each gene is either in a particular module, or not in that

module. Therefore, it can be beneficial to define a continuous measure of uncertainty of module assignment. This is valuable for genes that are near module boundaries. The module membership of each gene in a module is the expression profile of the gene and is the module eigengene of that module [288, 291].

3.20 Investigation of inhibitors targeting Inflammasome related targets

3.20.1 Background

Work by Lai and colleagues previously reported that hypercytokinemia in TB-IRIS is contributed by the activation of canonical and non-canonical inflammasomes, in which inhibition of inflammasomes by non-selective pan-Caspase inhibitor can significantly reduce the production of pro-inflammatory cytokines including IL-1α and IL-1β [25]. To better understand whether specific inhibition of inflammasomes or its downstream effectors (e.g. IL-1 cytokines or eicosanoids) can confer better protection in TB-IRIS than a non-specific anti-inflammatory agent such as prednisolone, a panel of anti-inflammasome inhibitors were assessed in comparison to prednisolone. The optimal concentrations of the experimental inhibitors were first determined with antigen-stimulated peripheral blood mononuclear cells (PBMC) from healthy donors, then their effect tested on PBMC collected from patients from the Pred-ART trial. Prednisolone, and a vehicle mock (e.g. DMSO) were used for benchmarking. Cell culture supernatants were collected for Luminex assay to measure secreted concentrations of pro- and anti-inflammatory cytokines and chemokines. A cell death assay (lactate dehydrogenase quantification) was performed to assess drug induced cytotoxicity.

3.20.2 Broth culture of Mycobacterium tuberculosis (H37Rv)

Mtb is classified as a class 3 pathogen that can cause severe disease for which therapeutic intervention is available. Due to its capacity to spread via aerosol and cause disease, its handling requires strict measures under biosafety level (BSL) III conditions where air flow is tightly regulated. The surface of the biosafety level II cabinet (BSCII) was decontaminated with 10% Incidin and 70% ethanol. All the material that was handled inside the BSC II including pipettes, pipette boxes, and culture flasks were decontaminated prior to being transported inside the BSCII. A pre-culture of H37Rv was prepared by inoculating a freezer stock in 7H9 with proper supplementation to a final volume of 10 mL in a 50 mL culture flask. The surface of the culture flask was decontaminated with 70% ethanol and carefully placed in a secondary container which was sealed in leak proof autoclavable waste bag. The double contained flask was carefully remove from the hood and incubated at 37 °C without shaking. The cultures were monitored daily for growth by measuring the OD_{600} using a spectrophotometer until it reached a value of 1. Approximately 0.5 mL of the pre-culture was inoculated in 10 mL sterile broth of properly supplemented 7H9 media. The culture flask was contained and incubated as previous and allowed to reach a final concentration (OD_{600}) of 0.5.

A total of 1 mL Mtb-H37Rv culture was aliquoted in sterile1.5 mL Eppendorf tubes and sealed with parafilm inside the BSCII.

3.20.3 Heat killing of Mtb-H37Rv

The parafilm sealed aliquots were safely transported outside the BSCII to a uniformly heated water bath. The cultures were heat killed at 80 ^{0}C for 2 hour and subsequently plated for colonies to ensure that there was no viable colonies. The heat killed cultures were safely transported out of the BSL III laboratory in an upright position and additionally contained in sterile double ziplock bags and stored at -80 ^{0}C in the BSL II laboratory for subsequent stimulation experiments.

3.20.4 Multiplicity of infection (MOI) determination

A titration of 3 different PBMC to Mtb-H37Rv ratios were set up to determine the optimal multiplicity of infection (MOI) that could induce a detectable cytokine response. Cells were recovered from cryopreservation as previously described and resuspended to a final concentration of approximately 250,000 cells/200 µL and stained for viability. Cells were seeded in a 96 well plate and four conditions were tested as follows: unstimulated cells and cells incubated with the different ratios of Mtb-H37Rv for 12 hours as follows: MOI of 1, 2 and 5, respectively. After 12 hours of incubation, the cells were sedimented by gradient centrifugation at 1200 rpm for 6 min and the supernatant collected and transferred to a sterile plate. The supernatants were tested for cytokine production using a custom 7-plex Luminex panel (Table 3.15).

Table 3.15*. Tabular list of 7-multiplexed analytes measured by Luminex, their class and function. Multiplexed analytes were measured by Luminex assay for optimization purposes following ex vivo cell culture of and stimulation of peripheral blood samples obtained at week 2 on ART from patients who developed paradoxical tuberculosis immune reconstitution inflammatory syndrome while enrolled in the TB-ART cohort study. Analytes represented proinflammatory cytokines, chemokine and proteases that were previous associated with paradoxical TB-IRIS.*

Analytes	**Class**	**Function**
IL-1α	Cytokine	Modulates inflammation

IL-1β	Cytokine	Modulates inflammation
IL-8	Cytokine	Chemo-attractant
IL-10	Cytokine	Activate CD4 lymphocytes
IL-18	Cytokine	Modulates inflammation
IFNγ	Cytokine	Activate innate immune cells
TNFα	Cytokine	Modulates inflammation

3.20.5 Cell number titration

PBMCs from one healthy participant were recovered from cryopreservation as previously described. A total of 200 µL of either 10 million cells/mL or in subsequent re-optimization, 1.25 million cells/mL which corresponds to 250,000 cells/200 µL were seeded for 5 different conditions. A total of 100 µL of RPMI supplemented with 2% FCS was added to the remaining wells. A 2-fold dilution series was performed by mixing 100 µL of the cells with 100 µL of properly supplemented RPMI. Similarly, heat killed Mtb-H37Rv was titrated in a sterile 96 well plate in a 1:1 ratio based on the highest cell concentration (250 000 cells/200 µL). The last four conditions were stimulated with a 1:1 dose of heat killed Mtb-H37Rv and treated with 5 nM optimized drug concentration of candidate drugs. The suspension was incubated for 12 hours, and the supernatant harvested by gradient centrifugation at 1800 rpm for 3 min. The cells were transferred to a new sterile plate and tested for drug mediated cytokine reduction by Luminex.

3.20.6 Optimization of the minimum amount of time required to induce a detectable cytokine response.

Participant PBMC were seeded in a sterile 96 well plate and allowed to recover from cryopreservation as previously described (see section 3.3). To determine the optimal time required to induce cytokine production, cells were stimulated with heat-killed Mtb-H37Rv for either 6 or 12 hours. Cells were sedimented by gradient centrifugation at 1800 rpm for 3 min. The supernatants were collected and stored in a sterile 96 well plate and used for multiple analyte detection by Luminex.

3.20.7 Determining dose dependent drug responses.

A total of 8 drugs were screened (7 FDA approved) including 2 pan-Caspase anti-inflammatory inhibitors (Z-VAD-FMK; Ac-VAD-CMK), 2 inflammatory lipids/eicosanoid inhibitors

(Naproxen; Celecoxib), 2 inflammasome inhibitors (Vx-765; Parthenolide-not FDA approved) and Anakinra - an IL-1 receptor antagonist which acts downstream of the inflammasome to block effector molecules. The capacity of the candidate drugs to reduce markers that are associated with inflammation was evaluated and compared to prednisolone which is the current drug of choice for treating inflammatory disorders including paradoxical TB-IRIS.

Briefly, cryopreserved PBMC from one healthy individual were rapidly thawed at 37 °C and subjected to two washes in RPMI media containing 20% FCS by gradient centrifugation at 1600 rpm for 6 min. PBMC were rested overnight (~12 hours) and were subsequently seeded to approximately 250 000 cells/200 µL. Dose responses were determined by stimulating PBMC with an optimized MOI of 1:1 of heat killed Mtb-H37Rv grown to OD_{600} 0.5. The cultures were subsequently treated with a panel of drugs at 6 standardized concentrations ranging from 1 µM; 500 nM; 100 nM; 50 nM; 25 nM and 5 nM for all drugs. Plates were incubated for 12 hours at 37 °C in the presence of 5% CO_2. Plates were subsequently spun down at 1800 rpm for 3 min for cell supernatant harvesting. A total of 180 µL of cell culture supernatants were stored at -80 °C for downstream detection of multiplexed analytes by Luminex, ELISA and the detection of the marker of cell death by lactate dehydrogenase assay. Cell pellets were resuspended in 200 µL Trizol and frozen at -80 °C for RNA extractions. Only two drugs showed competitive anti-inflammatory capacity (Table 3.16, parthenolide and anakinra) relative to prednisolone (**Figure 3.4**).

Table 3.16*. Inflammasome-related Inhibitors used in the ex vivo cell culture and stimulation of peripheral blood samples obtained at week 2 on ART from patients who developed paradoxical tuberculosis immune reconstitution inflammatory syndrome while enrolled in the Pred-ART trial.*

Inhibitors	**Final concentration used (nM)**	**Function**
Anakinra	5	IL-1 receptor blocker
Parthenolide	5	Anti-inflammatory agent derived from herb
Prednisolone	5	Anti-inflammatory agent with broad effects

Both parthenolide and anakinra were subsequently tested for the capacity to reduce markers of inflammation in PBMC samples obtained at week 2 on ART from patients that were enrolled in the Pred-ART trial

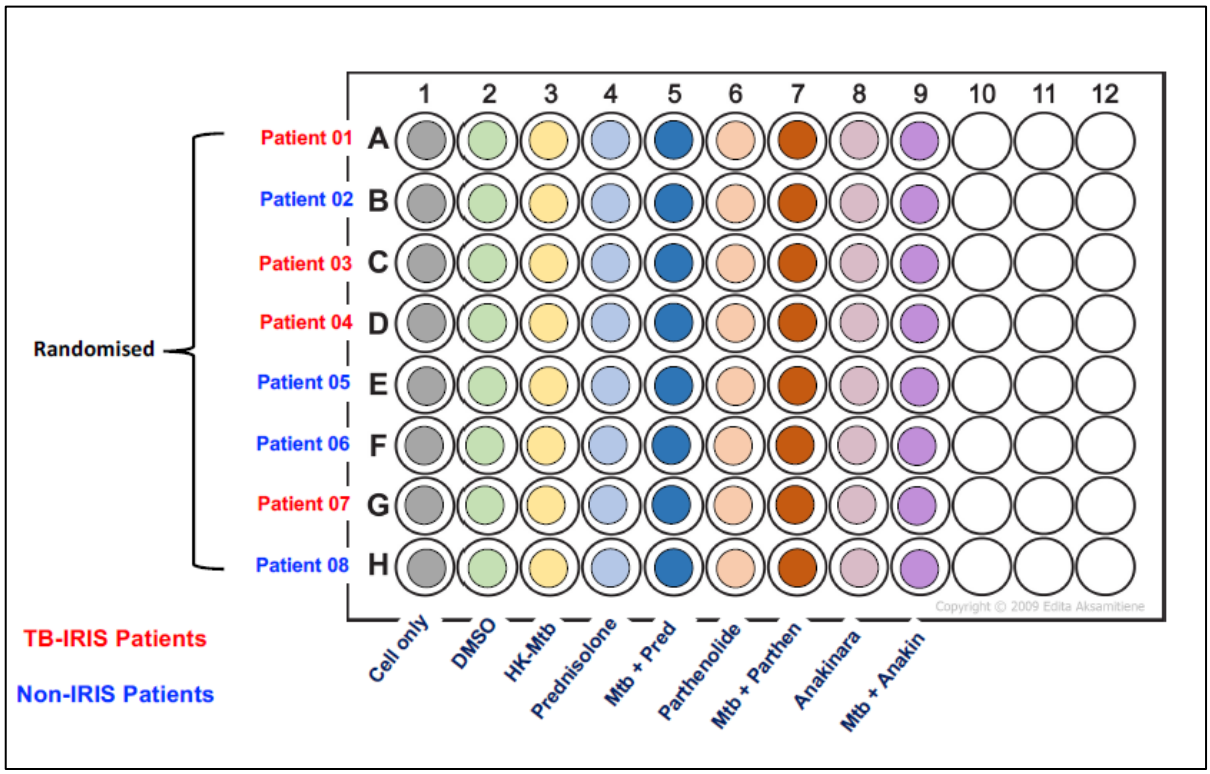

Figure 3.4. Schematic of the experimental design for the ex vivo cell culture of patient peripheral blood mononuclear cell *(PBMC). Patient PBMC were stimulated with heat-killed H37Rv and subsequently treated with drugs including parthenolide and anakinra. Prednisolone was used for benchmarking capacity to reduce markers of inflammation.*

3.21 Assays for downstream detection of analytes

3. 21.1 Luminex

3. 21.1.1 Sample preparation

Cell culture supernatants were diluted 2-fold in RD6-52 prior to use.

3. 21.1.2 Reagent preparations

All reagents were brought to ambient temperature before use.

3. 21.1.3 Wash buffer preparation

To prepare 500 mL of wash buffer, 20 mL of wash buffer concentrate was thoroughly mixed with 480mL of deionized or distilled water.

3. 21.1.4 Preparation of standards

The custom 15-multiplex kit (Table 3.17) of pro-inflammatory cytokines and chemokines and metalloproteinases was procured from R&D biosystems and contained six standards (B, E, R, A, X and C), magnetic beads/microparticle, calibrator diluent (RD6-52), sample-diluent (RD2-1), Biotinylated antibody, and PE streptavidin and plate sealers and a sterile, clear, flat bottom plate.

Table 3.17*. Tabular list of multiplexed analytes measured by luminex and their class and function. Multiplexed analytes were measured by Luminex assay following ex vivo cell culture of and stimulation of peripheral blood samples obtained at week 2 on ART from patients who developed paradoxical tuberculosis immune reconstitution inflammatory syndrome while enrolled in the Pred-ART trial. Analytes represented proinflammatory cytokines, chemokine and proteases that were previous associated with paradoxical TB-IRIS.*

Analytes	**Class**	**Function**
GM-CSF	Cytokine	Promotes innate cell differentiation
IL-1α	Cytokine	Modulates inflammation
IL-1β	Cytokine	Modulates inflammation
IL-6	Cytokine	Modulates inflammation
IL-8	Cytokine	Chemo-attractant
IL-10	Cytokine	Role in anti-inflammation
IL-12	Cytokine	Activate CD4 lymphocytes
IL-17	Cytokine	T cell and neutrophil activation
IL-18	Cytokine	Modulates inflammation
IFNα	Cytokine	Stimulate/inhibit immune function
IFNβ	Cytokine	Stimulate/inhibit immune function
IFNγ	Cytokine	Activate innate immune cells
MMP 9	Protease	Remodels extracellular matrix
MMP 10	Protease	Remodels extracellular matrix

TNFα	Cytokine	Modulates inflammation

Standards were prepared in duplicate as follows: the standards were reconstituted in 275, 225, 225, 250, 250 and 275 volumes (µL) of calibrator diluent RD6-52 respectively. The standards were allowed to equilibrate to ambient temperature for 15 minutes with gentle agitation at 300 rpm. A total of 100 µL of each reconstituted standard was added to a sterile 1.5 mL Eppendorf tube labelled S1 and topped up to 1 mL. A 1:3 dilution series was prepared by transferring 100µL of S1 to a sterile 1.5 mL Eppendorf tube labelled S2 containing 200 µL RD6-52 diluent and subsequently up to S7 as illustrated in the schematic below. Of note, standards were used within 1 hour of preparation.

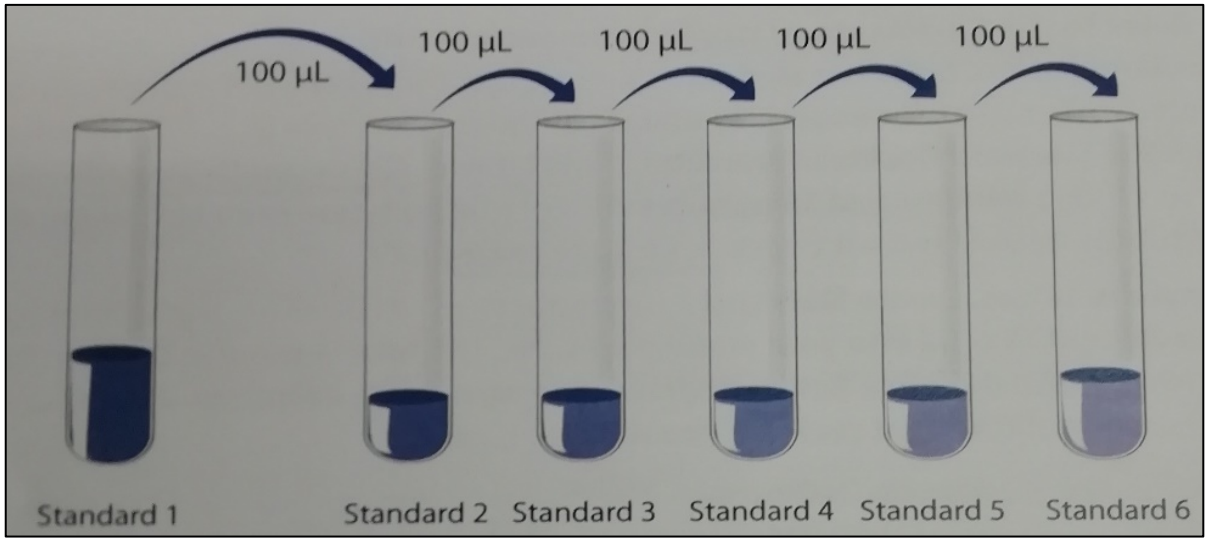

Figure 3.5. Diagrammatic illustration of preparation of standards for the 7-plex and 15-plex Luminex assay. *Standards were prepared by reconstituting in recommended calibrator diluent (RD6-52) and 100 µL of each standard transferred to a tube labelled S1 which was topped up to a final volume of 1 mL. A serial dilution was performed by transferring total volume of 100 µL of S1 to S2 and down to S7 to produce a 1:3 dilution.*

3. 21.1.5 Preparation of microparticle cocktail

The microparticle cocktail vial was centrifuged for 30 seconds at 1000 xg to pull down the mixture and subsequently vortexed for a minimum of 120 seconds to mix the contents of the vial. The microparticle cocktail was diluted in RD2-1 buffer according to the table below:

Table 3.18. *Required volumes for the preparation of microparticle or beads solution. Beads were prepared for 20 samples with 5 conditions per sample*

Number of wells used	Streptavidin-PE concentrate (µL)	Wash buffer (mL)
96	500	5
72	375	3.75
48	250	2.50
24	125	1.25

3. 21.1.6 Preparation of antibody cocktail

The antibody cocktail vial was centrifuged for 30 seconds at 1000 xg to pull down the mixture and subsequently vortexed for a minimum of 120 seconds to mix the contents of the vial. The antibody cocktail was diluted in RD2-1 buffer according to the table below:

Table 3.19. *Required volumes for the preparation of the antibody cocktail solution. The antibody cocktail was prepared for 20 samples with 5 conditions per sample*

Number of wells used	Streptavidin-PE concentrate (µL)	Wash buffer (mL)
96	500	5
72	375	3.75
48	250	2.50
24	125	1.25

3. 21.1.7 Preparation of Streptavidin PE

Streptavidin PE vial was centrifuged for 30 seconds at 1000 xg to pull down the mixture and subsequently vortexed for a minimum of 120 seconds to mix the contents of the vial. The Streptavidin PE mixture was diluted in wash buffer solution according to the table below:

Table 3.20*. Required volumes for the preparation of streptavidin-phycoerythrin (PE) solution. Streptavidin PE was prepared for 20 samples with 5 conditions per sample*

Number of wells used	Streptavidin-PE concentrate (µL)	Wash buffer (mL)
96	220	5.35
72	165	4
48	110	2.65

24	55	1.35

Approximately 50 µL of blank (RD6-52) standards and cell culture supernatants were added to appropriate wells of a sterile, flat and clear bottom 96 well plate. Approximately 50 µL of the microparticle cocktail was added to each well containing the blank, standards and diluted cell culture supernatants. The plate was covered with a plate sealer and incubated for 2 hours at ambient temperature in a horizontal orbital microplate shaker adjusted to 840 rpm. The plate was subsequently washed 3X in a magnetic automated microplate washer using approximately 100 µL wash buffer solution. Approximately 50 µL of the diluted biotin antibody cocktail was added to all wells and covered with a plate sealer and incubated for 1 hour at ambient temperature with shaking as previous. Washing was repeated as previous. A total of 50 µL of the diluted streptavidin-PE was added to each well and cover with a plate sealer and incubated for 30 minutes at ambient temperature with shaking as previous. Washing was repeated as previous and the microparticles were resuspended in 100 µL of wash buffer solution and incubated for 2 minutes with shaking as previous. The plate was acquired using Bio-Rad plate reader immediately.

3.22 Enzyme linked immunosorbent assays (ELISA) for Caspase-1, Azurocidin 1, Human neutrophil peptide1-3, Neutrophil elastase, and Myeloperoxidase.

ELISA for various analytes including caspase-1, azurocidin, human neutrophil peptide, neutrophil elastase and myeloperoxidase was conducted using blood plasma samples collected from participants that were enrolled in the Pred-ART study. Of note, all reagents and samples were brought to room temperature prior to use.

3.22.1 Preparation of Caspase-1 wash buffer solution.

A total of 20 mL of wash buffer concentrate was thoroughly mixed with 480 mL of distilled water to prepare 500 mL of wash buffer solution.

3.22.2 Preparation of Caspase-1 standards.

Caspase-1 standard was reconstituted in 1 mL volume of distilled water to generate a stock solution of 4000 pg/mL. The stock solution was allowed to stand for 15 minutes with gentle agitation to facilitate proper mixing. A dilution series of the standards was prepared as follows:

seven sterile1.5 mL Eppendorf tubes labelled Standard 1 to Standard 7 were prepared. Standard 1 (S1) was prepared by mixing 100 µL of the stock solution with 900µL of diluent RD5-5 to generate a 1:10 dilution. A total of 500 µL of the RD5-5 diluent was aliquoted to the remaining sterile 1.5 mL Eppendorf tubes labelled standard (S) 2-7, as illustrated below. The contents of S1 were thoroughly mixed prior to generating a 2-fold dilution series by transferring 500 µL of S1 to a tube labelled S2 and to each subsequent tube up to S7. Calibrator diluent RD5-5 was used as a blank. Of note, the standards were used within 30 minutes of preparation.

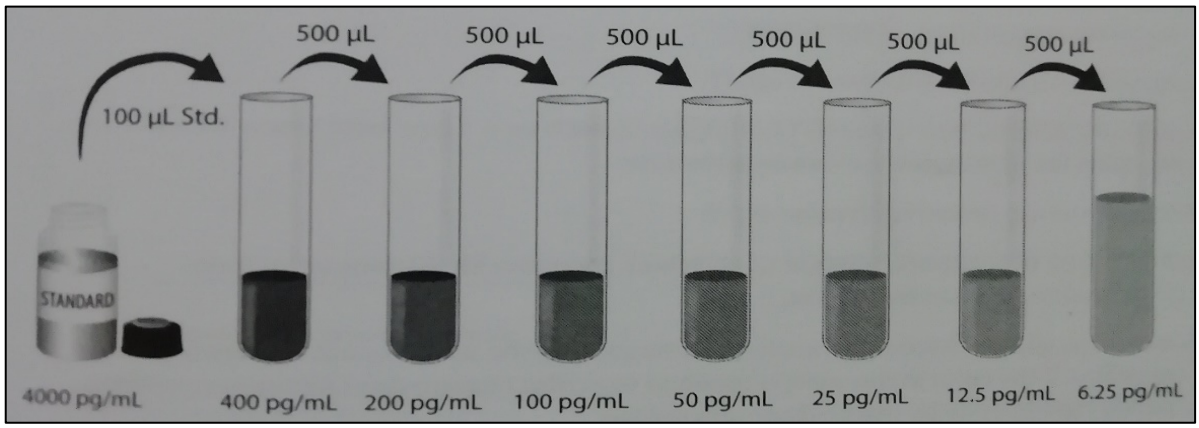

Figure3.6. Diagrammatic illustration of preparation of standards for the Caspase-1 enzyme linked immunosorbent assay*. Standards were prepared by reconstituting in recommended volume of calibrator diluent (RD5-5) and 100 µL of the standard transferred to a tube labelled S2. S2 was mixed thoroughly and 500 µL was transferred to a tube labelled S3 up to S7 to produce a 1:2 dilution series.*

3.22.3 Substrate solution

The kit contained color reagents A and B which are light sensitive and were mixed in equal volumes within 15 minutes of use. Briefly, approximately 50 µL of assay diluent (RD1W) was aseptically added to each well of the Caspase-1 coated plate. Approximately 100 µL of the blank, standards, and double filtered cell free supernatant for each experimental condition were added to appropriate wells that were pre-determined. The plate was covered with a plate sealer and incubated in the dark for 1.5 hours at ambient temperature without agitation. The plate was washed 3X in an automated plate washer in 100 µL wash buffer (20 mL wash buffer concentrate + 480 mL distilled water). Approximately 100µL of caspase-1 anti-serum was subsequently added to each well and the plate was subsequently covered with a sealer and incubated for 30 min at room temperature without agitation at 300 rpm. Washing was repeated

as previous and 100 µL of human caspase-1 conjugate was added to each well. The plate was secured with a sealer and incubated for 20 min at room temperature without agitation. Washing was repeated as previous and 200 µL of substrate solution was added to each well. The plate was sealed and protected from light and incubated for 20 minutes at ambient temperature. Approximately 50 µL of stop solution was added to each well following which the optical density was determined immediately using a Bio-RAD colorimetric microplate reader set at a wavelength of 450 nm.

3.22.4 Preparation of human neutrophil peptide (HNP)1-3 wash buffer solution.

A total of 30 mL of 40X wash buffer concentrate was thoroughly mixed with 1170 mL of distilled water to prepare 1200 mL of wash buffer solution.

3.22.5 Preparation of HNP1-3 dilution buffer.

Dilution buffer was prepared according to the manufacturer's instructions. Briefly, a total of 20 mL of 10X dilution buffer concentrate was mixed with 180 mL distilled water to generate 200 mL dilution buffer.

3.22.6 Preparation of HNP1-3 sample dilution buffer.

Sample dilution buffer was prepared according to manufacturer's instructions. Briefly, a total volume of 15 mL of 10X sample dilution buffer concentrate was thoroughly mixed with 135 mL of dilution buffer.

3.22.7 Preparation of HNP 1-3 standard solution.

Standard solution was prepared as directed in the instruction manual. Briefly, the standard was reconstituted in 581 µL of sample dilution buffer and labelled S1. Seven Eppendorf tubes labelled S2-S7 were aliquoted with 225 µL of sample dilution buffer. A total volume of 225 µL from S1 was serially diluted from S2-S7 to produce a 1:2 dilution series. Sample dilution buffer was used as a blank.

3.22.8 Preparation of HNP1-3 tracer solution.

The tracer solution was reconstituted in 1 mL of de-ionized water and subsequently diluted 1 part (mL) in 11 mL of dilution buffer.

3.22.9 Preparation of HNP1-3 streptavidin-peroxidase solution.

The streptavidin-peroxidase were spun down prior to use. A total of 250 µL of 100X streptavidin-peroxidase concentrate was mixed with 25 mL of dilution buffer.

3.22.10 Detection of plasma soluble HNP1-3 using enzyme linked immunosorbent assay.

The human neutrophil peptide (HNP)-1-3 enzyme linked immunosorbent assay (ELISA) kit was procured from Hycult Biotech™ and utilized for the quantitation of HNP1-3 in plasma samples (diluted in 10X in sample dilution buffer) from patients with paradoxical TB-IRIS and TB-non-IRIS controls prior to the initiation of ART (week 0) and at week 2 on ART. The HNP1-3 ELISA kit is a ready to use solid phase assay that is based on the sandwich principle. The assay was performed according to manufacturer's instructions. All reagents were equilibrated to ambient temperature prior to use; standards, dilution of samples, and all buffers were prepared according to the manufacturer's instructions. Briefly, a total volume of 100 µL of standards and samples were added to appropriate wells coated with the primary antibody and the plates were subsequently incubated for 1 hour at room temperature. The plates were washed four times in 400 µL wash buffer using an automated plate washer. A total volume of 100 µL of prediluted tracer solution was added to all the wells. The plates were sealed and incubated for 1 hour at room temperature and washing repeated as previous. A total volume of 100 µL of 3,3',5,5'-Tetramethylbenzidine (TMB) – a substrate for horseradish peroxidase (HRP), was added to all the wells; the plates were sealed and incubated in the dark at ambient temperature for 30 min. The reaction was stopped by adding 100 µL of stop solution and the solution gently mixed by swirling the plates. The absorbance was determined by reading the plate in an automated plate reader at absorbance wavelength 450 nm. The data was quality checked by an independent investigator and analyzed by plotting concentration values.

3.22.11 Preparation of azurocidin wash buffer solution.

A total of 20 mL of 20X wash buffer concentrate was thoroughly mixed with 380 mL of distilled water to prepare 400 mL of wash buffer solution.

3.22.12 Preparation of azurocidin assay diluent.

Assay diluent (5X) was diluted 5-fold in distilled water prior to use.

3.22.13 Preparation of standards for azurocidin.

The standard was reconstituted with approximately 400 µL of 1X assay diluent and labelled as S1as directed in the instruction manual. Seven Eppendorf tubes labelled S2-S7 were aliquoted with 270 µL of assay diluent. A total volume of 180 µL of dissolved S1 was serially diluted from S2-S7 to produce a 2.5 dilution series. Assay diluent was used as a blank.

3.22.14 Preparation of azurocidin1 streptavidin-HRP solution.

The streptavidin-HRP solution was spun down prior to use. The streptavidin-HRP solution was diluted 1000-fold by mixing 50 µL of streptavidin-HRP concentrate with 50 mL assay diluent.

3.22.15 Detection of plasma soluble azurocidin (Azu1) using enzyme linked immunosorbent assay.

A total volume of 100 µL of standards or 1:3 pre-diluted plasma samples (in assay diluent) were added to the Azu1 coated 96 well plate. The plates were sealed and left to incubate a room temperature with gentle agitation (650 rpm) for 2.5 hours. The plates were washed four times in 400 µL of wash buffer using an automated plate washer. A total of 100 µL of prepared biotin conjugate was added to each well; the plates sealed and the incubated for 1 hour as previous. The plates were washed as previous and 100 µL of streptavidin-HRP was added to each well; the plates were sealed and incubated for 45 min as previous. The plates were washed as previous and 100 µL of TMB substrate was added to each well; the plates were sealed and incubated in the dark for 30 min until the solution turned blue. A total volume of 50 µL stop solution was added to all wells to stop the reaction. The absorbance of each well was measured in an automated plate reader at 450 nm.

3.22.16 Preparation of neutrophil elastase wash buffer solution.

A total of 50 mL of 10X wash buffer concentrate was thoroughly mixed with 450 mL of distilled water to prepare 500 mL of neutrophil elastase wash buffer solution.

3.22.17 Preparation of standards for neutrophil elastase detection.

Standards were prepared according to the manufacturer's directions as follows: Seven Eppendorf tubes were labelled S2-S7 and 225 µL of provided assay diluent was aliquoted into each tube. A total volume of 225 µL of human neutrophil standard, reconstituted with 1 mL of assay diluent was added to S2 and serially diluted up to S7 to produce a 1:2 dilution series.

3.22.18 Detection of plasma soluble neutrophil elastase (NE) using enzyme linked immunosorbent assay.

A total volume of 100 µL of standards or 1:100 pre-diluted plasma samples (in assay diluent) were added to the NE coated 96 well plate. The plates were sealed and left to incubate a room temperature with agitation (900 rpm) for 1 hour. The adhesive strips were gently removed, and the plates were washed four times in 400 µL of wash buffer using an automated plate washer. A total of 150 µL of ready-made horse-reddish peroxidase (HRP) conjugate was added to all wells; the plates sealed and the incubated for 1 hour as previous. The adhesive strips were removed; and the plates were washed as previous and 200 µL of TMB substrate was added to all wells; the plates were sealed and incubated for 30 min as in the dark without shaking. A total volume of 50 µL stop solution was added to all wells to stop the reaction. The absorbance of each well was measured in an automated plate reader at 450 nm.

3.22.19 Preparation of myeloperoxidase wash buffer solution.

A total volume of 25 mL of 20X wash buffer concentrate was thoroughly mixed with 475 mL of distilled water to prepare 500 mL of myeloperoxidase wash buffer solution.

3.22.20 Detection of plasma soluble myeloperoxidase (MPO) using enzyme linked immunosorbent assay.

Human myeloperoxidase (MPO) ELISA kits were procured from Thermo-Fischer Scientific™ and employed for the *in vitro* quantitation of MPO in plasma samples from patients with paradoxical TB-IRIS and TB-non-IRIS controls prior to the initiation of ART (week 0) and at week 2 on ART. The ELISA kits are a ready to use solid phase assays that are based on the sandwich principle. The assays were performed according to manufacturer's instructions. All reagents were equilibrated to ambient temperature prior to use; standards, dilution of samples, and all buffers were prepared according to the manufacturer's instructions. Briefly, a total volume of 100 µL of distilled water was added to the sample wells and 50 µL of prediluted samples (1:50) were added to the appropriate wells. Plates were sealed and subsequently incubated with gentle shaking for 3 hours at room temperature. The plates were washed four times in 400 µL of wash buffer using an automated plate washer. A total volume of 100 µL of TMB substrate was added to all the wells; the plates were sealed and incubated in the dark at ambient temperature for 10 min. The reaction was stopped by adding 100 µL of stop solution and the solution gently mixed by swirling the plates. The absorbance was determined by reading the plate in an automated plate reader at absorbance wavelength 450 nm. The data was quality checked by an independent investigator and the data analyzed by plotting concentration values.

3.23 Lactate dehydrogenase (LDH) assay

Dying cells have a compromised duplex membrane and as a result release LDH which is an enzyme that is often used as a proxy to quantify cell death. The LDH assay kit was procured from Roche technologies and contained two components-vial 1 containing the catalyst and vial 2 containing the dye solution. Vial 1 was reconstituted in 1 mL of double distilled water and allowed to equilibrate to room temperature with gentle agitation for 10 minutes. A total of 50 µL cell free supernatant for all tested conditions was seeded into a 96 well plate. Approximately 250 µL of vial 1 was mixed with 11.25 mL of vial 2 shortly before use and 100 µL of the LDH solution was added to the supernatants and incubated in the dark at room temperature for 30 minutes. Cell death was quantified by reading the plate at a wavelength of 490 nm using a BioRad colorimetric plate reader.

3.24 Statistical analyses

For analyses, samples from TB-IRIS and TB-non-IRIS groups were classified into four categories based on sample timing in relation to ART: baseline (BL) include samples

collected within seven days before or on the day of ART initiation, Week 2 (W2)-samples collected between day 1 and 14 on ART, Week 4 (W4)-samples collected between day 15 and 30 on ART, Week 6 (W6) samples collected between day 31 and 65 on ART. Paired samples were analysed using the paired Wilcoxon ranked Student T test while the Mann-Whitney U test was used to compare unpaired samples for all time points between TB-IRIS and TB-non-IRIS groups. A p-value of 0.05 or less was considered statistically significant. All statistical analyses were performed using Prism (v8.0.2, GraphPad Software Inc, San Diego, CA, USA)

3.25 Software

3.25.1. Linux command line prompt

Command-line prompt scripting was used to upload raw data to the UCT servers and process it through the nf-core rnaseq pipeline.

3.25.2. R and R-studio

R studio was used to load the processed read count data, manipulate, and visualize it using various base and third-party packages from Bioconductor, GitHub and CRAN [276].

3.25.3. Graphpad Prism

Graphpad Prism was used for importing and visualizing data

Chapter 4 summary: Phenotypic profile of Mtb-specific Interferon-gamma producing CD4 T cells in HIV-immunosuppressed patients with paradoxical TB associated immune reconstitution inflammatory syndrome.

This chapter investigated the contribution of Mtb-specific interferon-gamma producing CD4 T cells to the immunopathology of paradoxical TB associated immune reconstitution inflammatory syndrome. This is done by characterizing the frequencies and phenotype of Mtb300-specific interferon gamma producing CD4 T cells and bulk CD4 T cells in peripheral blood of patients with HIV associated TB, who developed paradoxical TB-IRIS compared to those who did not (TB-non-IRIS controls).

4. BACKGROUND

Although antiretroviral therapy (ART) has substantially reduced HIV-1 related morbidity and mortality in people with HIV(PWH) and tuberculosis (TB) [293], TB-immune reconstitution inflammatory syndrome (TB-IRIS) frequently complicates management [12, 163]. TB-IRIS has an estimated incidence of 18% across cohorts and an attributable mortality rate of 2% [294].

Two forms of TB-IRIS are recognised: 1) Unmasking TB IRIS which occurs in patients with undiagnosed TB who present with severe inflammatory features of TB during the first 3 months of ART and 2) Paradoxical TB-IRIS which occurs in patients started on TB treatment before ART who experience recurrent, new or worsening symptoms and signs of TB within the first months of initiating ART [26, 295]. The major risk factors for paradoxical TB-IRIS include a low CD4 count prior to ART initiation, higher HIV-1 viral load, a short interval between TB treatment and ART initiation and disseminated TB [89, 296].

Innate immune responses including inflammasome activation [28, 30], monocyte and natural killer cell activation [235, 297], neutrophilia [297, 298] and dysregulation of the complement system in monocytes [236] have been associated with TB-IRIS. Elevated concentrations of proinflammatory cytokines [32, 299] and matrix degrading metalloproteinases [300] have been described at TB-IRIS onset. Moreover, monocyte subset frequency and circulating inflammatory mediators can independently predict TB-IRIS [182, 301]. Expansion of pathogen-specific CD4+ T cells has been observed in association with TB-IRIS [39, 302-304]. Pathogen-specific CD4+ T cells from patients with IRIS have been reported to be highly activated [305] and polyfunctional [306]. Recently, it was reported that immunosuppressed PWH, who were coinfected with *Mycobacterium avium* complex (MAC) and subsequently developed MAC-IRIS had higher expression of Eomesodermin (Eomes) compared with Tbet in MAC-specific IFNγ+CD4+ T cells at the onset of IRIS [307]. Eomes and Tbet are members of the T-box DNA binding family of transcription factors with structural similarities and overlapping expression [308]. Eomes is involved in the development of cytotoxic T lymphocyte activity [308] while Tbet is a Th-1 lineage-defining transcription factor [309].

Th-1 responses have been implicated in a mouse model of MAC-IRIS [302, 303]. Consequently, we capitalized on the existing mouse model of IRIS to investigate phenotypic CD4 T cell features that may be associated with IRIS in mice and compare these with findings in patients developing TB-IRIS in a prospective cohort study of immunosuppressed PWH and TB, initiating ART.

4.1 Methods

4.1.1 M. avium-IRIS induction in mice

C57BL/6J-[KO] TCRalpha mice (6-8 weeks old) were intravenously infected with $1x10^6$ colony-forming units of *M. avium* (strain SmT 2151). After at least 40 days, CD4 T cells were isolated from C57BL/6, B6.129S6-Tbx21tm1Glm/J mice (The Jackson Laboratory, Bar Harbor, ME), or $eomes^{fl/fl}CD4\text{-}CRE^{+}$ uninfected mice using positively selecting microbeads (Miltenyi Biotec, Auburn, CA), and $1x10^6$ cells were intravenously transferred into chronically infected T cell deficient mice. All mice were maintained and bred at NIAID, NIH, Bethesda, MD. All animals were housed at an Association for the Assessment and Accreditation of Laboratory Animal Care-approved facility at the NIAID according to the National Research Council's Guide for the Care and Use of Laboratory Animals

4.1.2 Participants in clinical study

Samples were obtained from PWH and TB initiating ART enrolled in a prospective observational study conducted at Brooklyn Chest Tuberculosis Hospital between May 2009 and November 2010 in Cape Town, South Africa [6]. All patients were ART naïve and those with rifampicin-resistant TB were excluded. TB diagnosis was based on smear, culture or clinical diagnosis. The first TB episode was treated with standard first line regimen of rifampicin (R), isoniazid (H), pyrazinamide and ethambutol for two months followed by four months of RH regimen. In patients with subsequent episodes, streptomycin was added for 2 months. TB-IRIS was diagnosed per International Network for the Study of HIV-associated IRIS (INSHI) criteria [26]. HIV-1 treatment included lamivudine and efavirenz with stavudine or tenofovir depending on guidelines at the time.

4.1.3 Patient Consent Statement

Written informed consent was obtained from all participants. The study design was approved by the Human Research Ethics Committee (HREC : 049/2009 and 809/2018) of the University of Cape Town. Clinical and other immunological findings from this cohort have been published [6, 27, 28].

4.1.4 PBMC isolation and stimulation

PBMC were isolated by Ficoll-Hypaque density gradient centrifugation (GE Healthcare® ALC-PK121R), cryopreserved and stored. Cryopreserved PBMC were thawed and rested at 37 °C in RPMI 1640 containing 10% heat-inactivated FCS for 4 hours prior to antigen stimulation. PBMC ($2x10^6$ cells) were stimulated with a peptide pool constituted of 300 Mtb-derived peptides (Mtb300, 1.5 µg/mL) [310] in the presence of anti-CD28 and anti-CD49d antibodies (both at 1 µg/ml, BD, Franklin Lakes, New Jersey) and brefeldin-A (10 µg/ml, Sigma, St Louis, Missouri) for 6 hours. Unstimulated cells, incubated with co-stimulatory antibodies and Brefeldin A only, were used as controls.

4.1.5 Cell staining and acquisition

Samples with a cell count of less than one million or a viability score of less than 20% were excluded. After stimulation, cells were washed, stained with a viability marker (Live/Dead® Fixable Near-InfraRed marker, Invitrogen, Carlsbad, California) for 10 minutes at room temperature and subsequently surface stained with the following antibodies: CD4-PerCP-cy5.5, PD1-BV421, HLA-DR-BV605, CD14-Allophycocyanin/H7, CD19-Allophycocyanin/H7 (all from Biolegend, San Diego, California) and CD8-Alexa700 (BD, Franklin Lakes, New Jersey) for 30 minutes at room temperature. Cells were fixed and permeabilized using the eBioscience Foxp3 fixation buffer for 30 minutes at room temperature and stained with IFNγ-BV711 (Biolegend), TNFα-FITC (Biolegend), granzyme B-BV510 (BD), Eomes-eFluor 660 (e-Bioscience, San Diego, California), Tbet-PEcy7 (e-Bioscience) and CD3-BV785 (Biolegend), for 45 minutes at 4 °C. Cells were washed and resuspended in 1% formaldehyde in PBS. Samples were acquired in the BD LSRII and data were analysed using FlowJo software version 9.9.6 (BD). The gating strategy is presented in **Figure 4** below**.**

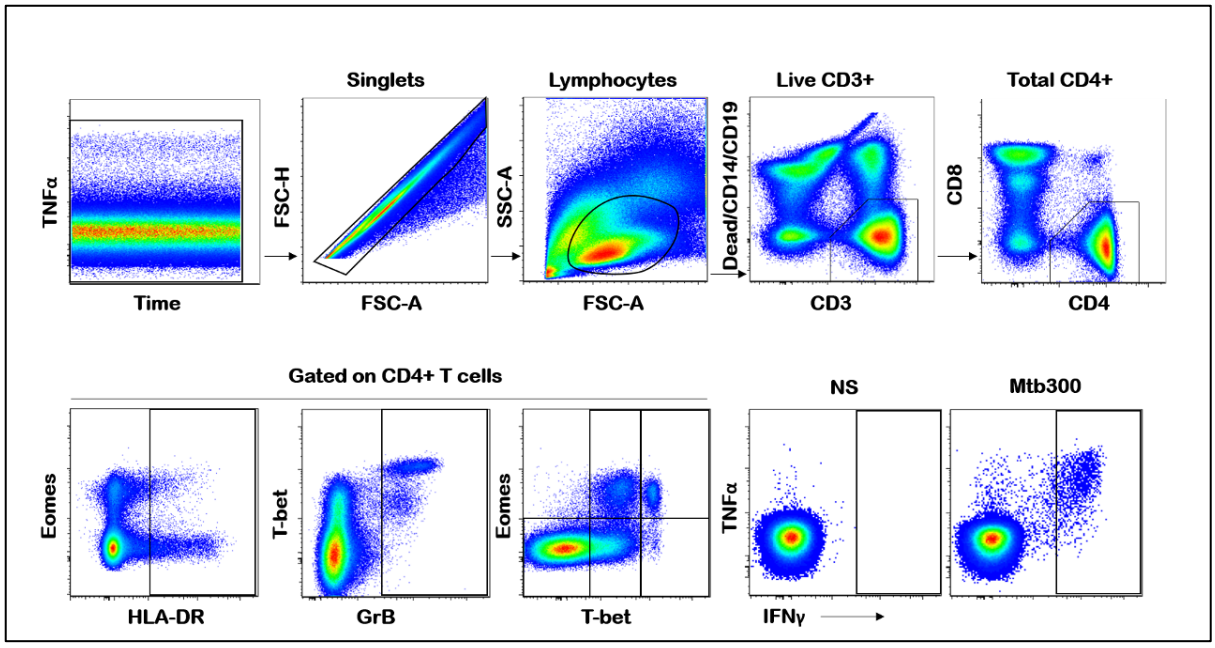

Figure 4. Representative gating strategy for the phenotypic characterization of IFNγ+CD4+ T cells. *To phenotype Mtb-specific IFNγ+CD4+ T cell responses, we gated on singlets (FSC-H vs FSC-A), lymphocytes (SSC-A vs FSC-A), live CD3+ cells(dead cells vs live CD3+) and on total CD4+ T cells.*

A positive Mtb-specific IFNγ response was defined as three-fold higher than the background measured in the presence of co-stimulatory antibodies without antigen. For the phenotypic analyses of Mtb-specific IFNγ+CD4+ T cells, only Mtb responses with more than 20 events were considered. Protocols were compliant with the guidelines for flow cytometry in immunological studies [311]. Although we analysed immunological characteristics of live cells, our cohort included 8 samples with a viability below 50% (median: 67%, [range: 96-22%]). Prior to assessing immunological phenotypic characteristics of our cohort, we ascertained whether sample viability affected immunological expression of markers (particularly Tbet and Eomes) in our cohort. There was no correlation between sample viability and the expression of Tbet and Eomes at all measured time points (data not shown).

4.1.6 Statistical analyses

For analyses, samples from TB-IRIS and non-IRIS groups were classified into four categories based on sample timing in relation to ART: Baseline (BL) include samples collected within seven days before or on the day of ART initiation, Week 2 (W2)-samples collected between

day 1 and 14 on ART, Week 4 (W4)-samples collected between day 15 and 30 on ART, Week 6 (W6) samples collected between day 31 and 65 on ART. Paired samples were analysed using the paired Wilcoxon ranked Student T test while the Mann-Whitney U test was used to compare unpaired samples for all time points between TB-IRIS and non-IRIS groups. A p-value of 0.05 or less was considered statistically significant. All statistical analyses were performed using Prism (v8.0.2, GraphPad Software Inc, San Diego, CA, USA).

4.2 RESULTS

4.2.1 Role of Eomes and Tbet in CD4 T cells during experimentally-induced IRIS

To model IRIS, T cell deficient (TCRα-/-) mice were infected with *M. avium*. This reproduced a lymphopenic host harbouring a mycobacterial infection. After 40-60 days, the mice were injected with CD4 T cells to mimic the reconstitution of T cells that occurs after ART **(Figure 4.1A)**.

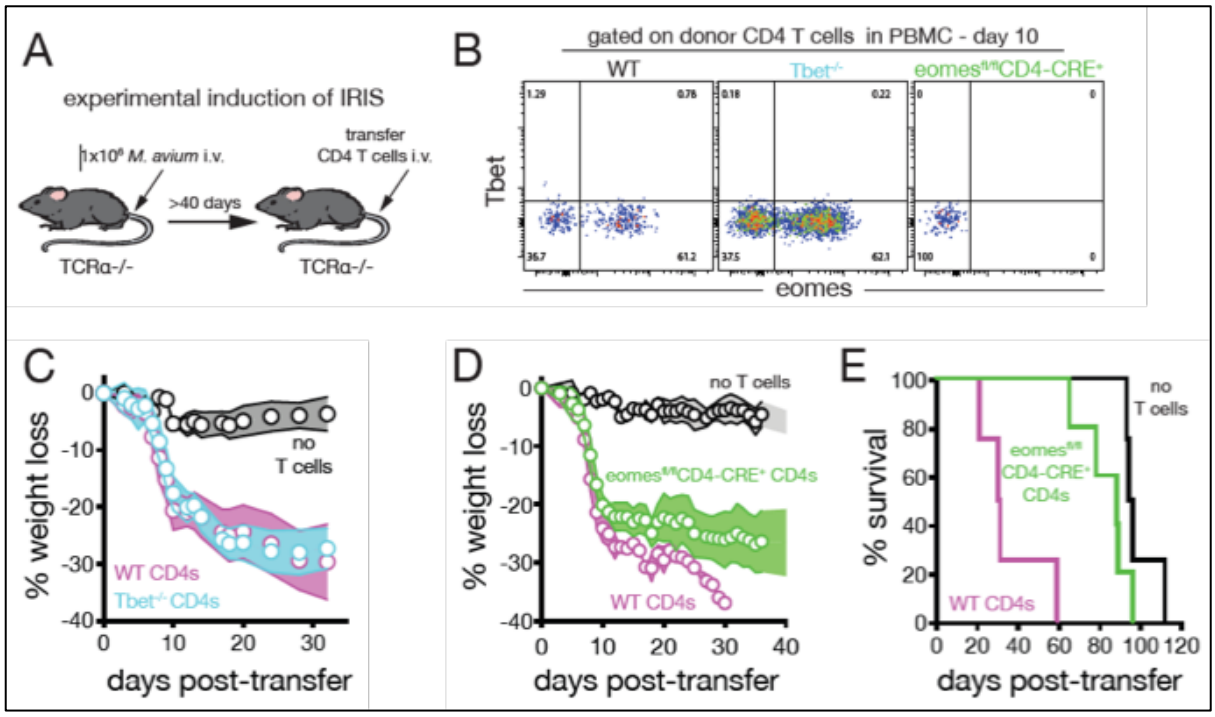

Figure 4.1. CD4 T cell expression of eomesodermin promotes mycobacterial IRIS in a murine model. ***A****. To model IRIS in mice, TCRα-/- mice harboring a chronic M. avium infection were injected with purified CD4 T cells from uninfected donor mice.* ***B****. M. avium infected TCRα-/- mice were injected with WT, Tbet-deficient or eomes-deficient CD4 T cells. The donor CD4 T cells (CD4+TCRβ+CD3+) were analyzed in the PBMC on day 10 post infection for the expression of Tbet and eomesodermin (plots are concatenated from n=8 mice/group).* ***C****. M. avium infected TCRα-/- mice were injected with either WT or Tbet-deficient CD4 T cells and monitored for weight loss (n=5 mice/group).* ***D.*** *M. avium infected TCRα-/- mice were injected with no T cells, WT or eomes-deficient CD4 T cells and monitored for weight loss.* ***E.*** *Survival of mice receiving WT or eomes-deficient CD4 T cells. n=4 to 5 mice/group. Error bars represent the standard deviation. Data are representative of at least 4 independent experiments each.*

To examine the expression of Eomes and Tbet in CD4+ T cells and their potential involvement in the murine model of IRIS, we injected mice with WT, Tbet$^{-/-}$, and Eomes deficient CD4 T cells and examined the donor CD4 T cells ten days post injection. We found that during murine IRIS, CD4 T cells surprisingly expressed little Tbet. Instead, a significant population of Eomes+ CD4+ T cells was observed **(Figure 4.1B)**. WT and Tbet$^{-/-}$ CD4+ T cells induced similar levels of weight loss **(Figure 4.1C)**. In contrast, recipients of Eomes deficient CD4+ T cells displayed less weight loss and longer survival compared to mice injected with WT CD4+ T cells **(Figure 4.1D, E)**. We concluded that, CD4+ T cells utilize Eomes but not Tbet, to drive *M. avium* IRIS in this animal model. These findings prompted us to next examine the role of Eomes expressing CD4+ T cells in human TB-IRIS.

4.2.2 Clinical characteristics of the cohort

Sufficient samples for immunological analyses were available for 43 HIV-1 infected inpatients being treated for TB when starting ART: 25 patients developed TB-IRIS and 18 patients did not (non-IRIS controls). The demographic and clinical characteristics of the two groups are summarized in **Table 4**.

Table 4. Clinical characteristics of patients who developed tuberculosis immune reconstitution inflammatory syndrome (TB-IRIS, n=25) and those who did not (non-IRIS, n=18). *TB: Tuberculosis, PTB: pulmonary TB , EPTB: extrapulmonary TB, IQR: interquartile range, ART: antiretroviral treatment, Hb: hemoglobin. The Wilcoxon rank sum test was used*

to compare all continuous variables and the Mann-Whitney test was used to compare categorical variables.

	TB-IRIS (n=25)	Non-IRIS (n=18)	p-value
Age [Median (IQR)] (years)	34 (22-52)	33 (24-55)	ns
Female sex [n (%)]	13 (52%)	12 (66%)	
Previous TB [n (%)]	15 (60%)	10 (55%)	
TB type [n (%)]			
PTB	4 (16%)	2 (11%)	
EPTB	4 (16%)	5 (27%)	
EPTB and PTB	17 (68%)	11 (61%)	
TB meningitis/neuroTB [n (%)]	7 (23%)	4 (21%)	
TB confirmation [n (%)]			
Cultured Mtb	9 (36%)	6 (33%)	
Smear	6 (24%)	2 (11%)	
Clinicoradiological	10 (40%)	10 (55%)	
Hb [Median (IQR)] (g/dL)	9.1 (6.4-13)	9.4 (5.9-14.0)	ns
CD4 nadir [Median (IQR)]	49 (11-209)	70 (4-272)	ns
CD4 count (cells/mm^3) at week 0 [Median (IQR)]	68 (21-521)	111 (4-662)	**0.009**
CD4 count (cells/mm^3) at week 4 [Median (IQR)]	164 (23-556)	276 (21-514)	ns
Log_{10} HIV VL at week 0 [Median (IQR)]	5.73 (3.96-7.78)	5.8 (4.21-7.15)	ns
Log_{10} HIV VL at week 4 [Median (IQR)]	2.72 (0-3.88)	2.68 (1.32-3.3)	ns
Duration TB treatment to ART [Median (IQR)] (days)	37 (14-99)	32 (13-91)	ns
Duration ART to TB-IRIS [Median (IQR)] (days)	15 (4-49)		
On steroid treatment at week 0 [n (%)]	7 (28)	4 (22)	ns

In both groups, over three-quarters of patients had evidence of extrapulmonary TB and around 20% had neurological TB, a common reason for TB patients in South Africa to be admitted to a TB hospital. Notably, 7/25 (28%) of TB-IRIS and 4/18 (22%) of non-IRIS patients were on treatment with corticosteroids at the time of starting ART, the most frequent indication being neurological TB. We previously demonstrated that corticosteroid therapy had no significant effect on the frequency of Mtb-specific CD4 T cells [33]. The median CD4 count at the start of ART was lower in TB-IRIS patients (median: 68 cells/mm^3) compared with non-IRIS patients (median 111 cells/mm^3) (p=0.009). The median duration of TB treatment before initiation of ART was similar for the groups (median 37 days in TB-IRIS versus 32 days in non-IRIS patients). The duration of ART prior to developing TB-IRIS symptoms was a median of 15 days. Additional clinical data is presented in **Table 4.1.**

***Table 4.1**. Individual patient duration to first TB-IRIS episode, symptom manifestation and steroid management. Different patients were on different combination of ART regimen including Stavudine (D4T), Lamivudine (3TC), Efavirenz (EFZ), Zidovudine (AZT) and Tenofovir (TDF).*

IRIS patient Identifier	ART regimen	Duration ART Start to TB-IRIS (days)	TB-IRIS system involvement	Steroids to Treat TB-IRIS	Duration from TB-IRIS onset to starting steroids (days)
IR 4011-3	D4T, 3TC, EFZ	6	Pulmonary, nodal, effusion and abdominal	Yes	9
IR 4035-1	AZT, 3TC, EFZ	42	Nodal, abdominal	No	
IR 4074-8	TDF, 3TC, EFZ	10	Pulmonary, nodal	Yes	5
IR 4071-5	TDF, 3TC, EFZ	8	Pulmonary, effusion, abdominal	No	
IR 4075-9	D4T, 3TC, EFZ	12	Abdominal	Yes	na
IR 4076-0	TDF, 3TC, EFZ	9	Nodal	No	
IR 4081-7	TDF, 3TC, EFZ	10	Abdominal	No	
IR 4108-1	TDF, 3TC, EFZ	9	Pulmonary, abdominal	No	
IR 4018-0	D4T, 3TC, EFZ	13	Pulmonary	Yes	4
IR 4020-4	D4T, 3TC, EFZ	30	Nodal	Yes	13
IR 4047-5	D4T, 3TC, EFZ	8	Pulmonary, abdominal	Yes	5
IR 4110-5	D4T, 3TC, EFZ	4	Pulmonary, abdominal	No	
IR 4052-2	TDF, 3TC, EFZ	13	Pulmonary, abdominal	No	
IR 4078-2	TDF, 3TC, EFZ	26	Neurological, pulmonary, abdominal	Yes	20
IR 4096-4	TDF, 3TC, EFZ	14	Pulmonary, abdominal	No	
IR 4115-0	AZT, 3TC, EFZ	26	Pulmonary	Yes	16
IR 4010-2	D4T, 3TC, EFZ	7	Nodal, abdominal	Yes	56
IR 4015-7	D4T, 3TC, EFZ	15	Pulmonary, abdominal	Yes	20
IR 4021-8	D4T, 3TC, EFZ	5	Pulmonary	Yes	2
IR 4036-2	D4T, 3TC, EFZ	7	Nodal, neurological	Yes	1
IR 4080-6	TDF, 3TC, EFZ	11	Neurological	Yes	na
IR 4085-1	TDF, 3TC, EFZ	14	Articular	Yes	na
IR 4088-4	TDF, 3TC, EFZ	49	Neurological	Yes	9
IR 4095-3	TDF, 3TC, EFZ	12	Pulmonary, abdominal	Yes	3
IR 4111-6	TDF, 3TC, EFZ	8	Abdominal	Yes	8

4.2.3 Expansion of Mtb-specific CD4+ T cells at TB-IRIS onset

For phenotypic analyses, we first compared the magnitude of Mtb-specific IFNγ+CD4+ T cell responses between the patient groups before the initiation of ART (Baseline), at week 2, 4 and 6 on ART. Representative examples of IFNγ production by CD4+ T cells following Mtb300 stimulation are presented in **Figure 4.2A**.

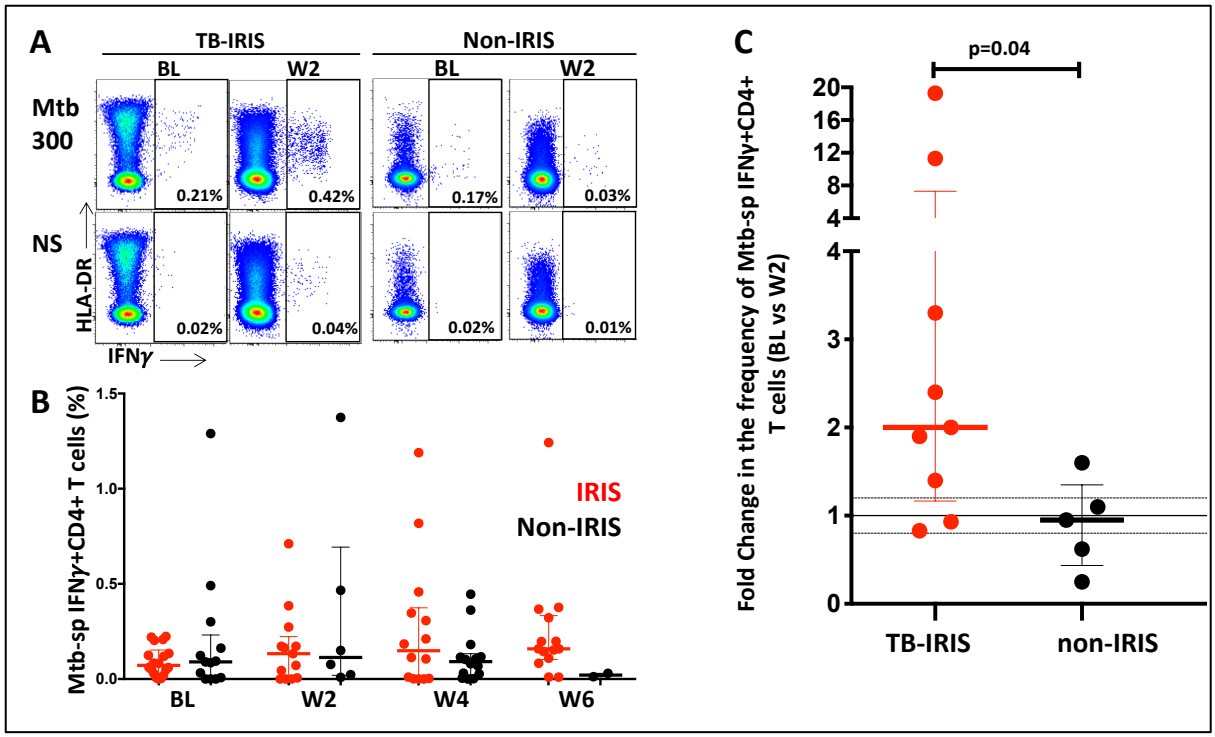

Figure 4.2. Frequencies of Mtb-specific IFNγ+CD4+ T cells in TB-IRIS and non-IRIS patients. ***A****, Representative flow plots of IFNγ production in response to Mtb peptide pool (Mtb300) and non-stimulated controls (NS) at baseline (BL, prior to initiation of antiretroviral therapy, ART) and 2 weeks on ART (W2).* ***B****, Frequencies of IFNγ producing CD4+ T cells in TB-IRIS (red) from baseline (BL, n= 16), through 2 weeks (W2, n= 9), 4 weeks (W4, n= 10) and 6 weeks (W6, n=12) and non-IRIS (black) from BL= 11, through W2, n= 4, W4, n= 8 and W6, n= 1 on ART.* ***C****, Fold change in the frequency of IFNγ+CD4+ T cells in TB-IRIS and non-IRIS patients between baseline (prior to ART) and 2 weeks on ART. The Wilcoxon ranked test was used for the statistical comparison of paired samples and the Mann-Whitney-U test was used for unpaired samples. Only statistically significant data with a p value of 0.05 or less are indicated on graphs.*

We observed no differences in the frequency of Mtb-specific IFNγ+CD4+ T cells between the two groups in cross-sectional comparisons at any time point **(Figure 4.2B)**. However, the fold change in Mtb-specific IFNγ+CD4+ T cell frequency between baseline and week 2 was significantly higher in the TB-IRIS group compared to the non-IRIS group (median fold change: 1.9 [IQR: 0.83-19.3]) and 0.9 [IQR: 0.25-1.6], respectively, p=0.04) **(Figure 4.2C)**. This significant increase was exclusively observed in TB-IRIS patients between baseline

(median: 0.08% [IQR: 0.0-0.2]) and 2 weeks on-ART (median: 0.13% [IQR: 0.0-0.71]) (p=0.039) **(Figure 4.3)**.

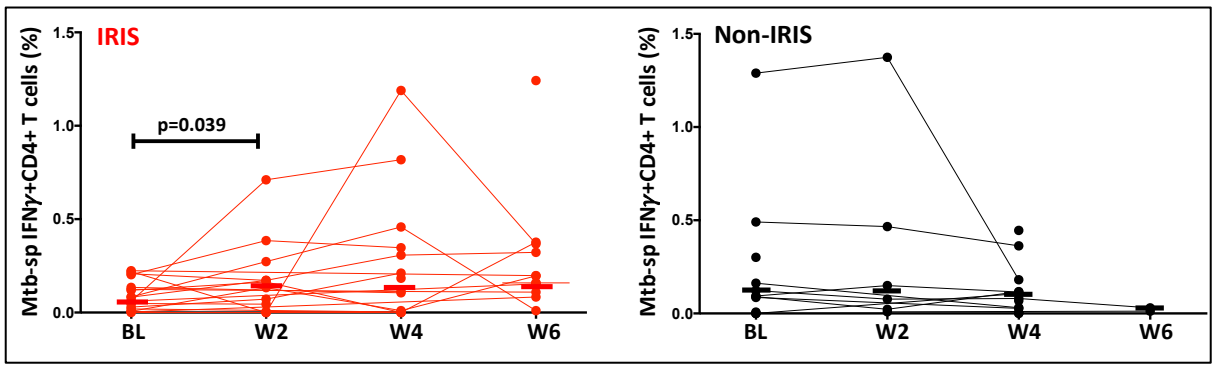

Figure 4.3. Frequencies of IFNγ producing CD4+ T cells in response to Mtb peptide pool (Mtb300) stimulation in TB-IRIS (red) at baseline (BL, n= 16), 2 weeks (W2, n= 9), 4 weeks (W4, n= 10) and 6 weeks (W6, n=12) and non-IRIS (black) at BL= 11, W2, n= 4, W4, n= 8 and W6, n= 1 after ART initiation. *The Wilcoxon ranked test was used for all statistical comparisons. Only statistically significant data with a p value of 0.05 or less are indicated on graphs.*

We next investigated the phenotype of Mtb-specific IFNγ+CD4+ T cell that could potentially characterise the role of these cells in the pathogenesis of TB-IRIS in humans.

4.2.4 No differences in the expression of Eomes or Tbet between patients with and without TB-IRIS at any tested time point

Based on our mouse model data and a recent report by Hsu *et al*. reporting that Eomes was significantly upregulated over Tbet in MAC-specific IFNγ+CD4 T cells of MAC-IRIS patients at disease onset [307], we determined whether these transcription factors were differentially expressed between TB-IRIS and non-IRIS patients.

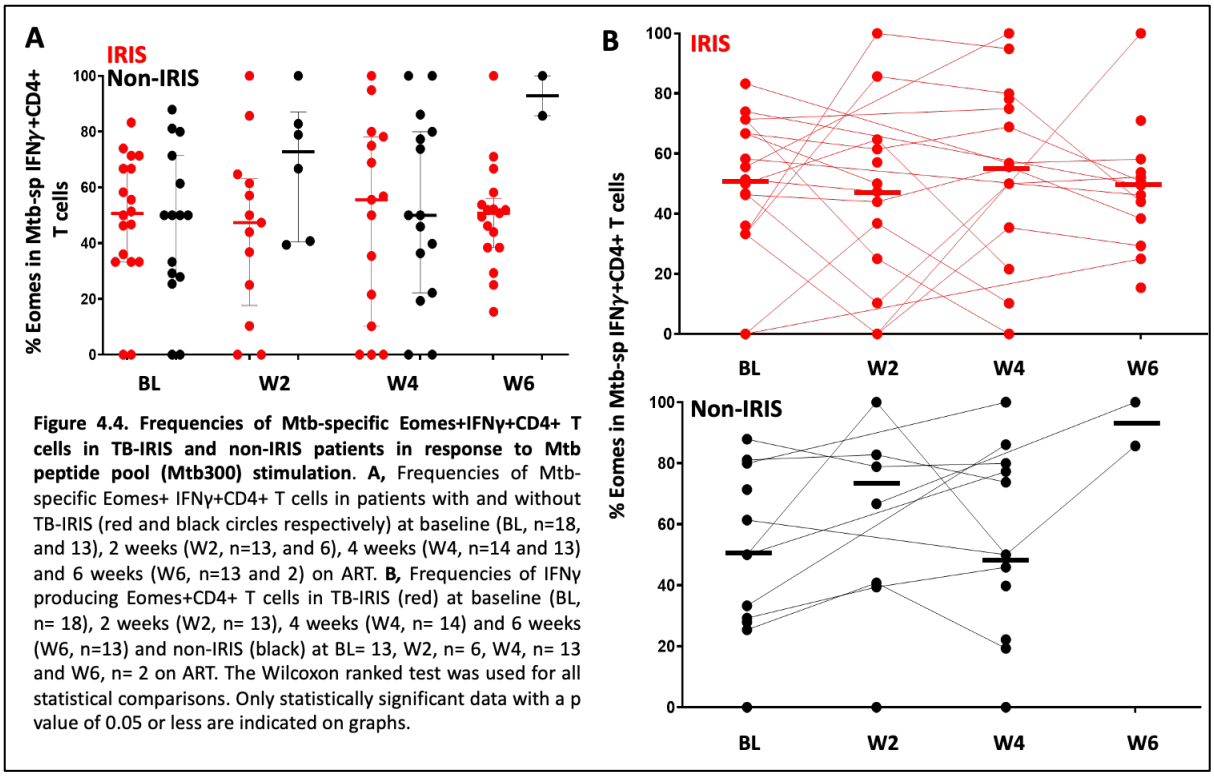

Figure 4.4. Frequencies of Mtb-specific Eomes+IFNγ+CD4+ T cells in TB-IRIS and non-IRIS patients in response to Mtb peptide pool (Mtb300) stimulation. A, Frequencies of Mtb-specific Eomes+ IFNγ+CD4+ T cells in patients with and without TB-IRIS (red and black circles respectively) at baseline (BL, n=18, and 13), 2 weeks (W2, n=13, and 6), 4 weeks (W4, n=14 and 13) and 6 weeks (W6, n=13 and 2) on ART. **B,** Frequencies of IFNγ producing Eomes+CD4+ T cells in TB-IRIS (red) at baseline (BL, n= 18), 2 weeks (W2, n= 13), 4 weeks (W4, n= 14) and 6 weeks (W6, n=13) and non-IRIS (black) at BL= 13, W2, n= 6, W4, n= 13 and W6, n= 2 on ART. The Wilcoxon ranked test was used for all statistical comparisons. Only statistically significant data with a p value of 0.05 or less are indicated on graphs.

We observed no differences in the frequency of Mtb-specific IFNγ+Eomes+CD4+ T cells between the two clinical groups at baseline or any time point on ART (**Figure 4.4**).

Eomes and Tbet expression in Mtb-specific IFNγ+CD4 T cells were highly variable between patients but not statistically different between the two groups at baseline **(Figure 4.5)** or any other time point (data not shown). The expression of Eomes in Mtb-specific IFNγ+CD4 T cells at baseline was approximately 50% and was comparable between the two groups (**Figure 4.5B)**.

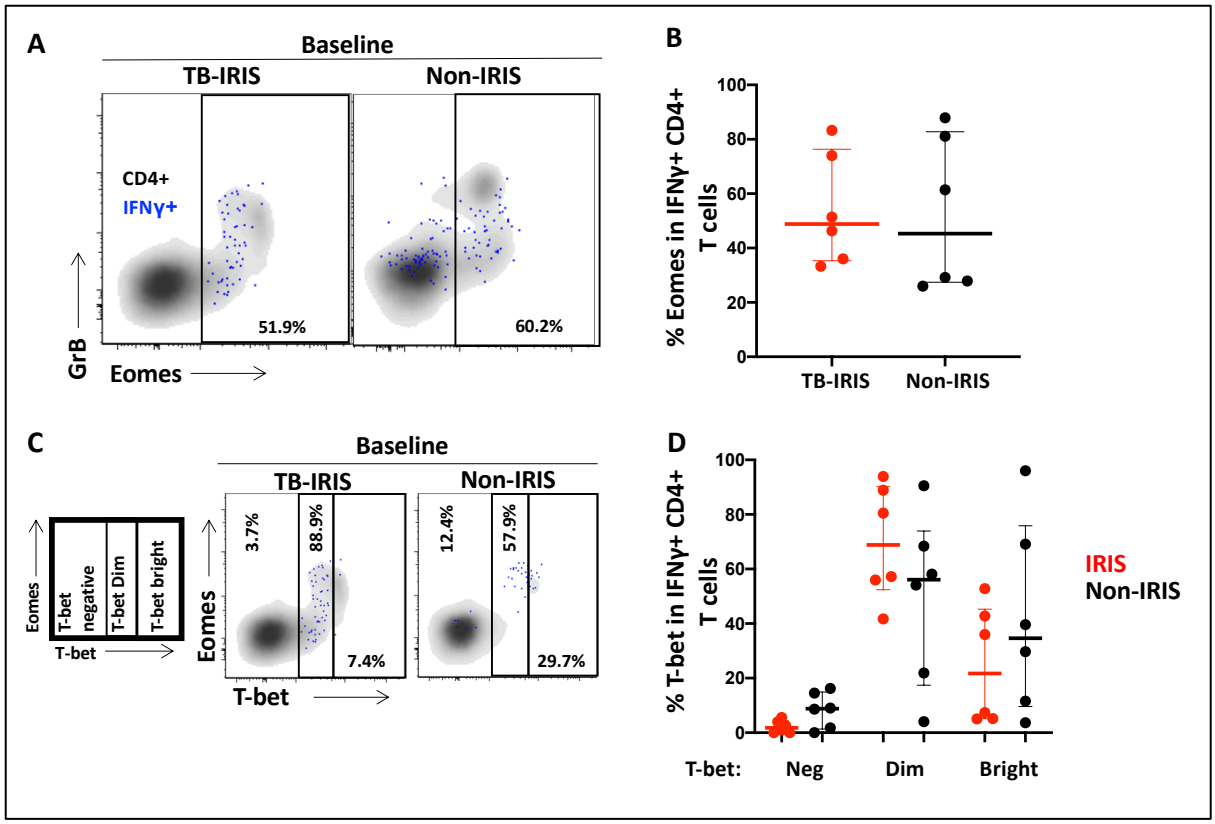

Figure 4.5. Eomes and T-bet expression on Mtb-specific IFNγ+CD4+ T cells in patients with and without TB-IRIS prior to initiation of antiretroviral therapy (ART) (BL). A, *Representative flow plot of the expression of Eomes on Mtb-specific IFNγ+CD4+ T cells (red) and total CD4+ T cells (black) in one TB-IRIS and one non-IRIS patient at BL.* ***B,*** *Summary plot of Eomes expression in Mtb-specific IFNγ+CD4+ T cells between TB-IRIS (n= 6) and non-IRIS patients (n= 6) at BL.* ***C,*** *Representative flow plot of the expression of differentiated T-bet subpopulations on Mtb-specific IFNγ+CD4+ T cells (red) and total CD4+ T cells (black) in one TB-IRIS and one non-IRIS patient at baseline.* ***D,*** *Summary plot of the T-bet expression in Mtb-specific IFNγ+CD4+ T cells between TB-IRIS (n= 6) and non-IRIS patients (n= 6) at BL. The Wilcoxon ranked test was used for all statistical comparisons. Only statistically significant data with a p value of 0.05 or less are indicated on graphs.*

Similarly, Tbet expression in Mtb-specific IFNγ+CD4+ T cells was comparable between TB-IRIS and non-IRIS groups; approximately 60% of cells expressed intermediate levels of Tbet (Tbet dim, Tbet+) and 25% expressed high Tbet levels at baseline **(**Tbet high, Tbet++, **Figure 4.5.C&D)**. Furthermore, Eomes expression on total CD4+ T cells in TB-IRIS patients was comparable to non-IRIS controls at all-time points **(Figure 4.6A&B)**.

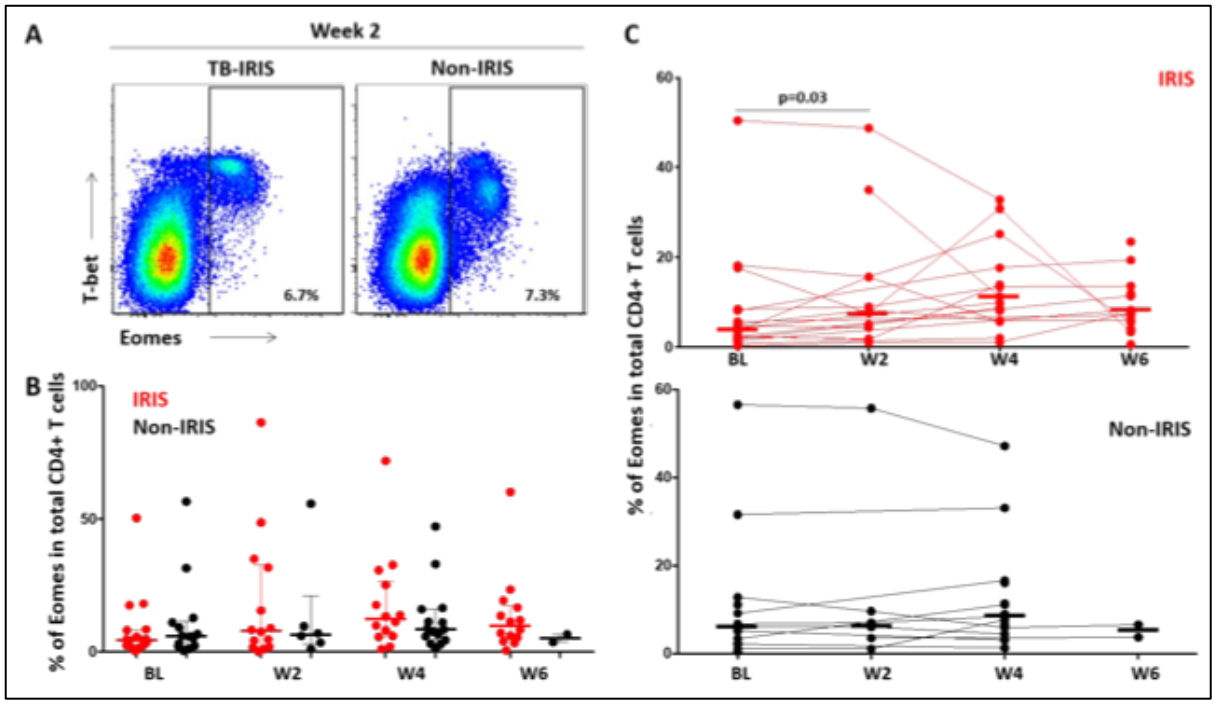

Figure 4.6. Eomes expression in total CD4+ T cells in patients with and without TB-IRIS*.A, Representative flow plot of Eomes expression in one patient with TB-IRIS and one non-IRIS patient in total CD4+ T cells two weeks post ART initiation.* ***B,*** *Cross sectional analyses of Eomes expression in total CD4+ T cells in patients with and without TB-IRIS at baseline (BL, n=18, and 13, respectively), 2 weeks (W2, n=13, and 6), 4 weeks (W4, n=14 and 13) and 6 weeks (W6, n=13 and 2) post-ART.* ***C,*** *Longitudinal analyses of the expression of Eomes in total CD4+ T cells in patients with TB-IRIS (top panel) and non-IRIS controls (bottom panel) from BL to 6 weeks post ART. The Wilcoxon ranked test was used for all statistical comparisons. Only statistically significant data with a p value of 0.05 or less are indicated on graphs.*

However, we did observe a modest increase in the frequency of CD4+ T cells expressing Eomes between baseline and week 2 (which corresponds to IRIS onset) in TB-IRIS patients (medians: 4.48% vs 7.6%, respectively, p=0.03). This was not observed in non-IRIS controls **(Figure 4.6C).** Previous studies have reported a higher frequency of both *M. avium* and Mtb-specific effector memory CD4 T cells in unmasking and paradoxical TB-IRIS patients compared to non-IRIS patients [305, 312]. Furthermore, a positive correlation between CD4+ T cell memory and Eomes expression is well established [308]. Therefore, it is possible that

the increase in Eomes expression observed in total CD4 T cells could be related to an expansion of effector cells.

Finally, Tbet expression on total CD4+ T cells was comparable between TB-IRIS and non-IRIS patients at baseline with no significant differences observed longitudinally on ART (data not shown).

In further analyses, we defined the co-expression of Eomes and Tbet, identifying five Eomes/Tbet subsets: Eomes-Tbet-, Eomes-Tbet+, Eomes+Tbet+, Eomes-Tbet++ and Eomes+Tbet++, as previously described [313] (**Figure 4.7A**). The distribution of these subpopulations within Mtb-specific IFNγ+CD4+ T cells was comparable between TB-IRIS and non-IRIS groups prior to ART initiation (i.e. baseline) **(Figure 4.7B)** and longitudinally on ART (data not shown).

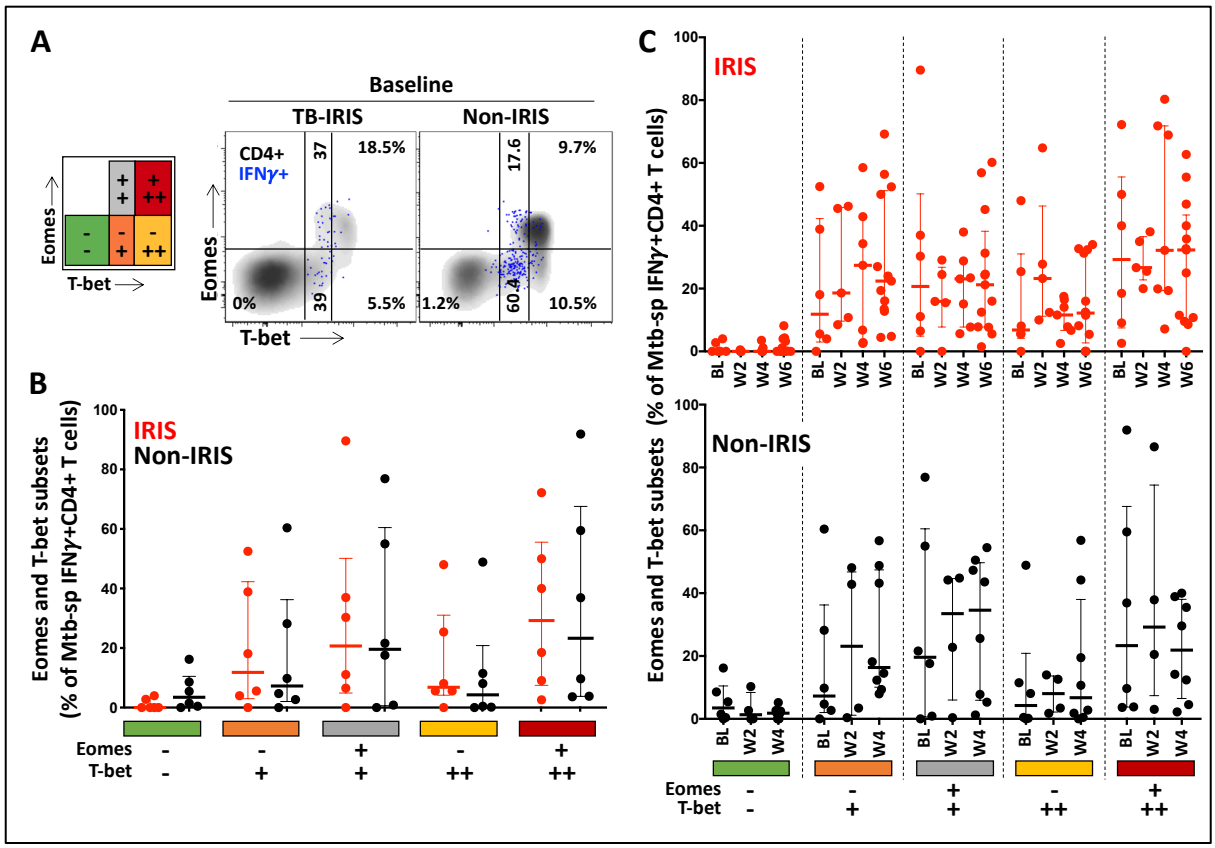

Figure 4.7. Eomes and T-bet expression profile in Mtb-specific IFNγ+CD4+ T cells in TB-IRIS and non-IRIS patients. ***A****, Representative flow plot of Eomes and T-bet expression on Mtb-specific IFNγ+CD4+ T cells (red) and total CD4+ T cells (black) in one TB-IRIS and one non-IRIS patient prior to ART initiation (BL).* ***B****, Distribution of Mtb-specific IFNγ+CD4+ T*

cells amongst distinct Eomes and T-bet subsets: (Eomes- T-bet-; Eomes- T-bet+; Eomes+ T-bet+; Eomes- T-bet++; Eomes+ T-bet++) in TB-IRIS (red, n= 6) and non-IRIS patients (black, n= 6) at BL. ***C****, Evolution of Eomes and T-bet profile in Mtb-specific IFNγ+CD4+ T cells in TB-IRIS from BL, (n= 6), through 2 weeks (W2, n= 5), 4 weeks (W4, n= 7) and 6 weeks (W6, n= 13) and non-IRIS patients (black) from BL, (n= 6), through 2 weeks (W2, n= 4) and 4 weeks (W4, n= 8) on-ART. The Wilcoxon ranked test was used for the statistical comparison of paired samples and the Mann-Whitney-U test was used for unpaired samples. Only statistically significant data with a p value of 0.05 or less are indicated on graphs.*

No significant changes in the distribution of Eomes and Tbet in Mtb-specific IFNγ+CD4+ T cells were observed over time within the two groups (**Figure 4.7C**).

However, in total CD4+ T cells there was a significant reduction in Eomes-Tbet- CD4+ T cells between baseline (median: 79.0%, IQR: 21.2-93.1) and week 2 (median: 65.5%, IQR: 15.3-84.4) (p=0.02) and baseline and week 4 (median: 54.5%, IQR: 21.8-94.5) (p=0.009) in TB-IRIS patients. These changes were countered by a progressive and significant increase in the proportion of Eomes-Tbet+ and Eomes+Tbet+ CD4+ T cells over the first 6 weeks of ART in TB-IRIS patients.

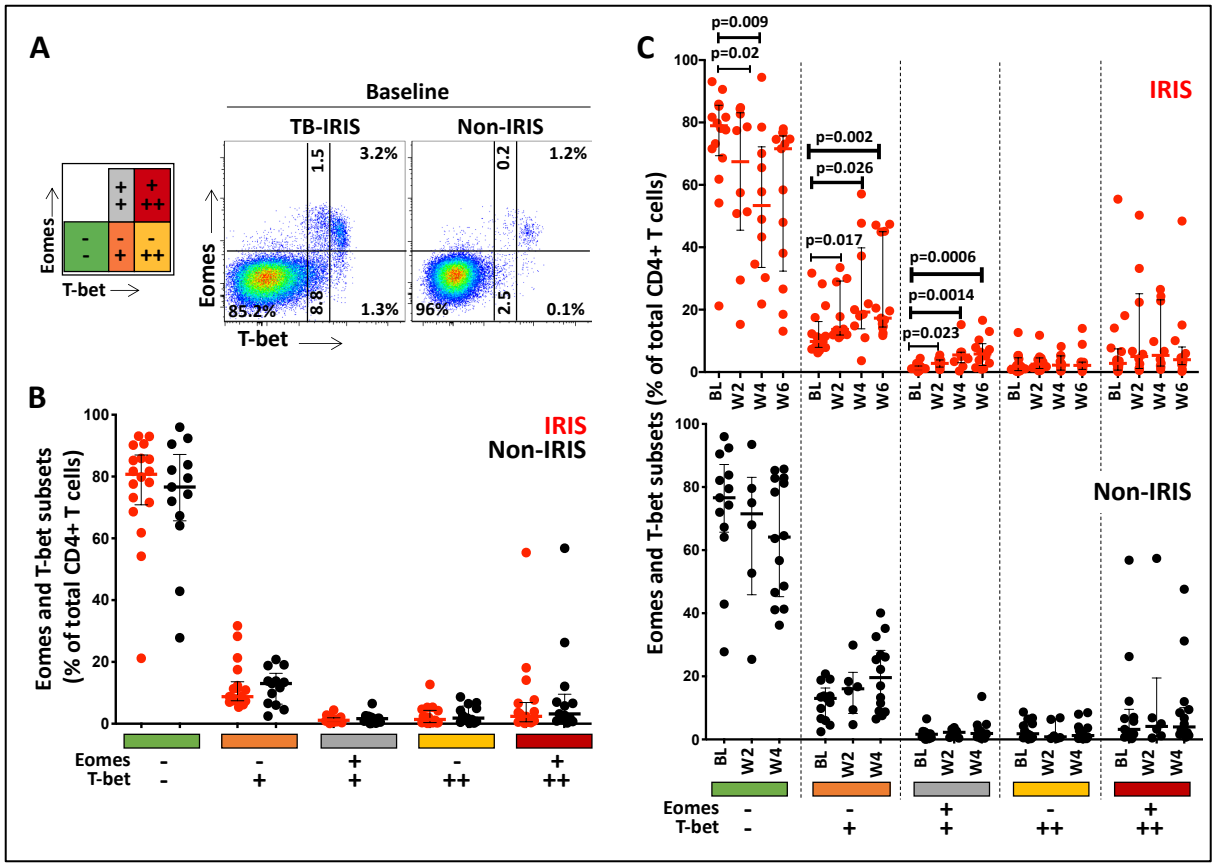

Figure 4.8. Eomes and T-bet co-expression in total CD4+ T cells in patients with and without TB-IRIS*. **A,** Representative flow plot of Eomes and T-bet co-expression in one patient with TB-IRIS and one non-IRIS patient in total CD4+ T cells two weeks on ART initiation. **B,** Cross sectional analyses of Eomes and T-bet co-expression in total CD4+ T cells in patients with and without TB-IRIS at baseline (BL, n=18, and 13, respectively), 2 weeks (W2, n=13, and 6), 4 weeks (W4, n=14 and 13) and 6 weeks (W6, n=13 and 2) on ART. **C,** Longitudinal analyses of the co-expression of Eomes and T-bet in total CD4+ T cells in patients with TB-IRIS (top panel) and non-IRIS controls (bottom panel) from BL to 6 weeks on ART. The Wilcoxon ranked test was used for all statistical comparisons. Only statistically significant data with a p value of 0.05 or less are indicated on graphs.*

Conversely, no changes over time were observed in the distribution of any of the Eomes/Tbet subsets in non-IRIS patients (**Figure 4.8C**).

4.2.5 Elevated HLA-DR expression at the time of TB-IRIS onset compared to non-IRIS controls

To further characterise the phenotype of Mtb-specific IFNγ+CD4+ T cell responses, we compared the activation profile (HLA-DR) and cytotoxic potential (Granzyme B) between TB-IRIS patients and non-IRIS controls. We observed high pre-ART HLA-DR expression in TB-IRIS (median: 71, [IQR: 45-78]) compared to non-IRIS patients (median: 39, [IQR: 23-58]), however, this was not statistically significant (p=0.18). Responses were characterized by a significantly higher expression of HLA-DR in TB-IRIS compared to non-IRIS patients at 2 weeks on ART (median: 79.3% [IQR: 66-96] and 40.9% [IQR: 27-56], respectively, p=0.016) **(Figure 4.9A&B)**.

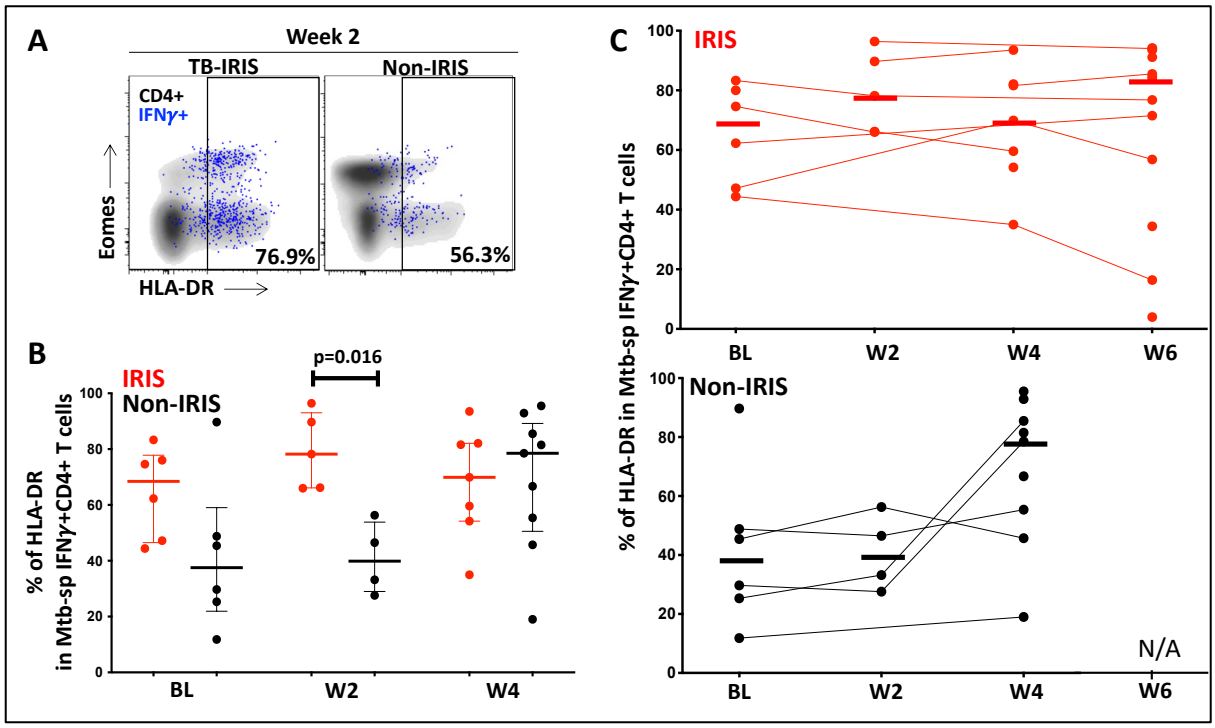

Figure 4.9. HLA-DR expression on Mtb-specific IFNγ+CD4+ T cells in TB-IRIS and non-IRIS patients*A, Representative flow plot of HLA-DR expression on Mtb-specific IFNγ+CD4+ T cells (red) and total CD4+ T cells (black) in one TB-IRIS and one non-IRIS patient at two weeks post ART initiation (W2).* ***B****, Expression of HLA-DR on Mtb-specific IFNγ+CD4+ T cells in TB-IRIS (red) from baseline (BL, n= 6), through 2 weeks (W2, n= 5), 4 weeks (W4, n= 7) and 6 weeks (W6, n= 13) and non-IRIS patients (black) from baseline (BL, n= 6), through 2 weeks (W2, n= 4), and 4 weeks (W4, n= 8) on-ART.* ***C****, Frequency of HLA-DR on Mtb-specific IFNγ+CD4+ T cells from baseline to 6 weeks on ART in TB-IRIS and non-IRIS patients. The Wilcoxon ranked test was used for the statistical comparison of paired samples and the Mann-*

Whitney-U test was used for unpaired samples. Only statistically significant data with a p value of 0.05 or less are indicated on graphs.

No significant changes over time were observed when data were analysed longitudinally for both groups respectively **(Figure 4.9C)**. However, we observed an increase in HLA-DR expression in total CD4+ T cells in TB-IRIS patients between baseline and week 2 (p=0.002) and week 4 (p=0.0005) and non-IRIS patients between baseline and week 4 (p=0.0098) **(Figure 4.10)**.

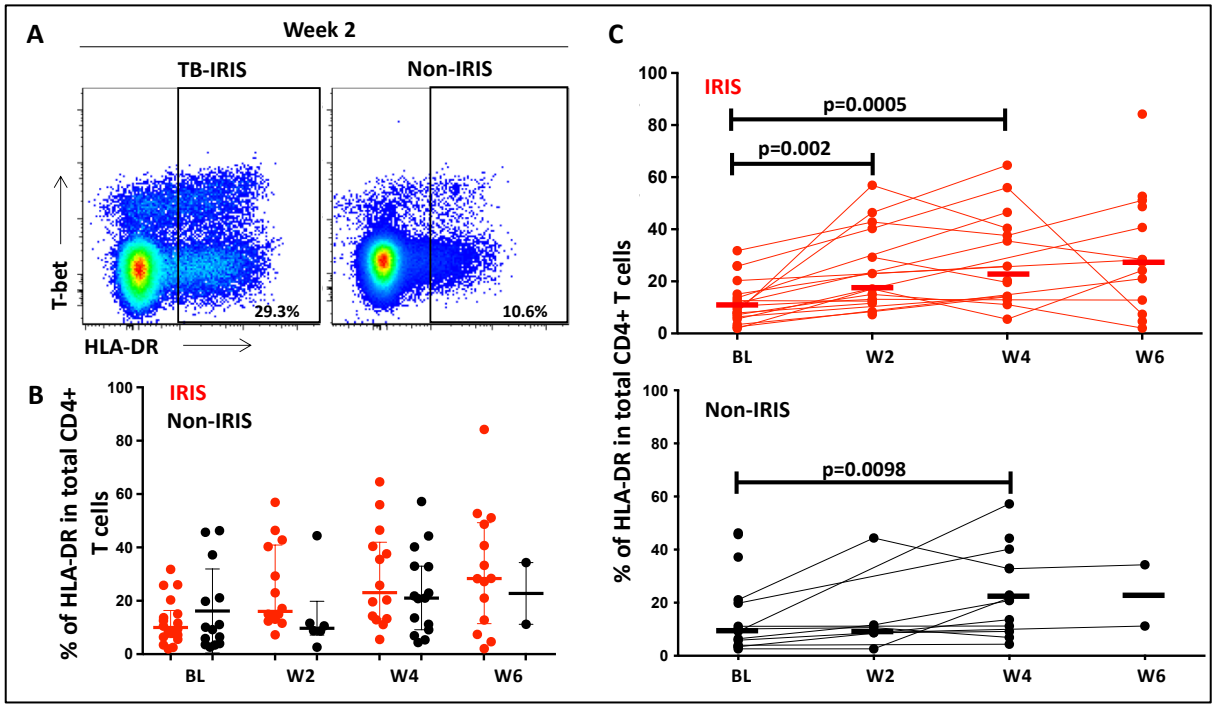

Figure 4.10. HLA-DR expression in total CD4+ T cells in patients with and without TB-IRIS. ***A,*** *Representative flow plot of HLA-DR expression in one patient with TB-IRIS and one non-IRIS patient in total CD4+ T cells two weeks post ART initiation.* ***B,*** *Cross sectional analyses of HLA-DR expression in total CD4+ T cells in patients with and without TB-IRIS at baseline (BL, n=18, and 13, respectively), 2 weeks (W2, n=13, and 6), 4 weeks (W4, n=14 and 13) and 6 weeks (W6, n=16 and 2) post-ART.* ***C,*** *Longitudinal analyses of the expression of HLA-DR in total CD4+ T cells in patients with TB-IRIS from BL, n= 18, W2, n= 13, W4, n= 14, W6, n= 13 and non-IRIS controls, BL, n= 13, W2, n= 6, W4, n= 13 and W6, n= 2 post*

ART. The Wilcoxon ranked test was used for all statistical comparisons. Only statistically significant data with a p value of 0.05 or less are indicated on graphs.

4.2.6 Elevated HLA-DR and granzyme B expression in Mtb-specific CD4 T cells co-expressing Eomes and Tbet in patients with TB-IRIS compared to non-IRIS controls

Finally, we investigated the activation and cytotoxic potential of Mtb-specific IFNγ+CD4+ T cells in relation to their transcription factor profile at the time of IRIS onset (Week 2).

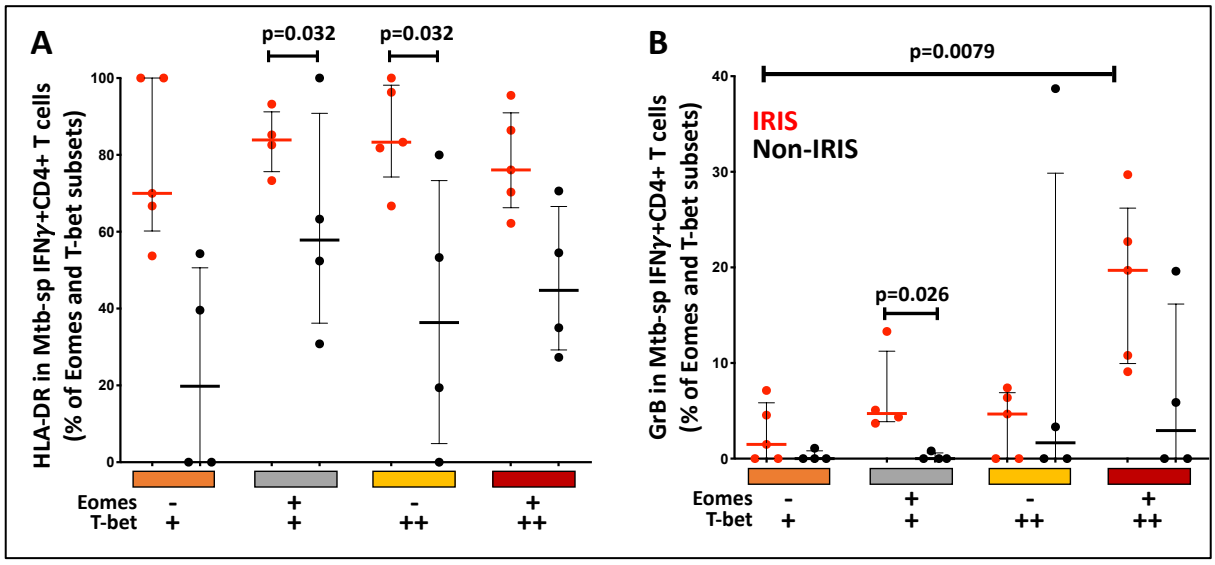

Figure 4.11. Expression of HLA-DR and granzyme B on Eomes and T-bet expressing subsets of Mtb-specific IFNγ+CD4+ T cells two weeks on ART. A*, Expression of HLA-DR and* ***B****, granzyme B on Eomes and T-bet subsets (Eomes-, T-bet+, Eomes+, T-bet+, Eomes-, T-bet++ and Eomes+, T-bet++) of Mtb-specific IFNγ+CD4+ T cells in TB-IRIS (red, n= 5), and non-IRIS patients (black, n= 4), 2 weeks on ART. The Mann-Whitney-U test was used for statistical comparison of unpaired samples. Only statistically significant data with a p value of 0.05 or less are indicated on graphs.*

While HLA-DR expression was comparable across the different Eomes and Tbet subsets in both groups, HLA-DR expression was higher in TB-IRIS compared with non-IRIS patients in specific Eomes/Tbet subsets, including Eomes+Tbet+ (median: 83.9% vs 57.9%, respectively;

p=0.032) and Eomes- Tbet++ (median: 83.3% vs 36.4%, respectively; p=0.032) (**Figure 4.11A**).

Notably, no differences in Granzyme B expression were observed in IFNγ+CD4 T cells between the two groups in cross-sectional comparisons **(Figure 4.12)**.

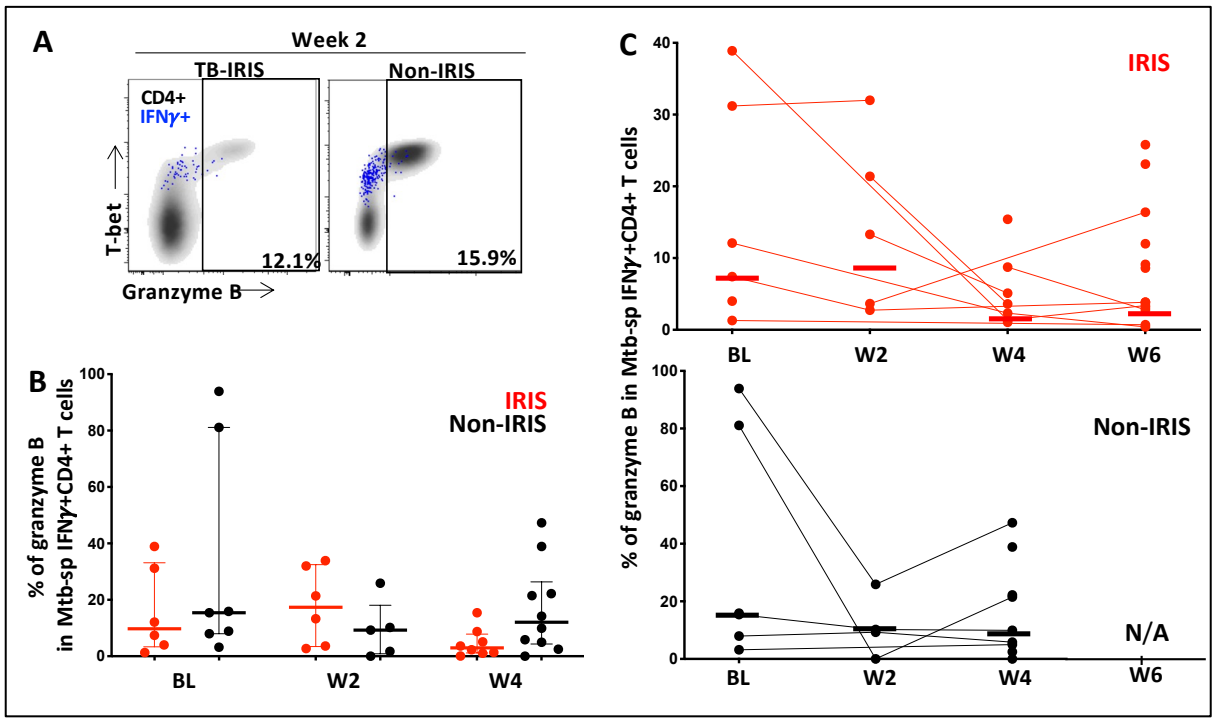

Figure 4.12. Granzyme B expression in Mtb-specific IFNγ+CD4+ T cells in TB-IRIS and non-IRIS patients*. **A,** Representative flow plot of granzyme B expression in Mtb-specific IFNγ+CD4+ T cells (red) and total CD4+ T cells (gray) in one TB-IRIS and one non-IRIS patient prior to ART initiation (at Baseline, BL). **B,** Expression of granzyme B in Mtb-specific IFNγ+CD4+ T cells in TB-IRIS (red) at baseline (BL, n= 6), 2 weeks (W2, n= 5), 4 weeks (W4, n= 7) and 6 weeks (W6, n= 13) and non-IRIS patients (black) at baseline (BL, n= 6), 2 weeks (W2, n= 4), and 4 weeks (W4, n= 8) post-ART. **C,** Expression of granzyme B in Mtb-specific IFNγ+CD4+ T cells from Baseline to 6 weeks post ART in TB-IRIS and non-IRIS patients. The Wilcoxon ranked test was used for all statistical comparisons. Only statistically significant data with a p value of 0.05 or less are indicated on graphs.*

However, Granzyme B expression was significantly higher in Eomes+Tbet+ Mtb-specific IFNγ+CD4+ T cells in patients with TB-IRIS compared to non-IRIS controls at week 2 on

ART (median: 4.7% vs 0%, respectively; p=0.026). There was also a trend towards higher Granzyme B expression in the Eomes+Tbet++ Mtb-specific IFNγ+CD4+ subset in patients with TB-IRIS compared to non-IRIS controls at week 2 (median: 19.7% vs 2.9%, respectively; p=0.063) **(Figure 4.11B)**. This trend was not observed at other time points (data not shown).

4.3 DISCUSSION

Hsu et al. recently reported that in HIV-1 and *M. avium* co-infected patients, *M. avium*-specific IFNγ+CD4+ T cells were characterized by higher expression of Eomes than Tbet at IRIS onset [307], suggesting potential involvement of Eomes in mycobacterial IRIS pathogenesis. While the functional role of Eomes is well established in CD8 T cells [308, 309], its role in CD4 T cells is less clear. Some reports implicate its expression in the pathogenesis of chronic inflammatory disorders [314-316], while others suggest a regulatory role in T cells [317]. Therefore, to define whether aberrant expression of transcription factors in CD4 T cell associate with the development of IRIS, we investigated the role of Eomes and Tbet in a experimentally-induced MAC-IRIS mouse model and compared the phenotype of Mtb-specific IFNγ+CD4+ T cells between HIV-associated TB patients who developed TB-IRIS and those who did not.

The MAC-IRIS mouse model showed that mimicking T cell reconstitution using Eomes knock-out CD4 T cells led to enhanced mice survival compared to wildtype, supporting the hypothesis that Eomes expression in CD4 T cells could play a role in IRIS pathogenesis [307]. However, while we demonstrated that Mtb-specific IFNγ+CD4+ T cells from TB-IRIS patients expressed high Eomes levels (~ 50%) that are comparable to those reported by Hsu et al. [307], we did not observe any difference in Eomes expression between TB-IRIS and non-IRIS patients. Several reasons could explain the disparity between our findings and the findings of Hsu et al. One notable difference is that the HIV-infected patients studied in the Hsu study had unmasking MAC-IRIS (10 out of 13) and were compared to HIV-uninfected patients with MAC infection. In this study, all patients with IRIS had paradoxical TB-IRIS and the control group was constituted of HIV-infected TB patients who did not develop TB IRIS after initiating ART. It is possible that the immunopathology of unmasking versus paradoxical IRIS is regulated by different mechanisms. It is also possible that differences in the underlying pathogen (MAC versus Mtb) may have contributed, but we think that this is unlikely given the considerable overlap in the inflammatory features and tissue pathology of IRIS related to these pathogens. Moreover, HIV infection itself may alter the expression of lineage defining transcription factor, as previously [318]. Hence, it would be of interest to define whether differential Eomes expression in unmasking MAC-IRIS patients is still observed when compared to HIV-infected matched control patients with MAC initiating ART. Nevertheless, as limited samples were included in both studies, larger cohorts are necessary to define the potential role of Eomes in unmasking and paradoxical IRIS.

The expression profile of Tbet in CD4+ T cells in this cohort mirrors that described by Knox *et al*. [319], where three distinct populations were discernible. Most Mtb-specific IFNγ+CD4+ T cells expressed Tbet with ~ 65% being Tbet dim and ~ 25% Tbet bright. Moreover, we found no significant differences in the co-expression profile of Eomes and Tbet in Mtb-specific IFNγ+CD4+ T cells at TB-IRIS onset or at other time points between the two clinical groups. However, the distribution of Eomes and Tbet subsets in total CD4+ T cells were altered on ART with increasing expression of both Tbet+ and Eomes/Tbet co-expressing CD4+ T cells in TB-IRIS patients on ART. Further studies are needed to confirm these observations and define their relevance.

In this cohort, TB-IRIS patients had significantly lower blood CD4 T cell counts compared to non-IRIS patients at baseline, as previously described [296, 320] and we observed a significant expansion in the frequency of Mtb-specific IFNγ+CD4+ T cells 2 weeks after the initiation of ART. Recently, Vignesh *et al*. described elevated pre-ART frequencies of Mtb-specific CD4 T cell responses which further expanded in TB-IRIS patients at disease onset [320]. We did not observe such differences at baseline in this or previous studies [304]. Clinical differences between the cohorts might account for these discrepancies.

Several studies have demonstrated that TB-IRIS is characterized by an increase in mycobacteria-specific CD4 T cell responses at disease onset [39, 320-323]. However, increased mycobacterial-specific CD4 T cell frequencies following ART is not systematically observed in all TB-IRIS patients, and pathogen-specific CD4 T cell expansion can also be observed in some non-IRIS patients [304]. This suggests that Mtb-specific CD4 T cell reconstitution upon ART is not the only mechanism involved in TB-IRIS pathogenesis. Current understanding suggests that paradoxical TB-IRIS is also partly driven by Mtb-primed innate immune responses, including inflammasome activation, being activated after ART initiation [28]. Mtb specific CD4 T cells may provide activation signals to the already primed innate immune cells resulting in a dysregulated inflammatory response

To further elucidate the contribution of Mtb-specific IFNγ+CD4+ T cells in TB-IRIS pathology, we characterised their phenotype in TB-IRIS patients. We demonstrated that Mtb-specific IFNγ+CD4 T cells of TB-IRIS patients had elevated HLA-DR expression prior to the initiation of ART and this was significantly upregulated in TB-IRIS patients at week 2 on ART compared to non-IRIS patients. Similarly, others have demonstrated that Mtb-specific CD4 T

cells are activated [305], and polyfunctional [306, 321], compared to non-IRIS controls at IRIS onset.

Consistent with our previous findings [304], we did not observe any significant differences in the expression of HLA-DR in total CD4+ T cells between the two clinical groups over time in a cross section analysis. However, like Antonelli *et al*, we observed increased HLA-DR expression in total CD4+ T cells of TB-IRIS patients from baseline to week 2 and 4 [305]. Similar observations were reported by Haridas et al. at the time of IRIS onset [324].

Lastly, Granzyme B expression was enriched in Eomes/Tbet co-expressing Mtb-specific IFNγ+CD4+ T cells at 2 weeks on ART in TB-IRIS patients. Although this represents a modest proportion of Eomes+Tbet+ cells, this is consistent with mouse data from experimental autoimmune encephalitis showing the capacity of Eomes+ IFNγ+CD4 T cells to acquire cytotoxic attributes [314]. Moreover, our group has previously shown TB-IRIS to be associated with increased transcript abundance and secretion of granzyme B by PBMC of TB-IRIS patients at week 2 on ART [325].

In conclusion, while the mouse model data suggested that CD4 T cell expression of Eomes promotes IRIS, there were no differences in the expression of Eomes or Tbet transcription factor in Mtb-specific IFNγ+ CD4 T cells between patients who developed TB-IRIS and non-IRIS controls. We found that TB-IRIS was associated with an increase of Mtb-specific CD4 T cells at onset. Moreover, increased expression of markers of immune activation and cytotoxicity in Mtb-specific CD4 T cell subsets in TB-IRIS patients suggests these cells may contribute to pathogenesis of TB-IRIS. Improved understanding of the pathophysiology of IRIS should enable the development of new diagnostic tools and better targeted treatments.

4.4 Study limitations

There were several limitations to this study. The number of samples analysed was limited, consequently, larger cohort studies are needed to verify these findings. We assessed responses in peripheral blood when clinical manifestations are often localized in tissue. Furthermore, the cell viability of the analysed samples was highly variable. To mitigate this potential technical issue, precautions were taken to include only live cells in our analysis, through stringent application of gates, excluding dead cells. Several patients with severe disease received corticosteroids prior to or while on ART, the main indications being neurological TB at TB diagnosis or the development of TB-IRIS after initiating ART. However, our previous findings suggest that corticosteroid treatment does not have a significant impact on *ex vivo* T cell functional responses in TB-IRIS patients [326]. Finally, MAC-IRIS animal model is a good model for studying the effects of reconstituting the immune system with MAC-specific CD4 lymphocytes. However, the model does not capture the complexity of the immunopathogenesis underpinning IRIS-related pathology, such as various innate immune responses which might be affected by ART, independently of CD4 lymphocyte reconstitution.

Chapter 5 summary: Functional transcriptomics of patients with paradoxical TB-IRIS and appropriate controls prior to and during early antiretroviral therapy

This chapter seeks to understand the molecular pathogenesis of paradoxical TB-IRIS by characterizing global gene expression in whole blood of patients who enrolled in the Pred-ART intervention trial. The chapter details cross sectional and longitudinal evaluation of differentially expressed genes in patients who were allocated either placebo or prophylactic prednisone who developed paradoxical TB-IRIS and TB-non-IRIS controls prior to the initiation of ART (week 0), at the median onset of inflammatory features (week 2) and post the resolution of inflammatory features (week 12) on ART. Differentially expressed genes were summarized into biological pathways using gene set enrichment analysis to decipher the cellular mechanisms that precede, underlie or reflect the resolution of paradoxical TB-IRIS at week 0, 2 and 12 respectively.

5. The development of paradoxical TB-IRIS

In patients with advanced HIV infection, TB is often disseminated with hematogenous spread to organs beyond the lungs [327]. Innate immune cells including macrophages, monocytes and neutrophils serve as a remaining immunological defense against Mtb replication in the absence of effective adaptive CD4 T cell mediated immune responses. This results in the activation of tissue resident macrophages enabling an extent of control of Mtb growth [30, 37, 39]. It is also common for Mtb to spread via the lymphatic system to the thoracic, cervical and mesenteric lymph nodes and establish nodal disease [328, 329]. Phagocytic cells sequester Mtb in the phagosome, where Mtb can subvert the immune responses by preventing phagosome maturation thereby continuing to replicate [330-332]. This interaction triggers the production of cytokines and chemokines resulting in the activation of the endothelial vessel wall and a chemokine gradient which causes the trafficking of immune cells to sites of Mtb infection [333, 334]. Immune cells in the vasculature follow the chemokine gradient and cross the endothelium to the site of infection to cause inflammation [335]. In advanced HIV, because of CD4 T cell deficiency and resultant impairment of multiple components of the immune response, Mtb infection is poorly controlled with high bacillary burden in tissues often accompanied by ill-formed granulomas and non-specific inflammation.

The initiation of ART results in the reversal of immune suppression over time, including the restoration of Mtb-specific CD4 immune cells [29, 39]. The production of interferon gamma by Mtb-specific CD4 T cells leads to the activation of already Mtb primed innate immune cells. In a context of high levels of Mtb antigen levels in infected tissues, this results in exaggerated inflammatory immune responses that manifest clinically as new or recurrent or worsening signs and symptoms of TB termed paradoxical TB-IRIS [29, 162].

Paradoxical TB-IRIS is the most common complication of combined ART and anti-TB treatment [6]. Paradoxical TB-IRIS is characterized by excessive inflammation and tissue damage [162]. Although it is usually a self-limiting disease, paradoxical TB-IRIS is potentially fatal with an attributable mortality rate of 2% [9]. Approximately 25% of patients with paradoxical TB-IRIS require hospitalization for diagnostic work-up and management [19]. This underscores its prominence as a public health concern. The diagnosis of paradoxical TB-IRIS is empiric, relying on the presence of inflammatory features and the exclusion of other causes for clinical deterioration [22]. Corticosteroids are the preferred treatment intervention for cases of paradoxical TB-IRIS with significant symptoms [21, 258, 336-339]. A major challenge associated with corticosteroids is that they result in immune suppression [340, 341].

For this reason, corticosteroids are prescribed with caution owing to their proclivity to cause Kaposi's sarcoma, especially in the context of advanced HIV induced immune suppression [339]. This highlights the need for safer drug options with alternative mechanisms of action to treat paradoxical TB-IRIS.

Recently, HIV clinical guidelines have shifted to advise early ART in patients with TB and low CD4 T-cell counts [160, 169]. This is projected to increase the incidence of paradoxical TB-IRIS, particularly in countries where HIV and TB are endemic.

5.1 Rationale

The incomplete understanding of the immunopathogenesis of paradoxical TB-IRIS is a bottleneck in the design of improved diagnostic, preventive and therapeutic strategies. This knowledge gap underscores the need for developing new research strategies that account for the complex and dynamic nature of biological systems.

Systems biology is one such strategy that integrates genome wide scale (omics) analysis such as DNA (genomics), RNA (transcriptomics), proteins (proteomics), lipids (lipidomics) and metabolites (metabolomics) with phenotypes [342, 343]. Systems biology is based on high throughput technology and high-performance computing [343]. This discovery approach improves on methods in which a single gene or an isolated linear molecular pathway is studied in isolation to understand its contribution to disease pathogenesis. Instead, systems biology hinges on the foundation that normal bodily function and/or malfunction, consists of a coordinated system that involves dynamic cross talk between a plethora of genes, proteins and metabolites that are spatially and temporally regulated.

This chapter describes the application of transcriptomics workflows to investigate the complexity of paradoxical TB-IRIS pathogenesis. This unbiased hypothesis-generating approach was also used to identify biological processes modulated by prednisone shown to be partially effective in TB-IRIS prevention in the placebo-controlled Pred-ART trial. RNA extracted from whole blood of participants in this trial was used including those who developed paradoxical TB-IRIS and controls who had HIV-associated TB but did not develop TB-IRIS after starting ART. This work aimed to better characterize the dysregulated hyper-inflammatory immune response that characterizes paradoxical TB-IRIS.

5.2 Objectives

- In those receiving placebo in the trial, to characterize the gene expression profile associated with TB-IRIS. To do this, significantly enriched biological pathways and their associated genes were identified in TB-IRIS cases compared to TB-non-IRIS control patients at baseline (week 0) and week 2 on ART.
- To identify biological pathways and genes modulated differentially by prednisone at week 2 on ART, in all patients and in the subgroup who developed TB-IRIS.
- To identify longitudinal changes in gene expression profile on ART in TB-IRIS cases by comparing profile at week 0 to that at week 2 on ART.
- To identify longitudinal changes in gene expression profile on ART in TB-non-IRIS controls by comparing profile at week 0 to that at week 2 on ART.

5.3 Materials and Methods

5.3.1 Patient recruitment and enrolment

This study was nested within the Pred-ART randomized-controlled trial for which the study protocol has been published and findings have been reported [21, 258]. The protocol for the Pred-ART trial was approved by the Human Research Ethics Committee of the Faculty of Health Sciences of the University of Cape Town. The Pred-ART trial enrolled HIV-positive patients with confirmed or probable drug susceptible TB starting ART with a CD4 count < 100 cells/μL. The population demographic included adult patients aged 18 and above recruited from four clinic sites in Khayelitsha, Cape Town, South Africa between August 2013 and February 2016. All patients provided written informed consent. A total of 240 patients were enrolled and randomized in a 1:1 ratio to receive either placebo or moderate dose prednisone for 4 weeks. This was a phase 3 trial which assessed the efficacy and safety of prednisone in preventing paradoxical TB-IRIS [21, 258]. At enrolment, patients had not initiated ART and 73% had microbiologically confirmed TB; the remainder had been empirically started on TB treatment. Patients were on standard first line antitubercular treatment for a median of 16 and 17 days for those allocated to received either prednisone or placebo respectively. A total of 120 patients were randomized to 40 mg/kg of prophylactic prednisone for 2 weeks which was then tapered down to 20 mg/kg for 2 weeks. The remaining 120 patients received identical placebo for 4 weeks from the initiation of ART [21, 258]. Both the participants and trial staff in the clinic were blinded to treatment allocation. Paradoxical TB-IRIS was defined according to the international network for the study of HIV associated IRIS (INSHI) criteria [22, 164, 344-346].

The incidence of TB-IRIS was 32.5% in the prednisone arm compared to 46.7% in the placebo arm. Further, no serious complications were recorded in the prednisone arm [21].

Peripheral blood samples were collected prior to ART initiation (week 0) and at 2, 4 and 12 weeks on ART in all consenting participants. Biological material including ribonucleic acid (RNA) and peripheral blood mononuclear cells (PBMCs) were extracted and cryogenically preserved for long term storage. RNA-sequencing technology was exploited for sequencing RNA samples available at week 0, 2 and 12 on ART. Computational biology and related workflows were applied on sequenced data to address several related objectives (refer to section 5.5).

Ethical approval for this sub-study was granted by the Human Research Ethics Committee of the Faculty of Health Sciences of the University of Cape Town (HREC ref: 136/2013).

5.3.2 Blood collection and processing

Whole blood was collected in PAXgene tubes from all consenting participants at week 0, 2, and 12 study visit and immediately transported at ambient temperature to the laboratory at the University of Cape Town for processing. Blood was stored at – 80 °C until extraction was performed.

5.3.3 RNA extraction procedure

The PAXgene 96 Blood RNA Kit offers high-throughput purification of cellular RNA in a manual format. RNA was extracted following manufactures guidelines and specifications. The blood samples (2.5 ml) had been collected in PAXgene Blood RNA Tubes (available from BD, cat. no. 762165). The PAXgene blood RNA tubes were centrifuged to pellet nucleic acids. The pellet was washed, and proteins were digested using proteinase K. Alcohol was added to adjust binding conditions. Lysates were applied to the PAXgene 96 filter plate and centrifuged to remove cell debris. The lysate was then applied to a PAXgene 96 RNA Plate. RNA extracts were shipped in dry ice by air to Francis Crick Institute, London, United Kingdom for library preparation and sequencing.

5.3.4 RNA library preparation

Sequencing libraries were constructed according to a standard next generation sequencing (NGS) protocol. Total RNA extracted from patient whole blood was constructed into short fragment length sequencing libraries using Ovation Universal Human Blood RNA-Seq preparation kit (Tecan Genomics, UK; product now discontinued) according to manufacturer's recommendations. RNA was reverse transcribed into cDNA before being fragmented mechanically using a Covaris E220 Focused Ultrasonicator and end paired to prevent re-ligation. Unique adapter indexes were conjugated to each fragment per sample to allow multiplexing. To enhance sequencing capacity on highly represented regions of the transcriptome, rRNA and globin RNA were depleted as part of the library construction step. The quantity and quality of the prepared library was assessed with Qubit fluorometer and TapeStation 2000, respectively.

5.3.5 RNA sequencing

High quality libraries were sequenced on the Illumina HiSeq 4000 platform at Francis Crick Institute, London, UK. To reduce batch effects, high throughput sequencing of samples collected prior to the initiation of ART (week 0), and samples collected at week 2 and 12 on ART were performed at once (refer to chapter 2 for comprehensive methods). A hard drive containing the raw data was shipped to the University of Cape Town, South Africa for bio-informatic analysis.

5.3.6 Handling raw data

Raw reads were uploaded to the UCT high performance computing (HPC) cluster network facility using command line shell scripting.

5.3.7 RNA sequencing analytical pipeline

Using Linux based command-line scripting, the Next-Flow RNA-sequencing (NFcore-RNA-seq) pipeline was used to quantify transcript expression across patient samples as outlined in more detail in chapter 3.

5.3.8 Data quality control

The nextflow core-RNA-seq pipeline has in-built quality control (QC) check points for each process. After running to completion, the pipeline produced a multi-QC report which was scrutinized for pipeline errors.

5.3.9 Downstream data analysis

Data was downloaded from UCT servers to a local computer where further downstream functional analyses of the gene expression data was performed using the R programming statistical language.

5.4 Results

The study design allowed for cross sectional and longitudinal data analyses of differentially abundant transcripts in samples from patients with paradoxical TB-IRIS and TB-non-IRIS controls prior to and during concurrent ART and prednisone or placebo intervention. Differential gene expression analysis was performed at each time point (week 0, 2, and 12). Transcripts were ranked by the differential gene expression score and subsequently summarized into biological pathways with the aid of gene set enrichment analysis (GSEA). Weighted gene co-expression network analysis was subsequently used to identify module eigengenes which significantly correlated with paradoxical TB-IRIS. Over representation analysis was then utilized to verify the GSEA findings.

5.4.1 Clinical characteristics of the cohort

Sufficient mRNA samples for differential gene expression analyses (DGEA) were available at week 0 (prior to ART initiation) for 225 of the 240 ambulatory, HIV-positive patients being treated for TB. Of the 225 participants, 92 developed paradoxical TB-IRIS and 133 did not (TB-non-IRIS controls). The demographic and clinical characteristics of the two groups are summarized in **Table 5**.

Table 5. Clinical characteristics of patients who developed tuberculosis-associated immune reconstitution inflammatory syndrome and controls (TB-IRIS, n=92) and those who did not (TB-non-IRIS, n=133).

Clinical characteristics	TB-IRIS (n=92)	TB-non-IRIS (n=133)	p-value
Age median[IQR]	34[21-57]	38[18-65]	0.007
Gender (Male) n(%)	56(61)	79(59)	0.31
TB confirmation			
Empirical n(%)	25 (27)	37 (27)	-
Smear n(%)	3 (3)	1 (0.8)	-
Culture n(%)	45 (48)	68 (51)	-
Xpert n(%)	22(23)	30 (22)	-
CD4 count week 0 median [IQR](cells/mm^3)	47[3-189]	53[1-233]	0.26
Log10 HIV VL at week 0	5.66	5.48	0.16
Hb (week 0)	9.8[6.5-13.7]	9.6[7.1-15]	0.61
Neutrophil count (week 0)	1.98[0.73-9.63]	2.22[0.49-5.75]	0.84
Median time to TB-IRIS onset in days [IQR]	12 [5-17.75]	NA	
On steroid treatment from week 0 (%)	36(39)	75(56)	-

Hb: Haemoglobin, HIV VL: Human immunodeficiency virus viral load, IQR: interquartile range, n: number (absolute count), %: Percentage, NA: not applicable. Non-parametric analysis (Mann-Whitney T-test) was used to compare unpaired discrete and categorical data.

Patients with paradoxical TB-IRIS were significantly younger than TB-non-IRIS controls. Thirty-nine percent of patients who developed paradoxical TB-IRIS received prednisone prophylaxis compared with 56% of controls. The median CD4 count and HIV viral load at the start of ART were similar in the two groups. Neutrophil counts and haemoglobin at baseline were also similar for the two groups. The median duration on ART prior to the development of paradoxical TB-IRIS was 12 days.

After analyzing the clinical characteristics of the Pred-ART sub-population, we characterized the gene expression signature of patient samples in both clinical groups at different time points. In this study, we had access to cryogenically preserved clinical material such as RNA extracted from peripheral blood of consenting patients that were enrolled in the Pred-ART clinical trial. The availability of samples prior to the onset of paradoxical TB-IRIS, at disease onset and post disease, provided a snapshot at every stage of the disease; thus enabling us to glean new understanding relating to the molecular events that occur in patients with paradoxical TB-IRIS. We leveraged the power of high throughput RNA sequencing technology. Finally, with the aid of this discovery approach, we uncovered the molecular processes modulated by prophylactic prednisone in all patients; as well as in patients who either developed TB-IRIS or did not while on prednisone prophylaxis. Of note, this is the largest transcriptomics study conducted in patients with paradoxical TB-IRIS to date. Discussed below are the findings from these analyses.

5.4.2 Placebo Week 0: TB-IRIS vs TB-non-IRIS

Characterizing early immunological processes that pre-exist ART initiation in patients who develop paradoxical TB-IRIS could be of benefit in aiding the development of novel targeted prevention strategies by identifying people at high risk of developing paradoxical TB-IRIS and in the rationale design of such prevention strategies. Recent gene expression studies have helped define biological processes involved in TB pathogenesis [342, 347]. Similar transcriptomics approaches and frameworks were applied in samples collected prior to the

initiation of ART (week 0) to investigate the gene expression signature and biological pathways that predict subsequent paradoxical TB-IRIS.

5.4.2.1 Differential gene expression analysis

Differential gene expression analysis (DGEA) was performed on samples collected from patients who developed paradoxical TB-IRIS and TB-non-IRIS controls at week 0. To model raw gene count data, a statistical count-based workflow called DESeq2 was adapted to derive and describe differentially expressed transcripts in samples from a total of 114 participants who received placebo, 56 of whom developed paradoxical TB-IRIS subsequently on ART (**see Table 5.1**).

***Table 5.1**: Summary of the number of the samples that were available by patient outcomes at different study visits, prior to ART initiation (week 0) up to week 12 on ART in patients allocated to either the placebo or prednisone arm.*

Time-point (weeks)	Number of samples Placebo/Prednisone (TB-IRIS)	Number of samples Placebo/Prednisone (TB-non-IRIS)	Total (Placebo/Prednisone)
Week 0	56/36	58/75	114/111
Week 2	44/26	51/69	95/95
Week 12	42/34	50/62	92/96

5.4.2.2 Exploratory analysis

Variance stabilized, normalized expression data, were assessed for quality and explored for patterns using principal component analysis (PCA). A total of 114 eigenvectors or principal components (PC) corresponding to the patient samples were generated. In Figure 5A the first 3 PCs or dimensions, which accounted for 99% of the cumulative variance, are shown. The figure also depicts the relative contribution of the first 10 samples to each PC, where the scale represents the proportion of variance contributed by each sample to each PC. PC1 accounted for 89.9% of the variance across all the samples (**Figure 5B**).

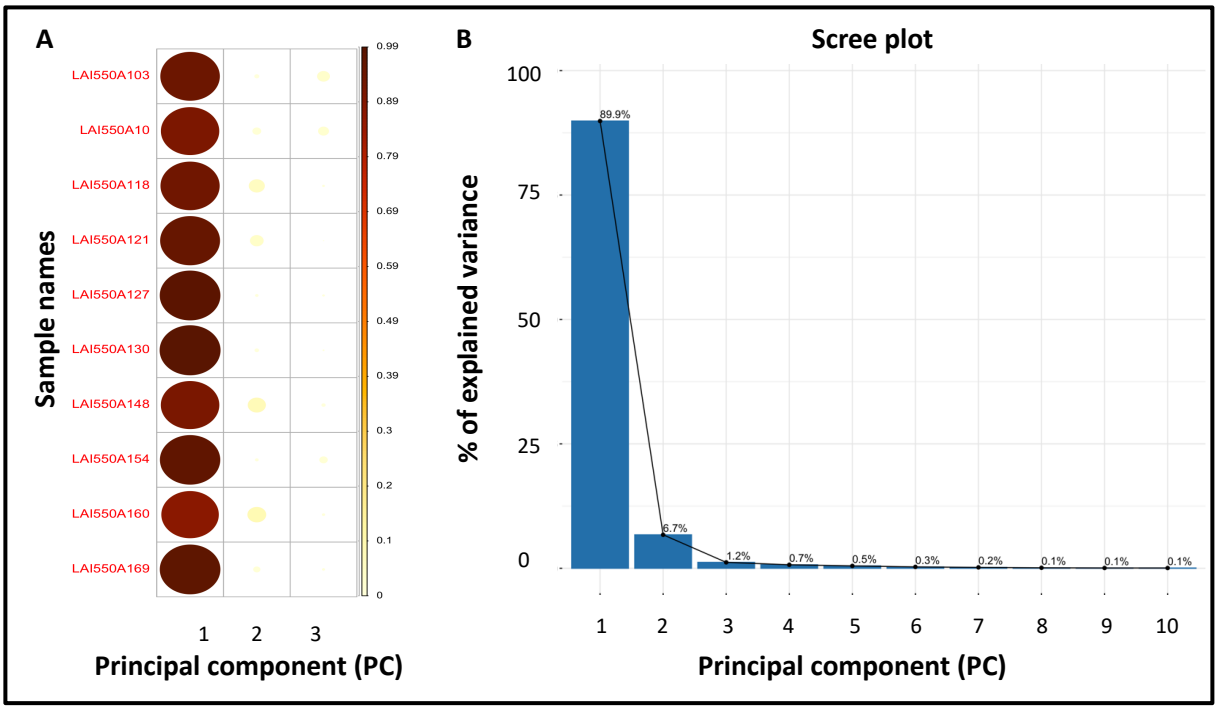

Figure 5. Principal component analysis (PCA) in a total of 114 samples collected from placebo allocated patients who later developed paradoxical TB-IRIS and TB-non-IRIS controls prior to the initiation of antiretroviral therapy (ART) (week 0). A. *The relative contribution of each sample to the cumulative variance across the first three principal components (PC) in an illustrative group of 10 samples.* ***B.*** *Scree plot showing the proportion of variance explained by each principal component (PC).*

PC1 and PC2 contributed 96.6% of the cumulative variance for all the samples (**Figure 5B**). Given this understanding, PCA was performed using the first 2 PCs for the 500 most variable genes between the two clinical groups across all samples at week 0 (**Figure 5A**). PC1 represents the linear combination of the Euclidean distances (eigenvalue) between transcripts across all 114 samples. PC1 maximizes the variability of the data when projected in the x-axis (42%). PC2 is orthogonal to PC1, and it describes the residual variance of PC1 (10%) (**Figure 5A&B**).

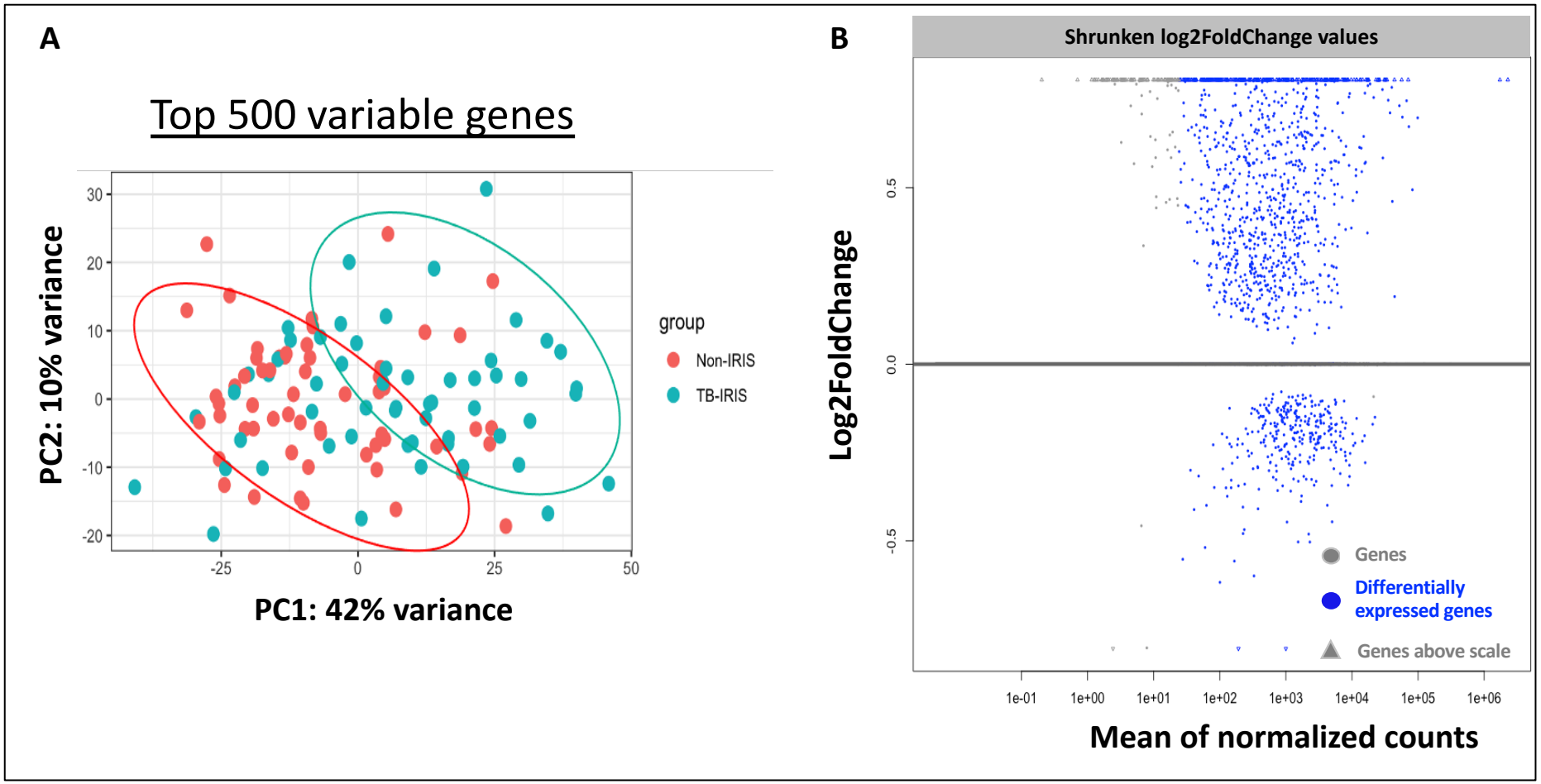

Figure 5.1. Exploratory data analysis for 114 samples collected from placebo-allocated patients who later developed paradoxical TB-IRIS and TB-non-IRIS controls prior to the initiation of antiretroviral therapy (ART). ***A.*** *Principal component analysis for the top 500 variable genes. PC1 contributed most of the variance. PC1 is a cluster predominated by samples from patients with paradoxical TB-IRIS, suggesting that there is more variation in gene expression in samples of patients with paradoxical TB-IRIS.* ***B.*** *Differential gene expression analysis to explore the distribution of*

differentially expressed genes (DEGs)across a spectrum of normalized base mean counts. DEGs were identified across the range of normalized base mean counts.

Since the axes of a PCA plot are ranked by order of importance (% of contributed variance), PC1 accounted for the most variance compared to PC2. PC1 is a cluster predominated by samples from patients with paradoxical TB-IRIS (**Figure 5.1A**). This suggests that patients with paradoxical TB-IRIS had more perturbations in gene expression at week 0, compared to TB-non-IRIS patients whose samples were used for benchmarking. Some samples from patients with paradoxical TB-IRIS clustered with some from patients who did not develop paradoxical TB-IRIS (TB-non-IRIS controls). This indicates the proximity of the eigenvalues and therefore, the similarities in gene expression in some patients between the two clinical groups at week 0. Additionally, despite the application of thresholds to exclude observations with low normalized base mean counts to reduce noise, several outliers were observed, and these typically had high variance (**Figure 5.1A**).

Following the evaluation of the similarities in gene expression between the samples, the magnitude of change in gene expression was assessed in relation to transcript abundance after adjusting for multiple hypothesis testing (FDR = 0.1) (**Figure 5.1B**). Each point represents a single gene; where blue shaded circles depict differentially expressed genes between patients who later developed TB-IRIS compared to those who did not; grey shaded circles depict genes with no change in gene expression and triangles represent gene expression values beyond the log2 fold change scale which ranged between [-1.8 and 2.5].

Figure 5.1B depicts the relationship between transcript abundance (base mean counts) and change in gene expression (log2foldchange). The figure illustrates the distribution of log2fold change values across a wide range of normalized base mean counts. Using differing thresholds to include transcripts based on large changes in gene expression (effect size threshold) leads to the loss of other significantly DEGs that do not satisfy the defined thresholds. This information was instrumental in choosing the functional analytical approach that factors in transcripts with small changes in gene expression that might nonetheless be important in the context of a coordinated immune response in a biological system. This pattern of transcript abundance and change in gene expression was also observed for DEGs identified at both week 2 and 12 on ART. The same relationship in gene expression and effect size has been reported in several RNA-seq studies [275].

Next, conventional false discovery rate (FDR = 0.05) thresholds were used to investigate gene expression profiles between the two clinical groups at week 0. A total of 1325 differentially expressed transcripts were identified in samples from patients with paradoxical TB-IRIS

compared to TB-non-IRIS controls at week 0. Of these, 978 transcripts were upregulated in samples collected from patients who later developed paradoxical TB-IRIS when compared to TB-non-IRIS controls. A total of 347 transcripts that were significantly downregulated in patients who later developed paradoxical TB-IRIS relative to TB-non-IRIS controls were also identified (**Figure 5.2A**). Collectively, DEGs were representative of genes encoding proteins in 3 subcellular compartments: genes encoding proteins that localize to the nucleus of cells; genes encoding mainly coding proteins and intracellular receptors that localize to the cytoplasm; and genes encoding transmembrane proteins and cell surface receptors. Many of the upregulated genes were those encoding proteins with diverse functions and localized to the cytoplasm. These included many genes that encode ribosomal proteins, mitochondrial proteins involved in the generation of ATP and the oxidation of Fe^{3+} containing proteins, genes encoding proteins that bind oxidized proteins, genes encoding defensins and antimicrobial peptides, genes encoding proteins involved in heme biosynthesis and porphyrin metabolism, and those encoding proteins involved in the transport of gas molecules. Lastly, interferon inducible genes and those involved in megakaryocyte differentiation were identified. Genes encoding proteins that localize to the nucleus included those involved in DNA repair and genes involved in the epigenetic regulation of gene expression. Among the genes that were downregulated were those encoding proteins involved in the process of inflammation and those that degrade aberrant proteins.

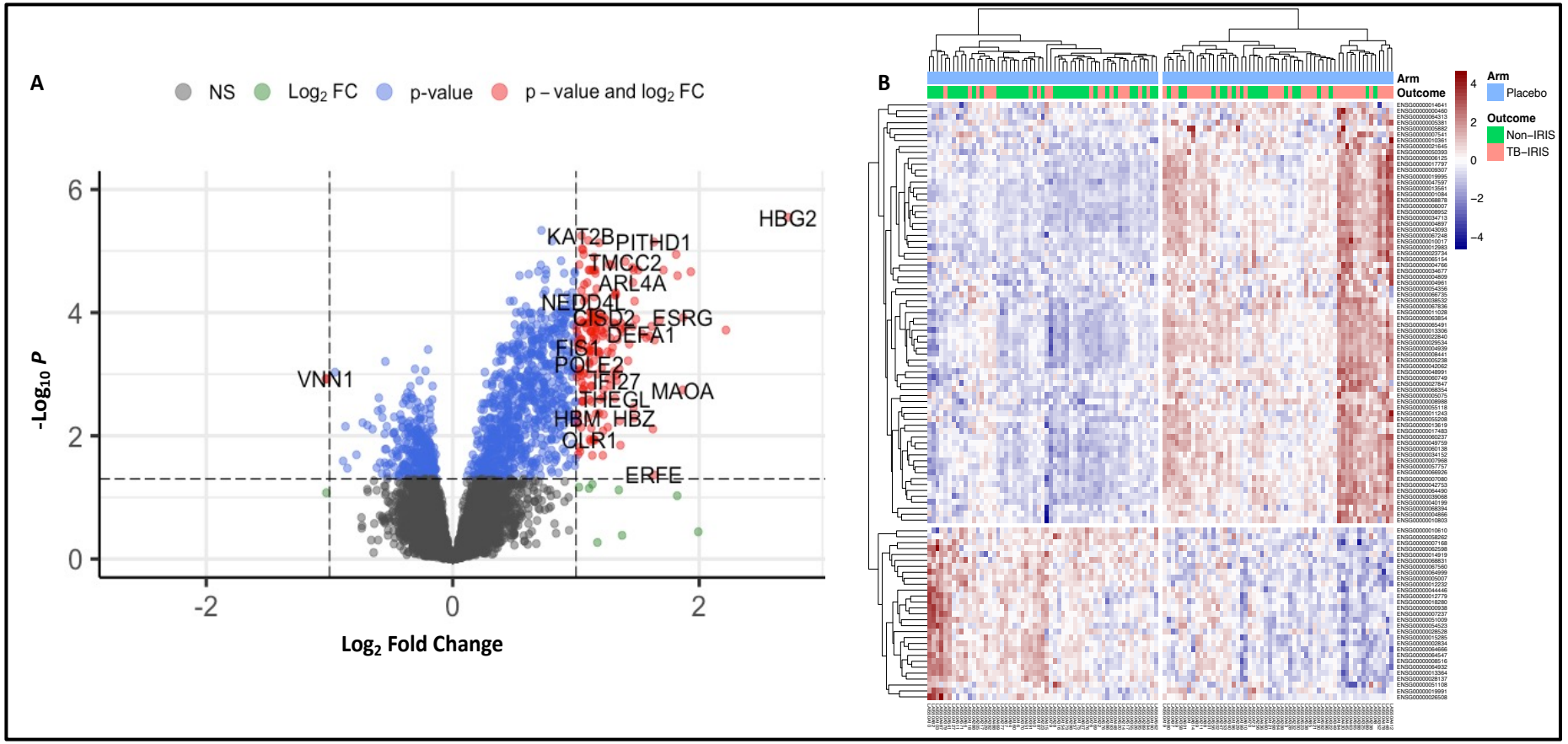

Figure 5.2. Differential gene expression analysis in 114 samples collected from placebo-allocated patients who later developed paradoxical TB-IRIS and TB-non-IRIS controls at week 0 prior to the initiation of antiretroviral therapy (ART). ***A,*** *Volcano plot showing differentially expressed genes (DEGs) in patient samples collected from the placebo arm at week 0. DEGs were defined by an adjusted p-value of less than or equal to 0.05.* ***B,*** *Visualization of the top 100 DEGs identified in samples from patients with paradoxical TB-IRIS (pink) and TB-non-IRIS control(green) at week 0. A*

total of 1325 transcripts were differentially expressed between the 2 clinical groups at week 0, with 978 genes being upregulated while 347 genes were downregulated in patients with paradoxical TB-IRIS.

Next, the top 100 of the 1325 DEGs were visualized using a heatmap to explore the gene expression profiles in the placebo allocated samples at week 0 based on paradoxical TB-IRIS outcome (**Figure 5.2B**). Figure 5.2B shows the top 100 DEGs in samples of patients who later developed paradoxical TB-IRIS (salmon) and TB-non-IRIS (green) controls at week 0. The rows represent the DEGs (red= upregulated, white = no change in gene expression, and blue = downregulated) and the columns represent deidentified patient sample (n =114).

In the context of clinical disease, these exploratory findings suggest that there is more perturbation in gene expression from samples of patients who eventually develop paradoxical TB-IRIS compared to TB-non-IRIS controls at week 0. Additionally, data were quite instructive with regards to choosing a well-suited workflow for subsequent functional enrichment analysis that could potentially include all the genes regardless of effect size contribution.

5.4.2.3 Gene set enrichment analysis

To identify and describe significantly enriched biological processes preceding the onset of paradoxical TB-IRIS, DEGs were ranked by log2fold change and summarized into biological pathways by conducting functional enrichment analysis using a threshold free statistical algorithm known as gene set enrichment analysis (GSEA) [282]. The GSEA algorithm accommodates a pre-ranked gene list and a curated gene set to functionally classify DEGs into biological pathways. The Reactome database provides gene sets that are curated based on multiple features including gene function. Described below, are the significantly enriched biological pathways and their attendant genes that precede the clinical onset of paradoxical TB-IRIS, at week 0 before ART was initiated.

5.4.2.3.1 Genes related to hypoxic stress and metabolic dysfunction were upregulated in samples collected from placebo-allocated patients who later developed paradoxical TB-IRIS compared to TB-non-IRIS controls prior to the initiation of ART.

Several biological pathways were identified that were significantly enriched in samples collected at week 0 from patients who later developed paradoxical TB-IRIS compared to TB-non-IRIS controls. *A priori* thresholds to define statistical significance including a normalized enrichment score (NES) greater or less than 0 and an FDR cut-off, of less or equal to 0.1, were used to define statistically enriched biological pathways as determined by the Kolmogorov-

Smirnov test [348]. In Figure 5.3, the 20 most significantly upregulated and downregulated biological processes at week 0 are shown. The biological pathways are discussed below largely in the context of the Reactome database from which they were curated and in relation to relevant published literature.

The top 5 biological pathways (eukaryotic translation elongation, eukaryotic translation initiation, response of eif2ak4 to amino acid deficiency, seleno-amino acid metabolism and nonsense mediated decay) largely represented upregulated genes encoding ribosomal proteins which are accessory to the 60S subunit of the eukaryotic ribosome (**Figure 5.3**). Ribosomes and their accessory proteins are confined to the cytoplasm of the cell where they facilitate the translation of mature mRNA into polypeptides; the elongation of the polypeptides and subsequent posttranslational modifications (i.e folding) into functional proteins [349]. rRNA constitute 90% of the total RNA species in the blood. Therefore, the abundance of the ribosomal proteins at week 0 in samples from patients who later developed paradoxical TB-IRIS and those who did not (TB-non-IRIS controls) likely reflects this fact. Consequently, we do not emphasize these findings although they were statistically enriched.

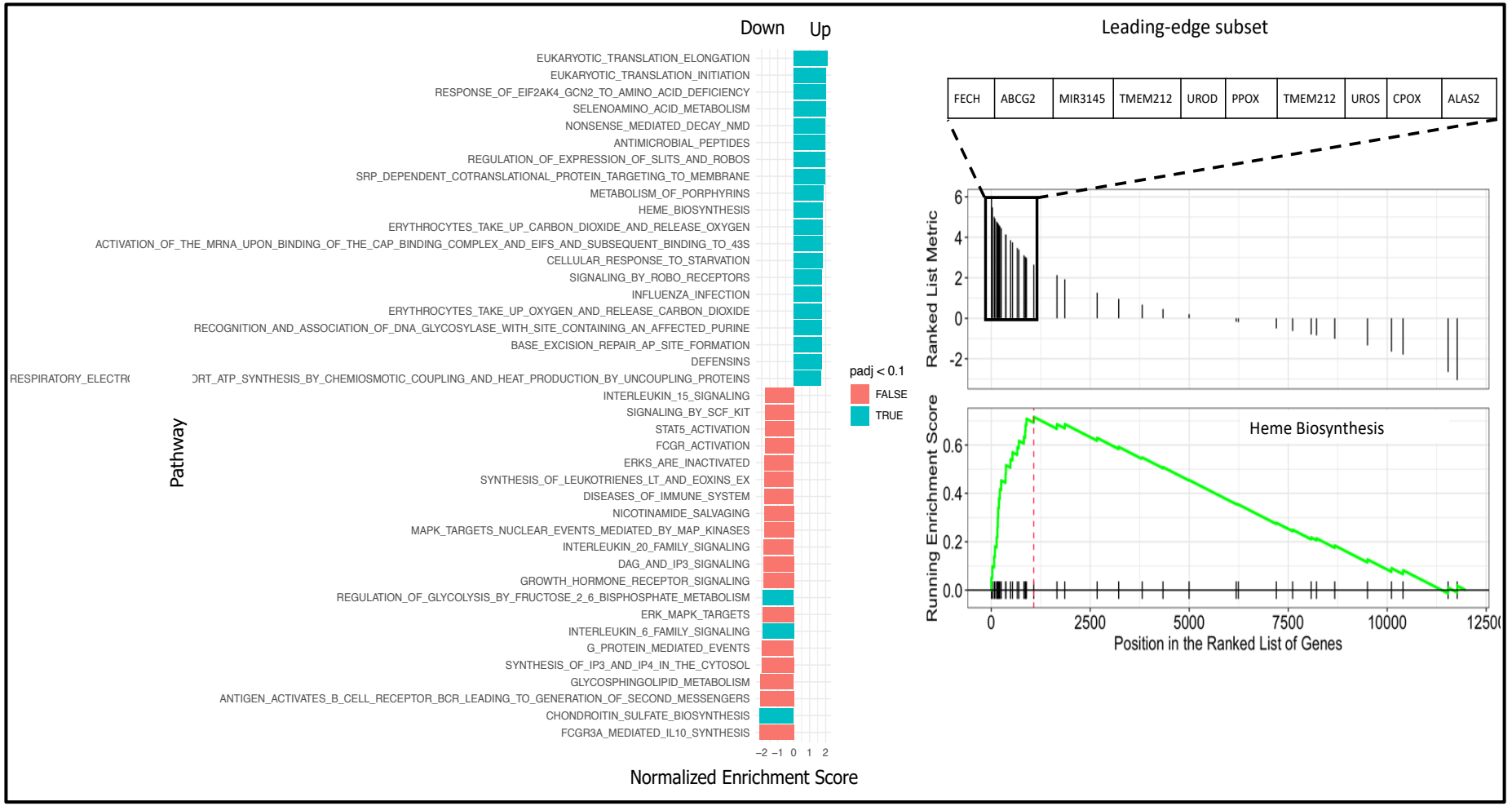

Figure 5.3.Gene set enrichment analysis in samples from placebo-allocated patients who later develop paradoxical TB-IRIS and TB-non-IRIS controls prior to the initiation of antiretroviral therapy (ART). *Significantly enriched pathways were defined by a normalized enrichment score greater than or less than 0 and an adjusted p-value of less or equal to 0.05. The right panel shows an enrichment plot for the heme biosynthetic pathway which*

is suggestive of adaptation to hypoxia in patients with paradoxical TB-IRIS compared to TB-non-IRIS controls at week 0. The red line depicts the enrichment score and the vertical black bars represent individual genes.

Several other biological pathways including heme biosynthesis, the transportation of oxygen and carbon dioxide, porphyrin metabolism and mitochondrial encoded proteins involved in the oxidation of Fe^{3+} containing proteins, were the most significantly upregulated in samples from patients who later developed paradoxical TB-IRIS compared to TB-non-IRIS controls at week 0 (**Figure 5.3**). The bottom right panel of Figure 5.3 depicts an enrichment plot for the heme biosynthesis biological pathway; the green line depicts the running enrichment score, while the red dotted line depicts the enrichment score which is defined as the maximum deviation of the running sum from zero [282, 350, 351]. The top right panel depicts the DESeq2 derived gene list that is ranked by the log2fold change metric. Each vertical bar represents an individual gene which add up to a gene set of 140 genes that comprise this biological pathway. The closely packed upright bars to the left of the enrichment score are the most upregulated genes that contribute significantly to the enrichment score. These are known as the leading-edge subset. Among the top 10 leading edge subset was ferrochelatase which catalyses the conversion of protoporphyrin IX to heme B [352].

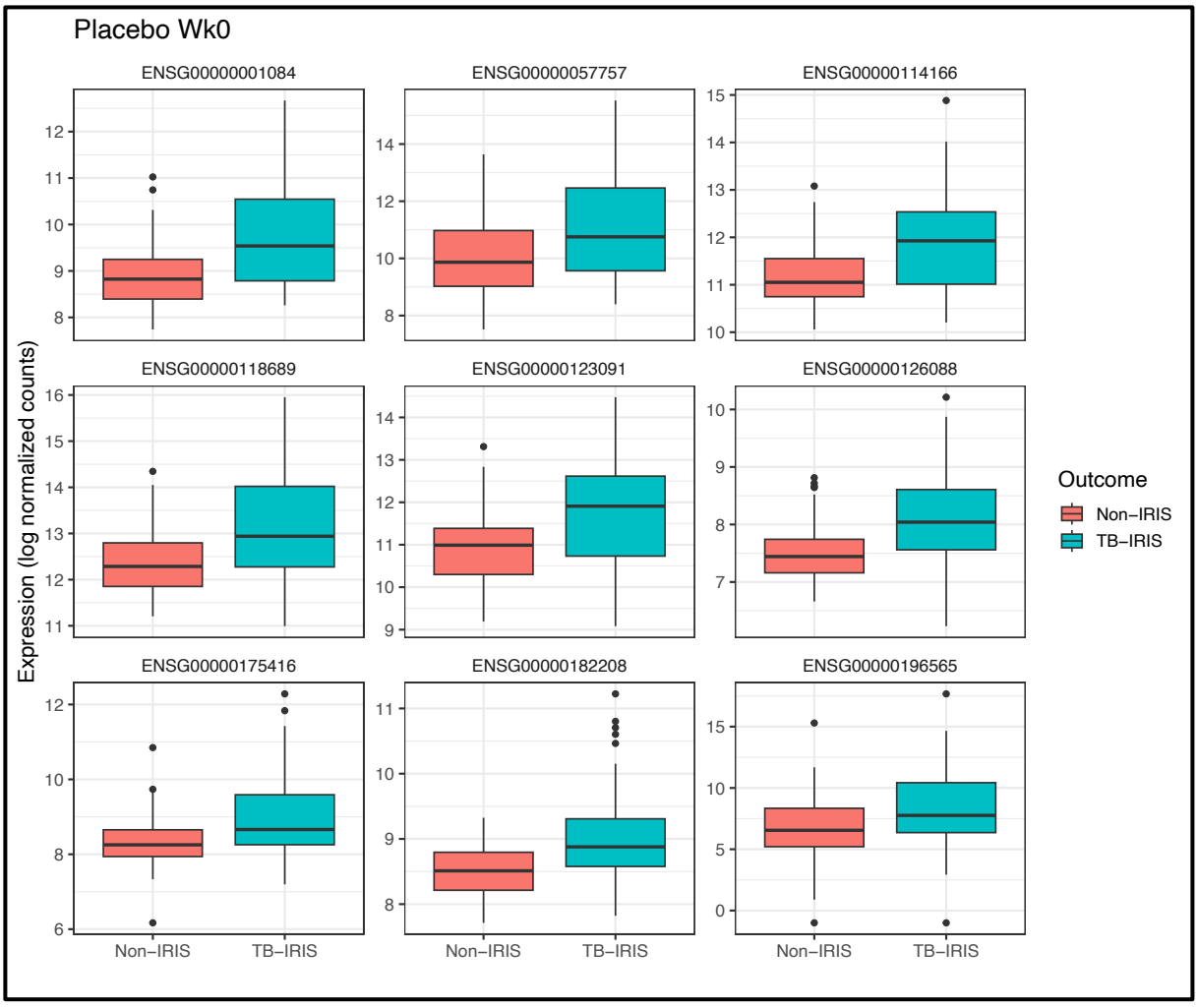

Figure 5.4. Gene expression of the top 9 transcripts identified with DESeq2 in samples from patients with paradoxical TB-IRIS and TB-non-IRIS controls at week 0*. glutamate-cysteine ligase catalytic subunit (GCLC), PITH domain containing 1 (PITHD1), lysine acetyltransferase 2B (KAT2B), forkhead box O3 (FOXO3), Ring finger protein 11 (RNF11), uroporphyrinogen decarboxylase (UROD), clathrin light chain B(CLTB), MOB kinase activator 2 (MOB2), hemoglobin subunit gamma 2 (HBG2)*

Figure 5.4 depicts the first 9 normalized expression counts that were stabilized for variance in samples collected at week 0 from patients who later developed TB-IRIS compared to those who did not. A short list of the significantly enriched genes and functions are listed in **Table 5.2** below.

Table 5.2.Gene names and function identified as part of heme biosynthesis and antimicrobial peptide pathways showing the leading edge subset that were significantly enriched (FDR = 0.1) in patients who later developed paradoxical TB-IRIS compared to TB-non-IRIS controls prior to the initiation of antiretroviral therapy.

Gene name	Symbol	Function
Heme biosynthesis leading edge subset		
Ferro chelatase	FECH	Encodes protein that catalyzes the insertion of iron into protoporphyrin IX in the heme biosynthesis pathway
ATP binding cassette subfamily G member 2	ABCG2	Encodes a protein that transports various molecules across extra- and intra-cellular membranes.
Hydroxy-methyl-bilane-synthase	HMBS	Encodes a member of the hydroxymethylbilane synthase superfamily, a third enzyme in the heme biosynthesis pathway
Amino levulinate synthase 2	ALAS2	Encoded gene catalyzes the first step in the heme biosynthetic pathway
Urod porphyrinogen decarboxylase	UROD	Encoded protein catalyses the conversion of urod-porphyrinogen to coproporphyrinogen through the removal of four carboxymethyl side chains
Protoporphyrinogen oxidase	PPOX	Encoded protein catalyzes the 6-electron oxidation of protoporphyrinogen IX to form protoporphyrin IX
Transmembrane protein 210	TMEM210	Predicted to be integral component of membrane
Uroporphyrinogen III synthase	UROS	Encoded protein catalyzes the fourth step of porphyrin biosynthesis in the heme biosynthetic pathway
Coproporphyrinogen oxidase	CPOX	Encoded protein catalyzes the stepwise oxidative decarboxylation of coproporphyrinogen III to protoporphyrinogen IX, a precursor of heme
Antimicrobial peptide leading edge subset		
Defensin alpha 1B	DEFA1B	Encoded protein is an antimicrobial and cytotoxic peptide, abundant in granules of neutrophils
Cathepsin G	CTSG	Encoded protein is a member of the peptidase S1 protein family, is found in azurophil granules of neutrophilic polymorphonuclear leukocytes
Defensin alpha1	DEFA1	Encoded protein is a member of the family of antimicrobial and cytotoxic peptides abundant in granules of neutrophils
Defensin alpha3	DEFA3	Encoded protein is a member of the family of antimicrobial and cytotoxic peptides abundant in granules of neutrophils
Defensin alpha4	DEFA4	Encoded protein is a member of the family of antimicrobial and cytotoxic peptides abundant in granules of neutrophils
Elastase neutrophil expressed	ELANE	Elastases form a subfamily of serine proteases that hydrolyze many proteins in addition to elastin
Proteinase 3	PRTN3	Encoded protein is involved in mature conventional dendritic cell differentiation; membrane protein ectodomain proteolysis; and neutrophil extravasation
Intelectin 1	ITLN 1	Encoded protein enables calcium ion binding activity, involved in positive regulation of glucose transport, protein phosphorylation
Cathelicidin antimicrobial peptide	CAMP	Encoded protein is a member of the antimicrobial peptide family contained in neutrophilic granules
Lipocalin 2	LCN2	A neutrophil encoded gelatinase that transports small hydrophobic molecules such as lipids, steroid hormones and retinoids
Lactotransferrin	LTF	Encoded protein is a member of the transferrin family of genes and its protein product is found in the secondary granules of neutrophils
Bactericidal permeability increasing protein	BPI	Gene encodes a lipopolysaccharide binding protein. It is associated with human neutrophil granules and has antimicrobial activity

The identified biological pathways largely reflect differential neutrophil gene expression and adaptation to metabolic stress and alterations in iron homeostasis in patients who later develop paradoxical TB-IRIS compared to TB-non-IRIS controls. The identified biological pathways reflect the physiologic and immunologic profile of patients at risk of developing paradoxical TB-IRIS. It is well established that patients with more advanced HIV-related immune suppression and more disseminated and severe TB before ART are at highest risk for developing paradoxical TB-IRIS [160]. The identified pathways likely reflect a consequence of these disease states. The upregulation of mitochondrial genes that are involved in the generation of ATP via the electron transport chain is consistent with increased oxidation of reduced metabolic equivalents that input protons across the cytoplasmic space for ATP synthesis [292, 353, 354]. ATP is the preferred metabolic currency of cells enabling them to maintain viability and execute their physiologic roles [355, 356]. Additionally, mitochondrial genes encoding proteins that catalyze the oxidation of Fe^{3+} containing proteins were upregulated in samples from patients who later developed paradoxical TB-IRIS compared to TB-non-IRIS controls. These findings likely reflect heightened metabolic and physiologic stress related to more severe immunosuppression and disseminated TB in the group who later developed paradoxical TB-IRIS.

The link between metabolic dysfunction and iron homeostasis is well established [357]. Iron is central to many biological processes including but not limited to DNA replication, and ATP synthesis via the electron transport chain which is resident in the phospholipid bilayer of mitochondria [357]. However, its main function is in the synthesis of hemoglobin to support the efficient delivery of oxygen to tissues [357]. Hypoferremia has been reported in TB disease [358]. Although potentially detrimental, hypoferremia is a host adaptation mechanism that deprives the invading *Mycobacterium tuberculosis* bacterium of reduced iron which is vital to its physiology [359-362]. The undesirable effect of hypoferremia is anemia, which can contribute to hypoxic stress [363]. Additionally, the loss of iron can occur through various physiological processes. Notably, most of the iron in the human body exists in complex within the prosthetic groups of hemoglobin which is a component of red blood cells [363]. As a result, the loss of iron can occur through the senescence of RBCs [364-366]. Additional iron reservoirs exist in RBC progenitors found in the bone marrow, the senescence of which leads to hypoferremia [364].

Tight regulation between iron availability in the context of infection and inflammation and the physiological response to hypoxia could both contribute to the gene expression profile

observed in patients who are at higher risk of developing paradoxical TB-IRIS related to more severe disseminated TB. As part of a possible coordinated response to tissue hypoxia, there was increased expression of genes encoding proteins involved in heme biosynthesis, porphyrin metabolism, and concomitant O2/CO2 uptake/release to maintain metabolic homeostasis.

Furthermore, we identified two biological pathways including antimicrobial peptides (AMPs) and defensins which were more significantly upregulated in patients who later developed paradoxical TB-IRIS compared to those who did not. The genes associated with these biological pathways are expressed preferentially in neutrophils and encode proteins involved in the innate host immune response to pathogens including *Mycobacterium tuberculosis*. The Reactome database defines the curated genes in these two pathways as coding for proteins with low molecular weight and broad antimicrobial spectrum against pathogenic microbes. These two pathways were significantly enriched in samples from patients who later developed paradoxical TB-IRIS compared to TB-non-IRIS controls prior to the initiation of ART. Increased expression of neutrophils in the context of hypoxia is well documented [367, 368].

Hypoxia triggers a physiological response involving transcriptional regulation to maintain oxygen levels through iron regulation under homeostatic conditions [369]. Tissue hypoxia may occur in the context of acute and/or chronic inflammation such in the case of HIV/TB co-infection, where two interacting disease states can cause severe inflammation resulting in hypoxia [370-373].

In TB disease, focal lesions of inflammation are known to be hypoxic and beneficial for Mtb survival [3, 374, 375]. Inflammation and tissue damage are triggers for neutrophil infiltration [376-378]. Neutrophils are a subset of innate immune cells that are found in circulation and rapidly traffic and extravasate to sites of infection, inflammation or tissue damage [379, 380]. Circulating innate immune cells (including monocytes and neutrophils) that extravasate to sites of inflammation where the gradient of oxygen is low are well adapted to function under reduced oxygen tension [381]. In this regard, infiltrating neutrophils have the capacity to directly increase their oxygen consumption to aid in the assembly of the nicotinamide adenine dinucleotide phosphate (NADPH) oxidase complex, superoxide dismutase and myeloperoxidase (MPO) to generate reactive oxygen species (ROS), hydrogen peroxide (H2O2) and hypochlorous acid (HClO), thereby depleting oxygen levels [381, 382].

Therefore, prior to the initiation of ART, there appears to be broad themes that describe the physiologic and immune state in the blood of patients who later develop paradoxical TB-IRIS

compared to TB-non-IRIS controls which include hypoxic stress, neutrophil activation and increased production of mediators of neutrophil microbial killing.

Three biological pathways were significantly downregulated in samples from patients who later developed paradoxical TB-IRIS compared to TB-non-IRIS controls: chondroitin sulfate biosynthesis, interleukin 6 family signaling and regulation of glycolysis metabolism.

Chondroitin is a linear heteropolysaccharide which consists of repeating disaccharide units of glucuronic acid and galactosamine. The latter is commonly sulfated at carbon 4 or 6 to form chondroitin sulfate (CS). This sugar moiety covalently attaches to proteins to form proteoglycans which are ubiquitous in animal tissue surfaces as well as vital components of the extracellular matrix. Proteoglycans are involved in a variety of biological processes including cell proliferation, cell migration and trafficking. Their activity is modulated by bioactive proteins including growth factors, morphogens, and cytokines. This implies that patients that are likely to develop paradoxical TB-IRIS might have impaired immune cell function including proliferation, mobility and signaling.

Although the chondroitin sulfate biosynthesis pathway is not sufficiently described in the Reactome database, this sulfated compound coats soft tissues and is a monomer of cartilaginous tissue in humans. The genes comprising the chondroitin sulfate biosynthetic gene set includes genes that encode proteins that function both in the cell nucleus and cytoplasm. Some of the genes that were downregulated included various genes encoding DNA polymerases that are central to the process of cell division and implications for epigenetic regulation of gene expression. Other downregulated genes encode cytoplasmic ubiquitinases which regulate other proteins such as proteins with high turn-over kinetics and aberrant proteins. These findings have not been reported previously in the context of paradoxical TB-IRIS.

Furthermore, the glycolytic energy generation pathway and associated genes were significantly downregulated in samples from patients who developed paradoxical TB-IRIS compared to TB-non-IRIS controls at week 0. Glycolytic reactions have been reported to be the main energy producing pathway in HIV-infected patients with severe pulmonary TB disease and in cases of pediatric tuberculous meningitis IRIS in what is known as the Warburg effect [214].

Lastly, IL-6 expression was significantly downregulated in patients who later developed paradoxical TB-IRIS compared to TB-non-IRIS controls. This may reflect impairment of certain proinflammatory responses in patients who develop paradoxical TB-IRIS prior to ART initiation. This is possibly due to the depletion of CD4 T cell immunity due to HIV-1 mediated

immune suppression, more so in patients who later develop paradoxical TB-IRIS. Mtb-specific CD4 T cell responses are critical for the activation of innate immune cells which are the remaining barrier of immunity during TB disease in advanced HIV [383, 384].

5.4.2.4 Weighted Gene Co-expression Network Analysis (WGCNA)

Next, we constructed gene networks using weighted gene co-expression network analysis from an expression matrix of samples collected prior to the initiation of ART in placebo allocated patients who later developed paradoxical TB-IRIS and those who did not (TB-non-IRIS controls). The strength behind WGCNA is in identifying transcripts with similar expression profiles and clustering them together to identify hub genes. These highly correlated genes are assumed to share overlapping functionality and as a result are very likely involved in the same biological pathway. We used the resulting modules that were highly correlated with genes that are predictive of paradoxical TB-IRIS to corroborate our initial findings using over representation analysis.

5.4.2.4.1 Network construction with WGCNA identified five module eigengenes that are significantly correlated with paradoxical TB-IRIS

Unsupervised learning approaches were used to identify and exclude a single outlier sample from a single TB-non-IRIS control at week 0 (**Figure 5.4A**). We constructed a network that satisfied the criteria for scale free topology by converting a gene expression matrix into a correlation matrix. A soft threshold (β value) of 12 was applied to the correlation matrix to generate a weighted adjacency matrix that was used for network construction (**Figure 5.4 B&C**).

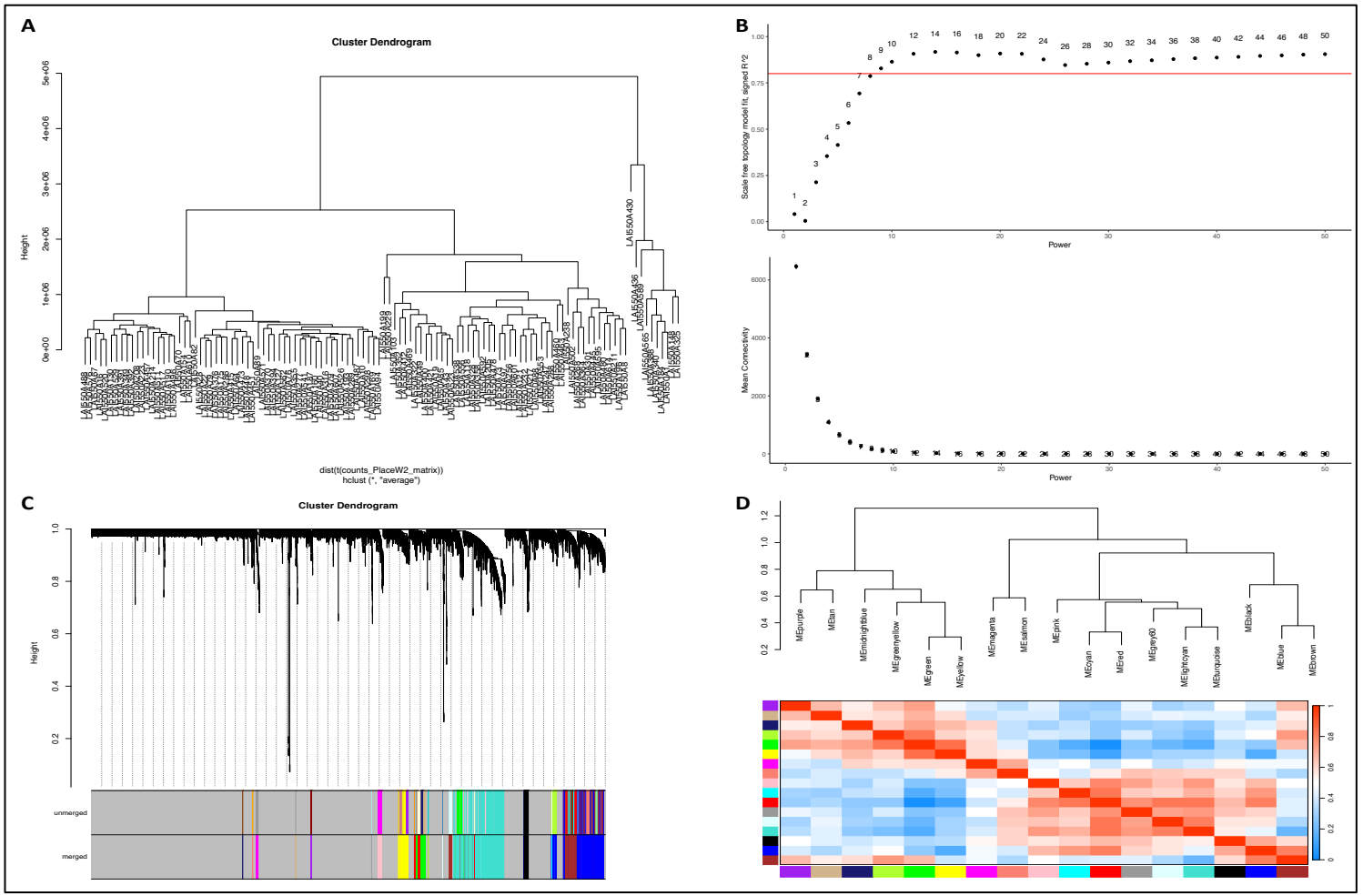

Figure 5.5. Weighted gene co-expression network analysis (WGCNA) in the placebo allocated samples from patients who later developed paradoxical TB-IRIS and TB-non-IRIS controls prior to the initiation of antiretroviral therapy (ART) at week 0*. A, Hierarchical clustering analysis identified one outlier sample (Red circles = excluded sample.* ***B,*** *Beta values for*

the network construction which satisfies scale free topology criteria. ***C,*** *Network construction with unsupervised hierarchical clustering of genes. Similar modules were merged (red box).* ***D,*** *heatmap cluster of the identified module eigengenes (ME).*

Next, a topological overlap matrix (TOM) and dissimilarity TOM (dissTOM) were created using TOM similarity and dissimilarity modules. Finally, module identification was performed by dynamic tree cutting, defining the minimum module size as 30. A threshold of 0.25 was used to merge modules with high similarity scores (**Figure 5.4 C**). Moreover, the values of gene significance (G.S) were used to calculate the association of individual genes with paradoxical TB-IRIS. Module Membership (M.M) was defined as the ME correlation as well as the gene expression profile for each module (**Figure 5.4 D**).

We identified 19 ME in this analysis, 3 of which were significantly predictive of paradoxical TB-IRIS (**Figure 5.5 A**). Three MEs in the following order, were highly and significantly correlated with paradoxical TB-IRIS, ME-blue (r = 0.96), ME-mid-night blue (r = 0.53) and ME-cyan (r = 0.45) (**Figure 5.5 A**). The number of genes comprising the turquoise, lightcyan and grey60 MEs are 1228, 148, and 221 respectively. The transcripts were largely involved in heme biosynthesis, neutrophil antimicrobial peptides, and O2/CO2 gas transport. These findings curated from the org.Hs.eg.db database, corroborated the similar pathways involved in hypoxic stress, neutrophil activation and epigenetic regulation which were identified by GSEA at week 0 in patients with paradoxical TB-IRIS compared to controls.

5.4.2.4.2 Identification of overrepresented pathways in samples from patients with paradoxical TB-IRIS

Next, three ME that were significantly correlated (FDR = 0.05) with paradoxical TB-IRIS were selected (ME-turquoise, ME-lightcyan and ME-grey60) and their associated genes (n = 425) and overrepresentation analysis (ORA) was performed to investigate the biological pathways that were significantly overrepresented in samples from patients who later developed paradoxical TB-IRIS (**Figure 5.5 A&B**).

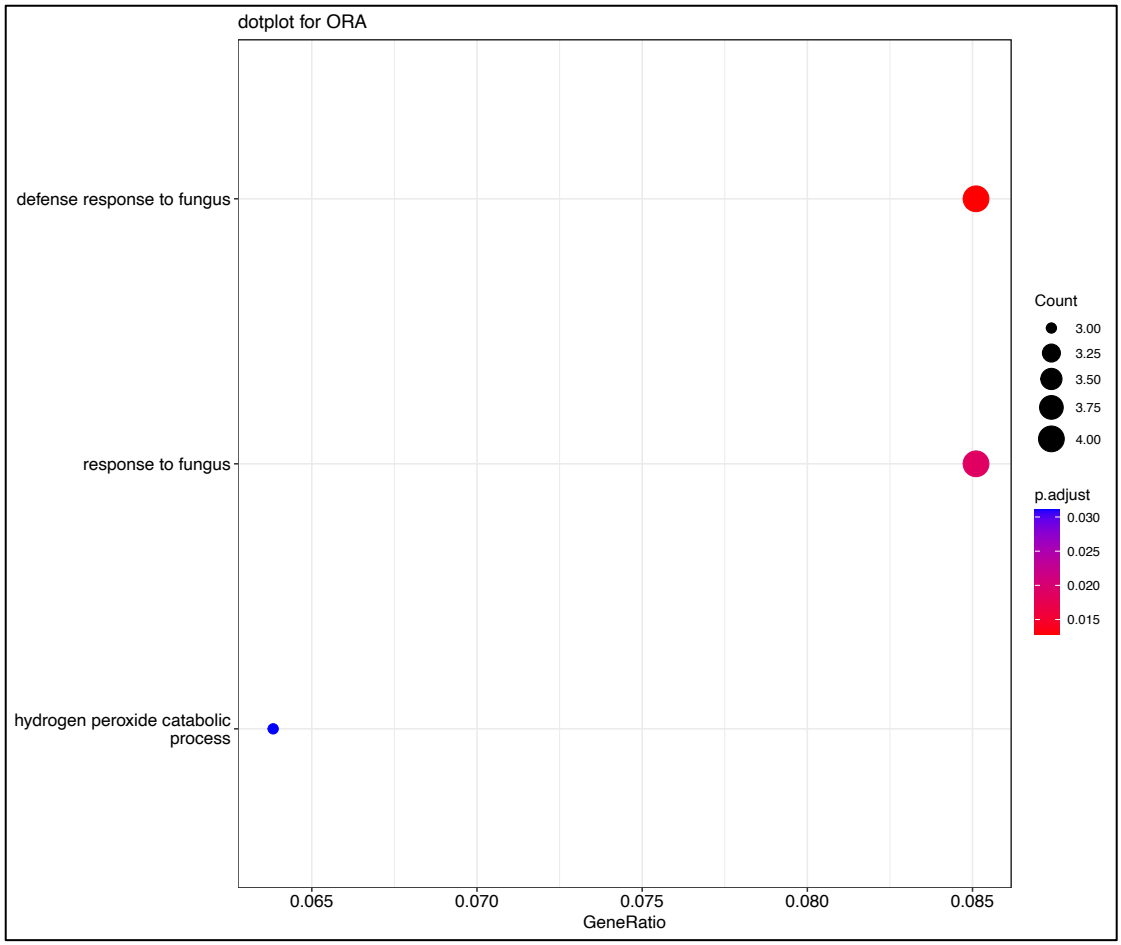

Figure 5.6. Over representation analysis (ORA) of transcripts belonging to the blue module eigengene (ME-blue) which was significantly correlated with paradoxical TB-IRIS*. ORA identified several pathways that corroborated our initial GSEA finding in patients with paradoxical TB-IRIS.*

The 3 biological pathways that were overrepresented in samples from patients who later developed TB-IRIS included detoxification of hydrogen peroxide which highlights the involvement of neutrophilic responses (**Figure 5.5**). This in part corroborates our initial GSEA findings. The identified pathways were involved in antimicrobial defense. The transcripts that formed part of these pathways were neutrophil genes involved in the upregulation of hydrogen peroxide and antimicrobial peptides.

5.4.2.5 Summary of findings for these analyses

Functional whole blood transcriptomics in samples from placebo-allocated patients who later developed paradoxical TB-IRIS compared to TB-non-IRIS controls identified DEGs prior to the initiation of ART (week 0).

Functional enrichment analysis using GSEA identified several biological processes that were enriched in samples from patients who later developed paradoxical TB-IRIS compared to TB-non-IRIS controls prior to the initiation of ART. Genes encoding neutrophil-related secondary granules which are released by exocytosis were upregulated in patients who later developed paradoxical TB-IRIS compared to those who did not. Additionally, over-representation analysis, which is more stringent in its method of identifying highly represented pathways, identified biological processes involving the detoxification of hydrogen peroxide, signaling the involvement of neutrophils and corroborating the GSEA findings. Additionally, transcripts involved in mediating homeostasis to hypoxic stress were other important biological processes that were significantly upregulated in samples from patients who later developed paradoxical TB-IRIS compared to those who did not. Hypoxic stress in the context of HIV-TB coinfection is likely by induced systemic inflammation and relates to innate immune cell trafficking including neutrophils. There was significant downregulation of genes in the IL-6 pathway in patients who later developed paradoxical TB-IRIS perhaps reflecting more severe pre-ART immune suppression in those who later developed paradoxical TB-IRIS. Lastly, chondroitin sulfate biosynthesis which is disaccharide that interacts with proteins to form proteoglycans which are components of the extracellular matrix which regulates many of the cell's activity was downregulated in patients who later developed paradoxical TB-IRIS compared to those who did not. The implication for this is many of the cell's functions such as proliferation, maturation and trafficking might be altered more so in patients that are predisposed to developing paradoxical TB-IRIS.

5.5 Placebo Week 2: TB-IRIS vs TB-non-IRIS

To gain better insight into the molecular events that are prominent at the time of the onset of paradoxical TB-IRIS symptoms, the gene expression profile of patients allocated to placebo who developed paradoxical TB-IRIS was compared to TB-non-IRIS controls allocated to placebo in samples collected at week 2 on ART, which is coincided with the median time of paradoxical TB-IRIS onset [21]. Subsequently, DGEA and functional enrichment analysis were conducted.

5.5.1 Differential gene expression analysis

Raw count data were modelled using DESeq2 to identify differentially abundant transcripts from a total of 95 samples collected from patients allocated to placebo in the Pred-ART trial who either developed paradoxical TB-IRIS or did not at week 2 on ART (**see Table 5.1**).

5.5.2 Exploratory analysis

Variance stabilized, normalized expression data, were assessed for quality and explored for patterns using PCA. A total of 95 eigenvectors or principal components (PC) corresponding to the patient samples were generated. Shown below are the first 3 PC which accounted for 98% of the cumulative variance (**Figure 5.7A**). Figure 5.7A depicts the relative contribution of each of the first 10 samples to each PC. The scale represents the proportion of variance contributed by each sample to each PC. Most importantly, PC1 accounted for 91.7% of the variance explained by all the samples (**Figure 5.7B**). PC1 and PC2 contributed almost 97% of the cumulative variance for all the samples (**Figure 5.7B**). Therefore, PCA was performed using the first 2 PCs for the 500 most variable genes between the two clinical groups across all samples (**Figure 5.8A**).

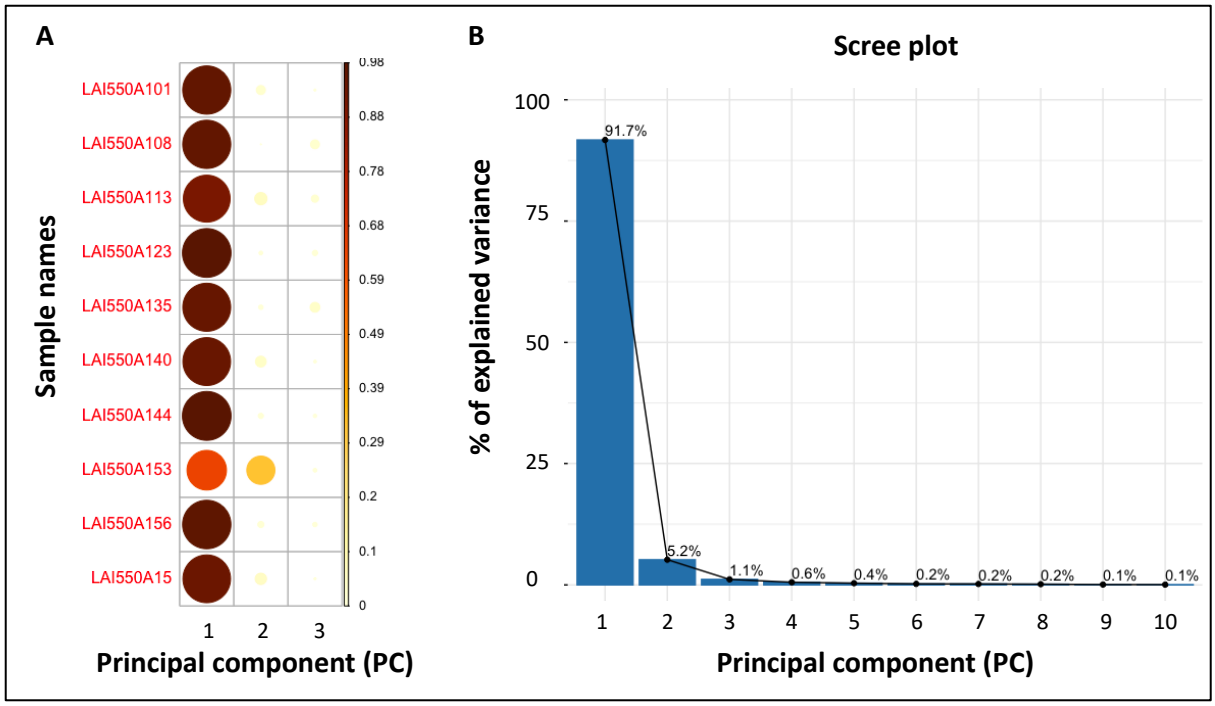

Figure 5.7. Principal component analysis (PCA) in a total of 95 samples collected from placebo allocated patients with paradoxical TB-IRIS and TB-non-IRIS controls at week 2 on ART. A. *The relative contribution of each of 10 selected samples to the cumulative variance across the first three principal components (PC).* ***B.*** *Scree plot showing the proportion of variance explained by each principal component (PC) across all samples.*

PC1 represents the linear combination of the Euclidean distances (eigenvalue) between transcripts across all 95 samples. It maximizes the variability of the data when projected in the x-axis (25%). PC2 is orthogonal to PC1, and it describes the residual variance of PC1 (13%) (**Figure 5.8A**).

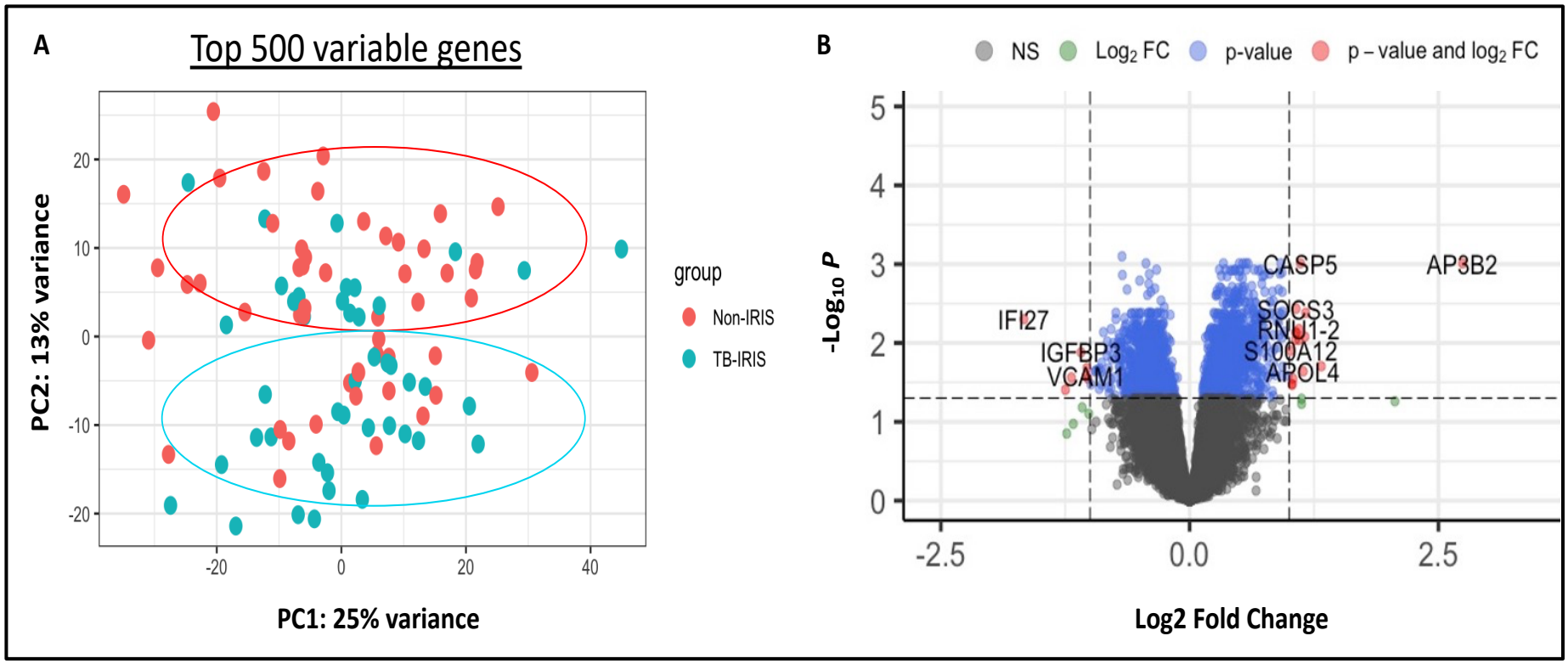

Figure 5.8. Exploratory data analysis for 95 samples collected from placebo allocated patients with paradoxical TB-IRIS and TB-non-IRIS controls at week 2 on ART. ***A.*** *Principal component analysis for the top 500 variable genes. PC1 contributed most of the variance. PC1 is a cluster predominated by samples from patients with paradoxical TB-IRIS, suggesting that there is more variation in gene expression from samples of patients with paradoxical TB-IRIS.* ***B.*** *Volcano plot showing differentially expressed genes (DEGs) in patient samples collected from the placebo arm at week 2 on ART. DEGs were defined by an adjusted p-value of less than or equal to 0.05 and log2 fold change greater than or equal to 1 or less than or equal to -1.*

PC1 accounted for most of the variance compared to PC2. PC1 is a cluster predominated by samples from patients who developed paradoxical TB-IRIS. This suggests that patients with paradoxical TB-IRIS had more perturbations in gene expression at week 2 on ART, compared to TB-non-IRIS patients. However, it is worth noting that some samples from patients who developed paradoxical TB-IRIS clustered with some from the TB-non-IRIS controls, indicating the proximity of the eigenvalues and therefore, the similarities in gene expression between the two clinical groups. Additionally, despite the application of thresholds to exclude observations with low normalized base mean to reduce noise, several outliers were observed, and these typically had high variance (**Figure 5.8A**).

Following the evaluation of the similarities in gene expression between the samples, differential gene expression analysis was performed to identify significantly upregulated and downregulated DEGs in samples from patients who developed paradoxical TB-IRIS and TB-non-IRIS control at week 2 on ART after adjusting for multiple testing (FDR = 0.05). A total of 2061 transcripts that were differentially expressed were identified. Of these, 1211 transcripts were upregulated while 850 were downregulated (**Figure 5.8B**). To explore the data further, we tested more conservative thresholds incorporating log2 fold change greater than or equal to 1 or less than or equal to -1 to identify a minimal biosignature. This dramatically collapsed the number of DEGs to 29 genes. A total of 21 transcripts were upregulated while 8 were downregulated in patients who developed paradoxical TB-IRIS (**Figure 5.9**). Many of the upregulated genes were directly linked to neutrophil activation & degranulation and caspase secretion. The downregulated genes were diverse in function and included, but were not limited to, immunoglobulin (Ig) like encoded proteins involved in pathogen recognition, Ig-like encoded proteins involved in the transport of insulin, and interferon alpha inducible genes.

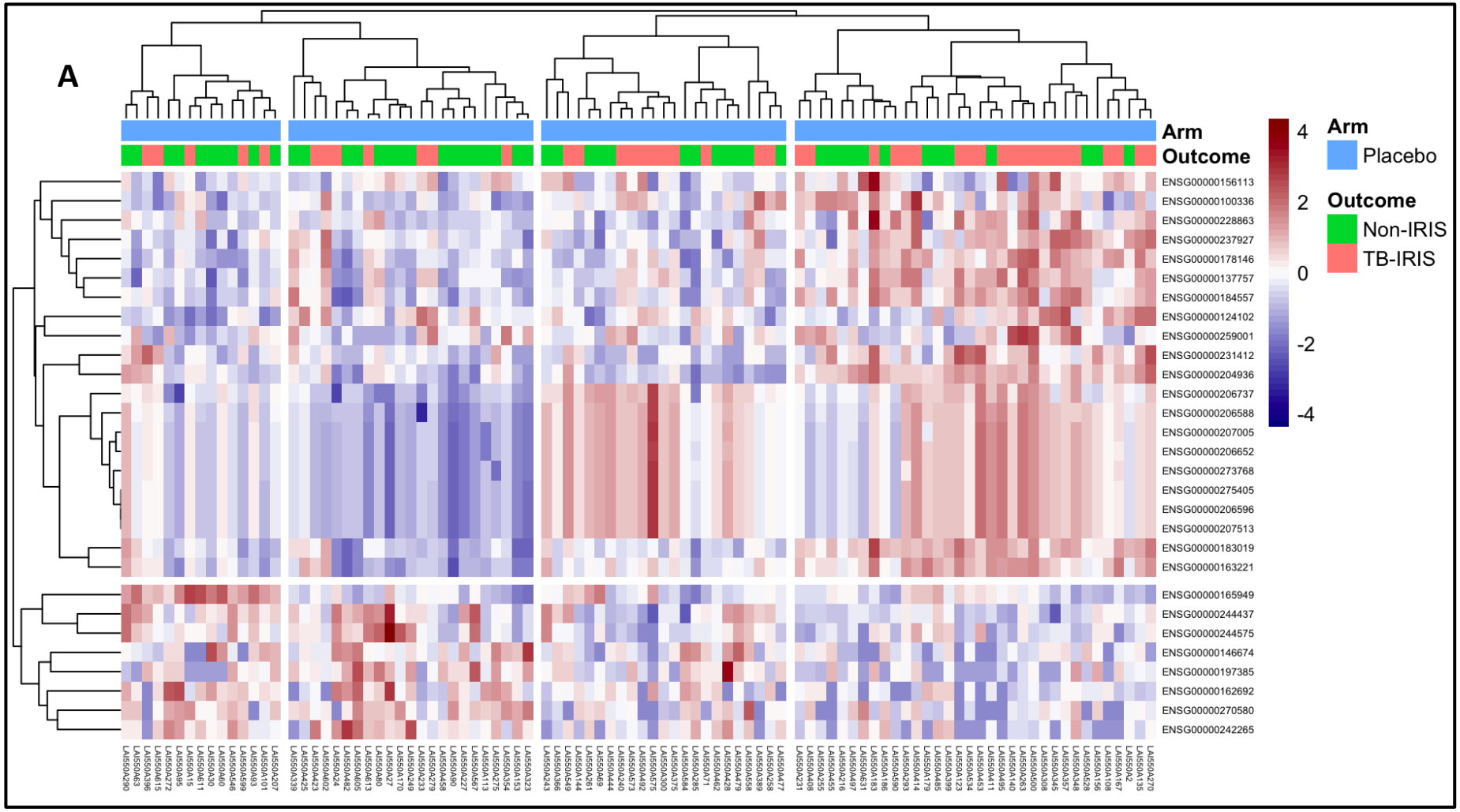
A
Arm
Outcome
ENSG00000156113
ENSG00000100336
ENSG00000228863
ENSG00000237927
ENSG00000178146
ENSG00000137757
ENSG00000184557
ENSG00000124102
ENSG00000259001
ENSG00000231412
ENSG00000204936
ENSG00000206737
ENSG00000206588
ENSG00000207005
ENSG00000206652
ENSG00000273768
ENSG00000275405
ENSG00000206596
ENSG00000207513
ENSG00000183019
ENSG00000163221
ENSG00000165949
ENSG00000244437
ENSG00000244575
ENSG00000146674
ENSG00000197385
ENSG00000162692
ENSG00000270580
ENSG00000242265
4
2
0
-2
-4
Arm
Placebo
Outcome
Non-IRIS
TB-IRIS

Figure 5.9. Differential gene expression analysis in 95 samples collected from placebo allocated patients with paradoxical TB-IRIS and TB-non-IRIS controls at week 2 on ART. A, *Visualization of 29 DEGs identified in samples from patients with paradoxical TB-IRIS (pink) and TB-non-IRIS control(green) at week 2 on ART. A total of 21 transcripts were upregulated and 8 transcripts were downregulated in samples from TB-IRIS patients.*

Next, we visualized the 29 DEGs using a heatmap to explore the gene expression profiles in the samples from placebo allocated patients collected from all patients at week 2 on ART (**Figure 5.9**). Clustering by columns (samples), did not reveal interesting patterns between TB-IRIS and TB-non-IRIS samples. However, in the clustering of rows (transcripts) there were mixed clusters that revealed 3 gene expression patterns: transcripts (n= 21) that were highly expressed (upregulated) predominantly in samples collected from patients who developed paradoxical TB-IRIS but not in samples from TB-non-IRIS controls; 8 transcripts that were upregulated in samples from TB-non-IRIS controls but were downregulated in most samples from patients who developed paradoxical TB-IRIS; and a small number of transcripts from both clinical groups that showed modest change in gene expression. (**Figure 5.9)**.

When relating these findings to the Pred-ART clinical data, these exploratory findings were rational: paradoxical TB-IRIS patients in this cohort had a spectrum of severity of clinical symptoms ranging from severe to mild with many of the patients having mild inflammatory features that were not markedly distinct from the TB pathology which afflicted TB-non-IRIS individuals. Of note, patients who developed severe paradoxical TB-IRIS symptoms were prescribed prednisone for treatment, but almost always after the week 2 visit.

Data from previous studies is different to what was observed in this study [15, 177]. The differences in the clustering patterns between this study and the findings reported by Lai and colleagues could potentially be due to the differences in the number of patient samples and the sequencing depth, but more likely due to the severity of inflammatory manifestations experienced by the paradoxical TB-IRIS patients enrolled in the TB-ART trial who were all hospitalized for TB treatment [177].

In this study, around three-times the number of samples using RNA-seq technology were analyzed compared to the previous study by Lai and colleagues, in which samples from the TB-ART observational study were analyzed using microarray technology [177]. Additionally, the hospitalized patients in that observational study were more severely ill with clinical manifestations involving multiple organ systems compared to the patients in this cohort [177]. This is consistent with the findings from a cohort of pediatric cases of paradoxical TB meningitis IRIS described by Rohlwink and colleagues [385].

5.5.3 Gene set enrichment analysis

To determine the functionality of the DESeq2 derived DEGs in patients who developed paradoxical TB-IRIS relative to TB-non-IRIS controls at week 2 on ART, all transcripts were pre-ranked by effect size. Functional enrichment analysis was computed with GSEA [282]. Described below, are the significantly enriched biological pathways and their attendant genes.

5.5.3.1 Neutrophil degranulation gene set is significantly upregulated in samples from patients with paradoxical TB-IRIS compared to TB-non-IRIS controls at week 2 on ART.

Several biological pathways were significantly enriched in samples collected from patients who developed paradoxical TB-IRIS compared to TB-non-IRIS controls at week 2 on ART. A normalized enrichment score (NES) greater or less than 0 and a false discovery rate (FDR) less or equal to 0.1 were used to define the level of statistical significance as determined by the Kolmogorov-Smirnov test. Shown in Figure 5.11 are the 20 most upregulated and downregulated biological processes that are likely involved in paradoxical TB-IRIS pathogenesis. The neutrophil degranulation gene set was the most significantly enriched biological pathway in samples from patients who developed paradoxical TB-IRIS compared to TB-non-IRIS controls at week 2 on ART (**Figure 5.11**). The bottom panel of Figure 5.11 depicts an enrichment plot for the neutrophil degranulation gene set; the green line depicts the running enrichment score, while the red dotted line depicts the enrichment score which is defined as the maximum deviation of the running sum from zero [282, 350, 351]. The top panel depicts the DESeq2 derived gene list that is ranked by the log2fold change metric. Each vertical bar represents individual genes which add up to a gene set of 452 genes that comprise this biological pathway. The closely packed upright bars before the enrichment score are the most upregulated genes that contribute significantly to the enrichment score. These are known as the leading-edge subset. Among the top 10 leading edge subset was CD177 which is a neutrophil specific glycoprotein involved in the activation of neutrophils (**Figure 5.10**) [386].

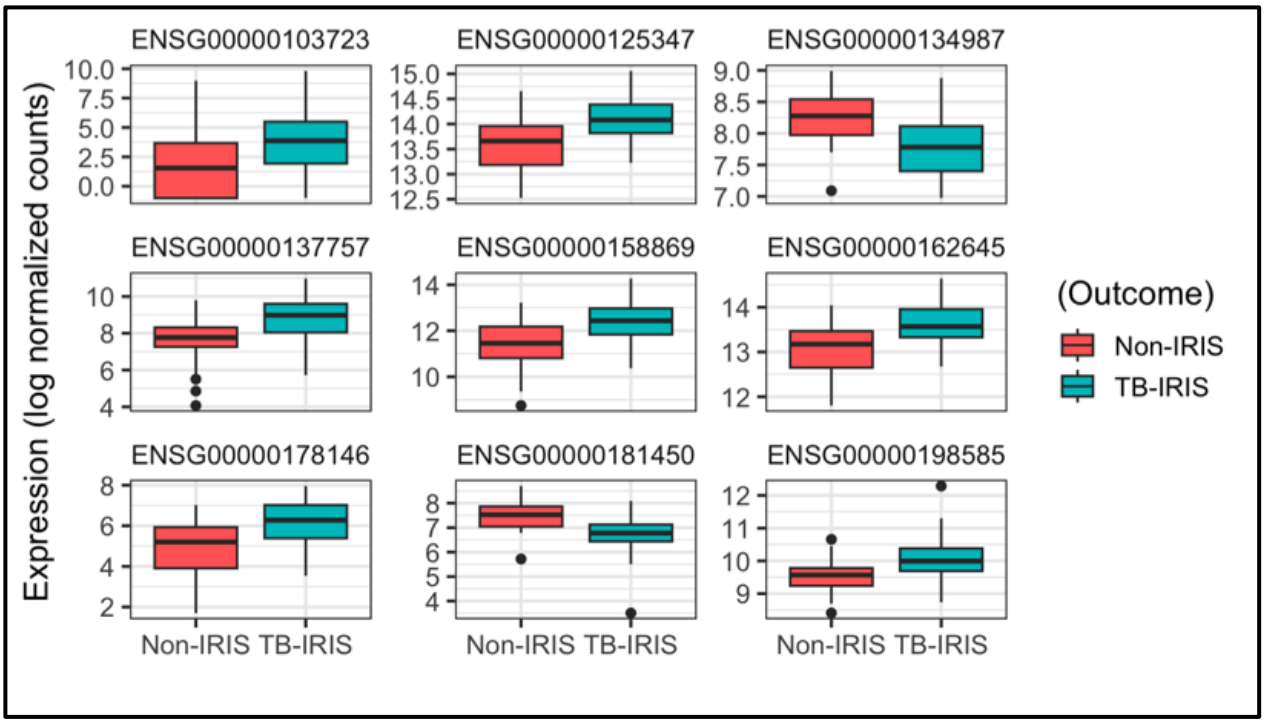

Figure 5.10. Gene expression of the top 9 differentially expressed transcripts identified with DESeq2 in samples comparing patients who developed paradoxical TB-IRIS and those who did not (TB-non-IRIS controls) at week 2 on ART. *From left to right AP3B2, IRF1, WDR36, CASP5, FCER1G, GBP2, RP1-232L22_B1, ZNF678, NUDT16.*

Other biological pathways that were significantly upregulated which are relevant to the pathogenesis of paradoxical TB-IRIS included antigen cross presentation, innate immune responses, interferon gamma signaling, interleukin-1 signaling and regulated necrosis (**Figure 5.11**). These findings are discussed in the context of peer reviewed literature below.

One of the key events that occurs early during the acute inflammatory response is the migration of leukocytes from the blood to the tissue at the site of infection or inflammation [204, 387-389]. Neutrophils and monocytes are the first innate immune cells to traffic to the site of infection and/or inflammation. The mechanism of this migration is a complex biological process involving inflammatory cytokines and kinases, chemokines and other chemotactic factors, and adhesion molecules [390]. All the three elements defined in Table 5.3 have distinct roles but function in concert to orchestrate the process of inflammation. Inflammatory cytokines such as TNFα, IL-1 family of cytokines, nitric oxide, and IL-6 activate the endothelium of the vessel wall, causing vasodilation and increased vascular permeability [391-

393]. The four cardinal signs of inflammation, heat, redness, swelling, and pain may characterize the onset of paradoxical TB-IRIS, especially when it involves peripheral lymph nodes. The first three are due to vasodilation and increased vascular permeability and can be explained by the action of the inflammatory cytokines on the vessel wall [392, 393].

Chemokines and other chemotactic factor such as IL-8, complement receptor 5a (C5A) and *N*-Formylmethionyl-leucyl-phenylalanine (FMLP), induce neutrophil and monocyte migration, while adhesion molecules such as selectins and integrins are important in promoting the adhesion of neutrophils and monocytes to the vascular endothelium [394-398]. Once immobile, the infiltrating leukocytes produce collagenase to disrupt the basement membrane resulting in trans-endothelial passage and extravasation [399, 400].

Table 5.3*.Gene names, symbols and function identified as part of neutrophil degranulation leading edge subset that was significantly enriched (FDR = 0.1) in patient samples with paradoxical TB-IRIS compared to TB-non-IRIS controls week 2 on antiretroviral therapy (ART)*

Gene name	Symbol	Function
Neutrophil Degranulation leading edge subset		
CD177 molecule	CD177	Gene encodes a glycosyl-phosphatidylinositol (GPI)-linked cell surface glycoprotein that plays a role in neutrophil activation
S100 calcium binding protein A12	S100A12	Involved in specific calcium-dependent signal transduction pathways and its regulatory effect on cytoskeletal components may modulate various neutrophil activities.
S100 calcium binding protein A09	S100A09	Involved in specific calcium-dependent signal transduction pathways and its regulatory effect on cytoskeletal components may modulate various neutrophil activities.
Mast cell expressed membrane protein 1	MCEMP1	Encoded gene involved in regulating mast cell differentiation or immune responses.
Elastase neutrophil expressed	ELANE	Elastases form a subfamily of serine proteases that hydrolyze many proteins in addition to elastin
Haptoglobin	HP	The protein encoded also functions to bind free plasma hemoglobin and exhibits antimicrobial activity against bacteria
Vanin1	VNN1	Encoded protein involved in hematopoietic cell trafficking
Heat shock protein family A1 member A	HSPA1A	Protein stabilizes existing proteins against aggregation and mediates the folding of newly translated proteins in the cytosol and in organelles
S100 calcium binding protein A08	S100A08	Involved in specific calcium-dependent signal transduction pathways and its regulatory effect on cytoskeletal components may modulate various neutrophil activities
S100 calcium binding protein A11	S100A11	Involved in specific calcium-dependent signal transduction pathways and its regulatory effect on cytoskeletal components may modulate various neutrophil activities
Defensin alpha4	DEFA4	Encoded protein is a member of the family of antimicrobial and cytotoxic peptides abundant in granules of neutrophils
Myeloperoxidase	MPO	Encodes a heme protein synthesized during myeloid differentiation that constitutes the major component of neutrophil azurophilic granules
TNF alpha induced protein 6	TNFAIP6	Encoded gene is important in the protease network associated with inflammation
S100 calcium binding protein P	S100P	Involved in specific calcium-dependent signal transduction pathways and its regulatory effect on cytoskeletal components may modulate various neutrophil activities
Cathelicidin antimicrobial peptide	CAMP	Encoded protein is a member of the antimicrobial peptide family contained in neutrophilic granules
Matrix metalloprotease 9	MMP9	Encoded protein remodels extracellular matrix
Matrix metalloprotease 8	MMP8	Encoded protein remodels extracellular matrix
Azurocidin 1	AZU1	Azurophil granules, specialized lysosomes of the neutrophil, contain at least 10 proteins implicated in the killing of microorganisms
PYD and CARD domains	PYCARD	Adaptors of the NLRC4 Inflammasome which function as intracellular pattern recognition receptor
Nuclear factor kappa beta 1	NFKB1	A transcription regulator that is activated by various intra- and extra-cellular stimuli such as cytokines, oxidant-free radicals, ultraviolet irradiation, and bacterial or viral products
Gasdermin D	GSDMD	Modulates the process of pyroptosis
Complement receptor 5 a	C5AR1	Facillitates the migration and activation of neutrophils
ADAM8 metallopeptidase domain	ADAM8	Encoded protein breaks down extracellular matrix

Previous studies have identified biological processes upstream of antigen presentation such as the upregulation of pattern recognition receptors (PRRs) in immune cells in samples of patients with paradoxical TB-IRIS at symptom onset [177]. PRRs recognize highly conserved structures of micro-organisms known as pathogen associated molecular patterns (PAMPs) such as components of the cell wall and nucleic acids [401, 402]. The main class of PRR is that of the toll like receptors (TLRs) which are found on cell membranes or intracellularly on the endosomal membrane [194, 403]. This endows them with the ability to recognize diverse extracellular and intracellular PAMPs [194, 404]. In a normal functioning cell, PRR-PAMP interaction leads to the internalization of Mtb through a process called phagocytosis [405, 406]. In the phagosome, the intact Mtb is digested into small peptides which are subsequently presented to CD4 T cells to activate adaptive immune cell responses [407]. Notably, although they are not professional phagocytes, neutrophils have the capacity to engulf Mtb, and present processed antigens to CD4 T cells to trigger an adaptive immune response [408-412]. This could potentially explain why some individuals develop paradoxical TB-IRIS as early as two days after initiating ART, while others develop paradoxical TB-IRIS weeks later. The differential onset of paradoxical TB-IRIS could be related to the half-life of neutrophils which is extended up to 11 days beyond the normal range during disease [413].

The process of antigen presentation leads to the production of interferon gamma (IFNγ) by CD4 T cells. Interestingly, IFNγ production was one of the biological pathways which was significantly upregulated in patients who developed paradoxical TB-IRIS compared to TB-non-IRIS controls at week 2 on ART (**Figure 5.11**). Several studies have reported higher frequencies of Mtb-specific CD4 T cells that produce interferon gamma in patients who developed paradoxical TB-IRIS compared to TB-non-IRIS controls at the onset of disease [29, 39]. Furthermore, once engaged, PRRs initiate a signaling cascade that culminates in the activation of transcription factors such as the NF-Kβ which mediates the process of inflammation as described previously [162, 177].

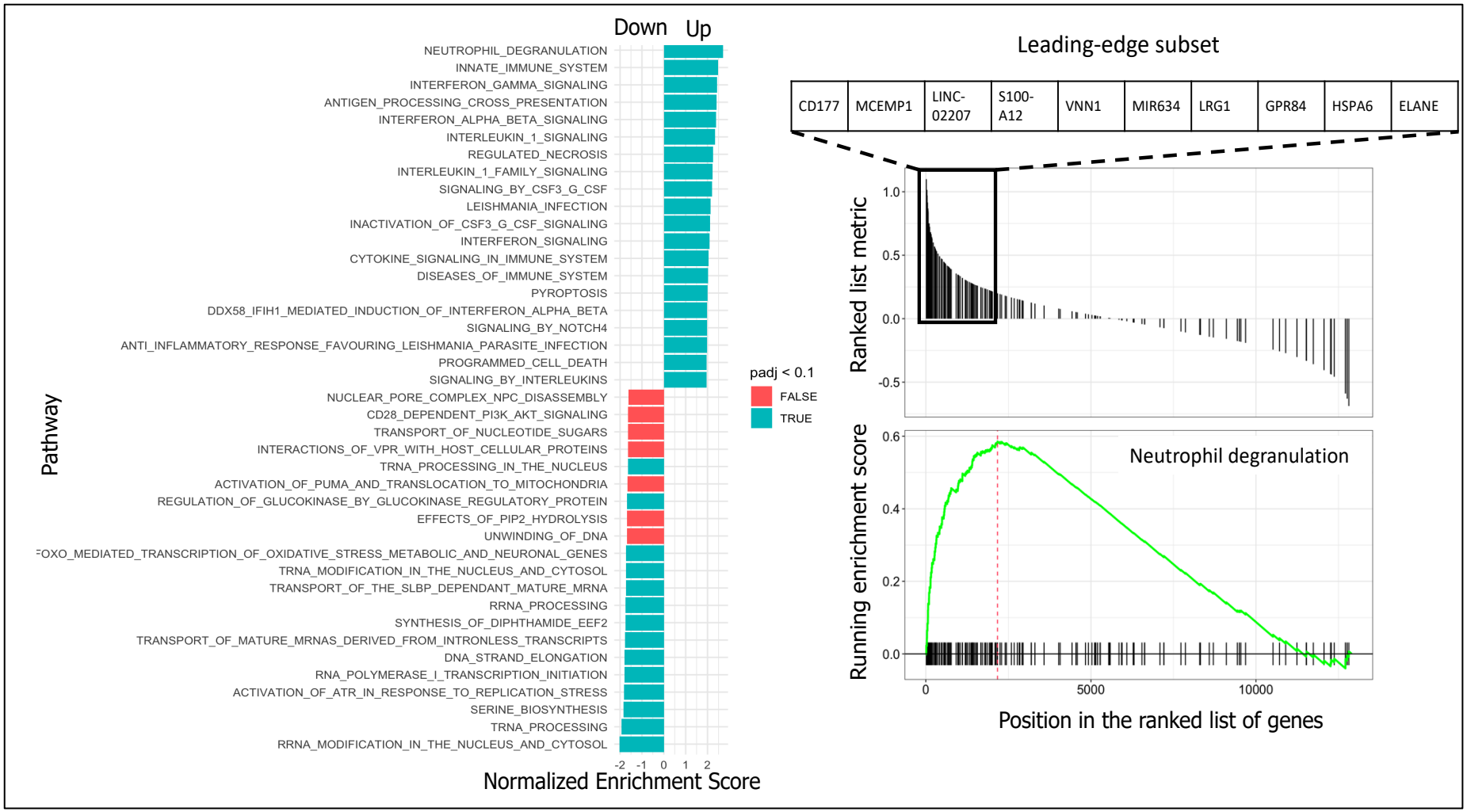

Figure 5.11.Gene set enrichment analysis in samples from placebo allocated patients with paradoxical TB-IRIS and TB-non-IRIS controls at week 2 on ART. *Significantly enriched pathways were defined by a normalized enrichment score greater than or less than 0 and adjusted p-value*

of less or equal to 0.05. The right panel shows an enrichment plot for the neutrophil degranulation pathway with the red line showing the enrichment score and the vertical black bars representing individual genes.

Additionally, Tadokera and colleagues reported statistically significant expression and serum secretion of IFNγ in patients with paradoxical TB-IRIS compared to TB-non-IRIS patients at TB-IRIS onset [162]. Evidence in the literature suggests that prior to the initiation of ART, TB-IRIS patients fail to mount adaptive immune responses due to HIV mediated CD4 T cell depletion [212]. The upregulation of interferon gamma signaling following the initiation of ART reported here is due to ART mediated HIV suppression, which results in in CD4 T cell recovery [39]. This leads to the activation of the Mtb primed innate immune cells culminating in an aberrant proinflammatory immune response [39, 162, 177]. To support this, previous reports detailed significant expression and secretion of proinflammatory cytokines including but not limited to IL-6, TNFα and IFNγ in patients with paradoxical TB-IRIS compared to TB-non-IRIS controls at the onset of symptoms [162].

Furthermore, the process of inflammation can be triggered and/or exacerbated by the release of danger associated molecular patterns (DAMPs) [414, 415]. DAMPs make up a broad category that include lipids originating from the nucleus, nucleic acids, and intracellular proteins, and other macromolecules originating from membrane enclosed organelles in the cytoplasm of cells [292, 414, 416]. Neutrophils can release DAMPs in a passive or active manner [417, 418]. They trap and kill Mtb through the release of their unpacked chromosomal DNA [414]. The extracellular chromosomal DNA is embedded with histones and often associates with antimicrobial proteins originating from neutrophil extracellular vesicles [419]. These are called neutrophil extracellular traps (NETs) and their passive release is toxic to Mtb [420]. Furthermore, the exocytosis of neutrophil vesicles through a process known as neutrophil degranulation exemplifies the active release of DAMPs by neutrophils.

Neutrophil degranulation was significantly enriched in patients who developed paradoxical TB-IRIS compared to TB-non-IRIS controls at week 2 on ART after correcting for multiple hypothesis testing (FDR = 0.1). In fact, this was true even with a much stringent FDR of 0.05 which assumes that 5% of the significantly enriched findings are false positives. The release of DAMPs activate intracellular PRRs which culminates in the upregulation of proinflammatory cytokines in a NF-κβ dependent manner [402, 421].

The NLRC4 inflammasome is an intracellular PRR that requires two stimuli for activation; typically, a priming signal such as a PAMP (i.e LPS) and an activation signal such as a DAMP [422]. The NLRC4 inflammasome was identified as one of the 800 transcripts that comprise the innate immune gene set which was significantly upregulated in samples of patients who

developed paradoxical TB-IRIS compared to TB-non-IRIS controls at week 2 on ART [162, 423]. The mature NLRC4 inflammasome recruits and activates caspase-1 which leads to the maturation of the IL-1 family of cytokines such as IL-1α, IL-1β and IL-18 which are potent mediators of inflammation [15, 177, 422]. In this way, inflammasomes amplify the inflammatory cascade in patients with paradoxical TB-IRIS [15, 30]. Therefore, it is likely that the active release of DAMPs through the process of neutrophil degranulation drives and/or exacerbates paradoxical TB-IRIS pathology.

Moreover, there is more evidence to suggest that the involvement of neutrophils is important in the pathogenesis of paradoxical TB-IRIS [239]. Some reports have described significantly higher proportions of neutrophils at TB-IRIS onset in patients who developed paradoxical TB-IRIS compared to TB-non-IRIS controls [239]. Others have characterized neutrophils and have shown that they have a variety of surface receptors which enable them to interact with various immune cells [424]. The implication is that they can alter their target cell and thereby modify its function. This can be beneficial or detrimental depending on the interaction and the cytokine milieu [386, 412, 425]. One study experimentally demonstrated the effect neutrophils have on macrophage function, stimulating production of proinflammatory cytokines and matrix metalloproteinases by macrophages [425]. Notably, a spectrum of proinflammatory cytokines and matrix metalloproteinases were reported to be significantly higher in samples from patients who developed paradoxical TB-IRIS compared to TB-non-IRIS controls at week 2 on ART [162]. Finally, the immunohistochemistry of clinical specimens from patients with paradoxical TB-IRIS supports the hypothesis that neutrophils are central to TB-IRIS immunopathology. Staining of markers of degranulation revealed the presence of neutrophil elastase in the pus exudates collected from patients with paradoxical TB-IRIS [239].

Similarly, several biological pathways that were significantly downregulated at week 2 on ART in samples from patients who developed paradoxical TB-IRIS compared to TB-non-IRIS controls were identified. rRNA modification in the nucleus and cytosol was the most significantly downregulated biological pathway at week 2 on ART. The leading-edge subset was largely representative of the genes involved in the complement pathway. This is in contrast with other findings reported in the literature [208]. Tran et al. reported the significant upregulation of the complement pathway at the time of paradoxical TB-IRIS onset. Notably, a smaller sample size compared to ours was analyzed by microarray technology by Tran et al.

Furthermore, other biological pathways reflected the downregulation of immune regulatory or check point cascades. Genes that encode serine/threonine kinases that mediate protein activation through phosphorylation which enable protein-protein interactions such as LIMK2 were significantly downregulated. In addition, genes that encode protein phosphatases such as PPP1R12B, PPP1R12B and PPP1CB that regulate the activity of other proteins by dephosphorylation were also significantly downregulated (**Figure 5.11**). Lastly, genes that encode proteins that belong to the RAS subfamily which belong to the RHO family of GTPases and localize to the membrane and cytosol to mediate intracellular signal transduction were among the genes that were downregulated in patients who developed paradoxical TB-IRIS compared to TB-non-IRIS patients at week 2 on ART.

5.5.4 Longitudinal gene expression analysis in patients with paradoxical TB-IRIS.

To follow up on the cross-section analysis, longitudinal changes in gene expression in patients who developed paradoxical TB-IRIS and in TB-non-IRIS controls respectively were investigated. This was achieved by performing pairwise comparisons in samples collected at week 0 and 2 on ART.

5.5.4.1 Differential gene expression analysis using DESeq2 at week 2 versus 0 in samples from patients with paradoxical TB-IRIS.

Differential gene expression analysis was performed on 100 samples from placebo allocated patients who developed paradoxical TB-IRIS between week 2 on ART and at week 0 prior to the initiation of ART with the aid of DESeq2 as previously described (**see Page 109, section 3.21.14**). We identified a total of 5912 DEGs between week 2 and week 0, after correcting for multiple hypothesis testing (FDR = 0.05). A total of 2614 genes were upregulated while 3298 were downregulated at week 2 compared to week 0 (**Figure 5.12A**).

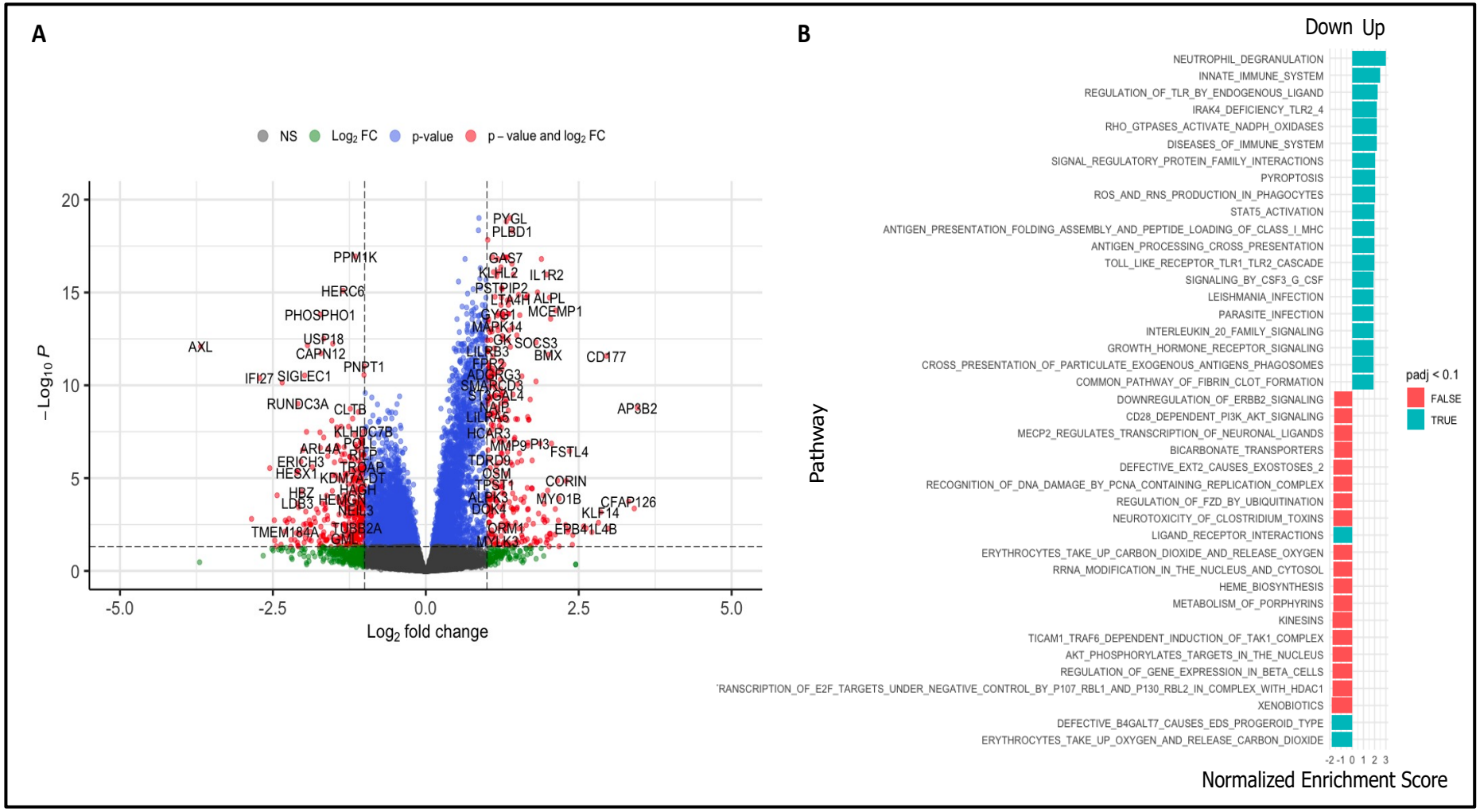

Figure 5.12. Longitudinal changes in gene expression in samples from patients with paradoxical TB-IRIS at week 2 on ART*. A, Differential gene expression analysis showing changes in gene expression in samples from patients with paradoxical TB-IRIS comparing gene expression at*

week 2 to that at week 0 in pairwise comparison. ***B,*** *Pathway analysis with gene set enrichment analysis identified enriched biological pathways in samples from patients who developed paradoxical TB-IRIS at week 2 on ART compared with week 0.*

Additionally, a more stringent threshold incorporating log2foldchange greater or equal to 1 or less or equal to -1 were explored to identify a minimal biosignature. This substantially reduced the number of DEGs to 834 genes. A total of 298 genes were upregulated while 536 genes were downregulated.

Among the genes that were significantly upregulated in the reduced DEG pool was CD177 which is an activation cell surface marker expressed chiefly on neutrophils. Other identified transcripts included IL-1 family of cytokines and receptors and the NLRC4 inflammasome that were differentially expressed at week 2 compared to week 0 in samples from patients who developed paradoxical TB-IRIS (**Figure 5.12**).

Among some of the genes that were downregulated were those encoding proteins involved in the shuttling of oxygen and carbon dioxide.

5.5.4.2 Functional enrichment analysis with GSEA

The DESeq2 derived gene list from samples of placebo-allocated patients who developed paradoxical TB-IRIS comparing week 2 on ART to week 0 were summarized into biological pathways using GSEA [282] (**Figure 5.12 B)**. Several biological pathways were significantly enriched. As with previous analysis, biological pathways with a NES greater or less than 0, and an FDR of less or equal to 0.1 were of interest. Of the top 5 biological pathways with a NES above 2, neutrophil degranulation, antigen cross presentation, interferon gamma signaling, interleukin-1 signaling and regulated necrosis were among the highly enriched. Generally, these reflected innate and adaptive immune responses and their cytokine and chemokine effectors with a neutrophil theme. For more detail, these were previously discussed in detail above under the cross-sectional comparisons where the findings were similar.

Furthermore, there were several biological pathways that were significantly downregulated in samples collected from patients with paradoxical TB-IRIS at week 2 on ART compared to week 0 prior to the initiation of ART (**Figure 5.12B)**. These generally reflected adaptation to hypoxic stress and metabolic homeostatic imbalance at week 2 compared to week 0. To the best of our knowledge, this is the first report to detail the longitudinal changes that occur in paradoxical TB-IRIS patients. Particularly as it relates to the biological processes that are downregulated at the time of TB-IRIS onset.

5.5.5 Longitudinal gene expression analysis in patients allocated placebo who did not develop paradoxical TB-IRIS.

Next the gene expression signature associated with "protection" in HIV-TB patients who were allocated placebo and did not develop paradoxical TB-IRIS upon initiating ART was investigated. This was achieved by conducting differential gene expression analysis longitudinally in samples collected at week 0 prior to the initiation of ART and at week 2 on ART in patients who did not develop paradoxical TB-IRIS (TB-non-IRIS controls).

5.5.5.1 Differential gene expression analysis using DESeq2 at week 2 versus 0 in samples from TB-non-IRIS patients.

Differential gene expression analysis was conducted on 109 samples derived from placebo allocated patients who did not develop paradoxical TB-IRIS (TB-non-IRIS controls) collected between week 2 (n = 51) on ART and at week 0 (n = 58) prior to the initiation of ART with the aid of DESeq2 as previously described (**see Page 109, section 3.21.14**). A modest number of DEGs (n = 52) were identified between week 2 and week 0 in samples from TB-non-IRIS controls after adjusting for multiple hypothesis testing (FDR = 0.05) (**Figure 5.13)**. A total of 14 transcripts were upregulated while 39 were downregulated at week 2 compared to week 0 (**Figure 5.13 A**).

Among the genes that were significantly upregulated was *defa1* which encodes a neutrophil antibacterial defensin protein. Other genes that were downregulated included *siglec 1* which is mainly expressed in various subtypes of macrophages and is associated with several inflammatory diseases; *hes4* which is a transcription factor and *usp 18* (**Figure 5.13A**). The modest change in gene expression in TB-non-IRIS controls following ART initiation probably reflects minimal immune activation. This is supported by previous experimental data [29].

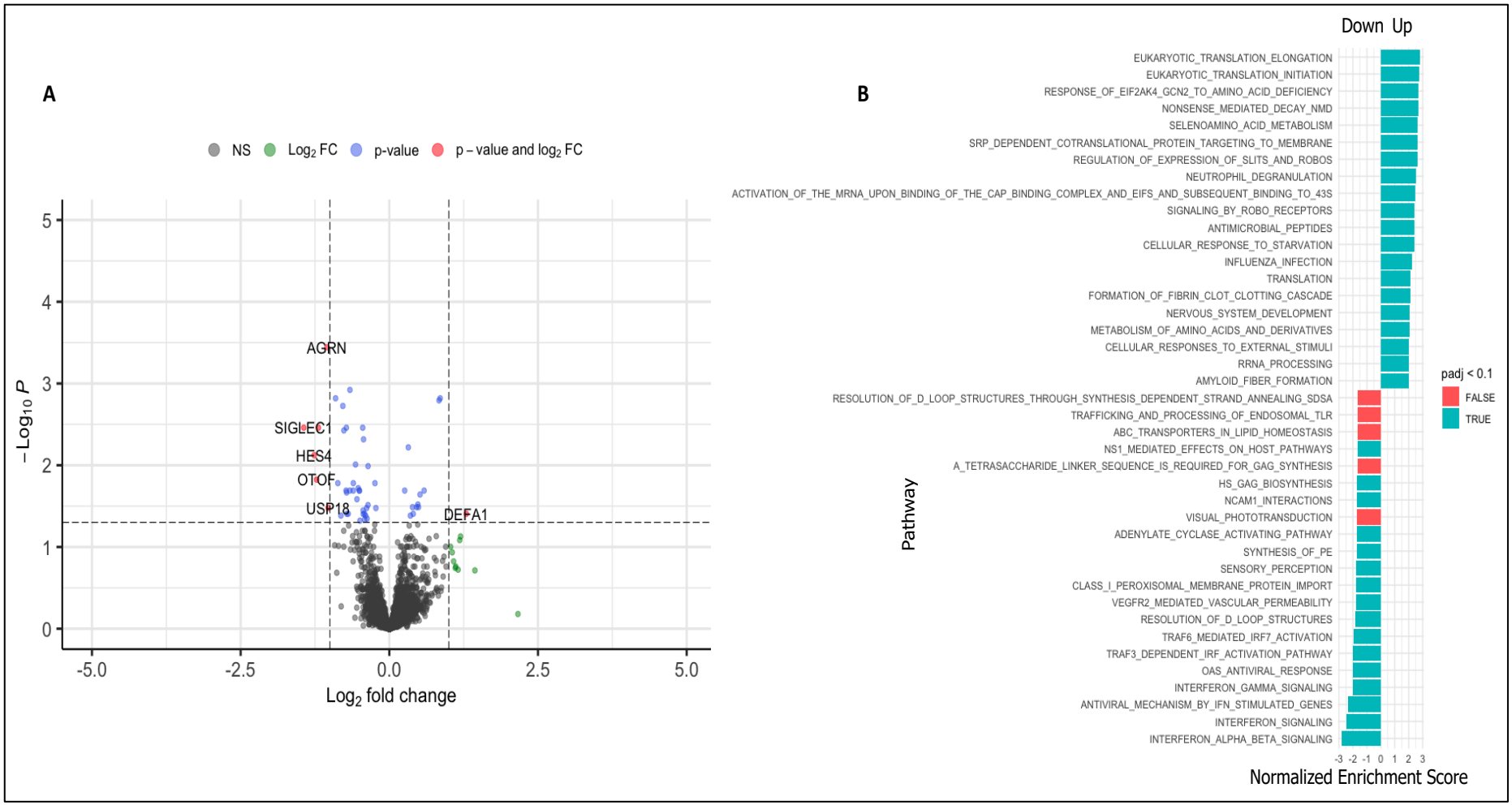

Figure 5.13. Longitudinal changes in gene expression in samples from TB-non-IRIS patients at week 2 on ART*. A, Differential gene expression analysis showing modest changes in gene expression in patients who did not develop paradoxical TB-IRIS comparing gene expression at week 2*

to that at week 0 in a pairwise comparison. B, Pathway analysis with gene set enrichment analysis identifies enriched biological pathways in samples from TB-non-IRIS patients at week 2 on ART compared with week 0.

5.5.5.2 Functional enrichment analysis with GSEA

The gene list derived from DESeq2 for samples collected from TB-non-IRIS patients longitudinally comparing week 2 on ART to week 0 were summarized into biological pathways using GSEA [282].

Several biological pathways were significantly enriched (**Figure 5.13 B)**. As with the previous analysis, biological pathways with a NES above or below 0 and a FDR of less or equal to 0.1 were considered when comparing DEGs at week 2 on ART relative to week 0 in patients who did not develop paradoxical TB-IRIS. Many of the biological pathways that were significantly upregulated included those involved in protein synthesis of the 60S subunit of the eukaryotic ribosomal RNA. Fibrin formation was among the biological pathways that were significantly upregulated in TB-non-IRIS patients at week 2 compared to week 0. Fibrin plays a role in the coagulation cascade and is a major component in the synthesis of the extracellular matrix. This implies that patients who did not develop paradoxical TB-IRIS are likely characterized by biological process involved in the biosynthesis and remodeling of the extracellular matrix which indicates tissue healing. Other notable pathways that were upregulated in these patients were neutrophil responses and there was notable absence of the genes that encode both adaptive immune responses and robust proinflammatory cytokine effectors which were detected in patients who developed paradoxical TB-IRIS.

Furthermore, there were several biological pathways that were significantly downregulated in samples collected from TB-non-IRIS patients at week 2 on ART versus week 0 (**Figure 5.13B**). The most predominant included interferon alpha/beta signaling, interferon signaling, interferon gamma signaling, antiviral mechanism by interferon stimulated genes and antiviral responses. These generally reflected the downregulation of antiviral responses, in the context of suppression of HIV replication by ART. To the best of my knowledge, this is the first report to detail the longitudinal changes that occur in TB-non-IRIS patients. Particularly as it relates to the biological processes that are downregulated in TB-non-IRIS patients at week 2 on ART. These findings could potentially point towards a protective biosignature in patients who do not develop paradoxical TB-IRIS.

Lastly, to identify the transcripts that are potentially associated with paradoxical TB-IRIS pathology or protection from it, DEGs between week 2 and week 0 were compared between the patients who developed paradoxical TB-IRIS and those who did not (TB-non-IRIS controls) respectively (**Figure 5.14**).

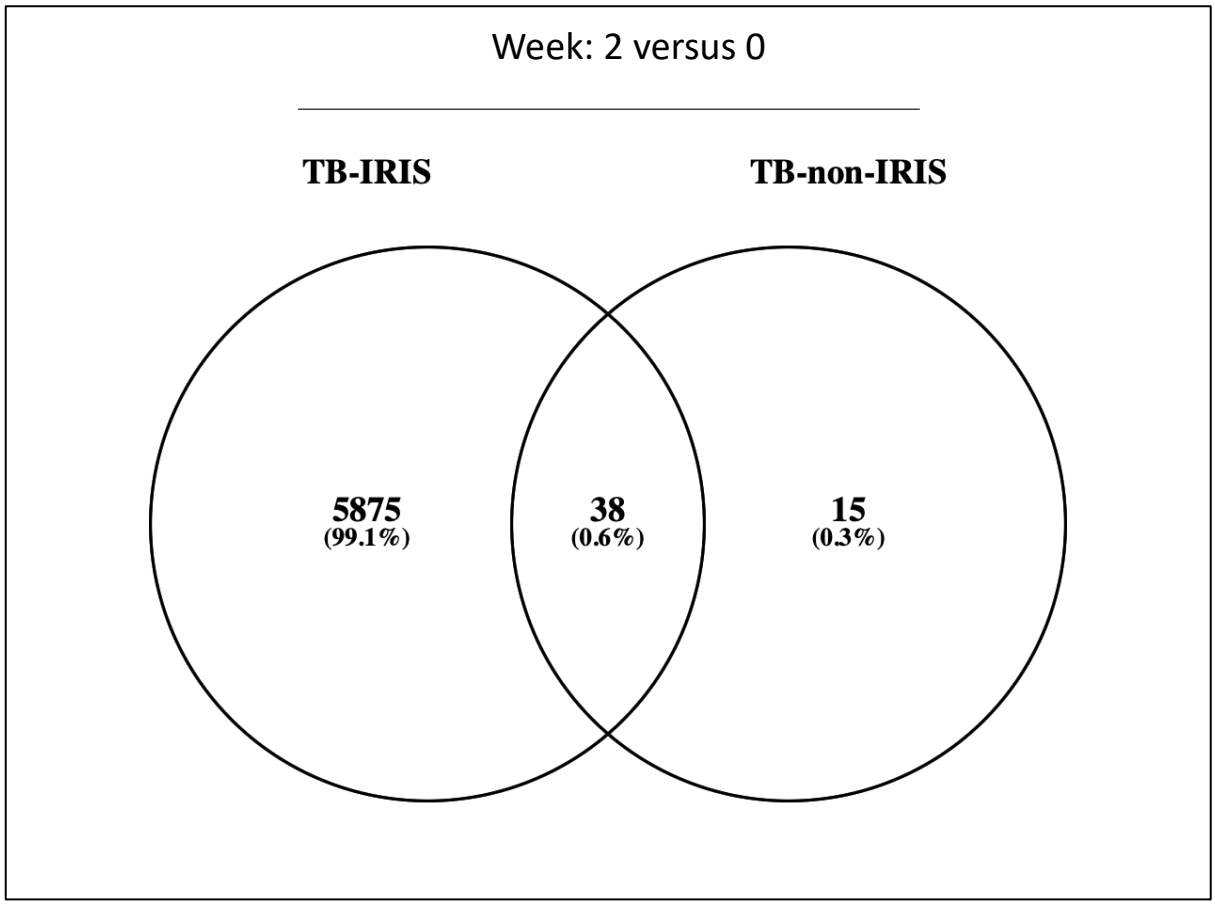

Figure 5.14. Overlap of differentially expressed genes in samples from patients with paradoxical TB-IRIS and TB-non-IRIS controls at week 2 on ART compared to week 0 prior to ART. *A total of 5875 and 32 transcripts were mutually exclusive in samples from patients with TB-IRIS and TB-non-IRIS controls respectively. A total of 38 differentially expressed genes were shared between the two clinical groups.*

A total of 5592 DEGs were identified between week 0 and week 2 in TB-IRIS patients compared to 53 DEGs in TB-non-IRIS controls, which indicated greater transcriptional perturbation in patients who developed paradoxical TB-IRIS at week 2 on ART (**Figure 5.14**). A total of 5574 differentially expressed transcripts were exclusively found in patients who developed paradoxical TB-IRIS compared to only 15 in TB-non-IRIS controls. A total of 38 transcripts were common in samples from patients with paradoxical TB-IRIS and TB-non-IRIS controls (**Figure 5.14**). The 15 genes that were mutually exclusive to TB-non-IRIS patients included among others several transcription factors and macrophage-specific surface markers.

5.5.6 Weighted Gene Co-expression Network Analysis (WGCNA)

Weighted gene co-expression networks were constructed from an expression matrix of patients who were allocated placebo who developed paradoxical TB-IRIS and those who did not at week 2 on ART. The strength behind WGCNA is identifying transcripts with similar expression profiles and clustering them together to identify hub genes. These highly correlated genes are assumed to share overlapping functionality and are consequently involved in the same biological pathways. The highly correlated modules were used to corroborate our initial findings using functional enrichment analysis with GSEA.

5.5.6.1. Network construction with WGCNA identifies five module eigengenes that are significantly correlated with paradoxical TB-IRIS

Unsupervised learning approaches were used to identify and exclude a single outlier sample from a patient with paradoxical TB-IRIS at week 2 on ART (**Figure 5.10A**). A network that satisfied the criteria for scale free topology was constructed by converting a gene expression matrix into a correlation matrix. A soft threshold (β value) of 12 was applied to the correlation matrix to generate a weighted adjacency matrix that was used for network construction (**Figure 5.10B&C**).

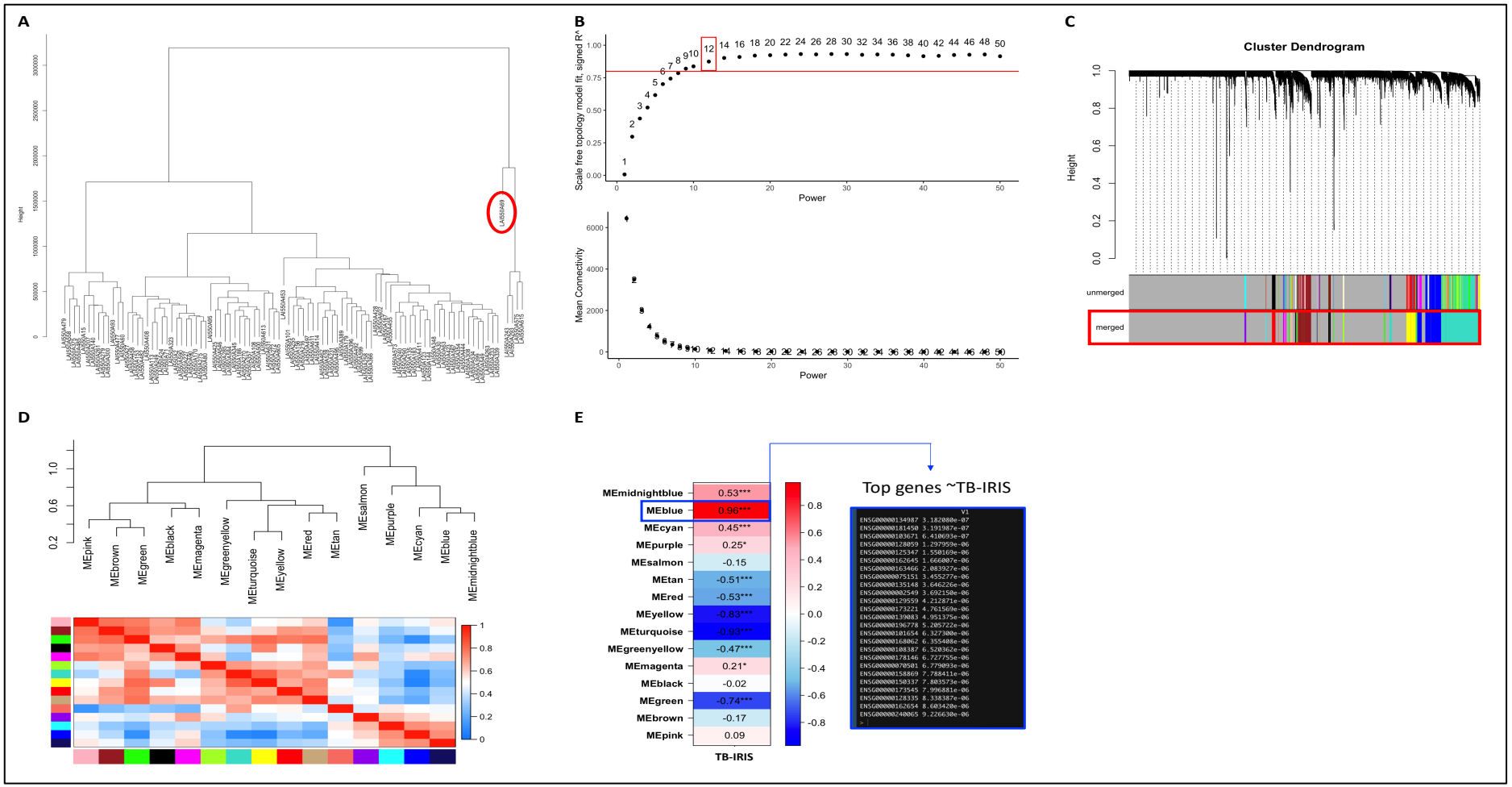

Figure 5.15. Weighted gene co-expression network analysis (WGCNA) in the samples from patients on placebo with paradoxical TB-IRIS and TB-non-IRIS controls on placebo at week 2 on ART*. A, Hierarchical clustering analysis identifies outlier sample (Red circles = excluded sample.* ***B,*** *Beta values for the construction of network which satisfies scale free topology criteria.* ***C,*** *Network construction with unsupervised hierarchical*

clustering of genes. Similar modules were merged (red box). ***D,*** *heatmap cluster of the identified module eigengenes (ME).* ***E,*** *Correlation matrix of each ME with paradoxical TB-IRIS and the top genes in the blue module which had a significant correlation with TB-IRIS.*

Next, a topological overlap matrix (TOM) and dissimilarity TOM (dissTOM) were created using TOM similarity and dissimilarity modules. Finally, module identification was performed by dynamic tree cutting, defining the minimum module size as 30. A threshold of 0.25 was used to merge modules with high similarity scores (**Figure 5.15 C**). Moreover, the values of gene significance (G.S) were used to calculate the association of individual genes with TB-IRIS. Module Membership (M.M) was defined as the ME correlation as well as the gene expression profile for each module (**Figure 5.15 D**).

A total of 15 ME were identified in this analysis, of which 5 were strongly associated with paradoxical TB-IRIS (**Figure 5.15 E**). Three MEs in the following order, had the highest correlation with paradoxical TB-IRIS: ME-blue (r = 0.96), ME-mid-night blue (r = 0.53) and ME-cyan (r = 0.45) (**Figure 5.15 E**). The number of genes comprising the blue, mid-night blue and cyan ME were 1228, 148, and 221, respectively. The transcripts in these MEs were largely involved in pathogen recognition, immune activation, innate intracellular immune cell signaling and the inflammatory cascade. ME-purple and ME-magenta were the remaining MEs that were significantly correlated with paradoxical TB-IRIS (r = 0.25 and 0.21 respectively) and had 94 and 131 genes respectively. The genes comprising these MEs were largely involved in adaptive immune responses, immune activation and the inflammatory signaling cascade.

5.5.6.2 Identification of overrepresented pathways in samples from patients with paradoxical TB-IRIS

Next, ME-blue and its attendant genes were selected and subjected to overrepresentation analysis (ORA) to investigate the biological pathways that were significantly overrepresented in samples from patients with paradoxical TB-IRIS at week 2 on ART (**Figure 5.16**).

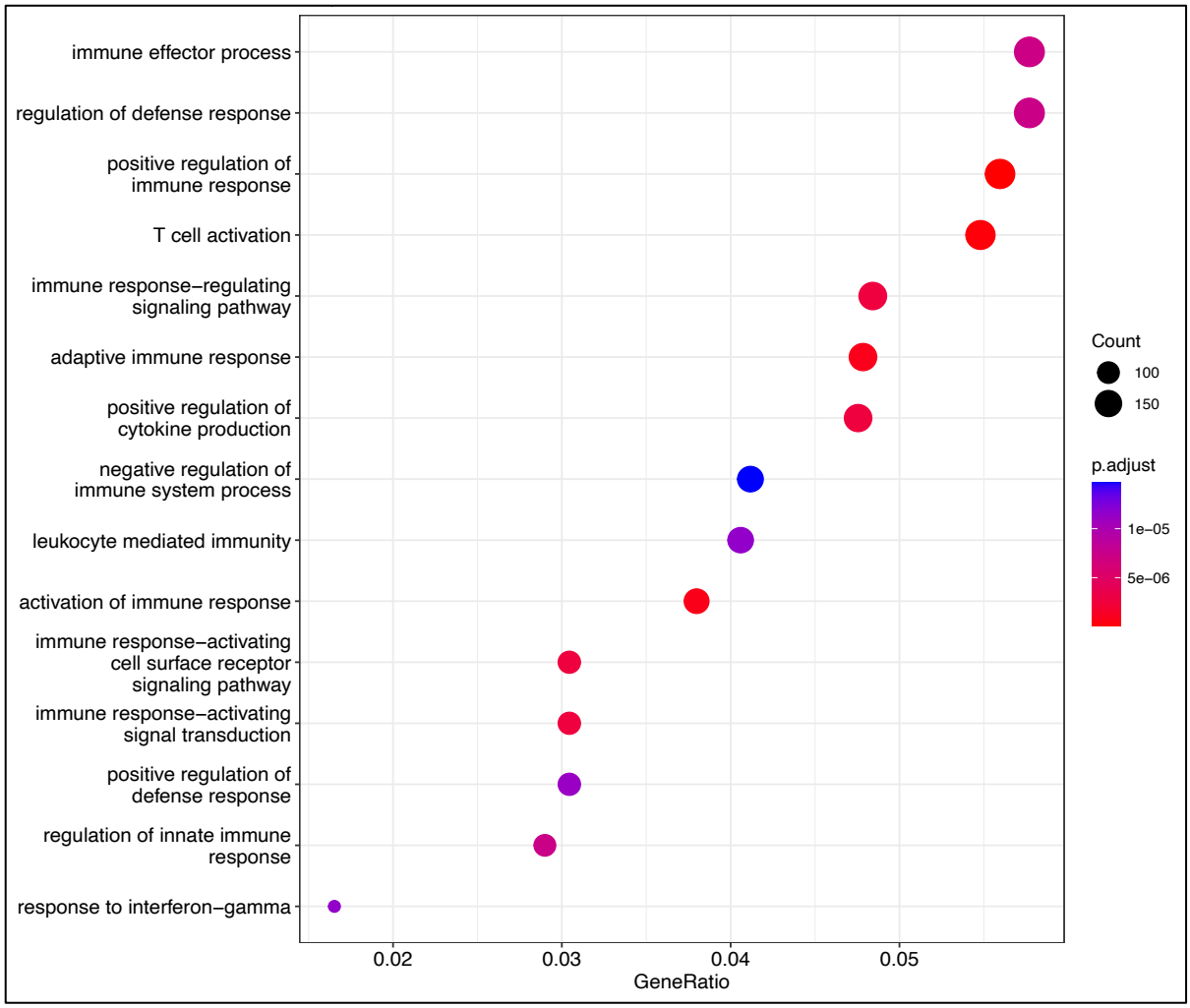

Figure 5.16. Over representation analysis (ORA) of transcripts belonging to the blue module eigengene (ME-blue) which was significantly correlated with paradoxical TB-IRIS*. ORA identified several pathways that corroborated the initial GSEA findings in patients with paradoxical TB-IRIS at week 2 on ART.*

Several biological pathways that were enriched in TB-IRIS patients at week 2 on ART were identified. These pathways included both innate and adaptative immune responses (**Figure 5.16**). This analysis corroborated our initial GSEA findings which identified significantly higher expression of transcripts involved in innate immune signaling, the involvement of neutrophil effector responses and transcripts involved in adaptive immune responses in patients who developed paradoxical TB-IRIS at week 2 on ART. Additionally, these findings are consistent with previous experimental observations which have been corroborated by others [15].

Following this, the interacting partners of T-Cell Activation WD Repeat-Containing Protein (*TA-WDRP/134430*) were investigated. *TA-WDRP/134430* was the most significantly expressed transcript in MEblue (**Figure 5.17**). This revealed several proteins that interact with *TA-WDRP* and these included proteins such as nucleolar complex associated 4 homolog (NOC4L), exosome component 1 (EXOSC1), BOP1 ribosomal biogenesis factor and UTP4 small subunit processome component. Validation studies are needed to confirm this interactome findings.

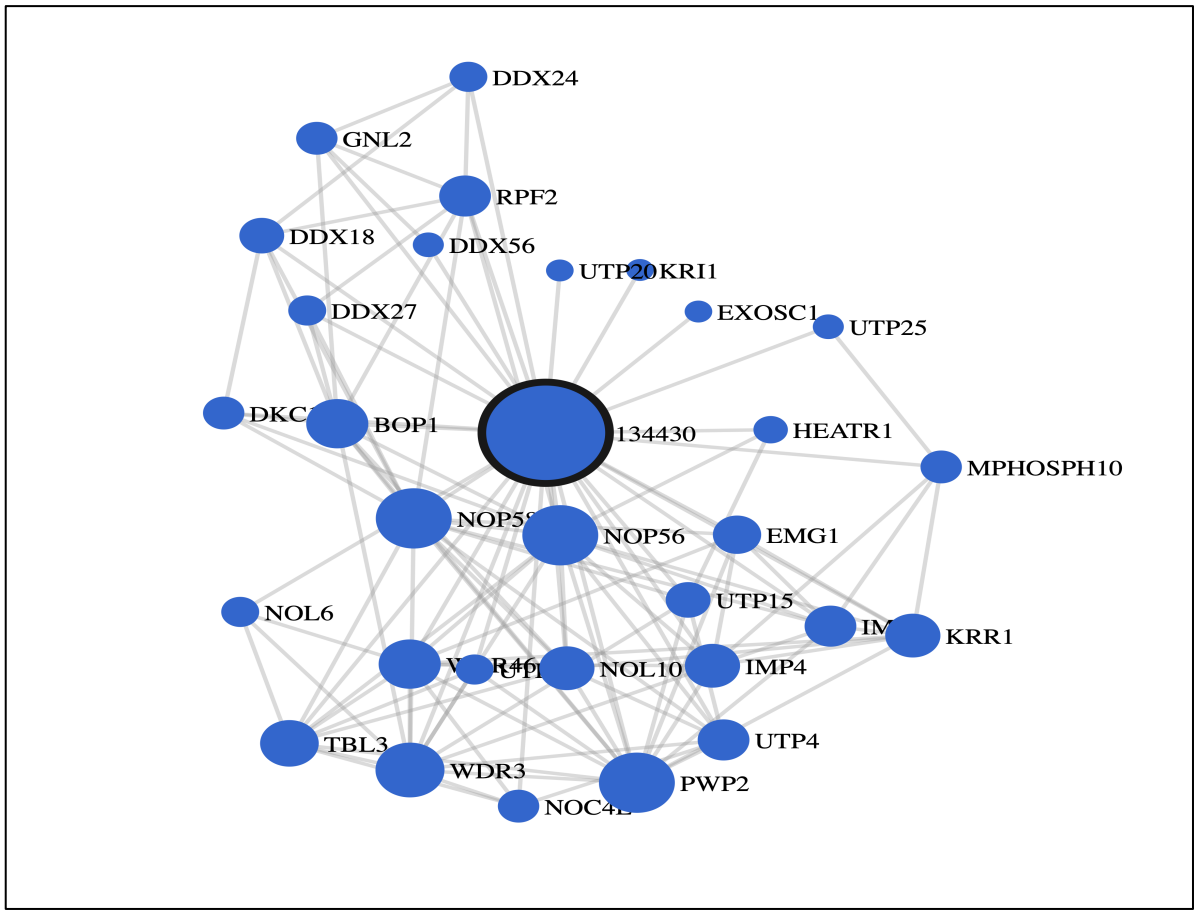

Figure 5.17*. Network analysis of the top gene T-Cell Activation WD Repeat-Containing Protein (TA-WDRP/134430) that was correlated with paradoxical TB-IRIS identified several interacting partners*

5.5.7 Summary of findings for these analyses

Using bulk RNA-sequencing, our exploratory analysis identified DEGs in whole blood samples comparing patients who developed paradoxical TB-IRIS to TB-non-IRIS controls at

week 2 on ART (which is the median time to symptom onset). Functional enrichment analysis was employed to identify biological processes that the pre-ranked gene list arising from DESeq2 were involved in. Findings revealed heightened cellular immune responses in patients with paradoxical TB-IRIS compared to TB-non-IRIS controls at disease onset. Importantly, responses were characterized by the upregulation of neutrophilic transcripts that are inflammatory and the downregulation of regulatory responses characterized by the genes that encode proteins that regulate other genes through phosphorylation, dephosphorylation or degradation. Such phosphoproteases and phosphatases act along the intracellular signaling cascade to modulate the inflammatory response. Furthermore, TB-IRIS patients had substantial changes in gene expression at week 2 compared to TB-non-IRIS patients. Samples from TB-non-IRIS patients showed modest changes in gene expression at week 2 on ART compared to week 0, unlike patients with TB-IRIS where substantial changes were noted, reflecting increased immune activation in patients with paradoxical TB-IRIS. Notably, there was a depletion of viral specific responses in TB-non-IRIS patients as indicated by the downregulation of interferon associated pathways and their attendant genes. Immune responses in these patients were characterized by the upregulation of genes encoding proteins that mediate wound healing and matrix formation. WGCNA analysis corroborated the gene set enrichment analysis and identified hub genes in the module eigengenes that were strongly correlated with paradoxical TB-IRIS. It is plausible that targeting the proteins related to these hub genes for therapeutic purposes could potentially alter the clinical course of patients at risk for developing TB-IRIS.

5.6 Placebo Week 12: TB-IRIS vs TB-non-IRIS

Paradoxical TB-IRIS is a self-limiting disease in most patients. In patients with mild disease, most will have symptom resolution without the need for hospitalization or therapeutic intervention [19]. A total of 92 samples from placebo allocated patients were collected at week 12 on ART from patients who had developed paradoxical TB-IRIS (n = 42) and those who had not (TB-non-IRIS controls, n = 50). Notably, a proportion of patients who were allocated placebo and developed paradoxical TB-IRIS (56/120) received prednisone for syndromic management. These samples were used to investigate the gene expression signature at week 12 on ART between cases and controls.

5.6.1 Differential gene expression analysis

Patient samples collected at week 12 on ART coincided with the median time to the resolution of the signs and symptoms associated with paradoxical TB-IRIS. Differential gene expression analysis (DGEA) was conducted using DESeq2 on all patient samples collected at week 12 on ART to study their gene expression signature (**see Table 5.1**).

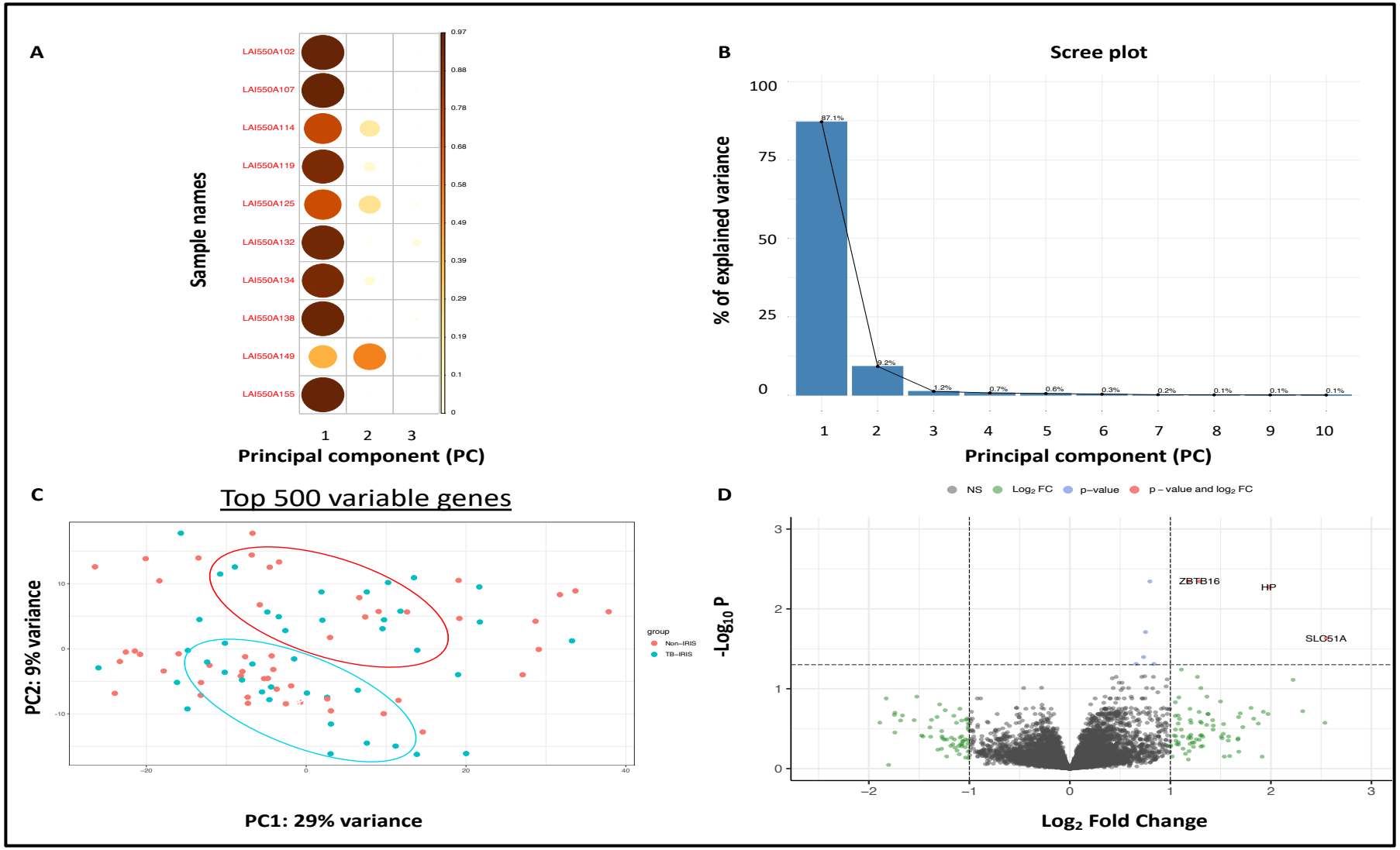
A
LAI550A102
LAI550A107
LAI550A114
LAI550A119
LAI550A125
LAI550A132
LAI550A134
LAI550A138
LAI550A149
LAI550A155
Sample names
1 2 3
Principal component (PC)
0.97
0.88
0.78
0.68
0.58
0.49
0.39
0.29
0.19
0.1
0
B
Scree plot
% of explained variance
100
75
50
25
0
87.1%
9.2%
1.2%
0.7%
0.6%
0.3%
0.2%
0.1%
0.1%
0.1%
1 2 3 4 5 6 7 8 9 10
Principal component (PC)
C
Top 500 variable genes
PC2: 9% variance
group
Non−IRIS
TB−IRIS
PC1: 29% variance
D
NS
Log2 FC
p−value
p − value and log2 FC
-Log10 P
ZBTB16
HP
SLC51A
Log2 Fold Change

***Figure 5.18**. **Exploratory data analysis in a total of 92 samples collected from placebo allocated patients with paradoxical TB-IRIS and TB-non-IRIS controls at week 12 on ART**. **A.** The relative contribution of each sample to the cumulative variance across the first three principal components (PC). **B.** Scree plot showing the proportion of variance explained by each principal component (PC). **C**. Principal component analysis for the top 500 variable genes. PC1 contributed most of the variance. PC1 is a mixed cluster of both TB-IRIS and TB-non-IRIS samples. **D**. Volcano plot showing differentially expressed genes in patient samples collected from the placebo arm at week 12 on ART. DEGs were defined by an adjusted p-value of less than or equal to 0.05.*

5.6.2 Exploratory analysis

The data were explored by computing principal component analysis (PCA) to assess patterns in gene expression across all samples using variance stabilized, normalized expression data. A total of 92 eigenvectors or principal components (PC) corresponding to the patient samples were generated. Shown above is the first 3 PC which accounted for 97% of the cumulative variance (**Figure 5.18A**). Figure 5.18A depicts the relative contribution of the first 10 samples to each PC. The scale represents the proportion of variance contributed by each sample to each PC. Most importantly, PC1 accounted for 87.1% of the variance explained by all the samples (**Figure 5.18 B**). Collectively, PC1 and PC2 contributed 96.3% of the cumulative variance for all the samples (**Figure 5.18B**).

PCA was subsequently computed using the first 2 PCs for the 500 most variable genes across all samples (**Figure 5.18C**). PC1 represents the linear combination of the Euclidean distances (eigenvalue) between transcripts across 92 samples. PC1 maximizes the variability of the data when projected in the x-axis (29%) and accounted for most of the variance compared to PC2. PC2 is orthogonal to PC1, and it describes the residual variance of PC1 (9%) (**Figure 5.18C**). PC1 is a mixed cluster of TB-IRIS and TB-non-IRIS, similarly for PC2. This indicates the proximity of the eigenvalues and therefore, the similarities in gene expression between the two clinical groups at week 12 on ART. (**Figure 5.18C**).

Following the evaluation of the similarities in gene expression between the samples, the differentially abundant transcripts were visualized between the two clinical groups at week 12 on ART. A total of 9 differentially expressed transcripts were identified in all samples at week 12 on ART after correcting for multiple hypothesis testing (FDR = 0.05). All the transcripts were upregulated in samples from patients with paradoxical TB-IRIS and were largely representative of the genes encoding proteins involved in extracellular matrix organization (**Figure 5.18D**).

5.6.3 Gene set enrichment analysis

To determine the functionality of the DESeq2 derived DEGs in patients with paradoxical TB-IRIS relative to the TB-non-IRIS controls at week 12 on ART, functional enrichment analysis

was conducted using GSEA [282]. Described below are the biological pathways and their attendant genes that were differentially expressed at week 12.

5.6.3.1 No differences in gene expression pathways in samples collected from patients who had developed paradoxical TB-IRIS and TB-non-IRIS controls at week 12 on ART.

Using GSEA, several upregulated biological pathways were identified in samples collected from patients with paradoxical TB-IRIS compared to TB-non-IRIS controls at week 12 on ART. However, none were statistically enriched between the two clinical groups after correcting for multiple comparisons (FDR = 0.1). This suggests disease resolution and similarities in gene expression between the two clinical groups by week 12 on ART. Several pathways such as collagen chain trimerization were upregulated but were not significantly enriched. This gene expression data coincides with the clinical progression by week 12 on ART when most paradoxical TB-IRIS patients had symptom resolution, either spontaneously or after treatment with prednisone. A substantial proportion of patients (46%) who developed acute inflammatory reactions were administered prednisone for syndromic management, and as such the effect of prednisone may have contributed to the narrowing of differences in gene expression by week 12. Prednisone is an anti-inflammatory corticosteroid that is used for the management of inflammatory diseases, including paradoxical TB-IRIS [19]. Prednisone may alter the course of paradoxical TB-IRIS by modifying gene expression in inflammation-related pathways.

Figure 5.19. Gene set enrichment analysis in samples from placebo allocated patients with paradoxical TB-IRIS and TB-non-IRIS controls at week 12 on ART*. Significantly enriched pathways were defined by a normalized enrichment score greater than or less than 0 and adjusted p-value of less or equal to 0.05. None of the identified pathways were significantly enriched in patients who had developed paradoxical TB-IRIS compared to those who had not at week 12 on ART.*

Similarly, several downregulated biological pathways were identified at week 12 on ART in samples collected from patients who had developed paradoxical TB-IRIS and TB-non-IRIS controls (**Figure 5.19**). However, none were significantly enriched. This implies that there are

no major differences in the gene expression signature between patients who had developed paradoxical TB-IRIS and TB-non-IRIS controls at week 12 on ART.

5.6.4 Summary of findings for these analyses

Differential gene expression analysis and functional enrichment analysis were successfully computed in samples from patients who had developed paradoxical TB-IRIS and TB-non-IRIS controls at week 12 on ART. Exploratory analysis and functional enrichment analysis of bulk RNA-sequencing data revealed no significant differences in the molecular signatures between patients who had paradoxical TB-IRIS disease and TB-non-IRIS controls at week 12 on ART. Based on clinical findings this is expected because for most patients significant paradoxical TB-IRIS symptoms have resolved either spontaneously or after initiation of corticosteroids for treatment, particularly those with severe manifestations. As such prednisone as treatment for paradoxical TB-IRIS could confound these findings, thereby rendering it a challenge to conclude if remission was part of natural history or due to prednisone treatment.

5.7 Prednisone Week 2: TB-IRIS vs TB-non-IRIS

The incidence of paradoxical TB-IRIS was reduced by 30% in the prednisone arm compared to the placebo arm in the Pred-ART clinical trial. Furthermore, prednisone prophylaxis was associated with decreased symptom severity in patients who developed paradoxical TB-IRIS [21]. However, prednisone prophylaxis did not offer complete protection from the development of paradoxical TB-IRIS. We next focused on identifying and describing the perturbations that prednisone prophylaxis had on the gene expression signature in patients who developed paradoxical TB-IRIS (n = 27) compared to those who did not (TB-non-IRIS controls: n = 68) at week 2 on ART.

5.7.1 Differential gene expression analysis

Prednisone is a corticosteroid with anti-inflammatory effects [426]. Since, all patients allocated to prednisone prophylaxis received treatment from study enrolment, the differences in gene expression between cases and controls who received prednisone were evaluated at week 2 which coincides with the median time to the onset of paradoxical TB-IRIS. Differential gene expression analysis (DGEA) was computed with the aid of DESeq2 in a total of n = 95 patient samples collected at week 2 on ART and prophylactic prednisone.

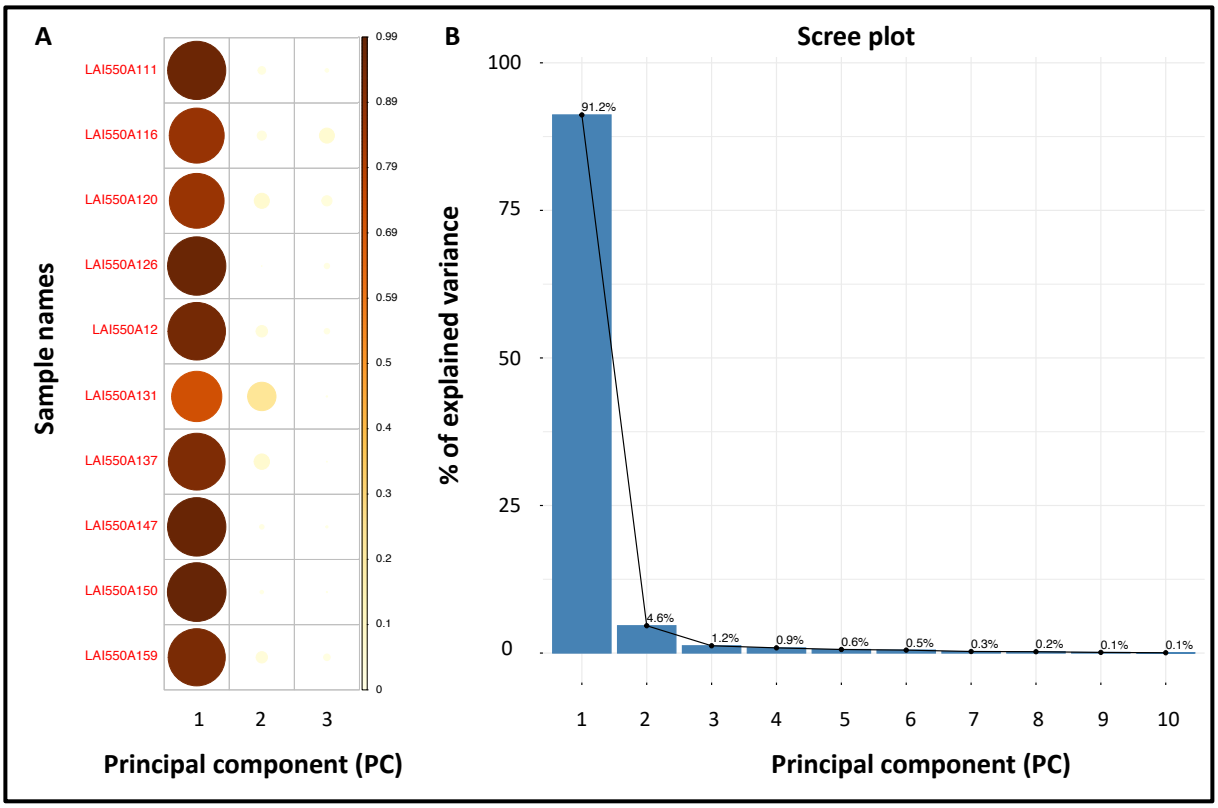

Figure 5.20. Exploratory data analysis in a total of 95 samples collected from patients with paradoxical TB-IRIS and TB-non-IRIS controls at week 2 on dual ART and prophylactic prednisone*. **A.** The relative contribution of each sample to the cumulative variance across the first three principal components (PC). **B.** Scree plot showing the proportion of variance explained by each principal component (PC).*

5.7.2 Exploratory analysis

Principal component analysis (PCA) was performed to explore patterns in gene expression across all samples using variance stabilized, normalized expression data. A total of 95 PC corresponding to the patient samples were generated. Shown in the figure above is the first 3 PCs which accounted for 99% of the cumulative variance (**Figure 5.20A**). Figure 5.20A depicts the relative contribution of the first 10 samples to each PC, where the scale represents the proportion of variance contributed by each sample to each PC. Most importantly, PC1 accounted for 91.2% of the variance explained by all the samples (**Figure 5.20B**). Collectively, PC1 and PC2 contributed 95.8% of the cumulative variance for all the samples (**Figure 5.20B**). Therefore, the first 2 PCs for the 500 most variable genes across all samples were used for dimensionality reduction (**Figure 5.21A**). PC1 represents the linear combination of the

Euclidean distances (eigenvalue) between transcripts across 95 samples. PC1 maximizes the variability of the data when projected on the x-axis (31%) and accounted for most of the variance compared to PC2. PC2 is orthogonal to PC1, and it describes the residual variance of PC1 (11%) (**Figure 5.21A**). PC1 describes a mixed cluster of TB-IRIS and TB-non-IRIS samples. Similarly, for PC2. This indicates the proximity of the eigenvalues and therefore, the similarities in gene expression between the two clinical groups at week 2 on dual ART and prednisone prophylaxis. (**Figure 5.21A**).

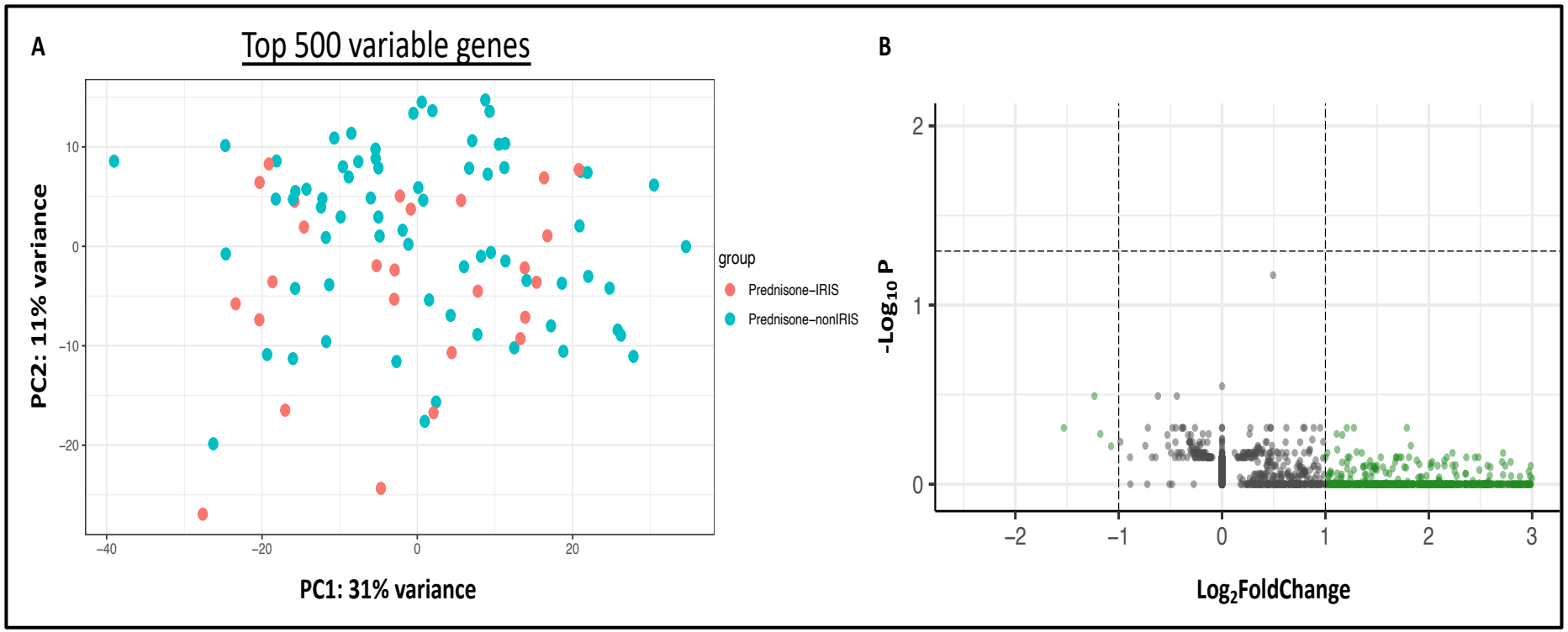

Figure 5.21. Exploratory data analysis in a total of 95 samples collected from patients with paradoxical TB-IRIS and TB-non-IRIS controls at week 2 on dual ART and prophylactic prednisone. ***A****. Principal component analysis for the top 500 variable genes. PC1 contributed most of the variance. PC1 is a mixed cluster of both TB-IRIS and TB-non-IRIS samples.* ***B****. Volcano plot showing differentially expressed genes in patient samples collected from the prednisone arm at week 2 on ART. DEGs were defined by an adjusted p-value of less than or equal to 0.05.*

To explore the data further, the list of differentially abundant transcripts between the two clinical groups at week 2 on dual ART and prednisone prophylaxis were visualized. There were no differentially abundant transcripts in the samples collected from patients with paradoxical TB-IRIS compared to TB-non-IRIS controls at week 2 after adjusting for multiple hypothesis testing (FDR = 0.05) (**Figure 5.21B**). This was an important finding, suggesting that prednisone significantly modulates gene expression in patients with HIV-associated TB during early ART substantially reducing differences in gene expression between patients who do and do not develop paradoxical TB-IRIS.

5.7.3 Gene set enrichment analysis

Many genes showed changes in gene expression as determined by effect size or log2 fold change in all samples but were not significant after correcting for multiple comparisons (FDR = 0.05). To infer the function, the pre-ranked genes were summarized into biological pathways using GSEA [282].

5.7.3.1 No differences in gene expression in samples collected from patients with paradoxical TB-IRIS and TB-non-IRIS controls at week 2 on concurrent ART and prednisone prophylaxis.

Using GSEA, we identified several upregulated biological pathways in samples collected from patients with paradoxical TB-IRIS compared to TB-non-IRIS controls at week 2 on concurrent ART and prednisone prophylaxis. However, none were significantly enriched between the two clinical groups after adjusting for multiple comparisons (FDR = 0.1). Despite not being significantly enriched, several pathways that were upregulated were involved in the regulation of immune signaling. These largely reflected the systemic effects of prednisone due to its pleiotropic nature (**Figure 5.22**).

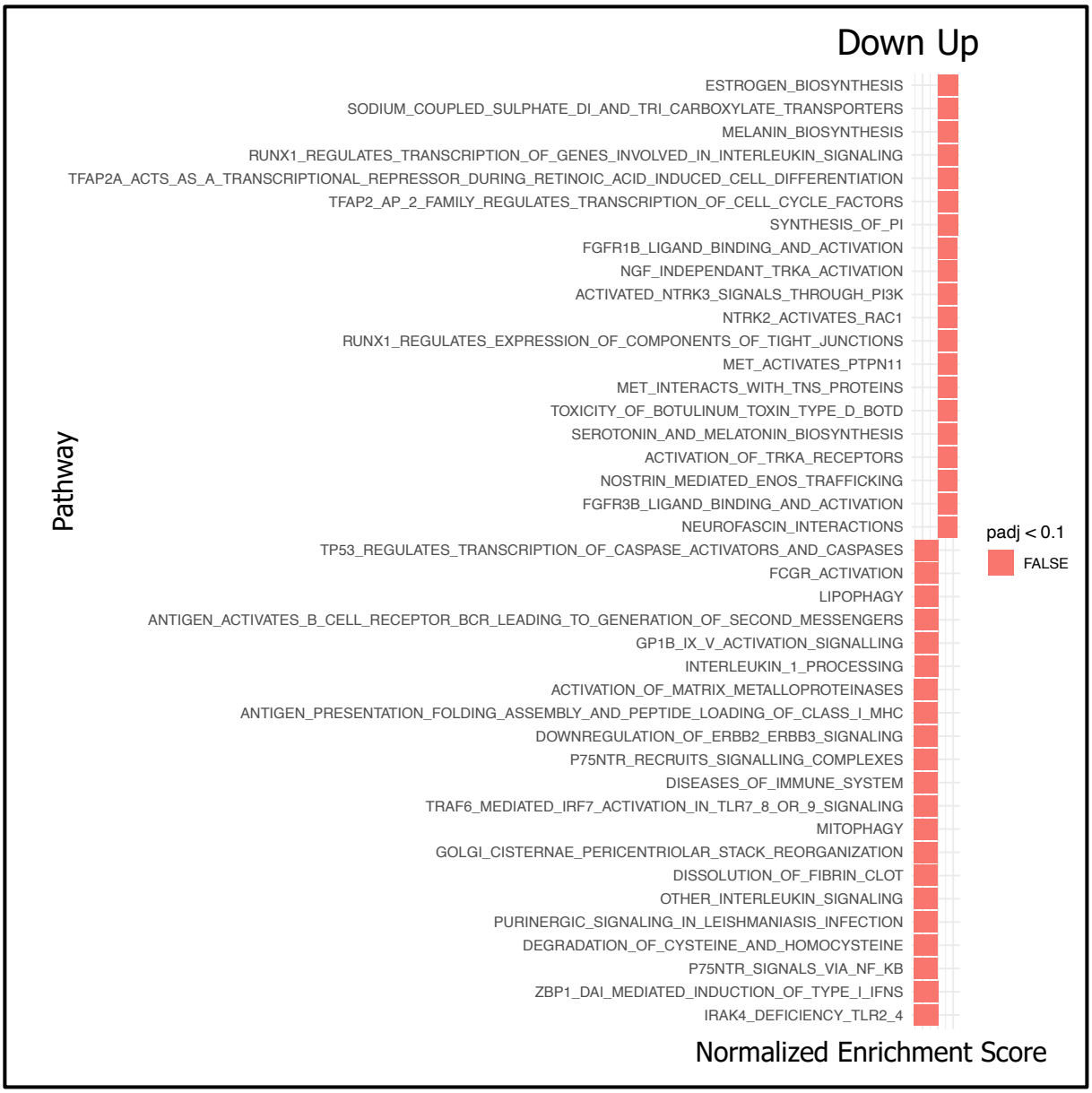

Figure 5.22.Gene set enrichment analysis in samples from patients with paradoxical TB-IRIS and TB-non-IRIS controls at week 2 on dual antiretroviral therapy (ART) and prophylactic prednisone*. Significantly enriched pathways were defined by a normalized enrichment score greater than or less than 0 and an adjusted p-value of less or equal to 0.1. Importantly, no significant differences in pathway enrichment were observed in patient samples from patients who developed paradoxical TB-IRIS and TB-non-IRIS controls at week 2 on dual ART and prophylactic prednisone.*

Similarly, several downregulated biological pathways were identified at week 2 on concurrent ART and prednisone prophylaxis in samples collected from patients who developed

paradoxical TB-IRIS and TB-non-IRIS controls (**Figure 5.22**). However, none were significantly enriched after adjusting for multiple hypothesis testing (FDR = 0.1).

The difference of these findings compared to the analyses of patients on placebo likely reflects the perturbation effect of prophylactic prednisone on the gene expression signature associated with paradoxical TB-IRIS. Notably, the clinical symptoms of patients who developed paradoxical TB-IRIS despite prednisone prophylaxis (likely reflecting degree of inflammation) were milder in the clinical trial compared to those who received placebo. This also aligns with the findings of a clinical trial that investigated higher doses of prednisone for the treatment of paradoxical TB-IRIS initiated after the onset of symptoms which reported more rapid symptom resolution and reduced duration of hospitalization and therapeutic procedures in patients who received prednisone versus placebo [19].

Furthermore, among the biological pathways which were downregulated despite not being statistically enriched in samples from patients with paradoxical TB-IRIS compared to TB-non-IRIS controls included interleukin-1 receptor associated kinase 4 (IRAK4) which forms part of the signaling cascade upstream of the nuclear factor kappa-light-chain-enhancer of activated B cells (NF-κβ) pathway [427]. NF-κβ is a global transcriptional regulator of gene expression that facilitates/mediates resistance to pathogens [428]. Noting that these pathways were enriched but not statistically significant after correcting for multiple comparisons, an explanation could be that prednisone exerts its anti-inflammatory effects along the NF-κβ signaling cascade to downregulate the expression of proinflammatory cytokines, chemokines and inflammatory lipids during paradoxical TB-IRIS [33]. Finally, considering that 40 mg daily prednisone (relatively low dose) was prescribed for 2 weeks and then tapered down to 20 mg daily for an additional 2 weeks, it is possible that a higher dose could potentially induce a more substantial effect on the gene expression in patients with paradoxical TB-IRIS and, as a corollary, potentially greater effect on reducing the incidence of paradoxical TB-IRIS.

5.7.4 Longitudinal gene expression analysis in patients who developed paradoxical TB-IRIS despite prophylactic prednisone

To follow up on the cross-section analysis, changes in gene expression that occur longitudinally up to week 2 on concurrent ART and prednisone prophylaxis were studied in patients with paradoxical TB-IRIS.

5.7.4.1 Differential gene expression analysis at week 2 versus 0 in samples from patients with paradoxical TB-IRIS who were on concurrent ART and prednisone prophylaxis

Differential gene expression analysis (DGEA) was computed in a total of 62 samples from patients who developed paradoxical TB-IRIS between week 2 and week 0 on dual ART and prednisone prophylaxis as previously described (**see Page 109, section 3.21.14**). A total of 3472 DEGs were identified between week 2 and week 0 after correcting for multiple comparisons (FDR = 0.05). A total of 1835 genes were upregulated while 1637 were downregulated at week 2 compared to week 0 (**Figure 5.23 A&B**).

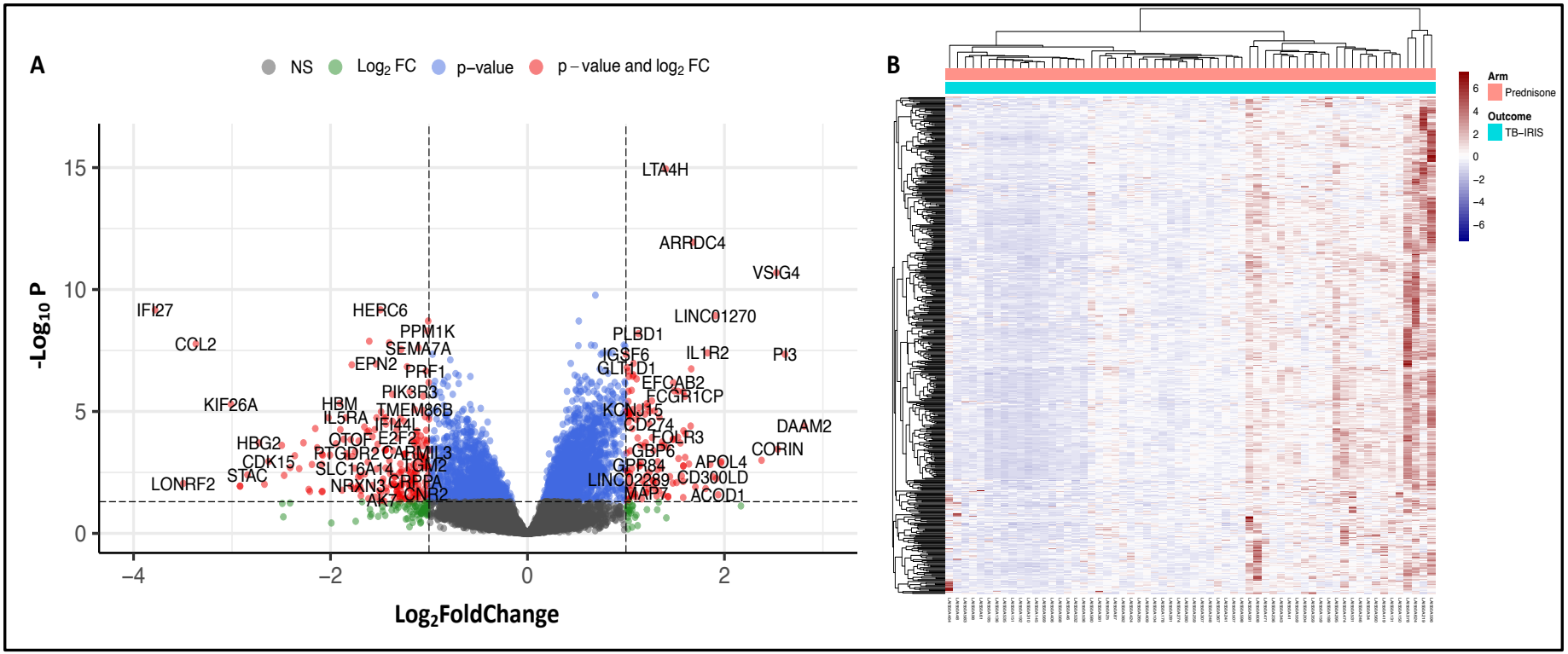

Figure 5.23. Longitudinal changes in gene expression (week 2 vs week 0) in a total of 62 samples collected from patients with paradoxical TB-IRIS on dual ART and prophylactic prednisone. ***A****. Volcano plot showing differentially expressed genes in prednisone treated patient samples between week 0 and week 2 on ART. DEGs (n = 3472) were defined by an adjusted p-value of less than or equal to 0.05.* ***B.*** *Heatmap of the top 500 DEGs identified in samples from patients with paradoxical TB-IRIS on dual ART and prophylactic prednisone at week 2 compared to week 0. A total of 3472 transcripts were differentially expressed between week 0 and week 2. 1835 genes were upregulated while 1637 were downregulated.*

Among the DEGs that were significantly upregulated was CD177 which is an activation cell surface marker expressed chiefly on neutrophils. Other identified genes included interleukin-1 receptors (IL-1R) and the NLRC4 inflammasome that were differentially expressed at week 2 compared to week 0 in samples from patients with paradoxical TB-IRIS on dual ART and prednisone (**Figure 5.23 A&B**). Additionally, leukotriene A4 hydrolase (LTA4H) transcript was one of the top significantly upregulated between week 0 and 2. LTA4H gene is an amino peptidase that catalyzes the conversion of LTA4 to LTB4. Single nucleotide polymorphisms in the LTA4H gene have been hypothesized to predispose patients to paradoxical TB-IRIS. The CC wildtype allele has been associated with lower incidence to paradoxical TB-IRIS, while the CT and TT variants were associated with higher incidence [429]. However Stek et al, recently demonstrated that the incidence of paradoxical TB-IRIS was similar in patients with different allelic frequencies in the LTA4H gene irrespective of prednisone prophylaxis, in another sub-study within the Pred-ART trial [430].

The transcripts that were downregulated were diverse in function. Among the prominent ones were genes that encode protein kinases involved in the regulation of other proteins through phosphorylation or dephosphorylation, genes encoding proteins involved in heme biosynthesis, chemokines and interleukin 5 receptor.

5.7.4.2 Functional enrichment analysis with GSEA

The DESeq2 derived gene list from samples collected between week 0 and 2 on ART and prophylactic prednisone in patients who developed paradoxical TB-IRIS were summarized into biological pathways using GSEA [282]. Several biological pathways were significantly enriched (**Figure 5.24)**. Biological pathways with a normalized enrichment score (NES) greater or equal to 0 or less or equal to 0, and an FDR of less or equal to 0.1 were of interest. The top 5 biological pathways with a NES above 2 were neutrophil degranulation, innate immune system, extracellular matrix organization, platelet aggregate plug formation and collagen formation.

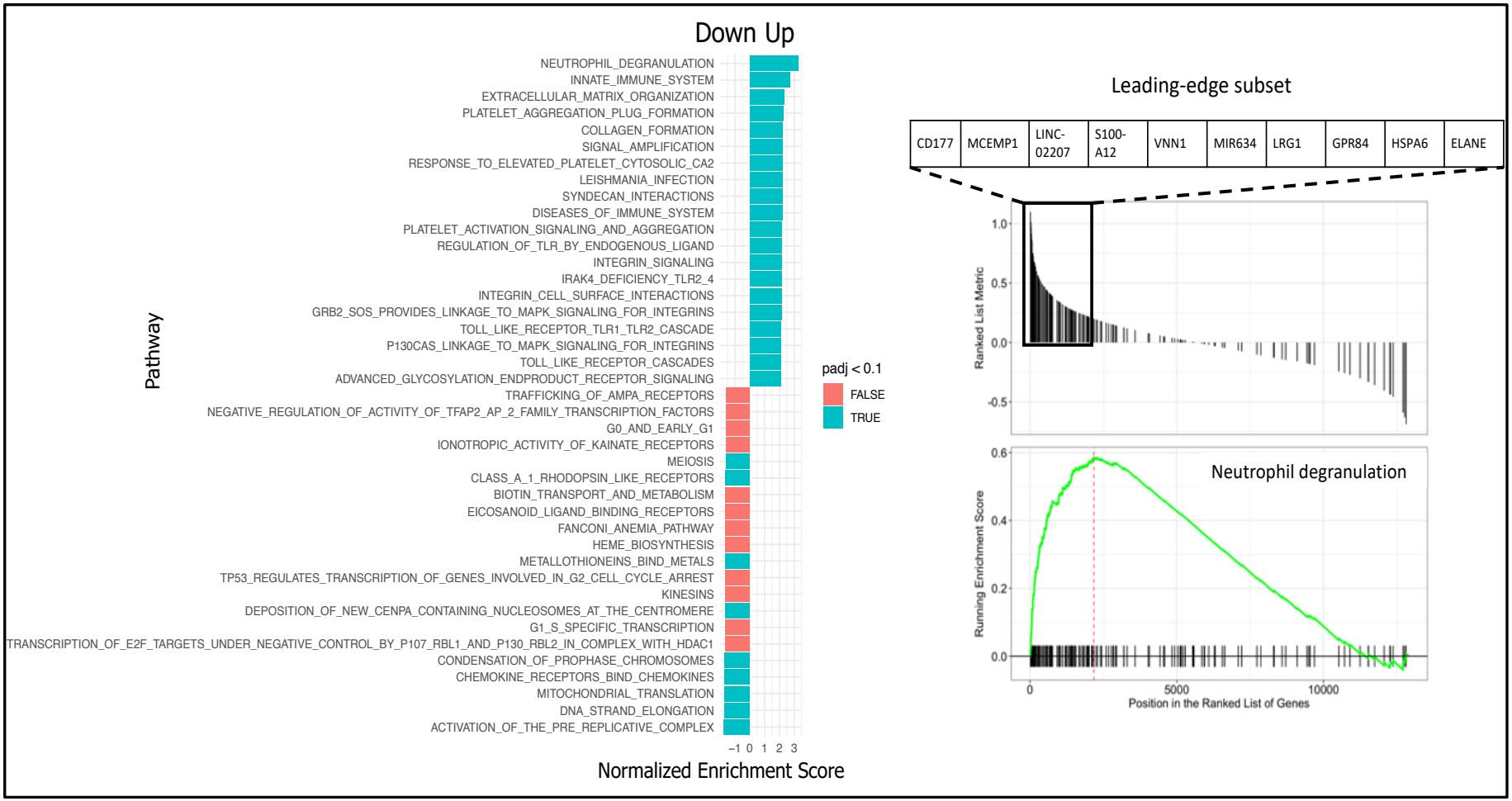

Figure 5.24. Functional enrichment with gene set enrichment analysis (GSEA) using a pre-ranked gene list and a curated gene set of canonical pathways from Reactome in samples from patients with paradoxical TB-IRIS comparing expression at week 2 on ART to week 0. *Pathway analysis identifies neutrophil degranulation as the most significantly enriched biological pathway in prednisone treated patient samples with*

paradoxical TB-IRIS up to week 2 longitudinally on ART. Identified pathways included biological processes such as collagen formation which are associated extracellular matrix remodelling and therefore may reflect response to tissue injury.

Prednisone is a synthetic glucocorticoid with potent inhibitory pharmacological activity [426, 431]. The involvement of neutrophils and their degranulation as the most significantly enriched biological pathway in samples from prednisone treated patients who nonetheless developed paradoxical TB-IRIS was therefore an interesting finding. The anti-inflammatory effects of prednisone on immune cells have been well documented, but prednisone may also [432, 433] favor the proliferation and maturation of neutrophils from the bone marrow and their subsequent vascular migration [434, 435]. This can result in higher-than-normal neutrophil counts. Notably, corticosteroids counter this with tight regulatory mechanisms. The molecular mechanisms underlying the regulation of corticosteroid induced neutrophil expansion entails the reduction in expression of neutrophil adhesion surface markers such as L-selectin which was identified in this analysis [436]. Reduced expression favor detachment of neutrophils from the vascular endothelium thereby increasing their rolling speed. Reduced L-selectin expression implies poor neutrophil transmigration at the site of inflammation and therefore reduced tissue accumulation of neutrophils resulting in less tissue inflammation and perhaps milder symptoms.

Prednisone induces the expression of other genes such as Annexin-A1 which encodes an anti-inflammatory peptide [437, 438]. Annexin-A1 was also significantly increased in patients who developed paradoxical TB-IRIS while on dual ART and prednisone prophylaxis. Increased expression of this gene also favors endothelial detachment of neutrophils, increasing their rolling speed and thus preventing extravasation into inflamed tissues. Additionally, the anti-inflammatory effects of the encoded protein contributes towards the resolution of inflammation and as a corollary, assists in the alleviation of severe disease [438].

Platelet aggregation was another biological pathway that was enriched at week 2 versus week 0 in samples of patients who developed paradoxical TB-IRIS despite prednisone prophylaxis. Platelets are anucleate cell fragments released by megakaryocytes whose primary function is to induce hemostasis through thrombosis [439, 440]. Notably, inflammatory stress induces platelet proliferation. Similarly to neutrophils, prednisone induces the proliferation and migration of platelets [441]. Interestingly, platelets interact with many cell types but their preferred partners are neutrophils [442, 443]. The pair synergistically contribute towards the maintenance of vascular and tissue integrity. Platelet P-selectin is a surface marker that interacts with its cognate ligand on neutrophils (P-selectin granulocyte ligand 1). The interaction is common following vessel injury or pathogen recognition [444, 445]. P-selectin-dependent platelet-neutrophil interaction recruits downstream integrin-dependent pathways

and culminates in neutrophil activation and transmigration [446]. Neutrophils interacting with platelets can either: (a) phagocytose them, quenching their thrombogenic and inflammatory potential; (b) progress to the generation of NETs [447, 448]. The latter may be related to the neutrophil degranulation gene set that was significantly enriched in peripheral blood in ART and prednisone treated patients who developed paradoxical TB-IRIS. Notably, the outcome of their interaction hinges on the metabolic state of neutrophils with increased risk of ischemic injury among the potential consequences [449].

Lastly, abnormal platelet-neutrophil ratios have unpredictable effects on vascular and immune cell homeostasis and are increasingly appreciated as targets for therapeutic intervention. The synergistic effect of platelets and neutrophils has not been described in the context paradoxical TB-IRIS and more research on this is needed in future studies.

Additionally, extracellular matrix organization (ECM) was longitudinally enriched in samples of patients who developed paradoxical TB-IRIS who received ART and prednisone. This potentially reflects a response to tissue injury in these patients. The ECM pathway is discussed in-depth in the next section because it was a prominent gene set in prednisone-treated patients who did not develop paradoxical TB-IRIS.

Furthermore, there were several biological pathways that were significantly downregulated in samples collected from patients who developed paradoxical TB-IRIS at week 2 compared to week 0 on dual ART and prednisone prophylaxis (**Figure 5.24)**. These generally reflected biological processes confined to the cell nucleus. Processes that are worth highlighting include the activation of the pre-replicative complex, DNA strand elongation, condensation of prophase chromosomes, meiosis, and deposition of new CENPA containing nucleosomes at the centromere among others.

The biological significance of genomic deoxyribonucleic acid (DNA) replication is to copy the genetic information from one generation of cells to another with high integrity [450]. DNA is resident in the nucleus of eukaryotic cells in a condensed form. Tight regulatory mechanisms exist to ensure compact packaging of the genetic material to fit inside the nucleus [451]. The DNA is condensed by tight coiling around an octamer of four core histone proteins into a compact polymer known as chromatin [451-453]. Chromatin is a dynamic structure that dictates access by cellular machineries to the genetic information in a localized manner [454]. By regulating access to the DNA, chromatin enables the accurate regulation of all genomic processes including DNA repair, DNA replication, and transcription [453]. These processes

require the reorganization of the chromatin structure through histone modifications, and the action of chromatin factors among others [455, 456]. This is known as epigenetic regulation and embodies the notion of modifying the function of genes without altering the genetic code [457, 458]. These epigenetic modifications facilitated primarily by histones, aid in extending the information potential of the genetic code and are potentially reversible and heritable [459].

The downregulation of these biological processes in patient samples who developed paradoxical TB-IRIS on dual ART and prednisone possibly may indicate the epigenetic changes resulting from prophylactic prednisone at week 2 on ART compared to week 0.

A subset of the genes that were downregulated at week 2 compared to week 0 and their function are listed in Table 5.4.

Table 5.4. Gene names, symbols and function of downregulated transcripts at week 2 compared to week 0 in patient samples who developed paradoxical TB-IRIS in patients while on prednisone prophylaxis. *The listed transcripts constituted part of the leading edge subset of the pre-replicative complex pathway which contained the most significantly downregulated gene set.*

Gene name	Symbol	Function
Lysine demethylase 7A	KDM7A	Encoded protein enables histone demethylase activity
Mitogen-activated protein kinase 2	MAP2K1	Encoded protein is involved in many cellular processes such as proliferation, differentiation, transcription regulation and development.
Mitogen-activated protein kinase 1	MAPK1	Encoded protein is involved in many cellular processes such as proliferation, differentiation, transcription regulation and development.
Mitogen-activated protein kinase 3	MAP3K1	Encoded protein is involved in many cellular processes such as proliferation, differentiation, transcription regulation and development.
Janus kinase 2	JAK2	Encoded protein plays a central role in cytokine and growth factor signalling
Tyrosine 3-monooxygenase/tryptophan 5-monooxygenase activation protein beta	YWHAB	Encoded protein may play a role in linking mitogenic signaling and the cell cycle machinery
Fibronectin	FN1	Encoded protein is involved in cell adhesion and migration processes including embryogenesis, wound healing, blood coagulation, host defense, and metastasis
Integrin subunit alpha 2b	ITGA2B	Encoded protein plays a crucial role in the blood coagulation system
Integrin subunit beta 3	ITGB3	Encoded protein participates in cell adhesion as well as cell-surface mediated signalling.
Angiotensin II receptor associated protein	AGTRAP	Encoded protein negatively regulates angiotensin II signaling.

5.7.5 Longitudinal gene expression analysis in patients who were allocated prophylactic prednisone who did not develop paradoxical TB-IRIS.

Next, the gene expression signature in patients who received prednisone prophylaxis and did not develop paradoxical TB-IRIS disease was investigated. This was achieved by computing DGEA longitudinally on dual ART and prednisone prophylaxis in samples collected at week 0 and at the median onset of paradoxical TB-IRIS (week 2) from TB-non-IRIS patients.

5.7.5.1 Differential gene expression analysis at week 2 versus 0 in samples from TB-non-IRIS patient samples who were on concurrent ART and prednisone prophylaxis.

Differential gene expression analysis (DGEA) was computed in a total of 144 TB-non-IRIS patient samples between week 2 (n = 69) and week 0 (n = 75) on concurrent ART and prednisone prophylaxis. A total of 2932 DEGs were identified between week 2 and week 0 after correcting for multiple comparisons (FDR = 0.05). A total of 1390 genes were upregulated while 1542 were downregulated at week 2 compared to week 0 (**Figure 5.25**).

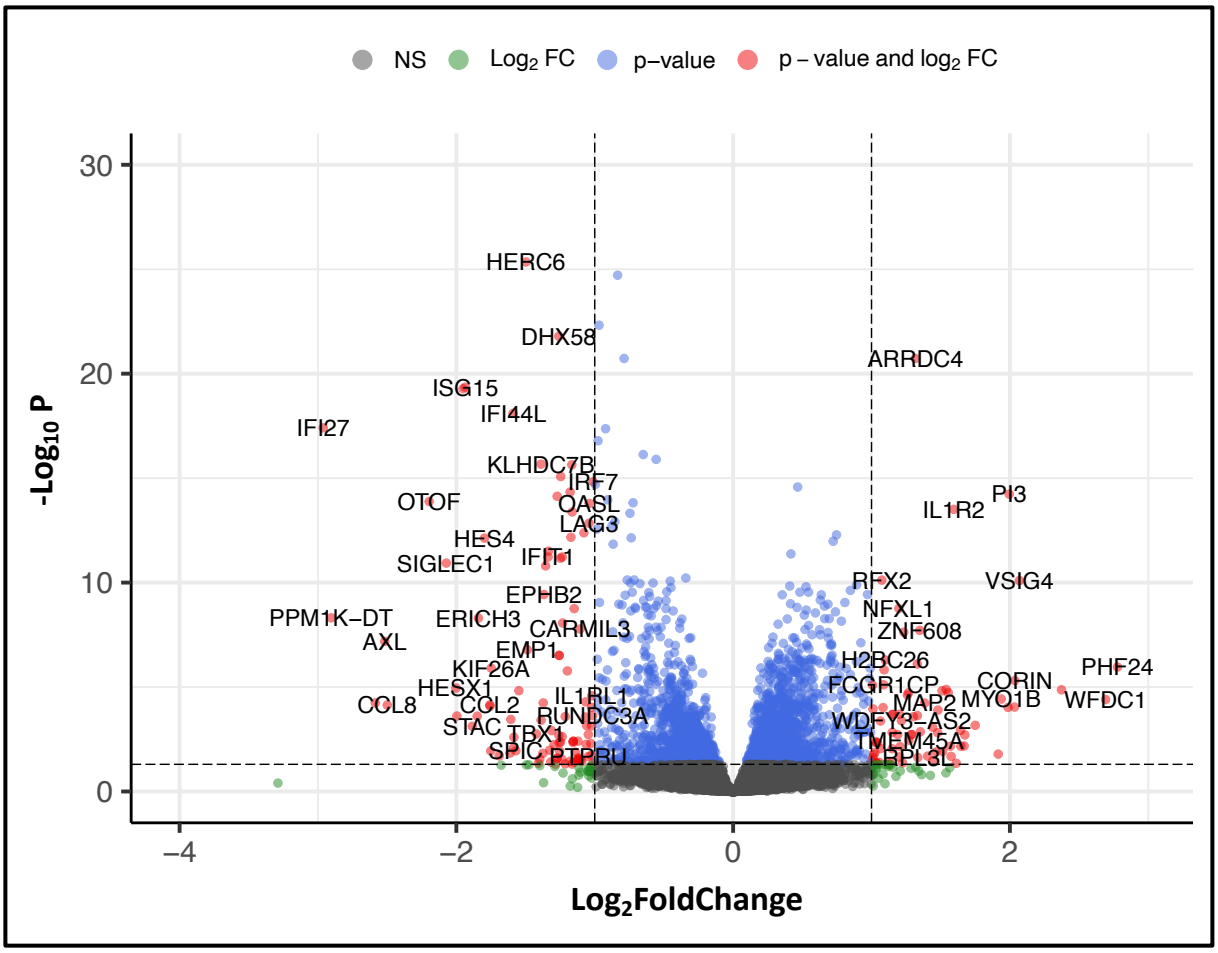

Figure 5.25. Longitudinal changes in gene expression in a total of 144 samples collected from TB-non-IRIS controls up to week 2 on dual ART and prophylactic prednisone*. Volcano plot showing differentially expressed genes in prednisone treated TB-non-IRIS patient samples between week 0 (n = 75) and week 2 (n = 69) on ART. DEGs (n = 2932) were defined by an adjusted p-value of less or equal to 0.05. A total of n = 1390 transcripts were upregulated while n = 1542 were downregulated after adjusting for multiple comparisons.*

Combined ART and prednisone induced the perturbation of many genes over the two weeks of therapy. One gene that was interestingly upregulated was a decoy receptor for the IL-1 family of cytokines (**Figure 5.25**). Engagement of this receptor leads to abortive IL-1 intracellular signaling [460]. Notably, many of the genes that were downregulated included those encoding proteins for viral specific responses and chemokine signaling (**Figure 5.25**). This is to be expected with effective ART that controls HIV replication rapidly.

5.7.5.2 Functional enrichment analysis with GSEA

The DESeq2 derived gene list from patient samples collected longitudinally between week 0 and week 2 in patients who did not develop paradoxical TB-IRIS while (TB-non-IRIS) on dual ART and prophylactic prednisone was summarized into biological pathways using GSEA [282]. Several biological pathways were significantly enriched (**Figure 5.24)**. The first 7 biological pathways contained the leading-edge subset comprising genes that mainly encode ribosomal proteins that are accessory to the 60S eukaryotic ribosome. These are important in the translation of processed and mature mRNA into polypeptides, and the subsequent elongation and folding into functional proteins [461]. Although these were significantly enriched, we do not emphasize these findings since rRNA constitute 90% of all the RNA species in peripheral blood [462].

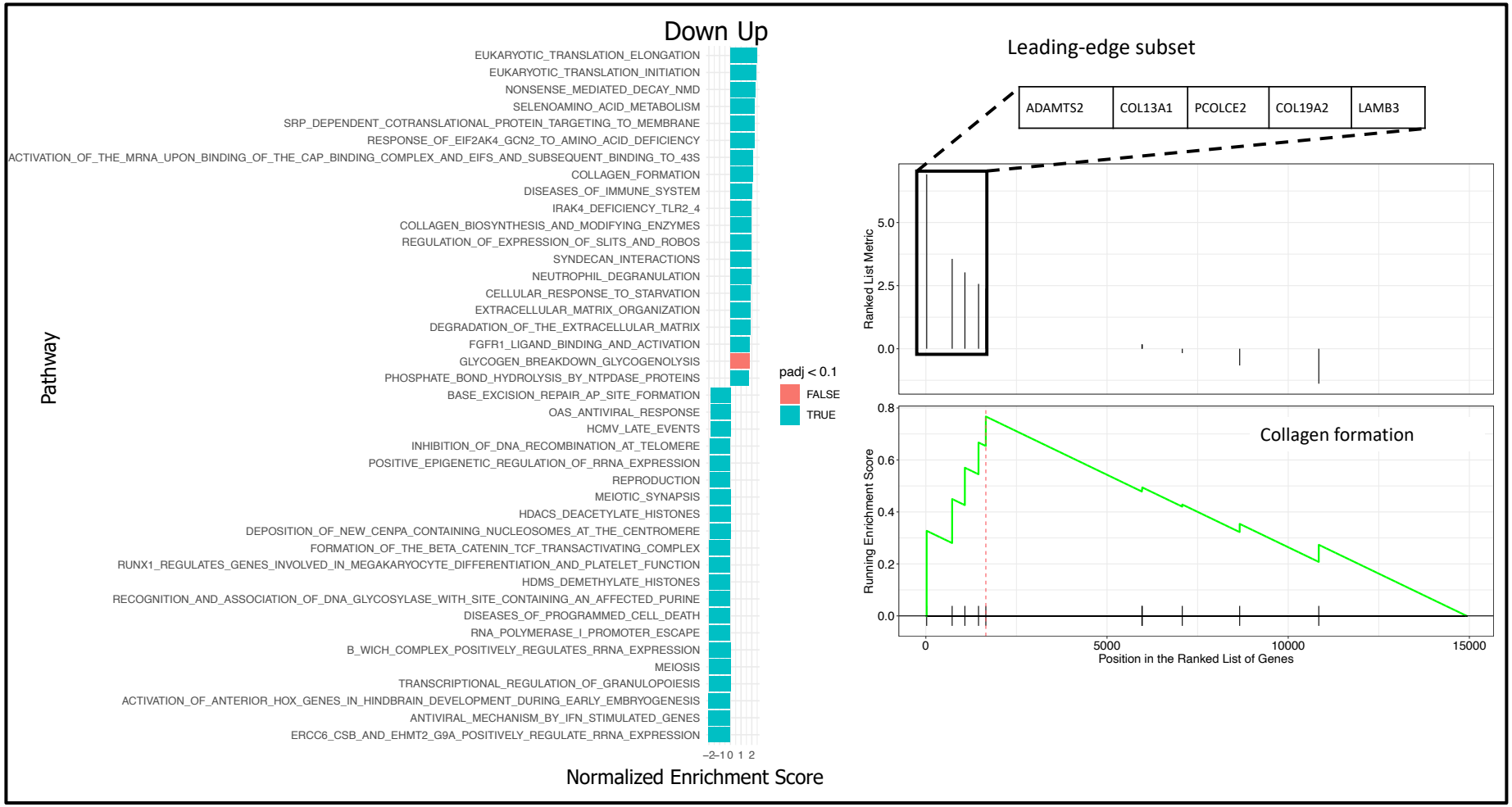

Figure 5.26. Functional enrichment with gene set enrichment analysis (GSEA) using a pre-ranked genelist and a curated gene set of canonical pathways from Reactome in samples from TB-non-IRIS up to week 2 on concurrent ART and prednisone prophylaxis*. Pathway analysis identifies collagen biosynthesis as the most significantly enriched biological pathway in prednisone treated patient samples who did not develop*

paradoxical TB-IRIS disease. The downregulated biological pathways largely represented biological processes involved in antiviral immune responses, granulocyte biosynthesis and epigenetic regulation of gene expression.

Interestingly, collagen formation and extracellular matrix organization were identified as the most significantly enriched biological pathways in 144 patient samples from TB-non-IRIS controls (**Figure 5.26**). The extracellular matrix (ECM) forms an environment surrounding cells. It has a complex and diverse composition of biochemically and structurally distinct macromolecules which have important functional characteristics [463-465]. These include but are not limited to proteins, proteoglycans, lipids and glycoprotein [466]. The main role of the ECM is to provide structural support, but it is versatile in the functions it can perform. For instance, the ECM partakes in rudimentary cell processes such as cell proliferation, adhesion, migration, cell differentiation and cell death [465]. Importantly, the function of the ECM is often shaped by its composition or architecture as it is a dynamic structure characterized by constant remodeling involving the synthesis and/or degradation of one or more of its many constituents [465, 467]. Furthermore, tight regulatory mechanisms of the ECM dynamics are required to ensure normal development, physiology, and robustness of organ systems [468]. In the context of paradoxical TB-IRIS, this suggest that the gene expression of patients who do not develop disease is characterized by ECM remodeling and in particular, the biosynthesis of collagen. Collagen is the main constituent of the extracellular matrix and its biosynthesis was enriched in TB-non-IRIS controls who received prednisone prophylaxis [469, 470].

Additionally, the downregulation of antiviral response and the biosynthesis of granulocytes which are implicated in the pathogenesis of paradoxical TB-IRIS were identified in patients who did not experience manifestation of paradoxical TB-IRIS who received prophylactic prednisone. Finally, the downregulation of the discussed biological pathways was associated with tissue healing and remodeling (**Figure 5.26**).

5.7.6 Gene overlap analysis of differentially expressed genes

5.7.6.1 Gene overlap analysis to compare the significant differentially expressed genes in prednisone treated patient samples who developed paradoxical TB-IRIS and those who did not (TB-non-IRIS controls) at week 2 on ART compared to week 0.

Furthermore, gene overlap analysis was performed to determine the genes that were exclusive between samples of prednisone treated patients who developed paradoxical TB-IRIS and TB-non-IRIS controls respectively at week 2 on ART compared to week 0. The aim of this analysis was to identify and describe the genes that are unique to each clinical group.

A total of 1684 differentially expressed transcripts that were shared between patient samples with paradoxical TB-IRIS compared to TB-non-IRIS controls at week 2 versus week 0 on concurrent ART and prophylactic prednisone were identified. More importantly a total of 1744 and 1033 transcripts were exclusively found in the samples of patients with paradoxical TB-IRIS and TB-non-IRIS controls respectively.

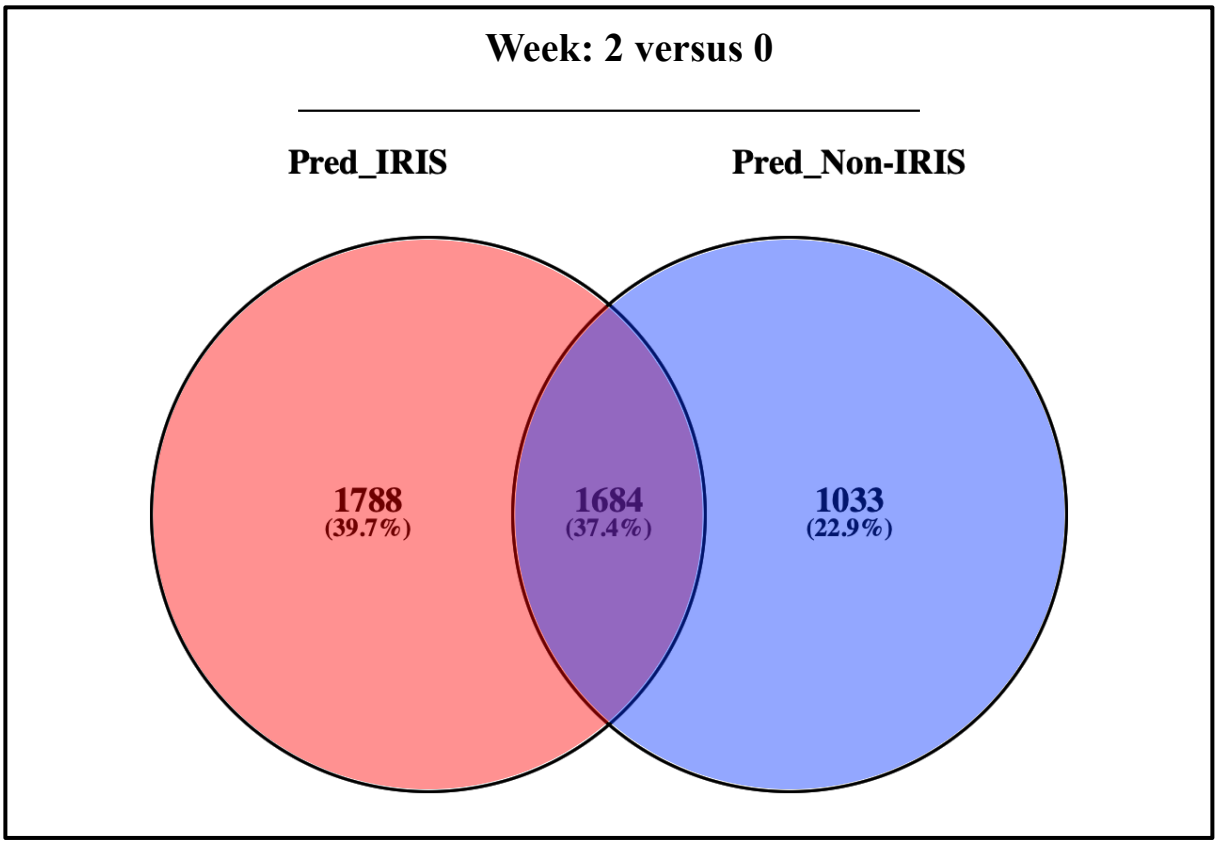

Figure 5.27. Gene overlap analysis of differentially expressed genes in prednisone treated patient samples with paradoxical TB-IRIS compared TB-non-IRIS controls at week 2 versus week 0 on ART*. Patients with paradoxical TB-IRIS had almost twice the number of differentially expressed genes despite prednisone prophylaxis compared to TB-non-IRIS controls.*

The number of DEGs were higher by nearly 2-fold in samples from patients with paradoxical TB-IRIS compared to TB-non-IRIS controls despite prophylactic prednisone. Samples of patients who developed paradoxical TB-IRIS were mainly significantly enriched for biological pathways involving neutrophils activation and degranulation while TB-non-IRIS patient

samples were mainly enriched for biological pathways including extracellular matrix organization.

5.7.5.6.2 Gene overlap analysis to compare significant differentially expressed genes comparing week 2 to week 0 samples in prednisone treated patient samples relative to placebo in patients who developed paradoxical TB-IRIS

Gene overlap analysis was computed to compare differentially expressed genes comparing week 2 to week 0 samples in patients who developed paradoxical TB-IRIS who received either placebo or prophylactic prednisone. The aim of this analysis was to identify genes that were upregulated at the time of paradoxical TB-IRIS onset despite prednisone prophylaxis.

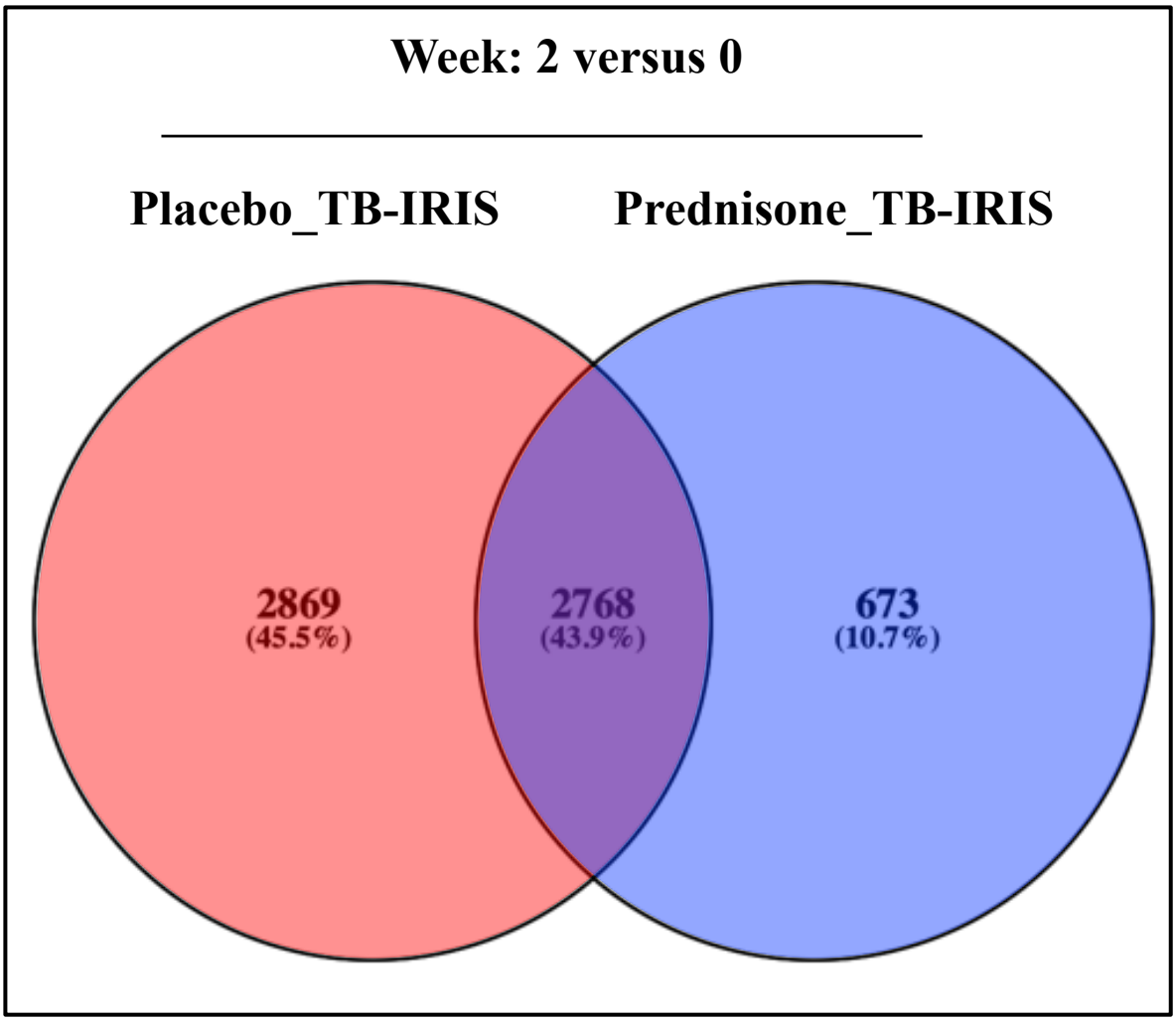

Figure 5.28. Gene overlap analysis in patient samples with paradoxical TB-IRIS who received either prednisone or placebo comparing week 0 and week 2 on ART*. Prednisone demonstrated at least a 4 fold reduction of the inflammatory mediators compared to placebo.*

A total of 2768 (43.9%) DEGs which were common between samples from paradoxical TB-IRIS patients who either received placebo or prednisone prophylaxis were identified. Furthermore, 2869 and 673 DEGs were exclusive to paradoxical TB-IRIS patients who were allocated placebo or prednisone prophylaxis respectively (**Figure 5.28**).

The genes exclusive to the placebo arm (45%) were diverse in function but with a common theme of genes of the innate immune system that encode receptors that form part of the proinflammatory intracellular signaling cascade, genes encoding inflammatory lipids, cytokines and chemokine respectively, intracellular PRRs, and transcription factors that modulate inflammation. Additionally, genes that encode signaling cytokines derived from the CD4 T cells constituted a proportion of the 45%. Notably, approximately 10% of the identified genes mapped exclusively to the prednisone intervention (**Figure 5.28**). This represents around

4-fold fewer genes compared with number of genes that were exclusively differentially expressed in the placebo arm. The list of genes mapping to the prednisone intervention mainly included genes that encode proteins of the extracellular matrix and those encoding proteins that are involved in neuronal development and signaling. Fewer genes associated with inflammation were in the prednisone gene list.

5.7.7 Summary of findings for these analyses

There were no DEGs when patient samples of paradoxical TB-IRIS patients were compared to those of TB-non-IRIS controls at week 2 on concurrent ART and prophylactic prednisone. These findings suggest that the prednisone intervention blunts the inflammatory gene expression signature associated with paradoxical TB-IRIS, despite some patients still developing clinical manifestations of TB-IRIS while on prednisone prophylaxis. Longitudinal gene expression analysis revealed robust transcriptional perturbation between week 0 and 2 on concurrent ART and prophylactic prednisone in patients with paradoxical TB-IRIS disease and in TB-non-IRIS controls. Functional classification of the DEGs identified a significant enrichment in the expression of neutrophils and platelet-associated genes at week 2 on dual ART and prednisone compared to week 0 in patients who developed paradoxical TB-IRIS. Additionally, epigenetic regulation of gene expression through methylation was significantly downregulated at week 2 compared to week 0 in these patients. Lastly, TB-non-IRIS controls showed upregulation of biological pathways that reflect the remodelling of the extracellular matrix involving the biosynthesis of the collagen polymer between week 0 and 2 on concurrent ART and prophylactic prednisone. Antiviral responses and interferon gene inducible responses as well as the synthesis of granulocytes whose cargo accommodates highly inflammatory and cytotoxic contents were significantly downregulated in TB-non-IRIS controls at week 2 compared to week 0. Lastly, genes associated epigenetic responses leading to the demethylation and deacetylation of other genes were downregulated in TB-non-IRIS controls who received concurrent ART and prednisone between week 0 and 2.

5.8 All patients at week 0: TB-IRIS vs TB-non-IRIS

To further explore the gene expression findings in patients who later developed paradoxical TB-IRIS and those who did not (TB-non-IRIS controls) at week 0, all patient samples (from placebo and prednisone allocated patients) were included, and the gene expression signature was investigated as described below.

5.8.1 Differential gene expression analysis

Differential gene expression analysis (DGEA) was computed for all samples collected from patients who later developed paradoxical TB-IRIS compared to TB-non-IRIS controls at week 0. To model raw gene count data, DESeq2 workflows were adapted to derive and describe differentially abundant transcripts in a total of n = 225 samples.

5.8.2 Exploratory analysis

Variance stabilized, normalized expression data, were assessed for quality and explored for patterns using principal component analysis (PCA). A total of 225 eigenvectors or principal components (PC) corresponding to the patient samples were generated. Shown below are the first 3 PC or dimensions, which accounted for 98% of the cumulative variance (**Figure 5.29 A**). Figure 5.29A depicts the relative contribution of the first 10 samples to each PC, where the scale represents the proportion of variance contributed by each sample to each PC. Most importantly, PC1 accounted for 90.3% of the variance explained by all the samples (**Figure 5.29 B**).

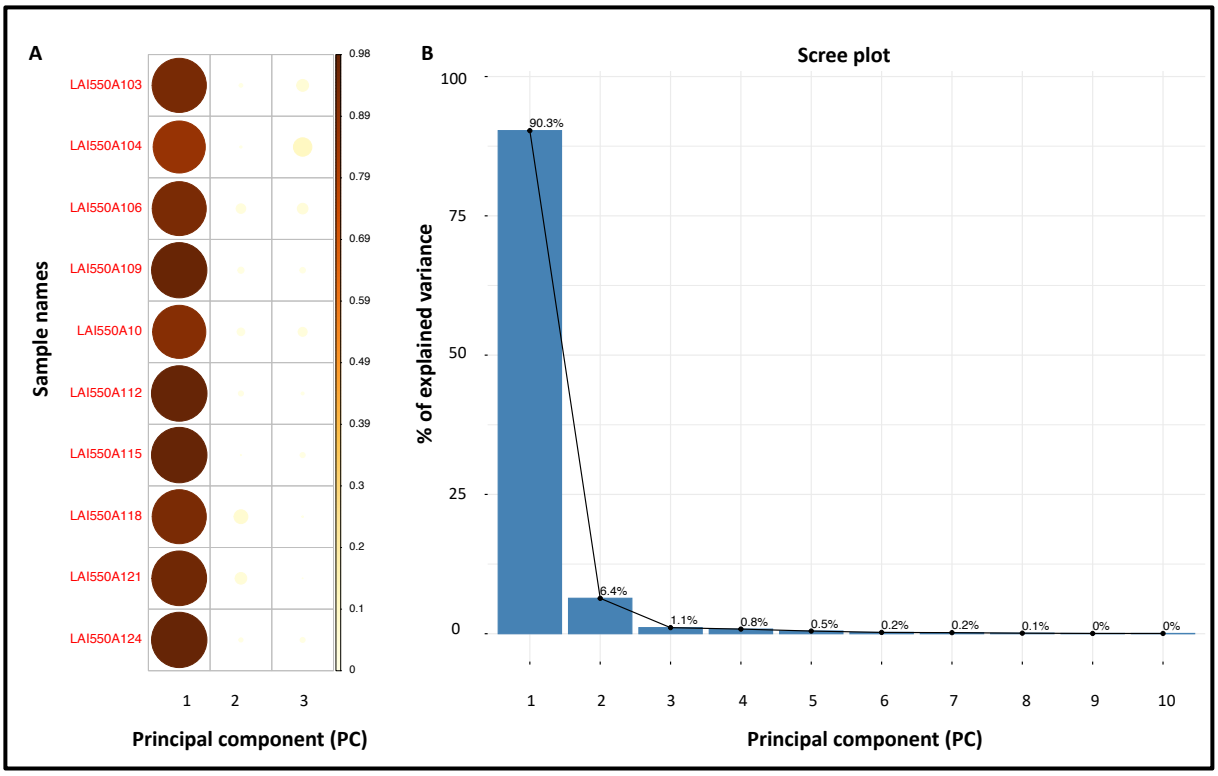

Figure 5.29. Exploratory data analysis for 225 samples collected from all patients with paradoxical TB-IRIS and TB-non-IRIS controls prior to the initiation of antiretroviral therapy (ART) and prednisone prophylaxis at week 0. ***A.*** *The relative contribution of each sample to the cumulative variance across the first three principal components (PC).* ***B.*** *Scree plot showing the proportion of variance explained by each PC.*

Collectively, PC1 and PC2 contributed 96.7% of the cumulative variance for all the samples (**Figure 5.29 B**). PCA was subsequently computed using the first 2 PCs for the 500 most variable genes across all samples (**Figure 5.30 A**). PC1 represents the linear combination of the Euclidean distances (eigenvalue) between transcripts across 225 samples. PC1 maximizes the variability of the data when projected in the x-axis (39%) and accounted for most of the variance compared to PC2 which is orthogonal to PC1. PC2 describes the residual variance of PC1 (9%) (**Figure 5.30 A&B**). PC1 is a mixed cluster of TB-IRIS and TB-non-IRIS patients, similarly for PC2. This indicates the proximity of the eigenvalues and therefore, the similarities in gene expression between the two clinical groups at week 0 (**Figure 5.30 A**).

Following the evaluation of the similarities in gene expression between all patient samples, the differentially abundant transcripts between the two clinical groups at week 0 were visualized. A total of 1036 differentially expressed transcripts were identified across all samples at week

0 after adjusting for multiple hypothesis testing (FDR of 0.05). A total of 876 transcripts were upregulated while 160 transcripts were downregulated in samples from patients who later developed paradoxical TB-IRIS compared to those who did not. (**Figure 5.30 B)**.

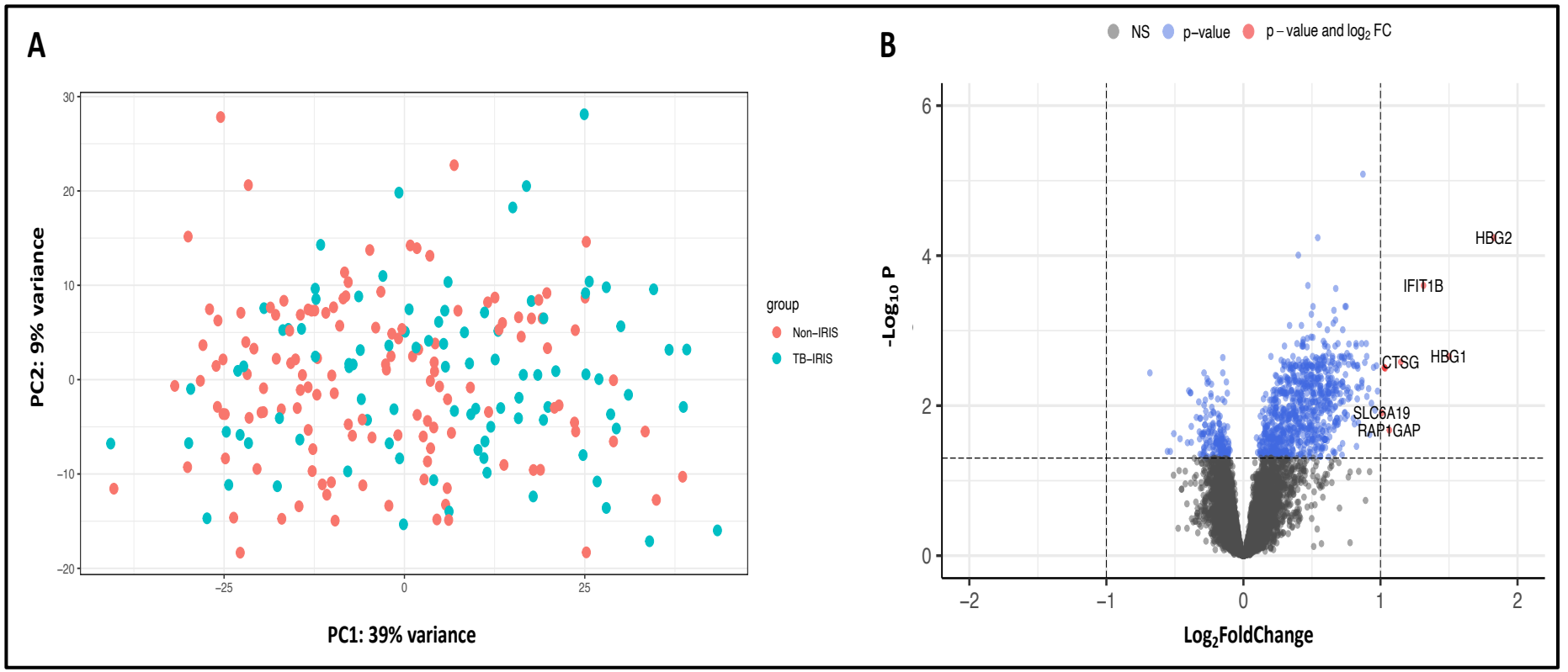

Figure 5.30. Exploratory data analysis for a total of 225 samples collected from patients who later developed paradoxical TB-IRIS and TB-non-IRIS controls prior to the initiation of antiretroviral therapy (ART) and prednisone prophylaxis or placebo (week 0). ***A***. *Principal component analysis for the top 500 variable genes. PC1 contributed most of the variance. Both PC1and PC2 are mixed clusters of TB-IRIS and TB-non-IRIS samples.* ***B***. *Volcano plot showing differentially expressed genes in patient samples collected from all patients (placebo and prednisone arm) at week 0. DEGs were defined by an FDR cut-off of 0.05 or less. A total of 1036 significant genes were identified.*

Next, the top 500 DEGs were visualized using a heatmap to explore the gene expression profiles in all patient samples collected at week 0 (**Figure 5.31**). Patient samples are represented as columns and the top500 transcripts as rows. A total of n= 1036 transcripts were differentially expressed showing significant upregulation in samples from patients with paradoxical TB-IRIS but not in TB-non-IRIS controls (**Figure 5.31**).

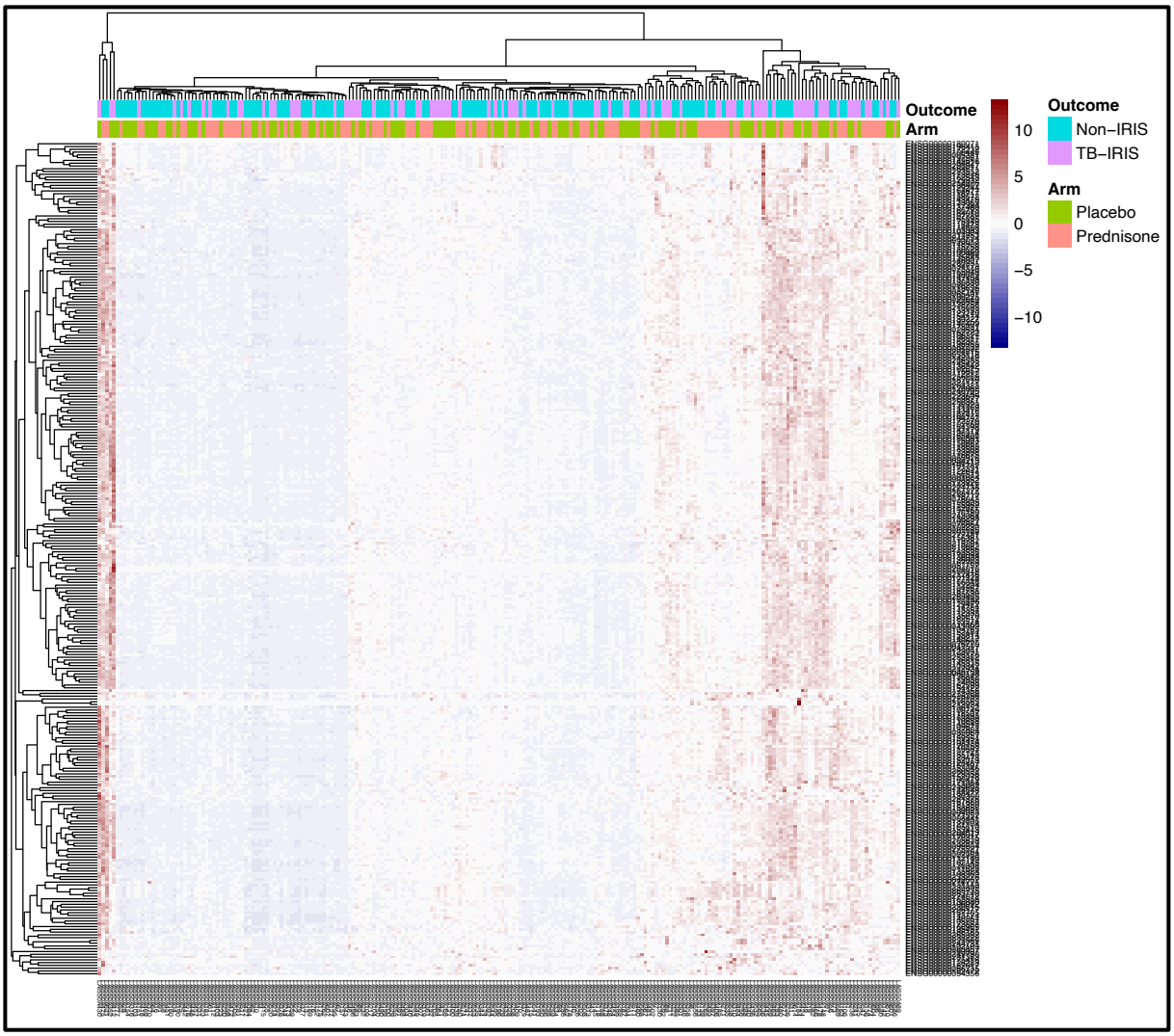

Figure 5.31. Differential gene expression analysis conducted on 225 patient samples (all patients - those who later received prednisone and those who later received placebo) taken prior to the initiation of antiretroviral therapy (ART) (week 0). A, *Visualization of the top 500 differentially expressed genes (DEGs) identified in samples from patients with paradoxical TB-IRIS (magenta) and TB-non-IRIS control(turquoise) at week 0. A total of 1036 transcripts were differentially expressed between the 2 clinical groups at week 0. A total of n =876 transcripts*

were upregulated while 160 transcripts were downregulated at week 0 in samples of patients who later developed paradoxical TB-IRIS versus non-TB-IRIS controls.

5.8.3 Gene set enrichment analysis

To identify and describe the significantly enriched biological pathways preceding the onset of paradoxical TB-IRIS, the list of DESeq2 derived DEGs was summarized into biological pathways by computing functional enrichment using gene set enrichment analysis (GSEA) [282]. Described below, are the significantly enriched biological pathways and their attendant genes that precede the acute inflammatory reactions that characterize paradoxical TB-IRIS. These are discussed in the context of both the Reactome database from which they are curated and peer review literature.

Figure 5.32 depicts the top 20 upregulated and downregulated biological pathways in 225 samples from patients who were assigned to receive either prednisone or placebo. Biological pathways were compared in those who later developed paradoxical TB-IRIS and in TB-non-IRIS controls at week 0, following adjusting for multiple hypothesis testing (FDR = 0.1). The top 20 upregulated pathways were statistically significant, while not all downregulated biological pathways were significant.

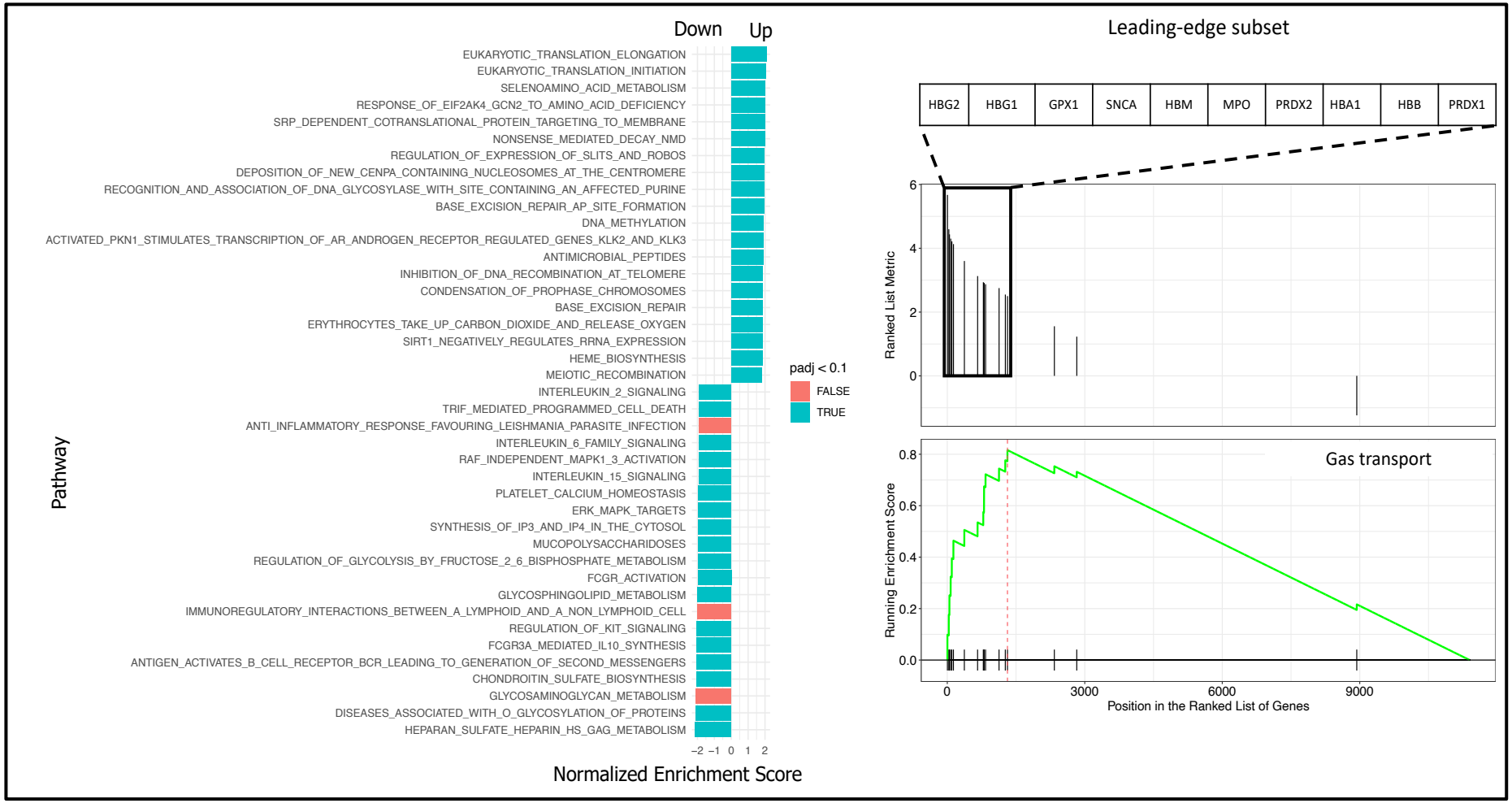

Figure 5.32. Functional enrichment with gene set enrichment analysis (GSEA) using a pre-ranked genelist and a curated gene set of canonical pathways from Reactome in 225 samples of patients comparing those who later developed paradoxical TB-IRIS to those who did not (TB-non-IRIS controls) prior to the initiation of antiretroviral therapy (ART) or week 0*. Pathway analysis identified the exocytosis of neutrophil secondary*

granules and adaptation to hypoxic stress as the most significantly enriched biological pathways in patient samples with paradoxical TB-IRIS compared to TB-non-IRIS controls week 0. Notably, processes involving prototypical inflammatory cytokines such as IL-6 were downregulated.

The upregulated gene sets were similar to the gene sets identified at week 0 when analyses were restricted to those who were allocated to receive placebo comparing patients who later developed paradoxical TB-IRIS with TB-non-IRIS controls (**Figure 5.32**). The increased power resulting from pooling all the samples from both the placebo and prednisone arms at week 0, likely resulted in the added identification of several gene sets such as those involved in DNA replication, DNA repair processes, and DNA methylation occurring in the nucleus of cells. The process of DNA replication and repair are highly conserved processes that accurately copy genetic information from generation to generation. This process involves chromatin disassembly and reassembly that is tightly regulated to ensure compact packaging of the genetic material into the nucleus while maintaining the epigenetic integrity of the information carried on histone proteins spooled by the genetic material [455]. Half of the histones that bind the genetic material during the process of DNA replication are from the parental chromatin and carry the parental epigenetic information, while the complementary half are *de novo* synthesized [471]. Much of the research conducted early in the mid 2000s endeavored to understand how the epigenetic information on the parental strand is inherited on the newly-synthesized histones in a DNA sequence-specific manner, to help maintain the flow of epigenetic information through cell divisions [459, 471]. It is possible that newly synthesized histones do not inherit parental epigenetic information with high integrity and thus predisposing to cellular malfunction and disease. Genes associated with DNA methylation, which is an epigenetic control mechanism, were significantly enriched in samples from patients with paradoxical TB-IRIS compared to TB-non-IRIS controls at week 0. This suggests epigenetic regulation may play a role in paradoxical TB-IRIS pathogenesis. This finding needs to be reproduced and explored in other clinical settings and study populations for verification and to better understand the mechanisms.

Furthermore, many genes that code for accessory proteins of the human 60S ribosomal RNA were differentially expressed in samples from patients with paradoxical TB-IRIS compared to TB-non-IRIS controls at week 0. Ribosomes partake in the process of protein synthesis occurring in the cytoplasm. Not much emphasis is placed on these finding since rRNA constitute 90% of the RNA species in the blood [461]. Their enrichment is probably a reflection of their abundance in peripheral blood.

Lastly, central processes characterizing paradoxical TB-IRIS compared to TB-non-IRIS controls prior to the initiation of ART include the exocytotic degranulation of secondary neutrophil vesicles and adaptation to hypoxic stress. These findings were previously discussed

in relation to Table 5.1. In Table 5.5 the transcripts that constituted the most significantly downregulated pathway (the heparan sulfate metabolic pathway) are listed. The associated genes comprised genes of the electron transport chain that leads to energy generation and recycling of redox equivalents. These were significantly downregulated in patients who later developed paradoxical TB-IRIS compared to TB-non-IRIS controls at week 0. This reinforces the notion that patients with paradoxical TB-IRIS disease may have mitochondrial metabolic dysfunction compared to TB-non-IRIS controls prior to ART initiation, perhaps due to more severe and extensive tuberculosis prior to initiating ART.

Table 5.5. Gene names, symbols and function of downregulated transcripts in samples across all patients at week 0*. The listed transcripts constituted part of the leading edge subset of the Heparan sulfate metabolism pathway that was most significantly downregulated in patients who later developed paradoxical TB-IRIS compared to TB-non-IRIS controls.*

Gene name	Symbol	Function
NADH:ubiquinone oxidoreductase subunit A1	NDUFA1	Encoded protein is an essential component of complex I of the respiratory chain, which transfers electrons from NADH to ubiquinone.
ECSIT signaling integrator	ECSIT	Encoded protein predicted to enable DNA-binding transcription factor activity and chromatin binding activity. Involved in regulation of oxidoreductase activity and regulation of protein complex stability.
NADH:ubiquinone oxidoreductase subunit A2	NDUFA2	The encoded protein is a subunit of the hydrophobic protein fraction of the NADH:ubiquinone oxidoreductase. May be involved in regulating complex I activity or its assembly via assistance in redox processes
NADH:ubiquinone oxidoreductase subunit A3	NDUFA3	Encoded protein is involved in mitochondrial respiratory chain complex I assembly
NADH:ubiquinone oxidoreductase subunit B3	NDUFB3	The encoded protein is an accessory subunit of the mitochondrial membrane respiratory chain NADH dehydrogenase
NADH:ubiquinone oxidoreductase complex assembly factor 3	NDUFAF3	The encoded protein is a mitochondrial complex I assembly protein that interacts with complex I subunits
NADH:ubiquinone oxidoreductase subunit B7	NDUFB7	The encoded protein is a subunit of the multi-subunit NADH:ubiquinone oxidoreductase (complex I). This protein has NADH dehydrogenase activity and oxidoreductase activity. It transfers electrons from NADH to the respiratory chain.
Mitochondrially encoded NADH:ubiquinone oxidoreductase core subunit 6	MT-ND6	Encoded protein enables NADH dehydrogenase (ubiquinone) activity
Mitochondrially encoded NADH:ubiquinone oxidoreductase core subunit 2	MT-ND2	Encoded protein enables NADH dehydrogenase (ubiquinone) activity
Mitochondrially encoded NADH:ubiquinone oxidoreductase core subunit 1	MT-ND1	Encoded protein enables NADH dehydrogenase (ubiquinone) activity

Of note, the same biological pathways remained significantly enriched in other curated databases (org.Hs.eg.db) which is a Bioconductor package for human genome-wide annotation.

5.8.4 WGCNA

Weighted gene co-expression network analysis (WGCNA) was conducted as previously described to identify genes that were highly correlated with paradoxical TB-IRIS. These could potentially be used to identify individuals at high risk for targeted intervention.

Six modules eigengenes (ME) that were highly correlated with paradoxical TB-IRIS were identified (ME: red, green, midnight blue, light green, tan and salmon). Subsequent analyses were conducted on the MEgreen due to highest correlation with paradoxical TB-IRIS (**Figure 5.33**).

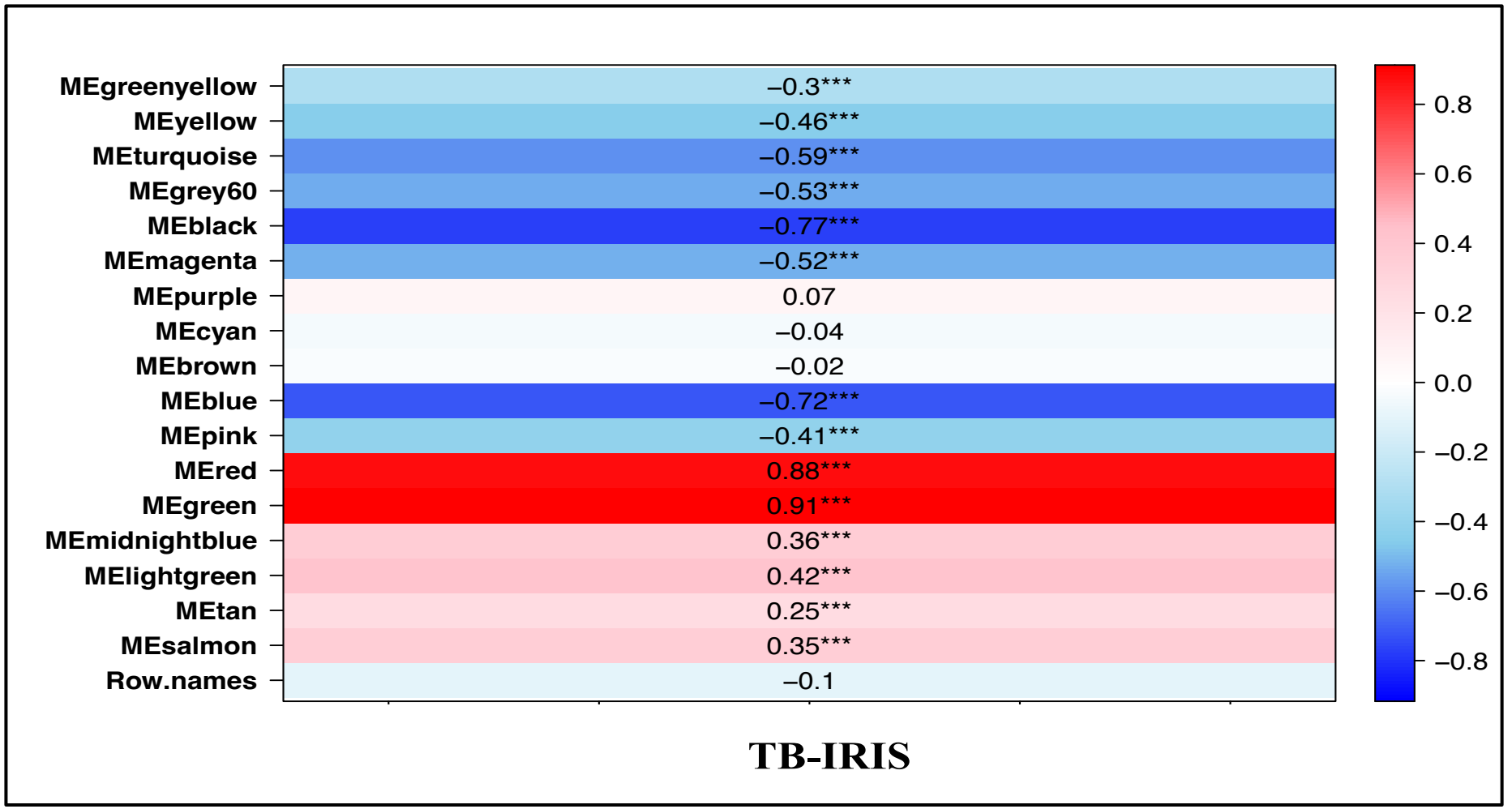

Figure 5.33. The identification of module eigengenes that are significantly correlated with paradoxical TB-IRIS using weighted gene co-expression network analysis in samples from all patients at week 0*. Six module eigengenes that were significantly correlated with paradoxical TB-IRIS disease at week 0 were identified. Subsequent analysis focused on MEgreen which was most significantly correlated with paradoxical TB-IRIS disease.*

The top 15 nodes in MEgreen were visualized to assess highly connected nodes. Gene ontology was performed on all the members of the module (n = 130) (**Figure 5.34**).

A

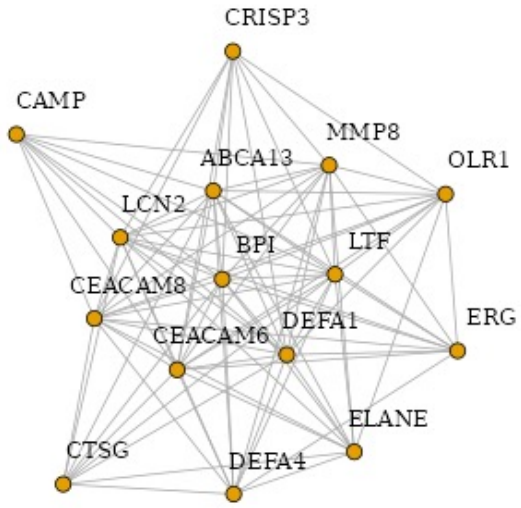

B

Pathways	Number of genes	Adj.Pval
Neutrophil activation and immune response	26	2.4e-18
Neutrophil mediated immunity	26	2.4e-18
Neutrophil activation	26	2.4e-18
Neutrophil degranulation	26	2.8e-18
Leukocyte degranulation	26	8.7e-18
Myeloid leukocyte mediated immunity	26	1.4e-18
Leukocyte activation involved in immune response	28	3.5e-17
Myeloid leukocyte activation	27	5.8e-17
Immune effector process	32	7.8e-17
Leukocyte mediated immunity	29	9.6e-17
Regulated exocytosis	28	1.4e-16
Leukocyte activation	33	9.7e-16
Exocytosis	28	3.3e-15
Cell activation	33	2.7e-14

Figure 5.34. Functional enrichment with weighted gene co-expression network analysis (WGCNA). A*. Visualization of the top 15 nodes in MEgreen. The module consists of n = 130 genes that were significantly correlated with paradoxical TB-IRIS.* ***B.*** *Gene ontology using ORA to summarise the module members into biological pathways. Several biological processes involving neutrophils were significantly enriched after correcting for multiple comparisons (FDR = 0.1).*

Several biological pathways involving neutrophils were among the top significantly enriched from the MEgreen that was significantly correlated with paradoxical TB-IRIS. These findings represent the basis for potentially developing biomarkers to identify those at highest risk for developing paradoxical TB-IRIS.

5.8.5 Summary of findings for these analyses

Whole blood derived gene expression profiles of all patients (both those assigned to prednisone and placebo) prior to the initiation of ART (week 0) were analyzed. The analyses identified

DEGs in those who later developed paradoxical TB-IRIS compared to TB-non-IRIS controls at week 0. A total of 1036 DEGs were identified between the two clinical groups and summarized them into biological pathways using GSEA and WGCNA. These were mainly representative of neutrophils and heme biosynthetic pathways in patients who later developed paradoxical TB-IRIS compared to those who did not prior to the initiation of ART.

5.9 All patients at week 2: Prednisone vs Placebo

To explore prednisone specific effects, the gene expression signature and biological pathways were compared in all patients who received prophylactic prednisone and all those who received placebo at week 2 on ART, which coincides with the median time for paradoxical TB-IRIS onset.

5.9.1 Differential gene expression analysis

Differential gene expression analysis (DGEA) was computed in all samples collected from patients at week 2 on ART comparing those receiving prednisone prophylaxis to placebo. To model raw gene count data, DESeq2 workflows were adapted to derive and describe differentially abundant transcripts at week 2, from a total of n = 190 patient samples.

5.9.2 Exploratory analysis

The data were explored by computing principal component analysis (PCA) to assess patterns in gene expression across all samples using variance stabilized, normalized expression data. A total of 190 eigenvectors or principal components (PC) corresponding to the number of patient samples were generated. Shown below are the first 3 PC which accounted for 99% of the cumulative variance (**Figure 5.35 A**). Figure 5.33A depicts the relative contribution of the first 10 samples to each PC. The scale represents the proportion of variance contributed by each sample to each PC. PC1 accounted for 91.4% of the variance explained by all the samples (**Figure 5.35 B**). Collectively, PC1 and PC2 contributed 96.3% of the cumulative variance for all the samples (**Figure 5.35 B**).

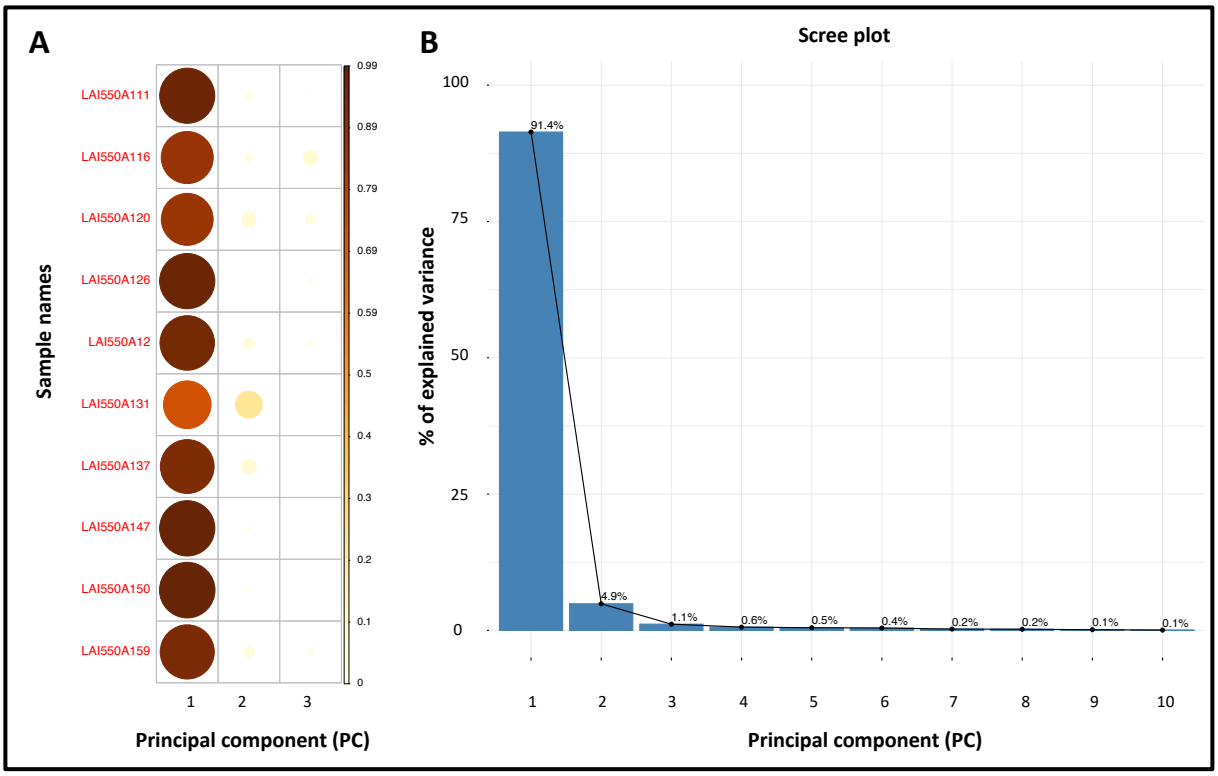

Figure 5.35. Exploratory data analysis for 190 samples from patients who received either prednisone prophylaxis or placebo at week 2 on antiretroviral therapy (ART). *A. The relative contribution of each sample to the cumulative variance across the first three principal components (PC).* ***B.*** *Scree plot showing the proportion of variance explained by each principal component (PC).*

Therefore, PCA was performed using the first 2 PCs for the 500 most variable genes across all samples (**Figure 5.35 A**). PC1 represents the linear combination of the Euclidean distances (eigenvalue) between transcripts across 190 samples. PC1 maximizes the variability of the data when projected in the x-axis (32%) and accounted for most of the variance compared to PC2. PC2 is orthogonal to PC1, and it describes the residual variance of PC1 (14%) (**Figure 5.35 A&B**). PC1 describes a mixed cluster of patients who received either prednisone prophylaxis or placebo. Similarly, for PC2. This indicates the proximity of the eigenvalues and therefore, the similarities in gene expression between the two clinical groups at week 2 on ART. (**Figure 5.35 A**).

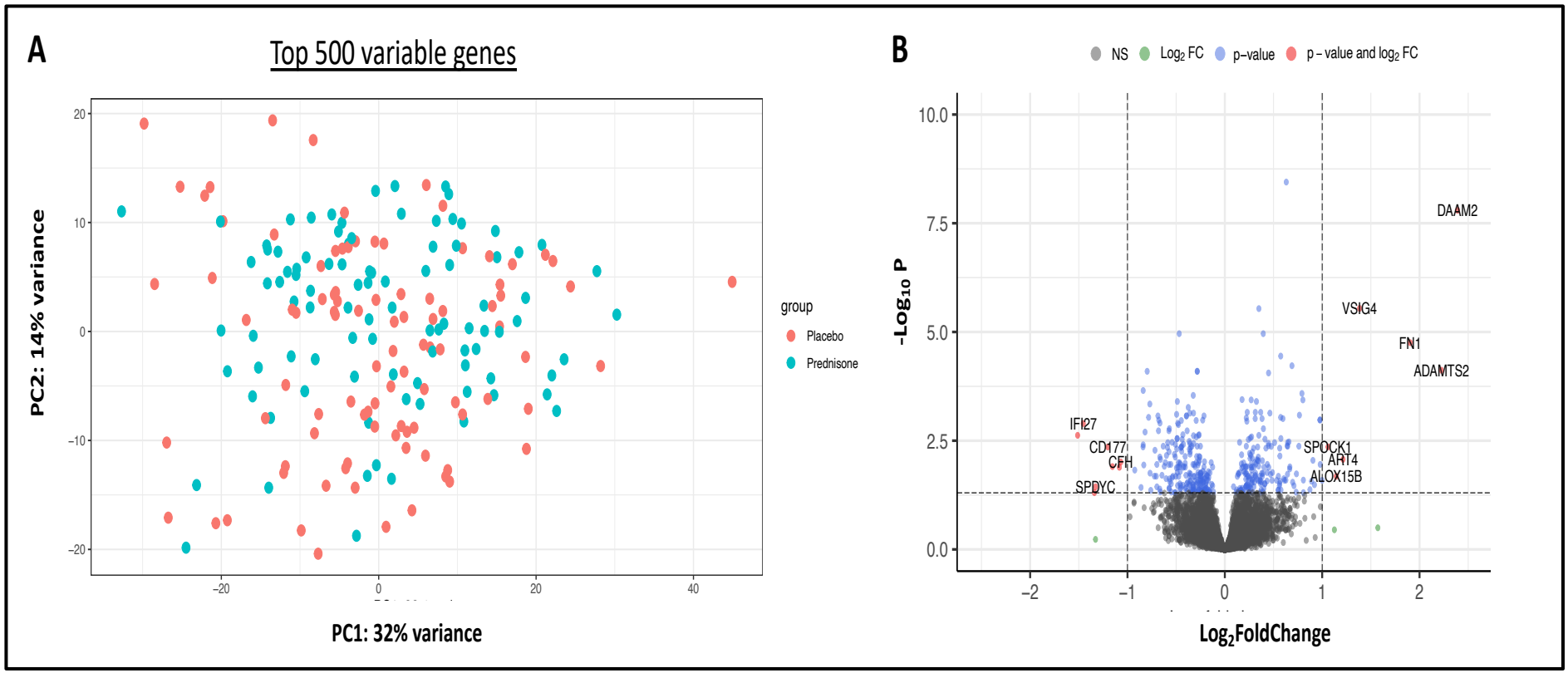

Figure 5.36. Exploratory data analysis on a total of 190 samples collected from all patients comparing those who received prophylactic prednisone to those who received placebo at week 2 on antiretroviral therapy (ART). *A. Principal component analysis for the top 500 variable genes. PC1 contributed most of the variance. Both PC1and PC2 are mixed clusters of patients receiving prednisone and placebo.* ***B****. Volcano plot showing differentially expressed genes in patient samples. DEGs were defined by an FDR of 0.05 or less. A total of 771 significant genes were identified.*

To explore the data further, the list of differentially abundant transcripts were visualized between the two intervention arms (prednisone vs placebo) in all patients at week 2 on ART. A total of 771 transcripts were differentially expressed after correcting for multiple hypothesis testing (FDR = 0.05). (**Figure 5.35 B**). A total of 293 transcripts were upregulated while 478 transcripts were downregulated. The upregulated genes were largely reflective of those encoding proteins involved in extracellular matrix remodeling. One transcript that was downregulated was a gene encoding a surface marker (CD177) for neutrophils.

We subsequently visualized the top 100 DEGs using a heatmap to explore the gene expression profiles in all patient samples comparing those receiving prednisone versus placebo at week 2 on ART (**Figure 5.36**).

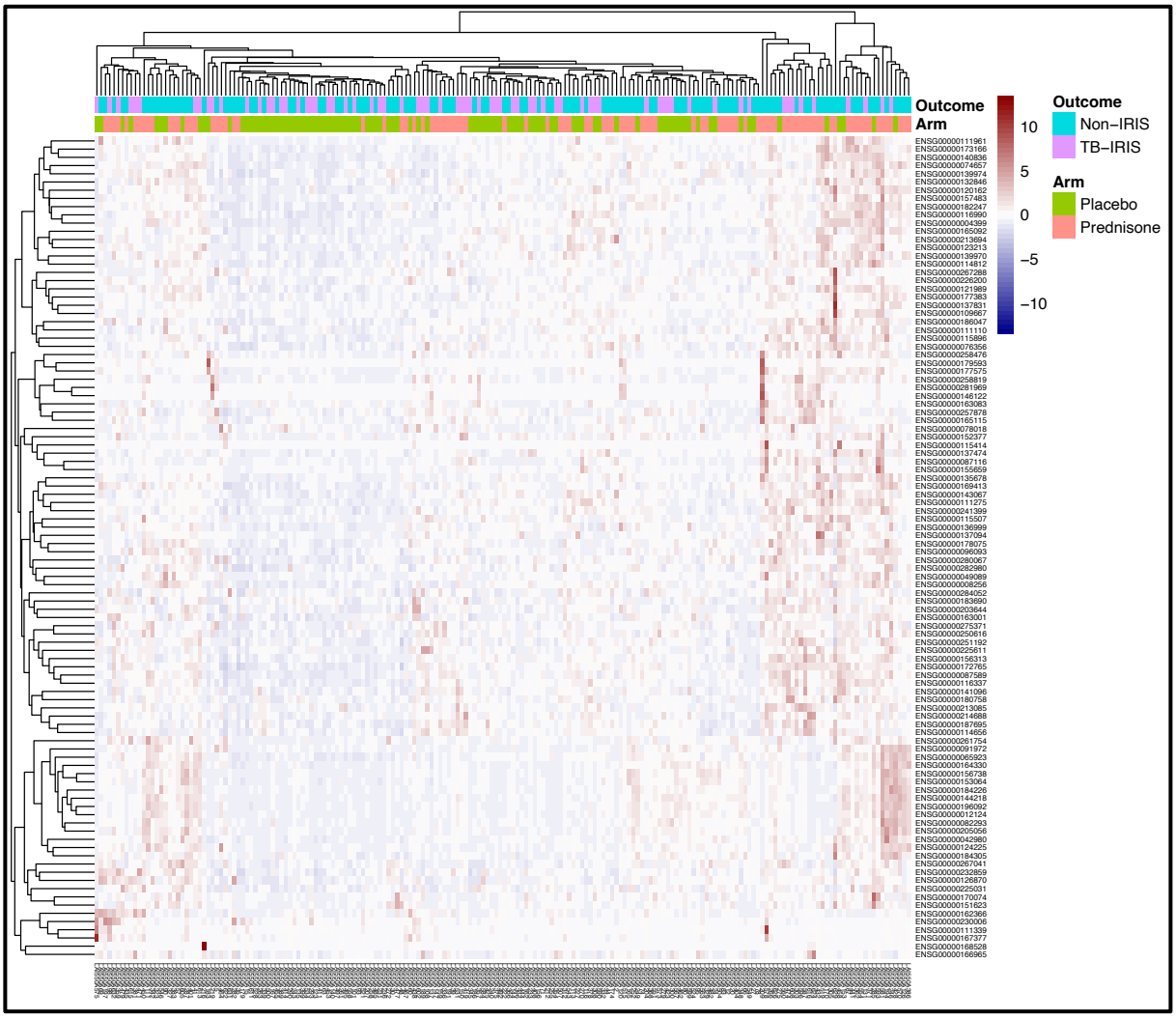

Figure 5.37. Differential gene expression analysis in 190 samples of patients who received prednisone prophylaxis compared to placebo at week 2 on antiretroviral therapy (ART).

Visualization of the top 500 differentially expressed genes (DEGs) identified in all patient samples. There was no clear differentiation in gene expression between patients who received either prophylactic prednisone or placebo.

Clustering both rows (genes) and samples revealed interesting patterns for both intervention arms; prophylactic prednisone modulated the perturbation of many transcripts relative to placebo and more transcripts were downregulated than upregulated (**Figure 5.37)**. The individual differentially expressed genes that are part of the leading-edge subset are further described in table 5.6.

Table 5.6.Gene names, symbols and function identified as part of extracellular matrix organization leading edge subset that were significantly enriched (FDR = 0.1) in all patient samples comparing those who received prophylactic prednisone to placebo at week 2 on antiretroviral therapy (ART).

Gene name	Symbol	Function
ECM organization leading edge subset		
Matrix metallopeptidase 8	MMP8	Encoded protein remodels extracellular matrix
Matrix metallopeptidase 9	MMP9	Encoded protein remodels extracellular matrix
Matrix metallopeptidase 25	MMP25	Encoded protein remodels extracellular matrix
Collagen type XIX alpha 1 chain	COL19A1	Encoded protein maintains the integrity of the extracellular matrix.
Collagen type IX alpha 2 chain	COL9A2	Encoded protein maintains the integrity of the extracellular matrix.
CEA cell adhesion molecule 8	CEACAM8	Involved in heterophilic cell-cell adhesion via plasma membrane cell adhesion molecules
ADAM metallopeptidase domain 09	ADAM9	The encoded protein implicated in a variety of biological processes involving cell-cell and cell-matrix interactions
ADAM metallopeptidase domain 17	ADAM17	The encoded protein implicated in a variety of biological processes involving cell-cell and cell-matrix interactions
Thrombospondin 1	THBS1	Encoded protein is an adhesive glycoprotein that mediates cell-to-cell and cell-to-matrix interactions.
Intercellular adhesion molecule 3	ICAM3	Encoded protein functions both as an adhesion molecule, and as a potent signalling molecule
Collagen beta(1-O) galactosyltransferase	COLGALT1	The encoded protein transfers galactose moieties to hydroxylysine residues of collagen and mannose binding lectin.
TIMP metallopeptidase inhibitor 1	TIMP1	Encoded protein inhibits matrix metalloproteinases (MMPs)
EGF containing fibulin extracellular matrix protein 2	EFEMP2	Encoded protein is necessary for elastic fiber formation and connective tissue development

Integrin subunit alpha X	ITGAX	gene encodes the integrin alpha X chain protein which dimerizes with ITGB2 to form a leukocyte-specific integrin referred to as inactivated-C3b. Important in the adherence of neutrophils and monocytes to stimulated endothelium cells, and in the phagocytosis of complement coated particles.
TIMP metallopeptidase inhibitor 2	TIMP2	Encoded protein inhibits matrix metalloproteinases (MMPs)
Integrin subunit alpha E	ITGAE	Encoded protein has a role in adhesion,
Elastin microfibril interfacer 2	EMILIN2	Encoded proteins enables extracellular matrix constituent conferring elasticity.
Integrin subunit alpha 1	ITGA1	Encoded protein heterodimerizes with the beta 1 subunit to form a cell-surface receptor for collagen and laminin.

5.9.3 Gene set enrichment analysis

To identify and describe the significantly enriched biological pathways modulated by prednisone prophylaxis when compared to placebo, the differentially abundant transcripts arising from DESEq2 were pre-ranked and summarized into biological pathways by computing functional enrichment using gene set enrichment analysis (GSEA) [282]. Described below, are the enriched biological pathways and their attendant genes that were identified after correcting for multiple hypothesis testing (FDR = 0.1). These are discussed in the context of the reactome database from which they are curated as well as peer reviewed literature.

Figure 5.38 depicts the top 20 upregulated and downregulated biological pathways at week 2 on ART that were all significantly enriched after adjusting for multiple hypothesis testing (FDR = 0.1) (**Figure 5.38**).

The first five biological pathways that were most upregulated in patients who were allocated prophylactic prednisone were dominated by genes that encode accessory proteins that associate with the eukaryotic 60S ribosomal RNA. Ribosomes are the site of protein synthesis which occurs in the cytoplasm. This potentially indicates the role of prednisone prophylaxis in modulating protein synthesis. The biological relevance of this is difficult to discern because the finding does not indicate the synthesis of which proteins is most affected. Ribosomal RNA constitute 90% of the total RNA species in the blood and the finding that ribosomal genes were most upregulated could relate to this.

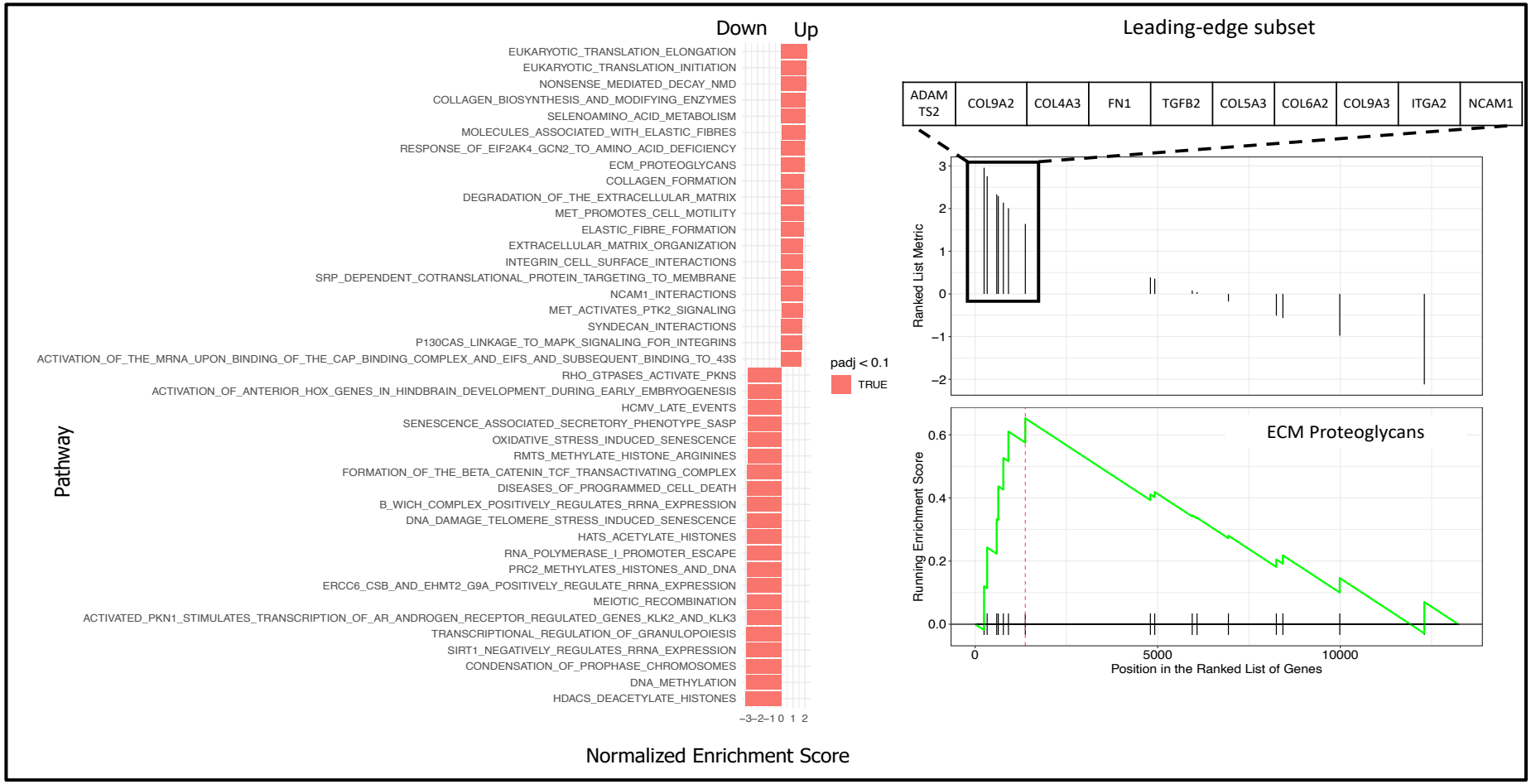

Figure 5.38. Functional enrichment with gene set enrichment analysis (GSEA) using a pre-ranked genelist and a curated gene set of canonical pathways from Reactome in samples from all patients (those that received prophylactic prednisone and those that received placebo) at week 2 on antiretroviral therapy (ART). *Pathway analysis identified the collagen formation and extracellular matrix organization pathways as the most significantly enriched biological pathways at week 2 on ART, in patients who received prednisone prophylaxis compared to those who received*

placebo. Notably, processes involving epigenetic regulation of gene expression were significantly downregulated in patients who received prednisone prophylaxis compared to those that received placebo.

Several other upregulated pathways that distinguish those receiving prednisone prophylaxis from placebo at week 2 on ART were identified (**Figure 5.38**). Pathways such as collagen formation, molecules associated with elastic fibers, extracellular matrix proteoglycans, elastic fiber formation, extracellular matrix organization, integrin cell surface interactions were among the biological pathways that were significantly upregulated by prednisone prophylaxis (**Figure 5.38**).

The extracellular matrix is a protein scaffold suspended in a semifluid environment of anionic proteoglycan polymers [464]. The main function of this protein mesh is to provide structural support for cells [463]. However, it performs other functions such as modulating cell behavior. There is a potential association between paradoxical TB-IRIS associated inflammation and tissue damage. Molecular evidence to support this includes the significant secretion of metalloproteinases in samples from patients with paradoxical TB-IRIS compared to TB-non-IRIS controls [162, 243, 472]. Clinical evidence for this is the frequent formation of pus collections at site of paradoxical TB-IRIS inflammation, particularly when lymph nodes are affected. These findings suggest prednisone prophylaxis may play a role in extracellular matrix damage remodeling and repair.

Furthermore, prophylactic prednisone increased the expression of neural cell adhesion molecule1 (NCAM1 interaction) pathway compared to placebo at week 2 on ART. This reflects the pleiotropic nature of effects of prednisone.

Several biological pathways that were significantly downregulated by prophylactic prednisone following adjustment for multiple comparisons (FDR = 0.1) were also identified at week 2 on ART. The downregulated biological pathways were largely representative of processes that occur in the cell nucleus, such as meiotic recombination, deacetylation of histones, DNA methylation and histone methylation among others. This data suggests that prophylactic prednisone plays a significant role in regulating epigenetic control mechanisms. Epigenetic regulation of gene expression and its significance was previously discussed in detail (see 5.7.6.3).

5.9.4 Summary of findings for these analyses

The gene expression profiles of patients who received prophylactic prednisone versus placebo were compared at week 2 on ART. A total of 771 DEGs were identified, and their pathway

membership was established using the curated Reactome database. The data suggests that prophylactic prednisone is associated with the upregulation of biological processes that are related with collagen biosynthesis and the remodeling of extracellular cellular matrix, suggesting a potential role in tissue remodeling and repair. Similarly, many biological pathways were significantly downregulated by prednisone and these were reflective of epigenetic regulation, compatible with the established mechanism of action of corticosteroids in regulating gene expression.

Chapter 6 outline: Neutrophil counts and plasma neutrophil markers in patients with paradoxical TB-IRIS and controls prior to the initiation of ART and longitudinally on ART

This chapter details the functional validation of the identified neutrophil signature in the transcriptomic analyses by analyzing blood measurements of absolute neutrophil counts at week 0, 2 and 12 on ART in patients who developed paradoxical TB-IRIS compared to those that did not (TB-non-IRIS controls). Further discussed are the longitudinal trends in absolute neutrophil counts, up to week 12 on ART in patients who developed paradoxical TB-IRIS and in TB-non-IRIS controls respectively. Enzyme linked immunosorbent assays were used to assess plasma soluble markers (human neutrophil peptide [HNP]-1-3, azurocidin, neutrophil elastase [NE] and myeloperoxidase [MPO]) associated with neutrophil degranulation at week 0 and 2 on ART, comparing TB-IRIS cases and controls. Multivariate analyses were applied to additionally evaluate whether observed soluble responses were a function of changes in absolute neutrophil counts. Finally, the chapter discusses the relevance of these findings.

6. Background

Leukocytes also known as white blood cells (WBC), collectively refer to the immune cellular fraction of the blood [473, 474]. WBC are synthesized *de novo* through haematopoiesis which defines the process of making blood cells and blood plasma [475, 476]. They are characterized by the lack of hemoglobin, the presence of a nucleus, and the capacity to move in blood and tissue [473, 477]. As part of the immune system, WBC are plentiful in the blood with normal counts ranging between 4000-11000 cells per microliter [478]. They originate from the bone marrow and move around the blood, home to different tissues and organs to protect the body against infections, diseases, and abnormal cellular functioning through a diverse range of effector functions [475]. WBC are classified into two major categories: agranulocytes and granulocytes based on the shape of their nucleus, size of the cell type and the presence of inclusion bodies [477]. This classification gives rise to five distinct WBC that collectively make up innate and adaptive immunity.

Innate immunity assumes the first line role in defending against injurious microbes. Neutrophils, a component of the innate immune system, have a pivotal function of combating the growth and spread of pathogenic microorganisms including fungi, bacteria and viruses [479]. However, their uncontrolled accumulation or improper activation is detrimental in a number of inflammatory diseases [480-482]. Therefore, the production, release and subsequent clearance of neutrophils must be tightly regulated to prevent self-induced injury. This has been described in rheumatoid arthritis and acute respiratory distress syndrome. The following sections discuss neutrophils and their characteristics.

6.1 Neutrophils

Neutrophils, also known as polymorphonuclear (PMN) leukocytes are myeloid cells characterized by the presence of multi-lobed or irregular shaped nuclei and the capacity to form bioactive laden secretory granules whose contents are released during infection or disease [477]. Neutrophils constitute up to 80% of circulating WBC and represent the body's first line of defence [483]. They are involved in the acute inflammatory response to bacterial infection and removal of pathogens through a variety of mechanism including phagocytosis, release of antimicrobial substances (e.g. peptides and enzymes) and formation of neutrophil extracellular traps (NETs).

6.1.1 The origin and maturation of neutrophils

The *de novo* synthesis of neutrophils occurs in haematopoietic cords of the venous sinuses in the bone marrow [413]. Agranulocytes and granulocytes arise from a common progenitor cell from which differentiation occurs [475, 484, 485]. Differentiation into granulocytes is a highly regulated process in which the coordinated expression of selective myeloid transcription factors (e.g. HoxB7 and STAT3), proteins (e.g. S100A9 and neutrophil elastase) and receptors (e.g. granulocyte-macrophage colony-stimulating factor (GM-CSF)) are required [486, 487]. Recent evidence suggest that Rac2 (a GTPase) also contributes to the formation of the myeloid lineage in haematopoietic cells [488].

The neutrophil population in the bone marrow is divided into three pools: the stem cell pool which consists of undifferentiated haematopoietic stem cells (HSC). The mitotic pool which make up the granulocytic progenitor cells that are undergoing proliferation and differentiation. Lastly, the post-mitotic pool which are fully differentiated mature neutrophils [489]. Not all mature neutrophils are released into the blood stream; in fact, a large storage pool of mature neutrophils is found in the bone marrow in what is called "the bone marrow reserve" [413, 489].

6.1.2 Mobilization and homeostasis

A mature neutrophil expresses high levels of G-CSF receptor, CXC chemokine receptor 4 (CXCR4), and low levels of G-protein coupled receptor on their surface [490]. Stromal-derived factor (SDF)-1 is a chemokine that is constitutively expressed by bone marrow stromal cells and serves as the main ligand for CXCR4. Signaling of the CXCR4/SDF-1 pair retains neutrophils in the post mitotic pool [491].

Following their maturation, neutrophils emigrate to the blood stream through the sinusoidal endothelium that separates the haematopoietic compartment from the blood circulation. They egress the sinusoidal endothelium through tight-fitting pores by trans-endothelial migration instead of passage through cell–cell junctions [492-494]. Neutrophils constitute 40-80% of the total WBC count making them the most abundant leukocytes in the blood [195, 483]. Neutrophils are highly mobile and eventually migrate into organs [495]. In fact, the lungs have the largest pool of marginated neutrophils in the body [496]. Neutrophil abundance, coupled with their brief circulating half-life (6–8h), necessitates a basal production rate of up to 10^{11} neutrophils per day by the bone marrow; the advantage of this rapid turnover to the host has clinical relevance as highlighted in cases of congenital or cyclic defects causing neutropenia resulting in the overgrowth of bacteria and other pathogenic microbes at the site of exposure or injury [482]. Neutrophil homeostasis is maintained by a fine-tuned balance between

granulopoiesis, bone marrow storage and release, intravascular margination, clearance and destruction [488, 492, 497-499].

6.1.3 Function

Neutrophils play a critical role in immune surveillance and are rapidly recruited to sites of infection or inflammation, where they eliminate invading pathogens through various mechanisms [380, 496, 500, 501]. Neutrophils contain at least four types of granules including primary or azurophilic granules, secondary or specific granules, tertiary and secretory granules [380, 500, 502]. The granules are armaments containing preformed enzymes and proteins that are biotoxic. Primary granules contain the most toxic cargo, which include among others elastases, myeloperoxidase, cathepsins, and defensins [501, 503]. Secondary and tertiary granules have overlapping cargo with lactoferrin and matrix metalloprotease-9 as distinct cargo between the two granule types [504]. The secretory vesicles of human neutrophils contain human serum albumin, indicating the presence of extracellular fluid taken up during phagocytosis [504].

Neutrophil degranulation is a processes by which the cargo inside the granules are released [501]. This process is initiated by receptor binding of the secretagogue which assembles the microtubule filaments and remodels the actin cytoskeleton of the granule causing it to migrate and fuse with the encapsulated pathogen or the target plasma membrane [504, 505]. This process depends on ATP and leads to a spike in intracellular calcium levels.

Neutrophils have phagocytic capacity which involves engulfing a pathogen and facilitating intracellular killing by releasing preformed bioactive granules in a process of degranulation and/or through the release of reactive oxygen species within the phagosome in a mode of killing known as respiratory burst. The type of released granule (with primary to tertiary granules ranging from most to least potent respectively) predicts the degree of damage caused to the pathogen [500, 501]. Alternatively, neutrophils can kill pathogens extracellularly mediated through cytokine secretion and cytotoxic mediators [506]. A mature neutrophil is endowed with high expression of plasma and granule membrane derived nicotinamide adenine dinucleotide phosphate (NADPH) oxidase, an enzyme that mediates oxidative stress [507, 508]. Oxidative stress is regulated via NADPH oxidase assembly to produce superoxide. Superoxide is highly reactive and is able to modify various molecules, including lipids, proteins, and nucleic acids hence, its microbicidal activity [508].

Lastly, neutrophils can eliminate pathogenic microbes through a particularly inflammatory process of cell death called NETosis. Death by NETosis releases the cell's chromosomal DNA which is complexed with histones that have microbicidal effect [509, 510]. NETosis can be triggered by several stimuli in addition to pathogenic microbes including nitric oxide, cytokines (IL8), activated endothelial cells and platelets [511].

However, the destructive capacity of these cells also raises the potential for neutrophils to damage healthy tissues, which occurs in many inflammatory diseases such as acute respiratory distress syndrome, inflammatory bowel disease, and rheumatoid arthritis [512, 513]. An important regulatory mechanism involves surface receptor triggering which leads to intracellular signaling, culminating in the activation of cell movement to modulate the release of granules.

In Chapter 5, the study which evaluated differentially abundant transcripts cross-sectionally and longitudinally up to week 12 on ART in patients who developed paradoxical TB-IRIS compared with TB-non-IRIS controls, found that paradoxical TB-IRIS was associated with gene expression suggesting increased neutrophil degranulation prior to the initiation of ART and at the median time of symptom onset, in patients that were allocated placebo. The objective of this chapter was to validate these findings using enzyme linked immuno-sorbent assay (ELISA) to measure plasma soluble markers of neutrophil function at protein level, as well as absolute neutrophil counts in blood of patients with paradoxical TB-IRIS and TB-non-IRIS controls from the Pred-ART intervention trial.

6.2 Methods

6. 2.1 Study cohort

This sub-study was nested in a previously completed double-blind, placebo randomized controlled trial that evaluated the efficacy of short course (4 weeks) prednisone given concurrently with ART in preventing paradoxical TB-IRIS. The clinical characteristics of the cohort were discussed in detail in chapter 5 (see section 5.4.1) and the findings of the trial were published [21, 252, 258, 346, 430].

6.2.2 Blood measurement of absolute neutrophil counts

Peripheral blood was collected from patients enrolled in the Pred-ART trial as previously described (see section 3.8.1). Bloods were transported to the National Health Laboratory Services (NHLS) laboratory for a complete blood count with differential. The number of neutrophils (cells/μL) were determined for each patient at week 0, 2 and 12 on ART.

6.2.3 Detection of plasma soluble human neutrophil peptide (HNP)1-3 using enzyme linked immunosorbent assay.

The human neutrophil peptide (HNP)-1-3 enzyme linked immunosorbent assay (ELISA) kit was procured from Hycult Biotech™ and utilized for the quantitation of HNP1-3 in plasma samples from patients with paradoxical TB-IRIS and TB-non-IRIS controls prior to the initiation of ART (week 0) and at week 2 on ART. The HNP1-3 ELISA kit is a ready to use solid phase assay that is based on the sandwich principle. The assay was performed according to manufacturer's instructions. All reagents were equilibrated to ambient temperature prior to use; standards, dilution of samples, and all buffers were prepared according to the manufacturer's instructions. Briefly, a total volume of 100 μL of standards and samples were added to appropriate wells coated with the primary antibody and the plates were subsequently incubated for 1 hour at room temperature. The plates were washed four times in 400 μL wash buffer using an automated plate washer. A total volume of 100 μL of prediluted tracer solution was added to all the wells. The plates were sealed and incubated for 1 hour at room temperature and washing repeated as previous. A total volume of 100 μL of 3,3',5,5'-tetramethylbenzidine (TMB) substrate was added to all the wells; the plates were sealed and incubated in the dark at ambient temperature for 30 min. The reaction was stopped by adding 100 μL of stop solution and the solution gently mixed by swirling the plates. The absorbance was determined by

reading the plate in an automated plate reader at absorbance wavelength 450 nm. The data was quality checked by an independent investigator and analyzed by plotting concentration values.

6.2.4 Detection of plasma soluble myeloperoxidase (MPO), azurocidin (Azu1) and neutrophil elastase using enzyme linked immunosorbent assay.

Human myeloperoxidase (MPO), azurocidin (Azu1) and neutrophil elastase (NE) ELISA kits were procured from Thermo-Fisher Scientific™ and employed for the *in vitro* quantitation of MPO, Azu1 and NE in plasma samples from patients with paradoxical TB-IRIS and TB-non-IRIS controls prior to the initiation of ART (week 0) and at week 2 on ART. The ELISA kits are a ready to use solid phase assays that are based on the sandwich principle. The assays were performed according to manufacturer's instructions. All reagents were equilibrated to ambient temperature prior to use; standards, dilution of samples, and all buffers were prepared according to the manufacturer's instructions. Briefly, a total volume of 100 µL of distilled water was added to the sample wells and 50 µL of prediluted samples were added to the appropriate wells. Plates were sealed and subsequently incubated with gentle shaking for 3 hours at room temperature. The plates were washed four times in 400 µL of wash buffer using an automated plate washer. A total volume of 100 µL of TMB substrate was added to all the wells; the plates were sealed and incubated in the dark at ambient temperature for 10 min. The reaction was stopped by adding 100 µL of stop solution and the solution gently mixed by swirling the plates. The absorbance was determined by reading the plate in an automated plate reader at absorbance wavelength 450 nm. The data was quality checked by an independent investigator and the data analyzed by plotting concentration values.

6.25 Samples and analytes

For assessment of plasma soluble mediators of neutrophils, limited samples were available. Furthermore, some plasma samples had dilution issues and these had to be excluded from the analyses. Table 6 below, specifies the number of samples (plasma or absolute neutrophil counts) that were available from week 0 up to week 12 on ART by intervention across clinical groups. Due to assay measurement technicalities, measurements for some analytes were not available. The lowest limit of detection was imputed for those values below this limit. For data that was above the upper limit of detection, the upper limit of detection was imputed. Of note, MPO measurements at week 0 were not available for approximately quarter of the patients. The lower limit of detection was imputed in such cases.

***Table 6**. Number of plasma samples and absolute neutrophil count results which were available at week 0, week 2, and at week 12 on ART representing the resolution of inflammatory symptoms.*

Plasma sample available at:	TB-IRIS placebo (n)	TB-IRIS prednisone (n)	TB-non-IRIS placebo (n)	TB-non-IRIS prednisone (n)
Week 0	36	26	34	48
Week 2	30	21	31	45
Absolute neutrophil counts available at:				
Week 0	56	39	64	81
Week 2	56	39	64	81
Week 12	56	39	64	81

6.2.6 Statistical analyses and software.

Cross-sectional and longitudinal data analysis were conducted on unpaired and paired samples respectively, collected from patients with paradoxical TB-IRIS and TB-non-IRIS controls from week 0 up to week 12 on ART. For unpaired cross-sectional analyses, the Mann-Whitney U test was used to compare medians between TB-IRIS patients and TB-non-IRIS controls at week 0 up to week 12 on ART. For longitudinal within-group analyses, the paired Wilcoxon ranked test was used to compare the medians at different time points for paradoxical TB-IRIS cases, and TB-non-IRIS controls separately. A p-value of 0.05 or less was considered as statistically significant. All data visualizations and statistical analyses were performed in the R statistical programming language.

6.3 Results

The clinical characteristics for the patients enrolled in the Pred-ART intervention trial were discussed in chapter 5 (see section 5.4.1). Figure 6 below summarizes the number of available plasma samples by intervention and disease outcome.

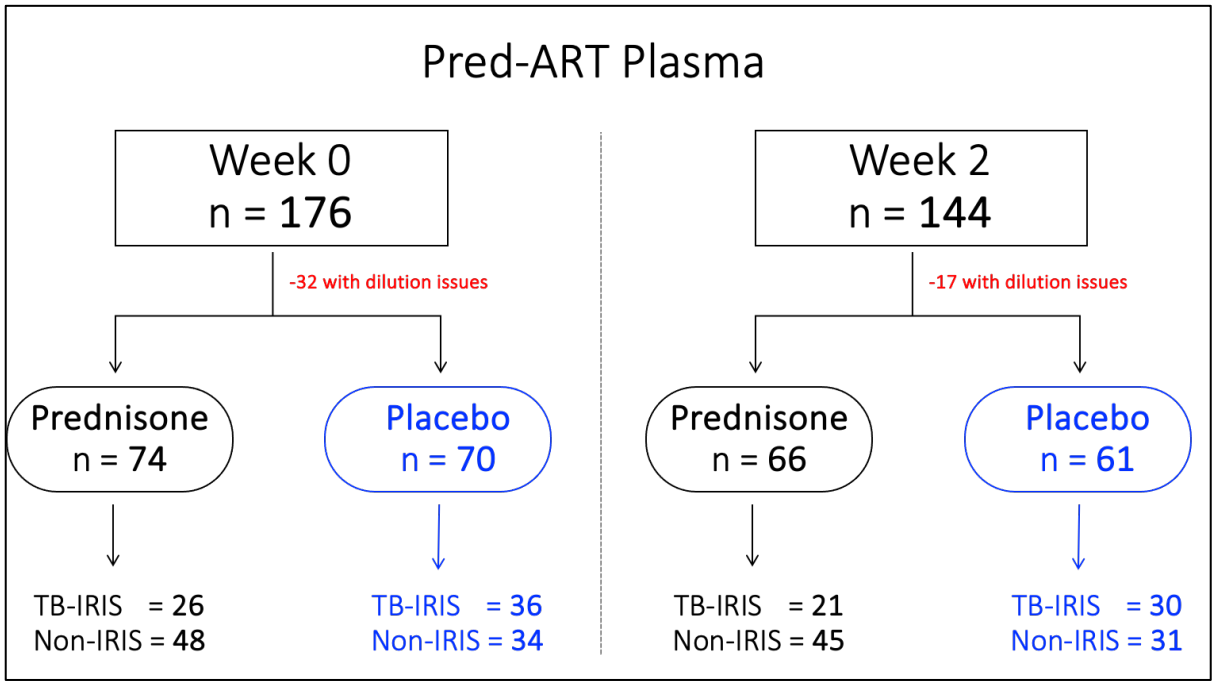

Figure 6. Diagram depicting the number of Pred-ART derived plasma samples that were available for use at week 0 and week 2 on ART. *Limited patient samples were available, showing the number of samples that were available by intervention and by outcome of paradoxical TB-IRIS*

6.3.1 Bulk analysis of absolute neutrophil counts and plasma soluble markers of neutrophils in patients allocated either placebo or prophylactic prednisone prior to the initiation of ART.

Peripheral blood from 240 participants was analyzed for absolute neutrophil counts (ANC) by differential count performed at the National Health Laboratory Services (NHLS) laboratory. The resultant ANC measurements were used to determine whether there was any association between neutrophilia and paradoxical TB-IRIS at different time points including week 0 (prior to ART initiation), week 2 (median duration to TB-IRIS onset) and week 12 (inflammatory symptoms had largely resolved). ANC measurements from those who did not develop paradoxical TB-IRIS were used as controls.

In patients that were allocated either placebo (black filled circles) or prednisone prophylaxis (brown filled circles) at week 0, no significant differences in ANC measurements were observed between participants who later developed paradoxical TB-IRIS (n = 95) and those who did not (TB-non-IRIS controls, n = 145) (**Figure 6.1)**.

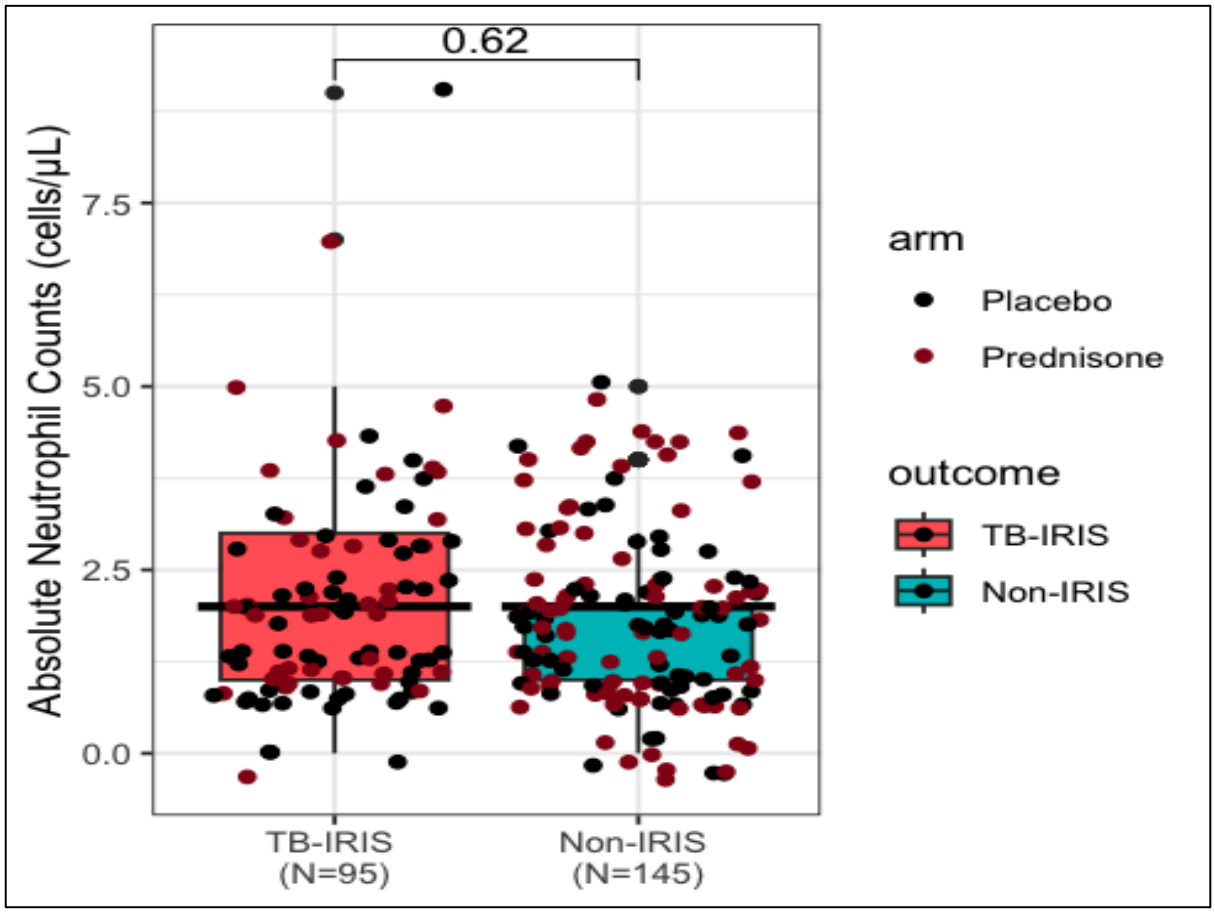

Figure 6.1. Evaluation of neutrophil counts in all patients prior to the initiation of antiretroviral therapy (ART) (week 0). *Evaluation of absolute neutrophil counts (ANC) at week 0 in all patients who later developed paradoxical TB-IRIS (Salmon; n = 95) and TB-non-IRIS controls (Turquoise; n = 145)*

Furthermore, plasma soluble analytes of neutrophils were assessed using a total of 144 plasma samples collected at week 0, from patients that later developed paradoxical TB-IRIS (n = 62) compared to those who did not (n = 82). Measured plasma soluble analytes included azurocidin (Azu1), human neutrophil peptide (HNP)-1-3, myeloperoxidase (MPO) and neutrophil elastase (NE) (**Figure 6.2)**.

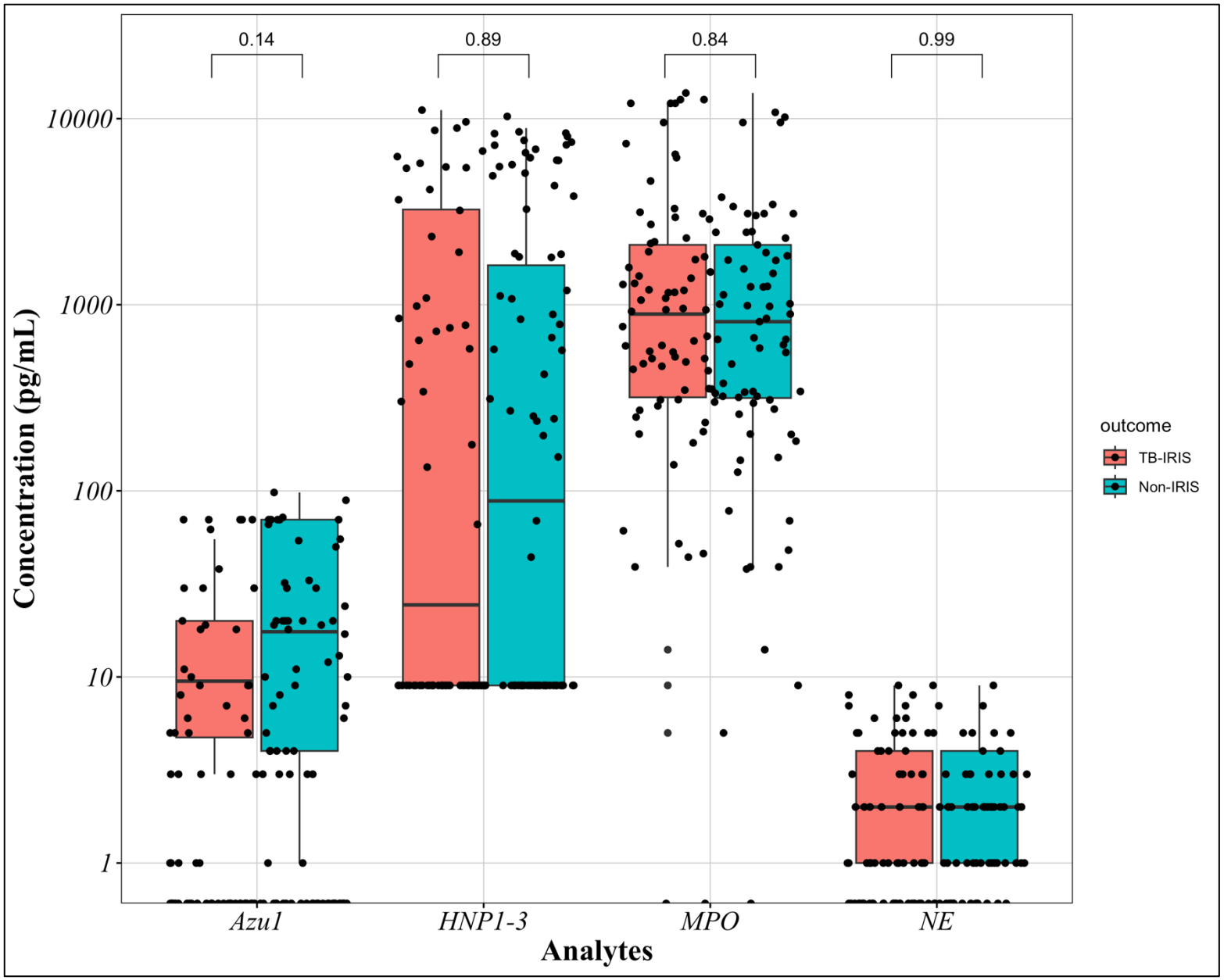
0.14
0.89
0.84
0.99
10000
1000
100
10
1
Concentration (pg/mL)
Azu1
HNP1-3
MPO
NE
Analytes
outcome
TB-IRIS
Non-IRIS

***Figure 6.2**. **Assessing plasma soluble markers of neutrophils in patients prior to the initiation of antiretroviral therapy (ART) (week 0).** Plasma concentrations of azurocidin (Azu1), human neutrophil peptide (HNP)1-3, myeloperoxidase (MPO) and neutrophil elastase in patients who later developed paradoxical TB-IRIS (Salmon, n=62) and TB-non-IRIS controls (Turquoise, n=82) at week 0. The Mann Whitney U-test was used to compare the medians between TB-IRIS patients and TB-non-IRIS controls. A p-value of less than or equal to 0.05 was considered statistically significant.*

There were no significant differences in the median plasma concentrations for Azu1, HNP1-3, MPO and NE in patients who later developed paradoxical TB-IRIS and those who did not (TB-non-IRIS controls) at week 0. (**Figure 6.2)**.

6.3.2 Investigating absolute neutrophil counts in patients allocated placebo and prednisone respectively prior to ART (week 0).

Measurements of absolute neutrophil counts from Pred-ART participants who later developed paradoxical TB-IRIS and those who did not, were stratified by intervention. The association between neutrophilia and paradoxical TB-IRIS was investigated at week 0. Measurements of absolute neutrophil counts in participants who were allocated either placebo or prednisone at week 0, who did not develop paradoxical TB-IRIS at later time points were used as controls. A total of 120 patients were analyzed for ANC at week 0 for each intervention (**Figure 6.3)**.

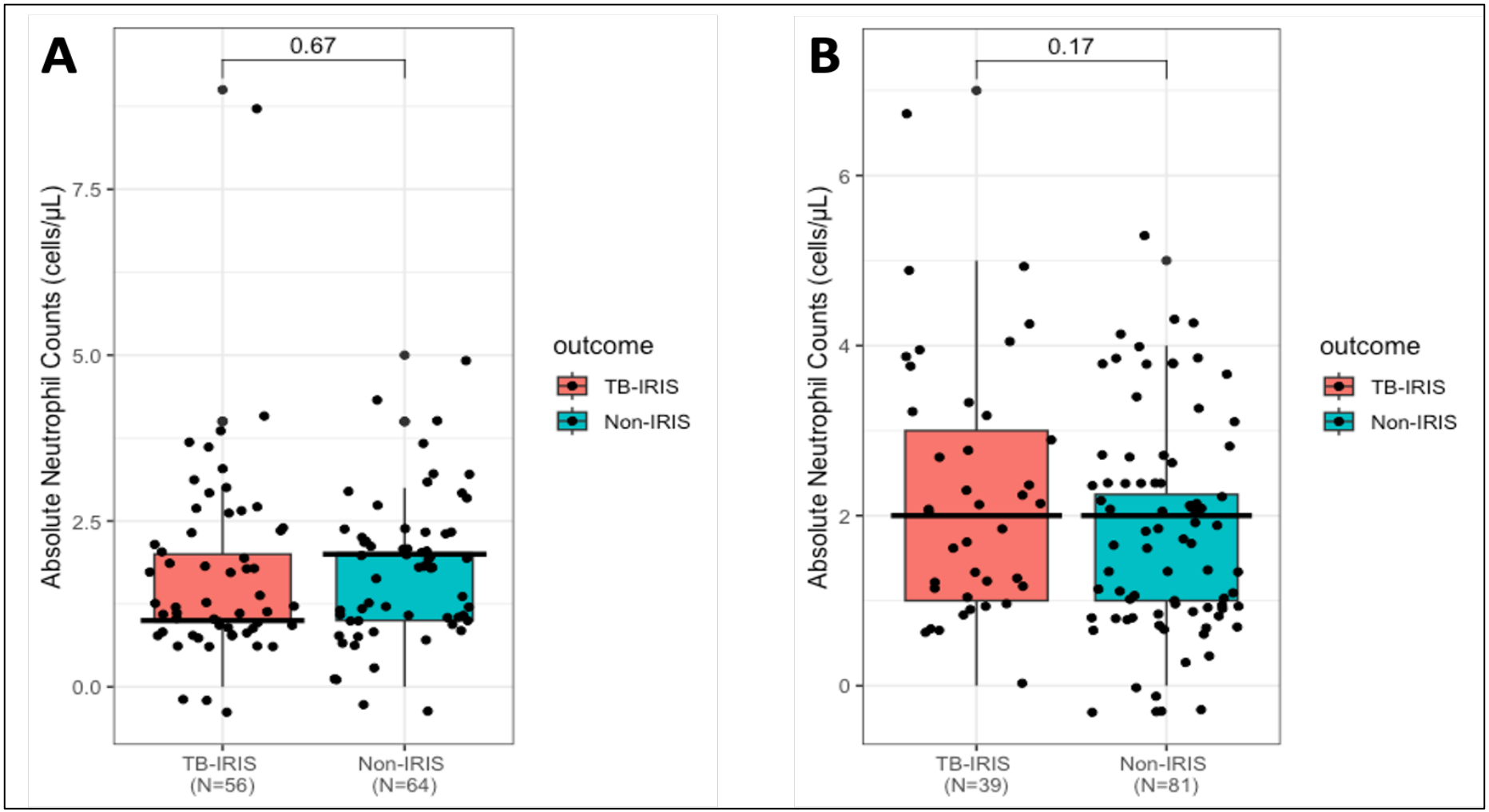

Figure 6.3*. Evaluation of neutrophil counts in patients prior to the initiation of antiretroviral therapy (ART) (week 0).** *Absolute neutrophil counts (ANC) at week 0 in patients allocated placebo* ***(A) *and prednisone* ***(B)*** *respectively who later developed paradoxical TB-IRIS (Salmon; n = 56 and 39) and those who did not (TB-non-IRIS controls ,Turquoise; n = 64 and 81).*

There were no significant differences in the measurements of ANC obtained from participants who were allocated placebo who later developed paradoxical TB-IRIS patients (n = 56) and those who did not (n = 64) **Figure 6.3A)**. Similarly, no significant differences in measurements of ANC were observed in participants that later developed paradoxical TB-IRIS patients (n = 39) and those who did not (n = 81) who were allocated prednisone at week 0 (**Figure 6.3B)**.

Pred-ART plasma samples from participants who were allocated placebo, who later developed paradoxical TB-IRIS (n = 36) were tested using ELISA for the presence of, and significant differences in soluble Azu1, HNP1-3, MPO, and NE at week 0. Plasma samples from participants who did not later develop paradoxical TB-IRIS (n = 34) were used as controls

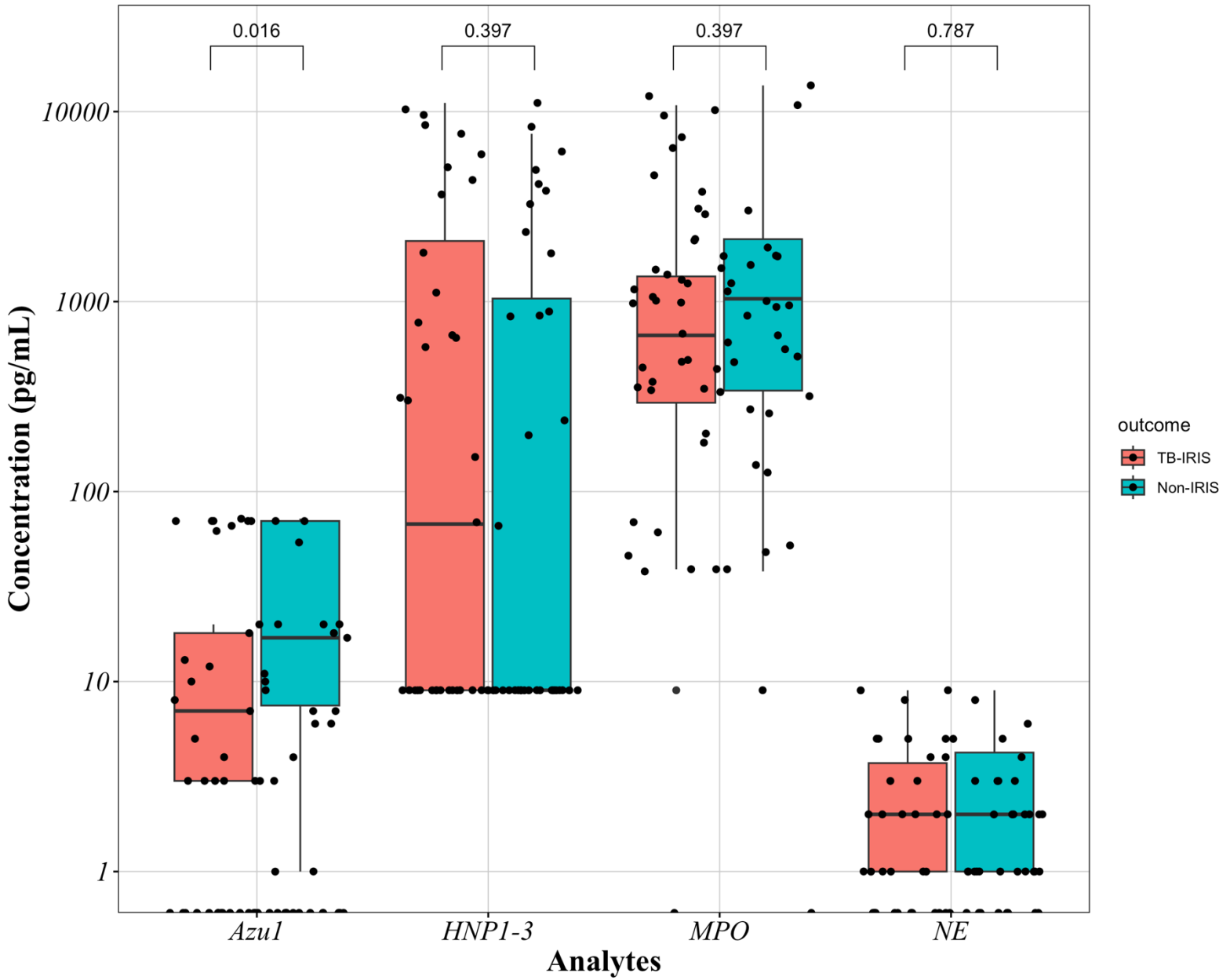
0.016
0.397
0.397
0.787
10000
1000
100
10
1
Concentration (pg/mL)
Azu1
HNP1-3
MPO
NE
Analytes
outcome
TB-IRIS
Non-IRIS

Figure 6.4. Evaluation of plasma soluble markers of neutrophils in patients allocated placebo prior to the initiation of antiretroviral therapy (ART) (week 0). *Plasma concentrations of azurocidin (Azu1), human neutrophil peptide, myeloperoxidase and neutrophil elastase in patients allocated placebo; who later developed paradoxical TB-IRIS (Salmon, n = 30) and in TB-non-IRIS controls (Turquoise, n = 31). The Mann Whitney U-test was used to compare the medians in plasma analytes between the two clinical groups. A p-value of less than or equal to 0.05 was considered statistically significant.*

Plasma levels of azurocidin were significantly lower at week 0 in participants who later developed paradoxical TB-IRIS (median = 3, IQR = 0-7) compared to those who did not (median = 7.5, IQR = 0-65). There were no significant differences in the median plasma concentrations for HNP1-3, MPO and NE in patients who later developed paradoxical TB-IRIS compared to TB-non-IRIS controls at week 0. However, a trend of lower MPO in patients who later developed paradoxical TB-IRIS was apparent compared to TB-non-IRIS controls (**Figure 6.4)**.

Notably, no significant differences were observed in plasma analytes in participants who later developed paradoxical TB-IRIS compared to TB-non-IRIS controls, who were allocated prednisone at week 0. Therefore, these data are not shown.

6.3.3 Cross section analysis of absolute neutrophil counts in all patients at week 2 on ART.

A total of 240 participants were allocated either placebo or prednisone intervention in the Pred-ART intervention trial. Measurements of absolute neutrophil counts (ANC) were available for each participant at week 2 on ART (**Figure 6.5)**. The association between neutrophilia and the onset of paradoxical TB-IRIS was investigated at week 2. Measurements of ANC in participants who were allocated either placebo or prednisone at week 2, who did not develop paradoxical TB-IRIS were used as controls.

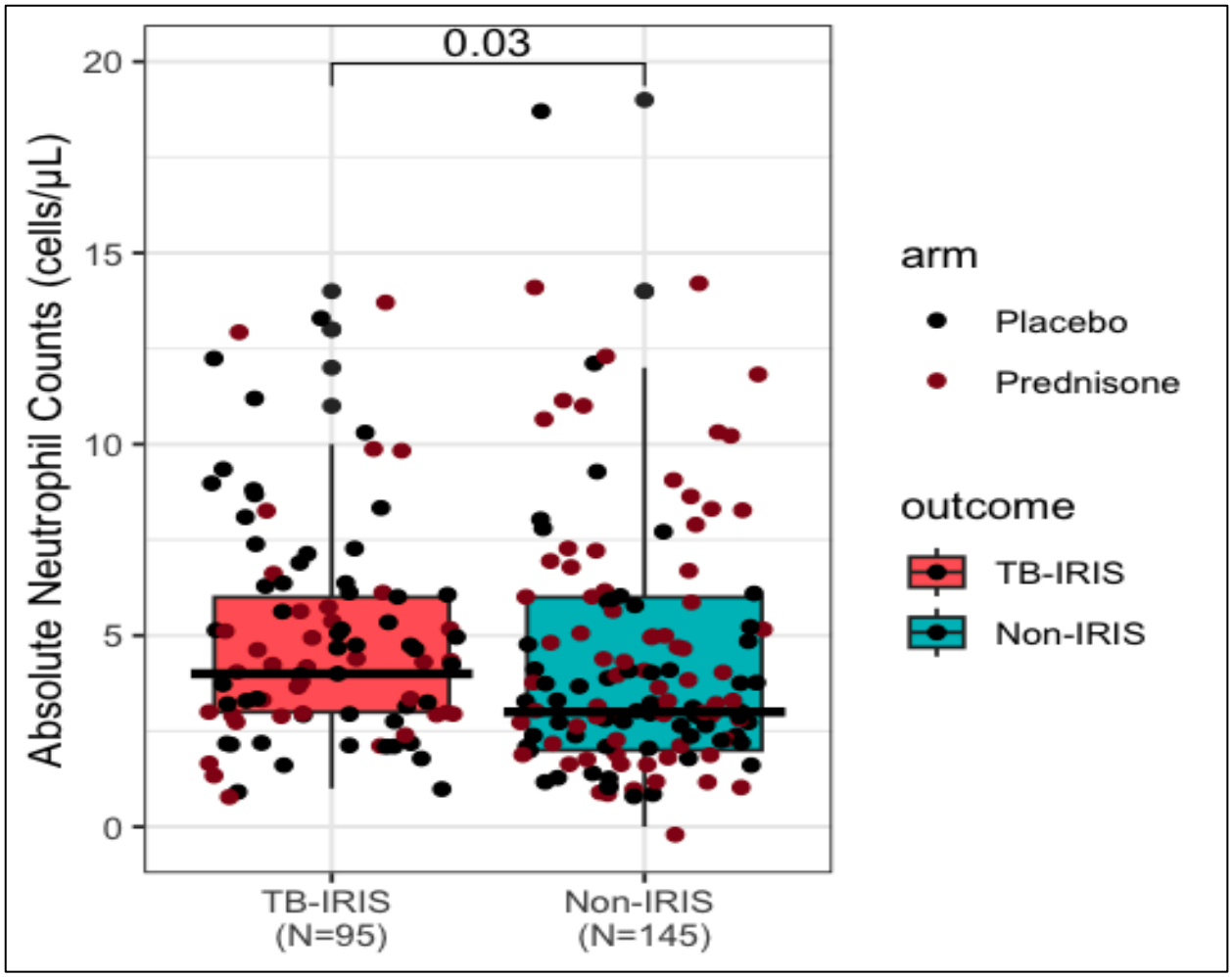

Figure 6.5. Evaluation of absolute neutrophil counts in patients that were allocated either placebo (black shaded circles) or prednisone prophylaxis (brown shaded circles) who developed paradoxical TB-IRIS *(Salmon; n = 95)* ***and those who did not (Non-IRIS,*** *turquoise; n = 145)* ***at week 2 of antiretroviral therapy (ART).***

Bulk measurements of ANC were significantly higher in patients who received either placebo or prophylactic prednisone, who developed paradoxical TB-IRIS (salmon, n = 95), compared to TB-non-IRIS controls (turquoise, n = 145) at week 2 on ART (**Figure** 6.5**)**.

6.3.4 Bulk analysis of plasma soluble markers of neutrophils in patients that received either prophylactic prednisone or placebo at week 2 on ART.

A total of 127 plasma samples were available from patients that received either prophylactic prednisone or placebo at week 2 on ART. The hypothesis that plasma soluble markers of neutrophils are associated with the development of paradoxical TB-IRIS with TB-non-IRIS

participants as controls was investigated (**Figure** 6.6). This analysis included samples from participants that received prednisone prophylaxis (n = 66) or placebo (n = 61).

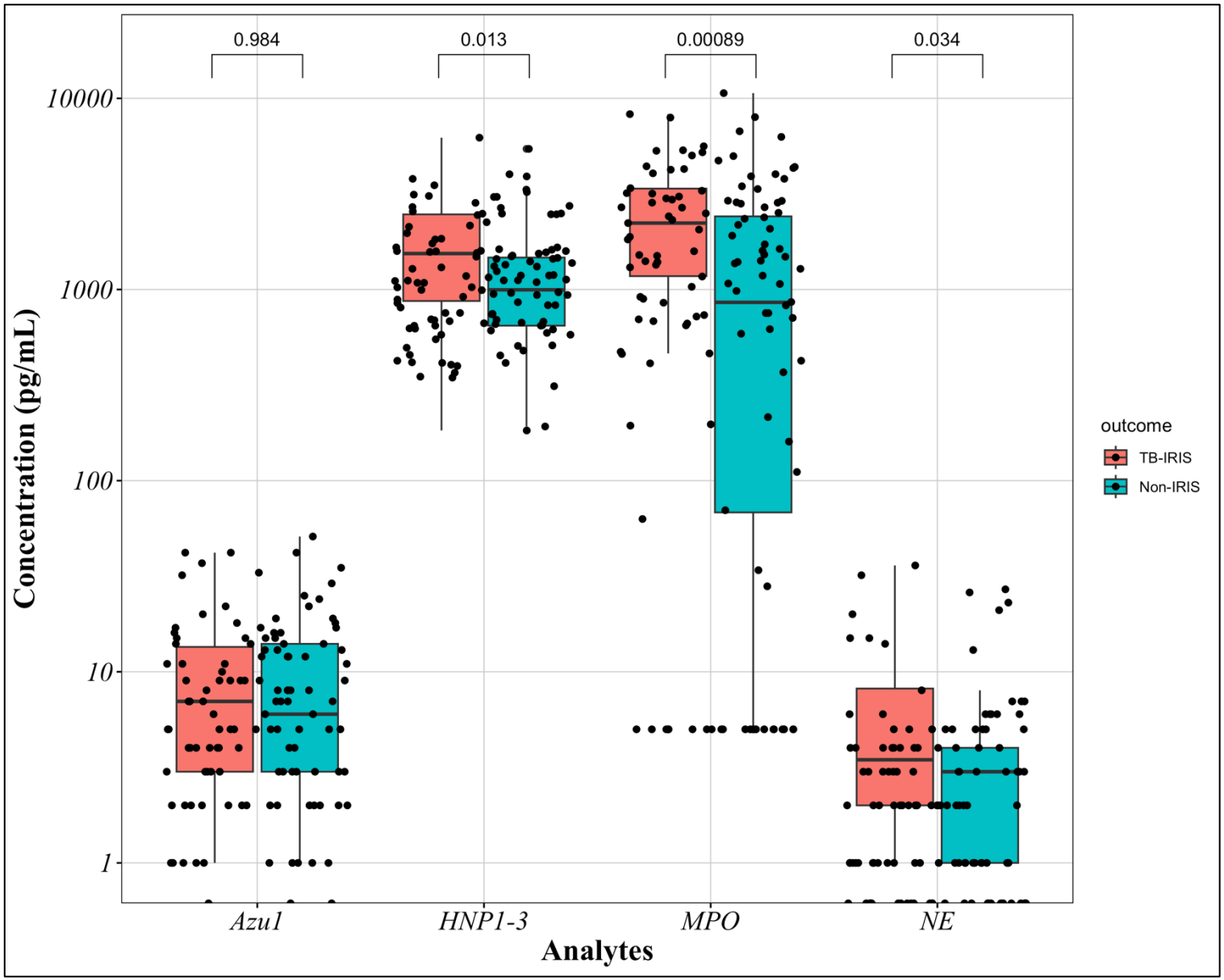
0.984
0.013
0.00089
0.034
10000
1000
100
10
1
Concentration (pg/mL)
Azu1
HNP1-3
MPO
NE
Analytes
outcome
TB-IRIS
Non-IRIS

Figure 6.6. Evaluation of plasma soluble markers of neutrophils in patients that received placebo or prophylactic prednisone at week 2 on antiretroviral therapy (ART)*. Plasma concentrations of azurocidin (Azu1), human neutrophil peptide (HNP)1-3, myeloperoxidase (MPO) and neutrophil elastase (NE) in patients at week 2 on ART; who developed paradoxical TB-IRIS (salmon, n = 51) and in TB-non-IRIS controls (turquoise, n = 76). The Mann Whitney U-test was used to compare the median concentrations of plasma analytes between the two clinical groups. A p-value of less than or equal to 0.05 was considered statistically significant.*

Plasma concentrations of HNP1-3, MPO and NE were significantly higher in patients who developed paradoxical TB-IRIS (HNP1-3: median = 1542, IQR = 872-2472), (MPO: median = 2226, IQR = 1179-3372), and (NE: median = 3, IQR = 1-6) compared to those who did not (HNP1-3: median = 996, IQR = 647-1469), (MPO: median = 856, IQR = 68-2413), (NE: median = 2, IQR = 0-4) (**Figure** 6.6). The median plasma concentrations for Azu1 were comparable in patients who developed paradoxical TB-IRIS and those that did not at week 2 on ART (**Figure** 6.6**)**.

6.3.5 Cross sectional analysis of absolute neutrophil counts in patients allocated placebo and prednisone respectively at week 2 on ART.

The association between neutrophilia and the onset of paradoxical TB-IRIS was evaluated by comparing measurements of ANC for a total of 120 participants that received placebo, a proportion of whom developed paradoxical TB-IRIS (56/120) and those who did not (n = 64) were used as controls.

Measurements of ANC were significantly higher at week 2 on ART (p = 0.0027), in participants that developed paradoxical TB-IRIS (n = 56; median = 5; IQR = 2.7 - 7.1) compared to those who did not (n = 64; median=2.7; IQR = 2 – 4.2) (**Figure** 6.7A**)**.

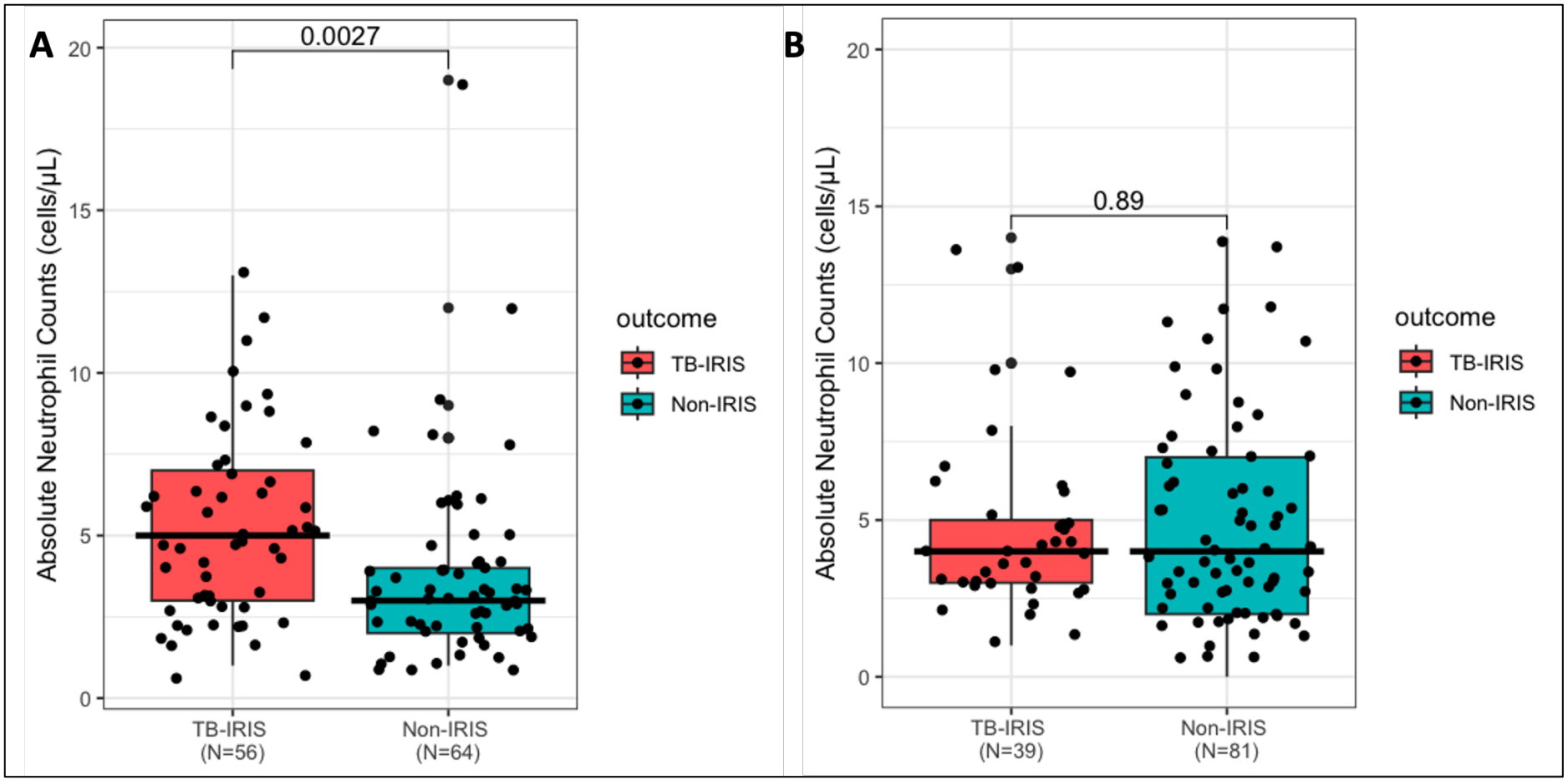

Figure 6.7. Evaluation of neutrophil counts in patients who received placebo and prednisone respectively at week 2 on antiretroviral therapy (ART). *Absolute neutrophil counts (ANC) at week 2 on ART in patients who received either placebo* ***(A)*** *or prednisone* ***(B)*** *respectively who developed paradoxical TB-IRIS (Salmon; n = 56 and 39) and those who did not (TB-non-IRIS controls ,Turquoise; n = 64 and 81). The Mann Whitney U-test was used to compare the median concentrations of plasma analytes between the two clinical groups. A p-value of less than or equal to 0.05 was considered statistically significant.*

However, no significant differences were observed in the ANC measurements of participants that received prednisone who developed paradoxical TB-IRIS patients (n = 39) and those who did not (n = 81) at week 2 on ART (**Figure** 6.7B).

6.3.6 Plasma soluble markers of neutrophils in patients who received placebo at week 2 on ART.

The hypothesis that participants who developed paradoxical TB-IRIS might potentially have increased neutrophil degranulation was tested by analyzing soluble Azu1, HNP1-3, MPO, and NE at week 2 on ART using plasma samples from participants that received placebo (n =61) (**Figure** 6.8**)**. Plasma from participants that received placebo at week 2 on ART but did not develop paradoxical TB-IRIS were used as controls.

The median plasma concentration of HNP1-3 and MPO were significantly higher in samples from patients who developed paradoxical TB-IRIS (n = 30; HNP1-3: median = 1602, IQR = 1015-2974) compared to TB-non-IRIS controls (n = 31; HNP1-3: median = 849, IQR = 647-1395) at week 2 on ART (**Figure** 6.8**)**.

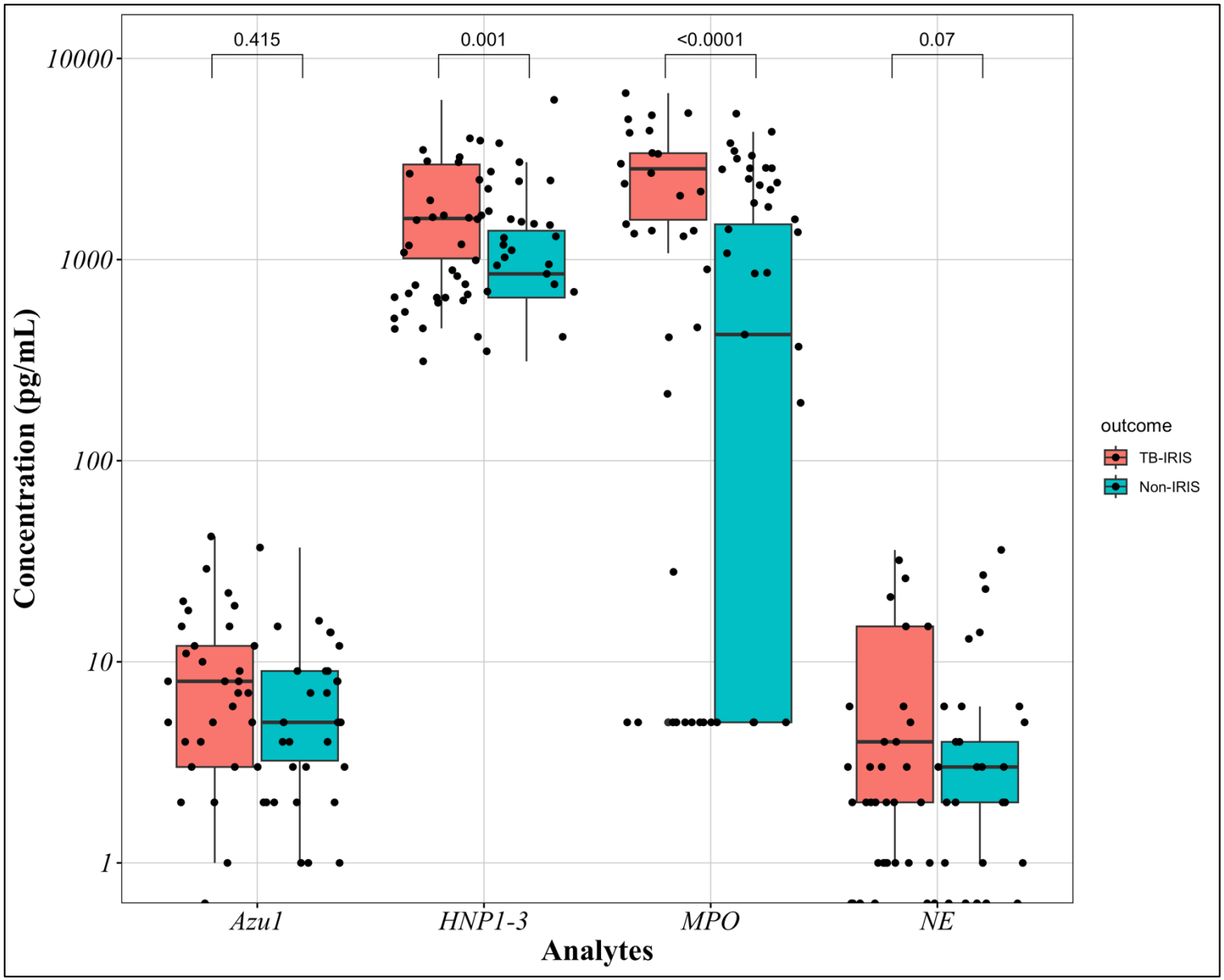
0.415
0.001
<0.0001
0.07
10000
1000
100
10
1
Concentration (pg/mL)
Azu1
HNP1-3
MPO
NE
Analytes
outcome
TB-IRIS
Non-IRIS

***Figure 6.8*. Evaluation of plasma soluble markers of neutrophils in participants that received placebo at week 2 on antiretroviral therapy (ART)**. *Plasma concentrations of azurocidin(Azu1), human neutrophil peptide (HNP)1-3 myeloperoxidase (MPO), and neutrophil elastase(NE) in participants that received placebo at week 2 on ART, who developed paradoxical TB-IRIS (salmon; n = 30) and in TB-non-IRIS controls (turquoise; n = 31). The Mann Whitney U-test was used to compare the median levels of plasma analytes between the two clinical groups. A p-value of less than or equal to 0.05 was considered statistically significant.*

Similarly, the median plasma concentration of MPO was significantly higher in patients who developed paradoxical TB-IRIS (n = 30; MPO: median = 2828, IQR = 1583-3381) compared to TB-non-IRIS controls (n = 31; MPO: median = 424, IQR = 5-1500) at week 2 on ART (**Figure** 6.8**).**

6.3.7 Plasma soluble markers of neutrophils in participants who received prednisone at week 2 on ART.

The effect of prednisone prophylaxis at week 2 on ART was evaluated on soluble plasma analytes of neutrophils including Azu1, HNP1-3, MPO and NE. Median concentration levels of the analytes in questions were compared in plasma samples from participants that developed paradoxical TB-IRIS (n = 21) and those that did not (n = 45) (**Figure** 6.9).

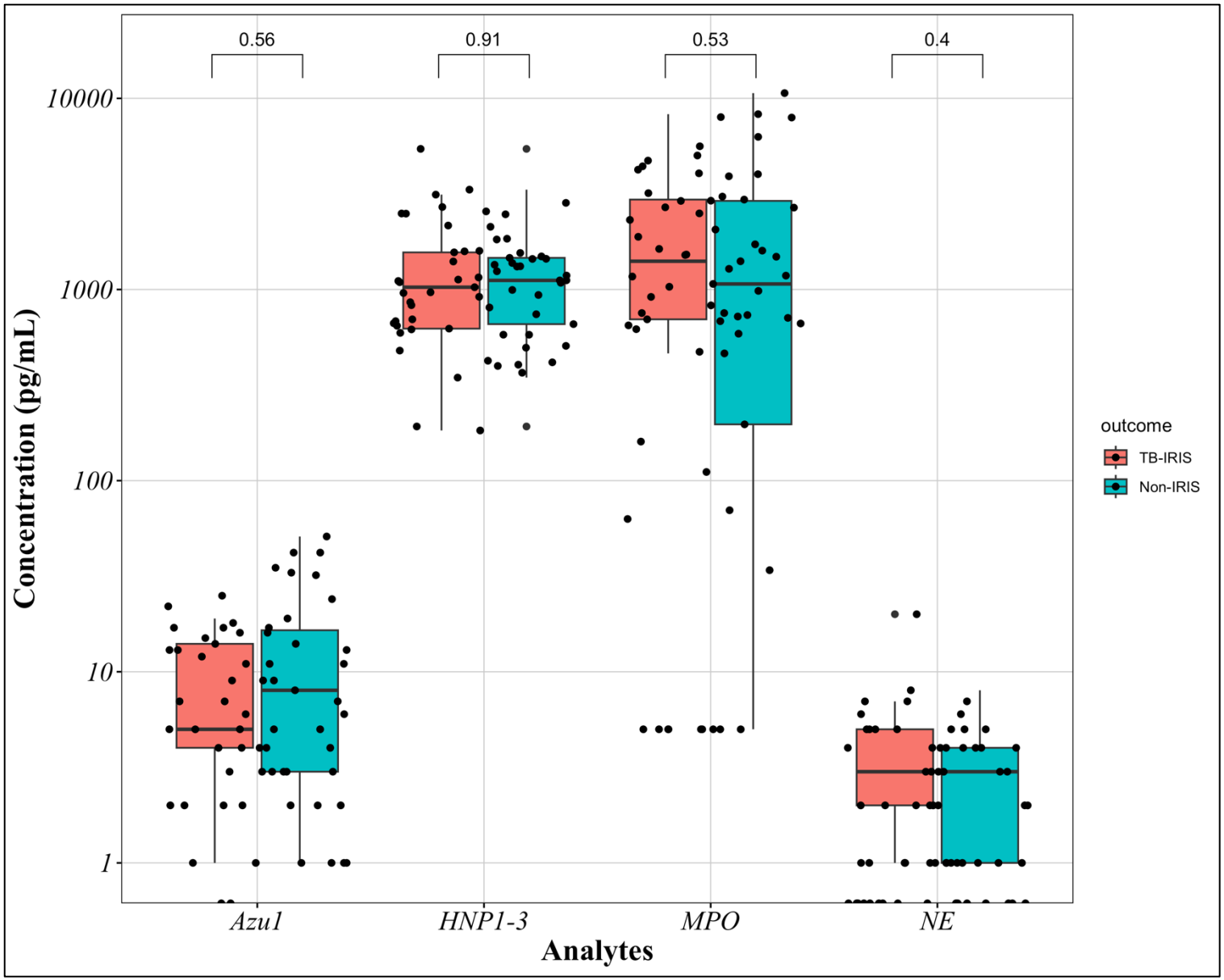
0.56
0.91
0.53
0.4
10000
1000
100
10
1
Concentration (pg/mL)
Azu1
HNP1-3
MPO
NE
Analytes
outcome
TB-IRIS
Non-IRIS

Figure 6.9*. *Evaluation of plasma soluble markers of neutrophils in participants that received prednisone at week 2 on antiretroviral therapy (ART). *Plasma concentrations of azurocidin (Azu1), human neutrophil peptide (HNP)1-3 myeloperoxidase (MPO), and neutrophil elastase(NE) in participants that received prednisone at week 2 on ART who developed paradoxical TB-IRIS (salmon, n = 21) and in TB-non-IRIS controls (turquoise, n = 45). The Mann Whitney U-test was used to compare median concentration levels between the two clinical groups. A p-value of less than or equal to 0.05 was considered statistically significant.*

Plasma levels of Azu1, HNP1-3, MPO, and NE were similar in plasma samples from participants who developed paradoxical TB-IRIS (n =21) compared to TB-non-IRIS controls (n = 45) who received concomitant prophylactic prednisone and ART at week 2 (**Figure 6.9)**. These data are consistent with the hypothesis that prednisone inhibits neutrophil degranulation and hence comparable levels of secreted plasma mediators of neutrophil degranulation were found in participants that developed paradoxical TB-IRIS compared to TB-non-IRIS controls.

6.3.8 Cross sectional and longitudinal comparison of absolute neutrophil counts in participants that received placebo who developed paradoxical TB-IRIS and those who did not at week 12 on ART.

In the Pred-ART intervention trial, week 12 represented a time point on ART at which most of the TB-IRIS manifestations had resolved despite the discontinuation of prednisone for treatment or prophylaxis. Measurements of ANC for a total of 120 participants were available for cross-section comparison between the two clinical groups at week 12 on ART.

There was no statistically significant difference in the ANC between participants who developed paradoxical TB-IRIS (n = 56) and TB-non-IRIS controls (n = 64) at week 12 on ART (**Figure 6.10A)**. Notably, some participants who were allotted placebo at week 0 who developed paradoxical TB-IRIS, received prednisone to treat inflammatory symptoms, but most had completed the treatment course before week 12.

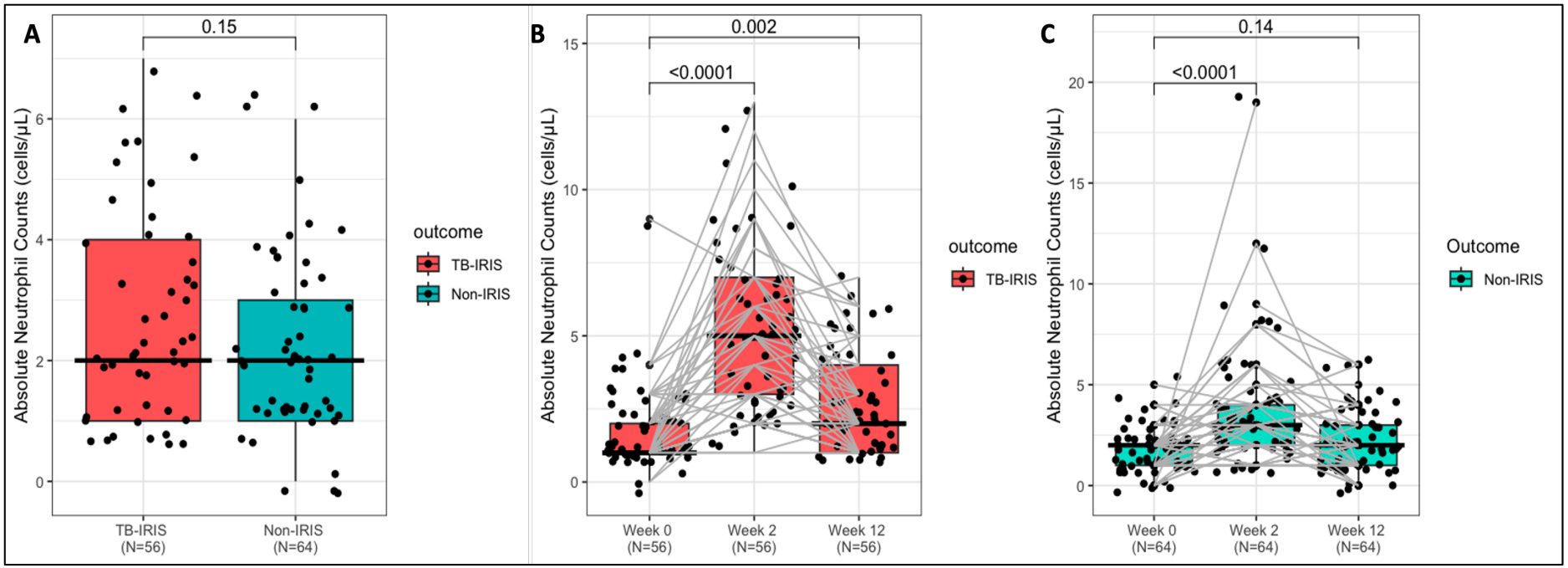

Figure 6.10. Longitudinal evaluation of absolute neutrophil counts in placebo allocated patient samples from week 0 up to week 12 on ART. *A. Cross-sectional analysis of absolute neutrophil counts (ANC) in placebo allocated participants who developed paradoxical TB-IRIS (salmon; n = 56) and TB-non-IRIS controls (turquoise; n = 64) at week 12 on ART.* ***B,C.*** *Longitudinal perturbations in absolute neutrophil counts in placebo allocated participants that developed paradoxical TB-IRIS and TB-non-IRIS controls respectively.*

Furthermore, longitudinal perturbation in ANC were evaluated in participants that were allocated placebo, some who developed paradoxical TB-IRIS (n = 56) and others who did not (TB-non-IRIS, n = 64). ANC were significantly higher at week 2 on ART in participants that developed paradoxical TB-IRIS and remained significantly high at week 12 on ART, compared to week 0 (**Figure 6.10B)**. Similarly, ANC were significantly high at week 2 on ART in TB-non-IRIS controls, but were reduced to levels comparable to week 0 at week 12 on ART. (**Figure 6.10C)**.

6.3.9. Cross sectional and longitudinal comparison of absolute neutrophil counts in participants that received prednisone, who developed paradoxical TB-IRIS and those who did not at week 12 on ART.

Cross-sectional comparison of measurements of ANC was carried out in a total of 120 participants that were allocated a 4-week course of prophylactic prednisone, some whom developed paradoxical TB-IRIS and others who did not.

There was no statistically significant difference in the ANC between patients who developed paradoxical TB-IRIS (salmon color, n = 39) and TB-non-IRIS controls (turquoise, n = 81) at week 12 on ART (**Figure** 6.11A**)**.

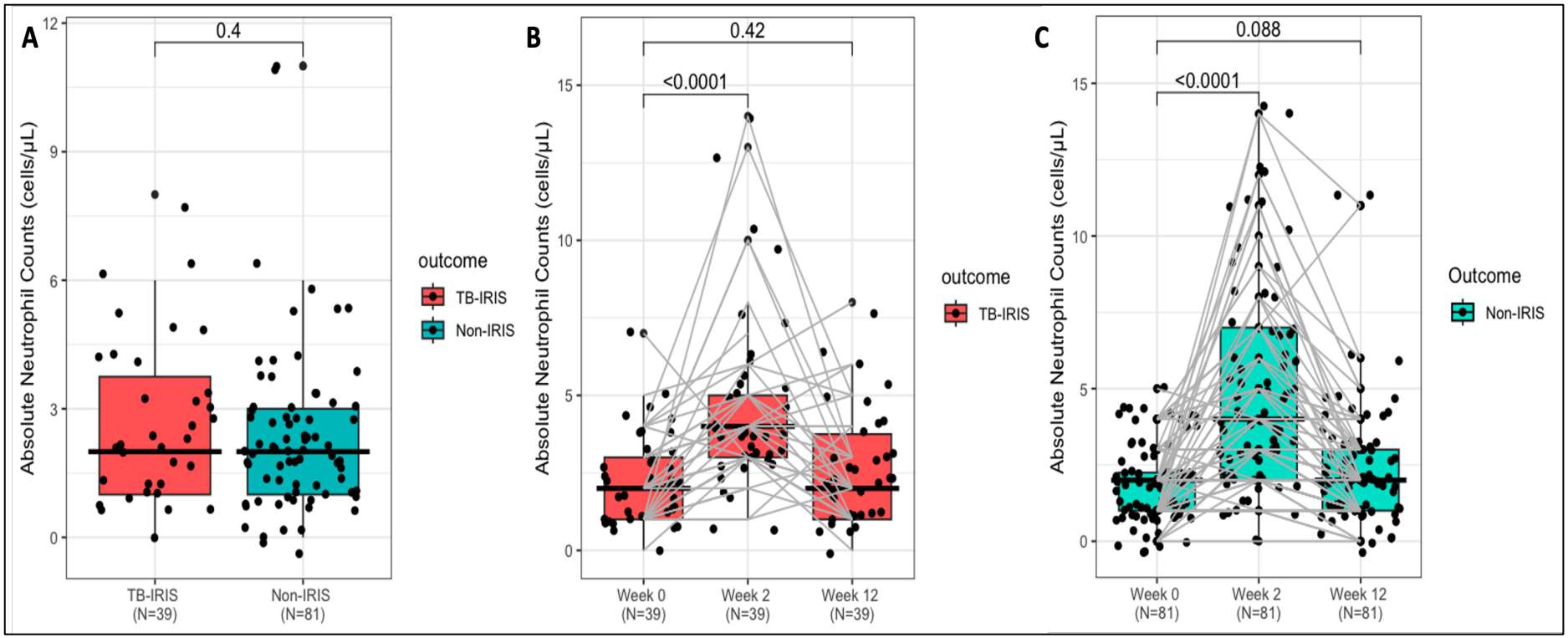

Figure 6.11. Longitudinal evaluation of absolute neutrophil counts in prednisone allocated patient samples from week 0 up to week 12 on ART. *A. Cross-sectional analysis of absolute neutrophil counts (ANC) in prednisone allocated TB-IRIS patients (salmon; n = 39) and TB-non-IRIS controls (turquoise; n = 81) at week 12 on ART.* ***B,C.*** *Longitudinal perturbations in absolute neutrophil counts in TB-IRIS patients and TB-non-IRIS controls respectively.*

Furthermore, longitudinal perturbations in ANC were determined for the two clinical groups respectively. ANC were significantly higher at week 2 longitudinally on ART in TB-IRIS patients who were allocated prednisone, however, ANC were reduced to levels comparable to baseline at week 12 on ART (**Figure 6.11B)**. A similar trend was observed for TB-non-IRIS control samples (**Figure 6.11C**).

6.3.10 Bulk absolute neutrophil counts at the median time of paradoxical TB-IRIS onset (week 2 on ART) in patients who were allocated placebo relative to prednisone.

To evaluate whether prednisone significantly increased ANC over and above the effect of TB-IRIS in this patient population, ANC measurements were evaluated at the median time of paradoxical TB-IRIS onset in patients who either received placebo or prednisone intervention.

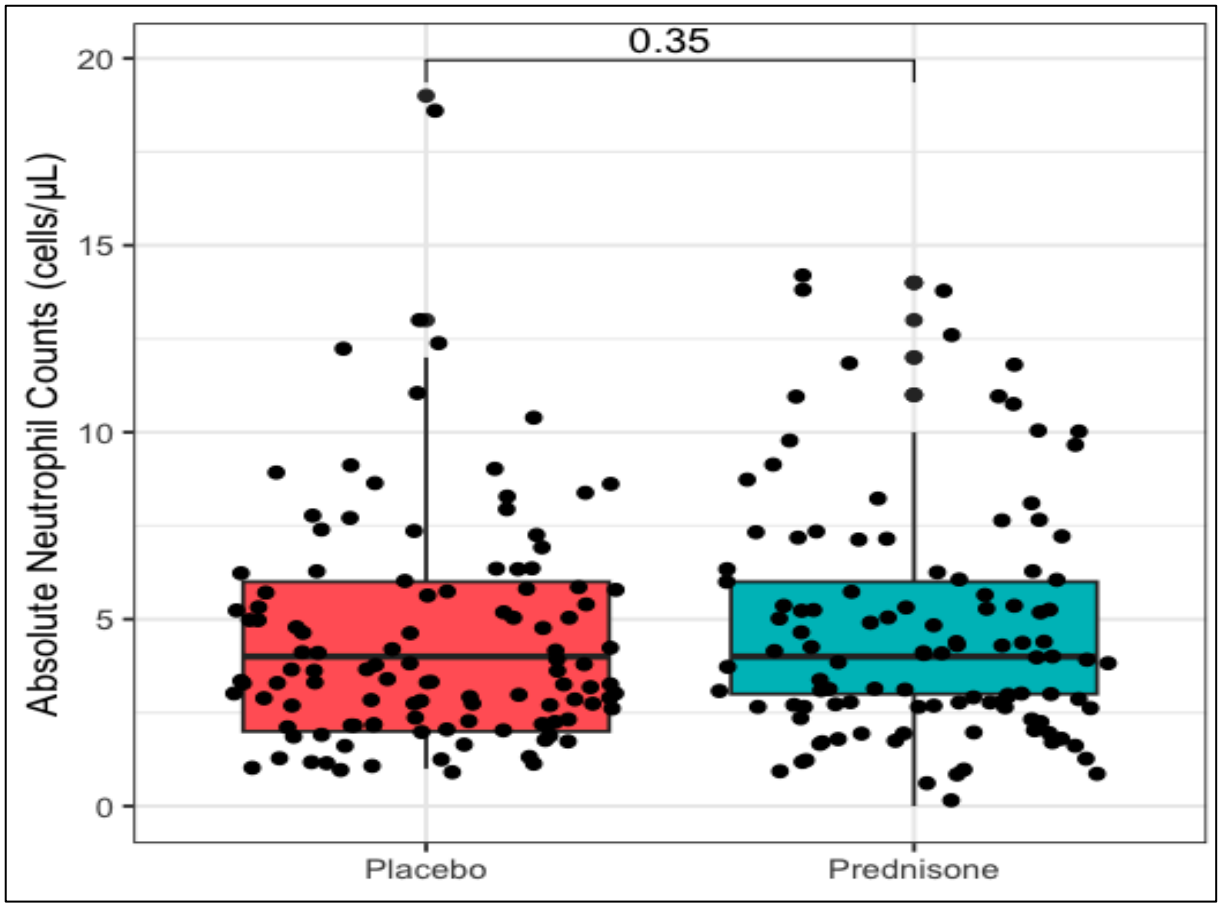

Figure 6.12. Absolute neutrophil counts (ANC) of patients that were allocated either placebo (salmon, n = 120) or prednisone (turquoise, n = 120) intervention at week 2 on ART*. The*

Mann-Whitney U-test was used to compare differences in medians of ANC. A p-value of 0.05 or less was considered statistically significant.

No significant differences were identified in the comparison of ANC of patients who were allocated placebo relative to prednisone at week 2 on ART (**Figure 6.12**).

6.3.11 Investigating the correlation between absolute neutrophil counts and plasma soluble analytes in TB-IRIS patients allocated placebo at week 2 on ART.

Finally, Pearson correlation analysis was conducted to evaluate the relationship between absolute neutrophil counts and the plasma soluble markers (HNP1-3, NE, Azu1 and MPO) at week 2 on ART in a total of 31 placebo allocated patients with paradoxical TB-IRIS (**Figure 6.13)**.

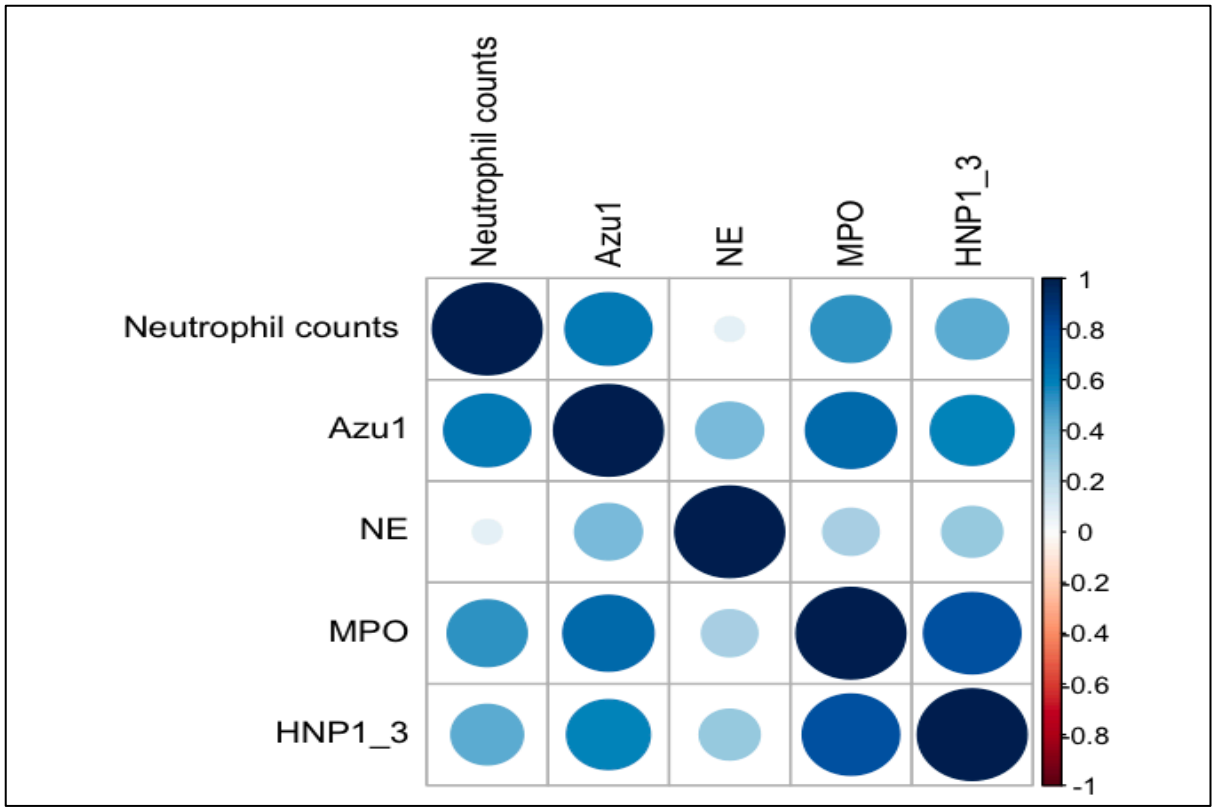

Figure 6.13. Investigating the correlation between absolute neutrophil counts and various plasma soluble analytes using the Pearson correlation. *Darker shade of blue indicates significant positive correlation whereas, darker hue of red reflect the opposite. The size of the shaded circle indicates a stronger association between the variables. Human neutrophil peptide 1-3 = HNP1-3, myeloperoxidase = MPO, azurocidin 1 = Azu1,and neutrophil elastase = NE.*

The scale on the right-hand side of the plot represents the Pearson correlation coefficient or R-value. Darker shades of blue indicate a strong correlation between the variables. The size of the circle coincides with statistical significance. Bigger circles correspond to smaller p-values and therefore indicate greater statistical significance. HNP1-3, MPO, and Azu1 were significantly correlated with absolute neutrophil counts in patients who developed paradoxical TB-IRIS.

6.4 Discussion

The findings from the RNA sequencing study (Chapter 5) indicated that the upregulation of genes involved in neutrophil degranulation preceded the onset of paradoxical TB-IRIS and may have an important role in its pathogenesis. Neutrophil counts in peripheral blood were analysed to evaluate the hypothesis that their absolute counts might be higher prior to the initiation of ART, as well as at the median onset of paradoxical TB-IRIS, in cases compared to controls. A mechanism for the latter could be that higher *Mycobacterium tuberculosis* antigen load at week 0, which is a risk factor for TB-IRIS development, might result in neutrophil counts being higher in cases compared to controls. Another related hypothesis was that there would be higher degranulation of neutrophil-derived primary granules in cases compared to controls at week 0 and week 2. Contents derived from primary granules of neutrophils including azurocidin, human neutrophil peptide, myeloperoxidase and neutrophil elastase were measured in plasma samples from cases and controls at week 0 and 2.

Contrary to one of the hypotheses, there was no significant difference in the absolute neutrophil counts between patients who later developed paradoxical TB-IRIS compared to those who did not at week 0. However, plasma levels of azurocidin at week 0 were significantly lower in patients who later developed paradoxical TB-IRIS compared to those who did not; including specifically in patients who were allocated placebo who later developed paradoxical TB-IRIS compared to those who did not. Azurocidin is a heparin binding protein that has an antimicrobial effect. Its role in innate immunity has been characterized as an alarmin that facilitates cell signaling. It is a chemoattractant and an inducer of monocytes and macrophages for enhanced phagocytosis and cytokine secretion, thereby enabling efficient bacterial

clearance [514]. Significantly lower plasma levels of azurocidin in patients who later developed paradoxical TB-IRIS may reflect greater immune dysfunction prior to the initiation of ART in these patients resulting in sub-optimal immune responses and impaired killing. Of all the constituents of the primary granules, azurocidin is unique in that it is the only protein stored in two different compartments and it exhibits unique kinetics. Azurocidin is released at early stages during neutrophil extravasation as well as at later stages when the neutrophil has reached the site of infection or inflammation [515]. This may allow azurocidin the spacio-temporal opportunity of early cross talk with cells in the bloodstream, the extravascular environment as well as the endothelial lining, thereby modulating their functionality. Lower levels of azurocidin may mean that this signalling is impaired in patients who later develop paradoxical TB-IRIS.

Notably, there was a trend towards lower MPO in patients who were allocated placebo who later developed paradoxical TB-IRIS compared to those who did not at week 0. This was not statistically significant. MPO comprises 5% dry weight in neutrophil derived primary granules indicating its abundance in these granules [516]. Additionally, it is present in smaller quantities in monocytes compared to neutrophils and it is lost during the monocyte transition to macrophages. It is released into the extracellular matrix during apoptosis, degranulation, NETosis and necrosis [517]. The ubiquity of MPO in other cell types makes it challenging to definitively evaluate its relation to neutrophil function in the context of paradoxical TB-IRIS at baseline.

The median concentrations of HNP1-3, MPO and NE were significantly higher at week 2 on ART in patients allocated placebo who developed paradoxical TB-IRIS compared to those who

did not. There appears to be a spatial target for most of the constituents of the primary granule and understanding this could help identify which are involved in the pathogenesis of paradoxical TB-IRIS. For instance, 90% of azurocidin is released at the site of infection while the remainder is released early during transmigration and later during the immune response [515]. HNP1-3 also known as defensins are antimicrobial peptides stored abundantly in the primary granules of neutrophils. HNPs lack enzymatic activity and depend on the induction of reactive oxygen species to eliminate pathogens. For instance, HNP can induce endothelial dysfunction by upregulating endothelial production of oxygen radicals [518]. They are prominently released into the phagolysosome, but can be released into the extracellular space in small quantities [360]. Additionally, HNP can stimulate eukaryotic cells, attract immune cells and have the capacity to be toxic to healthy cells [519]. Furthermore, MPO and NE constitute a substantial proportion of the contents of primary granules and are released into the extracellular space where they potentially cause severe cellular and tissue damage leading to distinct inflammatory pathologies [517, 520]. These attributes suggest that HNP1-3, MPO and NE play a role in the pathogenesis of various inflammatory diseases. Higher neutrophil counts, plasma soluble HNP1-3, NE, and MPO in patients who developed paradoxical TB-IRIS compared to TB-non-IRIS controls at week 2 on ART is suggestive of a role for neutrophils and their mediators in the immunopathogenesis of paradoxical TB-IRIS. A role for neutrophils in TB-IRIS has previously been suggested based on the findings of other studies [15, 16, 239, 241]. Marais and colleagues reported significant differences in the secretion of proinflammatory cytokines, chemokines and matrix metalloproteinases (soluble mediators secreted by neutrophils) at baseline as well as at the time of TBM-IRIS onset, in the

cerebrospinal fluid (CSF) compartment of patients who developed TB meningitis-IRIS compared to those who did not (TBM-non-IRIS controls) [241].

The increase in neutrophil counts may be accounted for by the degranulation of neutrophils at sites of inflammation which involve the release of biotoxic mediators that lead to the recruitment of more neutrophils [504]. Alternatively, higher *Mycobacterium tuberculosis* antigen load is a major risk factor and predictor of paradoxical TB-IRIS and may lead to the recruitment of more neutrophils and their degranulation [521, 522]. Furthermore, it is plausible that neutrophil death by NETosis and/or oxidative burst responses leads to secondary neutrophilia particularly in the context of high antigen load or uncleared bacterial niches during ART mediated immune recovery [379, 410, 523]. Lastly, in the acute stages of disease such as TB, the lifespan of neutrophils in blood is increased at least 2-fold [524]. Their improper accumulation during acute disease may lead to the release of chemotactic factors that mediate the egress of mature neutrophils from the mitotic pool in the bone marrow. Such instances likely account for the detrimental role of neutrophils that has been documented in both acute and chronic inflammatory diseases including Covid-19 [525]. Finally, neutrophils have an important regulatory role in the resolution of inflammation [526]. Neutrophilia and increased degranulation in this study are suggestive of heightened activation and/or impaired regulatory mechanisms of neutrophils in patients who develop paradoxical TB-IRIS.

In patients allocated to prednisone at week 2 on ART concentrations of Azu1 was lower in those who developed paradoxical TB-IRIS, but unlike those on placebo there were no differences in neutrophil count, HNP1-3, MPO and NE between paradoxical TB-IRIS cases and TB-non-IRIS controls. In the trial, prednisone reduced the incidence and severity of

paradoxical TB-IRIS and is plausible that in part this was due to prednisone modulating the effector functions and degranulation of neutrophils [527, 528]. No significant differences in ANC were observed in bulk analysis of patients that were allocated placebo compared to those who were allocated prednisone at the median time of paradoxical TB-IRIS symptoms manifestations. This could be due to the relatively low dose that was allocated patients that were enrolled in the Pred-ART trial.

6.5 Study limitations

Soluble neutrophil responses were measured in plasma derived from whole blood while inflammation associated paradoxical TB-IRIS is often localized in tissue and responses measured in blood may only partially reflect disease pathogenesis. It would have been beneficial to have samples at earlier timepoints on ART than 2 weeks to assess whether neutrophil responses associated with TB-IRIS preceded the onset of symptoms which would strengthen the case for their role in pathogenesis.

6.6 Conclusions

This study validated the RNA sequencing gene expression findings by evaluating absolute neutrophil counts and plasma soluble markers of neutrophils at week 0 prior to the initiation of ART, and at week 2 on ART. Absolute neutrophil counts peaked at week 2 on ART in TB-IRIS patients and TB-non-IRIS controls respectively and declined to levels comparable to baseline at week 12 in patients who did not develop paradoxical TB-IRIS. In patients receiving placebo,

neutrophil counts were significantly higher in paradoxical TB-IRIS cases than controls at week 2 on ART. In these patients, there was evidence of greater neutrophil degranulation in TB-IRIS cases than TB-non-IRIS controls at week 2 on ART, the time which coincides with the median time of TB-IRIS onset. These differences at week 2 were not seen in patients receiving prednisone, suggesting that prednisone might favorably modulate neutrophil responses in the context of TB-IRIS. There were few differences at baseline, prior to the initiation of ART. These findings together with those from the RNA sequencing study support the hypothesis that neutrophils and their degranulation products, in the context of early immune reconstitution on ART, contribute to the pathogenesis of paradoxical TB-IRIS.

Chapter 7 outline: Investigating the anti-inflammatory capacity of inflammasome-related targets in an *ex vivo* cell culture model using samples from patients with paradoxical TB-IRIS at week 2 on ART.

This chapter details the investigation of the anti-inflammatory capacity of two candidate drugs (anakinra and parthenolide) that target the inflammasome or its downstream effectors, compared to corticosteroid (prednisone) that is currently used in clinical practice to manage severe symptoms of paradoxical TB-IRIS. The preface of the chapter provides background on the role of the inflammasome in inflammation, and the interleukin-1 family of cytokines and their receptors which are potent modulators of inflammation. Subsequent sections detail the objectives of this sub-study prior to outlining the methods used for investigation. The methods involve *ex vivo* cell culture, stimulation, and concomitant treatment with candidate drugs to evaluate their capacity in reducing known mediators of inflammation in paradoxical TB-IRIS. The results section outlines several optimizations performed on peripheral blood mononuclear cells (PBMC) from healthy donors before piloting the cell culture system in PBMC from patients enrolled in the TB-ART observational study. The final section evaluates the cell culture model in PBMC collected at week 2 on ART from patients in the placebo arm enrolled in the Pred-ART intervention trial. Finally, the findings and the limitations of the study are discussed.

7. Background

Approximately 95% of living organisms require innate immune mechanisms for survival [529]. Innate immunity plays a pivotal role in initiating inflammation, a host defence mechanism whose dysregulation may cause tissue damage [530, 531]. Attempts to elucidate the mechanisms behind the pathogenesis of paradoxical TB-IRIS have implicated the dysregulation of innate immune signaling and responses [25, 30-32]. The prevailing paradigm of paradoxical TB-IRIS pathogenesis involves enhanced innate immune responses following partial reconstitution of the CD4 T cell compartment due to ART mediated inhibition of HIV replication [177, 532].

Previous transcriptomic data in our laboratory has identified the enrichment of innate immune cell signaling processes (i.e toll like receptor (TLR) and IL-1 signaling) in participants who developed paradoxical TB-IRIS compared to those who did not [25]. These innate pathways are associated with the elevated secretion of pro-inflammatory mediators as well as the upregulation of caspase activation and recruitment domain (CARD), a component of inflammasomes [25]. The involvement of the inflammasome in the pathogenesis of paradoxical TB-IRIS was also shown by Tan and co-workers, who reported on the aberrant activation of inflammasomes, which may arise from the lysis of infected cells in people with TB-IRIS, culminating in the release of Mtb antigens and endogenous danger associated molecular patterns (DAMP) in the surrounding milieu. Mtb antigens and DAMP activate soluble pattern recognition receptors (PRR) resulting in a vicious cycle of immune activation and cytokine production [30].

The mechanisms underpinning inflammasome-mediated pathology in other diseases are well described [533-535]. PRRs are receptors of the innate immune system and are responsible for pathogen surveillance as well as cellular health [536, 537]. Effective innate immune responses rely on the recognition of conserved pathogen-associated molecular patterns (PAMP) and DAMP derived from pathogenic microbes and endogenous stress respectively [402, 538]. PRR may occur as soluble molecules capable of detecting and binding intracellular pathogens and/or as surface receptors on immune cells. PRRs directly recognize conserved molecular structures on the surface of damaged senescent cells, apoptotic host cells as well as pathogens [401, 402]. PRR can be classified into 5 categories based on their protein domain homology. These include TLR, nucleotide oligomerization domain (NOD) like receptors (NLR), retinoic acid-inducible gene (RIG)-1 like receptors (RLRs), C-type lectin receptors (CLR) and absent in melanoma (AIM)-2 like receptors (ALR) [537]. Different classes of PRR either directly recognize pathogens and/or participate in intracellular signalling to initiate a cellular response [537].

The inflammasome is an intracellular protein complex involved in cytosolic immune surveillance, modulation of inflammatory effector responses, and inflammatory cell death through the regulation of caspase-1 activation [423]. It is ubiquitous in mammals and is assembled upon the detection of PAMP and/or DAMP [535, 539]. The NLRP3 is a member of the NLR family of PRR and is the best characterized inflammasome [423]. Two signals are required for the activation of the NLRP3 inflammasome in response to Mtb infection. First, the priming signal, typically through stimulation of transmembrane TLR by PAMP, followed by

signal relay to the C-terminal leucine rich repeats (LRR) domain of the scaffold NLRP3 protein. The signal induces increased expression of the NLRP3 scaffold protein, and other IL-1 family of cytokines via the translocation of the nuclear factor kappa light chain enhancer of activated B cells (NF-κβ) to the nucleus. The second signal is an activating signal, typically an endogenous/host-derived DAMP (i.e leaking of ATP or calcium ions) which facilitates NLRP3 inflammasome assembly and maturation [540-542]. The NLRP3 scaffold protein is characterized by three structural domains: the amino-terminal (N-terminal) pyrin domain containing two death fold domains, the central nucleotide binding oligomerization domain and the carboxy terminal LRR [543]. The active NLRP3 inflammasome begins with the recruitment of the apoptosis-associated spec-like protein containing a CARD (ASC). ASC is an adaptor protein characterized by two domains: the N-terminal PYD domain which is recruited to the pyrin domain of the NLRP3 scaffold protein and the C-terminal CARD domain. ASC oligomerization culminates in the recruitment of procaspase-1 via CARD-CARD interactions between the adapter and procaspase-1 [543, 544]. The autocatalytic activity of procaspase-1 generates a mature hetero-tetrameric caspase-1, whose function is to process zymogen pro-IL-1β and pro-IL-18 into biologically active cytokines [524]. In the absence of caspase-1, caspase-8 facilitates the redundant function of IL-1β and IL-18 maturation. In the presence of caspase-1, caspase-8 positively regulates caspase-1 activity [545].

Recently, the role of caspase-1 has been demonstrated to extend beyond pro-inflammatory cytokine processing and maturation. Caspase-1 is additionally involved in the induction of an inflammatory type of cell death called pyroptosis through the maturation of gasdermin D [546,

547]. The target for mature gasdermin D is the lipid bilayer membrane of infected cells. Upon binding, gasdermin D induces holes in the membrane leading to cell rupture and death [546]. Although this a specific and tightly regulated intracellular pathogen surveillance and response mechanism, its function may potentially be dysregulated during paradoxical TB-IRIS [30].

Furthermore, type I and II interferon (IFN) responses such as IFNα/IFNβ and IFNγ were upregulated at the median time of paradoxical TB-IRIS manifestation in those who developed paradoxical TB-IRIS compared to those who did not [162]. IFNα and IFNβ negatively regulate the activity of the NLRP3 inflammasome [544]. For other intracellular pathogens, type-I and type II IFN promote the expression of the absent in melanoma 2 (AIM2) inflammasome [544]. However, *in vitro* infection with virulent Mtb does not trigger AIM2 expression whereas infection with non-tuberculous mycobacteria does [548]. The type VII ESX-1 secretion system present in Mtb has been implicated in AIM2 inhibition [548]. This mechanism likely mediates intracellular Mtb survival in the absence of other pathogen surveillance mechanisms. The composition of AIM2 inflammasome includes the N-terminal PYD domain and the HIN200 domain which detects and binds double stranded DNA which in turn alleviates autoinhibition of AIM2 [549]. The PYD domain recruits the ASC adaptor protein which in turn recruits pro-caspase-1 via CARD-CARD interactions and the subsequent maturation of pro IL-1β and IL-18 and their secretion [549].

Therefore, inflammasomes function to regulate the maturation of caspases which in turn modulate necrotic cell death through gasdermin-D as well as the maturation of various members of the interleukin-1 (IL-1) family of cytokines [550] [423, 551]. The IL-1 family of cytokines are low molecular weight signalling proteins that are secreted in response to a vast array of stimuli and are potent orchestrators of the process of inflammation, a hallmark of paradoxical TB-IRIS [529]. The IL-1 superfamily comprises 11 cytokine members and 10 receptors. The cytokines and receptors in the IL-1 superfamily are classified into four distinct subfamilies which include the IL-1, IL-33, IL-36 and IL-18 subfamilies [552, 553]. This classification is based on each subfamily's recognition of its cognate receptor. The IL-18 subfamily uses a different co-receptor compared to all other subfamilies which share the IL-1 receptor accessory protein (RAcP) as their secondary receptor [553, 554].

The field of structural biology has enhanced our understanding concerning the functioning of the members in the IL-1 superfamily [555, 556]. The four divisions of the IL-1 superfamily respectively signal via distinct primary receptors [553]. The receptors are composed of three immunoglobulin like domains, one transmembrane domain and one toll-like-IL-1-receptor (TIR) domain [553, 555]. Signaling occurs when the cytokine binds its cognate receptor [554]. Interestingly, despite overlapping functionality within each subfamily, the extent of sequence concordance is relatively low. For example, for the IL-1 subfamily: IL-1β and IL-1α signal via the same IL-1R but share 25% sequence homology [557]. Notably, the members have a common beta coil fold which enables them to signal via the same primary receptor [558]. This

holds true for IL1- receptor antagonist (IL-1RA) which regulates the activity of IL-1β and IL-1α. The antagonist competes with the agonists for binding of the primary receptor, but the binding of the former precludes the recruitment of the co-receptor, thus inhibiting signal transduction [559].

The mechanism of signal initiation is highly conserved within the IL-1 superfamily. Typically, signal initiation follows a stepwise process where the agonist cytokine binds its cognate receptor. Collectively, the cytokine-receptor pair recruits a co-receptor leading to signal relay or its inhibition depending on whether it was the agonist or antagonist interaction [553, 559]. In the case of an agonist-receptor interaction, the toll/interleukin-1 receptor (TIR) domains of the two receptors located intracellularly are recruited, initiating an NF-κβ signal transduction cascade [560-562].

Members of the IL-1 superfamily are potent modulators of inflammation [531, 554], consequently, their activities are tightly regulated at multiple levels [563]. This includes regulation at gene transcription level, secretion of cytokines as zymogens, competitive inhibition through antagonist cytokine-primary receptor binding and engaging of agonist cytokines with decoy receptors [564, 565].
Of note, the IL-1 family of cytokines are induced by various stimuli including but not limited to toll like receptor agonists, cytokines and oxidative stress signals [566-568]. The majority of cytokines of the IL-1 superfamily are constitutively expressed in a variety of tissues including

the lungs, kidneys, epithelial, endothelial and stromal cells [552, 569]. Notably, the expression of both IL-1β and IL-18 is restricted to innate immune cells such as monocytes, macrophages and neutrophils [570, 571]. Most members of the IL-1 superfamily are secreted as inactive proenzymes with N-terminal domains of varying lengths [572]. Inflammasome-derived proteases such as caspases remove the N-terminal amino acids, creating mature, signaling competent cytokines [80, 573]. Upon activation, they bind to their cognate receptors to initiate a cascade of signalling events that culminate in a constitutive induction of proinflammatory cytokines [554]. The secretion of mature IL-1β, IL-1α and IL-18 occurs through the non-classical secretion system [549].

The IL-1 family of cytokines and receptors were implicated as central role players in a number of pathological inflammatory conditions including paradoxical TB-IRIS. For instance, the expression of IL-1β was higher in *ex vivo* cultured PBMC from patients with paradoxical TB-IRIS compared to TB-non-IRIS controls after 6 hours of stimulation with heat-killed Mtb [162]. Moreover, the secretion of the same was significantly higher in supernatants from *ex vivo* cultured PBMC samples of patients with paradoxical TB-IRIS compared to TB-non-IRIS controls [162]. Furthermore, in a discovery approach using transcriptomics, Lai and colleagues identified the enrichment of toll like receptors (TLR), antigen presentation and the involvement of the inflammasome in RNA samples from patients with paradoxical TB-IRIS compared to TB-non-IRIS controls at 2 weeks on ART, which coincides with the median time of paradoxical TB-IRIS onset [25]. TLR are important mediators of inflammation and share a

common intracellular signalling motif - the TIR - with the IL-1 family of receptors [559, 574, 575]. Furthermore, previous work has shown that hypercytokinemia in patient samples with paradoxical TB-IRIS is contributed by the activation of canonical and non-canonical inflammasomes, in which inhibition of inflammasomes by non-specific pan-caspase inhibitor (prednisone, which has broad anti-inflammatory effects) can significantly reduce production of pro-inflammatory cytokines including IL-1α and IL-1β [33, 340, 341].

To determine whether specific inhibition of inflammasomes or its downstream effectors significantly reduce markers associated with acute inflammation in patients with paradoxical TB-IRIS compared with a non-selective anti-inflammatory agent such as prednisone, the effect of two drugs were assessed: a specific-inflammasome target (parthenolide) and anakinra which exerts its anti-inflammatory effects downstream of the inflammasome by blocking IL-1 receptors. The two drugs were tested in a PBMC culture model of heat-killed Mtb-H37Rv stimulation with drug treatment, using patient samples from the Pred-ART intervention trial and showed the lowest dose dependent responses that significantly reduced mediators of inflammation compared to other tested inhibitors [21, 258, 576]. The cohort from which the samples in this sub-study were derived is the Pred-ART intervention trial and was discussed in detail in Chapter 3 and 5 (see section 3.8.1 and 5.4.1 respectively).

7.1 Objectives

The main objectives of this sub-study were to assess the following in an *ex vivo* cell culture model:

1. To determine the dose-dependent responses of several experimental and FDA approved inflammasome-related inhibitors using peripheral blood mononuclear cells (PBMC) from HIV uninfected, interferon gamma release assay (IGRA)-positive (Mtb sensitized/ 'healthy') participants.
2. To determine the cytotoxicity of the drug candidates using the lactate dehydrogenase (LDH) assay and the trypan blue stain for confirmatory purposes in the same 'healthy' participant samples.
3. To assess the anti-inflammatory capacity of the candidate drugs with the aid of the optimized *ex vivo* cell culture model using PBMC collected at week 2 on ART, from the placebo allocated participants which were enrolled in the Pred-ART intervention trial.

7.2 Methods

Ex vivo cell culture experimental workflows in conjunction with multiplex analyte detection systems were used to investigate the potency of several inflammasome-related drug candidates in PBMC from patients who were allocated placebo in the Pred-ART trial, some who developed paradoxical TB-IRIS (n = 10) and some who did not (TB-non-IRIS controls, n = 10). A series of optimizations were conducted prior to evaluating the candidate drugs in patient samples.

7.2.1 The isolation of peripheral blood mononuclear cells (PBMCs)

Peripheral blood mononuclear cells (PBMC) were isolated from one healthy donor, as well as patients enrolled in the Pred-ART trial from whole blood using gradient centrifugation using ficoll. Briefly, peripheral blood was collected in 10 mL ethylenediamine-tetraacetic acid (EDTA) tubes which were diluted in distilled water/phosphate buffer saline (PBS) in a ratio of 1:2 and thoroughly mixed. Approximately 20 mL of diluted blood was layered in 15 mL of ficoll and centrifuged at 1750 rpm for 20 min with the deceleration set to 0. The plasma was discarded and the PBMC layer was collected and transferred to a new 50 mL falcon tube. The PBMC layer was resuspended in 40 mL of rosewell park media (RPMI) supplemented with 10% fecal calf serum (FCS) and washed twice by gradient centrifugation at 400 xg for 10 min. Cells were kept in ice and were mixed with 20% freezing medium (8 mL dimethyl sulfoxide (DMSO) + 32 mL FCS) and aliquoted in 2 mL Sarstedt cryovials. The cells were subsequently kept at -80 ^{0}C overnight before being transferred to a liquid nitrogen tank for long term storage.

7.2.2 Recovery of PBMC from cryopreservation

PBMC were transported in wet ice from the liquid nitrogen tank and rapidly thawed at 37 ^{0}C in a water bath. Cells were transferred to a 50 mL falcon tube and resuspended in warm RPMI supplemented with 10% FCS. Cells were subjected to two rounds of washes by centrifugation at 1200 rpm for 6 min. Cells were resuspended to a concentration of 2 million cells/mL and used for various optimization experiments. Cell viability was tested using trypan blue staining. Cells were incubated at 37 ^{0}C in the presence of 5% CO_2 for 12 hours to recover. Cells were subsequently stimulated with Mtb-H37Rv and treated with candidate drugs.

7.2.3 Broth culture of Mycobacterium tuberculosis (Mtb-H37Rv)

Mtb-H37Rv was cultured in 7H9 with Middlebrook oleic albumin dextrose catalase (OADC) supplement to a final volume of 10 mL in a 50 mL culture flask and was allowed to reach a concentration of optical density (OD_{600}) of 0.5 without shaking at 37 ^{0}C. Briefly, a freezer stock of Mtb-H37Rv was seeded at OD_{600} 0.05 and allowed to reach a final concentration of OD_{600} 0.5. The surface of the culture flasks were wiped with 70% ethanol, carefully removed from the hood and transported for incubation at 37 ^{0}C without shaking. The cultures were monitored daily for growth by measuring the OD using a spectrophotometer. Once the cultures reached a final concentration OD_{600} of 0.5, a total of 1 mL Mtb culture was aliquoted in sterile1.5 mL Eppendorf tubes and sealed with parafilm inside biosafety level II cabinet (BSCII).

7.2.4 Heat killing of Mtb-H37Rv

The parafilm sealed aliquots were safely transported outside the class II biosafety cabinet (BSCII) to a uniformly heated water bath. The cultures were heat killed at 80 ^{0}C for 2 hour and subsequently plated for colonies to verify killing. The heat-killed cultures were safely transported out of the BSL III laboratory in a sterile double ziplock bag in an upright position, and stored at -80 ^{0}C in the BSL II laboratory for subsequent stimulation experiments.

7.3 Optimization of experimental conditions

7.3.1 Determining the multiplicity of infection.

The multiplicity of infection refers to the ratio of cells to infecting agent used for stimulation purposes. A titration of 3 different PBMC to Mtb-H37Rv ratios were set up to determine the optimal multiplicity of infection (MOI) that could induce a detectable cytokine response. Cells were recovered from cryopreservation as previously described (section 7.2.2) and resuspended to a final concentration of approximately 250 000/200 µL and stained for viability. Cells were seeded in a 96 well plate and four conditions were tested as follows: unstimulated cells and cells incubated with different ratios of Mtb-H37Rv for 12 hours as follows: 1:1, 1:2 and 1:5. After 12 hours of incubation, the cells were sedimented by gradient centrifugation at 1800 rpm for 3 min and the supernatant collected and transferred to a sterile 96 well plate. The supernatants were tested for cytokine production using a custom 7-plex Luminex panel which included interferon gamma (IFN-γ), interleukin (IL)-1α, IL-1β, IL-8, IL-10, IL-18, and tumor necrosis factor (TNF-α).

7.3.2 Cell number titration

PBMC from one healthy participant were recovered from cryopreservation as previously described (section 7.2.2). A total of 200 µL of either 10 million cells/mL or in subsequent re-optimization, 1.25 million cells/mL which corresponds to 250 000cells/200µL were seeded for 5 different conditions. A total of 100 µL of RPMI supplemented with 2% FCS was added to the remaining wells. A 2-fold dilution series was performed by mixing 100 µL of the cells with 100 µL of RPMI supplemented with 2% FCS. Similarly, heat killed Mtb-H37Rv was titrated in a sterile 96 well plate in a 1:1 ratio based on the highest cell concentration (250,000 cells/200 µL). The last four conditions were stimulated with a 1:1 dose of heat killed Mtb-H37Rv and treated with 5 nM optimized drug concentration of candidate drugs. The suspension was incubated for 12 hours, and the supernatant harvested by gradient centrifugation at 1800 rpm for 3 min. The cells were transferred to a new sterile 96 well plate and tested for drug mediated cytokine reduction by Luminex.

7.3.3 Assaying for the optimal/minimum time for sample stimulation.

Cells with poor viability release death factors the longer they are in culture and may even be killed by stimulation. This can trigger other cells in the same milieu to lose viability and die [577]. Because no viability data was stored for the Pred-ART samples which were used for the final analyses, the minimum duration of antigen stimulation required to induce the secretion of cytokines was tested. Patient PBMC from the TB-ART observational study were seeded in a

sterile 96 well plate and allowed to recover from cryopreservation as previously described (see section 7.2.2). To determine the optimal time required to induce cytokine production, cells were stimulated with heat-killed Mtb-H37Rv for either 6 or 12 hours. Cells were sedimented by gradient centrifugation at 1800 rpm for 3 min. The supernatants were collected and stored in a sterile 96 well plate and used for multiple analyte detection by Luminex.

7.3.4 Determining dose-dependent drug responses in PBMC from a healthy individual.

A total of 8 drugs were screened (7 FDA approved) including 2 pan-caspase anti-inflammatory inhibitors (Z-VAD-FMK; Ac-VAD-CMK), 2 inflammatory lipids/eicosanoid inhibitors (Naproxen; Celecoxib), 2 inflammasome inhibitors (Vx-765; Parthenolide-not FDA approved) and Anakinra - an IL-1 receptor antagonist which acts downstream of the inflammasome to block effector molecules. The capacity of the candidate drugs to reduce markers that are associated with inflammation was evaluated and compared to the broadly anti-inflammatory corticosteroid - prednisolone - which is used for the treatment and prevention of paradoxical TB-IRIS.

Briefly, cryopreserved PBMC from one healthy individual were rapidly thawed at 37 °C and washed twice in RPMI media containing 20% FCS by gradient centrifugation at 1200 rpm for 6 min. PBMC were rested overnight (~12 hours) and were subsequently seeded at 250,000 cells/200 µL. Dose responses were determined by stimulating PBMC with an optimized MOI of 1:1 of heat killed Mtb-H37Rv grown to OD_{600} 0.5. The cultures were subsequently treated

with a panel of drugs at 6 standardized concentrations ranging from 1 μM; 500 nM; 100 nM; 50 nM; 25 nM and 5 nM for all drugs. Plates were incubated for 12 hours at 37 °C in the presence of 5% CO_2. Plates were subsequently spun down (1800 rpm; 3 min) for cell supernatant harvesting. A total of 180 μL of cell culture supernatant was stored at -80 °C for downstream detection of multiplexed analytes by Luminex, enzyme linked immunosorbent assay (ELISA) and lactate dehydrogenase (LDH) to quantify cell death. Cell pellets were resuspended in 100 μL of Trizol and frozen at -80 °C for RNA extractions.

7.3.5 Cytokine detection by Luminex.

For analyte detection, a custom 7-plex for optimization and an extended 15-plex Luminex panel of pro-inflammatory cytokines, chemokines and metalloproteinases (GM-CSF, IL-1α, IL-β, IL-1RA, IL-6, IL-8, IL-10, IL-12, IL-17, IL-18, IFN-α, IFN-β, IFN-γ, MMP-9, MMP-10, TNF-α) that were significantly upregulated in patients with paradoxical TB-IRIS compared to TB-non-IRIS controls was used [162]. The standards were prepared fresh for each new assay according to the manufacturer's instruction (**see page 109, section 3.21.14**). Cell culture supernatants were thawed at room temperature. A total of 50 μL of cell culture supernatants were diluted 1:2 in RD6 buffer and incubated for 2 hours in the dark, in a rotary shaker with a 50 μL preparation of biotinylated beads. The plate was subsequently washed in 100 μL of wash buffer solution in an automated washer to avoid the loss of beads. The wash step was repeated twice prior to another incubation step in a 50 μL mixture of secondary antibody as previous for 1 hour. The plate was washed as previous and incubated as previous for 30 min in 50 μL of

streptavidin. The plate was washed as previous and resuspended in 100 µL of wash buffer and the beads mixed for 2 min prior to acquisition.

7.3.6 Piloting optimized conditions using samples from the TB-ART study.

The optimized parameters were piloted in a subset of PBMCs from patients who developed paradoxical TB-IRIS and those who did not (controls), who were previously enrolled in the TB-ART study. Due to a limited number of samples at week 2 on ART, which coincides with the onset of paradoxical TB-IRIS onset, samples collected at week 1 on ART were used.

7.3.7 Detection of caspase-1 by enzyme linked immune sorbent assay (ELISA)

The IL-1 family of cytokines are zymogens that are catalytically activated by caspase-1 which is a product of the inflammasome complex. The presence of caspase-1 was detected by ELISA. Briefly, anti-caspase-1 coated 96 well ELISA plate was incubated for 2 hours in the dark without mixing with 50 µL of supernatants from *ex vivo* cultured patient PBMC that were stimulated with heat killed Mtb-H37Rv and subsequently treated with 5nM of candidate drugs. The plate was washed in 100 µL of fresh wash buffer in an automated plate washer and incubated in the dark with 50 µL of secondary antibody. The plate was washed as previous and incubated with 50 µL of horse radish peroxidase for 20 min after which the reaction was stopped with 50 µL of 0.1% hydrochloric acid (HCl). Absorbance was measured at 490 nm and the results were analyzed in GraphPad Prism.

7.3.8 Evaluation of drug induced cytotoxicity by lactate dehydrogenase (LDH) assay or trypan blue viability staining.

Drug induced cell cytotoxicity was determined by both trypan blue staining and the lactate dehydrogenase assay. Damaged or dead cells have a compromised cell membrane integrity, and as a result, release markers of cell death, such as of LDH, and allow dye penetration. Briefly, a total of 50 µL of supernatant from the *ex vivo* PBMC culture model of heat killed Mtb stimulation and treatment with 3 candidate drugs were assayed for the release of LDH. In addition to the 5 conditions, cells incubated in 1% triton X-100 were used as a positive control. The plates were read at 490nm wavelength. The results were represented as percentage where the measure of cytotoxicity was calculated as the quotient of the difference of the positive control from the experimental condition divided by the difference of the positive control and the negative control multiplied by 100. For confirmation, approximately 20 µL of the drug treated cells condition was diluted in a 1:2 ratio with trypan blue dye. The suspension was mounted on a counting slide and the viability determined using an automated TC counter. For analysis, viability was plotted as percentage and median values were compared between the various drug-treated conditions relative to the untreated cell only condition.

7.3.9 Acquisition

The optimized protocol was tested on week 2 PBMC samples collected from placebo allocated participants in the Pred-ART intervention trial. Sample acquisition and analyte detection was

carried out using the Bio-Rad Luminex hardware running the Bio-Plex-200 software. The system was configured to exclude all doublets and to acquire at least 100,000 events.

7.4 Results

The clinical characteristics of the Pred-ART cohort whose samples were used in this sub-study were discussed previously in the results section of Chapter 5 (see section 5.4.1).

7.4.1 Optimization of multiplicity of infection using PBMC from one "healthy" individual.

The ideal ratio of PBMC to heat-killed Mtb-H37Rv otherwise known as the multiplicity of infection (MOI) to induce a detectable cytokine response was determined. Assaying for a range of PBMC to heat killed-H37Rv ratios revealed that an MOI of 1 induced the highest concentration for several cytokines over a 12-hour incubation period compared to other tested MOI for IFN-γ, TNF-α, IL-6 and IL-1α among others (**Figure 7**).

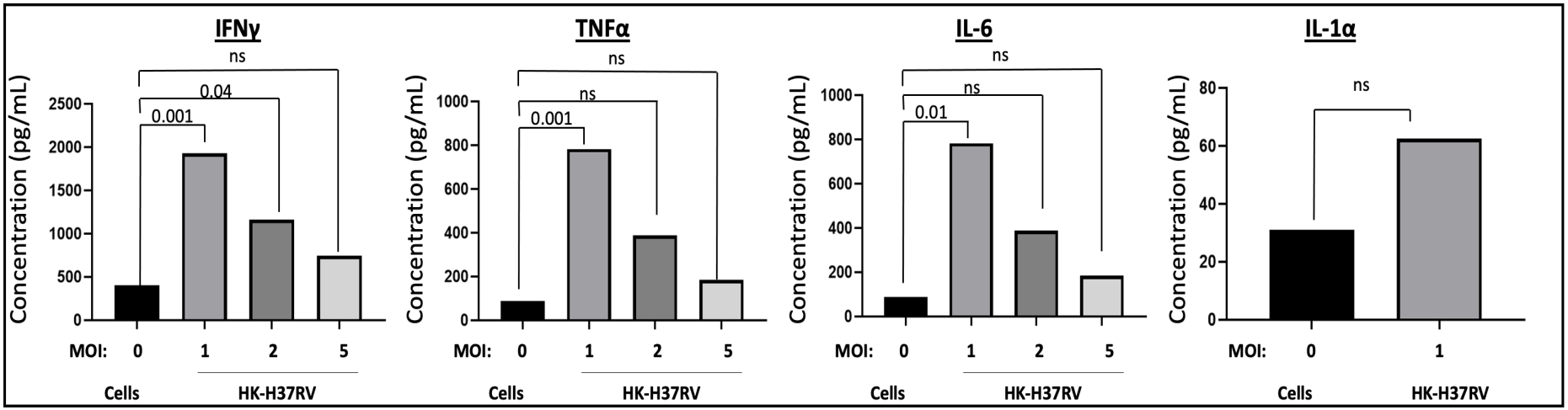

Figure 7. Testing a range of multiplicity of infections (MOI) (0-5) to determine which MOI is associated with optimal cytokine induction over a 12-hour incubation period with heat-killed Mycobacterium tuberculosis laboratory strain (H37Rv). *Multiple analyte detection was performed by Luminex. An MOI of 1:1 induced the highest concentration for multiple cytokines. A p-value of 0.05 or less was considered statistically significant; ns = not significant.*

The length of incubation together with a higher infective dose (higher number of Mtb bacilli) of heat killed-H37Rv likely reduces the viability of cells, thus resulting in lower concentrations for IFN-γ, TNF-α, IL-6 and IL-1α. The concentration of IL-1α at an MOI of 2 and 5 were below the limit of detection and are therefore not shown (Figure 7).

7.4.2 Determination of dose dependent drug responses of both pan-caspase and inflammasome specific inhibitors.

The lowest dose dependent drug response concentration that was tested for all drug candidates was 5 nM. Two inhibitors (parthenolide and anakinra) demonstrated low dose drug responses comparable to the current standard of care for paradoxical TB-IRIS (prednisolone) Figure 7.1.

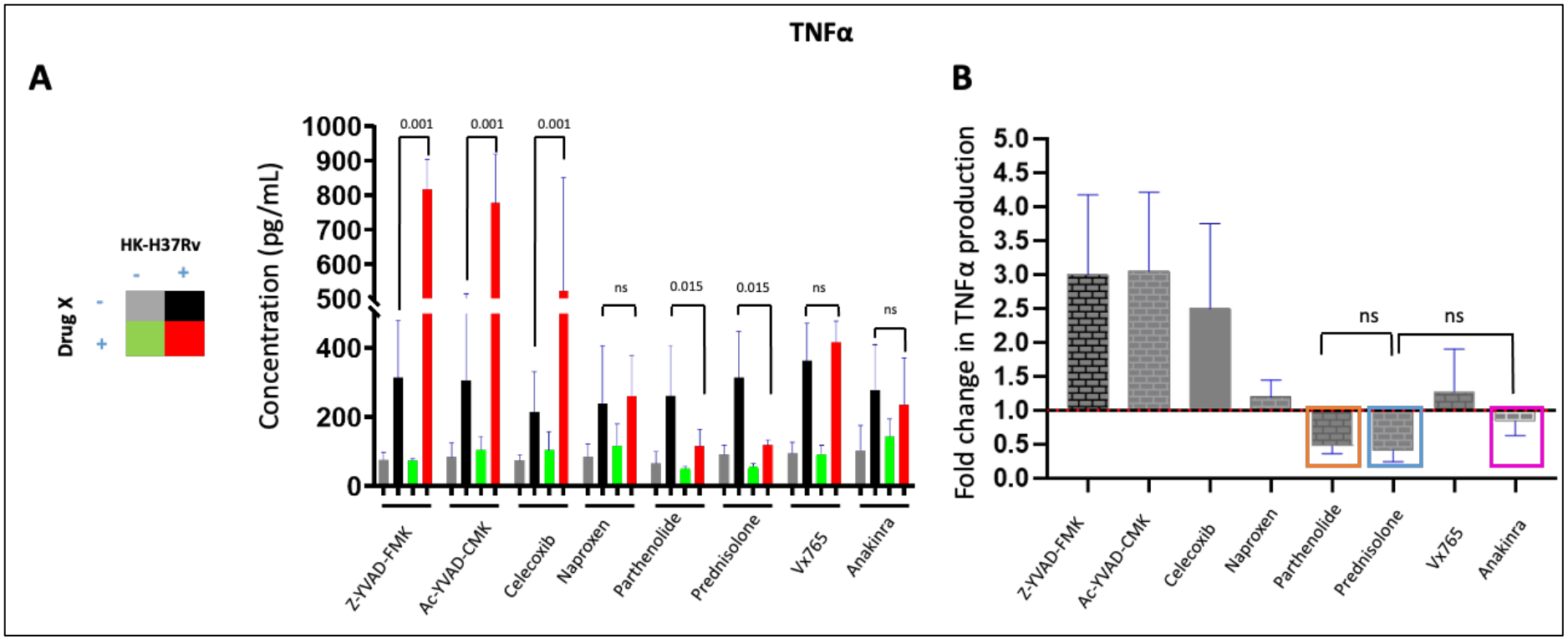

Figure 7.1. Determination of dose dependent-drug effect for a total of 7 inflammasome specific drug candidates compared to prednisolone in a healthy participant with immune sensitization to Mycobacterium tuberculosis. *Drug concentrations ranging from 100 □M-5nM were tested for the capacity to reduce several markers that are associated with inflammation. A drug concentration of 5 nM of parthenolide and anakinra were comparable in anti-inflammatory activity against TNF-α to the current standard of care (prednisolone). A p-value of 0.05 or less was considered statistically significant; ns = not significant.*

Parthenolide and anakinra significantly reduced TNF-α and other markers of inflammation (not shown) in a single healthy participant when compared to prednisolone. The experiment was performed in triplicate (single biological repeat done in triplicate).

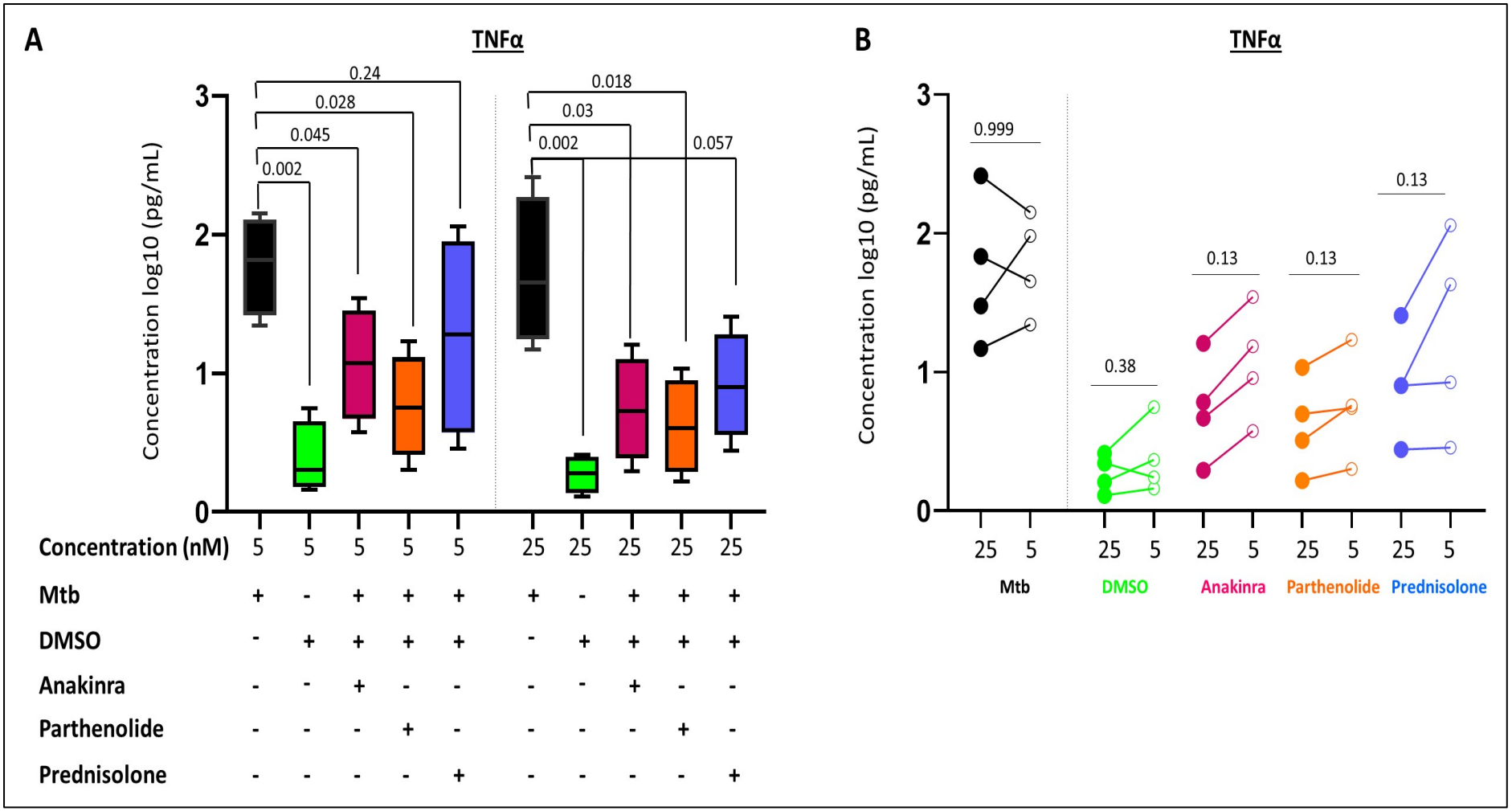

Figure 7.2. Comparison of the two lowest dose dependent drug responses for anakinra, parthenolide and prednisolone by enzyme linked immunosorbent assay (ELISA). A, *Testing of 5 nM of the candidate drugs in ex vivo cell culture model of stimulation and drug treatment for*

effect in reducing concentration of TNF-α. ***B,*** *Testing of 25 nM of the candidate drugs in ex vivo cell culture model of stimulation and drug treatment for effect in reducing concentration of TNF-α. A p-value of 0.05 or less was considered statistically significant.*

Furthermore, we determined whether there were differences in the reduction of pro-inflammatory cytokines between the candidate drugs at 25 and 5 nM concentrations respectively. There was no statistically significant difference between the two tested concentrations and their ability to reduce markers of inflammation in a total of 4 patient PBMC collected at week 1 on ART in patients who developed paradoxical TB-IRIS who were enrolled in the TB-ART study (**Figure** 7.2).

7.4.3 Safety profile of the inhibitors

To determine whether 25 nM drug concentration induced significantly higher drug cellular toxicity compared to the 5 nM drug concentration, lactate dehydrogenase assay was chosen as the assay of choice.

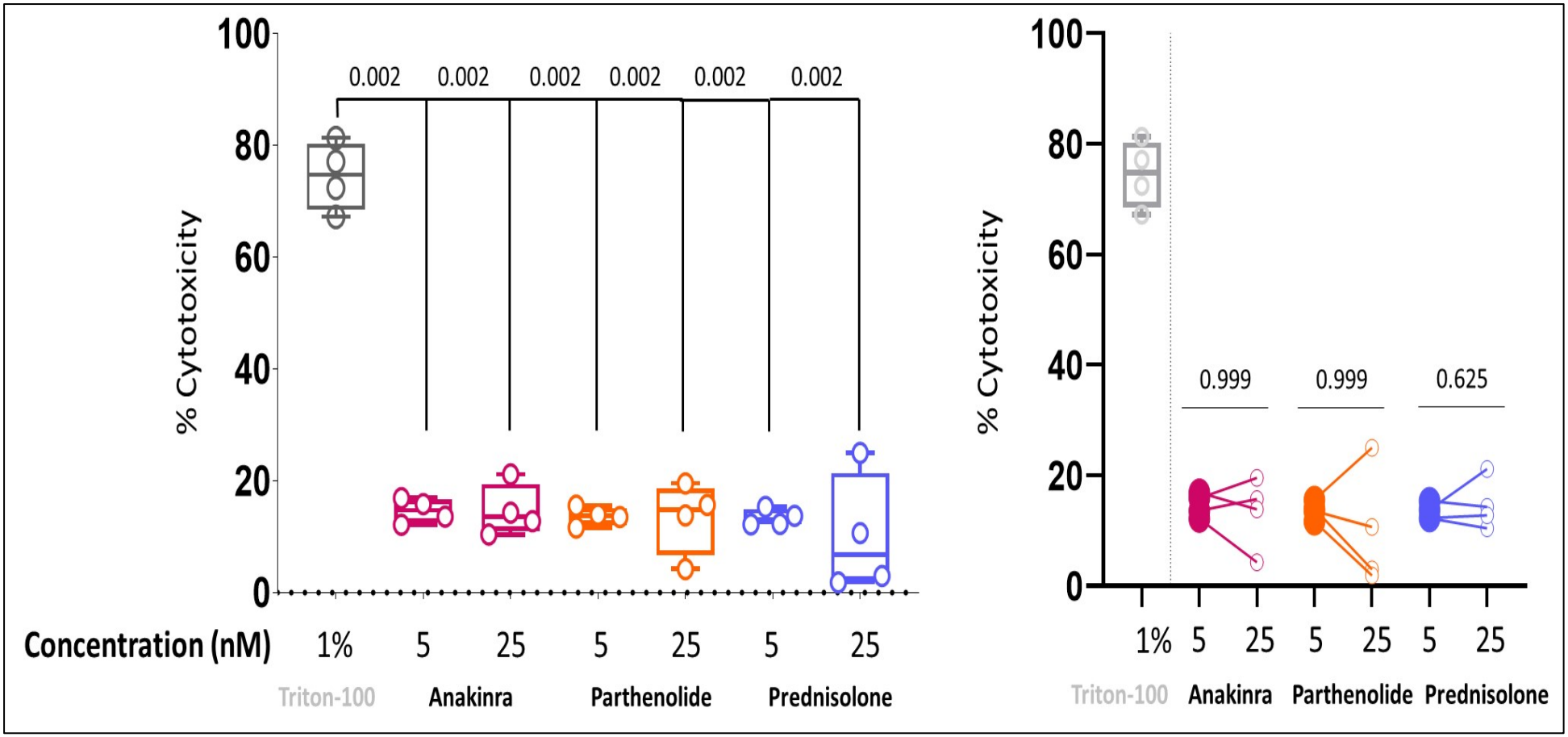

Figure 7.3. Investigating drug induced cytotoxicity between 5 nM and 25 nM drug concentrations using the lactate dehydrogenase (LDH) assay*. Triton X-100 (1%) was highly toxic to cells as determined by the release of LDH. However, no differences in drug cytotoxicity were detected for all 3 drug candidates for the tested drug concentrations. A p-value of 0.05 or less was considered statistically significant.*

A final volume to volume concentration of 1% triton-X-100 served as a positive control to confirm loss of membrane integrity resulting in trypan blue penetration. Notably, the 5 and 25 nM drug concentrations were both associated with numerically small but statistically significant toxicity compared to the untreated samples. However, there was no significant differences in the percentage of trypan blue penetration in PBMC treated with the 3 respective drugs (**Figure** 7.3). This finding suggests that the 25 nM drug concentration for all three drug candidates did not induce significant cytotoxicity compared to 5 nM drug concentration. The 5nM drug concentration was chosen for all subsequent/ final testing in patient PBMC.

7.4.4 Determining the minimum number of cells that allowed for multiplexed analyte detection.

The cell numbers for the stored patient samples enrolled in the Pred-ART trial were generally low and highly variable. As such, we explored by cell number titration, the minimum number of cells that permitted for multiplexed analyte detection by Luminex using PBMC from a 'healthy' participant.

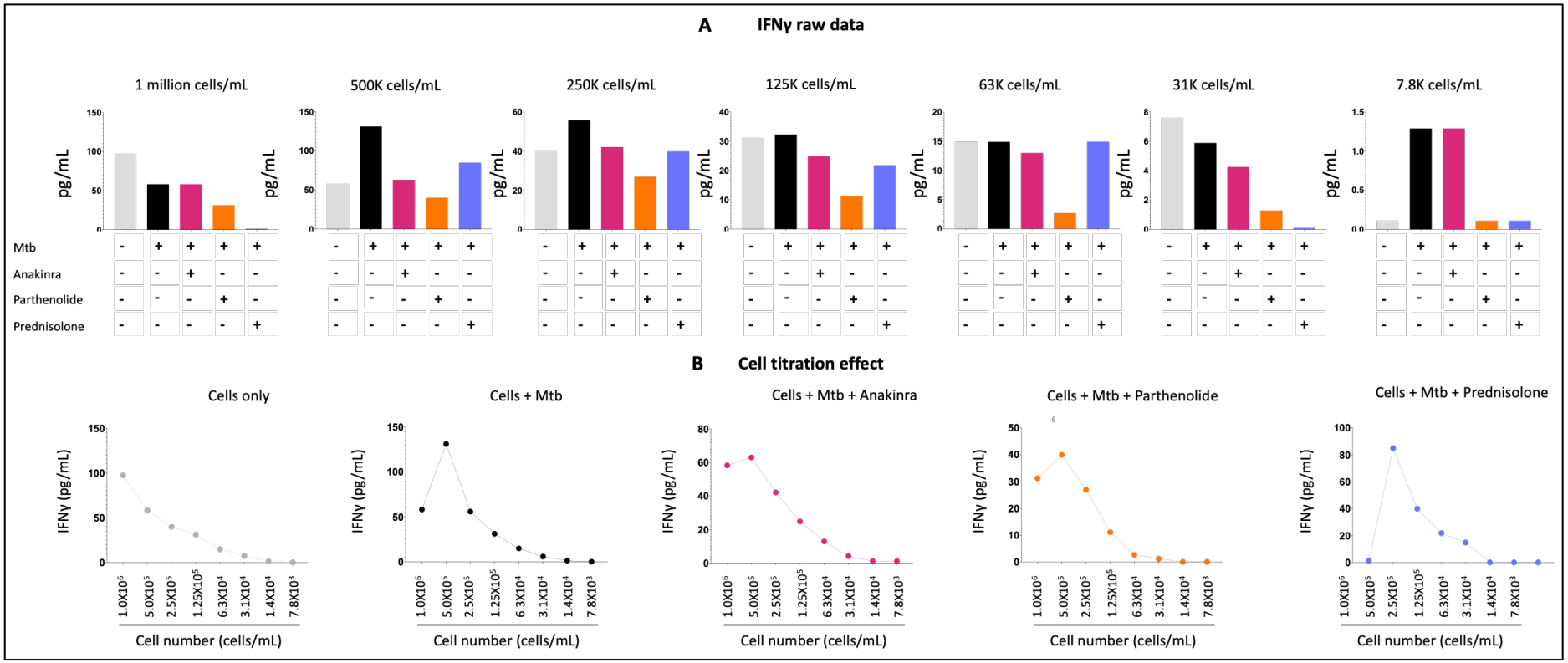

Figure 7.4. Determination of the lowest number of cells that allowed for muti-analyte detection using Luminex*. **A,** Ex vivo PBMC culture conditions including unstimulated control signifying background cytokine secretion (Grey), heat-killed Mycobacterium tuberculosis laboratory strain (H37Rv) stimulation condition-induces cytokine production (Black) and treatment with anakinra (Purple), parthenolide (Orange) and prednisolone (Blue) respectively- measure was ability of drug to reduce interferon gamma (IFN-γ) secretion. **B,** Titration effect for IFN-γ for the lowest dilution.*

Panel A of Figure 7.4 shows the experimental conditions including the unstimulated and untreated cells, cells stimulated with heat killed-H37Rv, heat killed-H37Rv stimulated cells and subsequently treated with anakinra, parthenolide or prednisolone respectively. The major concern was that the stimulation conditions did not show a consistent predicted effect in certain titration conditions. This cast doubt on the reliability of the findings, particularly as it relates to the treatment condition. It raised concerns about whether anticipated stimulation had occurred in certain experiments. However, when plotting the titration effect for each condition individually, it was apparent that the effect of titration was present (**Figure** 7.4 Panel B). To determine the minimum number of cells that permitted a detectable cytokine response, the heat-killed-H37Rv stimulated, and drug-treated conditions were used to make an assessment. From this data, no definitive conclusion regarding the lowest number of cells that allowed for a detectable cytokine response could be made due to the high background in the unstimulated condition.

Therefore, to troubleshoot the high level of background that was observed in the unstimulated condition, experiments were repeated with the aim of further optimizing the titration results. PBMC culture stimulation and treatment were repeated as previously albeit with washing after overnight recovery. The cultures were subsequently stimulated and treated with the 3 candidate drugs as previous using PBMC from a ‘healthy’ participant.

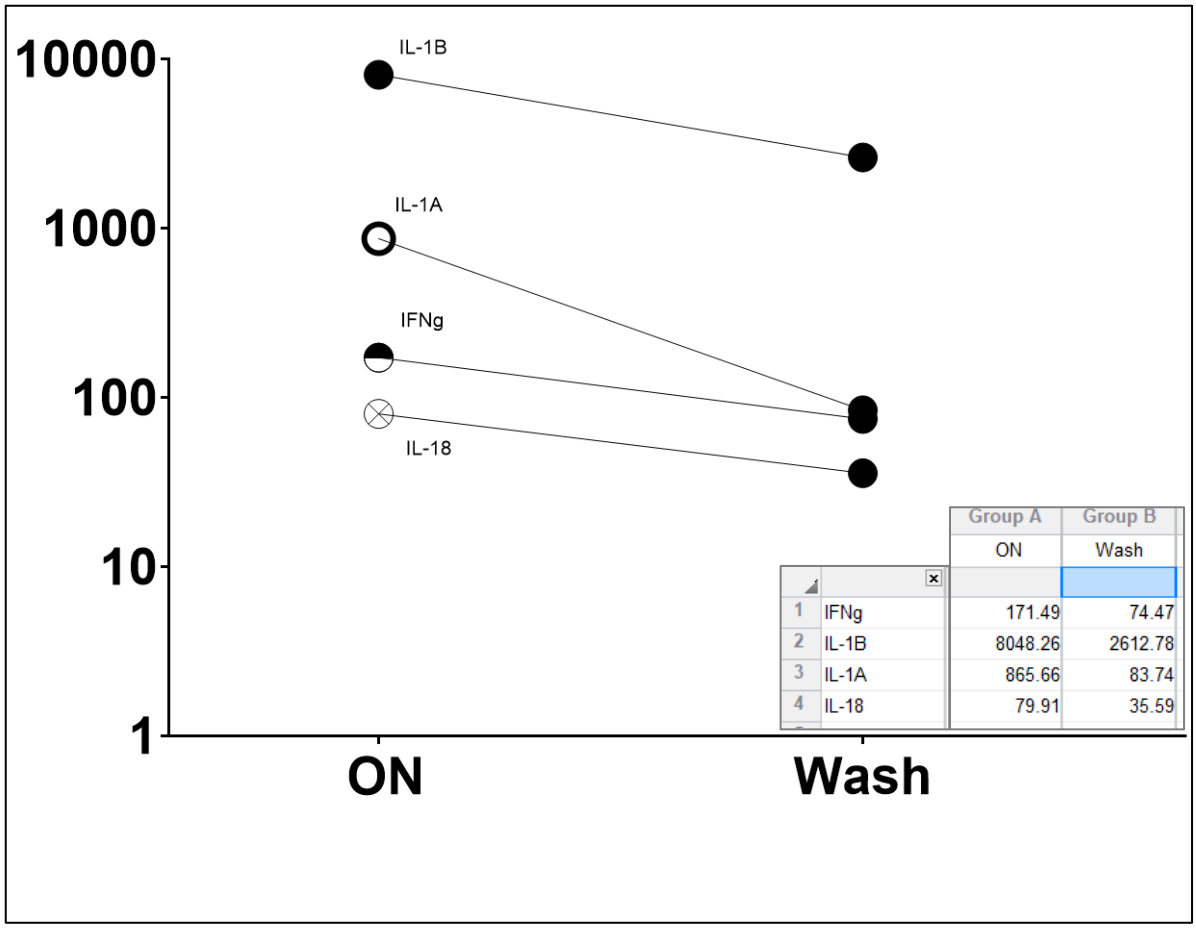

Figure 7.5. Troubleshooting to address the high level of background in untreated samples. *Cells were processed and rested overnight for recovery from cryopreservation. Cells were washed after recovery or left unwashed. Supernatants were collected and multiple analytes were measured using Luminex. Washed cells showed a reduction in the level of background cytokine secretion*

It was concluded that washing the cultures after overnight recovery reduced background cytokine secretion for all measured analytes (**Figure** 7.5). For subsequent stimulation and drug-treatment experiments, the washing step was incorporated following overnight recovery from cryo-preservation.

Stimulation and concomitant drug treatment experiments were repeated to verify the validity of various culture conditions including, reduced background, the effect of stimulation and the titration effect. Titration experiments were repeated as previously with minor modifications to the protocol. The expected stimulation effect and reduced background was observed (**Figure** 7.6). In an *ex vivo* cell culture model of PBMC from one healthy participant, 5nM parthenolide

significantly reduced several markers of inflammation (including IFN-γ, TNF-α, IL-1α, IL-1β, IL-6 and IL-18) measured by Luminex compared to the equivalent of anakinra and prednisolone (**Figure** 7.6B).

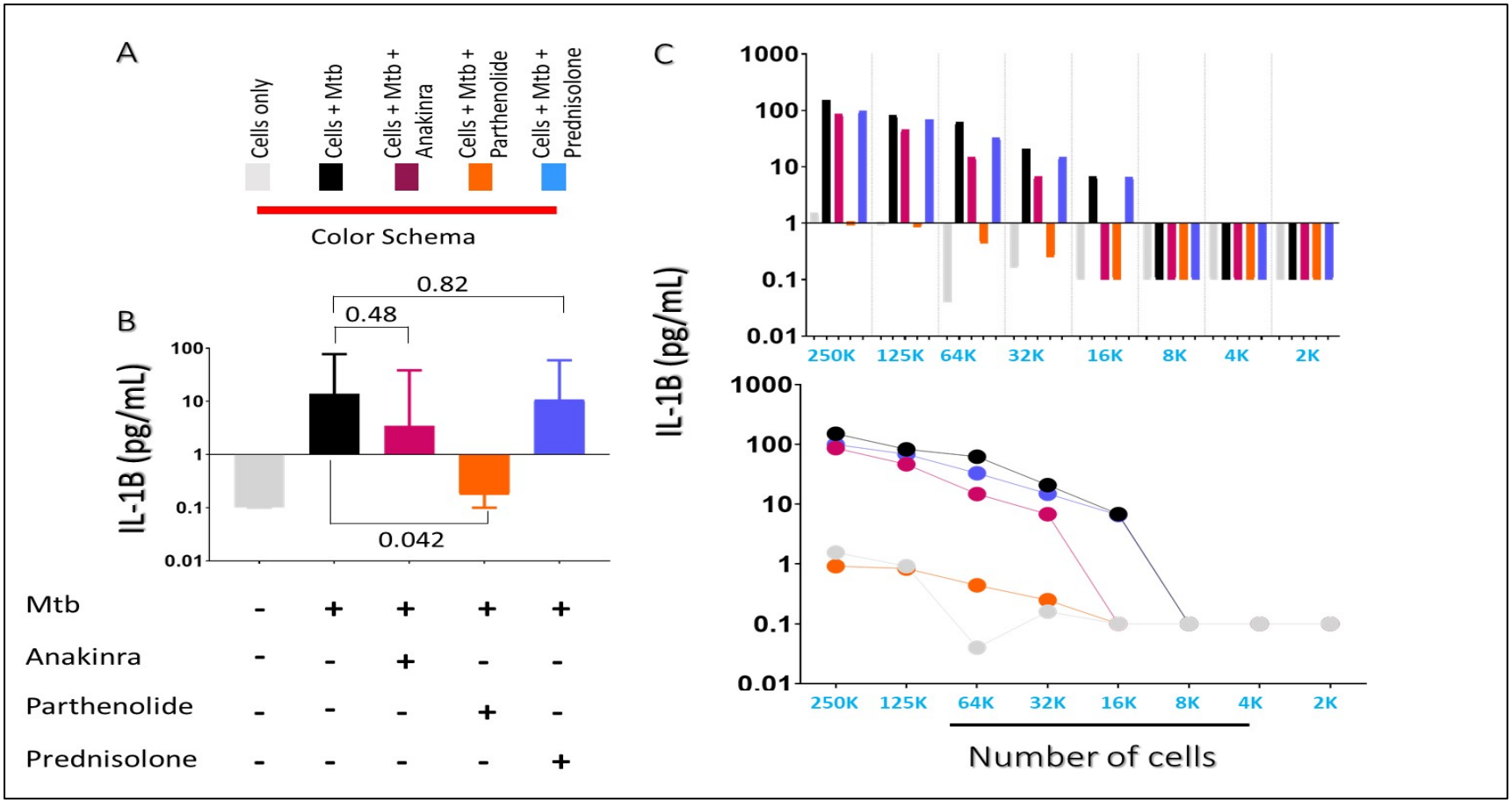

Figure 7.6. Determination of the lowest number of cells that allowed for multi-analyte detection using Luminex. A, *Color scheme describing the experimental conditions.* ***B,*** *Ex vivo peripheral blood mononuclear cells (PBMC) culture conditions including unstimulated control signifying background cytokine secretion (Grey), heat-killed Mycobacterium tuberculosis laboratory strain (H37Rv) stimulation condition-induces cytokine production (Black) and treatment with anakinra (Purple), parthenolide (Orange) and prednisolone (Blue) respectively- reduce interleukin (IL)-1β secretion. PBMC were seeded at 250 000 cells/200 µL and diluted 2-fold*

to the lowest concentration; all dilutions were exposed to corresponding dilutions of 5 nM treatment with candidate drugs. ***C,*** *Titration effect for IL-1β for the lowest dilution*

The main finding was that 32 000 cells/200 µL was sufficient to detect markers of inflammation using Luminex in an *ex vivo* cell culture model of stimulation and drug treatment (**Figure** 7.6C). Therefore, this data suggests that Luminex is sensitive enough to detect multiplexed pro-inflammatory analytes from this cell culture model between 250 000 cells/200 µL and 32 000 cells/200 µL cell ranges.

7.4.5 Determining the optimal stimulation time for detecting cytokine/chemokine secretion.

Given that PBMC samples from our cohort had been cryogenically preserved, it was observed that the longer they stayed in culture, the more they lost viability despite proper supplementation. Because of this, the length of stimulation and whether longer culture times were associated with increased cytokine secretion were evaluated (**Figure** 7.7).

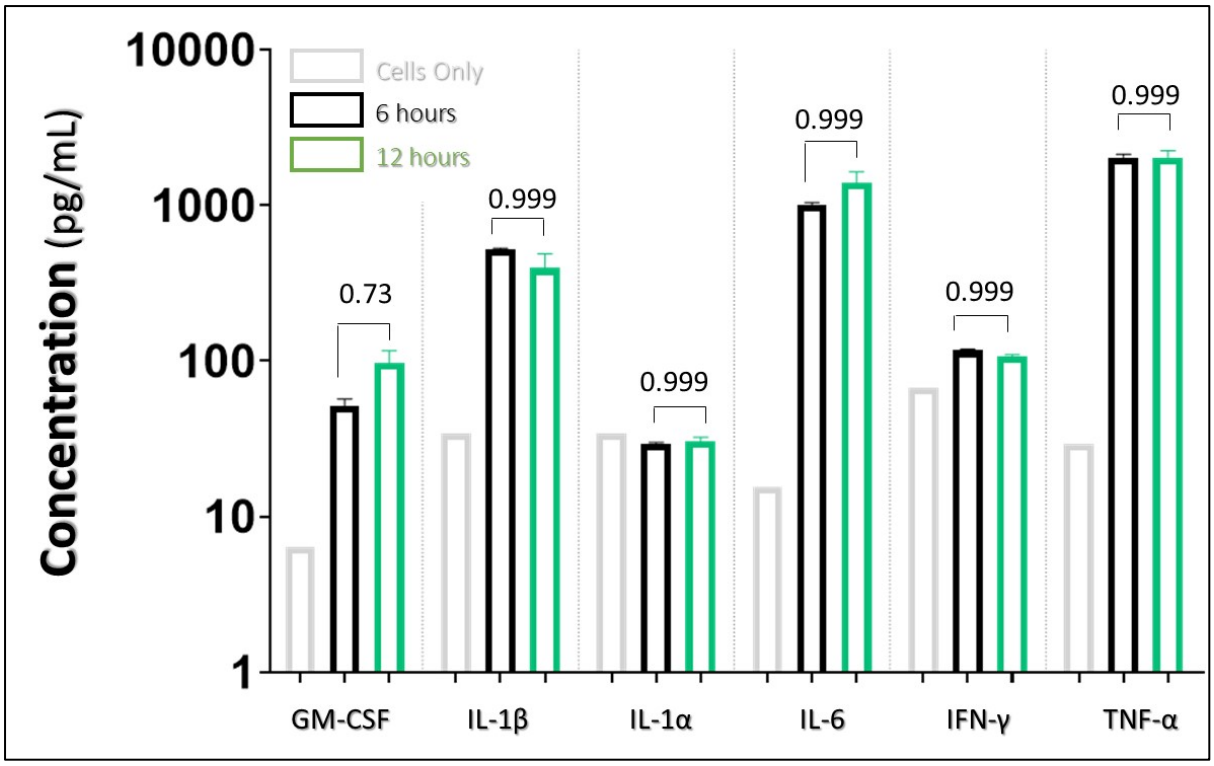

Figure 7.7. Ex vivo cell culture to determine the differences in cytokine induction between 6 and 12 hours of heat-killed stimulation with laboratory strain of Mycobacterium tuberculosis (H37Rv) at an MOI of 1. Peripheral blood mononuclear cell (PBMC) culture supernatants were assayed for several analytes using Luminex*. There were no significant*

differences in the concentration of several measured cytokines between the two tested time points. A p-value of 0.05 or less was considered statistically significant.

There were no statistically significant differences in cytokine secretion between cells propagated for 6 hours compared to those propagated for 12 hours at an MOI of 1 (**Figure** 7.7). This was a single independent experiment with two technical repeats using a sample from one patient who developed paradoxical TB-IRIS. In the finalized and optimized protocol, stimulation time was reduced to 8 hours in subsequent assays.

7.4.6 Piloting the optimized protocol in an ex vivo cell culture model of heat killed Mtb stimulation and drug treatment using PBMC samples from patients enrolled in the TB-ART observational clinical study.

The optimized protocol was piloted in an *ex vivo* cell culture model of PBMC collected at week 1 on ART for a total of 4 patient samples from the TB-ART observational study [19]. Of note, although the time to paradoxical TB-IRIS onset was a median of 2 weeks on ART for the TB-ART cohort, the time to paradoxical TB-IRIS onset for each participant was variable ranging between 3-17 days. Notably, 2 of the 4 selected TB-IRIS samples were from patients who developed paradoxical TB-IRIS at week 1 on ART. There were no significant differences in the reduction of TNF-α and other pro-inflammatory cytokines (not shown) between TB-IRIS (n=4) and TB-non-IRIS controls (n=4) when the different interventions were compared (**Figure** 7.8). Both parthenolide and anakinra had similar trends in reducing TNF-α concentration in samples from patients who developed paradoxical TB-IRIS. However, this was not statistically different when compared to prednisolone, potentially due to small sample size (**Figure** 7.8).

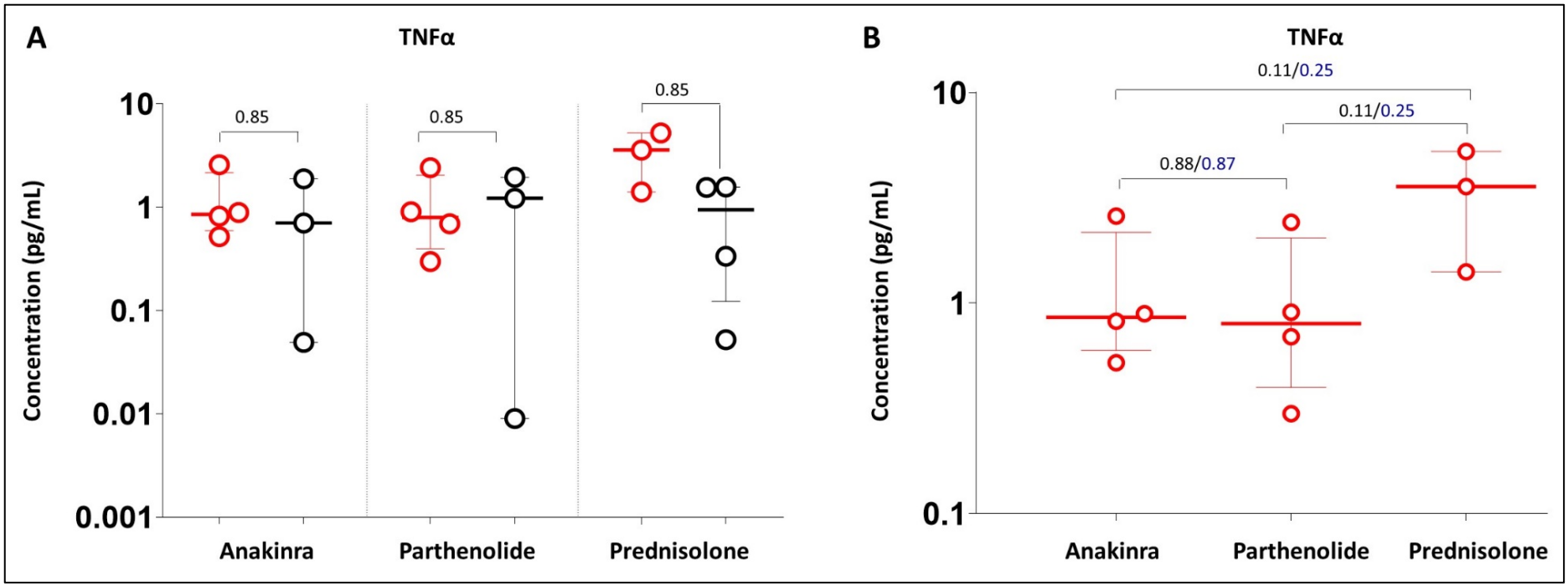

***Figure** 7.8. Detection of TNFα by Luminex assay in an ex vivo cell culture model of peripheral blood mononuclear cells (PBMC) stimulation and drug treatment in 8 patient samples from the TB-ART observational study who either developed paradoxical TB-IRIS or did not at week 2 on antiretroviral therapy (ART). **A,** Cross-section comparison of TNF-α concentrations in supernatants of PBMC samples from patients who developed paradoxical TB-IRIS (open red circles, n = 4) and those who did not (open black circles, n = 4). PBMC were stimulated with an MOI of 1 using heat-killed Mycobacterium tuberculosis laboratory strain (H37Rv) and subsequently treated with 5 nM of anakinra, parthenolide or prednisolone. **B,** TNF-α concentrations in supernatants of PBMC samples from patients who developed paradoxical TB-IRIS (open red circles, n = 4). A p-value of 0.05 or less was considered statistically significant; ns = not significant. Black font of p-value is for paired data and blue font is for unpaired statistical analysis.*

7.4.7 Drug mediated ex vivo reduction of proinflammatory mediators in PBMC samples collected from patients enrolled in the Pred-ART intervention trial.

Finally, the optimized protocol of the *ex vivo* cell culture model of heat-killed Mtb stimulation and concomitant inhibition was evaluated on PBMC samples collected at week 2 on ART; from patients who were allocated placebo, who developed paradoxical TB-IRIS and TB-non-IRIS controls enrolled in the Pred-ART intervention trial. The drug candidates were evaluated for their efficacy to reduce known markers of inflammation using an expanded, custom Luminex panel (15 analytes) comprising pro-inflammatory cytokines, chemokines, growth factors and metalloproteinases which have previously been shown to be upregulated at the onset of paradoxical TB-IRIS [162, 472].

After processing and recovering a total of 20 PBMC samples (n = 10) of patients with paradoxical TB-IRIS and samples (n = 10) of patients who were TB-non-IRIS controls from cryopreservation for 8 hours, the samples were assessed for cell counts. Samples had a median cell count of 780 000 cells/mL with an interquartile range (IQR) of 84 000 – 1 800 000 cells/mL (**Figure** 7.9). Only 1/20 samples satisfied a predefined threshold (1 250 000 cells/mL) that allowed seeding of 250 cells/ 200 µL. However, the remaining samples had sufficient cell numbers that allowed for detection of cytokines by Luminex within the predefined limits of detection. (**Figure** 7.9).

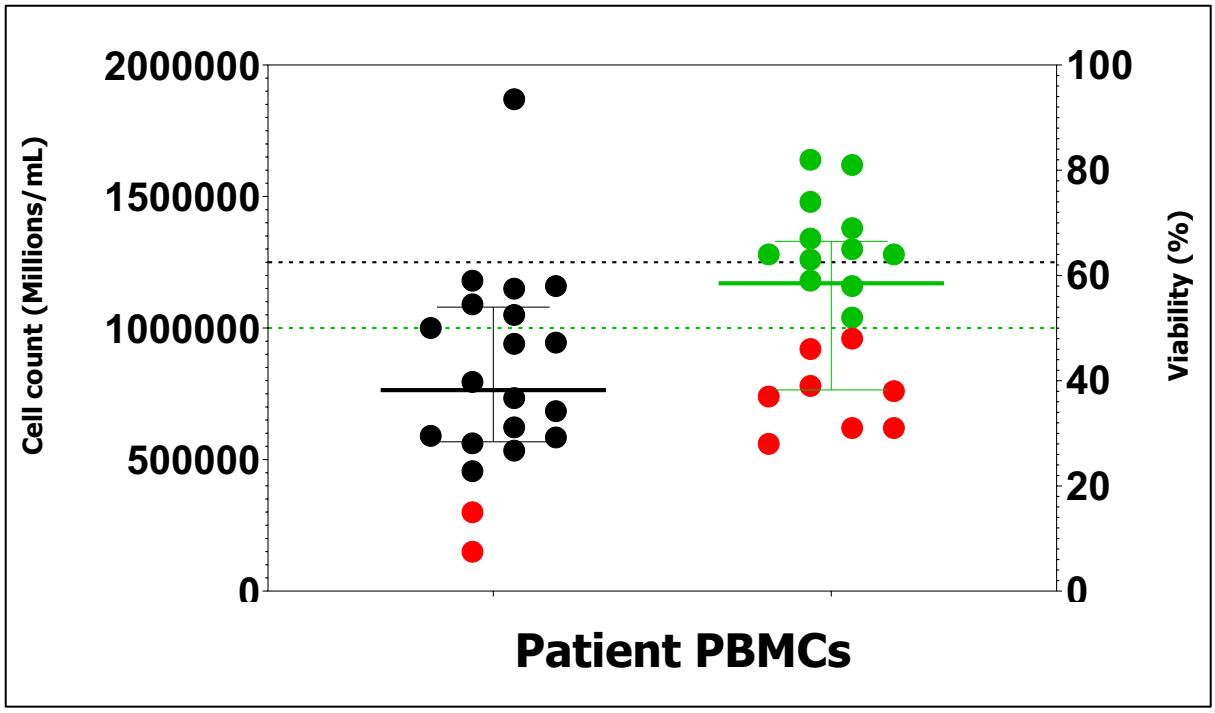

Figure 7.9. Determination of Pred-ART patient sample cell numbers and cell viability 8 hours after recovery from cryo-preservation*. Black closed circles depict patient sample cell numbers that fell within the pre-defined threshold that allow for multi-analyte detection by Luminex. The horizontal dotted black line depicts the ideal cell number threshold (1.25 million cells/mL). The horizontal dotted green line depicts the pre-defined viability threshold of 50%. The green closed circles represent samples with a viability above the 50% threshold while the red closed circles depict samples that fell below the cell number or cell viability thresholds.*

Furthermore, the viability of the samples was assessed. PBMC samples had a median viability of 59% and an IQR of 35-82% (**Figure** 7.9). A total of 11/ 20 samples met the predefined viability cut-off (dotted green line) of 50% (**Figure** 7.9).

Table 7 summarizes 15 cytokines measured by Luminex in samples collected at week 2 on ART from the placebo arm of patients enrolled in the Pred-ART intervention trial. Notably, candidate drugs significantly reduced various markers associated with inflammation when compared to the stimulation-only condition (**Table** 7). Moreover, anakinra and parthenolide significantly reduced IL-1 family of cytokines compared to prednisolone within groups (TB-IRIS or TB-non-IRIS)

Table 7. Summary of ex vivo drug treatment responses in the presence of heat killed Mycobacterium tuberculosis (H37Rv) antigen stimulation using peripheral blood mononuclear cells (PBMC) collected at the median time of paradoxical TB-IRIS onset (week 2) from patients derived from the placebo arm of the Pred-ART intervention trial. *Showing responses from participants who developed paradoxical TB-IRIS only.*

Measured analytes	Mtb stimulation	Anakinra treatment[a]	Parthenolide treatment[b]	Prednisolone treatment[c]	p-value
GM-CSF median (IQR)	1318(1157-1484)	452(318-544)	506(433-623)	581(448-759)	0.0001[a] 0.0001[b] 0.0001[c]
IL-6 median (IQR)	8022 (6943-8848)	1847 (1099-2667)	679.6(330.6-1826)	968.8(669-2655)	0.0001[a] 0.0001[b] 0.0001[c]
IL-10 median (IQR)	952.7 (904.1-1024)	248.8(182.1-409.4)	305.8(154.4-395.2)	276.1(230.2-380.3)	0.0001[a] 0.0001[b] 0.0001[c]
IL-12 median (IQR)	8290 (7925-8779)	2858 (970-3920)	963.2(731.4-1199)	2022(1438-4251)	0.0001[a] 0.0001[b] 0.0001[c]
IL-1α median (IQR)	1678 (1562-1873)	394.6(328.6-583.3)	524.3(381.6-571.1)	773.6(585.8-877.2)	0.0001[a] 0.0001[b] 0.0001[c]
IL-1β median (IQR)	7176 (6519-7851)	1156(878.1-1886)	694.2(322.1-1190)	1721(576.6-2502)	0.0001[a] 0.0001[b] 0.0001[c]
TNFα median (IQR)	4773 (4217-5452)	714.9(121.8-1890)	476.1(213.6-1663)	773.6(147.9-1703)	0.0001[a] 0.0001[b] 0.0001[c]
IFNγ median (IQR)	4815 (4405-5416)	380.2(300.2-500.4)	338.3(162-41.8)	408.7(263.2-480.5)	0.0001 [a] 0.0001[b] 0.0001[c]
IFNα	1000 (953.4-1033)	707.8(646.6-820.3)	425(370-507.6)	497(377.3-519.4)	0.0002 [a] 0.0001[b]

median (IQR)					0.0001[c]
IFNβ median (IQR)	2.9 (0.73-4.35)	0.86(0.40-3.2)	1.41(0.35-3.3)	0.81(0.40-2.1	0.08[a] 0.22[b] 0.06[c]
MMP1 median (IQR)	4931(4533-5650)	400.3(258.4-530.2)	285.7(217.4-445.7)	366.8(298.4-504.2)	0.0001[a] 0.0001[b] 0.0001[c]
MMP10 median (IQR)	3749(3528-4310)	184.1(123.8-336.6)	180.6(108.3-263.2)	202.3(116.9-350)	0.0001 [a] 0.0001[b] 0.0001[c]

A total of 15 inflammatory mediators which were previously shown to be upregulated at paradoxical TB-IRIS manifestation were measured in the presence of inflammasome targeting drugs (anakinra and parthenolide) relative to a corticosteroid used for the management of severe inflammatory feaures of paradoxical TB-IRIS (prednisolone). Interleukin (IL)-6, 8, 10, 12, 17, 18, receptor antagonist (RA), 1α, 1β, interferon (IFN-) α, β, γ, tumor necrosis factor (TNF-)α, and metalloproteinase (MMP) 9 and 10 were measured in a multiplexed fashion using samples derived from the placebo arm of the Pred-ART trial collected at week 2 on ART. Summary statistics are reported as medians and interquartile ranges (IQR) between the heat killed H37Rv stimulation and candidate drug treatment (anakinra and parthenolide, relative to prednisolone). Data for 3 cytokines (IL-1RA, IL-17 and IL-18) where some values from paradoxical TB-IRIS or TB-non-IRIS group were missing are not shown because the values were above the limit of detection for most patients. Superscript a, b and c represent the p-value between the stimulation only condition and anakinra, parthenolide and prednisolone respectively.

7.4.8 Exploratory analysis of Luminex measured TNF-α raw data from 20 Pred-ART samples.

Cell culture supernatants were analyzed for soluble markers associated with inflammation. A total of 6 conditions were tested for each of the 20 patient samples as illustrated in Figure 7.10A. Highlighted in Figure 7.10 is the raw data for the experiment for the first 4 patient samples indicating TNF-α induction by heat killed-H37Rv stimulation (black bar) and drug-mediated TNF-α reduction by anakinra (purple bar), parthenolide (orange bar) relative to prednisolone (blue bar) (**Figure 7.**10B). Furthermore, anakinra and parthenolide were effective

as reflected in the proportion of log-fold reduction by TB-IRIS stratification compared to prednisolone (**Figure 7.**10C). This was a common trend for the remaining 14 analytes. Notably, anakinra was particularly potent at reducing cytokines that signal via interleukin 1 receptor (IL-1R) such as IL-1α, and IL-1β.

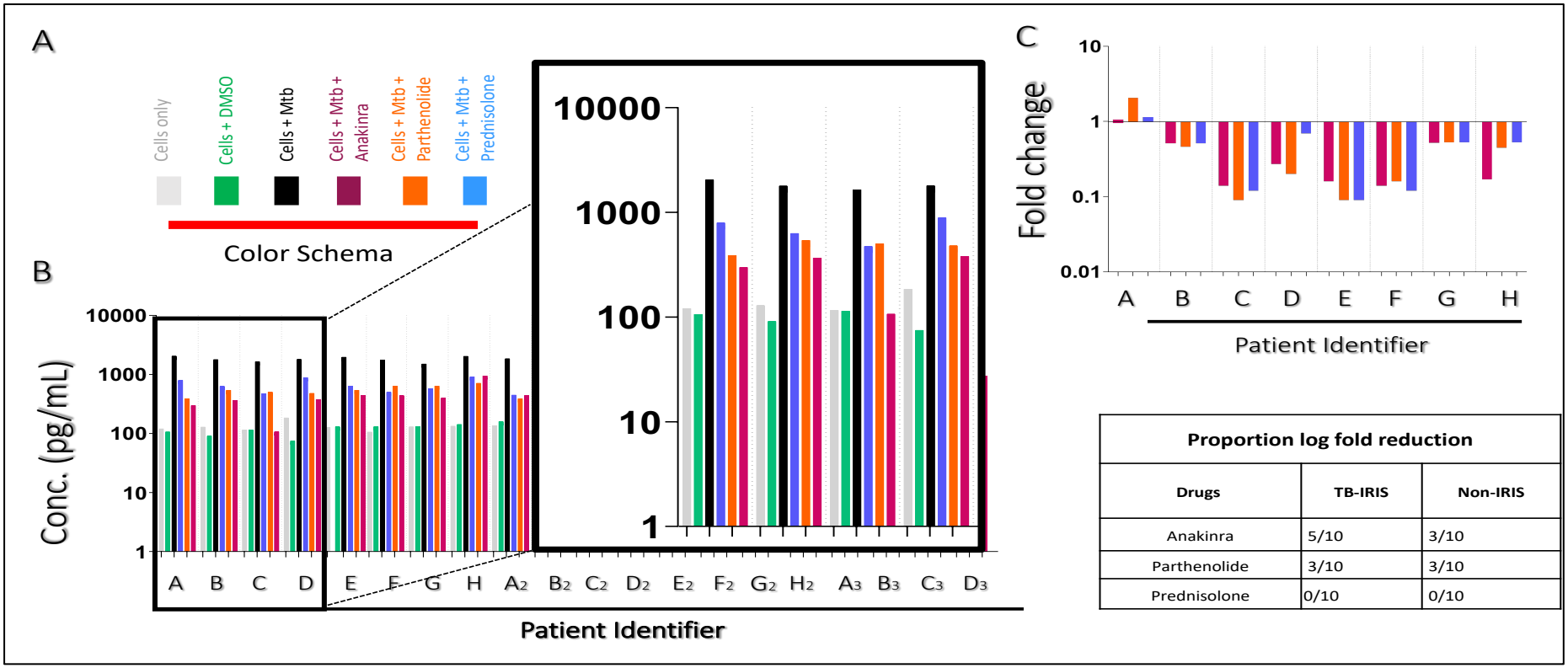

Proportion log fold reduction		
Drugs	**TB-IRIS**	**Non-IRIS**
Anakinra	5/10	3/10
Parthenolide	3/10	3/10
Prednisolone	0/10	0/10

Figure 7.10. Detection of TNF-α by Luminex in an ex vivo cell culture model of peripheral blood mononuclear cells (PBMC) stimulation and drug treatment in 20 patient samples from the placebo arm of the Pred-ART trial who either developed paradoxical TB-IRIS or did not at week 2 on antiretroviral therapy (ART). ***A,*** *Color scheme of the experimental conditions.* ***B,*** *Exvivo PBMC culture conditions including unstimulated control signifying background cytokine secretion (Grey), heat-killed Mycobacterium tuberculosis laboratory strain (H37Rv) stimulation condition-induces cytokine production (Black), dimethyl sulfoxide vehicle control (DMSO; Green) and treatment with 5 nM of anakinra (Purple), parthenolide (Orange) and prednisolone (Blue) respectively.* ***C,*** *Log2Fold change (LFC) values for 8/20 sample subset. LFC values were calculated by taking the difference between the black and the grey bars divided by the difference of the drug treatment in the presence of the*

stimulation and drug only condition. The table shows the proportion with at least one log10 fold reduction of TNF-α for the 3 drug candidates stratified by paradoxical TB-IRIS outcome

Figure 7.10 is consistent with the expected kinetics of the Mtb stimulation and drug treatment. The stimulation condition triggered at least one log-fold cytokine induction in most of the 15 analytes that were measured using the Luminex assay. Treatment with candidate drugs reduced the inflammatory mediators in all analytes.

7.4.9 Anakinra and parthenolide significantly reduces IL-1α compared to prednisolone in TB-IRIS patients at week 2 on ART.

Figure 7.11 illustrates the anti-inflammatory effect of the three drug candidates on the concentration levels of IL-1α in the presence of heat killed-H37Rv stimulation compared to the stimulation only condition. Anakinra significantly reduced IL-1α concentration levels compared to heat killed-H37Rv stimulation condition (median: 394.6; IQR: 328.6-583.3 and median: 1678.6; IQR: 1562-1873, respectively) in 20 patient samples taken at week 2 on ART (**Figure** 7.11A). Moreover, anakinra significantly reduced IL-1α concentration levels when compared to parthenolide (median: 524.3; IQR: 381.6-571.1) and prednisolone (median: 773.6; IQR: 585.8-877.2) (**Figure** 7.11A). In a cross-section analysis, patients were stratified by paradoxical TB-IRIS outcome. No differences were observed in the heat-killed-H37Rv stimulation condition between the two groups (**Figure** 7.11B). Similarly, none of the 3 drug candidates significantly reduced IL-1α concentration levels in samples of patients who developed paradoxical TB-IRIS compared to TB-non-IRIS controls (**Figure** 7.11B).

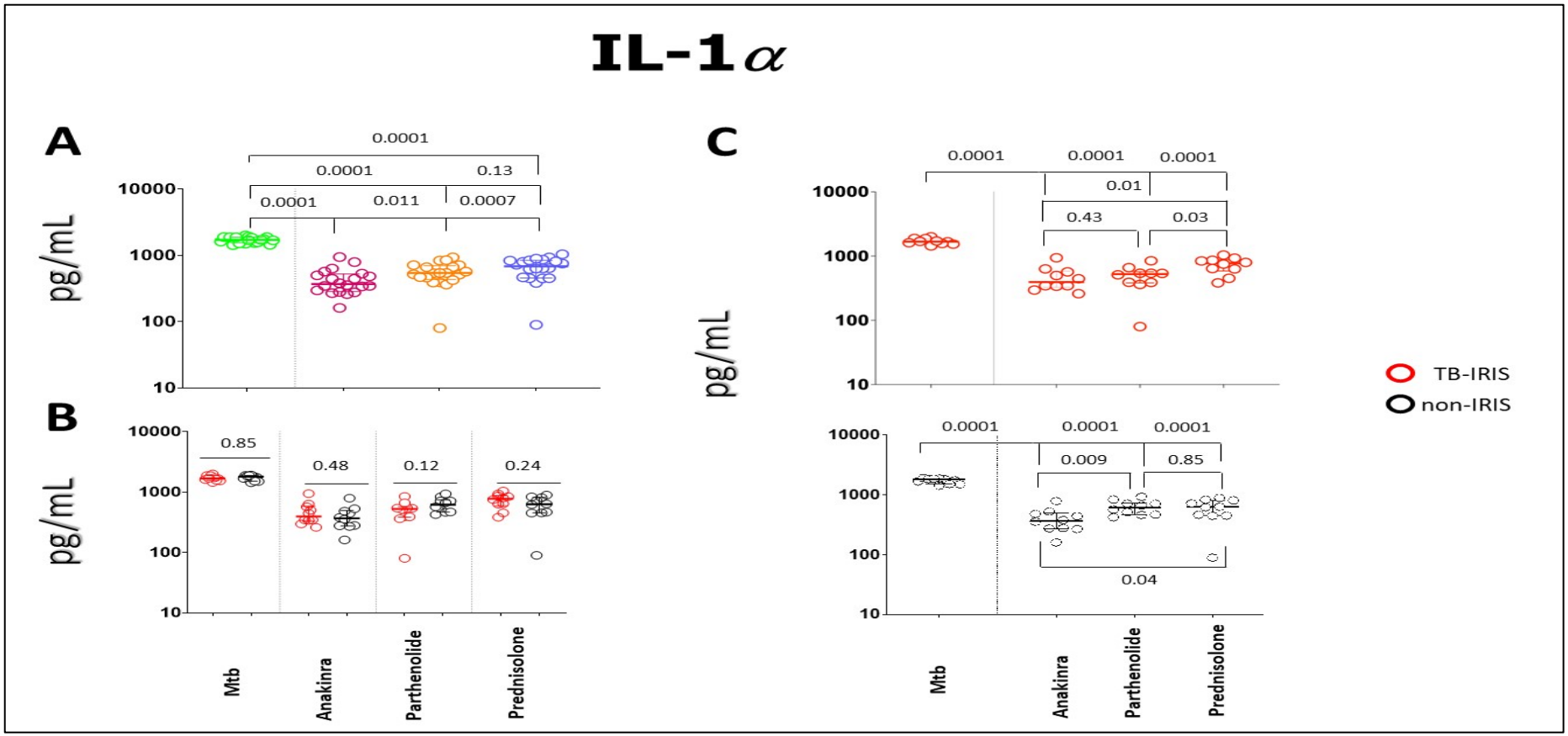

Figure 7.11. Drug mediated reduction of interleukin (IL)-1α in supernatants derived from exvivo cell culture model of heat killed H37Rv stimulation in a total of 20 placebo allocated patient samples from the Pred-ART intervention trial at week 2 on antiretroviral therapy A, *Significant reduction of IL-1α concentration levels by 5nM of anakinra, parthenolide and prednisolone respectively in presence of heat-killed H37Rv compared to the heat-killed H37Rv stimulation alone condition.* ***B,*** *Cross-section analysis of 5 nM of the three drug candidates in reducing IL-1α levels in patient samples stratified by paradoxical TB-IRIS outcome.* ***C,*** *Effect of 5 nM anakinra, parthenolide or prednisolone in reducing*

IL-1α in samples from patients who developed paradoxical TB-IRIS (red) and TB-non-IRIS controls (black) respectively. A p-value of 0.05 or less was considered statistically significant; ns = not significant

Finally, anakinra significantly reduced IL-1α compared to prednisolone in samples from patients who developed paradoxical TB-IRIS (**Figure** 7.11C). Similarly, anakinra significantly reduced IL-1α compared to parthenolide and prednisolone respectively in samples from TB-non-IRIS controls (**Figure** 7.11C). Notably, parthenolide significantly reduced IL-1α concentration levels compared to prednisolone in samples from patients who developed paradoxical TB-IRIS but not in samples from TB-non-IRIS controls (**Figure** 7.11C).

7.4.10 Parthenolide significantly reduced IL-1β compared to prednisolone in TB-IRIS patients at week 2 on ART.

The effect of reducing IL-1β induction through stimulation with heat-killed H37Rv and concomitant inhibition with 5 nM anakinra, parthenolide and prednisolone is illustrated in Figure 7.12. All three drug candidates respectively reduced IL-1β levels significantly compared to the heat killed-H37Rv stimulation condition in 20 placebo allocated patient samples from the Pred-ART intervention trial (**Figure** 7.12A). In a cross-section analysis, patients were stratified by paradoxical TB-IRIS outcome. IL-1β concentrations of the stimulation condition were similar in samples from patients who developed paradoxical TB-IRIS compared to those who did not (**Figure** 7.12B). Parthenolide but not anakinra or prednisolone significantly reduced IL-1β levels in samples from patients who developed paradoxical TB-IRIS compared to those who did not (**Figure** 7.12B).

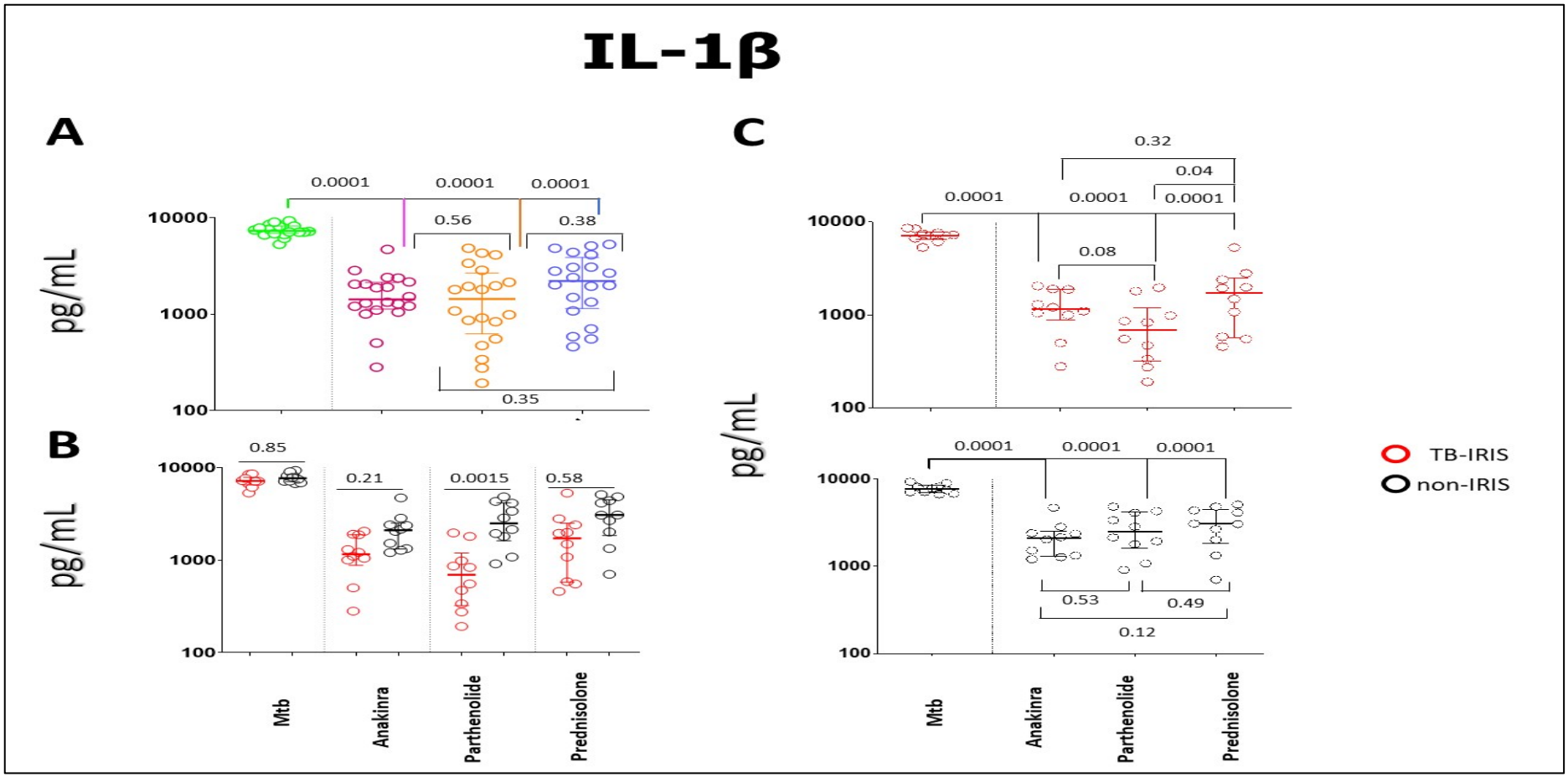

Figure 7.12. Drug mediated reduction of interleukin (IL)-1β in supernatants derived from ex vivo cell culture model of heat killed H37Rv stimulation in a total of 20 patient samples derived from the Pred-ART intervention trial at week 2 on antiretroviral therapy (ART). ***A,*** *Significant reduction of IL-1β concentrations by 5nM of anakinra, parthenolide and prednisolone respectively in the presence of heat-killed H37Rv compared to the heat-killed H37Rv stimulation alone condition.* ***B,*** *Effect of 5 nM of each drug candidate in reducing IL-1β levels in patient*

samples stratified by paradoxical TB-IRIS outcome. ***C,*** *The effect of 5 nM of each drug candidate in samples from patients who developed paradoxical TB-IRIS (red) and TB-non-IRIS controls (black) respectively. A p-value of 0.05 or less was considered statistically significant.*

Finally, parthenolide significantly reduced IL-1β levels (median: 859; IQR: 389.1-1062) compared to prednisolone (median: 1721; IQR: 760.6-2502) in samples from patients who developed paradoxical TB-IRIS (**Figure** 7.12C). There was no significant difference in the reduction of IL-1β between anakinra and parthenolide or prednisolone. Reductions in IL-1β concentrations were comparable between all three drug candidates in samples from TB-non-IRIS controls (**Figure** 7.12C).

7.4.11 Parthenolide and prednisolone significantly reduced caspase-1 compared to anakinra at week 2 on ART in samples from TB-IRIS patients.

The effect of reducing caspase-1 induction through stimulation with heat-killed H37Rv and concomitant inhibition with 5 nM anakinra, parthenolide and prednisolone is illustrated in Figure 7.13. Prednisolone (median = 0.58, IQR = 0.45-0.62) and parthenolide (median = 0.45, IQR = 0.40-0.58) respectively reduced caspase-1 levels significantly compared to the heat killed-H37Rv stimulation condition (median = 0.74, IQR = 0.62-0.85) in samples from 20 placebo allocated participants in the Pred-ART intervention trial (**Figure** 7.13A). In a cross-section analysis, patients were stratified by paradoxical TB-IRIS outcome. Caspase-1 concentrations in the heat-killed-H37RV stimulation condition were comparable between samples from patients who developed paradoxical TB-IRIS compared to TB-non-IRIS controls (**Figure** 7.13B). Similarly, there were no significant differences in the reduction of caspase-1 between all three drug candidates in samples from patients who developed paradoxical TB-IRIS and TB-non-IRIS controls (**Figure** 7.13B).

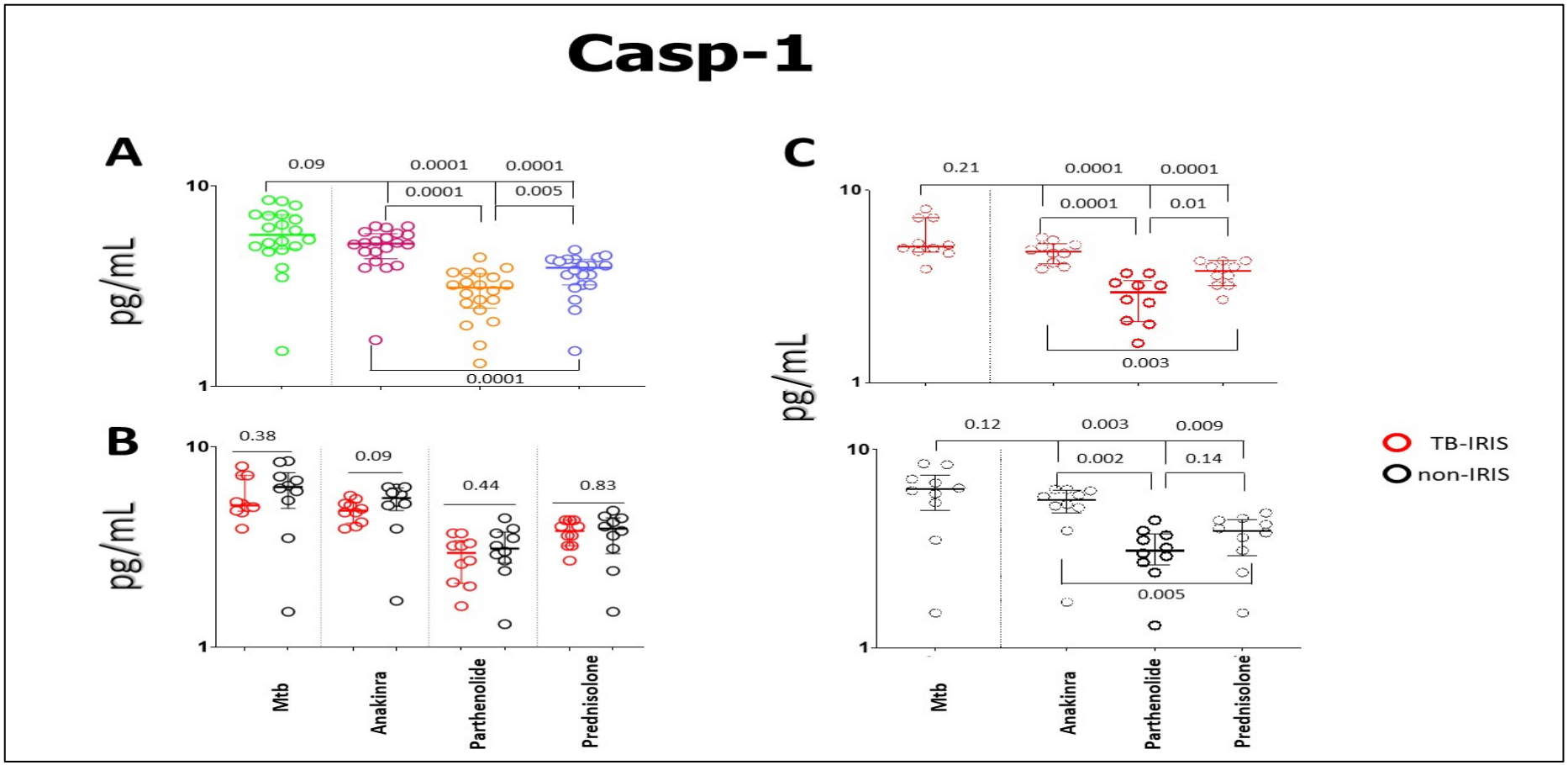

Figure 7.13. Drug mediated reduction of caspase-1 in supernatants derived from an ex vivo cell culture model of heat killed H37Rv stimulation in a total of 20 patient samples derived from the Pred-ART intervention trial at week 2 on antiretroviral therapy (ART)*. **A,** Significant reduction of caspase-1 by 5nM of parthenolide and prednisolone respectively but not anakinra in presence of heat-killed H37Rv compared to the heat-killed H37Rv stimulation condition. **B,** The effect of 5 nM of each drug candidate in reducing caspase-1 in patient samples stratified by paradoxical TB-*

IRIS outcome. ***C,*** *Effect of 5 nM of each drug candidate in reducing caspase-1 in samples from patients who developed paradoxical TB-IRIS (red) and TB-non-IRIS controls (black) respectively. A p-value of 0.05 or less was considered statistically significant*

Finally, parthenolide significantly reduced caspase-1 (median = 0.45, IQR = 0.27-0.51) compared to either anakinra (median = 0.7, IQR = 0.62-0.75) or prednisone (median = 0.50; IQR = 0.47-0.62) in samples from patients who developed paradoxical TB-IRIS (**Figure** 7.13C). Parthenolide significantly reduced caspase-1 (median = 0.46, IQR = 0.37-0.51) compared to anakinra (median =0.72, IQR = [0.62- 0.80) but not prednisolone in samples from TB-non-IRIS controls (**Figure** 7.13C). Prednisolone significantly reduced caspase-1 (median =0.51, IQR = 0.35-0.6) in samples from TB-non-IRIS controls compared to anakinra treated samples (median = 0.72, IQR = 0.62- 0.80) (**Figure** 7.13C).

7.4.12 All three drug candidates significantly reduced plasma levels of IL-6 in all patients at week 2 on ART, but parthenolide was more effective in reducing IL-6 concentrations in samples of patients that developed paradoxical TB-IRIS.

IL-6 is a critical marker of inflammation and the capacity of the candidate drugs to reduce its secretion in supernatants was investigated. Figure 7.14 illustrates concentrations of IL-6 following stimulation of 20 placebo allocated patient PBMC with heat-killed-H37Rv and concomitant inhibition with 5 nM of either anakinra, pathernolide or prednisolone. All three drug candidates significantly reduced IL-6 concentration levels compared to the heat-killed-H37Rv stimulation condition (**Figure** 7.14A). The magnitude of IL-6 reduction by the three drug candidates was comparable (**Figure** 7.14A). In a cross-section analysis, patients were stratified by paradoxical TB-IRIS outcome. IL-6 levels in the heat-killed-H37RV stimulation condition were comparable between samples from patients who developed paradoxical TB-IRIS compared to TB-non-IRIS controls (**Figure** 7.14B). Similarly, IL-6 levels were comparable in the presence of the three drug candidates in samples from patients who developed paradoxical TB-IRIS compared to those who did not (**Figure** 7.14B).

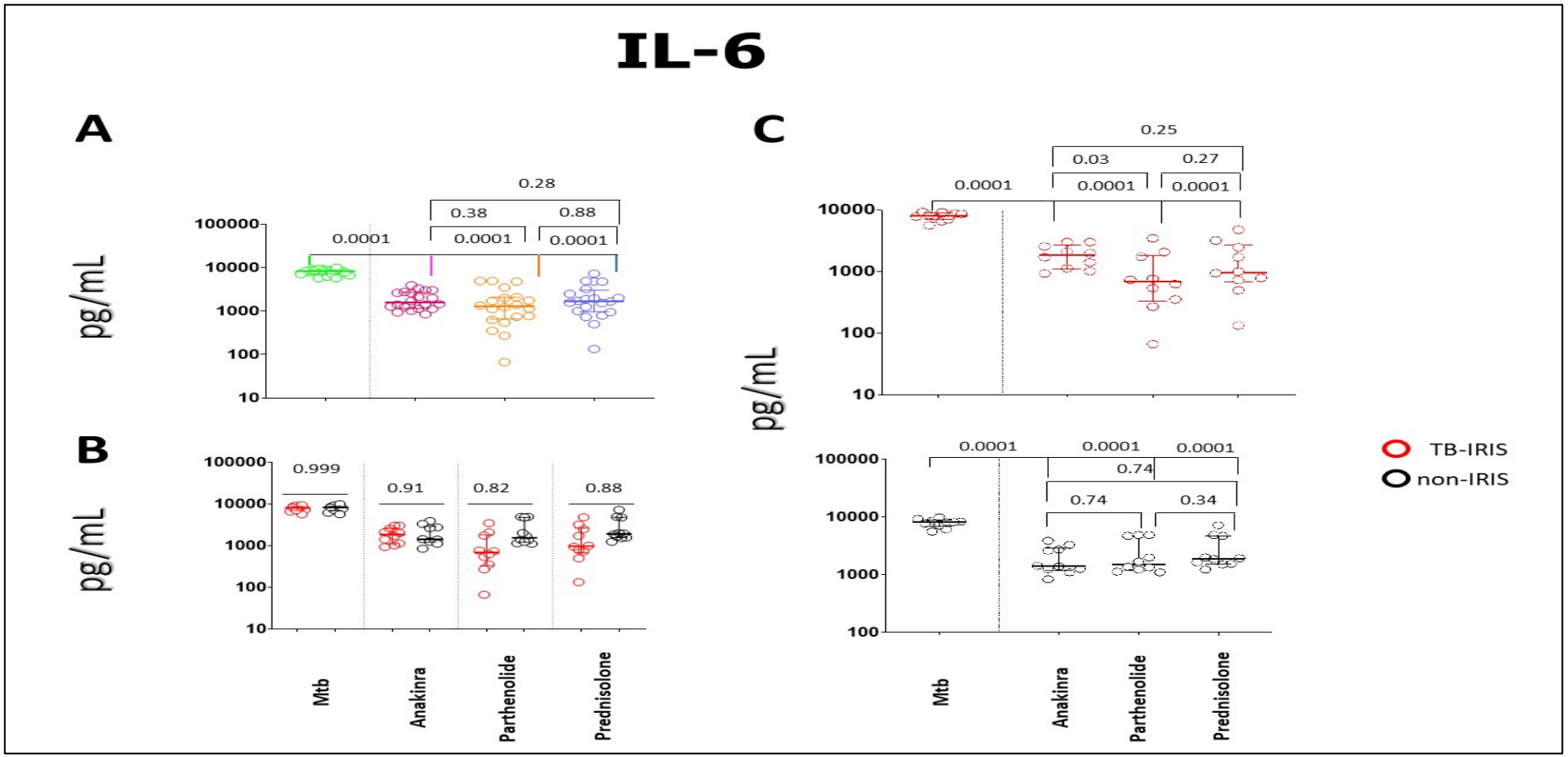

Figure 7.14. Drug mediated reduction of interleukin (IL)-6 in supernatants derived from an ex vivo cell culture model of heat killed H37Rv stimulation in a total of 20 placebo allocated patient samples derived from the Pred-ART intervention trial at week 2 on antiretroviral therapy (ART). ***A,*** *Significant reduction of IL-6 by 5nM of anakinra, parthenolide or prednisolone in presence of heat-killed H37Rv compared to the heat-killed H37Rv stimulation condition.* ***B,*** *The effect of 5 nM of each drug candidate in reducing IL-6 in patient samples stratified by paradoxical TB-*

IRIS outcome. ***C,*** *Effect of 5 nM of each drug candidates in sample from patients who developed paradoxical TB-IRIS (red) and TB-non-IRIS controls (black) respectively. A p-value of 0.05 or less was considered statistically significant*

Finally, parthenolide significantly reduced IL-6 (median:679.6; IQR = 330.6-1826) compared to anakinra (median:1847; IQR = 1099.6-2667) in samples from patients who developed paradoxical TB-IRIS (**Figure** 7.14C). There was no significant difference in the reduction of IL-6 between parthenolide and prednisolone. Similarly, there was no significant difference in the reduction of IL-6 between anakinra and prednisolone in samples collected from patients who developed paradoxical TB-IRIS (**Figure** 7.14C). The reduction in IL-6 concentrations was comparable between all three drug candidates in samples from TB-non-IRIS controls at week 2 on ART (**Figure** 7.14C).

7.5 Discussion

In this sub-study, all three drug candidates significantly reduced various markers of inflammation. While anakinra was effective in reducing IL-1 family of cytokines, parthenolide had much broader anti-inflammatory activity, reducing several markers of inflammation including IL-6.

Inflammasome dependent maturation of IL-1 cytokines is an important feature of many inflammatory disorders and thus an attractive target for therapeutic intervention. Several studies have shown that directly inhibiting the inflammasome by blocking its assembly or by regulating its phosphorylation and/or ubiquitination is the most effective strategy. The relevance of IL-1 cytokines and receptors as modulators of inflammation cannot be overstated and has been extensively documented [529, 531, 552, 554, 570]. Therefore, this study evaluated the capacity of inflammasome-related targets relative to prednisolone, an anti-inflammatory corticosteroid that is commonly used in clinical practice, to reduce pro-inflammatory cytokines in response to stimulation with heat-killed-H37Rv in an *ex vivo* culture model of PBMC. The choice of measured cytokines included primarily IL-1 ligands and other upregulated cytokines at the median time of TB-IRIS manifestation.

Although all 3 candidate drugs (anakinra, parthenolide and prednisolone) significantly reduced pro-inflammatory cytokines compared to the untreated controls, the lack of statistical significance between inflammasome-related targets (anakinra and parthenolide) relative to the benchmark (prednisolone) in the TB-ART samples (used for piloting optimized experimental conditions) can be attributed to several factors. First, the number of patient samples used (n = 8) to pilot the assay were limited and thus reduced statistical power. Secondly, the median time of paradoxical TB-IRIS manifestation in the TB-ART cohort was 2 weeks on ART; the patient samples selected for piloting optimized experimental condition were taken at week 1 on ART (due to limited sample availability), which for half of the patients was prior to the onset of paradoxical TB-IRIS.

The anti-inflammatory effect of the candidate drugs was tested in an expanded sample size of 20 patient samples with and without paradoxical TB-IRIS from the Pred-ART intervention trial. The capacity of anakinra, parthenolide and prednisolone (the candidate drugs) to reduce pro-inflammatory cytokines in all patients was successfully investigated. Candidate drugs reduced the

measured pro-inflammatory analytes when compared to the heat killed Mtb-H37Rv stimulation control, without exception. However, a similar comparison between the candidate drugs did not reveal significant differences in a cross-sectional analysis for several analytes except for IL-1β. This finding was not unexpected presumably because, the drugs target the same signaling cascades or pathway in both TB-IRIS and TB-non-IRIS patients.

The significant reduction of IL-1β in a cross-sectional comparison by parthenolide compared to anakinra and prednisolone was surprising. The margin of IL-1β reduction was notably variable among patients who developed paradoxical TB-IRIS whose samples were treated with parthenolide. Therefore, the lower IL-1β outlier values may be contributing to a significance of the p-value.

Notably, both anakinra and parthenolide were effective at reducing several of the assessed pro-inflammatory analytes that mediate inflammation. Several explanations can be raised to account for the potency of both parthenolide and anakinra as anti-inflammatory agents in the *ex vivo* cell culture experiments. Parthenolide belong to the germacranolide class of therapeutics. It is a sequiterpene lactone that occurs naturally in herbs that are indigenous to specific geographic regions [578]. Parthenolide has a documented potent anti-inflammatory and anticancer effects [579]. Parthenolide targets multiple steps in the inflammatory cascade including the inhibition of multiple steps that are integral to the maturation of the inflammasome. Two major mechanisms have been described for parthenolide. First, parthenolide inhibits the activation of IκB kinase which regulates the activation of the NF-κB transcription factor [580]. The NF-κB is a transcription factor that mediates the process of inflammation by inducing the expression of IL-1 cytokines, TNF-α, and IL-6 which were reported to be significantly upregulated in patients with paradoxical TB-IRIS relative to controls [162]. Parthenolide was shown to directly bind to NF-κβ, thereby preventing its interaction with DNA. This results in the inhibition of the NF-κβ pathway in a dose dependent manner [580]. In a mouse model of dextran sulfate sodium induced colitis, parthenolide was shown to block the activation of the NLRP3 inflammasome by inhibiting the upstream priming signal thereby preventing its assembly [581]. Its mechanism of action was shown to target the ATPase activity of the nucleotide-binding oligomerization domain which facilitates oligomerization of the inflammasome through CARD-CARD interactions [581, 582].

Additionally, some findings that contrast our findings relate to analytes that are not regulated by parthenolide or anakinra. Liu and colleagues recently characterized the mechanism of action underlying parthenolide using mouse bone marrow derived macrophages (BMDM) and THP-1 cell line. Treatment of both BMDM and THP-1 cultures with parthenolide following lipopolysaccharide (LPS) stimulation had no effect on IL-6 and TNFα reduction; whereas the same significantly reduced IL-1β, caspase 1 and the NLRP3 scaffold protein [581]. Notably, IL-6 and TNF-α are under the transcriptional regulation of NF-kβ and not the inflammasome. Preincubation with parthenolide followed by stimulation with LPS was associated with a dose dependent reduction in the secretion of IL-1β and the NLRP3 scaffold protein; while preincubation with LPS followed by parthenolide treatment was not associated with any changes [581]. These data suggests that pretreatment with parthenolide regulates NF-kβ activity while post treatment with parthenolide does not. It is noteworthy that these experiments were conducted in mice and may not be representative of what happens in humans. Moreover, the authors did not repeat the parthenolide pretreatment (which is similar to our concomitant stimulation and treatment experimental design) experiments measuring IL-6 and TNF-α for which they saw no effect of parthenolide.

On the other hand, anakinra is an FDA approved biologic with a demonstrable anti-inflammatory activity [583, 584] and routinely used in patients with rheumatoid arthritis [50, 585-587]. Other studies have also corroborated its anti-inflammatory capacity in cases of severe SARS-CoV2 disease which is characterized by hyperinflammation [588-590]. Moreover, the safety of anakinra has also been established in humans [35, 591]. Anakinra is a competitive inhibitor that acts upstream of the release of mature IL-1 cytokines [592]. It acts by binding the IL-1 receptor thereby antagonizing IL-1α and/or IL-1β signaling which drives the inflammatory cascade [593]. The described mechanism of action is consistent with the observations made in this study where anakinra was most effective in inhibiting cytokines that signal via the IL-1 receptor and displayed poor inhibitory capacity in reducing other cytokines such as IL-6 and TNF-α that do not signal via the IL-1receptor. IL-1 family of cytokines follow an autocrine paradigm of signaling, resulting in a positive feedback loop. Therefore inhibiting the IL-1RI breaks the feedback mechanism resulting in a reduction of their soluble secretion [584, 594-596].

Therefore, both anakinra and parthenolide were comparable in reducing IL-1 cytokines compared to prednisolone in these experiments. Parthenolide was potent in reducing other cytokines such as IL-6, TNF-α which are induced by IL-1α. Future studies could test the anti-inflammatory capacity of other non-immunosuppressive drugs that were not investigated in this study. Collecting cell pellets for RNA sequencing in similar experiments and performing pathway analysis could elucidate the mechanisms of action of these drugs

7.6 Limitations

A limited number of samples were tested for the pilot study (n = 8). Additionally, half of the samples from patients who developed paradoxical TB-IRIS (n = 4) were collected at week 1 on ART, while the onset of inflammatory reactions were recorded at a median of week 2 on ART. Although several studies assessing the *in vitro* activity and efficacy of parthenolide against several inflammatory disorders, it has not been tested in humans. Therefore, its thorough pharmacokinetic and pharmacodynamic characterization is required to receive FDA approval for use in clinical settings, which makes Anakinra a more attractive option for clinical evaluation.

The study design involved the use of *ex vivo* cell culture model to assess the activity of several drugs that target the inflammasome. This is a reductive model that does not factor into consideration, the interaction of different cell types that may be present in a biological system. Therefore, these findings may not truly reflect the pharmacodynamics of the tested drugs in a biological system. Additionally, specific activators of the inflammasome were not used, instead, Mtb cell lysate containing various antigens and inflammatory lipids to activate both canonical and non-canonical inflammasomes was used. Lastly, the inflammasome is robustly induced in neutrophils, but these assays were conducted in PBMC.

7.7 Conclusions

Parthenolide is potent at reducing pro-inflammatory cytokines and its *ex vivo* activity suggests that it is also potent at inhibiting the inflammasome. Although it was associated with high variability between patients, anakinra was effective at reducing downstream ligands of the IL-1 receptor, namely, IL-1α and IL-1β which are known drivers of inflammation. Its availability in the market makes it a desirable candidate for repurposing for the treatment of IRIS-related complications or for targeted prevention. However, robust evidence that these interventions might be efficacious in the context of paradoxical TB-IRIS, would have to be generated by conducting a RCT to assess the efficacy of these inhibitors.

Chapter 8 summary: Discussion, conclusions, and future direction.

This chapter provides a chapter-by-chapter summary, discussion of the original work and highlights the significance of the findings in the context of existing literature. Additionally, the chapter summarizes all the work with a conclusion section and ends with recommendations for future work to build on the current findings.

8. Background

This thesis comprises seven chapters that can be summarized into two overarching themes:

1. The involvement of neutrophils, functional *Mycobacterium tuberculosis* (Mtb) specific activated CD4 lymphocytes, as well as aberrant inflammasome activation as mediators of the immunopathogenesis of paradoxical TB-IRIS.

2. The demonstration of the *in vitro* efficacy of inflammasome related inhibitors in modulating the hyperinflammatory state that characterizes paradoxical TB-IRIS.

The section below provides a chapter-by-chapter summary of the main findings and their significance.

8.1 Phenotypic characterization of Mtb-specific CD4 T cells in people who develop paradoxical TB-IRIS.

A hallmark of paradoxical TB-IRIS includes the partial reconstitution of Mtb-specific CD4 T cells within 3 months of initiating antiretroviral therapy (ART). For a while, bulk CD4 T cell reconstitution after the initiation of ART was postulated to be the cause of paradoxical TB-IRIS; until it was shown that similar reconstitution of the CD4 compartment occurred in some individuals matched for age and CD4 count who did not develop paradoxical TB-IRIS [37]. In chapter 4, flow cytometry was used to phenotype CD4 lymphocytes in peripheral blood mononuclear cells (PBMC) in a murine model of IRIS and patients living with HIV-associated TB who developed paradoxical TB-IRIS compared to those who did not.

Work by Hsu and colleagues characterized reconstituting *Mycobacterium avium* (MAC)-specific interferon (IFNγ+) producing CD4 T cells, reported significantly higher frequencies of cells expressing Eomesodermin (Eomes) in HIV-1 immunosuppressed patients with MAC coinfection, who later developed MAC-IRIS compared to HIV infected individuals who did not develop MAC-IRIS [40]. Eomes is a Tbox transcription factor that is mainly expressed in cytotoxic lymphocytes such as antigen specific CD8 T cells, CD8 T cells with memory phenotype and natural killer cells [308]. The potential significance of this is that reconstituting MAC-specific CD4 T cell responses may have altered transcription factor profiles that imbues them with the potential to be cytotoxic; thus, implicating them in MAC-IRIS mediated immunopathology. In this thesis, this hypothesis

was explored in the context of paradoxical TB-IRIS. In experiments conducted by collaborators, a murine model of MAC-IRIS was used for deep phenotypic analysis of *Mycobacterium avium*-specific CD4 T cells. In experiments conducted in Cape Town, peripheral blood mononuclear cells (PBMC) from human participants who were enrolled in the TBART observational study that integrated anti-tuberculosis therapy and ART were used to validate the findings from the study by Hsu and colleagues and the murine experiments. Eomes knockout (KO) mice were associated with increased survival following adoptive transfer of wildtype CD4 T cells compared to littermate mice. This implied that the presence of Eomes conferred pathogenicity in wildtype mice and corroborated the findings of Hsu and colleagues. These findings were further investigated in human PBMC from patients enrolled in an observational study that evaluated adverse events of integrated antituberculosis therapy and ART in patients admitted to a TB hospital.

Phenotypic analysis of CD4 lymphocytes responses revealed that reconstituting Mtb-specific CD4 T cells were functional with the ability to produce multiple cytokines such as IFN-γ and TNF-α. The relative frequency of Mtb-specific, IFN-γ producing CD4 lymphocytes was significantly higher in patients who developed paradoxical TB-IRIS compared to those who did not, at the median onset of clinical symptoms.

Transcription factor profiling of Mtb-specific IFN-γ producing CD4 T cells in patients who developed paradoxical TB-IRIS revealed that they expressed Eomes, something that had not been shown previously. However, the relative frequency of Mtb-specific IFN-γ+, Eomes+ CD4 lymphocytes were comparable between patients who developed paradoxical TB-IRIS and those who did not. This contrasted with the findings of Hsu and colleagues as well as the observations in mice. Conversely, bulk relative frequencies of Eomes+ CD4 T cells were significantly higher in patients who developed paradoxical TB-IRIS compared to those who did not at week 2 on ART.

One of the key findings included the observation that, Mtb-specific, IFN-γ producing CD4 T cell responses from patients who developed paradoxical TB-IRIS highly expressed the marker of immune activation called HLADR. The relative frequency of Mtb-specific, IFN-γ+ HLADR+ CD4 lymphocytes were significantly higher in samples from patients who developed paradoxical TB-IRIS compared to those who did not at week 2 on ART.

Lastly, relative frequency of Mtb-specific, IFNγ+ granzyme B+ CD4 T cell responses that co-express Eomes and Tbet were significantly higher in patients that developed paradoxical TB-IRIS compared to those who did not at week 2 on ART. The significance of this is, IFN-γ producing, Mtb-specific CD4 lymphocytes that co-express Eomes and Tbet might have more cytotoxic potential in patients who develop paradoxical TB-IRIS at week 2 on ART than those who do not.

High Eomes expression in functional Mtb-specific CD4 lymphocytes was a novel finding in the context of paradoxical TB-IRIS. However, contradicting observations regarding the relative frequencies of Eomes expressing pathogen-specific IFN-γ producing CD4 lymphocytes between the murine model of IRIS, patients that develop paradoxical MAC-IRIS and paradoxical TB-IRIS, may reflect different regulation of pathogen-specific CD4 T cells in underlying opportunistic pathogens causing IRIS manifestations. Hyper immune activation in patients who develop paradoxical TB-IRIS is likely due to high antigen load which predisposes individuals to developing IRIS. These findings suggests that greater immune activation and CD4 T cell reconstitution in individuals who develop paradoxical TB-IRIS are important aspects of TB-IRIS pathology but may not be the sole mediators underpinning the pathogenesis of paradoxical TB-IRIS.

8.2 Functional transcriptomics in samples obtained at week 0, 2 and 12 on ART in participants who developed paradoxical TB-IRIS

Gene expression studies have greatly advanced the understanding of paradoxical TB-IRIS immunopathogenesis. Chapter 5 reported the application of bulk RNA-sequencing workflows in whole blood samples to identify differentially expressed genes and summarize them into biological pathways.

Using biological samples from the PredART interventional trial, chapter 5 investigated the potential biological pathways and cellular mechanisms that underlie the pathogenesis of paradoxical TB-IRIS using unbiased hypothesis generating approaches.

Ribonucleic acid (RNA) extracted from whole blood obtained from consenting participants that were enrolled in the PredART intervention trial who either developed paradoxical TB-IRIS or not, were prepared for RNA sequencing to study differences in global gene expression profiles and mine new insights about the pathogenesis of paradoxical TB-IRIS.

The prospective design of the PredART trial was exploited by conducting cross-sectional and longitudinal analysis of the RNA-seq data to characterize the biosignature of patients who developed paradoxical TB-IRIS and those who did not at week 0, 2 and 12.

Patients who were allocated either placebo or prednisone at week 0 who later developed paradoxical TB-IRIS were characterized by the significant upregulation of transcripts encoding neutrophil derived antimicrobial peptides and biological pathways suggestive of prevailing metabolic dysfunction; while transcripts that were significantly downregulated included those encoding cellular transcripts of the cytoskeleton which modulates biological processes involving cellular proliferation, maturation, and migration. These findings imply that patients that are likely to develop paradoxical TB-IRIS are characterized by severe inflammation, and impaired innate immune cell function including proliferation, mobility and signaling. No prior studies exist that have defined the cellular and molecular features in patients that predispose to developing paradoxical TB-IRIS.

Characterization of gene expression profiles was carried out in patients who were allocated either placebo or prophylactic prednisone who subsequently developed paradoxical TB-IRIS and those who did not. The onset of paradoxical TB-IRIS was variable with a median of 14 days. Notably, some patients who were allocated placebo, who developed paradoxical TB-IRIS, received prednisone for syndromic management - typically after the 14-day time point. The latter were characterized by the upregulation of innate immune signaling pathways. The most significantly enriched biological pathway in patients who developed paradoxical TB-IRIS compared to those who did not, was neutrophil degranulation.

The second most enriched biological pathway in patients who developed paradoxical TB-IRIS compared to those who did not at week 2 on ART was the innate immune pathway. The transcripts associated with this pathway included 800 transcripts representing all cellular subsets of the innate immunity, their surface and soluble receptors as well transcription factors, cytokines, and morphogens. Transcripts of the NLRC4 inflammasome, gasdermin D, Caspase-1 and IL-1β were significantly upregulated in patients who developed paradoxical TB-IRIS compared to those who did not, at week 2 on ART.

Other biological pathways that were significantly upregulated in samples from patients that developed paradoxical TB-IRIS compared to those who did not at week 2 on ART included interleukin 1 signaling, type I and II interferon signaling [162].

Similarly, pathway analysis longitudinally on ART in samples of patients that developed paradoxical TB-IRIS revealed the same biological processes including neutrophil degranulation, IL-1 cytokine signaling and type I as well as type II signaling and pyroptosis at week 2 on ART compared to week 0 prior to the initiation of ART. These findings indicated the involvement of the inflammasome as the underlying mechanism for severe inflammation in patients that developed paradoxical TB-IRIS. Pathways that were significantly downregulated included heme biosynthesis and the shuttling of respiratory gases such as oxygen and carbon dioxide. This reflects the potential restoration of homeostasis at a biochemical level.

Pathway analysis in TB-non-IRIS controls revealed several biological processes that were significantly upregulated in samples from these patients including but not limited to epigenetic modulation of gene expression, collagen biosynthesis-a major component of the extracellular matrix and the remodeling of the cytoskeleton which modulates biological processes including cell proliferation, motility and immune responses. Significantly downregulated biological pathways included interferon stimulated genes responses and antiviral responses.

No differentially abundant transcripts were observed at week 12 on ART between participants who developed paradoxical TB-IRIS and those who did not. The comparable pattern in gene expression suggests disease resolution in patients that developed paradoxical worsening of TB. However, since a proportion of patients received prednisone as a treatment at the onset of paradoxical TB-IRIS, it is challenging to conclude whether the resolution of TB-IRIS symptoms were a result of prednisone treatment or spontaneous resolution.

Similarly, no differentially expressed transcripts were identified in samples from patients who developed paradoxical TB-IRIS compared to those who did not, at week 2 on ART who were allocated prophylactic prednisone at the initiation of ART.

Prednisone prophylaxis had an effect of normalizing the gene expression signature associated with paradoxical TB-IRIS in patients who were allocated prednisone at week 0. Like other

glucocorticoids, prednisone is a pleiotropic molecule that has systemic effects with potent anti-inflammatory activity in patients who previously developed paradoxical TB-IRIS [33].

The involvement of neutrophils in IRIS related pathologies is not novel and was previously described in patients with paradoxical tuberculous meningitis IRIS, which is a severe form paradoxical TB-IRIS involving the central nervous system [241]. Neutrophils are the most abundant immune cells in the body and are the first line of defense against noxious agents. Their improper accumulation or dysfunction has been long associated with several inflammatory diseases [376, 382, 482]. The exact mechanisms involving neutrophils in the immunopathogenesis of paradoxical TB-IRIS points towards two potential mechanisms as suggested by the gene expression findings. First the process of neutrophil degranulation which involves pathogen clearance mediated by cytotoxic cargo residing in neutrophil granulytic bags [380, 517]. These contain preformed biotoxic enzymes, and antimicrobial peptides which when mobilized in excess, can result in collateral tissue damage. This is one plausible mechanism as it was shown in chapter 6 that at the time of symptom manifestation, people who develop paradoxical TB-IRIS have higher neutrophil counts and soluble markers of degranulation compared to those who do not develop TB-IRIS.

The second potential mechanism that is inherent in neutrophils involves the inflammasome. The inflammasome is an intracellular pattern recognition receptor that is sensitive to danger, chromatin, and pathogen associated molecular patterns. It functions to activate caspases and gasdermin D which leads to the maturation of the interleukin 1 family of cytokines as well as mediating pyroptosis which is a necrotic cell death. Inflammasome markers were also enriched in patients who developed paradoxical TB-IRIS at week 2 on ART. The involvement of gene modules that are central to the activation and maturation of the inflammasome such as pyroptosis and IL-1β among others have been extensively described and experimentally validated in other studies [15, 25, 30-32, 177, 379]. The abundance of these transcripts in samples from patients who developed paradoxical TB-IRIS compared to those who did not at week 2 on ART potentially highlights the significance the inflammasome, as a foundational mechanism in the pathogenesis of paradoxical TB-IRIS. Mechanistically, the inflammasome is primed and activated by danger and pathogen associated molecular patterns. A mature inflammasome, activates caspases which in turn activate IL-1 family of cytokines including IL-1β and IL-1α which are potent modulators of inflammation.

Many studies have demonstrated that soluble cytokines of the interleukin 1 family which are potent modulators of inflammation are significantly higher in patients who developed paradoxical TB-IRIS compared to those who do not, at the median time of TB-IRIS onset [162]. Caspases additionally activate gasdermin D which facilitates the necrotic rupture of cells which release viable *M. tuberculosis* and danger associated molecular patterns. This may create a cyclic loop that amplifies the inflammatory cascade that characterizes paradoxical TB-IRIS [539].

8.3 Evaluating absolute neutrophil counts and soluble markers of neutrophils in plasma samples collected at week 0 and 2 on ART, from patients who developed paradoxical TB-IRIS and those who did not.

Findings from chapter 5 suggested that neutrophil degranulation and aberrant intracellular signaling were central to the pathogenesis of paradoxical TB-IRIS. Chapter 6 investigated this further by evaluating the association between absolute neutrophil counts (ANC) collected at week 0, 2 and 12 on ART and paradoxical TB-IRIS. Moreover, the association between neutrophil degranulation and paradoxical TB-IRIS was tested by measuring plasma soluble markers associated with or specific to neutrophils at week 0 and 2 on ART. Absolute neutrophil counts were significantly higher in patients who developed paradoxical TB-IRIS compared to those who did not, at week 2 on ART. Soluble markers of neutrophils including human neutrophil peptide1-3, neutrophil elastase, and myeloperoxidase were measured by enzyme linked immunosorbent assay (ELISA) and were significantly higher in samples from patients who developed paradoxical TB-IRIS compared to those who did not, at week 2 on ART. Additionally, absolute neutrophil counts were significantly correlated with the concentrations of plasma soluble neutrophil mediators.

8.4 Investigating the anti-inflammatory capacity of inflammasome-related targets in an ex vivo cell culture model using samples from patients with paradoxical TB-IRIS at week 2 on ART

Gene expression data in chapter 5, as well as findings from other studies suggest that the aberrant expression of canonical and non-canonical inflammasomes may specifically underpin the

pathogenesis of paradoxical TB-IRIS [25, 30]. Chapter 7 detailed the evaluation of several inflammasome related drugs and their capacity to reduce known molecular markers of inflammation.

A total of 8 inflammasome related inhibitors were evaluated, 2 of which had significantly low dose dependent responses (anakinra, parthenolide) were evaluated further for the capacity to reduce known markers of inflammation in an *ex vivo* cell culture model and benchmarked against the standard of care (prednisolone). Both Anakinra and Parthenolide significantly reduced IL1 family of cytokines compared to prednisolone. IL1 cytokines are known modulators of inflammation and their activation depend on the action of a mature inflammasome. Additionally, parthenolide was effective in reducing other cytokines (other than IL1 cytokines) that are associated with hyper inflammation in paradoxical TB-IRIS compared to prednisolone.

While parthenolide is potent and shows remarkable inhibition in our *ex vivo* cell culture model, it has not been evaluated in clinical trials. Anakinra on the other hand is a biologic that has been extensively tested across different inflammatory conditions and has been approved by the Food and Drug Administration. This makes it a suitable anti-inflammatory candidate, with a known safety profile, that could potentially be repurposed for the treatment or prevention of paradoxical TB-IRIS.

8.5 Conclusions

This thesis included the largest transcriptomic study conducted in patients who developed paradoxical TB-IRIS to investigate the cellular and molecular mechanisms that underpin the pathophysiology of paradoxical TB-IRIS. The prospective nature of the study allowed us to address knowledge gaps regarding the immune signaling that potentially precede the manifestations of paradoxical TB-IRIS. Prior to ART, patients who developed TB-IRIS later were characterized by impaired neutrophil degranulation, inflammation and recovery from metabolic dysfunction prior to the initiation of ART. Across the studies, at the week 2 which coincides with the median onset of paradoxical TB-IRIS, patient samples were characterized by neutrophilia, neutrophil degranulation, reconstitution of the CD4 lymphocyte compartment, Type I and II interferon signaling, and IL1 family of cytokine signaling which specifically implicates inflammasome mediated pathology in TB-IRIS. The use of prednisone for prevention of

paradoxical TB-IRIS had an effect of inducing epigenetic changes related to remodeling of the cellular cytoskeleton as well as the extracellular matrix which control the behavior of cells. Corticosteroids like prednisone have been shown to reduce the degranulation of neutrophils and it is expected that a higher dose of prednisone could potentially reduce the incidence of paradoxical TB-IRIS significantly.

Together, these findings support a model of paradoxical TB-IRIS pathogenesis where early post-ART changes in neutrophil trafficking, and degranulation, as well as activated and exuberant Mtb-specific IFNγ+ CD4 T cell recovery, lead to hypercytokinemia mediated through the inflammasome and resulting in systemic and local inflammation. Given the downstream consequences of phagocyte activation, Th-1 lymphocyte recovery and cytosolic recognition of danger and pathogen associated molecular patterns via the inflammasome following ART in persons with disseminated TB, the production of IFNγ, IL-12, IL-1β and other proinflammatory cytokines, likely together cause the excessive inflammatory response that is characteristic of paradoxical TB-IRIS. Consistent with this, specific inhibition of the inflammasome was associated with significant reduction of several proinflammatory cytokines including IL-1β and IL-1α.

This data can be used to develop a biosignature that can potentially be used to identify individuals who are at high risk of developing paradoxical TB-IRIS for targeted prevention as well as for developing a biosignature that can diagnose individuals with paradoxical TB-IRIS.

8.6 Future directions

The use of systems biology approaches to explore the immune mediators of paradoxical TB-IRIS provides numerous avenues for selecting future therapeutics and predictive algorithms which can have real impact on the clinical outcomes for patients who develop paradoxical TB-IRIS. Peripheral blood is easily accessible and was used to study the mechanism associated with the pathogenesis of paradoxical TB-IRIS in humans. However, clinical manifestations are often localized and whole blood responses may not represent tissue/organ level immune responses.

In chapter 4, transcription factor profiling of functional Mtb-specific CD4 lymphocytes in peripheral blood mononuclear cells revealed no significant differences between cases and controls.

However significantly higher frequencies in bulk CD4 lymphocytes were observed in patients that developed paradoxical TB-IRIS compared to those who did not, at median onset of clinical manifestations. Since bulk CD4 T cells encompasses all CD4 lymphocyte subsets, future studies can advance this study by conducting similar transcription factor profiling in memory subsets of CD4 T cells using more patient samples. The premise for this is Eomes expression could increase as CD4 lymphocytes gain memory phenotype.

As has been noted in other studies, specific CD4 T cell clonotypes may be preferentially expanded during TB disease. Since reconstitution of the CD4 lymphocyte compartment is a defining feature of paradoxical TB-IRIS, it is possible that specific Mtb-specific clonotypes are preferentially expanded in paradoxical TB-IRIS and thereby contributing to disease. Single cell RNA sequencing, sequencing the TCR of Mtb-specific CD4 lymphocytes in conjunction and spatial transcriptomics workflows could be used successfully to study CD4 clonotypes that are selectively expanded [597].

Neutrophils were implicated in the pathogenesis of paradoxical TB-IRIS. Additionally, aberrant inflammasome activation is likely one of the mechanisms that mediate pathology in people that develop paradoxical TB-IRIS. In chapter 7, specific inhibition of the inflammasome reduced markers of inflammation in an *ex vivo* cell culture model. It has been established that neutrophils express the inflammasome more than other antigen presenting cells [598]. Future studies should consider advancing this work by isolating neutrophils in patients that develop paradoxical TB-IRIS and evaluating the inhibition of the inflammasome directly on neutrophils instead of using peripheral blood mononuclear cells. Also, future phase I clinical trials could be conducted to assess the appropriate dosage and safety of parthenolide in healthy volunteers.

Moreover, the exact mechanisms of inflammasome inhibition by the candidate drugs used in this study remain obscure. To study their exact mechanism of action, future studies can pick up on the *ex vivo* cell culture experiments by collecting cell culture pellets and lysing them for RNA extractions. RNA sequencing could be performed on the RNA extracts and pathway analysis carried out to investigate biological pathways or signaling cascades that are modulated by each inhibitor.

Finally, a major impediment in understanding cellular and biological mechanisms underpinning the pathogenesis of paradoxical TB-IRIS is the lack of clinical specimen at the site of clinical

manifestation. Tissues release DNA which can be recovered in plasma and is called cell free DNA. The field of oncology has successfully established protocols and workflows for studying gene expression at the site of disease by sequencing cell free DNA.

Adapting similar workflows and technologies to study gene expression at the site of clinical manifestation in people who develop paradoxical TB-IRIS is ideal, and promises to advance the agenda of unravelling the mechanisms of TB-IRIS pathogenesis [599, 600]. Future studies should explore this technique to gain better insights about gene expression at tissue level.

8.6 Bibliography

1. Organization WH. Global tuberculosis report 2022. **2022**.
2. Chengalroyen MD, Beukes GM, Gordhan BG, et al. Detection and quantification of differentially culturable tubercle bacteria in sputum from patients with tuberculosis. American journal of respiratory and critical care medicine **2016**; 194:1532-40.
3. Barry 3rd CE, Boshoff HI, Dartois V, et al. The spectrum of latent tuberculosis: rethinking the biology and intervention strategies. Nature Reviews Microbiology **2009**; 7:845-55.
4. Migliori G, Tiberi S. WHO drug-resistant TB guidelines 2022: what is new. Int J Tuberc Lung Dis **2022**; 26:590-1.
5. Sonnenberg P, Glynn JR, Fielding K, Murray J, Godfrey-Faussett P, Shearer S. How soon after infection with HIV does the risk of tuberculosis start to increase? A retrospective cohort study in South African gold miners. Journal of Infectious Diseases **2005**; 191:150-8.
6. Van der Plas H, Meintjes G, Schutz C, et al. Complications of antiretroviral therapy initiation in hospitalised patients with HIV-associated tuberculosis. PLoS One **2013**; 8:e54145.
7. Pooranagangadevi N, Padmapriyadarsini C. Treatment of tuberculosis and the drug interactions associated with HIV-TB co-infection treatment. Frontiers in Tropical Diseases **2022**; 3:834013.
8. Müller M, Wandel S, Colebunders R, Attia S, Furrer H, Egger M. IeDEA Southern and Central Africa. Immune reconstitution inflammatory syndrome in patients starting antiretroviral therapy for HIV infection: a systematic review and meta-analysis. Lancet Infect Dis **2010**; 10:251-61.
9. Namale PE, Abdullahi LH, Fine S, Kamkuemah M, Wilkinson RJ, Meintjes G. Paradoxical TB-IRIS in HIV-infected adults: a systematic review and meta-analysis. Future microbiology **2015**; 10:1077-99.
10. Haddow LJ, Moosa M-YS, Mosam A, Moodley P, Parboosing R, Easterbrook PJ. Incidence, clinical spectrum, risk factors and impact of HIV-associated immune reconstitution inflammatory syndrome in South Africa. PloS one **2012**; 7:e40623.
11. Yang H, Liu Q, Wu Y, He K, Zeng Q, Liu M. Paradoxical tuberculosis-associated immune reconstitution inflammatory syndrome in initiating ART among HIV-Infected patients in China-risk factors and management. BMC infectious diseases **2024**; 24:5.
12. Breen R, Smith C, Bettinson H, et al. Paradoxical reactions during tuberculosis treatment in patients with and without HIV co-infection. Thorax **2004**; 59:704-7.
13. Benson CA, Kaplan JE, Masur H, Pau A, Holmes KK. Treating opportunistic infections among HIV-infected adults and adolescents; recommendations from CDC, the National Institutes of Health, and the HIV Medicine Association/Infectious Diseases Society of America. **2004**.
14. Bana TM, Lesosky M, Pepper DJ, et al. Prolonged tuberculosis-associated immune reconstitution inflammatory syndrome: characteristics and risk factors. BMC Infectious Diseases **2016**; 16:1-12.
15. Marais S, Lai RP, Wilkinson KA, Meintjes G, O'Garra A, Wilkinson RJ. Inflammasome activation underlying central nervous system deterioration in HIV-associated tuberculosis. The Journal of infectious diseases **2017**; 215:677-86.
16. Marais S, Scholtz P, Pepper D, Meintjes G, Wilkinson R, Candy S. Neuroradiological features of the tuberculosis-associated immune reconstitution inflammatory syndrome. The International journal of tuberculosis and lung disease **2010**; 14:188-96.
17. Agarwal U, Kumar A, Behera D, French MA, Price P. Tuberculosis associated immune reconstitution inflammatory syndrome in patients infected with HIV: meningitis a potentially life threatening manifestation. AIDS Research and Therapy **2012**; 9:1-6.
18. Meintjes G, Sonderup MW. A practical approach to the diagnosis and management of paradoxical tuberculosis immune reconstitution inflammatory syndrome: TB-associated immune reconstitution inflammatory syndrome is seen after the initiation of antiretroviral therapy. Continuing Medical Education **2011**; 29.

19. Meintjes G, Wilkinson RJ, Morroni C, et al. Randomized placebo-controlled trial of prednisone for paradoxical TB-associated immune reconstitution inflammatory syndrome. AIDS (London, England) **2010**; 24:2381.
20. Mayosi BM, Ntsekhe M, Bosch J, et al. Prednisolone and Mycobacterium indicus pranii in tuberculous pericarditis. New England Journal of Medicine **2014**; 371:1121-30.
21. Meintjes G, Stek C, Blumenthal L, et al. Prednisone for the prevention of paradoxical tuberculosis-associated IRIS. New England Journal of Medicine **2018**; 379:1915-25.
22. Meintjes G, Lawn SD, Scano F, et al. Tuberculosis-associated immune reconstitution inflammatory syndrome: case definitions for use in resource-limited settings. The Lancet infectious diseases **2008**; 8:516-23.
23. Campbell I, Dyson A. Lymph node tuberculosis: a comparison of various methods of treatment. Tubercle **1977**; 58:171-9.
24. Stek C, Schutz C, Blumenthal L, et al. Preventing paradoxical tuberculosis-associated immune reconstitution inflammatory syndrome in high-risk patients: Protocol of a randomized placebo-controlled trial of prednisone (PredART trial). JMIR research protocols **2016**; 5.
25. Lai RP, Meintjes G, Wilkinson KA, et al. HIV–tuberculosis-associated immune reconstitution inflammatory syndrome is characterized by Toll-like receptor and inflammasome signalling. Nature communications **2015**; 6:8451.
26. Meintjes G, Lawn SD, Scano F, et al. Tuberculosis-associated immune reconstitution inflammatory syndrome: case definitions for use in resource-limited settings. Lancet Infec Dis **2008**; 8:516-23.
27. Conesa-Botella A, Meintjes G, Coussens AK, et al. Corticosteroid therapy, vitamin D status, and inflammatory cytokine profile in the HIV-tuberculosis immune reconstitution inflammatory syndrome. Clin Infect Dis **2012**; 55:1004-11.
28. Lai RP, Meintjes G, Wilkinson KA, et al. HIV–tuberculosis-associated immune reconstitution inflammatory syndrome is characterized by Toll-like receptor and inflammasome signalling. Nat Commun **2015**; 6:8451.
29. Moseki RM, Barber DL, Du Bruyn E, et al. Phenotypic Profile of Mycobacterium tuberculosis-Specific CD4 T-Cell Responses in People With Advanced Human Immunodeficiency Virus Who Develop Tuberculosis-Associated Immune Reconstitution Inflammatory Syndrome. In: Open Forum Infectious Diseases. Oxford University Press US:ofac546.
30. Tan HY, Yong YK, Shankar EM, et al. Aberrant inflammasome activation characterizes tuberculosis-associated immune reconstitution inflammatory syndrome. The Journal of Immunology **2016**; 196:4052-63.
31. Tan HY, Yong YK, Andrade BB, et al. Plasma interleukin-18 levels are a biomarker of innate immune responses that predict and characterize tuberculosis-associated immune reconstitution inflammatory syndrome. Aids **2015**; 29:421-31.
32. Tan DB, Lim A, Yong YK, et al. TLR2-induced cytokine responses may characterize HIV-infected patients experiencing mycobacterial immune restoration disease. Aids **2011**; 25:1455-60.
33. Meintjes G, Skolimowska KH, Wilkinson KA, et al. Corticosteroid-modulated immune activation in the tuberculosis immune reconstitution inflammatory syndrome. American journal of respiratory and critical care medicine **2012**; 186:369-77.
34. Conesa-Botella A, Meintjes G, Coussens AK, et al. Corticosteroid therapy, vitamin D status, and inflammatory cytokine profile in the HIV-tuberculosis immune reconstitution inflammatory syndrome. Clinical infectious diseases **2012**; 55:1004-11.
35. Fleischmann RM, Tesser J, Schiff MH, et al. Safety of extended treatment with anakinra in patients with rheumatoid arthritis. Annals of the rheumatic diseases **2006**; 65:1006-12.

36. Goldbach-Mansky R. Blocking interleukin-1 in rheumatic diseases: Its initial disappointments and recent successes in the treatment of autoinflammatory diseases. Annals of the New York Academy of Sciences **2009**; 1182:111-23.
37. Meintjes G, Wilkinson KA, Rangaka MX, et al. Type 1 helper T cells and FoxP3-positive T cells in HIV–tuberculosis-associated immune reconstitution inflammatory syndrome. American journal of respiratory and critical care medicine **2008**; 178:1083-9.
38. Bourgarit A, Carcelain G, Samri A, et al. Tuberculosis-associated immune restoration syndrome in HIV-1-infected patients involves tuberculin-specific CD4 Th1 cells and KIR-negative γδ T cells. The Journal of Immunology **2009**; 183:3915-23.
39. Bourgarit A, Carcelain G, Martinez V, et al. Explosion of tuberculin-specific Th1-responses induces immune restoration syndrome in tuberculosis and HIV co-infected patients. Aids **2006**; 20:F1-F7.
40. Hsu DC, Breglio KF, Pei L, et al. Emergence of polyfunctional cytotoxic CD4+ T cells in Mycobacterium avium immune reconstitution inflammatory syndrome in human immunodeficiency virus-infected patients. Clinical Infectious Diseases **2018**; 67:437-46.
41. Travers A, Muskhelishvili G. DNA structure and function. The FEBS journal **2015**; 282:2279-95.
42. Storey JD, Madeoy J, Strout JL, Wurfel M, Ronald J, Akey JM. Gene-expression variation within and among human populations. The American Journal of Human Genetics **2007**; 80:502-9.
43. Churko JM, Mantalas GL, Snyder MP, Wu JC. Overview of high throughput sequencing technologies to elucidate molecular pathways in cardiovascular diseases. Circulation research **2013**; 112:1613-23.
44. Kukurba KR, Montgomery SB. RNA sequencing and analysis. Cold Spring Harbor Protocols **2015**; 2015:pdb. top084970.
45. Abubakar I, Tillmann T, Banerjee A. Global, regional, and national age-sex specific all-cause and cause-specific mortality for 240 causes of death, 1990-2013: a systematic analysis for the Global Burden of Disease Study 2013. Lancet **2015**; 385:117-71.
46. Kim J, Park Y, Kim Y, et al. Miliary tuberculosis and acute respiratory distress syndrome. The International Journal of Tuberculosis and Lung Disease **2003**; 7:359-64.
47. Patterson B, Wood R. Is cough really necessary for TB transmission? Tuberculosis **2019**; 117:31-5.
48. Bussi C, Gutierrez MG. Mycobacterium tuberculosis infection of host cells in space and time. FEMS microbiology reviews **2019**; 43:341-61.
49. Baussano I, Williams BG, Nunn P, Beggiato M, Fedeli U, Scano F. Tuberculosis incidence in prisons: a systematic review. PLoS medicine **2010**; 7:e1000381.
50. Balasubramanian V, Wiegeshaus E, Taylor B, Smith D. Pathogenesis of tuberculosis: pathway to apical localization. Tubercle and Lung Disease **1994**; 75:168-78.
51. Sakamoto K. The pathology of Mycobacterium tuberculosis infection. Veterinary pathology **2012**; 49:423-39.
52. Ernst JD. Macrophage receptors for Mycobacterium tuberculosis. Infection and immunity **1998**; 66:1277-81.
53. Boni FG, Hamdi I, Koundi LM, Shrestha K, Xie J. Cytokine storm in tuberculosis and IL-6 involvement. Infection, Genetics and Evolution **2022**; 97:105166.
54. Yogo N, Furukawa C, Hayano S. Paediatric progressive primary tuberculosis. Journal of Clinical Tuberculosis and Other Mycobacterial Diseases **2022**; 28.
55. Comstock GW. Epidemiology of tuberculosis. American Review of Respiratory Disease **1982**; 125:8-15.
56. Dempers J, Sens MA, Wadee SA, Kinney HC, Odendaal HJ, Wright CA. Progressive primary pulmonary tuberculosis presenting as the sudden unexpected death in infancy: a case report. Forensic science international **2011**; 206:e27-e30.
57. Dheda K, Schwander SK, Zhu B, van Zyl-Smit RN, Zhang Y. The immunology of tuberculosis: from bench to bedside. Respirology **2010**; 15:433-50.

58. Cobat A, Gallant CJ, Simkin L, et al. Two loci control tuberculin skin test reactivity in an area hyperendemic for tuberculosis. Journal of Experimental Medicine **2009**; 206:2583-91.
59. Morrison J, Pai M, Hopewell PC. Tuberculosis and latent tuberculosis infection in close contacts of people with pulmonary tuberculosis in low-income and middle-income countries: a systematic review and meta-analysis. The Lancet infectious diseases **2008**; 8:359-68.
60. Houben RM, Dodd PJ. The global burden of latent tuberculosis infection: a re-estimation using mathematical modelling. PLoS medicine **2016**; 13:e1002152.
61. Silva Miranda M, Breiman A, Allain S, Deknuydt F, Altare F. The tuberculous granuloma: an unsuccessful host defence mechanism providing a safety shelter for the bacteria? Journal of Immunology Research **2012**; 2012.
62. Aly S, Wagner K, Keller C, et al. Oxygen status of lung granulomas in Mycobacterium tuberculosis-infected mice. The Journal of Pathology: A Journal of the Pathological Society of Great Britain and Ireland **2006**; 210:298-305.
63. Ramakrishnan L. Revisiting the role of the granuloma in tuberculosis. Nature Reviews Immunology **2012**; 12:352-66.
64. Bafica A, Scanga CA, Feng CG, Leifer C, Cheever A, Sher A. TLR9 regulates Th1 responses and cooperates with TLR2 in mediating optimal resistance to Mycobacterium tuberculosis. The Journal of experimental medicine **2005**; 202:1715-24.
65. Peddireddy V, Doddam SN, Ahmed N. Mycobacterial dormancy systems and host responses in tuberculosis. Frontiers in immunology **2017**; 8:84.
66. Swaminathan S, Narendran G. HIV and tuberculosis in India. Journal of biosciences **2008**; 33:527-37.
67. Winter JR, Smith CJ, Davidson JA, et al. The impact of HIV infection on tuberculosis transmission in a country with low tuberculosis incidence: a national retrospective study using molecular epidemiology. BMC medicine **2020**; 18:1-15.
68. Parandhaman DK, Narayanan S. Cell death paradigms in the pathogenesis of Mycobacterium tuberculosis infection. Frontiers in cellular and infection microbiology **2014**; 4:31.
69. Moraco AH, Kornfeld H. Cell death and autophagy in tuberculosis. In: Seminars in immunology. Elsevier:497-511.
70. Butler RE, Brodin P, Jang J, et al. The balance of apoptotic and necrotic cell death in Mycobacterium tuberculosis infected macrophages is not dependent on bacterial virulence. PLoS one **2012**; 7:e47573.
71. Keane J, Balcewicz-Sablinska MK, Remold HG, et al. Infection by Mycobacterium tuberculosis promotes human alveolar macrophage apoptosis. Infection and immunity **1997**; 65:298-304.
72. Upadhyay S, Mittal E, Philips J. Tuberculosis and the art of macrophage manipulation. Pathog Dis 76: fty037, **2018**.
73. Ferrari G, Langen H, Naito M, Pieters J. A coat protein on phagosomes involved in the intracellular survival of mycobacteria. Cell **1999**; 97:435-47.
74. Chen M, Gan H, Remold HG. A mechanism of virulence: virulent Mycobacterium tuberculosis strain H37Rv, but not attenuated H37Ra, causes significant mitochondrial inner membrane disruption in macrophages leading to necrosis. The Journal of Immunology **2006**; 176:3707-16.
75. Anes E, Pires D, Mandal M, Azevedo-Pereira JM. ESAT-6 a Major Virulence Factor of Mycobacterium tuberculosis. Biomolecules **2023**; 13:968.
76. Zhai W, Wu F, Zhang Y, Fu Y, Liu Z. The immune escape mechanisms of Mycobacterium tuberculosis. International journal of molecular sciences **2019**; 20:340.
77. Derrick SC, Morris SL. The ESAT6 protein of Mycobacterium tuberculosis induces apoptosis of macrophages by activating caspase expression. Cellular microbiology **2007**; 9:1547-55.
78. Sreejit G, Ahmed A, Parveen N, et al. The ESAT-6 protein of Mycobacterium tuberculosis interacts with beta-2-microglobulin (β2M) affecting antigen presentation function of macrophage. PLoS pathogens **2014**; 10:e1004446.

79. Nisa A, Kipper FC, Panigrahy D, Tiwari S, Kupz A, Subbian S. Different modalities of host cell death and their impact on Mycobacterium tuberculosis infection. American Journal of Physiology-Cell Physiology **2022**; 323:C1444-C74.
80. Zhang M, Qi Y, Li H, et al. AIM2 inflammasome mediates Arsenic-induced secretion of IL-1 β and IL-18. Oncoimmunology **2016**; 5:e1160182.
81. Cain KP, McCarthy KD, Heilig CM, et al. An algorithm for tuberculosis screening and diagnosis in people with HIV. New England Journal of Medicine **2010**; 362:707-16.
82. Moodley N, Velen K, Saimen A, Zakhura N, Churchyard G, Charalambous S. Digital Chest Radiography Enhances Screening Efficiency for Pulmonary Tuberculosis in Primary Health Clinics in South Africa. Clinical Infectious Diseases **2022**; 74:1650-8.
83. Soares TR, de Oliveira RD, Liu YE, et al. Evaluation of chest X-ray with automated interpretation algorithms for mass tuberculosis screening in prisons: A cross-sectional study. The Lancet Regional Health–Americas **2023**; 17.
84. Kiazyk S, Ball T. Tuberculosis (TB): Latent tuberculosis infection: An overview. Canada Communicable Disease Report **2017**; 43:62.
85. Helb D, Jones M, Story E, et al. Rapid detection of Mycobacterium tuberculosis and rifampin resistance by use of on-demand, near-patient technology. Journal of clinical microbiology **2010**; 48:229-37.
86. Mechal Y, Benaissa E, El Mrimar N, et al. Evaluation of GeneXpert MTB/RIF system performances in the diagnosis of extrapulmonary tuberculosis. BMC infectious Diseases **2019**; 19:1-8.
87. Dorman SE, Chihota VN, Lewis JJ, et al. Performance characteristics of the Cepheid Xpert MTB/RIF test in a tuberculosis prevalence survey. **2012**.
88. Boldi M-O, Denis-Lessard J, Neziri R, et al. Performance of microbiological tests for tuberculosis diagnostic according to the type of respiratory specimen: A 10-year retrospective study. Frontiers in Cellular and Infection Microbiology **2023**; 13:1131241.
89. Shelburne SA, Visnegarwala F, Darcourt J, et al. Incidence and risk factors for immune reconstitution inflammatory syndrome during highly active antiretroviral therapy. AIDS **2005**; 19:399-406.
90. Campelo TA, Cardoso de Sousa PR, Nogueira LdL, Frota CC, Zuquim Antas PR. Revisiting the methods for detecting Mycobacterium tuberculosis: what has the new millennium brought thus far? Access Microbiology **2021**; 3:000245.
91. Getahun H, Sculier D, Sismanidis C, Grzemska M, Raviglione M. Prevention, diagnosis, and treatment of tuberculosis in children and mothers: evidence for action for maternal, neonatal, and child health services. Journal of Infectious Diseases **2012**; 205:S216-S27.
92. Esposito S, Tagliabue C, Bosis S. Tuberculosis in children. Mediterranean journal of hematology and infectious diseases **2013**; 5.
93. Franco-Paredes C, Rouphael N, del Rio C, Santos-Preciado JI. Vaccination strategies to prevent tuberculosis in the new millennium: from BCG to new vaccine candidates. International journal of infectious diseases **2006**; 10:93-102.
94. Luca S, Mihaescu T. History of BCG vaccine. Maedica **2013**; 8:53-8.
95. REPRESENTATIVES L. The Role of BCG Vaccine in the Prevention and Control of Tuberculosis in the United States A Joint Statement by the Advisory Council for the Elimination of Tuberculosis and the Advisory Committee on Immunization Practices. MMWR Recomm Rep **1996**; 45:1-18.
96. Li J, Zhao A, Tang J, et al. Tuberculosis vaccine development: from classic to clinical candidates. European Journal of Clinical Microbiology & Infectious Diseases **2020**; 39:1405-25.
97. Calmette A. Preventive vaccination against tuberculosis with BCG: SAGE Publications, **1931**.
98. Kuan R, Muskat K, Peters B, Arlehamn CSL. BCG vaccine efficacy, immune correlates of protection and antigen-specific T cell responses. Journal of internal medicine **2020**; 288:651.

99. Andersen P, Doherty TM. The success and failure of BCG—implications for a novel tuberculosis vaccine. Nature Reviews Microbiology **2005**; 3:656-62.
100. Trunz BB, Fine P, Dye C. Effect of BCG vaccination on childhood tuberculous meningitis and miliary tuberculosis worldwide: a meta-analysis and assessment of cost-effectiveness. The Lancet **2006**; 367:1173-80.
101. Colditz GA, Berkey CS, Mosteller F, et al. The efficacy of bacillus Calmette-Guerin vaccination of newborns and infants in the prevention of tuberculosis: meta-analyses of the published literature. Pediatrics **1995**; 96:29-35.
102. Norouzi S, Aghamohammadi A, Mamishi S, Rosenzweig SD, Rezaei N. Bacillus Calmette-Guérin (BCG) complications associated with primary immunodeficiency diseases. Journal of Infection **2012**; 64:543-54.
103. Rodrigues LC, Diwan VK, Wheeler JG. Protective effect of BCG against tuberculous meningitis and miliary tuberculosis: a meta-analysis. International journal of epidemiology **1993**; 22:1154-8.
104. Arregui S, Sanz J, Marinova D, Martín C, Moreno Y. On the impact of masking and blocking hypotheses for measuring the efficacy of new tuberculosis vaccines. PeerJ **2016**; 4:e1513.
105. Palmer CE, Long MW. Effects of infection with atypical mycobacteria on BCG vaccination and tuberculosis. American review of respiratory disease **1966**; 94:553-68.
106. Brandt L, Feino Cunha J, Weinreich Olsen A, et al. Failure of the Mycobacterium bovis BCG vaccine: some species of environmental mycobacteria block multiplication of BCG and induction of protective immunity to tuberculosis. Infection and immunity **2002**; 70:672-8.
107. Oettinger T, Jørgensen M, Ladefoged A, Hasløv K, Andersen P. Development of the Mycobacterium bovis BCG vaccine: review of the historical and biochemical evidence for a genealogical tree. Tubercle and lung disease **1999**; 79:243-50.
108. Rangaka MX, Wilkinson RJ, Boulle A, et al. Isoniazid plus antiretroviral therapy to prevent tuberculosis: a randomised double-blind, placebo-controlled trial. The Lancet **2014**; 384:682-90.
109. Churchyard GJ, Fielding KL, Lewis JJ, et al. A trial of mass isoniazid preventive therapy for tuberculosis control. New England Journal of Medicine **2014**; 370:301-10.
110. Smieja M, Marchetti C, Cook D, Smaill FM, Group CID. Isoniazid for preventing tuberculosis in non-HIV infected persons. Cochrane database of systematic reviews **1996**; 2019.
111. Ayieko J, Abuogi L, Simchowitz B, Bukusi EA, Smith AH, Reingold A. Efficacy of isoniazid prophylactic therapy in prevention of tuberculosis in children: a meta–analysis. BMC infectious diseases **2014**; 14:1-10.
112. Hamada Y, Ford N, Schenkel K, Getahun H. Three-month weekly rifapentine plus isoniazid for tuberculosis preventive treatment: a systematic review. The International Journal of Tuberculosis and Lung Disease **2018**; 22:1422-8.
113. Huang H-L, Lee M-R, Lee C-H, et al. One-month daily and three-month weekly rifapentine plus isoniazid are comparable in completion rate and safety for latent tuberculosis infection in non-HIV Population: a randomized controlled trial. Clinical Microbiology and Infection **2024**; 30:1410-7.
114. Rabahi MF, Silva JLRd, Ferreira ACG, Tannus-Silva DGS, Conde MB. Tuberculosis treatment. Jornal Brasileiro de Pneumologia **2017**; 43:472-86.
115. Hijjar MA, Gerhardt G, Teixeira GM, Procópio MJ. Retrospect of tuberculosis control in Brazil. Revista de Saúde Pública **2007**; 41:50-7.
116. Rosenblatt MB. Pulmonary tuberculosis: evolution of modern therapy. Bulletin of the New York Academy of Medicine **1973**; 49:163.
117. Sharma SK, Mohan A. Tuberculosis: From an incurable scourge to a curable disease-journey over a millennium. The Indian journal of medical research **2013**; 137:455.
118. Blomberg B, Spinaci S, Fourie B, Laing R. The rationale for recommending fixed-dose combination tablets for treatment of tuberculosis. Bulletin of the world health organization **2001**; 79:61-8.

119. Sumartojo E. When tuberculosis treatment fails. Am Rev Respir Dis **1993**; 147:e20.
120. Seung KJ, Keshavjee S, Rich ML. Multidrug-resistant tuberculosis and extensively drug-resistant tuberculosis. Cold Spring Harbor perspectives in medicine **2015**; 5.
121. Jang JG, Chung JH. Diagnosis and treatment of multidrug-resistant tuberculosis. Yeungnam University Journal of Medicine **2020**; 37:277-85.
122. Dheda K, Gumbo T, Maartens G, et al. The epidemiology, pathogenesis, transmission, diagnosis, and management of multidrug-resistant, extensively drug-resistant, and incurable tuberculosis. The lancet Respiratory medicine **2017**; 5:291-360.
123. Liang L, Wu Q, Gao L, et al. Factors contributing to the high prevalence of multidrug-resistant tuberculosis: a study from China. Thorax **2012**; 67:632-8.
124. Oelofse S, Esmail A, Diacon A, et al. Pretomanid with bedaquiline and linezolid for drug-resistant TB: a comparison of prospective cohorts. The International Journal of Tuberculosis and Lung Disease **2021**; 25:453-60.
125. Kharsany AB, Karim QA. HIV infection and AIDS in sub-Saharan Africa: current status, challenges and opportunities. The open AIDS journal **2016**; 10:34.
126. Hill AR, Premkumar S, Brustein S, et al. Disseminated tuberculosis in the acquired immunodeficiency syndrome era. American Review of Respiratory Disease **2012**.
127. Corbett EL, Watt CJ, Walker N, et al. The growing burden of tuberculosis: global trends and interactions with the HIV epidemic. Archives of internal medicine **2003**; 163:1009-21.
128. Opeodu O, Ogunrinde T. Mode of transmission of HIV/Aids: Perception of dental patients in a nigerian teaching hospital. Journal of the West African College of Surgeons **2015**; 5:1.
129. Moyo E, Moyo P, Murewanhema G, Mhango M, Chitungo I, Dzinamarira T. Key populations and Sub-Saharan Africa's HIV response. Frontiers in Public Health **2023**; 11:1079990.
130. Pawlowski A, Jansson M, Sköld M, Rottenberg ME, Källenius G. Tuberculosis and HIV co-infection. PLoS pathogens **2012**; 8:e1002464.
131. Getahun H, Gunneberg C, Granich R, Nunn P. HIV infection—associated tuberculosis: the epidemiology and the response. Clinical Infectious Diseases **2010**; 50:S201-S7.
132. Sathekge M, Maes A, Van de Wiele C. FDG-PET imaging in HIV infection and tuberculosis. In: Seminars in nuclear medicine. Elsevier:349-66.
133. Drain PK, Bajema KL, Dowdy D, et al. Incipient and subclinical tuberculosis: a clinical review of early stages and progression of infection. Clinical microbiology reviews **2018**; 31:10.1128/cmr. 00021-18.
134. Achkar JM, Jenny-Avital ER. Incipient and subclinical tuberculosis: defining early disease states in the context of host immune response. Journal of Infectious Diseases **2011**; 204:S1179-S86.
135. Schutz C, Meintjes G, Almajid F, Wilkinson RJ, Pozniak A. Clinical management of tuberculosis and HIV-1 co-infection: Eur Respiratory Soc, **2010**.
136. Chopra K, Singh S. Tuberculosis: newer diagnostic tests: applications and limitations. Indian Journal of Tuberculosis **2020**; 67:S86-S90.
137. Lawn SD, Kerkhoff AD, Vogt M, Wood R. HIV-associated tuberculosis: relationship between disease severity and the sensitivity of new sputum-based and urine-based diagnostic assays. BMC medicine **2013**; 11:1-10.
138. Södersten E, Ongarello S, Mantsoki A, et al. Diagnostic accuracy study of a novel blood-based assay for identification of tuberculosis in people living with HIV. Journal of clinical microbiology **2021**; 59:10.1128/jcm. 01643-20.
139. Shah M, Hanrahan C, Wang ZY, et al. Lateral flow urine lipoarabinomannan assay for detecting active tuberculosis in HIV-positive adults. Cochrane Database of Systematic Reviews **2016**.
140. Bjerrum S, Schiller I, Dendukuri N, et al. Lateral flow urine lipoarabinomannan assay for detecting active tuberculosis in people living with HIV. Cochrane Database of Systematic Reviews **2019**.

141. Pai M, Menzies D. Interferon-γ release assays: what is their role in the diagnosis of active tuberculosis? Clinical infectious diseases **2007**; 44:74-7.
142. Cattamanchi A, Smith R, Steingart KR, et al. Interferon-gamma release assays for the diagnosis of latent tuberculosis infection in HIV-infected individuals–a systematic review and meta-analysis. Journal of acquired immune deficiency syndromes (1999) **2011**; 56:230.
143. Rangaka MX, Wilkinson KA, Glynn JR, et al. Predictive value of interferon-γ release assays for incident active tuberculosis: a systematic review and meta-analysis. The Lancet infectious diseases **2012**; 12:45-55.
144. Herrera V, Perry S, Parsonnet J, Banaei N. Clinical application and limitations of interferon-γ release assays for the diagnosis of latent tuberculosis infection. Clinical infectious diseases **2011**; 52:1031-7.
145. Dorman SE, Belknap R, Graviss EA, et al. Interferon-γ release assays and tuberculin skin testing for diagnosis of latent tuberculosis infection in healthcare workers in the United States. American journal of respiratory and critical care medicine **2014**; 189:77-87.
146. Gennaro ML. Immunologic diagnosis of tuberculosis. Clinical infectious diseases **2000**; 30:S243-S6.
147. Kunst H. Diagnosis of latent tuberculosis infection: the potential role of new technologies. Respiratory medicine **2006**; 100:2098-106.
148. Wyndham-Thomas C, Corbière V, Dirix V, et al. Key role of effector memory CD4+ T lymphocytes in a short-incubation heparin-binding hemagglutinin gamma interferon release assay for the detection of latent tuberculosis. Clinical and Vaccine Immunology **2014**; 21:321-8.
149. Deeks SG, Lewin SR, Havlir DV. The end of AIDS: HIV infection as a chronic disease. The lancet **2013**; 382:1525-33.
150. Vella S, Schwartländer B, Sow SP, Eholie SP, Murphy RL. The history of antiretroviral therapy and of its implementation in resource-limited areas of the world. Aids **2012**; 26:1231-41.
151. Saag MS, Benson CA, Gandhi RT, et al. Antiretroviral drugs for treatment and prevention of HIV infection in adults: 2018 recommendations of the International Antiviral Society–USA Panel. Jama **2018**; 320:379-96.
152. Maenza J, Flexner C. Combination antiretroviral therapy for HIV infection. American family physician **1998**; 57:2789-98.
153. Worthington RJ, Melander C. Combination approaches to combat multidrug-resistant bacteria. Trends in biotechnology **2013**; 31:177-84.
154. Mahtab S, Coetzee D. Influence of HIV and other risk factors on tuberculosis. South African Medical Journal **2017**; 107:428-38.
155. Cain KP, Anekthananon T, Burapat C, et al. Causes of death in HIV-infected persons who have tuberculosis, Thailand. Emerging infectious diseases **2009**; 15:258.
156. Dodd PJ, Knight GM, Lawn SD, Corbett EL, White RG. Predicting the long-term impact of antiretroviral therapy scale-up on population incidence of tuberculosis. PloS one **2013**; 8:e75466.
157. Lawn SD, Harries A, Williams B, et al. Antiretroviral therapy and the control of HIV-associated tuberculosis. Will ART do it?[Unresolved issues]. The international journal of tuberculosis and lung disease **2011**; 15:571-81.
158. Meintjes G, Brust JC, Nuttall J, Maartens G. Management of active tuberculosis in adults with HIV. The Lancet HIV **2019**; 6:e463-e74.
159. Lawn SD, Meintjes G, McIlleron H, Harries AD, Wood R. Management of HIV-associated tuberculosis in resource-limited settings: a state-of-the-art review. BMC medicine **2013**; 11:1-16.
160. Abdool Karim SS, Naidoo K, Grobler A, et al. Integration of antiretroviral therapy with tuberculosis treatment. New England Journal of Medicine **2011**; 365:1492-501.
161. Blanc F-X, Sok T, Laureillard D, et al. Earlier versus later start of antiretroviral therapy in HIV-infected adults with tuberculosis. New England Journal of Medicine **2011**; 365:1471-81.

162. Tadokera R, Meintjes G, Skolimowska KH, et al. Hypercytokinaemia accompanies HIV–tuberculosis immune reconstitution inflammatory syndrome. European Respiratory Journal **2011**; 37:1248-59.
163. French MA, Price P, Stone SF. Immune restoration disease after antiretroviral therapy. AIDS **2004**; 18:1615-27.
164. Van Rie A, Sawry S, Link-Gelles R, et al. Paradoxical tuberculosis-associated immune reconstitution inflammatory syndrome in children. Pediatric pulmonology **2016**; 51:157-64.
165. French M, Lenzo N, John M, et al. Immune restoration disease after the treatment of immunodeficient HIV-infected patients with highly active antiretroviral therapy. HIV medicine **2000**; 1:107-15.
166. Lawn SD, Myer L, Bekker L-G, Wood R. Tuberculosis-associated immune reconstitution disease: incidence, risk factors and impact in an antiretroviral treatment service in South Africa. Aids **2007**; 21:335-41.
167. Ratnam I, Chiu C, Kandala N-B, Easterbrook P. Incidence and risk factors for immune reconstitution inflammatory syndrome in an ethnically diverse HIV type 1–infected cohort. Clinical Infectious Diseases **2006**; 42:418-27.
168. Kuritzkes DR, Ribaudo HJ, Squires KE, et al. Plasma HIV-1 RNA dynamics in antiretroviral-naive subjects receiving either triple-nucleoside or efavirenz-containing regimens: ACTG A5166s. The Journal of infectious diseases **2007**; 195:1169-76.
169. Uthman OA, Okwundu C, Gbenga K, et al. Optimal timing of antiretroviral therapy initiation for HIV-infected adults with newly diagnosed pulmonary tuberculosis: a systematic review and meta-analysis. Annals of internal medicine **2015**; 163:32-9.
170. Organization WH. Global Tuberculosis Report. Geneva: World Health Organization; 2014. Contract No: WHO/HTM/TB **2016**.
171. Organization WH. Guidelines for managing advanced HIV disease and rapid initiation of antiretroviral therapy, July 2017. Guidelines for managing advanced HIV disease and rapid initiation of antiretroviral therapy, July 2017, **2017**.
172. Organization WH. Consolidated guidelines on the use of antiretroviral drugs for treating and preventing HIV infection: recommendations for a public health approach. **2013**.
173. Bahr N, Boulware DR, Marais S, Scriven J, Wilkinson RJ, Meintjes G. Central nervous system immune reconstitution inflammatory syndrome. Current infectious disease reports **2013**; 15:583-93.
174. Török ME, Yen NTB, Chau TTH, et al. Timing of initiation of antiretroviral therapy in human immunodeficiency virus (HIV)–associated tuberculous meningitis. Clinical infectious diseases **2011**; 52:1374-83.
175. De D, Sarkar RN, Phaujdar S, Bhattacharyya K, Pal HK. Incidence and risk factors of immune reconstitution inflammatory syndrome in HIV-TB coinfected patients. The Brazilian Journal of Infectious Diseases **2011**; 15:553-9.
176. Kumarasamy N, Chaguturu S, Mayer KH, et al. Incidence of immune reconstitution syndrome in HIV/tuberculosis-coinfected patients after initiation of generic antiretroviral therapy in India. JAIDS Journal of Acquired Immune Deficiency Syndromes **2004**; 37:1574-6.
177. Lai RP, Meintjes G, Wilkinson RJ. HIV-1 tuberculosis-associated immune reconstitution inflammatory syndrome. In: Seminars in immunopathology. Springer:185-98.
178. Fishman JE, Saraf-Lavi E, Narita M, Hollender ES, Ramsinghani R, Ashkin D. Pulmonary tuberculosis in AIDS patients: transient chest radiographic worsening after initiation of antiretroviral thrapy. American Journal of Roentgenology **2000**; 174:43-9.
179. Narendran G, Oliveira-de-Souza D, Vinhaes CL, et al. Multifocal tuberculosis-associated immune reconstitution inflammatory syndrome–a case report of a complicated scenario. BMC Infectious Diseases **2019**; 19:1-5.

180. Valentin L, DiNardo A, Chiao E, Woc-Colburn L, Nachiappan A. Case Report: Tuberculosis IRIS: a mediastinal problem. F1000Research **2013**; 2.
181. Musselwhite LW, Andrade BB, Ellenberg SS, et al. Vitamin D, D-dimer, interferon γ, and sCD14 levels are independently associated with immune reconstitution inflammatory syndrome: a prospective, international study. EBioMedicine **2016**; 4:115-23.
182. Haddow LJ, Dibben O, Moosa M-YS, Borrow P, Easterbrook PJ. Circulating inflammatory biomarkers can predict and characterize tuberculosis-associated immune reconstitution inflammatory syndrome. Aids **2011**; 25:1163-74.
183. Michailidis C, Pozniak AL, Mandalia S, Basnayake S, Nelson MR, Gazzard BG. Clinical characteristics of IRIS syndrome in patients with HIV and tuberculosis. Antiviral therapy **2005**; 10:417-22.
184. Kassa E, Enawgaw B, Gelaw A, Gelaw B. Effect of anti-tuberculosis drugs on hematological profiles of tuberculosis patients attending at University of Gondar Hospital, Northwest Ethiopia. BMC hematology **2016**; 16:1-11.
185. Eticha T, Kassa E. Non-adherence to anti-TB drugs and its predictors among TB/HIV co-infected patients in Mekelle, Ethiopia. Journal of Bioanalysis & Biomedicine **2014**; 6.
186. Meintjes G, Rangaka MX, Maartens G, et al. Novel relationship between tuberculosis immune reconstitution inflammatory syndrome and antitubercular drug resistance. Clinical infectious diseases **2009**; 48:667-76.
187. Wells CD, Cegielski JP, Nelson LJ, et al. HIV infection and multidrug-resistant tuberculosis—the perfect storm. The Journal of infectious diseases **2007**; 196:S86-S107.
188. Makhado NA, Matabane E, Faccin M, et al. Outbreak of multidrug-resistant tuberculosis in South Africa undetected by WHO-endorsed commercial tests: an observational study. The Lancet Infectious Diseases **2018**; 18:1350-9.
189. Havlir DV, Getahun H, Sanne I, Nunn P. Opportunities and challenges for HIV care in overlapping HIV and TB epidemics. Jama **2008**; 300:423-30.
190. Singanayagam A, Sridhar S, Dhariwal J, et al. A comparison between two strategies for monitoring hepatic function during antituberculous therapy. American journal of respiratory and critical care medicine **2012**; 185:653-9.
191. Stern A, Green H, Paul M, Vidal L, Leibovici L. Prophylaxis for Pneumocystis pneumonia (PCP) in non-HIV immunocompromised patients. Cochrane database of systematic reviews **2014**.
192. Maze MJ, Bassat Q, Feasey NA, Mandomando I, Musicha P, Crump JA. The epidemiology of febrile illness in sub-Saharan Africa: implications for diagnosis and management. Clinical Microbiology and Infection **2018**; 24:808-14.
193. Goncalves PH, Montezuma-Rusca JM, Yarchoan R, Uldrick TS. Cancer prevention in HIV-infected populations. In: Seminars in oncology. Elsevier:173-88.
194. Kawai T, Akira S. The role of pattern-recognition receptors in innate immunity: update on Toll-like receptors. Nature immunology **2010**; 11:373-84.
195. Rosales C. Neutrophils at the crossroads of innate and adaptive immunity. Journal of Leucocyte Biology **2020**; 108:377-96.
196. Geldmacher C, Schuetz A, Ngwenyama N, et al. Early depletion of Mycobacterium tuberculosis-specific T helper 1 cell responses after HIV-1 infection. The Journal of infectious diseases **2008**; 198:1590-8.
197. Du Bruyn E, Wilkinson RJ. The immune interaction between HIV-1 infection and Mycobacterium tuberculosis. Microbiology Spectrum **2016**; 4:4.6. 40.
198. Chaudhry A, Das SR, Hussain A, et al. The Nef protein of HIV-1 induces loss of cell surface costimulatory molecules CD80 and CD86 in APCs. The Journal of Immunology **2005**; 175:4566-74.
199. Bell LC, Noursadeghi M. Pathogenesis of HIV-1 and Mycobacterium tuberculosis co-infection. Nature Reviews Microbiology **2018**; 16:80-90.

200. Noursadeghi M, Tsang J, Miller RF, et al. Genome-Wide Innate Immune Responses in HIV-1-Infected Macrophages Are Preserved Despite Attenuation of the NF-κB Activation Pathway. The Journal of Immunology **2009**; 182:319-28.
201. Patel NR, Zhu J, Tachado SD, et al. HIV impairs TNF-α mediated macrophage apoptotic response to Mycobacterium tuberculosis. The Journal of Immunology **2007**; 179:6973-80.
202. Naing C, Mak JW, Maung M, Wong SF, Kassim AIBM. Meta-analysis: the association between HIV infection and extrapulmonary tuberculosis. Lung **2013**; 191:27-34.
203. Mayer-Barber KD, Barber DL. Innate and adaptive cellular immune responses to Mycobacterium tuberculosis infection. Cold Spring Harbor perspectives in medicine **2015**; 5:a018424.
204. O'Garra A, Redford PS, McNab FW, Bloom CI, Wilkinson RJ, Berry MP. The immune response in tuberculosis. Annual review of immunology **2013**; 31:475-527.
205. Scriba TJ, Coussens AK, Fletcher HA. Human immunology of tuberculosis. Microbiology spectrum **2017**; 5:10.1128/microbiolspec. tbtb2-0016-2016.
206. Geri G, Passeron A, Heym B, et al. Paradoxical reactions during treatment of tuberculosis with extrapulmonary manifestations in HIV-negative patients. Infection **2013**; 41:537-43.
207. Robbins GK, Spritzler JG, Chan ES, et al. Incomplete reconstitution of T cell subsets on combination antiretroviral therapy in the AIDS Clinical Trials Group protocol 384. Clinical Infectious Diseases **2009**; 48:350-61.
208. Lage SL, Wong C-S, Amaral EP, et al. Classical complement and inflammasome activation converge in CD14highCD16-monocytes in HIV associated TB-immune reconstitution inflammatory syndrome. PLoS Pathogens **2021**; 17:e1009435.
209. Meintjes G, Scriven J, Marais S. Management of the immune reconstitution inflammatory syndrome. Current HIV/AIDS Reports **2012**; 9:238-50.
210. Nusbaum RJ, Calderon VE, Huante MB, et al. Pulmonary tuberculosis in humanized mice infected with HIV-1. Scientific reports **2016**; 6:21522.
211. Barber DL, Andrade BB, McBerry C, Sereti I, Sher A. Role of IL-6 in Mycobacterium avium–associated immune reconstitution inflammatory syndrome. The Journal of Immunology **2014**; 192:676-82.
212. Barber DL, Andrade BB, Sereti I, Sher A. Immune reconstitution inflammatory syndrome: the trouble with immunity when you had none. Nature reviews Microbiology **2012**; 10:150-6.
213. Barber DL, Mayer-Barber KD, Antonelli LR, et al. Th1-driven immune reconstitution disease in Mycobacterium avium–infected mice. Blood, The Journal of the American Society of Hematology **2010**; 116:3485-93.
214. Lai RP, Cortes T, Marais S, et al. Transcriptomic characterization of tuberculous sputum reveals a host Warburg effect and microbial cholesterol catabolism. Mbio **2021**; 12:e01766-21.
215. Khan TA, Mazhar H, Saleha S, Tipu HN, Muhammad N, Abbas MN. Interferon-gamma improves macrophages function against M. tuberculosis in multidrug-resistant tuberculosis patients. Chemotherapy research and practice **2016**; 2016:7295390.
216. Wilson H, de Jong BC, Peterson K, et al. Skewing of the CD4+ T-Cell Pool Toward Monofunctional Antigen-Specific Responses in Patients With Immune Reconstitution Inflammatory Syndrome in The Gambia. Clinical infectious diseases **2013**; 57:594-603.
217. Ravimohan S, Tamuhla N, Nfanyana K, et al. Robust reconstitution of tuberculosis-specific polyfunctional CD4+ T-cell responses and rising systemic interleukin 6 in paradoxical tuberculosis-associated immune reconstitution inflammatory syndrome. Clinical Infectious Diseases **2016**; 62:795-803.
218. Elliott JH, Vohith K, Saramony S, et al. Immunopathogenesis and diagnosis of tuberculosis and tuberculosis-associated immune reconstitution inflammatory syndrome during early antiretroviral therapy. The Journal of infectious diseases **2009**; 200:1736-45.

219. Haridas V, Pean P, Jasenosky LD, et al. TB-IRIS, T-cell activation, and remodeling of the T-cell compartment in highly immunosuppressed HIV-infected patients with TB. Aids **2015**; 29:263-73.
220. Van Kaer L, Parekh VV, Wu L. Invariant natural killer T cells: bridging innate and adaptive immunity. Cell and tissue research **2011**; 343:43-55.
221. Paolini R, Bernardini G, Molfetta R, Santoni A. NK cells and interferons. Cytokine & growth factor reviews **2015**; 26:113-20.
222. Kumar V, Delovitch TL. Different subsets of natural killer T cells may vary in their roles in health and disease. Immunology **2014**; 142:321-36.
223. Bendelac A, Savage PB, Teyton L. The biology of NKT cells. Annu Rev Immunol **2007**; 25:297-336.
224. Bennstein SB. Unraveling natural killer T-cells development. Frontiers in immunology **2018**; 8:1950.
225. Gapin L, Matsuda JL, Surh CD, Kronenberg M. NKT cells derive from double-positive thymocytes that are positively selected by CD1d. Nature immunology **2001**; 2:971-8.
226. Shissler SC, Webb TJ. The ins and outs of type I iNKT cell development. Molecular immunology **2019**; 105:116-30.
227. Sullivan BA, Nagarajan NA, Wingender G, et al. Mechanisms for glycolipid antigen-driven cytokine polarization by Vα14i NKT cells. The journal of immunology **2010**; 184:141-53.
228. Conradie F, Foulkes AS, Ive P, et al. Natural Killer cell activation distinguishes M. tuberculosis-mediated immune reconstitution syndrome (IRIS) from chronic HIV and HIV-MTB co-infection. Journal of acquired immune deficiency syndromes (1999) **2011**; 58:309.
229. Wilkinson KA, Walker NF, Meintjes G, et al. Cytotoxic mediators in paradoxical HIV–tuberculosis immune reconstitution inflammatory syndrome. The Journal of Immunology **2015**; 194:1748-54.
230. Walker NF, Opondo C, Meintjes G, et al. Invariant natural killer T-cell dynamics in human immunodeficiency virus–associated tuberculosis. Clinical Infectious Diseases **2020**; 70:1865-74.
231. Tibúrcio R, Narendran G, Barreto-Duarte B, et al. Frequency of CXCR3+ CD8+ T-lymphocyte subsets in peripheral blood is associated with the risk of paradoxical tuberculosis-associated immune reconstitution inflammatory syndrome development in advanced HIV disease. Frontiers in Immunology **2022**; 13:873985.
232. Goovaerts O, Jennes W, Massinga-Loembé M, et al. Lower pre-treatment T cell activation in early- and late-onset tuberculosis-associated immune reconstitution inflammatory syndrome. PloS one **2015**; 10:e0133924.
233. Goovaerts O, Massinga-Loembé M, Ondoa P, et al. Increased KLRG1 and PD-1 expression on CD8 T lymphocytes in TB-IRIS. PLoS One **2019**; 14:e0215991.
234. Pean P, Nouhin J, Ratana M, et al. High Activation of γδ T cells and the γδ2pos T-cell subset is associated with the onset of tuberculosis-associated immune reconstitution inflammatory syndrome, ANRS 12153 CAPRI NK. Frontiers in immunology **2019**; 10:2018.
235. Tran HTT, Van den Bergh R, Vu TN, et al. The role of monocytes in the development of Tuberculosis-associated Immune Reconstitution Inflammatory Syndrome. Immunobiology **2014**; 219:37-44.
236. Tran HT, Van den Bergh R, Loembé MM, et al. Modulation of the complement system in monocytes contributes to tuberculosis-associated immune reconstitution inflammatory syndrome. Aids **2013**; 27:1725-34.
237. Andrade BB, Singh A, Narendran G, et al. Mycobacterial antigen driven activation of CD14++ CD16− monocytes is a predictor of tuberculosis-associated immune reconstitution inflammatory syndrome. PLoS pathogens **2014**; 10:e1004433.
238. Oliver BG, Elliott JH, Price P, Phillips M, Cooper DA, French MA. Tuberculosis after commencing antiretroviral therapy for HIV infection is associated with elevated CXCL9 and CXCL10 responses to Mycobacterium tuberculosis antigens. JAIDS Journal of Acquired Immune Deficiency Syndromes **2012**; 61:287-92.

239. Nakiwala JK, Walker NF, Diedrich CR, et al. Neutrophil activation and enhanced release of granule products in HIV-TB immune reconstitution inflammatory syndrome. Journal of acquired immune deficiency syndromes (1999) **2018**; 77:221.
240. Ma J, Zhao F, Su W, et al. Zinc finger and interferon-stimulated genes play a vital role in TB-IRIS following HAART in AIDS. Personalized Medicine **2018**; 15:251-69.
241. Marais S, Wilkinson KA, Lesosky M, et al. Neutrophil-associated central nervous system inflammation in tuberculous meningitis immune reconstitution inflammatory syndrome. Clinical infectious diseases **2014**; 59:1638-47.
242. Church P, Judson MA. Paradoxical Reactions and the Immune Reconstitution Infl ammatory Syndrome. Tuberculosis and Nontuberculous Mycobacterial Infections **2021**:509-21.
243. Walker NF, Wilkinson KA, Meintjes G, et al. Matrix degradation in human immunodeficiency virus type 1–Associated tuberculosis and tuberculosis immune reconstitution inflammatory syndrome: a prospective observational study. Clinical Infectious Diseases **2017**; 65:121-32.
244. Ravimohan S, Tamuhla N, Steenhoff AP, et al. Immunological profiling of tuberculosis-associated immune reconstitution inflammatory syndrome and non-immune reconstitution inflammatory syndrome death in HIV-infected adults with pulmonary tuberculosis starting antiretroviral therapy: a prospective observational cohort study. The Lancet Infectious diseases **2015**; 15:429-38.
245. Narendran G, Jyotheeswaran K, Senguttuvan T, et al. Characteristics of paradoxical tuberculosis-associated immune reconstitution inflammatory syndrome and its influence on tuberculosis treatment outcomes in persons living with HIV. International Journal of Infectious Diseases **2020**; 98:261-7.
246. Pepper DJ, Marais S, Maartens G, et al. Neurologic manifestations of paradoxical tuberculosis-associated immune reconstitution inflammatory syndrome: a case series. Clinical Infectious Diseases **2009**; 48:e96-e107.
247. Sumatoh HR, Oliver BG, Kumar M, et al. Mycobacterial antibody levels and immune restoration disease in HIV patients treated in South East Asia. Biomarkers in medicine **2011**; 5:847-53.
248. Simonney N, Dewulf G, Herrmann J-L, et al. Anti-PGL-Tb1 responses as an indicator of the immune restoration syndrome in HIV-TB patients. Tuberculosis **2008**; 88:453-61.
249. Naidoo K, Yende-Zuma N, Padayatchi N, et al. The immune reconstitution inflammatory syndrome after antiretroviral therapy initiation in patients with tuberculosis: findings from the SAPiT trial. Annals of internal medicine **2012**; 157:313-24.
250. Worodria W, Massinga-Loembe M, Mazakpwe D, et al. Incidence and predictors of mortality and the effect of tuberculosis immune reconstitution inflammatory syndrome in a cohort of TB/HIV patients commencing antiretroviral therapy. JAIDS Journal of Acquired Immune Deficiency Syndromes **2011**; 58:32-7.
251. Auld SC, Maenetje P, Ravimohan S, et al. Declines in lung function after antiretroviral therapy initiation in adults with human immunodeficiency virus and tuberculosis: a potential manifestation of respiratory immune reconstitution inflammatory syndrome. Clinical Infectious Diseases **2020**; 70:1750-3.
252. Stek C, Allwood B, Du Bruyn E, et al. The effect of HIV-associated tuberculosis, tuberculosis-IRIS and prednisone on lung function. European Respiratory Journal **2020**; 55.
253. Gopalan N, Chandrasekaran P, Swaminathan S, Tripathy S. Current trends and intricacies in the management of HIV-associated pulmonary tuberculosis. AIDS research and therapy **2016**; 13:1-19.
254. Hardwick C, White D, Morris E, Monteiro E, Breen R, Lipman M. Montelukast in the treatment of HIV associated immune reconstitution disease. Sexually transmitted infections **2006**; 82:513-4.
255. Gill PK. Rapid isolation of peripheral blood mononuclear cells from whole blood with ficoll hypaque density centrifugation. J Int Res Med Pharm Sci **2019**; 14:17-20.
256. Hønge BL, Petersen MS, Olesen R, Møller BK, Erikstrup C. Optimizing recovery of frozen human peripheral blood mononuclear cells for flow cytometry. PloS one **2017**; 12:e0187440.

257. Lindestam Arlehamn CS, McKinney DM, Carpenter C, et al. A quantitative analysis of complexity of human pathogen-specific CD4 T cell responses in healthy M. tuberculosis infected South Africans. PLoS pathogens **2016**; 12:e1005760.
258. Stek C, Schutz C, Blumenthal L, et al. Preventing paradoxical tuberculosis-associated immune reconstitution inflammatory syndrome in high-risk patients: protocol of a randomized placebo-controlled trial of prednisone (PredART Trial). JMIR Research Protocols **2016**; 5:e6046.
259. Technologies T. Universal Plus, Total RNA-Seq with NuoQuant. Online:30.
260. Stoddart D, Heron AJ, Mikhailova E, Maglia G, Bayley H. Single-nucleotide discrimination in immobilized DNA oligonucleotides with a biological nanopore. Proceedings of the National Academy of Sciences **2009**; 106:7702-7.
261. Hyman RW, Jiang H, Fukushima M, Davis RW. A direct comparison of the KB™ Basecaller and phred for identifying the bases from DNA sequencing using chain termination chemistry. BMC research notes **2010**; 3:1-4.
262. Ewels PA, Peltzer A, Fillinger S, et al. The nf-core framework for community-curated bioinformatics pipelines. Nature biotechnology **2020**; 38:276-8.
263. Di Tommaso P, Chatzou M, Floden EW, Barja PP, Palumbo E, Notredame C. Nextflow enables reproducible computational workflows. Nature biotechnology **2017**; 35:316-9.
264. Andrews S. FastQC, A Quality control tool for high throughput sequence data. BibSonomy[(accessed on 17 March 2022)] Available online: https://www bibsonomy org/bibtex/f230a919c34360709aa298734d63dca3 **2015**; 1.
265. Smith T, Heger A, Sudbery I. UMI-tools: modeling sequencing errors in Unique Molecular Identifiers to improve quantification accuracy. Genome research **2017**; 27:491-9.
266. Kopylova E, Noé L, Touzet H. SortMeRNA: fast and accurate filtering of ribosomal RNAs in metatranscriptomic data. Bioinformatics **2012**; 28:3211-7.
267. Dobin A, Davis CA, Schlesinger F, et al. STAR: ultrafast universal RNA-seq aligner. Bioinformatics **2013**; 29:15-21.
268. Patro R, Duggal G, Love MI, Irizarry RA, Kingsford C. Salmon provides fast and bias-aware quantification of transcript expression. Nature methods **2017**; 14:417-9.
269. Li H, Handsaker B, Wysoker A, et al. 1000 genome project data processing subgroup. The sequence alignment/map format and SAMtools. Bioinformatics **2009**; 25:2078-9.
270. Kovaka S, Zimin AV, Pertea GM, Razaghi R, Salzberg SL, Pertea M. Transcriptome assembly from long-read RNA-seq alignments with StringTie2. Genome biology **2019**; 20:1-13.
271. Quinlan AR, Hall IM. BEDTools: a flexible suite of utilities for comparing genomic features. Bioinformatics **2010**; 26:841-2.
272. Wang L, Wang S, Li W. RSeQC: quality control of RNA-seq experiments. Bioinformatics **2012**; 28:2184-5.
273. Ewels P, Magnusson M, Lundin S, Käller M. MultiQC: summarize analysis results for multiple tools and samples in a single report. Bioinformatics **2016**; 32:3047-8.
274. Anders S, Huber W. Differential expression analysis for sequence count data. Nature Precedings **2010**:1-.
275. Love MI, Huber W, Anders S. Moderated estimation of fold change and dispersion for RNA-seq data with DESeq2. Genome biology **2014**; 15:1-21.
276. R Core Team R. R: A language and environment for statistical computing: R foundation for statistical computing Vienna, Austria, **2013**.
277. Maćkiewicz A, Ratajczak W. Principal components analysis (PCA). Computers & Geosciences **1993**; 19:303-42.
278. Kolde R, Kolde MR. Package 'pheatmap'. R package **2015**; 1:790.

279. Abatangelo L, Maglietta R, Distaso A, et al. Comparative study of gene set enrichment methods. BMC bioinformatics **2009**; 10:1-12.
280. Maciejewski H. Gene set analysis methods: statistical models and methodological differences. Briefings in bioinformatics **2014**; 15:504-18.
281. Ebrahimpoor M, Spitali P, Hettne K, Tsonaka R, Goeman J. Simultaneous enrichment analysis of all possible gene-sets: unifying self-contained and competitive methods. Briefings in bioinformatics **2020**; 21:1302-12.
282. Subramanian A, Kuehn H, Gould J, Tamayo P, Mesirov JP. GSEA-P: a desktop application for Gene Set Enrichment Analysis. Bioinformatics **2007**; 23:3251-3.
283. Subramanian A, Tamayo P, Mootha VK, et al. Gene set enrichment analysis: a knowledge-based approach for interpreting genome-wide expression profiles. Proceedings of the National Academy of Sciences **2005**; 102:15545-50.
284. Liberzon A, Birger C, Thorvaldsdóttir H, Ghandi M, Mesirov JP, Tamayo P. The molecular signatures database hallmark gene set collection. Cell systems **2015**; 1:417-25.
285. Liberzon A, Subramanian A, Pinchback R, Thorvaldsdóttir H, Tamayo P, Mesirov JP. Molecular signatures database (MSigDB) 3.0. Bioinformatics **2011**; 27:1739-40.
286. Croft D, O'kelly G, Wu G, et al. Reactome: a database of reactions, pathways and biological processes. Nucleic acids research **2010**; 39:D691-D7.
287. Benjamini Y, Hochberg Y. Controlling the false discovery rate: a practical and powerful approach to multiple testing. Journal of the Royal statistical society: series B (Methodological) **1995**; 57:289-300.
288. Zhang B, Horvath S. A general framework for weighted gene co-expression network analysis. Statistical applications in genetics and molecular biology **2005**; 4.
289. Van Dam S, Vosa U, van der Graaf A, Franke L, de Magalhaes JP. Gene co-expression analysis for functional classification and gene–disease predictions. Briefings in bioinformatics **2018**; 19:575-92.
290. Ruan J, Dean AK, Zhang W. A general co-expression network-based approach to gene expression analysis: comparison and applications. BMC systems biology **2010**; 4:1-21.
291. Horvath S. Weighted network analysis: applications in genomics and systems biology. Springer Science & Business Media, **2011**.
292. Zhao RZ, Jiang S, Zhang L, Yu ZB. Mitochondrial electron transport chain, ROS generation and uncoupling. International journal of molecular medicine **2019**; 44:3-15.
293. Suthar AB, Lawn SD, Del Amo J, et al. Antiretroviral therapy for prevention of tuberculosis in adults with HIV: a systematic review and meta-analysis. PLoS Med **2012**; 9:e1001270.
294. Namale PE, Abdullahi LH, Fine S, Kamkuemah M, Wilkinson RJ, Meintjes G. Paradoxical TB-IRIS in HIV-infected adults: a systematic review and meta-analysis. Future Microbiol **2015**; 10:1077-99.
295. Colebunders R, John L, Huyst V, Kambugu A, Scano F, Lynen L. Tuberculosis immune reconstitution inflammatory syndrome in countries with limited resources. Int J Tuberc Lung Dis **2006**; 10:946-53.
296. Vignesh R, Swathirajan CR, Solomon SS, Shankar EM, Murugavel KG. Risk factors and frequency of tuberculosis-associated immune reconstitution inflammatory syndrome among HIV/Tuberculosis co-infected patients in Southern India. Indian J Med Microbiol **2017**; 35:279.
297. Conradie F, Foulkes AS, Ive P, et al. Natural Killer cell activation distinguishes M. tuberculosis-mediated immune reconstitution syndrome (IRIS) from chronic HIV and HIV-MTB co-infection. AIDS (1999) **2011**; 58:309.
298. Marais S, Meintjes G, Pepper DJ, et al. Frequency, severity, and prediction of tuberculous meningitis immune reconstitution inflammatory syndrome. Clin Infect Dis **2013**; 56:450-60.
299. Tadokera R, Meintjes G, Skolimowska KH, et al. Hypercytokinaemia accompanies HIV–tuberculosis immune reconstitution inflammatory syndrome. Eur Respir J **2011**; 37:1248-59.
300. Tadokera R, Meintjes GA, Wilkinson KA, et al. Matrix metalloproteinases and tissue damage in HIV-tuberculosis immune reconstitution inflammatory syndrome. Eur J immunol **2014**; 44:127-36.

301. Andrade BB, Singh A, Narendran G, et al. Mycobacterial antigen driven activation of CD14++ CD16− monocytes is a predictor of tuberculosis-associated immune reconstitution inflammatory syndrome. PLoS Pathog **2014**; 10:e1004433.
302. Barber DL, Mayer-Barber KD, Antonelli LR, et al. Th1-driven immune reconstitution disease in *Mycobacterium avium*-infected mice. Blood **2010**; 116:3485-93.
303. Barber DL, Andrade BB, Sereti I, Sher A. Immune reconstitution inflammatory syndrome: the trouble with immunity when you had none. Nat Rev Microbiol **2012**; 10:150-6.
304. Meintjes G, Wilkinson KA, Rangaka MX, et al. Type 1 helper T cells and FoxP3-positive T cells in HIV–tuberculosis-associated immune reconstitution inflammatory syndrome. Am J Respir Crit Care Med **2008**; 178:1083-9.
305. Antonelli LR, Mahnke Y, Hodge JN, et al. Elevated frequencies of highly activated CD4+ T cells in HIV+ patients developing immune reconstitution inflammatory syndrome. Blood **2010**; 116:3818-27.
306. Mahnke YD, Greenwald JH, DerSimonian R, et al. Selective expansion of polyfunctional pathogen-specific CD4+ T cells in HIV-1–infected patients with immune reconstitution inflammatory syndrome. Blood **2012**; 119:3105-12.
307. Hsu DC, Breglio KF, Pei L, et al. Emergence of polyfunctional cytotoxic CD4+ T Cells in *Mycobacterium avium* immune reconstitution inflammatory syndrome in human immunodeficiency virus-infected patients. Clin Infect Dis **2018**; 67:437-46.
308. Pearce EL, Mullen AC, Martins GA, et al. Control of effector CD8+ T cell function by the transcription factor Eomesodermin. Science **2003**; 302:1041-3.
309. Szabo SJ, Kim ST, Costa GL, Zhang X, Fathman CG, Glimcher LH. A novel transcription factor, T-bet, directs Th1 lineage commitment. Cell **2000**; 100:655-69.
310. Lindestam Arlehamn CS, McKinney DM, Carpenter C, et al. A quantitative analysis of complexity of human pathogen-specific CD4 T cell responses in healthy *M. tuberculosis* infected South Africans. PLoS Pathog **2016**; 12:e1005760.
311. Cossarizza A, Chang HD, Radbruch A, et al. Guidelines for the use of flow cytometry and cell sorting in immunological studies. Eur J Immunol **2019**; 49:1457-973.
312. Silveira-Mattos PS, Narendran G, Akrami K, et al. Differential expression of CXCR3 and CCR6 on CD4+ T-lymphocytes with distinct memory phenotypes characterizes tuberculosis-associated immune reconstitution inflammatory syndrome. Scientific reports **2019**; 9:1-9.
313. Buggert M, Tauriainen J, Yamamoto T, et al. T-bet and Eomes are differentially linked to the exhausted phenotype of CD8+ T cells in HIV infection. PLoS pathogens **2014**; 10:e1004251.
314. Raveney BJ, Oki S, Hohjoh H, et al. Eomesodermin-expressing T-helper cells are essential for chronic neuroinflammation. Nat Commun **2015**; 6:8437.
315. Chemin K, Ramsköld D, Diaz-Gallo LM, et al. EOMES-positive CD4+ T cells are increased in PTPN22 (1858T) risk allele carriers. Eur J Immunol **2018**; 48:655-69.
316. Mazzoni A, Maggi L, Siracusa F, et al. Eomes controls the development of Th17-derived (non-classic) Th1 cells during chronic inflammation. Eur J Immunol **2019**; 49:79-95.
317. Gruarin P, Maglie S, De Simone M, et al. Eomesodermin controls a unique differentiation program in human IL-10 and IFN-γ coproducing regulatory T cells. Eur J Immunol **2019**; 49:96-111.
318. Schiralli Lester GM, Henderson AJ. Mechanisms of HIV transcriptional regulation and their contribution to latency. Molecular biology international **2012**; 2012.
319. Knox JJ, Cosma GL, Betts MR, McLane LM. Characterization of T-bet and eomes in peripheral human immune cells. Front Immunol **2014**; 5:217.
320. Vignesh R, Kumarasamy N, Lim A, et al. TB-IRIS after initiation of antiretroviral therapy is associated with expansion of preexistent Th1 responses against *Mycobacterium tuberculosis* antigens. AIDS (1999) **2013**; 64:241.

321. Ravimohan S, Tamuhla N, Nfanyana K, et al. Robust reconstitution of tuberculosis-specific polyfunctional CD4+ T-cell responses and rising systemic interleukin 6 in paradoxical tuberculosis-associated immune reconstitution inflammatory syndrome. Clin Infect Dis **2015**; 62:795-803.
322. Tieu HV, Ananworanich J, Avihingsanon A, et al. Immunologic markers as predictors of tuberculosis-associated immune reconstitution inflammatory syndrome in HIV and tuberculosis coinfected persons in Thailand. AIDS research and human retroviruses **2009**; 25:1083-9.
323. Elliott JH, Vohith K, Saramony S, et al. Immunopathogenesis and diagnosis of tuberculosis and tuberculosis-associated immune reconstitution inflammatory syndrome during early antiretroviral therapy. J Infect Dis **2009**; 200:1736-45.
324. Haridas V, Pean P, Jasenosky LD, et al. TB-IRIS, T-cell activation, and remodeling of the T-cell compartment in highly immunosuppressed HIV-infected patients with TB. AIDS **2015**; 29:263-73.
325. Wilkinson KA, Walker NF, Meintjes G, et al. Cytotoxic Mediators in Paradoxical HIV–Tuberculosis Immune Reconstitution Inflammatory Syndrome. J Immunol **2015**; 194:1748-54.
326. Meintjes G, Skolimowska KH, Wilkinson KA, et al. Corticosteroid-modulated immune activation in the tuberculosis immune reconstitution inflammatory syndrome. AM J Respir Crit Care Med **2012**; 186:369-77.
327. Lawn SD, Wood R, Wilkinson RJ. Changing concepts of "latent tuberculosis infection" in patients living with HIV infection. Clinical and Developmental Immunology **2011**; 2011.
328. Rodriguez-Takeuchi SY, Renjifo ME, Medina FJ. Extrapulmonary tuberculosis: pathophysiology and imaging findings. Radiographics **2019**; 39:2023-37.
329. Leeds IL, Magee MJ, Kurbatova EV, et al. Site of extrapulmonary tuberculosis is associated with HIV infection. Clinical Infectious Diseases **2012**; 55:75-81.
330. Welin A, Raffetseder J, Eklund D, Stendahl O, Lerm M. Importance of phagosomal functionality for growth restriction of Mycobacterium tuberculosis in primary human macrophages. Journal of innate immunity **2011**; 3:508-18.
331. Tailleux L, Neyrolles O, Honoré-Bouakline S, et al. Constrained intracellular survival of Mycobacterium tuberculosis in human dendritic cells. The Journal of Immunology **2003**; 170:1939-48.
332. Van der Wel N, Hava D, Houben D, et al. M. tuberculosis and M. leprae translocate from the phagolysosome to the cytosol in myeloid cells. Cell **2007**; 129:1287-98.
333. Toossi Z. The inflammatory response in Mycobacterium tuberculosis infection. Inflammation **2001**:139-51.
334. Madan-Lala R, Peixoto KV, Re F, Rengarajan J. Mycobacterium tuberculosis Hip1 dampens macrophage proinflammatory responses by limiting toll-like receptor 2 activation. Infection and immunity **2011**; 79:4828-38.
335. Park SA, Hyun Y-M. Neutrophil extravasation cascade: what can we learn from two-photon intravital imaging? Immune network **2016**; 16:317-21.
336. Schutz C, Davis AG, Sossen B, et al. Corticosteroids as an adjunct to tuberculosis therapy. Expert review of respiratory medicine **2018**; 12:881-91.
337. Prasad K, Singh MB, Ryan H, Group CID. Corticosteroids for managing tuberculous meningitis. Cochrane Database of Systematic Reviews **1996**; 2016.
338. Thwaites G, Fisher M, Hemingway C, Scott G, Solomon T, Innes J. British Infection Society guidelines for the diagnosis and treatment of tuberculosis of the central nervous system in adults and children. Journal of infection **2009**; 59:167-87.
339. Lanzafame M, Vento S. Tuberculosis-immune reconstitution inflammatory syndrome. Journal of Clinical Tuberculosis and Other Mycobacterial Diseases **2016**; 3:6-9.
340. Barnes PJ. Anti-inflammatory actions of glucocorticoids: molecular mechanisms. Clinical science **1998**; 94:557-72.

341. Barnes PJ. How corticosteroids control inflammation: quintiles prize lecture 2005. British journal of pharmacology **2006**; 148:245-54.
342. Walzl G, Haks MC, Joosten SA, Kleynhans L, Ronacher K, Ottenhoff TH. Clinical immunology and multiplex biomarkers of human tuberculosis. Cold Spring Harbor perspectives in medicine **2015**; 5:a018515.
343. Kitano H. Systems biology: a brief overview. science **2002**; 295:1662-4.
344. Manosuthi W, Van Tieu H, Mankatitham W, et al. Clinical case definition and manifestations of paradoxical tuberculosis-associated immune reconstitution inflammatory syndrome. Aids **2009**; 23:2467-71.
345. Haddow LJ, Moosa M-YS, Easterbrook PJ. Validation of a published case definition for tuberculosis-associated immune reconstitution inflammatory syndrome. Aids **2010**; 24:103-8.
346. Stek C, Buyze J, Menten J, et al. Diagnostic accuracy of the INSHI consensus case definition for the diagnosis of paradoxical tuberculosis-IRIS. Journal of Acquired Immune Deficiency Syndromes (1999) **2021**; 86:587.
347. Esmail H, Lai RP, Lesosky M, et al. Complement pathway gene activation and rising circulating immune complexes characterize early disease in HIV-associated tuberculosis. Proceedings of the National Academy of Sciences **2018**:201711853.
348. Karson M. Handbook of Methods of Applied Statistics. Volume I: Techniques of Computation Descriptive Methods, and Statistical Inference. Volume II: Planning of Surveys and Experiments. IM Chakravarti, RG Laha, and J. Roy, New York, John Wiley; 1967, $9.00: Taylor & Francis, **1968**.
349. Stults DM, Killen MW, Pierce HH, Pierce AJ. Genomic architecture and inheritance of human ribosomal RNA gene clusters. Genome research **2008**; 18:13-8.
350. Korotkevich G, Sukhov V, Budin N, Shpak B, Artyomov MN, Sergushichev A. Fast gene set enrichment analysis. BioRxiv **2016**:060012.
351. Shi J, Walker MG. Gene set enrichment analysis (GSEA) for interpreting gene expression profiles. Current Bioinformatics **2007**; 2:133-7.
352. Chau TT, Ishigaki M, Kataoka T, Taketani S. Ferrochelatase catalyzes the formation of Zn-protoporphyrin of dry-cured ham via the conversion reaction from heme in meat. Journal of agricultural and food chemistry **2011**; 59:12238-45.
353. Lapuente-Brun E, Moreno-Loshuertos R, Acín-Pérez R, et al. Supercomplex assembly determines electron flux in the mitochondrial electron transport chain. Science **2013**; 340:1567-70.
354. Manoj KM. Aerobic respiration: Criticism of the proton-centric explanation involving rotary adenosine triphosphate synthesis, chemiosmosis principle, proton pumps and electron transport chain. Biochemistry insights **2018**; 11:1178626418818442.
355. Martin WF, Thauer RK. Energy in ancient metabolism. Cell **2017**; 168:953-5.
356. Yoon J-Y, Yoon J-Y. Cell Metabolism. Tissue Engineering: A Primer with Laboratory Demonstrations **2022**:33-54.
357. Renassia C, Peyssonnaux C. New insights into the links between hypoxia and iron homeostasis. Current opinion in hematology **2019**; 26:125.
358. Dasaradhan T, Koneti J, Kalluru R, et al. Tuberculosis-associated anemia: a narrative review. Cureus **2022**; 14.
359. Nairz M, Dichtl S, Schroll A, et al. Iron and innate antimicrobial immunity—depriving the pathogen, defending the host. Journal of Trace Elements in Medicine and Biology **2018**; 48:118-33.
360. Stefanova D, Raychev A, Arezes J, et al. Endogenous hepcidin and its agonist mediate resistance to selected infections by clearing non–transferrin-bound iron. Blood, The Journal of the American Society of Hematology **2017**; 130:245-57.
361. Gold BS. The Mycobacterium tuberculosis IdeR: A dual-functional regulator of iron metabolism and virulence. New York University, **2001**.

362. Silva-Gomes S, Vale-Costa S, Appelberg R, Gomes MS. Iron in intracellular infection: to provide or to deprive? Frontiers in Cellular and Infection Microbiology **2013**; 3:96.
363. Beaumont C, Delaby C. Recycling iron in normal and pathological states. In: Seminars in hematology. Elsevier:328-38.
364. Clark MR. Senescence of red blood cells: progress and problems. Physiological reviews **1988**; 68:503-54.
365. de Back DZ, Kostova EB, van Kraaij M, van den Berg TK, Van Bruggen R. Of macrophages and red blood cells; a complex love story. Frontiers in physiology **2014**; 5:9.
366. Straat M, van Bruggen R, de Korte D, Juffermans NP. Red blood cell clearance in inflammation. Transfusion Medicine and Hemotherapy **2012**; 39:353-60.
367. Lodge KM, Cowburn AS, Li W, Condliffe AM. The impact of hypoxia on neutrophil degranulation and consequences for the host. International journal of molecular sciences **2020**; 21:1183.
368. Hoenderdos K, Lodge KM, Hirst RA, et al. Hypoxia upregulates neutrophil degranulation and potential for tissue injury. Thorax **2016**; 71:1030-8.
369. Michiels C. Physiological and pathological responses to hypoxia. The American journal of pathology **2004**; 164:1875-82.
370. Bartels K, Grenz A, Eltzschig HK. Hypoxia and inflammation are two sides of the same coin. Proceedings of the National Academy of Sciences **2013**; 110:18351-2.
371. Bucşan AN, Veatch A, Singh DK, et al. Response to hypoxia and the ensuing dysregulation of inflammation impacts mycobacterium tuberculosis pathogenicity. American journal of respiratory and critical care medicine **2022**; 206:94-104.
372. Prosser G, Brandenburg J, Reiling N, Barry III CE, Wilkinson RJ, Wilkinson KA. The bacillary and macrophage response to hypoxia in tuberculosis and the consequences for T cell antigen recognition. Microbes and infection **2017**; 19:177-92.
373. Kaufmann SH, Dorhoi A. Inflammation in tuberculosis: interactions, imbalances and interventions. Current opinion in immunology **2013**; 25:441-9.
374. Wayne LG, Sohaskey CD. Nonreplicating persistence of Mycobacterium tuberculosis. Annual Reviews in Microbiology **2001**; 55:139-63.
375. Rustad TR, Sherrid AM, Minch KJ, Sherman DR. Hypoxia: a window into Mycobacterium tuberculosis latency. Cellular microbiology **2009**; 11:1151-9.
376. Persson YAZ, Blomgran-Julinder R, Rahman S, Zheng L, Stendahl O. Mycobacterium tuberculosis-induced apoptotic neutrophils trigger a pro-inflammatory response in macrophages through release of heat shock protein 72, acting in synergy with the bacteria. Microbes and infection **2008**; 10:233-40.
377. Ravimohan S, Kornfeld H, Weissman D, Bisson GP. Tuberculosis and lung damage: from epidemiology to pathophysiology. European respiratory review **2018**; 27.
378. Almeida FM, Ventura TL, Amaral EP, et al. Hypervirulent Mycobacterium tuberculosis strain triggers necrotic lung pathology associated with enhanced recruitment of neutrophils in resistant C57BL/6 mice. PloS one **2017**; 12:e0173715.
379. Tan S-Y, Weninger W. Neutrophil migration in inflammation: intercellular signal relay and crosstalk. Current opinion in immunology **2017**; 44:34-42.
380. Burn GL, Foti A, Marsman G, Patel DF, Zychlinsky A. The neutrophil. Immunity **2021**; 54:1377-91.
381. D'Ignazio L, Bandarra D, Rocha S. NF-κB and HIF crosstalk in immune responses. The FEBS journal **2016**; 283:413-24.
382. Hsu BE, Shen Y, Siegel PM. Neutrophils: orchestrators of the malignant phenotype. Frontiers in immunology **2020**; 11:1778.
383. McLaughlin TA, Khayumbi J, Ongalo J, et al. CD4 T cells in Mycobacterium tuberculosis and schistosoma mansoni Co-infected individuals maintain functional TH1 responses. Frontiers in immunology **2020**; 11:127.

384. Green AM, DiFazio R, Flynn JL. IFN-γ from CD4 T cells is essential for host survival and enhances CD8 T cell function during Mycobacterium tuberculosis infection. The Journal of Immunology **2013**; 190:270-7.
385. Rohlwink UK, Figaji A, Wilkinson KA, et al. Tuberculous meningitis in children is characterized by compartmentalized immune responses and neural excitotoxicity. Nature Communications **2019**; 10:3767.
386. Bayat B, Werth S, Sachs UJ, Newman DK, Newman PJ, Santoso S. Neutrophil transmigration mediated by the neutrophil-specific antigen CD177 is influenced by the endothelial S536N dimorphism of platelet endothelial cell adhesion molecule-1. The Journal of Immunology **2010**; 184:3889-96.
387. Eruslanov EB, Lyadova IV, Kondratieva TK, et al. Neutrophil responses to Mycobacterium tuberculosis infection in genetically susceptible and resistant mice. Infection and immunity **2005**; 73:1744-53.
388. Lyadova IV. Neutrophils in tuberculosis: heterogeneity shapes the way? Mediators of inflammation **2017**; 2017.
389. Muller WA. Getting leukocytes to the site of inflammation. Veterinary pathology **2013**; 50:7-22.
390. Chen L, Deng H, Cui H, et al. Inflammatory responses and inflammation-associated diseases in organs. Oncotarget **2018**; 9:7204.
391. Sprague AH, Khalil RA. Inflammatory cytokines in vascular dysfunction and vascular disease. Biochemical pharmacology **2009**; 78:539-52.
392. Szmitko PE, Wang C-H, Weisel RD, de Almeida JR, Anderson TJ, Verma S. New markers of inflammation and endothelial cell activation: Part I. Circulation **2003**; 108:1917-23.
393. Zhang C. The role of inflammatory cytokines in endothelial dysfunction. Basic research in cardiology **2008**; 103:398-406.
394. Mantovani A, Dejana E. Cytokines as communication signals between leukocytes and endothelial cells. Immunology today **1989**; 10:370-5.
395. Joyce DE, Nelson DR, Grinnell BW. Leukocyte and endothelial cell interactions in sepsis: relevance of the protein C pathway. Critical care medicine **2004**; 32:S280-S6.
396. Galley H, Webster N. The immuno-inflammatory cascade. British journal of anaesthesia **1996**; 77:11-6.
397. Galley HF, Webster NR. Physiology of the endothelium. British journal of anaesthesia **2004**; 93:105-13.
398. Luster AD. Chemokines—chemotactic cytokines that mediate inflammation. New England Journal of Medicine **1998**; 338:436-45.
399. Muller WA. Leukocyte–endothelial-cell interactions in leukocyte transmigration and the inflammatory response. Trends in immunology **2003**; 24:326-33.
400. Panés J, Perry M, Granger DN. Leukocyte-endothelial cell adhesion: avenues for therapeutic intervention. British journal of pharmacology **1999**; 126:537.
401. Amarante-Mendes GP, Adjemian S, Branco LM, Zanetti LC, Weinlich R, Bortoluci KR. Pattern recognition receptors and the host cell death molecular machinery. Frontiers in immunology **2018**; 9:2379.
402. Mogensen TH. Pathogen recognition and inflammatory signaling in innate immune defenses. Clinical microbiology reviews **2009**; 22:240-73.
403. Kawasaki T, Kawai T. Toll-like receptor signaling pathways. Frontiers in immunology **2014**; 5:461.
404. Harding CV, Boom WH. Regulation of antigen presentation by Mycobacterium tuberculosis: a role for Toll-like receptors. Nature Reviews Microbiology **2010**; 8:296-307.
405. Hossain M, Norazmi M-N. Pattern recognition receptors and cytokines in Mycobacterium tuberculosis infection—the double-edged sword? BioMed research international **2013**; 2013.

406. Mortaz E, Adcock IM, Tabarsi P, et al. Interaction of pattern recognition receptors with Mycobacterium tuberculosis. Journal of clinical immunology **2015**; 35:1-10.
407. Harriff MJ, Purdy GE, Lewinsohn DM. Escape from the phagosome: the explanation for MHC-I processing of mycobacterial antigens? Frontiers in immunology **2012**; 3:40.
408. Ishikawa F, Miyazaki S. New biodefense strategies by neutrophils. Archivum immunologiae et therapiae experimentalis **2005**; 53:226-33.
409. Lin A, Loré K. Granulocytes: new members of the antigen-presenting cell family. Frontiers in immunology **2017**; 8:1781.
410. Yang C-W, Strong BS, Miller MJ, Unanue ER. Neutrophils influence the level of antigen presentation during the immune response to protein antigens in adjuvants. The Journal of Immunology **2010**; 185:2927-34.
411. Blomgran R, Ernst JD. Lung neutrophils facilitate activation of naive antigen-specific CD4+ T cells during Mycobacterium tuberculosis infection. The Journal of Immunology **2011**; 186:7110-9.
412. Kalyan S, Kabelitz D. When neutrophils meet T cells: beginnings of a tumultuous relationship with underappreciated potential. European journal of immunology **2014**; 44:627-33.
413. Summers C, Rankin SM, Condliffe AM, Singh N, Peters AM, Chilvers ER. Neutrophil kinetics in health and disease. Trends in immunology **2010**; 31:318-24.
414. Chen GY, Nuñez G. Sterile inflammation: sensing and reacting to damage. Nature Reviews Immunology **2010**; 10:826-37.
415. Medzhitov R. Inflammation 2010: new adventures of an old flame. Cell **2010**; 140:771-6.
416. Denning N-L, Aziz M, Gurien SD, Wang P. DAMPs and NETs in sepsis. Frontiers in immunology **2019**; 10:2536.
417. Murao A, Aziz M, Wang H, Brenner M, Wang P. Release mechanisms of major DAMPs. Apoptosis **2021**; 26:152-62.
418. Kaczmarek A, Vandenabeele P, Krysko DV. Necroptosis: the release of damage-associated molecular patterns and its physiological relevance. Immunity **2013**; 38:209-23.
419. Fischle W, Wang Y, Allis CD. Histone and chromatin cross-talk. Current opinion in cell biology **2003**; 15:172-83.
420. Duarte TA, Noronha-Dutra AA, Nery JS, et al. Mycobacterium tuberculosis-induced neutrophil ectosomes decrease macrophage activation. Tuberculosis **2012**; 92:218-25.
421. Nofi CP, Wang P, Aziz M. Chromatin-Associated Molecular Patterns (CAMPs) in sepsis. Cell Death & Disease **2022**; 13:700.
422. Gross O, Thomas CJ, Guarda G, Tschopp J. The inflammasome: an integrated view. Immunological reviews **2011**; 243:136-51.
423. Wawrocki S, Druszczynska M. Inflammasomes in Mycobacterium tuberculosis-driven immunity. Canadian Journal of Infectious Diseases and Medical Microbiology **2017**; 2017.
424. Futosi K, Fodor S, Mócsai A. Reprint of Neutrophil cell surface receptors and their intracellular signal transduction pathways. International immunopharmacology **2013**; 17:1185-97.
425. Krotova K, Khodayari N, Oshins R, Aslanidi G, Brantly ML. Neutrophil elastase promotes macrophage cell adhesion and cytokine production through the integrin-Src kinases pathway. Scientific reports **2020**; 10:15874.
426. Puckett Y, Gabbar A, Bokhari AA. Prednisone. **2018**.
427. Kusiak A, Brady G. Bifurcation of signalling in human innate immune pathways to NF-kB and IRF family activation. Biochemical Pharmacology **2022**:115246.
428. Salminen A, Huuskonen J, Ojala J, Kauppinen A, Kaarniranta K, Suuronen T. Activation of innate immunity system during aging: NF-kB signaling is the molecular culprit of inflamm-aging. Ageing research reviews **2008**; 7:83-105.

429. Narendran G, Kavitha D, Karunaianantham R, et al. Role of LTA4H polymorphism in tuberculosis-associated immune reconstitution inflammatory syndrome occurrence and clinical severity in patients infected with HIV. PLoS One **2016**; 11:e0163298.
430. Stek C, Shey M, Mnika K, et al. Relationship Between LTA4H Promotor Polymorphism and Tuberculosis-Associated Immune Reconstitution Inflammatory Syndrome and Its Prevention With Prednisone. In: Open Forum Infectious Diseases. Oxford University Press US:ofad379.
431. Bergmann TK, Barraclough KA, Lee KJ, Staatz CE. Clinical pharmacokinetics and pharmacodynamics of prednisolone and prednisone in solid organ transplantation. Clinical pharmacokinetics **2012**; 51:711-41.
432. Ronchetti S, Ricci E, Migliorati G, Gentili M, Riccardi C. How glucocorticoids affect the neutrophil life. International journal of molecular sciences **2018**; 19:4090.
433. Cain DW, Cidlowski JA. Immune regulation by glucocorticoids. Nature Reviews Immunology **2017**; 17:233-47.
434. Cavalcanti DMdH, Lotufo CMdC, Borelli P, Ferreira ZS, Markus RP, Farsky SHP. Endogenous glucocorticoids control neutrophil mobilization from bone marrow to blood and tissues in non-inflammatory conditions. British journal of pharmacology **2007**; 152:1291-300.
435. Cavalcanti DM, Lotufo CM, Borelli P, et al. Adrenal deficiency alters mechanisms of neutrophil mobilization. Molecular and cellular endocrinology **2006**; 249:32-9.
436. Lund-Johansen F, Terstappen LW. Differential surface expression of cell adhesion molecules during granulocyte maturation. Journal of leukocyte biology **1993**; 54:47-55.
437. Buckingham JC, John CD, Solito E, et al. Annexin 1, glucocorticoids, and the neuroendocrine–immune interface. Annals of the New York Academy of Sciences **2006**; 1088:396-409.
438. Strausbaugh HJ, Rosen SD. A potential role for annexin 1 as a physiologic mediator of glucocorticoid-induced L-selectin shedding from myeloid cells. The Journal of Immunology **2001**; 166:6294-300.
439. Thon JN, Montalvo A, Patel-Hett S, et al. Cytoskeletal mechanics of proplatelet maturation and platelet release. Journal of Cell Biology **2010**; 191:861-74.
440. Machlus KR, Italiano Jr JE. The incredible journey: From megakaryocyte development to platelet formation. Journal of Cell Biology **2013**; 201:785-96.
441. Wagner DD, Burger PC. Platelets in inflammation and thrombosis. Arteriosclerosis, thrombosis, and vascular biology **2003**; 23:2131-7.
442. Maugeri N, Rovere-Querini P, Manfredi AA. Disruption of a regulatory network consisting of neutrophils and platelets fosters persisting inflammation in rheumatic diseases. Frontiers in Immunology **2016**; 7:182.
443. Semple JW, Italiano JE, Freedman J. Platelets and the immune continuum. Nature Reviews Immunology **2011**; 11:264-74.
444. Maugeri N, Evangelista V, Celardo A, et al. Polymorphonuclear leukocyte-platelet interaction: role of P-selectin in thromboxane B2 and leukotriene C4 cooperative synthesis. Thrombosis and haemostasis **1994**; 72:450-6.
445. Page C, Pitchford S. Neutrophil and platelet complexes and their relevance to neutrophil recruitment and activation. International immunopharmacology **2013**; 17:1176-84.
446. Kornerup KN, Salmon GP, Pitchford SC, Liu WL, Page CP. Circulating platelet-neutrophil complexes are important for subsequent neutrophil activation and migration. Journal of applied physiology **2010**.
447. Clark SR, Ma AC, Tavener SA, et al. Platelet TLR4 activates neutrophil extracellular traps to ensnare bacteria in septic blood. Nature medicine **2007**; 13:463-9.
448. Maugeri N, Rovere-Querini P, Evangelista V, et al. Neutrophils phagocytose activated platelets in vivo: a phosphatidylserine, P-selectin, and β2 integrin–dependent cell clearance program. Blood, The Journal of the American Society of Hematology **2009**; 113:5254-65.

449. Zhang S, Bories G, Lantz C, et al. Immunometabolism of phagocytes and relationships to cardiac repair. Frontiers in Cardiovascular Medicine **2019**; 6:42.
450. Alberts B. DNA replication and recombination. Nature **2003**; 421:431-5.
451. Alberts B, Johnson A, Lewis J, Raff M, Roberts K, Walter P. Chromosomal DNA and its packaging in the chromatin fiber. Molecular Biology of the Cell 4th edition: Garland Science, **2002**.
452. Luger K, Dechassa ML, Tremethick DJ. New insights into nucleosome and chromatin structure: an ordered state or a disordered affair? Nature reviews Molecular cell biology **2012**; 13:436-47.
453. Kornberg RD. Chromatin Structure: A Repeating Unit of Histones and DNA: Chromatin structure is based on a repeating unit of eight histone molecules and about 200 DNA base pairs. Science **1974**; 184:868-71.
454. Nair N, Shoaib M, Sørensen CS. Chromatin dynamics in genome stability: roles in suppressing endogenous DNA damage and facilitating DNA repair. International journal of molecular sciences **2017**; 18:1486.
455. Cutter AR, Hayes JJ. A brief review of nucleosome structure. FEBS letters **2015**; 589:2914-22.
456. Robusti G, Vai A, Bonaldi T, Noberini R. Investigating pathological epigenetic aberrations by epi-proteomics. Clinical Epigenetics **2022**; 14:145.
457. Wilson AG. Epigenetic regulation of gene expression in the inflammatory response and relevance to common diseases. Journal of periodontology **2008**; 79:1514-9.
458. Santos K, Mazzola T, Carvalho H. The prima donna of epigenetics: the regulation of gene expression by DNA methylation. Brazilian Journal of Medical and Biological Research **2005**; 38:1531-41.
459. Budhavarapu VN, Chavez M, Tyler JK. How is epigenetic information maintained through DNA replication? Epigenetics & chromatin **2013**; 6:1-7.
460. Malek TR, Castro I. Interleukin-2 receptor signaling: at the interface between tolerance and immunity. Immunity **2010**; 33:153-65.
461. Doudna JA, Rath VL. Structure and function of the eukaryotic ribosome: the next frontier. Cell **2002**; 109:153-6.
462. Chomczynski P, Wilfinger WW, Eghbalnia HR, Kennedy A, Rymaszewski M, Mackey K. Inter-individual differences in RNA levels in human peripheral blood. PLoS One **2016**; 11:e0148260.
463. Hynes RO. The extracellular matrix: not just pretty fibrils. Science **2009**; 326:1216-9.
464. Har-El R, Tanzer ML. Extracellular matrix 3: evolution of the extracellular matrix in invertebrates. The FASEB journal **1993**; 7:1115-23.
465. Karamanos NK, Theocharis AD, Piperigkou Z, et al. A guide to the composition and functions of the extracellular matrix. The FEBS journal **2021**; 288:6850-912.
466. Hutter H, Vogel BE, Plenefisch JD, et al. Conservation and novelty in the evolution of cell adhesion and extracellular matrix genes. Science **2000**; 287:989-94.
467. Travascio F. Composition and function of the extracellular matrix in the human body. BoD–Books on Demand, **2016**.
468. Trojanowska M. Ets factors and regulation of the extracellular matrix. Oncogene **2000**; 19:6464-71.
469. Kielty CM, Grant ME. The collagen family: structure, assembly, and organization in the extracellular matrix. Connective tissue and its heritable disorders: molecular, genetic, and medical aspects **2002**:159-221.
470. Ricard-Blum S, Ruggiero F. The collagen superfamily: from the extracellular matrix to the cell membrane. Pathologie Biologie **2005**; 53:430-42.
471. Campos EI, Stafford JM, Reinberg D. Epigenetic inheritance: histone bookmarks across generations. Trends in cell biology **2014**; 24:664-74.
472. Tadokera R, Meintjes GA, Wilkinson KA, et al. Matrix metalloproteinases and tissue damage in HIV-tuberculosis immune reconstitution inflammatory syndrome. European Journal of Immunology **2014**; 44:127-36.

473. Tigner A, Ibrahim SA, Murray I. Histology, white blood cell. **2020**.
474. Athens J. Blood: leukocytes. Annual review of physiology **1963**; 25:195-212.
475. Rieger MA, Schroeder T. Hematopoiesis. Cold Spring Harbor perspectives in biology **2012**; 4:a008250.
476. Frenette PS, Mayadas TN, Rayburn H, Hynes RO, Wagner DD. Susceptibility to infection and altered hematopoiesis in mice deficient in both P-and E-selectins. Cell **1996**; 84:563-74.
477. Prinyakupt J, Pluempitiwiriyawej C. Segmentation of white blood cells and comparison of cell morphology by linear and naïve Bayes classifiers. Biomedical engineering online **2015**; 14:1-19.
478. Blumenreich MS. The white blood cell and differential count. Clinical Methods: The History, Physical, and Laboratory Examinations 3rd edition **1990**.
479. Mayadas TN, Cullere X, Lowell CA. The multifaceted functions of neutrophils. Annual Review of Pathology: Mechanisms of Disease **2014**; 9:181-218.
480. Sagiv JY, Voels S, Granot Z. Isolation and characterization of low-vs. high-density neutrophils in cancer. The Tumor Microenvironment: Methods and Protocols **2016**:179-93.
481. Jasper AE, McIver WJ, Sapey E, Walton GM. Understanding the role of neutrophils in chronic inflammatory airway disease. F1000Research **2019**; 8.
482. Zhang L, Yuan Y, Xu Q, Jiang Z, Chu C-Q. Contribution of neutrophils in the pathogenesis of rheumatoid arthritis. Journal of Biomedical Research **2020**; 34:86.
483. Kraus RF, Gruber MA. Neutrophils—From bone marrow to first-line defense of the innate immune system. Frontiers in immunology **2021**; 12:767175.
484. Doulatov S, Notta F, Laurenti E, Dick JE. Hematopoiesis: a human perspective. Cell stem cell **2012**; 10:120-36.
485. Orkin SH, Zon LI. Hematopoiesis: an evolving paradigm for stem cell biology. Cell **2008**; 132:631-44.
486. Sasmono RT, Ehrnsperger A, Cronau SL, et al. Mouse neutrophilic granulocytes express mRNA encoding the macrophage colony-stimulating factor receptor (CSF-1R) as well as many other macrophage-specific transcripts and can transdifferentiate into macrophages in vitro in response to CSF-1. Journal of Leucocyte Biology **2007**; 82:111-23.
487. Ye P, Rodriguez FH, Kanaly S, et al. Requirement of interleukin 17 receptor signaling for lung CXC chemokine and granulocyte colony-stimulating factor expression, neutrophil recruitment, and host defense. The Journal of experimental medicine **2001**; 194:519-28.
488. Gomez JC, Soltys J, Okano K, Dinauer MC, Doerschuk CM. The role of Rac2 in regulating neutrophil production in the bone marrow and circulating neutrophil counts. The American journal of pathology **2008**; 173:507-17.
489. Dancey J, Deubelbeiss KA, Harker LA, Finch CA. Neutrophil kinetics in man. The Journal of clinical investigation **1976**; 58:705-15.
490. Root RK, Dale DC. Granulocyte colony-stimulating factor and granulocyte-macrophage colony-stimulating factor: comparisons and potential for use in the treatment of infections in nonneutropenic patients. The Journal of infectious diseases **1999**; 179:S342-S52.
491. Zuelzer WW, Evans RK, Goodman J. Myelokathexis—a new form of chronic granulocytopenia: report of a case. New England Journal of Medicine **1964**; 270:699-704.
492. Burdon PC, Martin C, Rankin SM. Migration across the sinusoidal endothelium regulates neutrophil mobilization in response to ELR+ CXC chemokines. British journal of haematology **2008**; 142:100-8.
493. Weiss L. Transmural cellular passage in vascular sinuses of rat bone marrow. Blood **1970**; 36:189-208.
494. Campbell FR. Ultrastructural studies of transmural migration of blood cells in the bone marrow of rats, mice and guinea pigs. American Journal of Anatomy **1972**; 135:521-35.
495. Chabot-Richards D, George T. Leukocytosis. International journal of laboratory hematology **2014**; 36:279-88.

496. Hogg JC. Neutrophil kinetics and lung injury. Physiological reviews **1987**; 67:1249-95.
497. Lawrence SM, Corriden R, Nizet V. The ontogeny of a neutrophil: mechanisms of granulopoiesis and homeostasis. Microbiology and Molecular Biology Reviews **2018**; 82:10.1128/mmbr. 00057-17.
498. Rosmarin AG, Yang Z, Resendes KK. Transcriptional regulation in myelopoiesis: Hematopoietic fate choice, myeloid differentiation, and leukemogenesis. Experimental hematology **2005**; 33:131-43.
499. Bratton DL, Henson PM. Neutrophil clearance: when the party is over, clean-up begins. Trends in immunology **2011**; 32:350-7.
500. Hurst JK. What really happens in the neutrophil phagosome? Free Radical Biology and Medicine **2012**; 53:508-20.
501. Borregaard N, Cowland JB. Granules of the human neutrophilic polymorphonuclear leukocyte. Blood, The Journal of the American Society of Hematology **1997**; 89:3503-21.
502. Haslett C, Savill J, Meagher L. The neutrophil. Current opinion in immunology **1989**; 2:10-8.
503. Othman A, Sekheri M, Filep JG. Roles of neutrophil granule proteins in orchestrating inflammation and immunity. The FEBS journal **2022**; 289:3932-53.
504. Lacy P. Mechanisms of degranulation in neutrophils. Allergy, Asthma & Clinical Immunology **2006**; 2:1-11.
505. Cicchetti G, Allen PG, Glogauer M. Chemotactic signaling pathways in neutrophils: from receptor to actin assembly. Critical Reviews in Oral Biology & Medicine **2002**; 13:220-8.
506. Nguyen GT, Green ER, Mecsas J. Neutrophils to the ROScue: mechanisms of NADPH oxidase activation and bacterial resistance. Frontiers in cellular and infection microbiology **2017**; 7:373.
507. Abo A, Webb M, Grogan A, Segal A. Activation of NADPH oxidase involves the dissociation of p21 rac from its inhibitory GDP/GTP exchange protein (rhoGDI) followed by its translocation to the plasma membrane. Biochemical Journal **1994**; 298:585-91.
508. Winterbourn CC, Kettle AJ, Hampton MB. Reactive oxygen species and neutrophil function. Annual review of biochemistry **2016**; 85:765-92.
509. Brinkmann V, Reichard U, Goosmann C, et al. Neutrophil extracellular traps kill bacteria. science **2004**; 303:1532-5.
510. Martinelli S, Urosevic M, Daryadel A, et al. Induction of genes mediating interferon-dependent extracellular trap formation during neutrophil differentiation. Journal of Biological Chemistry **2004**; 279:44123-32.
511. Neeli I, Khan SN, Radic M. Histone deimination as a response to inflammatory stimuli in neutrophils. The Journal of Immunology **2008**; 180:1895-902.
512. Wéra O, Lancellotti P, Oury C. The dual role of neutrophils in inflammatory bowel diseases. Journal of clinical medicine **2016**; 5:118.
513. Chatham W, Edberg J, Kimberley R. The role of neutrophils in rheumatoid arthritis. Rheumatoid arthritis: new frontiers in pathogenesis and treatment New York: Oxford University Press, Inc **2000**:101-12.
514. Soehnlein O, Kai-Larsen Y, Frithiof R, et al. Neutrophil primary granule proteins HBP and HNP1–3 boost bacterial phagocytosis by human and murine macrophages. The Journal of clinical investigation **2008**; 118:3491-502.
515. Tapper H, Karlsson A, Mörgelin M, Flodgaard H, Herwald H. Secretion of heparin-binding protein from human neutrophils is determined by its localization in azurophilic granules and secretory vesicles. Blood, The Journal of the American Society of Hematology **2002**; 99:1785-93.
516. Klebanoff SJ. Myeloperoxidase: friend and foe. Journal of leukocyte biology **2005**; 77:598-625.
517. Kessenbrock K, Krumbholz M, Schönermarck U, et al. Netting neutrophils in autoimmune small-vessel vasculitis. Nature medicine **2009**; 15:623-5.
518. Kougias P, Chai H, Lin PH, Yao Q, Lumsden AB, Chen C. Neutrophil antimicrobial peptide α-defensin causes endothelial dysfunction in porcine coronary arteries. Journal of vascular surgery **2006**; 43:357-63.

519. Panyutich AV, Voitenok NN, Lehrer RI, Ganz T. An enzyme immunoassay for human defensins. Journal of immunological methods **1991**; 141:149-55.
520. Pham CT. Neutrophil serine proteases fine-tune the inflammatory response. The international journal of biochemistry & cell biology **2008**; 40:1317-33.
521. Walker NF, Stek C, Wasserman S, Wilkinson RJ, Meintjes G. The tuberculosis-associated immune reconstitution inflammatory syndrome: recent advances in clinical and pathogenesis research. Current Opinion in HIV and AIDS **2018**; 13:512.
522. Walker NF, Meintjes G, Wilkinson RJ. HIV-1 and the immune response to TB. Future virology **2013**; 8:57-80.
523. Yang H, Biermann MH, Brauner JM, Liu Y, Zhao Y, Herrmann M. New insights into neutrophil extracellular traps: mechanisms of formation and role in inflammation. Frontiers in immunology **2016**; 7:302.
524. O'Donnell JA, Kennedy CL, Pellegrini M, et al. Fas regulates neutrophil lifespan during viral and bacterial infection. Journal of Leucocyte Biology **2015**; 97:321-6.
525. Herrero-Cervera A, Soehnlein O, Kenne E. Neutrophils in chronic inflammatory diseases. Cellular & Molecular Immunology **2022**; 19:177-91.
526. Phillipson M, Kubes P. The neutrophil in vascular inflammation. Nature medicine **2011**; 17:1381-90.
527. Liu L, Wang Y, Zhou J, et al. Rapid non-genomic inhibitory effects of glucocorticoids on human neutrophil degranulation. Inflammation research **2005**; 54:37-41.
528. Buttgereit F, Scheffold A. Rapid glucocorticoid effects on immune cells. Steroids **2002**; 67:529-34.
529. Dinarello CA. Interleukin-1 in the pathogenesis and treatment of inflammatory diseases. Blood, The Journal of the American Society of Hematology **2011**; 117:3720-32.
530. Janeway Jr CA, Medzhitov R. Innate immune recognition. Annual review of immunology **2002**; 20:197-216.
531. Dinarello CA. Overview of the IL-1 family in innate inflammation and acquired immunity. Immunological reviews **2018**; 281:8-27.
532. Quinn CM, Poplin V, Kasibante J, et al. Tuberculosis IRIS: pathogenesis, presentation, and management across the spectrum of disease. Life **2020**; 10:262.
533. Colarusso C, Terlizzi M, Molino A, Pinto A, Sorrentino R. Role of the inflammasome in chronic obstructive pulmonary disease (COPD). Oncotarget **2017**; 8:81813.
534. Spel L, Martinon F. Inflammasomes contributing to inflammation in arthritis. Immunological reviews **2020**; 294:48-62.
535. Yang Y, Wang H, Kouadir M, Song H, Shi F. Recent advances in the mechanisms of NLRP3 inflammasome activation and its inhibitors. Cell death & disease **2019**; 10:128.
536. Suresh R, Mosser DM. Pattern recognition receptors in innate immunity, host defense, and immunopathology. Advances in physiology education **2013**; 37:284-91.
537. Li D, Wu M. Pattern recognition receptors in health and diseases. Signal transduction and targeted therapy **2021**; 6:291.
538. Tang D, Kang R, Coyne CB, Zeh HJ, Lotze MT. PAMP s and DAMP s: Signal 0s that spur autophagy and immunity. Immunological reviews **2012**; 249:158-75.
539. Zheng D, Liwinski T, Elinav E. Inflammasome activation and regulation: toward a better understanding of complex mechanisms. Cell discovery **2020**; 6:36.
540. dos Santos G, Kutuzov MA, Ridge KM. The inflammasome in lung diseases. American Journal of Physiology-Lung Cellular and Molecular Physiology **2012**; 303:L627-L33.
541. Shaw PJ, McDermott MF, Kanneganti T-D. Inflammasomes and autoimmunity. Trends in molecular medicine **2011**; 17:57-64.
542. Davis BK, Wen H, Ting JP-Y. The inflammasome NLRs in immunity, inflammation, and associated diseases. Annual review of immunology **2011**; 29:707-35.

543. Broz P, Dixit VM. Inflammasomes: mechanism of assembly, regulation and signalling. Nature Reviews Immunology **2016**; 16:407.
544. Briken V, Ahlbrand SE, Shah S. Mycobacterium tuberculosis and the host cell inflammasome: a complex relationship. Frontiers in cellular and infection microbiology **2013**; 3:62.
545. Philip NH, Dillon CP, Snyder AG, et al. Caspase-8 mediates caspase-1 processing and innate immune defense in response to bacterial blockade of NF-κB and MAPK signaling. Proceedings of the National Academy of Sciences **2014**; 111:7385-90.
546. Aglietti RA, Dueber EC. Recent insights into the molecular mechanisms underlying pyroptosis and gasdermin family functions. Trends in immunology **2017**; 38:261-71.
547. Denes A, Lopez-Castejon G, Brough D. Caspase-1: is IL-1 just the tip of the ICEberg? Cell death & disease **2012**; 3:e338.
548. Shah S, Bohsali A, Ahlbrand SE, et al. Cutting edge: Mycobacterium tuberculosis but not nonvirulent mycobacteria inhibits IFN-β and AIM2 inflammasome–dependent IL-1β production via its ESX-1 secretion system. The Journal of Immunology **2013**; 191:3514-8.
549. Guo H, Callaway JB, Ting JP. Inflammasomes: mechanism of action, role in disease, and therapeutics. Nature medicine **2015**; 21:677.
550. Mayer-Barber KD, Barber DL, Shenderov K, et al. Cutting edge: caspase-1 independent IL-1β production is critical for host resistance to Mycobacterium tuberculosis and does not require TLR signaling in vivo. The Journal of Immunology **2010**; 184:3326-30.
551. Teresa Cruz M, Ferreira I, Liberal J, D Martins J, Silva A, Miguel Neves B. Inflammasome in dendritic cells immunobiology: implications to diseases and therapeutic strategies. Current drug targets **2017**; 18:1003-18.
552. Garlanda C, Dinarello CA, Mantovani A. The interleukin-1 family: back to the future. Immunity **2013**; 39:1003-18.
553. Dinarello C, Arend W, Sims J, et al. IL-1 family nomenclature. Nature immunology **2010**; 11:973-.
554. Dinarello CA. Immunological and inflammatory functions of the interleukin-1 family. Annual review of immunology **2009**; 27:519-50.
555. Fields JK, Günther S, Sundberg EJ. Structural basis of IL-1 family cytokine signaling. Frontiers in immunology **2019**; 10:1412.
556. Krumm B, Xiang Y, Deng J. Structural biology of the IL-1 superfamily: Key cytokines in the regulation of immune and inflammatory responses. Protein Science **2014**; 23:526-38.
557. Rivers-Auty J, Daniels MJ, Colliver I, Robertson DL, Brough D. Redefining the ancestral origins of the interleukin-1 superfamily. Nature communications **2018**; 9:1156.
558. **!!! INVALID CITATION !!! [18, 21, 22]**.
559. O'Neill L. Signal transduction pathways activated by the IL-1 receptor/toll-like receptor superfamily. Toll-Like Receptor Family Members and Their Ligands **2002**:47-61.
560. Bankers-Fulbright JL, Kalli KR, McKean DJ. Interleukin-1 signal transduction. Life sciences **1996**; 59:61-83.
561. Martin M, Falk W. The interleukin-1 receptor complex and interleukin-1 signal transduction. European cytokine network **1997**; 8:5-17.
562. O'neill L. Interleukin-1 signal transduction. International Journal of Clinical and Laboratory Research **1995**; 25:169-77.
563. Marucha PT, Zeff RA, Kreutzer DL. Cytokine regulation of IL-1 beta gene expression in the human polymorphonuclear leukocyte. Journal of immunology (Baltimore, Md: 1950) **1990**; 145:2932-7.
564. Netea MG, van de Veerdonk FL, van der Meer JW, Dinarello CA, Joosten LA. Inflammasome-independent regulation of IL-1-family cytokines. Annual review of immunology **2015**; 33:49-77.
565. Muñoz-Wolf N, Lavelle EC. A Guide to IL-1 family cytokines in adjuvanticity. The FEBS journal **2018**; 285:2377-401.

566. Bont Nd, Netea MG, Rovers C, et al. LPS-Induced Release of IL-1 β, IL-1Ra, IL-6, and TNF-α in Whole Blood from Patients with Familial Hypercholesterolemia: No Effect of Cholesterol-Lowering Treatment. Journal of interferon & cytokine research **2006**; 26:101-7.
567. Pioli PA, Weaver LK, Schaefer TM, Wright JA, Wira CR, Guyre PM. Lipopolysaccharide-induced IL-1β production by human uterine macrophages up-regulates uterine epithelial cell expression of human β-defensin 2. The Journal of Immunology **2006**; 176:6647-55.
568. Hsu H-Y, Wen M-H. Lipopolysaccharide-mediated reactive oxygen species and signal transduction in the regulation of interleukin-1 gene expression. Journal of Biological Chemistry **2002**; 277:22131-9.
569. Weber A, Wasiliew P, Kracht M. Interleukin-1 (IL-1) pathway. Science signaling **2010**; 3:cm1-cm.
570. Cavalli G, Colafrancesco S, Emmi G, et al. Interleukin 1α: a comprehensive review on the role of IL-1α in the pathogenesis and treatment of autoimmune and inflammatory diseases. Autoimmunity reviews **2021**; 20:102763.
571. Li W, Yamamoto H, Kubo S, Okamura H. Modulation of innate immunity by IL-18. Journal of reproductive immunology **2009**; 83:101-5.
572. Monteleone M, Stow JL, Schroder K. Mechanisms of unconventional secretion of IL-1 family cytokines. Cytokine **2015**; 74:213-8.
573. Sahoo M, Ceballos-Olvera I, del Barrio L, Re F. Role of the Inflammasome, IL-1 ùõΩ, and IL-18 in Bacterial Infections. TheScientificWorldJournal **2011**; 11:2037-50.
574. Rock FL, Hardiman G, Timans JC, Kastelein RA, Bazan JF. A family of human receptors structurally related to Drosophila Toll. Proceedings of the National Academy of Sciences **1998**; 95:588-93.
575. Heguy A, Baldari C, Macchia G, Telford J, Melli M. Amino acids conserved in interleukin-1 receptors (IL-1Rs) and the Drosophila toll protein are essential for IL-1R signal transduction. Journal of Biological Chemistry **1992**; 267:2605-9.
576. Zasłona Z, Pålsson-McDermott EM, Menon D, et al. The induction of pro–IL-1β by lipopolysaccharide requires endogenous prostaglandin E2 production. The Journal of Immunology **2017**; 198:3558-64.
577. Ali Burak O, Geyik C. From viability to cell death: claims with insufficient evidence in high-impact cell culture studies. **2022**.
578. Kwok BH, Koh B, Ndubuisi MI, Elofsson M, Crews CM. The anti-inflammatory natural product parthenolide from the medicinal herb Feverfew directly binds to and inhibits IκB kinase. Chemistry & biology **2001**; 8:759-66.
579. Mathema VB, Koh Y-S, Thakuri BC, Sillanpää M. Parthenolide, a sesquiterpene lactone, expresses multiple anti-cancer and anti-inflammatory activities. Inflammation **2012**; 35:560-5.
580. Saadane A, Masters S, DiDonato J, Li J, Berger M. Parthenolide inhibits IκB kinase, NF-κB activation, and inflammatory response in cystic fibrosis cells and mice. American journal of respiratory cell and molecular biology **2007**; 36:728-36.
581. Liu L, Feng L, Gao J, et al. Parthenolide targets NLRP3 to treat inflammasome-related diseases. International Immunopharmacology **2023**; 119:110229.
582. Juliana C, Fernandes-Alnemri T, Wu J, et al. Anti-inflammatory compounds parthenolide and Bay 11-7082 are direct inhibitors of the inflammasome. Journal of Biological Chemistry **2010**; 285:9792-802.
583. Baskar S, Klein AL, Zeft A. The use of IL-1 receptor antagonist (anakinra) in idiopathic recurrent pericarditis: a narrative review. Cardiology Research and Practice **2016**; 2016.
584. Bresnihan B, Alvaro-Gracia JM, Cobby M, et al. Treatment of rheumatoid arthritis with recombinant human interleukin-1 receptor antagonist. Arthritis & Rheumatism **1998**; 41:2196-204.
585. Mertens M, Singh JA. Anakinra for rheumatoid arthritis. Cochrane database of systematic reviews **2009**.
586. Mertens M, Singh JA. Anakinra for rheumatoid arthritis: a systematic review. The Journal of rheumatology **2009**; 36:1118-25.

587. Cavalli G, Dinarello CA. Anakinra therapy for non-cancer inflammatory diseases. Frontiers in pharmacology **2018**; 9:1157.
588. Huet T, Beaussier H, Voisin O, et al. Anakinra for severe forms of COVID-19: a cohort study. The Lancet Rheumatology **2020**; 2:e393-e400.
589. King A, Vail A, O'Leary C, et al. Anakinra in COVID-19: important considerations for clinical trials. The Lancet Rheumatology **2020**; 2:e379-e81.
590. Khani E, Shahrabi M, Rezaei H, Pourkarim F, Afsharirad H, Solduzian M. Current evidence on the use of anakinra in COVID-19. International Immunopharmacology **2022**:109075.
591. Kyriazopoulou E, Panagopoulos P, Metallidis S, et al. An open label trial of anakinra to prevent respiratory failure in COVID-19. Elife **2021**; 10:e66125.
592. Vitale A, Rigante D, Lucherini OM, et al. Biological treatments: new weapons in the management of monogenic autoinflammatory disorders. Mediators of Inflammation **2013**; 2013.
593. Van Tassell BW, Toldo S, Mezzaroma E, Abbate A. Targeting interleukin-1 in heart disease. Circulation **2013**; 128:1910-23.
594. Kary S, Burmester G. Anakinra: the first interleukin-1 inhibitor in the treatment of rheumatoid arthritis. International journal of clinical practice **2003**; 57:231-4.
595. Arend WP. The mode of action of cytokine inhibitors. The Journal of Rheumatology Supplement **2002**; 65:16-21.
596. Bresnihan B. The prospect of treating rheumatoid arthritis with recombinant human interleukin-1 receptor antagonist. BioDrugs **2001**; 15:87-97.
597. Szabo PA, Levitin HM, Miron M, et al. Single-cell transcriptomics of human T cells reveals tissue and activation signatures in health and disease. Nature communications **2019**; 10:4706.
598. Bakele M, Joos M, Burdi S, et al. Localization and functionality of the inflammasome in neutrophils. Journal of Biological Chemistry **2014**; 289:5320-9.
599. Albitar M, Zhang H, Charifa A, et al. Combining cell-free RNA with cell-free DNA in liquid biopsy for hematologic and solid tumors. Heliyon **2023**; 9.
600. Wang J, Huang J, Hu Y, et al. Terminal modifications independent cell-free RNA sequencing enables sensitive early cancer detection and classification. Nature Communications **2024**; 15:156.